

DISS. ETH NO. 25006

# **Kinetic and Mechanistic Investigation of the Potassium Acyltrifluoroborate Ligation Reaction**

A thesis submitted to attain the degree of

DOCTOR OF SCIENCES of ETH ZURICH

(Dr. sc. ETH Zurich)

Presented by

**SARA DA ROS**

M.Sc. UZH in Chemistry

Born on 04.11.1988

Citizen of Hauptwil-Gottshaus, Thurgau, Switzerland

Accepted on the recommendation of

Prof. Dr. Jeffrey W. Bode, examiner

Prof. Dr. Simon M. Ametamey, co-examiner

2018



*This thesis is dedicated to my parents Markus and Silvia Da Ros.*



*“Education is the most powerful weapon which you can use to change the world.”*

*Nelson Mandela (1918 – 2013)*



---

## Acknowledgements

First and foremost, I would like to thank RPOF. DR. JEFFREY W. BODE for giving me the opportunity to work in his research group and for the supervision of my graduate studies throughout the past three and a half years. I am not only grateful for his support but also the freedom he gave me to pursue my own ideas.

I would like to express my sincere gratitude to PROF. DR. SIMON M. AMETAMEY for accepting the co-examination of my doctoral thesis. His valuable comments and corrections are highly appreciated and substantially improved this thesis. I would also like to thank him for the fruitful collaboration on the KAT radiolabeling project and the many stimulating discussions over the past years.

MARIO KESSINGER is greatly acknowledged for his assistance with organizational and administrative tasks. I would like to thank him for his kind and welcoming nature and for always offering a helping hand when needed.

During my doctoral thesis I was fortunate to be actively engaged in various research collaborations. A special thank goes to my collaborators ERWIN LAM for providing outstanding calculations and the many helpful discussions, HAZEM AHMED for the collaboration on the KAT radiolabeling project and the insightful afternoon in the radiolabeling laboratory and DR. ADRIEN H. MARCHAND for his expertise in mass spectrometry and the days we spent together performing mass experiments.

Additionally, I want to thank all past and present members of the BODE group. Special thanks goes to DR. DMITRY MAZUNIN and DR. GABOR ERŐS for their time and valuable advice especially at the beginning of my doctoral studies. I would like to thank YI-CHUNG DZENG for his inexhaustible interest in my research project and the many stimulating discussions. Furthermore, I am grateful to DR. TOMOYA SHIRO and ALBERTO OSUNA GÁLVEZ for the countless scientific and non-scientific discussions we shared during our time together in Lab F314. I would also like to thank SIMON BALDAUF, GÁBOR BOROSS, DR. BENEDIKT WANNER and DR. FLORIAN ROHRBACHER for the fun times during casual after-work beers and many good group trip memories. I am especially grateful to DR. STÉPHANIE ANTUNES, MARIE PERRIN and ANKITA RAY for their strong support and enthusiasm.

This thesis could have never been realized without the excellent infrastructure and analytical experts at ETH Zurich. Accordingly, I want to thank the past and present NMR service team with RENÉ ARNOLD, RAINER FRANKENSTEIN, PHILIPP ZUMBRUNNEN, STEPHAN BURKHARDT and DR. MARC-OLIVER EBERT, the MS service team with LOUIS BERTSCHI, OSWALD L. GRETER, PETER KÄLIN, DANIEL WIRZ, ROLF HÄFLIGER, DR. XIANGYANG ZHANG and DR. BERTRAN GERRITS and the SMOCC-team with DR. NILS TRAPP and MICHAEL SOLAR. Furthermore, I would like to thank the whole SCHALTER- and ENTSORGUNGS team.

THOMAS MÄDER is greatly acknowledged for the thorough safety education I enjoyed during my time at ETH and as the Bode group's safety representative.

Besides my doctoral studies I had the exceptional opportunity to be an active board member of various ETH organizations. On this occasion, I would like to thank all present and former members of the SOCIETY FOR WOMEN IN NATURAL SCIENCES (WINS) and the UNION OF THE ASSISTANTS AT THE CHEMICAL LABORATORIES OF ETH ZURICH (VAC).

I am especially grateful to my former supervisors and chemistry mentors, DR. ANNA POTIER and DR. XIAOHUI HE for their constant effort to teach me invaluable experimental and theoretical skills, for their time and patience and all their enthusiasm during my education. Both of you have been a true inspiration.

Furthermore, I would like to express my deepest gratitude to the whole team of the GENOMICS INSTITUTE OF THE NOVARTIS RESEARCH FOUNDATION (GNF). Being part of the drug discovery division and working among so many bright and energetic scientists could not have prepared me better for starting my doctoral studies.

I consider myself fortunate to be surrounded by many wonderful friends who have supported me during the past years. Special thanks goes to DR. ANGELO FREI, DR. CEREN YILMAZ, DR. FLORIAN HODEL, CÉDRIC SCHAACK, DR. MICHAEL LÖPFE, JESSICA ROBERTS and SILKE SCHEER for their constant motivation and believe in me. Your friendship and support are invaluable to me.

Von Herzen möchte ich mich auch bei meinen Studienkollegen KRISTINA SIEBERTZ, LEONARD VON ECKHARDSTEIN, MINE KREMER, TINA SCHREIER, DR. LAURA LANDER UND DR. NIKLAS VON WOLFF für die tolle Zeit während des Bachelor und Masterstudiums bedanken und die gute Freundschaft die uns seither verbindet.



Mein besonderer Dank gilt meinen Eltern, MARKUS und SILVIA DA ROS, meinem Bruder, SANDRO DA ROS, und meiner ganzen Familie. Danke für eure Unterstützung während meines gesamten Studiums.

Zuletzt möchte ich mich bei DR. CHRISTIAN EBNER für die grenzenlose Unterstützung und für das kritische Korrekturlesen dieser Arbeit bedanken. Danke für die vielen Gespräche und dein unnachgiebiger Glaube an mich. Du holst stets das Beste aus mir heraus und dafür liebe und schätze ich dich.

## **Publications**

S. Da Ros, A. Linden, K. K. Baldrige, J. S. Siegel

### **Boronic Esters of Corannulene: Potential Building Blocks toward Icosahedral Supramolecules**

*Org. Chem. Front.* **2015**, *2*, 626-633.

X. He, S. Da Ros, J. Nelson, X. Zhu, T. Jiang, B. Okram, S. Jiang, P.-Y. Michellys, M. Iskandar, S. Espinola, Y. Jia, B. Bursulaya, A. Kreuzsch, M.-Y. Gao, G. Spraggon, J. Baaten, L. Clemmer, S. Meeusen, D. Huang, R. Hill, V. Nguyen-Tran, J. Fathman, B. Liu, T. Tuntland, P. Gordon, T. Hollenbeck, K. Ng, J. Shi, L. Bordone, H. Liu

### **Identification of Potent and Selective RIPK2 Inhibitors for the Treatment of Inflammatory Diseases**

*ACS Med. Chem. Lett.* **2017**, *8*, 1048-1053.

S. Da Ros, E. Lam, K. N. Houk, J. W. Bode

### **Improved Kinetics and Advanced Mechanistic Insight of the Chemoselective Amide Bond Forming Ligation Reaction between Potassium Acyltrifluoroborates and Hydroxylamines**

*Manuscript in preparation.*

## **Poster and Oral Presentations**

### **EuCheMS Chemistry Congress**

Poster Presentation, Prague, Czech Republik, August 2012

### **GNF Chemistry Meeting**

Oral Presentation, La Jolla, California, US, February 2013

### **Academic Exchange Collaboration and Research (AECOR) Symposium**

Oral Presentation, Zurich, Switzerland, November 2017

---

## Table of Contents

Acknowledgements.....	i
Publications.....	iv
Poster and Oral Presentations.....	iv
Table of Contents.....	v
Abstract.....	ix
Zusammenfassung .....	xii
List of Abbreviations, Acronyms and Symbols.....	xvi
<b>Chapter 1 Introduction.....</b>	<b>1</b>
1 Introduction .....	3
1.1 Proteins – The Essence of Biological Life.....	3
1.2 Protein Modification.....	6
1.3 Protein Bioconjugation and Polymerization .....	6
1.3.1 Bioorthogonal Ligation Reactions .....	8
1.3.1.1 Oxime and Hydrazone Ligation.....	11
1.3.1.2 Pictet-Spengler Ligation .....	12
1.3.1.3 Staudinger Ligation .....	12
1.3.1.4 Copper-Catalyzed Azide-Alkyne 1,3-Dipolar Cycloaddition .....	14
1.3.1.5 Strain-Promoted Azide-Alkyne 1,3-Dipolar Cycloaddition.....	15
1.3.1.6 Tetrazine Ligation.....	16
1.3.1.7 Thiol-Maleimide Ligation .....	17
1.3.1.8 Native Chemical Ligation .....	18
1.3.1.9 $\alpha$ -Ketoacid-hydroxylamine Ligation .....	19
1.3.2 Limitations of Bioorthogonal Ligation Reactions .....	20
1.3.3 The Importance of Reaction Kinetics .....	21
1.4 Potassium Acyltrifluoroborate (KAT) Ligation .....	22
1.4.1 Synthesis of Potassium Acyltrifluoroborates (KATs).....	22
1.4.2 Synthesis of Hydroxylamines .....	26
1.4.3 Synthetic Limitations and Applications of Potassium Acyltrifluoroborates .....	28
1.5 Concluding Remarks.....	31
1.6 References.....	32

---

<b>Chapter 2 First Generation of Acyltrifluoroborates with Enhanced KAT Ligation Kinetics.....</b>	<b>51</b>
2 First Generation of Acyltrifluoroborates with Enhanced KAT Ligation Kinetics.....	53
2.1 Research Goal and Rationale .....	53
2.2 Strategies for the Improvement of KAT Ligation Kinetics .....	54
2.3 Design of Novel Acyltrifluoroborates .....	54
2.3.1 Strategy I – Modification of the KAT Moiety .....	56
2.3.2 Strategy II – Modification of the KAT Backbone.....	58
2.4 Pyridyl Acyltrifluoroborates.....	60
2.4.1 Initial Kinetic Investigations .....	60
2.4.2 Substitution Effects .....	66
2.4.3 Variable pH Kinetic Studies.....	73
2.4.4 Specific Acid Catalysis vs. General Acid Catalysis .....	75
2.5 Concluding Remarks.....	76
2.5.1 References.....	77
<b>Chapter 3 Mechanistic Investigations of the KAT Ligation.....</b>	<b>79</b>
3 Mechanistic Investigations of the KAT Ligation .....	81
3.1 Introductory Remarks.....	81
3.2 Reaction Profile of the KAT Ligation .....	82
3.3 Potential Mechanistic Pathways.....	86
3.4 DFT Calculations.....	88
3.5 Determination of Activation Parameters.....	96
3.6 The Important Role of Acid in KAT Ligation Kinetics .....	97
3.7 Concluding Remarks.....	98
3.8 References.....	99
<b>Chapter 4 Application of Pyridyl KATs in Radiolabeling .....</b>	<b>103</b>
4 Application of Pyridyl KATs in Radiolabeling .....	105
4.1 Introduction .....	105
4.1.1 General Remarks .....	105
4.1.2 Positron Emission Tomography .....	105

---

4.2	Project Goal and Rationale .....	107
4.3	Synthesis of KATs for Radiolabeling.....	108
4.4	Radiolabeling of KATs.....	109
4.5	KAT Ligation Using Radiolabeled Pyridyl KATs.....	113
4.6	Incorporation of Labeled Pyridyl KATs into Peptides and Proteins.....	114
4.7	Concluding Remarks.....	115
4.8	References.....	116
<b>Chapter 5 Second Generation of Acyltrifluoroborates with Enhanced KAT Ligation Kinetics .....</b>		<b>121</b>
5	Second Generation of Acyltrifluoroborates with Enhanced KAT Ligation Kinetics	123
5.1	Introductory Remarks.....	123
5.2	From Pyridine to Other Heterocyclic Acyltrifluoroborates .....	124
5.3	Kinetics of Quinoline KATs.....	126
5.4	Synthesis and Functionalization of Quinoline KATs .....	133
5.5	Concluding Remarks.....	135
5.6	References.....	135
<b>Chapter 6 Conclusion and Outlook.....</b>		<b>137</b>
6	Conclusion and Outlook.....	139
6.1	Conclusion .....	139
6.2	Outlook.....	141
6.2.1	Application of Pyridyl KAT Ligation in Bioconjugation.....	141
6.2.2	Potential Applications of Quinoline KAT Ligation .....	142
6.3	References.....	143
<b>Chapter 7 Experimental Procedures and Characterization Data.....</b>		<b>145</b>
7	Experimental Procedures and Characterization Data.....	147
7.1	General Methods.....	147
7.2	Experimental Procedures and Characterization Data .....	150
7.3	Kinetic Procedures and Data .....	181
7.4	References.....	253

---

<b>Chapter 8 Spectroscopic Data and DFT Calculations .....</b>	<b>259</b>
8 Spectroscopic Data and DFT Calculations .....	261
8.1 NMR Spectroscopic Data.....	261
8.2 DFT Calculations.....	324
Curriculum Vitae.....	xxii

## Abstract

In 2012, BODE and MOLANDER reported a novel amide bond forming ligation reaction between potassium acyltrifluoroborates (KATs) and *O*-acylhydroxylamines (Scheme I). This chemoselective and bioorthogonal ligation reaction, commonly referred to as the KAT ligation, has great potential to fulfill all the requirements necessary to enable the efficient conjugation of biomolecules. The reaction operates in water at room temperature, without the need for additional reagents or catalysts, forms stable and naturally occurring amide bond linkages and has been shown to produce only non-toxic byproducts. In addition, the KAT ligation displays fast reaction kinetics under acidic conditions and has successfully been applied in the PEGylation, lipidation and biotinylation of unprotected peptides. However, recent studies have shown that the KAT ligation suffers from a significant decrease in reaction rates at elevated pH values (>pH 5), which up to date renders this ligation reaction inefficient for the equimolar conjugation of large biomolecules under physiological conditions.



**Scheme I** KAT ligation reaction between potassium acyltrifluoroborates and *O*-acylhydroxylamines.

In an effort to expand the utility of the KAT ligation for biological applications, we envisioned the development of improved ligation kinetics at physiological pH. In the first part of this thesis, we identified 2-pyridyl KATs as a novel generation of acyltrifluoroborates with enhanced overall ligation kinetics by up to two orders of magnitude compared to traditionally used aryl KATs (Figure I).

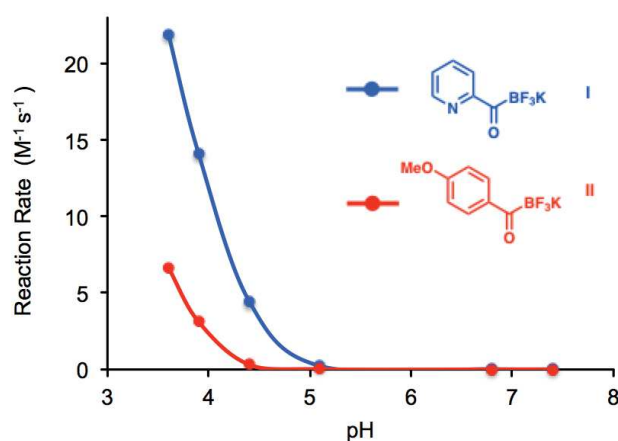


**Figure I** Comparison of KAT ligation rates between pyridyl and aryl KATs over a selected pH range.

Real time NMR kinetic studies of a panel of more than 30 acyltrifluoroborates under deuterated aqueous conditions at physiological pH (pH 5.1 – 7.4) were conducted and the resulting second-order rate constants were evaluated. The kinetic data indicates that the pyridyl nitrogen at the ortho position of the acyltrifluoroborate group plays a key role in enhancing the reaction kinetics by acting as proton acceptor/donor during the course of the ligation reaction (Figure 2).

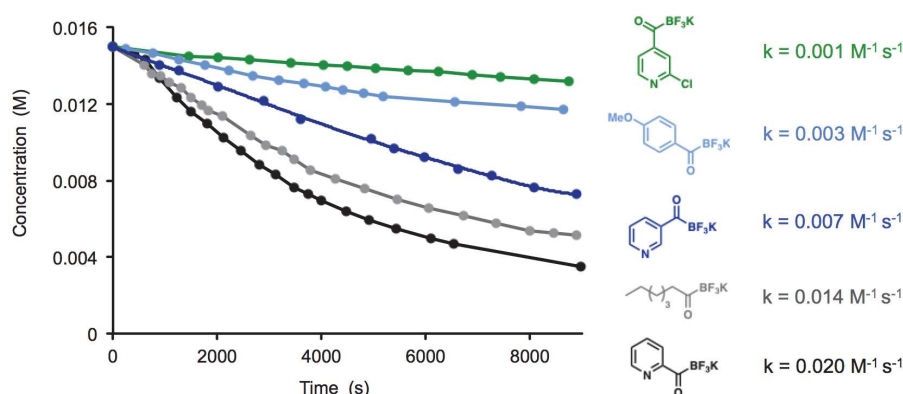
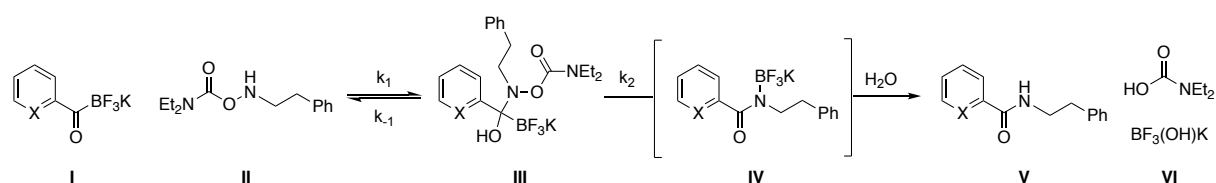


**Figure II** Comparison of KAT ligation rates between various KAT species.

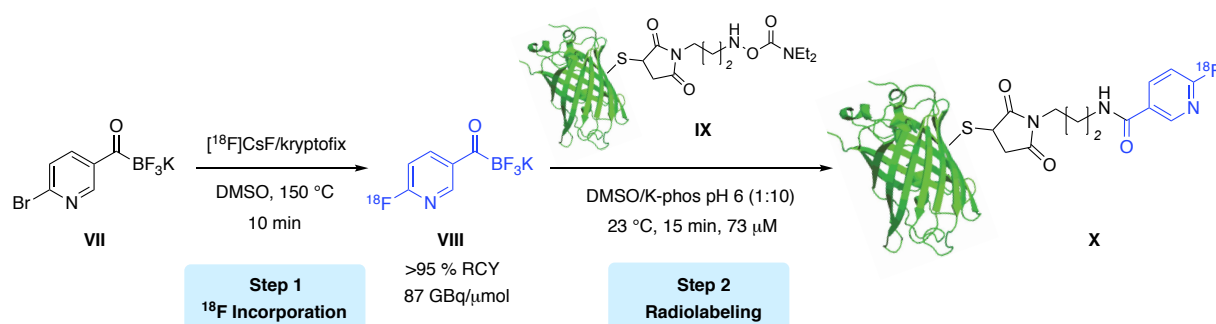
In the second part of this thesis, extensive experimental and computational mechanistic studies provided an in-depth understanding of the KAT ligation mechanism. Detailed analysis of the reaction profile by real time  $^1\text{H}$  NMR disclosed that the KAT ligation proceeds via a rate determining pre-equilibrium in lieu of following traditional second-order kinetics (Scheme II). The rate-determining step of the ligation reaction was found to be the breakdown of the tetrahedral intermediate **III** ( $k_2$ ). Furthermore, we postulate that the ligation mechanism proceeds via nucleophilic attack of hydroxylamine **II** to the carbonyl carbon of the KAT **I** resulting in a tetrahedral addition intermediate **III**. Concerted elimination of **III** further leads to a *N*-trifluoroboryl species **IV**, which is short-lived and thus rapidly collapses to the desired amide product **V**. Noteworthy, it was discovered that 2-pyridyl KATs enable proton transfer under mildly acidic conditions and thus facilitate the rate-determining breakdown of the tetrahedral intermediate.



**Scheme II** Postulated KAT ligation mechanism.



In the third part of this thesis, pyridyl KATs were identified as suitable candidates for radiolabeling. Rapid introduction of  $^{18}\text{F}$  into 6-bromo-nicotinoyltrifluoroborate **VII** was achieved by nucleophilic aromatic substitution in a single step (Scheme III). In addition, it was shown that  $^{18}\text{F}$ -labeled 6-fluoro-nicotinoyltrifluoroborate **VIII** is prone to undergo KAT ligation reactions with hydroxylamines in acidic aqueous media or rat plasma at room temperature. This paved the way for the  $^{18}\text{F}$ -labeling of larger molecules, such as a model peptide and superfolder green fluorescent protein (sfGFP) **IX**, bearing hydroxylamines.



**Scheme III** Radiolabeling of pyridyl KAT **VII** and incorporation of labeled pyridyl KAT **VIII** into sfGFP by KAT ligation.

The advanced mechanistic insight of the KAT ligation allowed for further structural fine-tuning of potassium acyltrifluoroborates and led us to the discovery of new *N*-heterocyclic KATs with even faster ligation rates. In the last part of this thesis, we demonstrate that 8-quinoline KATs are superior potassium acyltrifluoroborates with second-order rate constants of up to  $4.8 \text{ M}^{-1} \text{ s}^{-1}$  at pH 6.8 (Figure III). Hence, 8-quinoline KATs display a rate increase  $>1000$  fold compared to state-of-the-art aryl KATs.

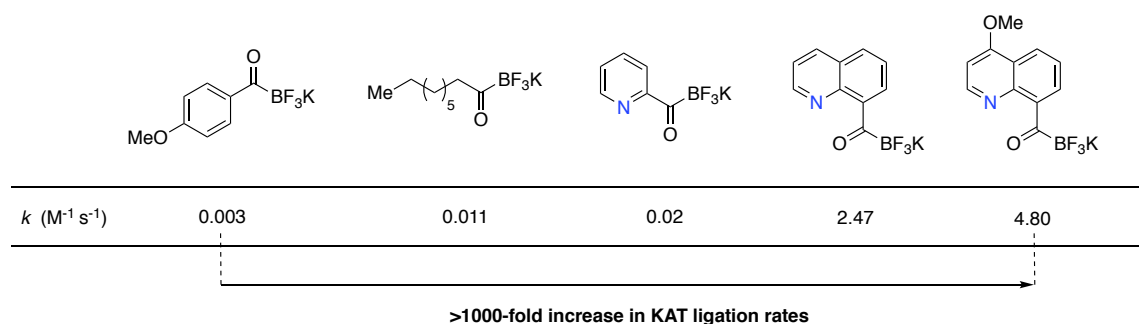
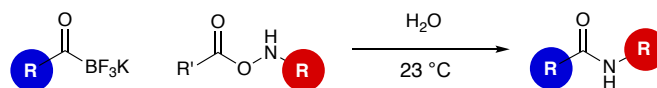


**Figure III** Comparison of KAT ligation kinetics of different KAT species.

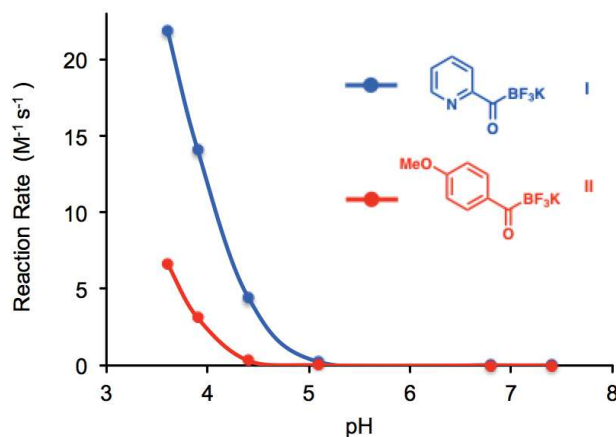
## Zusammenfassung

Im Jahre 2012 veröffentlichten BODE und MOLANDER eine neuartige Ligationsreaktion um Amidbindungen zwischen Kalium Acyltrifluoroboraten (KATs) und O-Acylhydroxylaminen zu bilden (Schema I). Diese chemoselektive und bioorthogonale Ligationsreaktion, welche auch als KAT Ligation bezeichnet wird, hat grosses Potenzial alle Voraussetzungen zu erfüllen, welche nötig sind um eine effiziente Konjugation von Biomolekülen zu ermöglichen. Die Reaktion verläuft in Wasser bei Raumtemperatur, benötigt keine zusätzlichen Reagenzien und Katalysatoren, bildet stabile und natürlich vorkommende Amidverknüpfungen und produziert nur ungiftige Nebenprodukte. Zusätzlich zeigt die KAT Ligation unter sauren Bedingungen eine schnelle Reaktionskinetik und wurde schon erfolgreich in der PEGylierung, Lipidierung und Biotinylierung ungeschützter Peptide angewandt. Neue Studien haben jedoch gezeigt, dass die KAT Ligation eine signifikante Reduktion der Reaktionsgeschwindigkeit bei erhöhten pH Werten (>pH 5) aufweist. Aus diesem Grund ist die KAT Ligationsreaktion bis heute ungeeignet für die equimolare Konjugation grosser Biomoleküle unter physiologischen Bedingungen.



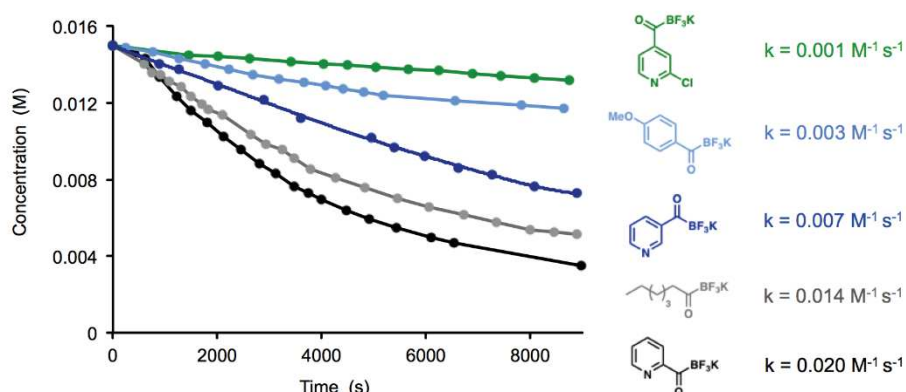
**Schema I** KAT Ligationsreaktion zwischen Kalium Acyltrifluoroboraten und O-Acylhydroxylaminen.

In einem Versuch, den Nutzen der KAT Ligation für biologischen Anwendungen zu erweitern, haben wir uns zum Ziel gesetzt, die Kinetik der Ligation bei physiologischem pH zu verbessern. Im ersten Teil dieser Thesis wurde mit den 2-pyridyl KATs eine neue Generation Acyltrifluoroborate entwickelt, welche eine Erhöhung der Ligationskinetik in einer Grössenordnung von einem Faktor 2 im Vergleich zu den traditionell eingesetzten Aryl KATs zeigen (Figur I).



**Figur I** Vergleich der KAT Ligationsreaktion von Pyridyl KAT und Aryl KAT über eine ausgewählte pH Bandbreite.

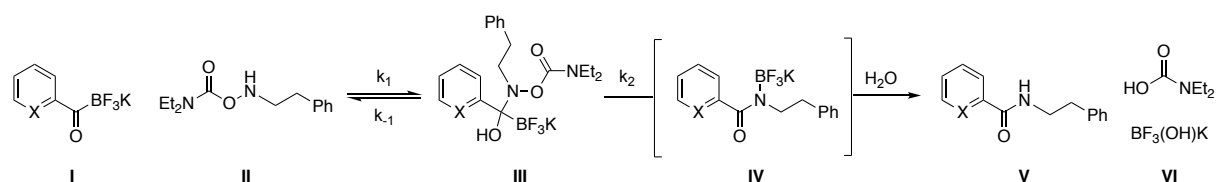
Echtzeit kinetische NMR Studien wurden mit einer Auswahl von über 30 Acyltrifluorboraten unter deuteriert-wässrigen Bedingungen bei physiologischem pH (pH 5.1 - 7.4) durchgeführt und die daraus resultierenden Geschwindigkeitskonstanten zweiter Ordnung ermittelt. Die kinetischen Daten zeigen, dass der Pyridin-Stickstoff in der *ortho*-Position der Acyltrifluorborat-Gruppe eine äusserst massgebliche Rolle bei der Verbesserung der Reaktionskinetik spielt, indem dieser während der Ligationsreaktion als Protonen-Donor/Akzeptor agiert (Figur II).



**Figur II** Vergleich von KAT Ligationsgeschwindigkeitskonstanten verschiedener KAT Spezies.

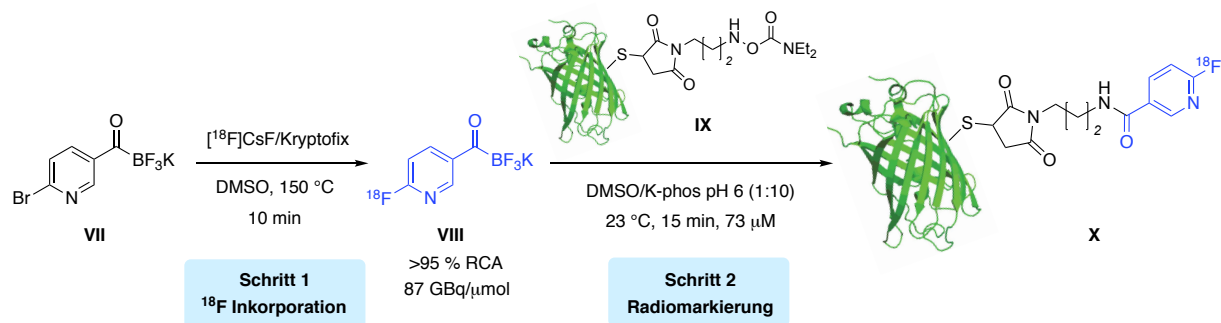
Im zweiten Teil dieser Thesis geben ausführliche experimentelle und theoretische mechanistische Studien ein tiefgreifendes Verständnis über den Mechanismus der KAT Ligationsreaktion. Eine genaue Analyse des Reaktionsprofils durch Echtzeit  $^1\text{H-NMR}$  Spektroskopie offenbarte, dass die KAT Ligationsreaktion über ein geschwindigkeitsbestimmendes vorgelagertes Gleichgewicht abläuft, welches durch eine Kinetik zweiter Ordnung bestimmt

ist (Schema II). Es wurde ermittelt, dass der geschwindigkeitsbestimmende Schritt der Ligationsreaktion im Zerfall des tetraedrischen Intermediates **III** ( $k_2$ ) besteht. Des Weiteren postulieren wir, dass der Mechanismus der Ligationsreaktion über einen nukleophilen Angriff des Hydroxylamins **II** auf den Carbonylkohlenstoff des KATs **I** abläuft, was zur Bildung des tetraedrischen Intermediates **III** führt. Eine konzertierte Eliminierung des tetraedrischen Additionsintermediates **III** führt dann zu einer *N*-Trifluoroboryl-Spezies, welche sehr kurzlebig ist und daher schnell zum gewünschten Amidprodukt **V** kollabiert. Bemerkenswerterweise wurde entdeckt, dass die 2-Pyridyl KATs unter gering sauren Bedingungen einen Protonentransfer ermöglichen und somit den geschwindigkeitsbestimmenden Zerfall des tetraedrischen Intermediates erleichtern.



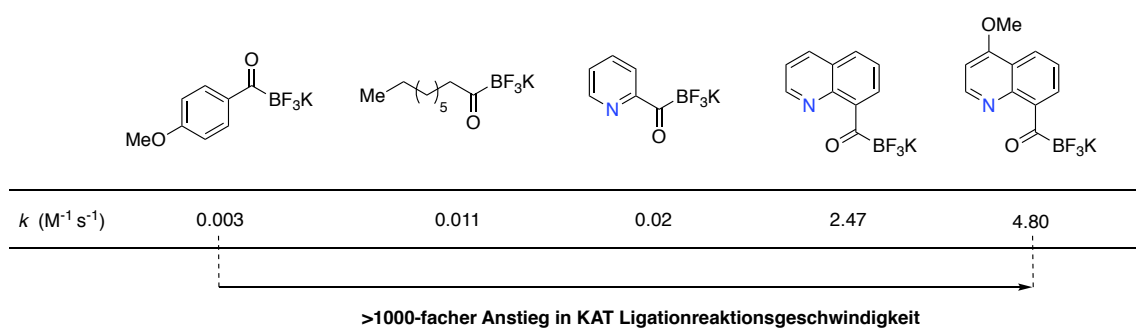
**Schema II** Postulierter Mechanismus der KAT Ligationsreaktion.

In einem dritten Teil dieser Thesis wurden die Pyridyl KATs als geeignete Kandidaten für radioaktive Markierungsstudien identifiziert. Eine rasche Einführung von  $^{18}\text{F}$  in 6-Bromnicotinoyltrifluorborat **VII** wurde in einem einzigen Schritt durch nukleophile aromatische Substitution erreicht (Schema III). Zusätzlich wurde gezeigt, dass  $^{18}\text{F}$ -markiertes 6-Fluornicotinoyltrifluorborat **VIII** dazu neigt eine KAT Ligationsreaktion mit Hydroxylaminen im sauren wässrigen Milieu oder in Rattenplasma bei Raumtemperatur einzugehen. Diese Entdeckung ermöglichte die  $^{18}\text{F}$  Markierung von grösseren Molekülen, wie beispielsweise Modellpeptiden und des grün-fluoreszierenden Proteins (sfGFP) **IX** mit eingebauter Hydroxylamin-Funktionalität.



**Schema III** Radioaktive Markierung von Pyridyl KAT **VII** und Einführung des  $^{18}\text{F}$ -markierten Pyridyl KATs **VIII** in sfGFP mittels KAT Ligationsreaktion.

Der fortgeschrittene mechanistische Einblick in die KAT Ligation ermöglichte weitere strukturelle Feinabstimmungen der Kalium Acyltrifluoroborate, was uns zur Entdeckung neuer *N*-heterozyklischer KATs mit noch schnelleren Ligationsraten brachte. Im letzten Teil dieser Thesis zeigen wir, dass 8-Quinolin KATs überlegene Kalium Acyltrifluoroborate sind, mit Geschwindigkeitskonstanten zweiter Ordnung von bis zu  $4.6 \text{ M}^{-1} \text{ s}^{-1}$  bei pH 6.8 (Figur III). Somit zeigen 8-Quinolin KATs im Vergleich zu den gängigen Aryl KATs einen >1000-fachen Anstieg der Reaktionsgeschwindigkeit.



**Figur III** Vergleich der KAT Ligationskinetiken verschiedener KAT Spezies.

---

## List of Abbreviations, Acronyms and Symbols

### *Abbreviations and Acronyms*

Ac	acetyl
app	apparent
arom	aromatic
aq	aqueous
atm	atmosphere
b	broad
BARAC	biarylazacyclooctynone
BCN	bicyclononyne
BirA	biotin ligase
Bn	benzyl
Boc	<i>tert</i> -butoxycarbonyl
BTTAA	2-[4-{{bis[(1- <i>tert</i> -butyl-1 <i>H</i> -1,2,3-triazol-4-yl)methyl]amino)methyl} -1 <i>H</i> -1,2,3-triazol-1-yl]acetic acid
BTTEs	2-[4-{{bis[(1- <i>tert</i> -butyl-1 <i>H</i> -1,2,3-triazol-4-yl)methyl]amino)-methyl} -1 <i>H</i> -1,2,3-triazol-1-yl]ethyl hydrogen sulfate
BTTP	3-[4-{{bis[(1- <i>tert</i> -butyl-1 <i>H</i> -1,2,3-triazol-4-yl)methyl]amino}methyl}} -1 <i>H</i> -1,2,3-triazol-1-yl]propanol
Bu	butyl
Bz	benzoyl
C	Celsius
c	centi, concentration
cal	calorie
calcd	calculated
cat	catalytic
Cbz	carboxybenzyl
CD	circular dichroism
<i>cf</i>	<i>confer</i>
conc	concentrated
COSY	correlation spectroscopy
Cp	cyclopentadienyl

---

CuAAC	copper-catalyzed azide-alkyne cycloaddition
Cyp	cyclopropene
d	doublet, days
d.r.	diastereomeric ratio
DABCO	1,4-diazabicycloundec-7-ene
DCC	dicyclohexylcarbodiimide
DCH	1,3-dichloro-5,5-dimethylhydantoin
DFT	density functional theory
Dha	dihydroalanine
DIBO	4-dibenzocyclooctynol
DIFO	difluorinated cyclooctyne
DMAP	4-dimethylaminopyridine
DMF	<i>N,N</i> -dimethylformamide
DMSO	dimethylsulfoxide
DQF	double-quantum filtered
<i>ee</i>	enantiomeric excess
EI	electron ionization
equiv	equivalents
ESI	electron spray ionization
Et	ethyl
ETH	<i>Eidgenössische Technische Hochschule</i>
<i>et al.</i>	<i>et alia</i>
Fmoc	fluorenylmethoxycarbonyl
FT	fourier transform
g	gram
h	hour
HATU	1-[bis(dimethylamino)methylene]-1 <i>H</i> -1,2,3-triazolo[4,5- <i>b</i> ]pyridinium 3-oxid hexafluorophosphate
HMBC	heteronuclear multiple bond coherence
HMPA	hexamethylphosphortriamide
HPLC	high performance liquid chromatography
HR	high resolution
HRMS	high resolution mass spectrometry

HSQC	heteronuclear single quantum coherence
Hz	Hertz
<i>i</i>	<i>iso</i>
IC <sub>50</sub>	half maximal inhibitory concentration
iEDDA	inverse electron-demand Diels–Alder cycloaddition
Ig	immunoglobulin
IR	infrared
J	Joule
<i>J</i>	coupling constant
k	kilo, rate constant
KAHA	-ketoacid hydroxylamine
KAT	potassium acyltrifluoroborate
L	liter
M	molar, mega
<i>M</i>	molecular ion
m	milli, meter, multiplet or unresolved
<i>m</i>	<i>meta</i>
MALDI	matrix-assisted laser desorption/ionization
Me	methyl
Mes	mesityl
MIDA	<i>N</i> -methyliminodiacetic acid
min	minute
MS	molecular sieves, mass spectrometry
Ms	methanesulfonyl
m.p.	melting point
m/z	mass to charge ratio
n	nano
<i>n</i>	<i>normal</i>
<i>n</i> BuLi	<i>n</i> -butyllithium
NMR	nuclear magnetic resonance
NOE	nuclear <i>Overhauser</i> effect\
Nor	norbornene
n.d.	not determined



---

<i>o</i>	<i>ortho</i>
OCT	cyclooctyne
Opr	5-oxaproline
ORTEP	oak ride thermal ellipsoid plot
Tf	triflate
Ozt	oxazetidine
<i>p</i>	<i>para</i>
pH	negative decadic logarithm of hydrogen ion concentration
Ph	phenyl
pK <sub>a</sub>	negative decadic logarithm of the acid dissociation constant
PLP	pyridoxal-5'-phosphate
ppm	parts per million
Pr	propyl
pre-mRNA	precursor messenger ribonucleic acid
PTM	post-translational modifications
PyBOP	benzotriazol-1-yl-oxytripyrrolidinophosphonium hexafluorophosphate
q	quartet
quant.	quantitative
RCY	radiochemical yield
ROS	reactive oxygen species
RT	room temperature
s	singlet, second
sat	saturated
sfGFP	superfolder green fluorescent protein
SPAAC	strain-promoted azide-alkyne cycloaddition
SPPS	solid phase peptide synthesis
T	temperature
t	triplet, time
<i>t</i>	<i>tert</i>
TBAF	tetra- <i>n</i> -butylammonium fluoride
TBDPS	<i>tert</i> -butyldiphenylsilyl
TBS	<i>tert</i> -butyldimethylsilyl
TBTA	Tris[(1-benzyl-1 <i>H</i> -1,2,3-triazol-4-yl)methyl]amine

TCO	<i>trans</i> -cyclooctene
TEOTA	tris[(1-(2-ethoxy-2-oxoethyl)-1 <i>H</i> -1,2,3-triazol-4-yl)methyl]amine
TFA	trifluoroacetic acid
THF	tetrahydrofuran
TGase	transglutaminase
THPTA	tris[(1-hydroxy-propyl-1 <i>H</i> -1,2,3-triazol-4-yl)methyl]amine
TIPS	triisopropylsilyl
TLC	thin layer chromatography
TMS	trimethylsilyl
TMTH	tetramethylthiacycloheptyne
Ts	<i>p</i> -toluenesulfonyl
UAA	unnatural amino acid
UV	ultraviolet
X	halogen atom

**Symbols**

°	degree
Å	Ångström
δ	chemical shift in ppm
μ	micro
v	wavenumber
%	per cent





# ***Chapter 1***

---

***Introduction***

---



# 1 Introduction

## 1.1 Proteins – The Essence of Biological Life

Proteins are one of the most abundant macromolecules in nature and essential to all biological life on earth.<sup>1</sup> They perform a broad diversity of functions in living organisms and are key actors in the regulation, repair and protection of cellular processes. In the human body, proteins are divided into different classes according to their respective functions (Figure 1.1).

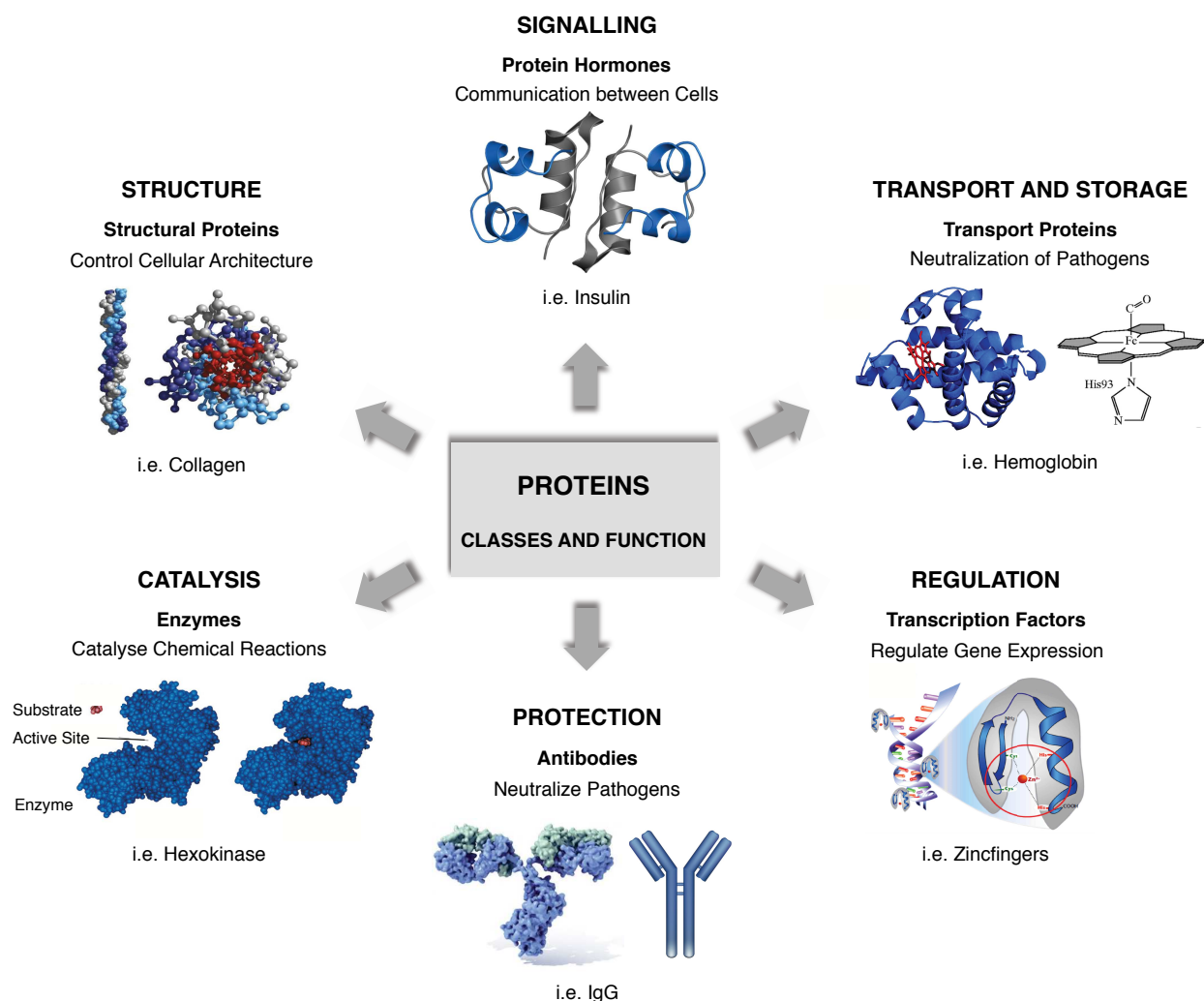


**Figure 1.1** Different classes of proteins and their respective functions in the human body.<sup>2</sup>

Protein hormones are signalling molecules transmitting information responsible for the communication between cells. Transport proteins relocate ions and small molecules within a living organism. Transcription factors regulate gene expression by selectively binding to

specific DNA sequences. Antibodies, also known as immunoglobulins, represent the backbone of the adaptive immune system by selectively recognizing and binding antigens of invading pathogens. Enzymes, such as hexokinase, act as catalysts for a large majority of chemical reactions in the cell. Structural proteins, i.e. collagen, provide structural components and control the cellular architecture.

Proteins are complex molecular structures comprising one or more polypeptides with a defined chemical sequence.<sup>3</sup> Each polypeptide is composed of a chain of amino acid residues, which are covalently linked via amide bonds. Figure 1.2 depicts the 21 different proteinogenic  $\alpha$ -amino acids, which exist in eukaryotes.

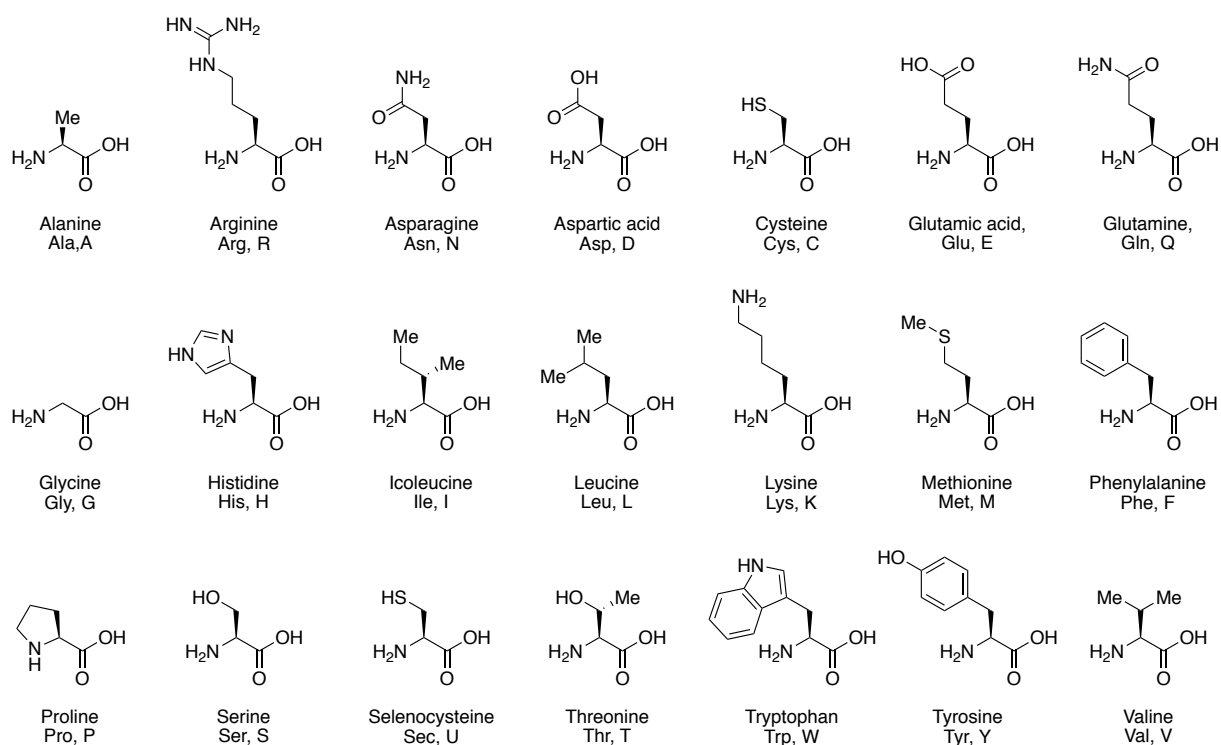


**Figure 1.2** The 21 proteinogenic  $\alpha$ -amino acid residues of eukaryotes with one and three-letter codes.

The biological activity of proteins is mainly dictated by their three-dimensional structure and spatial arrangement of functional groups. The structure of proteins is historically characterized by four different conformational levels (Figure 1.3). The primary structure describes the linear polypeptide – a particular sequence of amino acid residues linked by amide bonds. Certain sections of this linear polypeptide sequence can adopt highly regular local substructures through hydrogen bonding, i.e.  $\alpha$ -helices and  $\beta$ -sheets, also referred to as secondary structures. Upon higher-order interactions secondary structures arrange into three-dimensional tertiary structures. Some proteins are composed of multiple polypeptide chains



and their quaternary structure describes the convoluted interaction between those polypeptide chains to form a larger protein assembly.

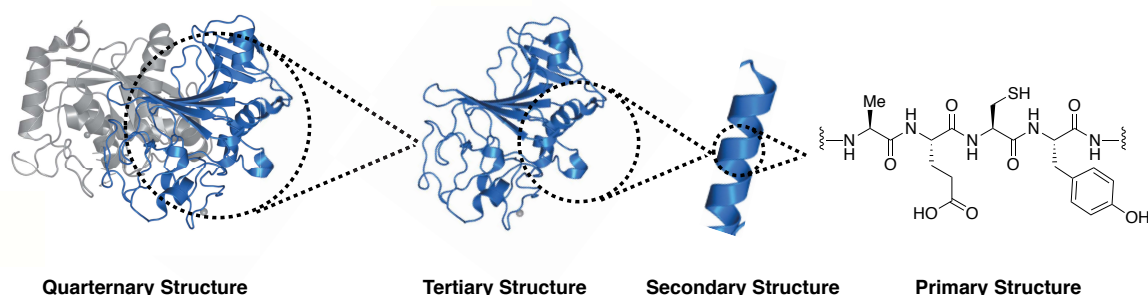


**Figure 1.3** The four different levels of the protein structure.<sup>4</sup>

Further levels of protein complexity arise from splicing of pre-mRNA transcripts prior to translation or by post-translational modifications (PTM). Over billions of years of evolution, nature has developed an intricate machinery to post-translationally modify specific amino acids and thus covalently introduce versatile functional groups into proteins after their ribosomal synthesis.<sup>5</sup> Once introduced, these functional groups may reversibly or irreversibly alter the structure and stability of proteins. In fact, naturally occurring PTMs play important roles in fine-tuning the physiochemical properties of proteins, modulating enzymatic activity, controlling protein-protein recognition and imparting enzymes with chemical functionalities that are not present in the standard set of proteinogenic amino acids, such as acylation, methylation, glycosylation, phosphorylation, ubiquitination. Glycosylation, for example, is a process that allows the attachment of carbohydrates to proteins and is known to improve the solubility of proteins in water and modulate ligand–receptor interactions.<sup>6</sup> Phosphorylation of serine, threonine or tyrosine residues regulates enzymes by enabling them to switch between their active and inactive states.<sup>7</sup> In a similar manner, the formation of complex protein assemblies is promoted or prevented. Furthermore, ubiquitination alters the cellular location of proteins and marks them for degradation.<sup>8,9,10</sup> Collectively, these examples highlight nature’s ability to create immense biological diversity by remodelling structure and function of existing proteins through PTM.

Due to the diverse role of proteins in almost all biological contexts and also the fact that not all cellular processes and their key players are well understood, the study and manipulation of protein functions are not only of significant importance to fundamental scientific research, but also critical to the development of prospective biotechnological and biomedical applications.

## 1.2 Protein Modification

Over the past decades, organic chemists have designed and developed a plethora of synthetic strategies and tools to achieve engineering of target proteins with unique functional groups or site-specific labeling of small molecule functional probes (Figure 1.4).<sup>11,12</sup> While only few strategies harness the selectivity of enzymatic reactions<sup>13</sup>, i.e. biotine ligase (BirA)<sup>14</sup> or transglutaminase (TGase),<sup>15</sup> the majority of approaches involve the modification of proteinogenic amino acids or aim at the incorporation and manipulation of unnatural amino acids.<sup>16,17</sup> Selected applications include expression profiling of proteins containing unnatural amino acids, detection of cell-surface carbohydrates via azide functionalities, and pull downs of small molecule enzyme inhibitors. The goal of these applications is mainly the detection or identification of a specific biomolecule in a pool of many other biological molecules.

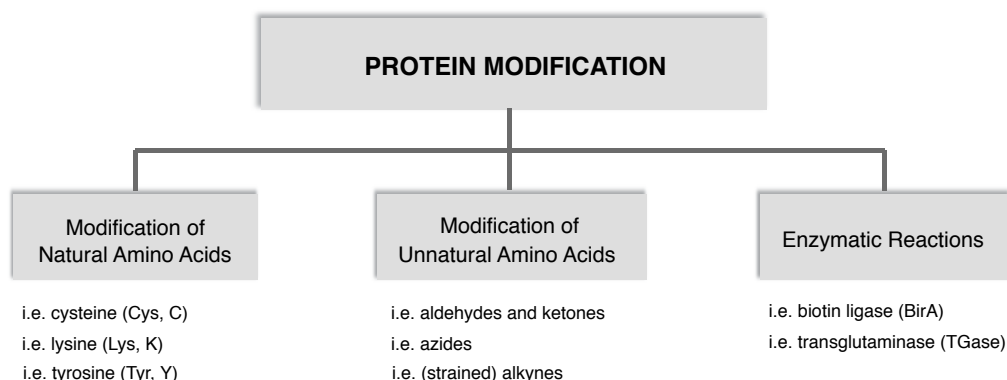


**Figure 1.4** An overview of different protein modification strategies.

## 1.3 Protein Bioconjugation and Polymerization

Recent advances in protein modification have transformed the fields of organic chemistry and chemical biology by facilitating the site-specific functionalization and labeling of proteins with small molecules or peptides. Yet, the covalent ligation of stoichiometric quantities of large molecules (>10'000 MW) for applications such as protein-polymer conjugation,<sup>18</sup> protein-protein conjugation<sup>19</sup> or the synthesis of more complex, oligomeric biomolecular architectures<sup>20</sup> remains one of the major contemporary challenges (Figure 1.5).<sup>21,22</sup> The conjugation of two large molecules at near equimolar stoichiometry is particularly demanding in organic chemistry, as it requires the use of suitable chemoselective ligation reactions with fast second order ligation kinetics.<sup>12,23,24</sup> Due to the high molecular weight and limited

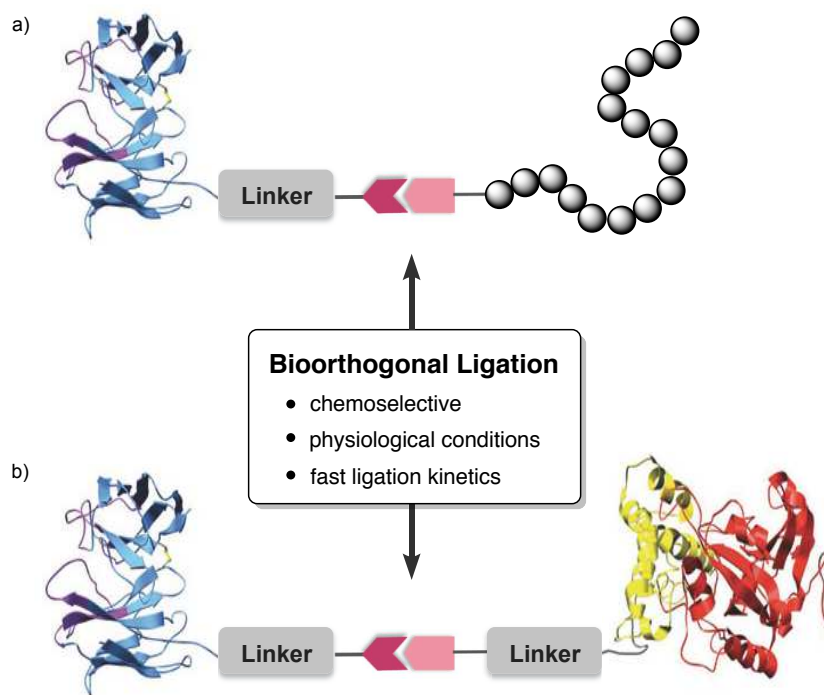
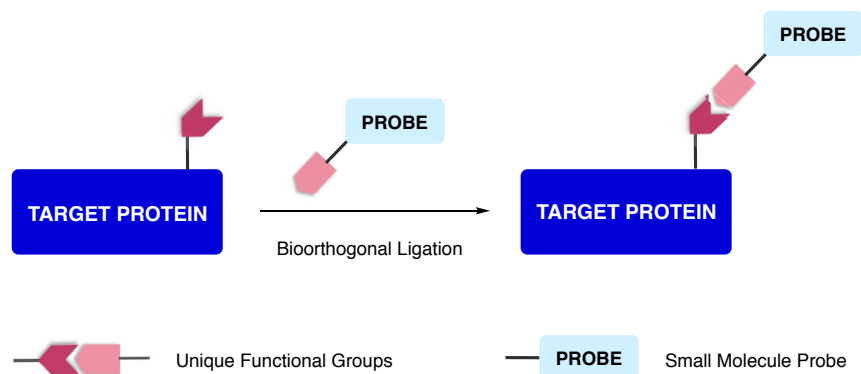


**Figure 1.5** Schematic representation of a) protein-polymer conjugation and b) protein-protein conjugation by the use of suitable bioorthogonal ligation reactions.<sup>25</sup>

solubility of most large molecules, the preparation of concentrated reaction solutions is limited. While most organic reactions optimally proceed at around 100 – 200  $\mu\text{M}$ , even small proteins are typically soluble at merely 20  $\mu\text{M}$  or less. This 10'000-fold dilution leads to rate attenuations of four orders of magnitude compared to small molecule chemistry. To compensate for the slow reaction kinetics of most known bioorthogonal ligation methods, protein modifications, such as the site-specific labeling of a biomolecule with a small chemical probe, are typically performed using a large excess of the small molecule reactant. This allows good conversions not only if the rates of the reactions are slow but also if one of the ligation partners suffers from stability issues under aqueous conditions. However, the conjugation of two proteins should ideally proceed with satisfying yields close to stoichiometric fashion, since recombinant proteins are often precious compounds, which are limited by difficulties of accessibility and purification. Yet, only few bioorthogonal, intermolecular reactions are fast enough to undergo site-specific protein-polymer or protein-protein conjugations in equimolar stoichiometry. The following subchapters provide a brief overview of the most common bioorthogonal ligation and their respective limitations.

### 1.3.1 Bioorthogonal Ligation Reactions

Bioorthogonal ligations enable the covalent bond forming reaction between two chemoselective ligation partners with unique functional groups under aqueous conditions and in presence of all naturally occurring functionalities in living organisms (Scheme 1.1).<sup>26</sup>



**Scheme 1.1** Bioorthogonal ligation reaction for the functionalization of a target protein with incorporated UAA.

A ligation reaction classifies as bioorthogonal if the following crucial criteria are fulfilled

- **Chemoselectivity:** The ligation reaction must proceed with high selectivity between two unique functional groups to produce a stable, covalent bond. Furthermore, the reaction must tolerate the presence of other reactive functional moieties.
- **Biological inertness:** Starting materials and the resulting covalent linkage must not display undesired reactivity with biological systems.
- **Compatibility and stability under physiological conditions:** The ligation reaction must proceed in aqueous media at room temperature and physiological pH. Starting materials and ligation products must be stable under physiological conditions.
- **Toxicity:** Reaction partners and ligation product, as well as possible side products, must be non-toxic for organisms.
- **Kinetics:** The reaction must proceed with fast reaction rates at low millimolar to micromolar concentrations and stoichiometric amounts of ligation partners.
- **Accessibility:** The chemoselective functional groups must be easily accessible by chemical synthesis and capable of being incorporated into biomolecules via genetic or chemical protein engineering.

The term 'bioorthogonal chemistry' was first introduced and defined by BERTOZZI in 2003.<sup>27</sup> However, the modern concept of bioorthogonal ligation reactions dates back to the year 1990, when RIDEOUT and coworkers demonstrated the selective condensation of hydrazines with aldehydes to exploit the assembly of toxins derived from inactive prodrugs within living cells.<sup>28</sup> Ever since, bioorthogonal reactions have significantly impacted the field of classical organic chemistry by not only facilitating site-selective modification of proteins with small molecule probes but also conjugation of larger biomolecules.<sup>29,30</sup> On these grounds, bioorthogonal reactions have found broad application in all areas of chemical biology.<sup>31</sup> Selected examples include the site-specific protein labeling with fluorophores or affinity probes,<sup>32</sup> cell surface modification,<sup>33,34</sup> protein-protein conjugation,<sup>35,36</sup> and drug development, such as antibody-drug conjugates are shown in Figure 1.6.<sup>37,38</sup>

In contrast to most chemical strategies for the modification of natural amino acids, which are limited to *in vitro* applications, bioorthogonal ligation reactions also allow for site-selective modification of target proteins *in vivo*.<sup>39</sup>

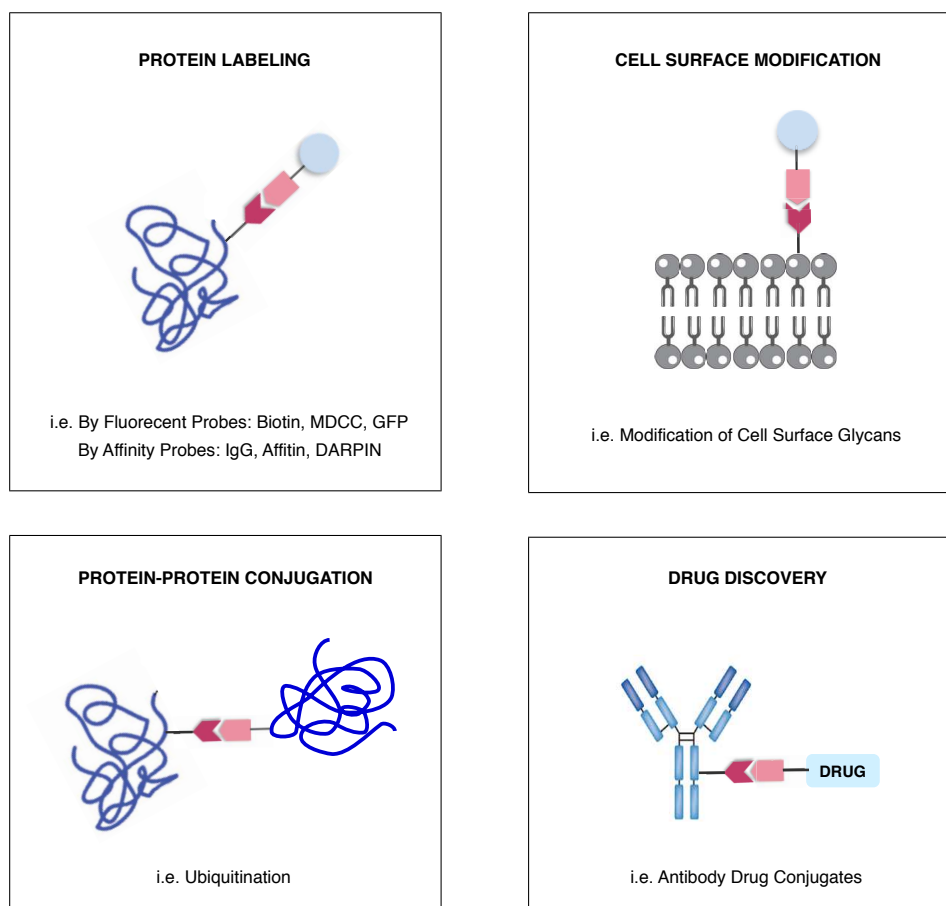
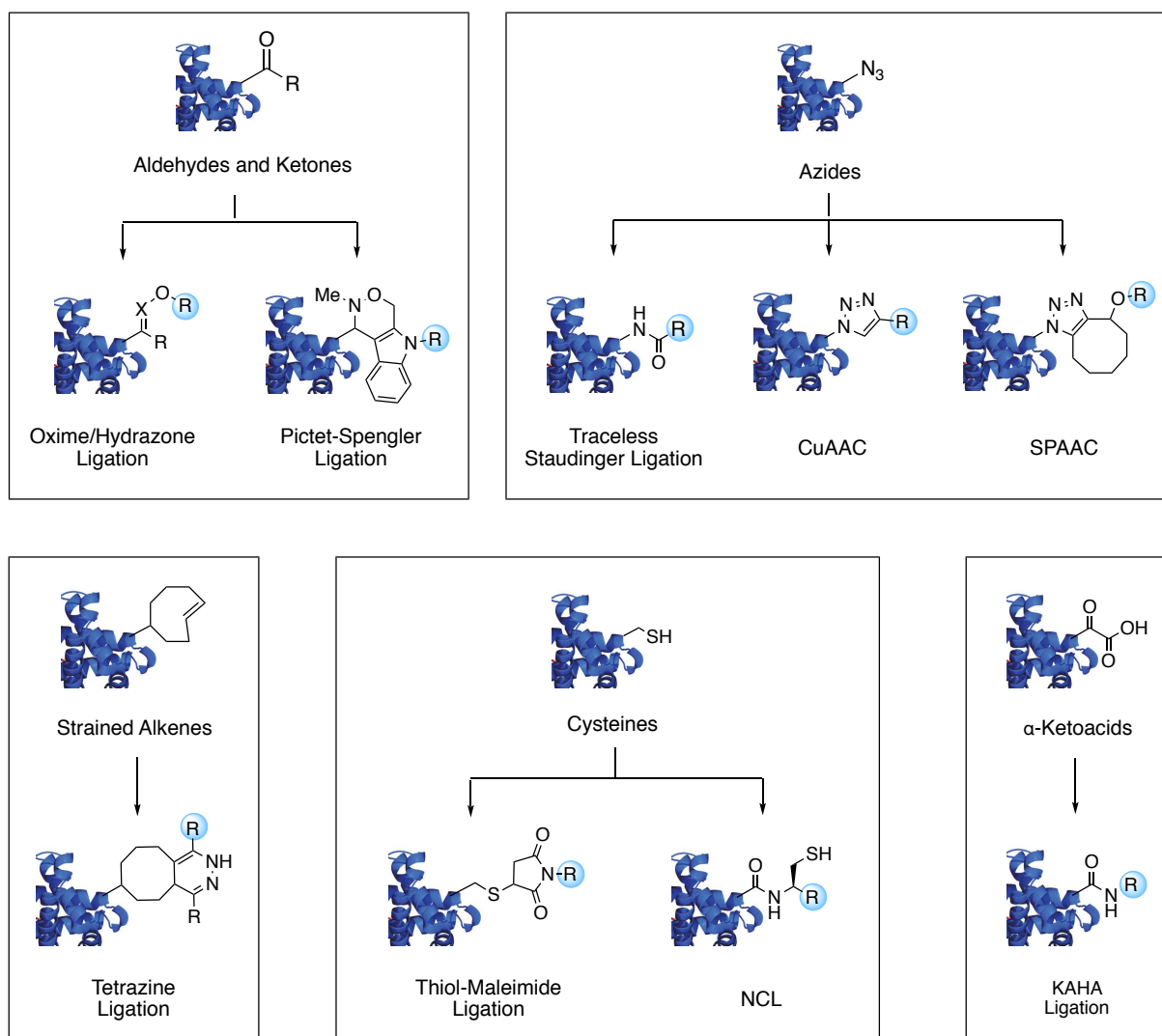


**Figure 1.6** Applications of bioorthogonal ligation reactions for the site-selective modification and conjugation of proteins.

Over the past 30 years, a number of bioorthogonal ligation reactions exploiting various functional groups have been reported.<sup>40,41</sup> Well-established and unique functional groups for chemoselective ligations include aldehydes, ketones, azides, alkynes, alkenes, ketoacids etc. Scheme 1.2 gives an overview of the commonly employed bioorthogonal ligation reactions which will be discussed in detail in the following subsections.

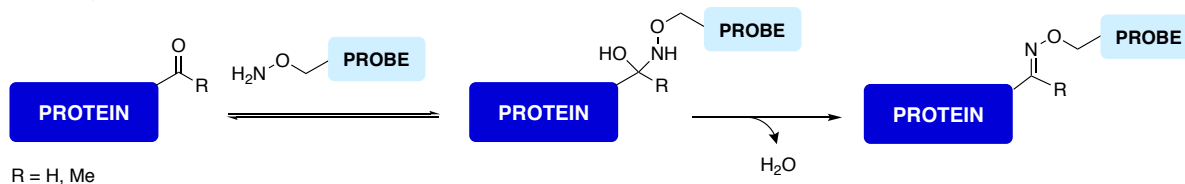


**Scheme 1.2** Overview of well-established bioorthogonal ligation reactions and their corresponding functional groups.

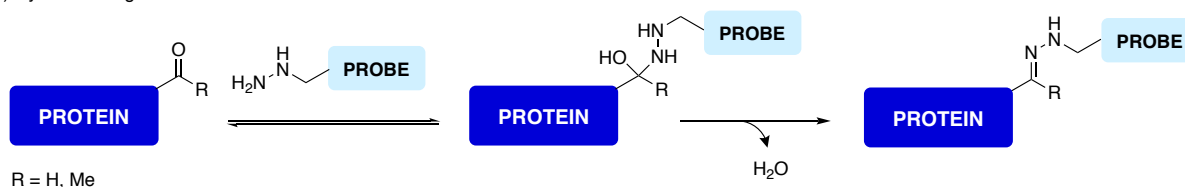
### 1.3.1.1 Oxime and Hydrazone Ligation

One of the earliest bioorthogonal reactions is the condensation of aldehydes and ketones with hydroxylamines or hydrazines leading to the formation of stable oximes and hydrazones, respectively (Scheme 1.3). To date, this ligation reaction has successfully been applied in peptide chemistry, site-specific *in vitro* protein-protein<sup>42</sup> or cell surface protein labeling.<sup>43,44</sup>

a) Oxime Ligation



b) Hydrazone Ligation



**Scheme 1.3** a) Oxime ligation between aldehydes or ketones and hydroxylamines. b) Hydrazone ligation between aldehydes or ketones and hydrazines.

Oxime and hydrazone ligations are highly pH dependent and rapidly proceed under acidic conditions (pH 4–5), however these ligation reactions are slow ( $k = 1 \times 10^{-3} \text{ M}^{-1} \text{ s}^{-1}$ ) at physiological pH.<sup>45</sup> Although aniline (**1**) was identified as a nucleophilic catalyst for the reaction,<sup>46</sup> rate acceleration is moderate and high catalyst concentrations are required.<sup>47,48</sup> To overcome these shortcomings, a new-generation of bifunctional catalysts, such as anthranilic acids, tetrazoles and phosphanilates, have been reported (Figure 1.7).<sup>49,50,51</sup> Recent kinetic studies by KOOL and coworkers disclosed that structural modifications on aldehyde and hydroxylamine/hydrazine substrates impact the reaction rates and lead to accelerated ligations.<sup>52</sup>

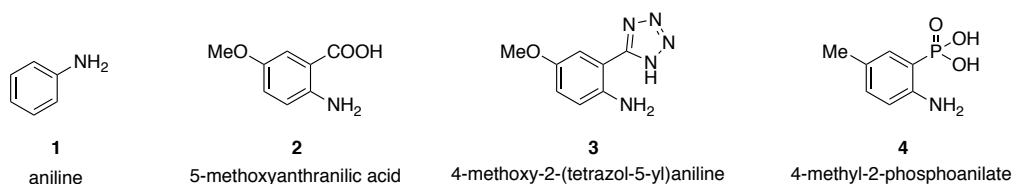
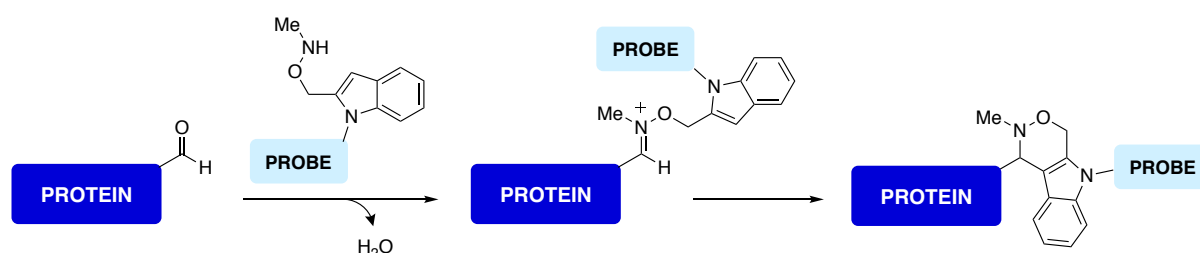


**Figure 1.7** Catalysts for oxime and hydrazone ligation.

### 1.3.1.2 Pictet-Spengler Ligation

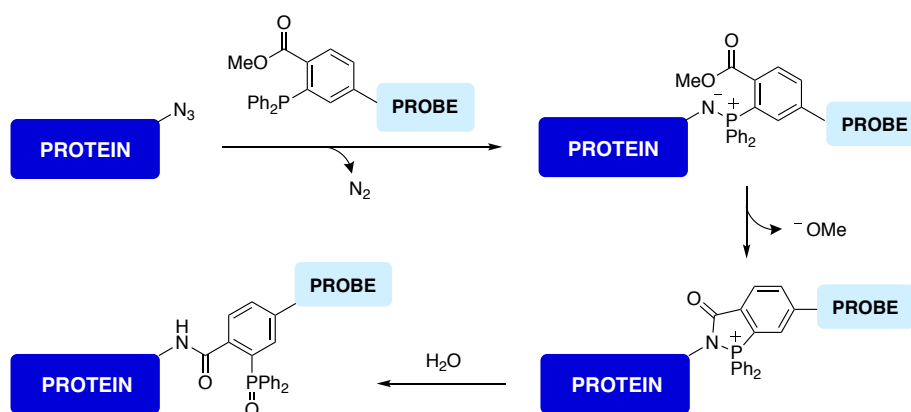
In 2013, BERTOZZI and co-workers introduced the Pictet-Spengler ligation based on the long-known Pictet-Spengler reaction<sup>53</sup> between aldehydes and  $\beta$ -arylethylamine, i.e. tryptamine (Scheme 1.4).<sup>54</sup> This ligation comprises the condensation of aldehyde and alkoxyamine to form an intermediate oxyiminium ion, which can subsequently undergo intramolecular C–C bond formation with the indole nucleophile to form a hydrolytically stable oxacarboline product.



**Scheme 1.4** Pictet-Spengler ligation reaction between aldehydes and tryptamines.

### 1.3.1.3 Staudinger Ligation

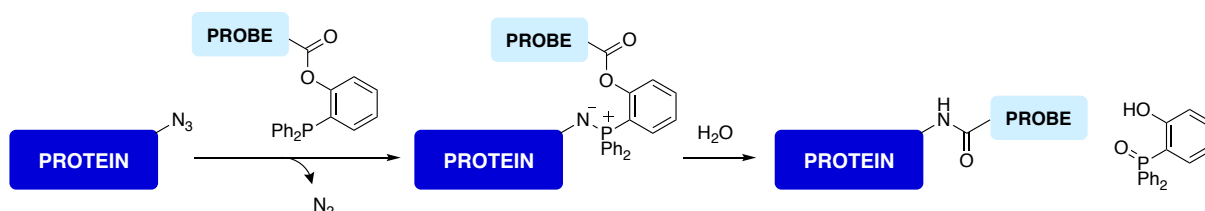
The Staudinger ligation is a modification of the classic Staudinger reaction<sup>55</sup> between azides and phosphines. Trapping of the aza-ylide intermediate by an ester group in the *ortho*-position of an aromatic substituent allows the formation of a five-membered ring intermediate, which upon hydrolysis yields a stable amide bond (Scheme 1.5).<sup>56,57</sup> The rate-determining step of the ligation reaction was identified to be the initial nucleophilic attack of the azide to the phosphine<sup>58</sup>. As a result, reaction rates are dependent on the electronic properties of both ligation partners, phosphine and azide moiety. In general, reaction kinetics were shown to be extremely slow with second-order rate constants of about  $10^{-3} \text{ M}^{-1} \text{ s}^{-1}$ .<sup>59</sup>



**Scheme 1.5** The Staudinger ligation reaction.

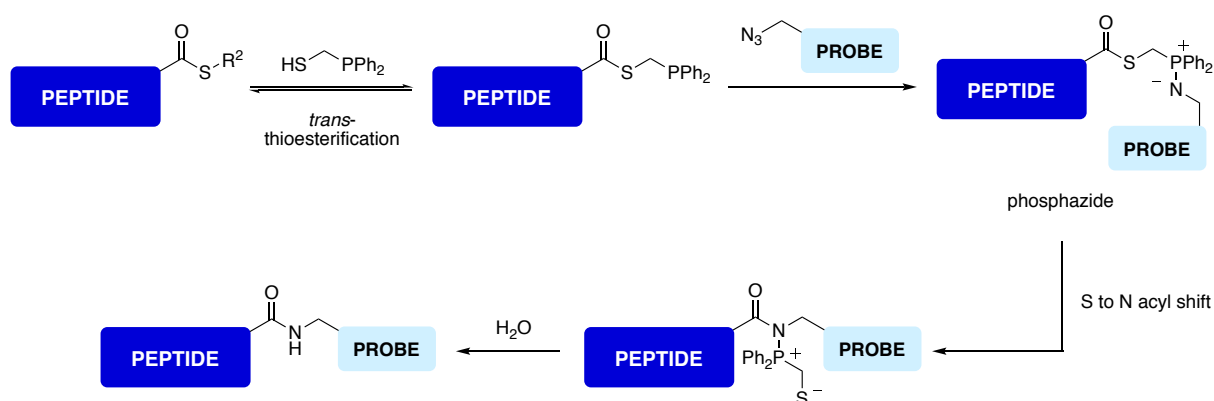


In 2000, BERTOZZI reported a traceless Staudinger ligation reaction. In this variant, a cleavable linker between the ester group and triphenylphosphine moiety was introduced (Scheme 1.6).<sup>60</sup> Upon amide bond formation, the linker is eliminated as a leaving group resulting in the formation of the desired amide product and triphenylphosphine oxide after hydrolysis.



**Scheme 1.6** Traceless Staudinger ligation developed by BERTOZZI.

In the same year, RAINES reported an alternative method for a traceless Staudinger ligation employing thioesters as substrates (Scheme 1.7).<sup>61</sup> In a first step, the thioester undergoes *trans*-thioesterification with diphenylphosphinethanethiol, similarly to NCL (*cf.* Chapter 1.2.3.8), followed by azide addition. The resulting phosphazide can rearrange via a S to N acyl shift, which upon hydrolysis liberates the desired ligation product and phosphine oxide.<sup>62</sup>

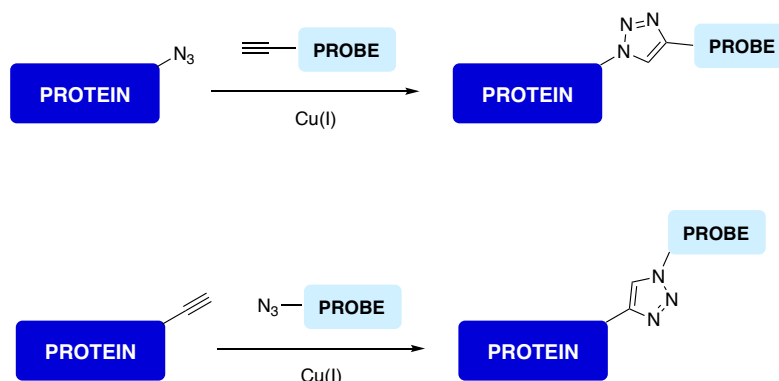


**Scheme 1.7** Traceless Staudinger ligation developed by RAINES.

Beside slow reaction kinetics Staudinger ligations suffer from poor stability of the phosphine reagents. In living systems phosphines can slowly undergo oxidations and presumably be metabolized *in vitro* by cytochrome P450. For these reasons, phosphine ligation partners are typically used in excess at relatively high concentrations.

### 1.3.1.4 Copper-Catalyzed Azide-Alkyne 1,3-Dipolar Cycloaddition

Besides Staudinger ligation, azides can also undergo 1,3-dipolar Huisgen cycloadditions with alkynes to yield stable tetrazine linkages at elevated temperature and pressure. In 2002, almost 40 years after the initial discovery by HUISGEN, SHARPLESS<sup>63</sup> and MELDAL<sup>64</sup> independently reported a copper(I)-catalyzed variant of the 1,3-dipolar azide-alkyne cycloaddition (CuAAC), commonly referred to as ‘click chemistry’ (Scheme 1.8).<sup>65</sup> This ligation reaction exclusively yields 1,4-substituted triazole isomers, whereas the uncatalyzed version delivers 1,4 and 1,5-isomers in almost equal ratio. Furthermore, it readily proceeds under mild conditions in aqueous media and at ambient temperature. CuAAC takes advantage of the formation of a dinuclear copper intermediate to activate both terminal alkynes and azides and is up to five magnitudes faster in reaction rates compared to its uncatalyzed counterpart.<sup>66</sup> Ligation rates are dependent on multiple parameters, including the nature of reactants, copper-catalysts and ligands. Second-order rate constants were shown to be in the range between  $1\text{-}2\text{ M}^{-1}\text{ s}^{-1}$ , when excess copper was employed.<sup>59</sup>



**Scheme 1.8** Copper-catalyzed azide-alkyne cycloaddition between azides and alkynes.

One of the major drawbacks of CuAAC is the cytotoxicity of Cu(I),<sup>67</sup> which is caused by Cu(I)-mediated generation of reactive oxygen species (ROS) from O<sub>2</sub> in living organisms.<sup>68</sup> In addition, copper complexes have also been found to induce changes in cellular metabolism. Recently, the use of water-soluble ligands including **5-10** has been shown to not only accelerate the ligation rate but also to reduce the apparent copper-associated cytotoxicity by complexing copper or serving as reductants to protect cells from ROS (Figure 1.8).<sup>69</sup> In combination with these ligands, CuAAC ligation reactions have successfully been applied in the site-specific labeling of bioconjugates in *Escherichia coli* and living mammalian cells,<sup>70,71</sup>

as well as for the monitoring of enzyme activities.<sup>72,73</sup> Nevertheless, it has been observed that different ligand environments of complexes continue to affect metabolism and uptake, thus leading to an undesired perturbation in cellular function.<sup>74</sup>

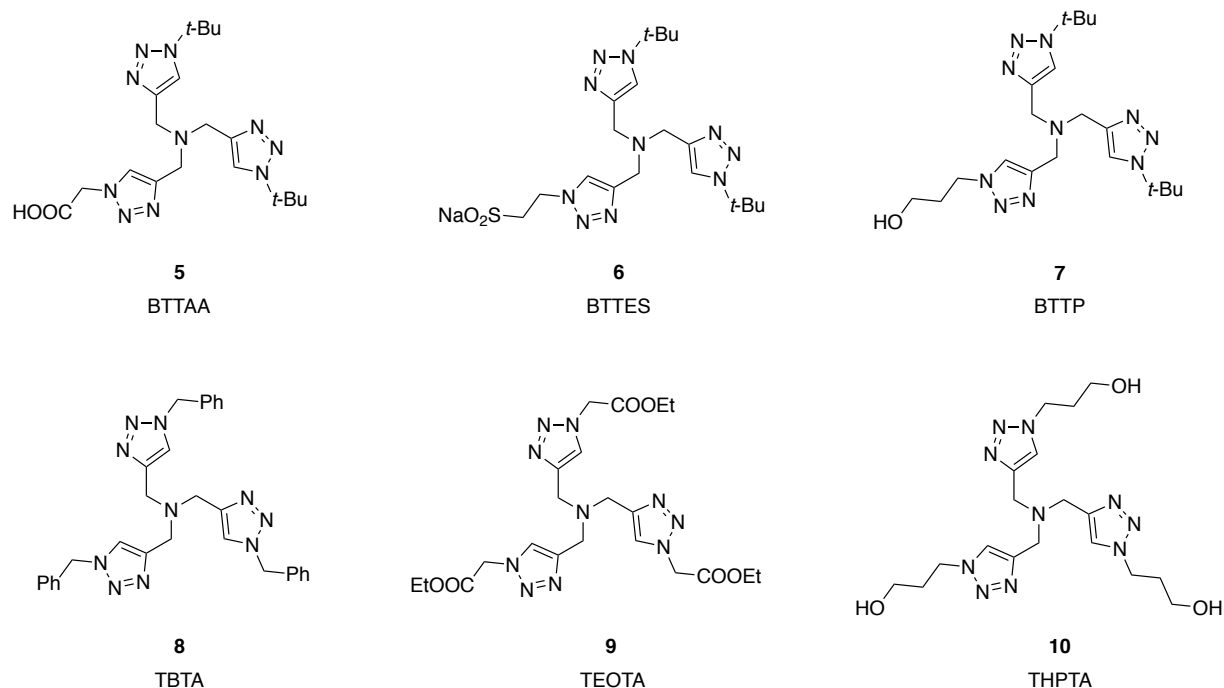
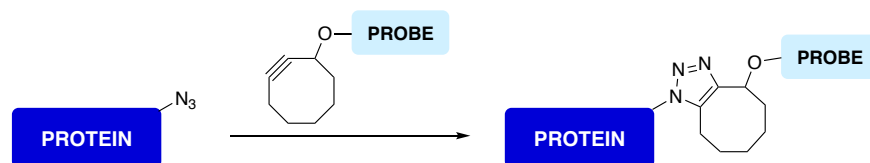


**Figure 1.8** A selection of water-soluble ligands for copper(I) coordination in CuAAC.

### 1.3.1.5 Strain-Promoted Azide-Alkyne 1,3-Dipolar Cycloaddition

In 2004, BERTOZZI and coworkers introduced the first strain-promoted azide-alkyne 1,3-dipolar cycloaddition (SPAAC), in which the ring strain of cyclooctyne was exploited as the driving force of the reaction (Scheme 1.9).<sup>75</sup> Due to the strain release, this cycloaddition proceeds under mild and copper-free conditions without the need for any additional catalysts or ligands. Furthermore, the reaction showed no cytotoxicity in living organisms. In its original format, the SPAAC reaction displayed relatively slow reaction kinetics, similar to the Staudinger ligation, with rate constants on the scale of  $10^{-3} \text{ M}^{-1} \text{ s}^{-1}$ .<sup>59</sup>



**Scheme 1.9** Strain-promoted azide-alkyne 1,3-dipolar cycloaddition between azides and strained alkynes.

Additional efforts in the field have led to the development of novel cyclooctyne derivatives **11-16** with improved reaction kinetics (Figure 1.9).<sup>76,77</sup> Recently, tetramethylthia-cycloheptyne (TMTH, **16**) was reported displaying ligation rates of up to  $4 \text{ M}^{-1} \text{ s}^{-1}$ .<sup>78</sup>

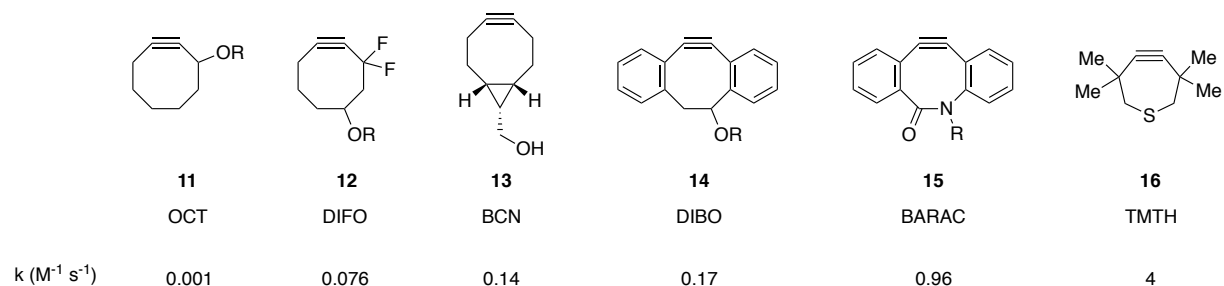
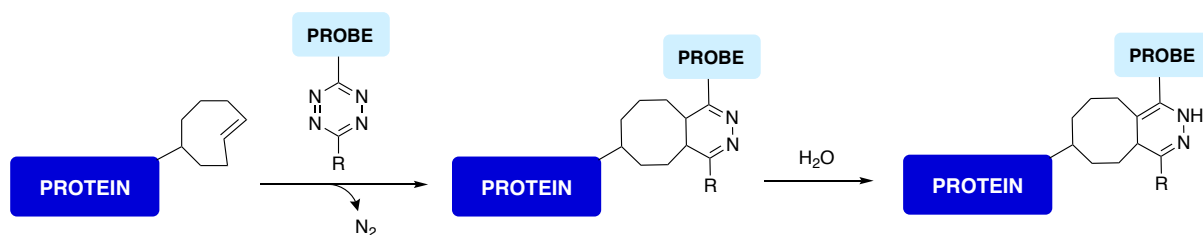


**Figure 1.9** A selection of cycloalkyne derivatives for SPAAC.

Enhanced ligation rates and other superior properties of the newly developed cyclooctyne derivatives led to a multitude of biological applications. Difluorinated derivative **12**<sup>79</sup> facilitates the rapid bioconjugation of fluorescent probes, i.e. biotin, to azido-functionalized glycoproteins for dynamic *in vivo* imaging of glycan trafficking in living cells<sup>80</sup> and developing zebrafish.<sup>81</sup> In a similar fashion, 4-dibenzocyclooctynol derivatives were used to generate metabolically labeled glycoconjugates for live cell imaging.<sup>82</sup> The biaryl substituents of **14** do not only increase ring strain but also provide additional bulkiness which impedes unselective reactions with other biomolecules. In an effort to address the strongly lipophilic character of most strained cyclooctynes, dimethoxy-substituted azacyclooctyne (DIMAC, **15**) was prepared. The increased hydrophilicity and water solubility of **15** was found to reduce non-specific binding events and consequently improves the sensitivity of azide detection.<sup>83</sup>

### 1.3.1.6 Tetrazine Ligation

In 2008, FOX<sup>84</sup> and HILDEBRAND<sup>85</sup> independently reported a new class of bioorthogonal reaction based on the inverse-electron-demand Diels-Alder reaction (IEDDA) between a tetrazine and a strained *trans*-cyclooctene (TCO) (Scheme 1.10).



**Scheme 1.10** Tetrazine ligation reaction between tetrazine and strained alkenes.

The reaction was found to proceed with extremely fast ligation rates in the range of  $10^3 - 10^6 \text{ M}^{-1} \text{ s}^{-1}$  under physiological conditions. Noteworthy, the resulting tetrazine linkages are stable towards hydrolysis. Owing to the remarkable reactivity and fast kinetics, this type of cycloaddition has found broad applications in all areas of protein labeling and bioconjugation, but most importantly, in live animal imaging. In addition to TCOs **17**, several strained alkenes and alkynes have been developed for tetrazine ligations, i.e. cyclopropenes (Cyp, **18**),<sup>86</sup> norbornenes (Nor, **19**)<sup>87</sup> and BCNs (**20**),<sup>88</sup> exhibiting comparably fast ligation kinetics (Figure 1.10).

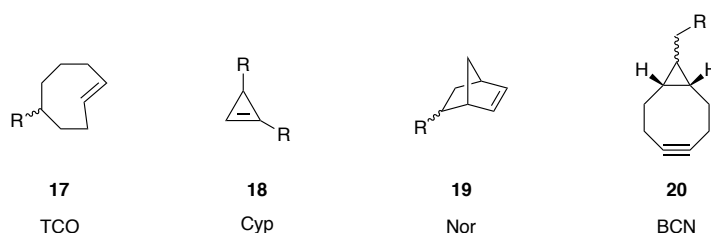
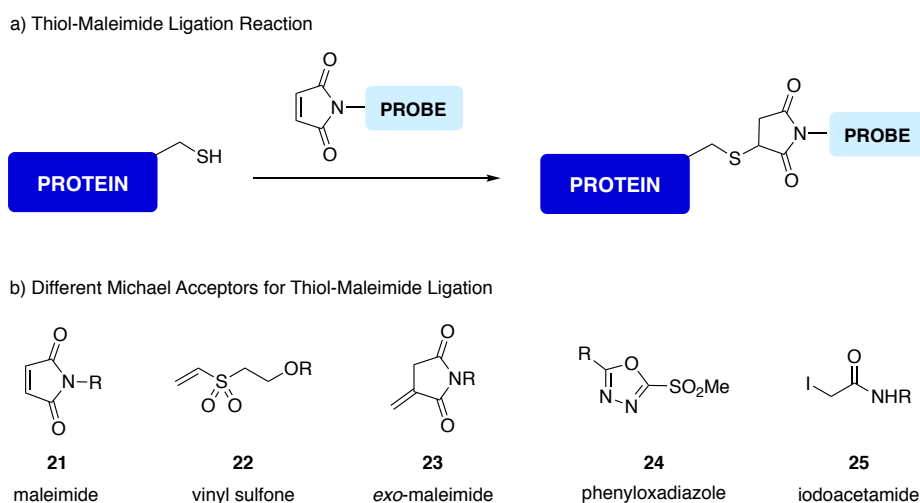


**Figure 1.10** A selection of cycloalkyne and cycloalkyne derivatives for SPAAC.

### 1.3.1.7 Thiol-Maleimide Ligation

The thiol-maleimide ligation is the reaction between thiols and  $\alpha,\beta$ -unsaturated carbonyl compounds, i.e. maleimids, providing succinimide (Scheme 1.11, a). Even though thiols naturally occur in cysteine side chains and are thus technically not bioorthogonal functional groups, the thiol-maleimide ligation has found a variety of applications in chemistry, biology<sup>89</sup> and material science.<sup>90</sup>

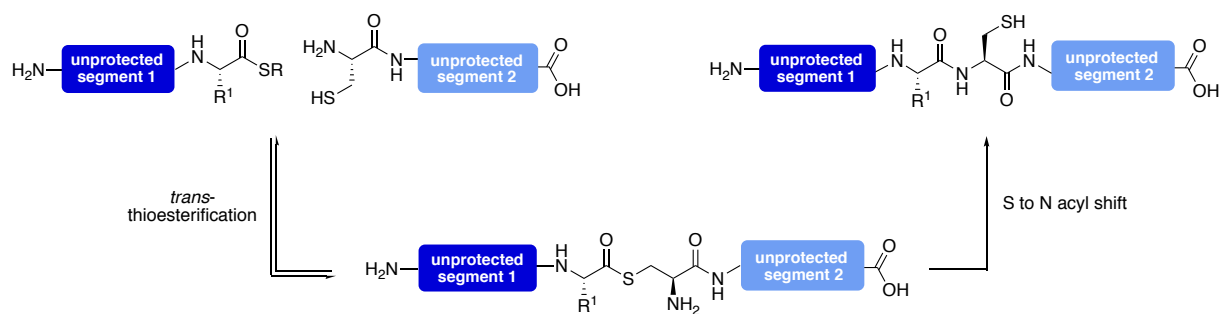


**Scheme 1.11** a) Thiol-maleimide ligation between surface-exposed cysteins and maleimides. b) A selection of different Michael acceptors for thiol-maleimide ligation.

The thiol-maleimide ligation proceeds with extremely fast reaction rates of up to  $700 \text{ M}^{-1} \text{ s}^{-1}$  at physiological pH.<sup>59,91</sup> However, the major limitation of this ligation reaction is the linker stability. Succinimides are prone to undergo hydrolytic ring-opening in aqueous buffers or retro-Michael reactions followed by conjugation to other thiols, i.e. albumin or glutathione, *in vivo*.<sup>92</sup> It has been found that ligation products from *N*-aryl-substituted maleimides are more susceptible to hydrolysis compared to that of their *N*-alkyl-substituted counterparts.<sup>93</sup> To overcome these limitations, several other Michael acceptors, including vinyl sulfones **22**, *exo*-maleimides **23**, phenyloxadiazoles **24** and iodoacetamides **25**, have been reported over the years exhibiting improved stability of the formed thioether conjugate (Scheme 1.11 b).<sup>94,95</sup>

### 1.3.1.8 Native Chemical Ligation

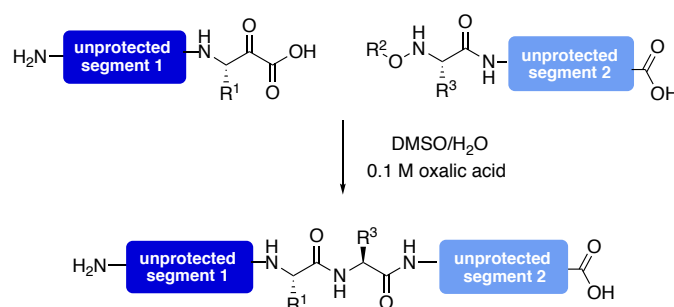
The native chemical ligation (NCL) was first reported by KENT and coworkers in 1994. The reaction showcases the chemoselective ligation between C-terminal thioesters and N-terminal cysteines resulting in the formation of natural amide bonds (Scheme 1.12). In the initial step of NCL, the cysteine moiety undergoes reversible *trans*-thioesterification with a thioester. In a second step, an intramolecular S to N acyl shift takes place resulting in the formation of the amide bond. In general, the reaction proceeds in aqueous media at pH 7-8 and ambient temperature. Rate constants for the reaction were determined to be between  $0.07\text{-}0.2 \text{ M}^{-1} \text{ s}^{-1}$ .<sup>59,96</sup> NCL consequently displays the current state of the art in protein synthesis. The reaction has been used in the synthesis of a diverse panel of proteins, such as of human interleukin 8 (IL-8),<sup>97</sup> erythropoietin,<sup>98,99</sup> HIV-1 protease,<sup>100</sup> and F-ATPase.<sup>101</sup> NCL is also a frequently used tool in the synthesis of dendrimers<sup>102</sup> or in the synthesis of high molecular weight collagen-like polymers.<sup>103</sup>



**Scheme 1.12** Native chemical ligation between thioesters and thiols.

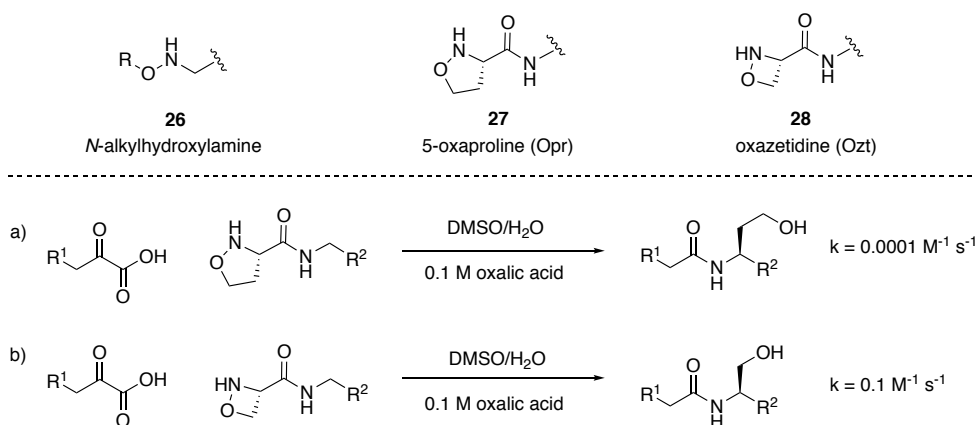
### 1.3.1.9 $\alpha$ -Ketoacid-hydroxylamine Ligation

In 2006, BODE and coworkers reported the  $\alpha$ -ketoacid-hydroxylamine (KAHA) ligation – a new type of chemoselective amide bond forming reaction involving a decarboxylative condensation of *N*-alkylhydroxylamines with  $\alpha$ -ketoacids,<sup>104</sup> referred to as the KAHA ligation (Scheme 1.13). The reaction proceeds under aqueous acidic conditions without the requirement for any additional reagents or catalysts. Importantly, the only byproducts formed are CO<sub>2</sub> and water.



**Scheme 1.13**  $\alpha$ -Ketoacid hydroxylamine (KAHA) ligation between  $\alpha$ -ketoacids and hydroxylamines.

The KAHA ligation is predominantly used for the chemical synthesis of proteins.<sup>105</sup> The utility of this reaction was first demonstrated in the synthesis of glucagon-like peptide GLP-1.<sup>106</sup> Further optimization studies led to the discovery of alternative cyclic hydroxylamines exhibiting enhanced ligation kinetics, such as 5-oxaproline **27** (Opr) and oxazetidine **28** (Ozt) (Scheme 1.14). While Opr **27** still displays relatively slow reaction rates, Ozt **28** exhibits faster reaction kinetics at micromolar concentrations and neutral pH with second-order rate constants on the scale of 0.1 M<sup>-1</sup> s<sup>-1</sup>. However, in comparison to *N*-alkylhydroxylamine and Opr (**27**), Ozt (**28**) unfortunately suffers from poor stability in solution.



**Scheme 1.14** Overview of suitable hydroxyl amines for KAHA ligation and their associated rate constants.

### 1.3.2 Limitations of Bioorthogonal Ligation Reactions

Despite the immense benefit and indispensable utility of bioorthogonal ligation reactions in the site-specific modification and labeling of proteins with small molecules or peptides,<sup>107</sup> the efficient covalent ligation of stoichiometric quantities of large molecules for desirable applications, such as protein-protein or protein polymer conjugation,<sup>108</sup> as well as the synthesis of oligomeric biomolecules,<sup>109,110</sup> remains one of the major contemporary challenges in the field. This is due to the fact that established chemoselective ligation reactions are hampered by at least one of the four general limitations:

- 1) Heterogeneous product formation due to limited site-selectivity<sup>111,112,113</sup>
- 2) Instability of ligation products or reactants<sup>114</sup>
- 3) Incompatibility with physiological conditions
- 4) Slow reaction kinetics<sup>115</sup>

One of the major boundaries that prevent bioorthogonal reactions, such as native chemical ligation (NCL), KAHA ligation and oxime/hydrazone ligation reactions, from their broader application are the slow reaction rates at physiological pH. In a few cases, such as in the oxime and hydrazone ligation or the copper-catalyzed azide-alkyne 1,3-dipolar cycloadditions (CuAAC), reaction rates can significantly be accelerated by the use of catalysts, i.e. bifunctional aniline or copper(I) respectively. Generally, however, it must be noted that the use of catalysts or other additives in bioorthogonal ligation reactions is undesirable as additional complexity is added and cytotoxic side effects are observed.<sup>74</sup>

Another restrictive criteria for bioorthogonal ligation reactions is the stability and nature of the ligation product. As an example, thiol-maleimide conjugation reactions suffer from insufficient stability of the succinimide ligation product, which is prone to undergo imide hydrolysis and retro-Michael reactions.<sup>92</sup> Furthermore, strain-promoted azide-alkyne 1,3-dipolar cycloadditions (SPAAC) and tetrazine ligation produce large, non-native linkages, which may perturb protein or metabolic function. Yet, the few existing ligation reactions that form native and stable amide bonds, such as native chemical ligation and KAHA ligation, suffer from particularly slow ligation kinetics.

In consideration of the shortcomings of the presented bioorthogonal reactions, new amide bond forming ligation chemistries are required that exhibit rate constants that are fast enough for the efficient synthesis of physiologically stable bioconjugates.



### 1.3.3 The Importance of Reaction Kinetics

Bioorthogonal ligation reactions can predominantly be described by standard second-order reaction kinetics. This means that the reaction is proportional to the concentration of both ligation partners. By virtue of their large molecular weight (>10 kD), proteins and other biomolecules must typically be manipulated under highly dilute reaction concentrations (<100  $\mu\text{M}$ ), which leads to rate attenuation of a factor of up to  $10^4$  compared to small molecule chemistry. As demonstrated by DAWSON and RAINES,<sup>116</sup> the conjugation of large molecules in the micromolar regime must display fast reaction rates with rate constants above  $10 \text{ M}^{-1} \text{ s}^{-1}$  to reach quantitative conversion (Figure 1.11). For achieving satisfying conversion rate constants larger than  $0.1 \text{ M}^{-1} \text{ s}^{-1}$  are required.

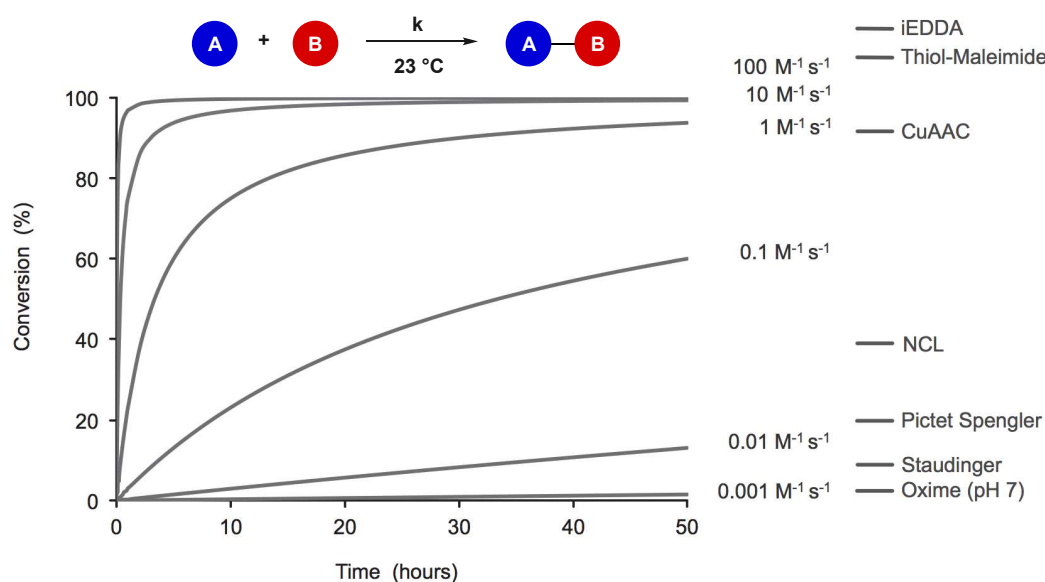
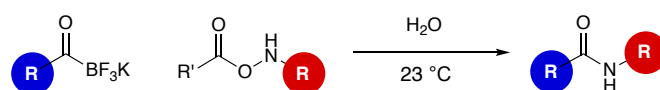


**Figure 1.11** Graphical representation of conversion over time for different reaction rates and ranking of common bioorthogonal ligation strategies at an initial concentration of  $50 \mu\text{M}$ .

Most bioorthogonal ligation reactions, such as native chemical ligation, Staudinger ligation, oxime/hydrazone ligation and KAHA ligation, exhibit reaction kinetics on the scale of  $10^{-3} - 10^{-1} \text{ M}^{-1} \text{ s}^{-1}$ . As a consequence, these reactions often require hours to days without ever reaching full conversion. While this is inconvenient for reactions *in vitro*, it is strongly limiting for *in vivo* applications. To compensate for the slow ligation kinetics of most established ligation methods to date, protein modifications are typically performed using a large excess of the small molecule reactant.<sup>117</sup> Due to limited accessibility and cumbersome purification of proteins, but also because of cost and waste reasons, the conjugation of two proteins should ideally proceed in stoichiometric fashion and good yield.

## 1.4 Potassium Acyltrifluoroborate (KAT) Ligation

In 2012, BODE and MOLANDER reported a novel amide bond forming ligation reaction between potassium acyltrifluoroborates (KATs) and *O*-acylhydroxylamines (Scheme 15).<sup>118</sup> This chemoselective and bioorthogonal ligation reaction satisfies almost all of the requirements previously mentioned for the efficient conjugation of biomolecules (*cf.* Chapter 1.2.4). It proceeds under aqueous conditions at room temperature without the need for additional reagents or catalysts and tolerates all common unprotected functional groups. In addition, the reaction forms stable and naturally occurring amide bond linkages and has been shown to produce only non-toxic byproducts.

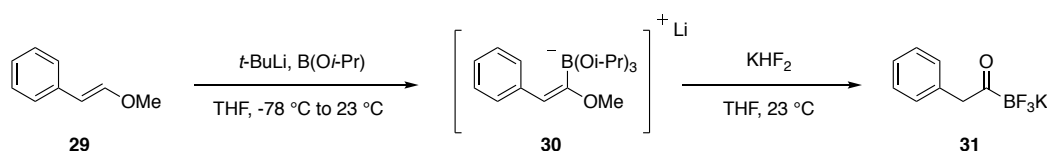


- Bioorthogonal
- Room temperature
- No additives
- Stable Linker
- Fast Kinetics

**Scheme 1.15** KAT ligation between acyltrifluoroborates and *O*-acylhydroxylamines.

### 1.4.1 Synthesis of Potassium Acyltrifluoroborates (KATs)

Due to lack of accessibility, potassium acyltrifluoroborates have thus far represented one of the most understated classes of boron compounds. It was only in 2010 that MOLANDER reported the first synthesis of a potassium acyltrifluoroborate **31** via a hydrolysis-fluorination sequence of borylvinyl ether intermediate **30** (Scheme 1.16).<sup>119</sup> However, this route could not be extended to the preparation of other KAT species.

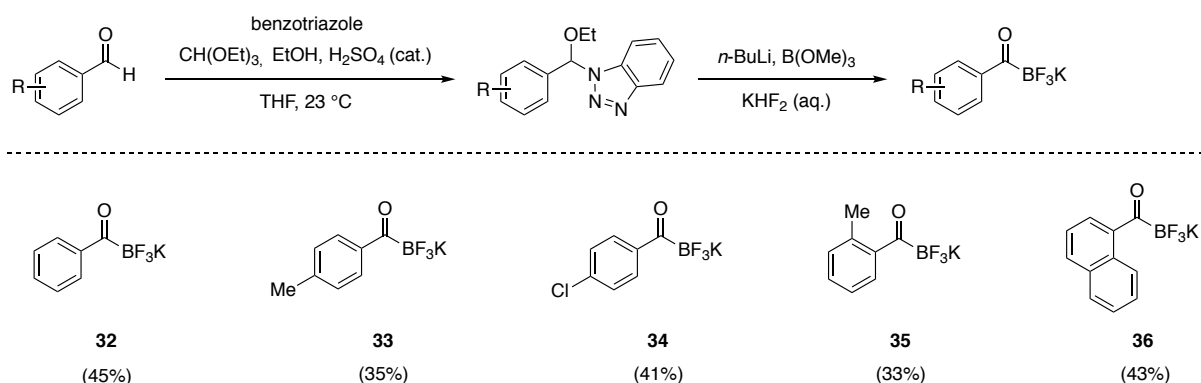


**Scheme 1.16** First synthesis of a potassium acyltrifluoroborate reported by MOLANDER.

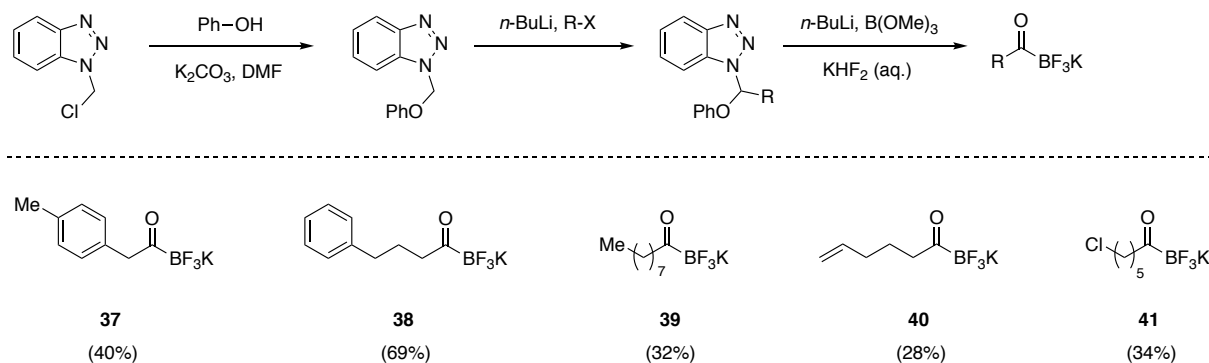
A milestone in the field was the work of BODE *et. al.*, who established multiple robust protocols for the efficient synthesis of a variety of KATs in satisfying yields. In an early report in 2012, BODE described two benzotriazole-mediated procedures for the preparation of over 10 examples of different aromatic and aliphatic KATs starting from the respective aldehydes

(Scheme 1.17).<sup>120</sup> The reaction proceeds in two steps taking advantage of KATRITZKY'S benzotriazole-based ethoxy-*N,O*-acetals<sup>121,122</sup> which upon treatment with *n*-butyllithium lead to the formation of acyl anions. Subsequent trapping with trimethyl borate followed by hydrolysis with aqueous  $\text{KHF}_2$  afforded aromatic KATs in moderate yields. Additionally, the replacement of ethoxy-*N,O*-acetals with phenoxy-*N,O*-acetals allowed the expansion of the substrate scope to alkyl KAT products.

a) Benzotriazole Route for the Synthesis of Aromatic KATs



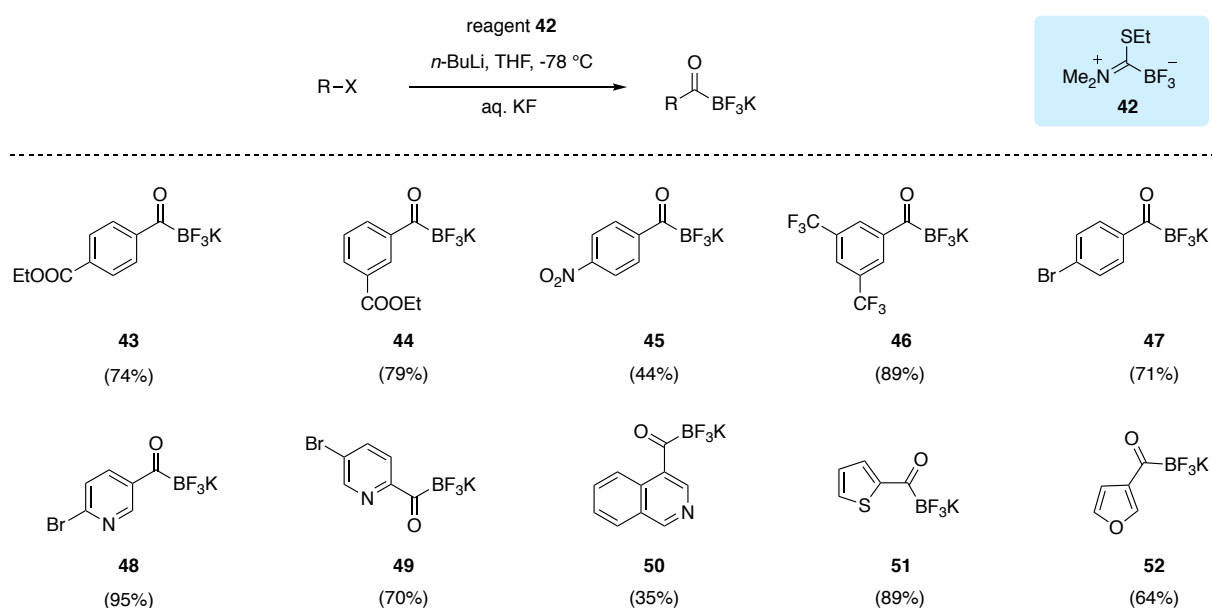
b) Benzotriazole Route for the Synthesis of Aliphatic KATs



**Scheme 1.17** Benzotriazole-mediated synthesis of KATs developed by BODE. a) Synthesis of aromatic KATs via *N,O*-acetals. b) aliphatic KATs. Reaction yields are given in parenthesis.

In an attempt to improve the overall yield, BODE and coworkers developed reagent **42**, also referred to as BODE KAT REAGENT, for the convenient one-pot synthesis of KATs starting from aryl or heteroaryl halides (Scheme 1.18).<sup>123</sup> The reaction proceeds via initial lithiation of an aryl halide with *n*-butyllithium followed by trapping with reagent **42**. Upon hydrolysis with aqueous KF the desired KAT products were collected by filtration in good to excellent yields. The reaction has proven to be particularly useful for the synthesis of aryl

KAT derivatives decorated with base-sensitive functional groups, which are prone to hydrolysis, i.e. esters.



**Scheme 1.18** One-pot KAT synthesis starting from aryl or heteroaryl halides via the BODE KAT REAGENT.

This reagent-based approach has evolved as the new standard in the synthesis of aromatic and heteroaromatic potassium acyltrifluoroborates and its broad utility entailed the commercialization of a selection of KATs,<sup>124</sup> as well as the BODE KAT REAGENT.<sup>125</sup>

In an effort to expand the synthetic repertoire of KATs, BODE *et. al.* recently developed the synthesis of bifunctional KAT species bearing additional, easily-modifiable functional groups for further orthogonal derivatization (Figure 1.12).<sup>126</sup> In presence of the KAT functionality, **54** and **55** were shown to participate in a chemoselective CuAAC with terminal alkyne or azide-substituted rhodamine dyes respectively. Furthermore, acylation of **58** with coumarin halides was demonstrated to be equally chemoselective.

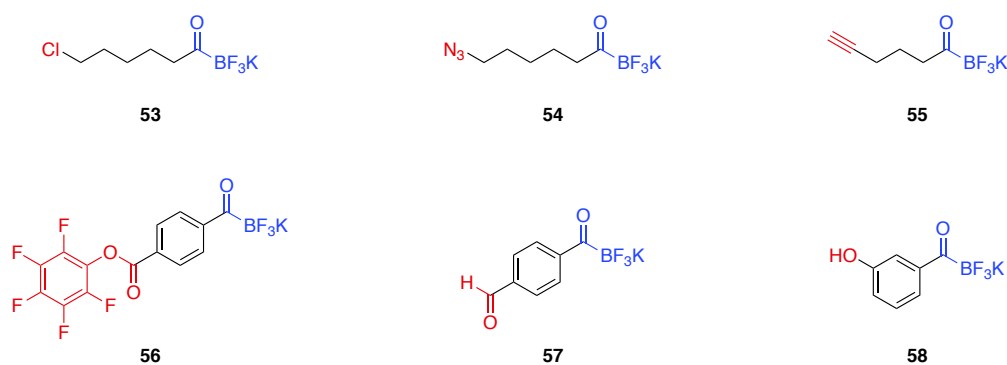
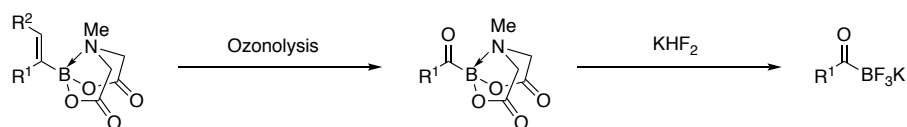


**Figure 1.12** A selection of bifunctional KAT species reorted by BODE and coworkers.

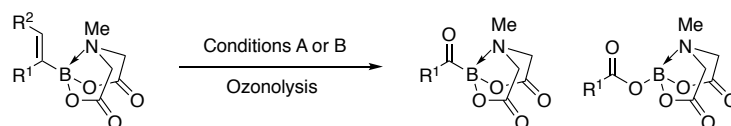
Recently, ITO and BODE reported an alternative synthetic methodology for the preparation of functionalized KATs via ozonolysis of alkenyl MIDA boronates followed by hydrolysis and fluorination of the intermediate acyl MIDA boronate with  $\text{KHF}_2$  in high yields (Scheme 1.19).<sup>127</sup>



**Scheme 1.19** KAT synthesis starting from ozonolysis of alkenyl MIDA boronates followed by

The ozonolysis conditions allowed the transformation of substrates including various functional groups such as ketones, esters, ethers, and amino groups (Table 1.1).

**Table 1.1** Substrate scope for the ozonolysis of alkenyl MIDA boronates

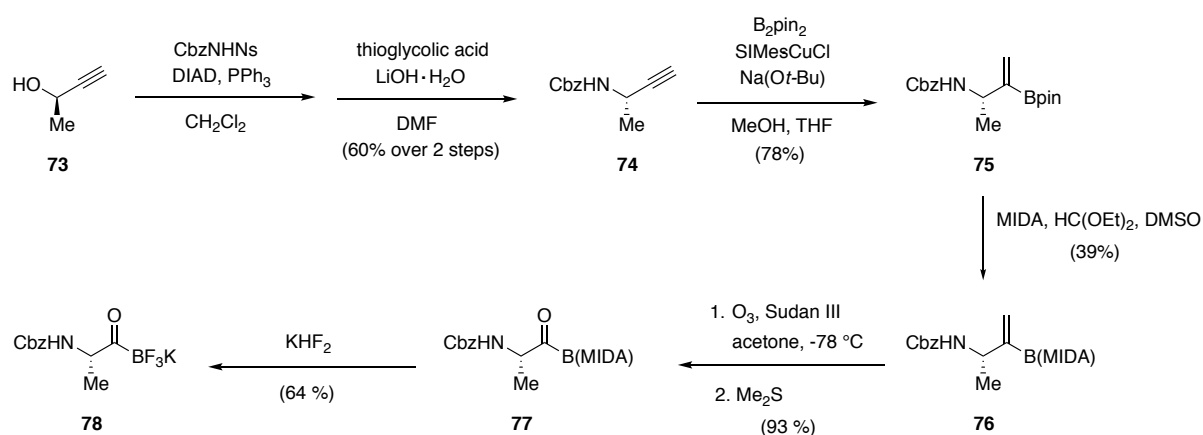


Entry	Substrate	Product	Conditions <sup>[a]</sup>	Yield <sup>[b]</sup>	Product Ratio <sup>[c]</sup>
1			A	84	>95:<5
2			A B	88 88	85:15 >95:<5
3			A B	85 81	93:7 95:5
4			A B	84 80	82:18 85:15
5			A	66	74:26
6			A	91	95:5
7 <sup>[d]</sup>			A	65	93:7

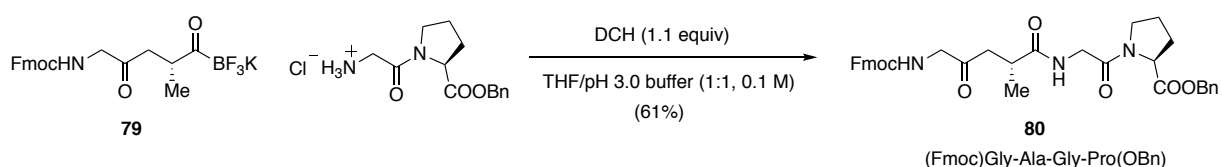
[a] Conditions: A) Substrate (0.3 mmol),  $\text{O}_3$ , acetone,  $-78\text{ }^\circ\text{C}$ , then excess  $\text{Me}_2\text{S}$ . B) Substrate (0.3 mmol),  $\text{O}_3$ , pyridine (0.3 equiv), acetone,  $-78\text{ }^\circ\text{C}$ . [b] Yields of combined isolated products are reported. [c] Product ratios were determined from the crude reaction mixture by  $^{11}\text{B}$ -NMR spectroscopy. [d] 0.03 mol % of Sudan III was added.<sup>128</sup>

Most importantly, this methodology enabled the synthesis of  $\alpha$ -amino acylboronates which include asymmetric carbon centers, with high enantiospecificity and good configurational stability. Beside glycine-derived  $\alpha$ -amino acylboronates **70** and **72**, also a synthetic route towards L-alanine-derived acylboronates **78** was described (Scheme 1.20, a). Furthermore, **79** was shown to undergo peptide coupling with a benzyl protected Gly-Pro dipeptide salt in presence of DCH as chlorinating agent. The diastereomeric ratio of ligation product **80** was found to be 98:2 indicating that  $\alpha$ -amino acylboronates are configurationally stable under these ligation conditions (Scheme 1.20, b).

a) Synthetic Route towards L-Alanine-Derived Acyltrifluoroborate



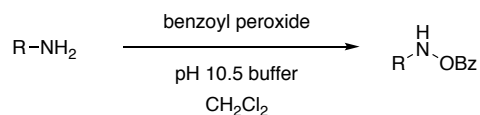
b) Application of L-Alanine-Derived Acyltrifluoroborate in Peptide Synthesis



**Scheme 1.20** a) Synthetic preparation of a Cbz-protected L-alanine-derived acyltrifluoroborate **78**. b) Peptide coupling of a Gly-L-Ala-derived acyltrifluoroborate dipeptide in presence of DCH as chlorinating agent.

### 1.4.2 Synthesis of Hydroxylamines

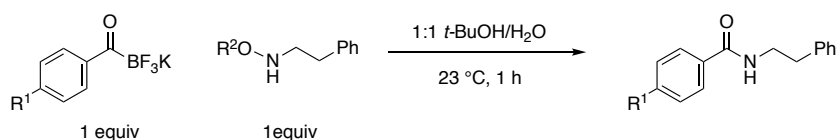
In the initial version of the KAT ligation *O*-benzoyl hydroxylamines were used as ligation partners.<sup>118</sup> As shown in Scheme 1.21, these hydroxylamines are usually prepared according to the method of PHANSTIEL starting from the respective primary amines by treatment with benzoyl peroxide under biphasic conditions.<sup>129</sup>



**Scheme 1.21** Synthesis of *O*-benzoyl hydroxylamines by PHANSTIEL.

However, it was found that *O*-benzoyl hydroxylamines show stability issues under various reaction conditions, particularly in presence of primary and secondary amines. To address this issue, BODE and coworkers evaluated the relative stability and reactivity of a panel of *O*-substituted hydroxylamines **81-89** in a KAT ligation (*cf.* Chapter 1.3) with stoichiometric amounts of KAT by the aid of different additives (Table 1.2).<sup>130</sup>

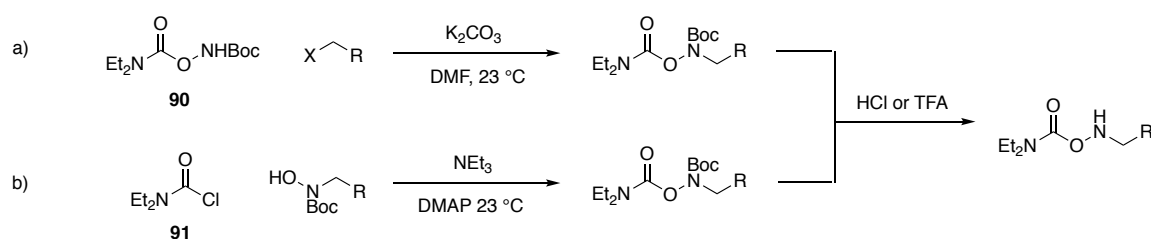
**Table 1.2** Reactivity and stability evaluation of different *O*-substituted hydroxylamines.



Entry	Hydroxylamine	Relative Reactivity	Stability to 1° amines <sup>[a]</sup>	Stability to 2° amines <sup>[b]</sup>	Stability in acid <sup>[c]</sup>
1		NR	–	–	–
2		NR	–	–	–
3		NR	–	–	–
4		14	–	–	–
5		100	no	no	yes
6		117	no	no	no
7		124	no	no	no
8		78	no	no	no
9		87	yes	yes	yes

Reactions were monitored by LC-MS. The following additives were added: [a] 2-Phenylethylamine (10 equiv), DMF, 23 °C, 1 h. [b] 20% Piperidine in DMF, *N*-Boc derivatives of the corresponding hydroxylamine were used as substrates, 23 °C, 24 h. [c] 50% TFA in CH<sub>2</sub>Cl<sub>2</sub>, 23 °C, 3 h.

After extensive screening, *N,N*-diethylcarbamoylhydroxylamine **89** was found to be a superior hydroxylamine with significantly increased stability and similar reactivity to the *O*-benzoyl derivative **85**. There are two main approaches for the synthesis of *N,N*-diethylcarbamoylhydroxylamines. One approach involves the alkylation of Boc-protected *N,N*-diethylcarbamoyl hydroxylamine **90** with alkylhalides in presence of base (Scheme 1.22, a). The other strategy comprises acylation of Boc-protected *N*-alkyl hydroxylamines with *N,N*-diethylcarbamoylchloride **91** under basic conditions. Both routes lead to the same *N*-Boc-protected intermediate, which upon acidic deprotection with hydrochloric acid or trifluoroacetic acid yields the desired *N,N*-diethylcarbamoylhydroxylamines in good overall yields (Scheme 1.22, b).



**Scheme 1.22** Synthetic strategies towards the preparation of *N,N*-diethylcarbamoylhydroxylamines. a) Alkylation of Boc-protected carbamoylhydroxylamines with alkylhalides. b) Acylation of Boc-protected *N*-alkylhydroxylamines with *N,N*-diethylcarbamoylchloride. Both strategies are followed by acidic deprotection.

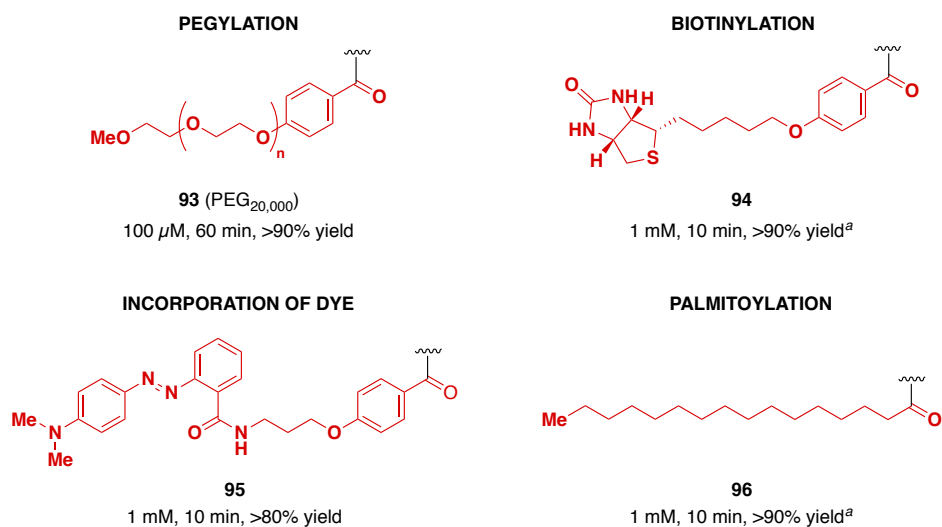
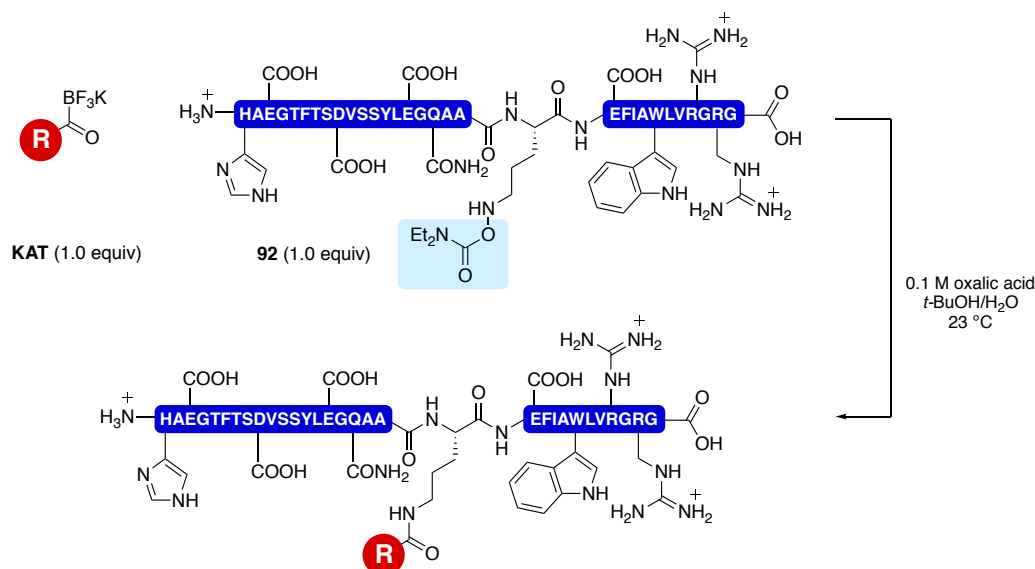
### 1.4.3 Synthetic Limitations and Applications of Potassium Acyltrifluoroborates

Naturally occurring, human glucagon like-peptide 1 (GLP-1) has a very short half-life of ca. 2 minutes *in vivo*, and over the years many efforts have been undertaken to improve its pharmacokinetic properties by structural modification.<sup>131,132</sup> As an example, the palmitoylated form of GLP-1 was shown to prolong plasma half-life to 13 hours and is an approved and marketed drug for type II diabetes mellitus therapy.<sup>133</sup>

In 2014, BODE and NODA reported KAT ligation as a tool for the chemoselective functionalization of GLP-1 analogue **92** enabling site-specific biotinylation, PEGylation, palmitoylation and incorporation of aza-dyes (Scheme 1.23).<sup>130</sup> **92** is a 31 amino acid residue peptide, which was prepared by standard Fmoc-SPPS. For ligation purposes a hydroxylamine moiety was incorporated into one of the side chains. The reaction of **92** and the respective functionalized **KAT** moiety was performed with all side chains unprotected in water at equimolar ratios and concentrations of either 1 mM or 100  $\mu\text{M}$ . The KAT ligation proceeds with remarkable chemoselectivity. Additionally, high reaction rates of up to



$20 \text{ M}^{-1} \text{ s}^{-1}$  at pH 3 were measured. Importantly, it was found that the presence of water is essential for efficient ligation. When the reaction was performed in anhydrous organic solvents, in the absence of water, extremely slow ligation rates were observed.

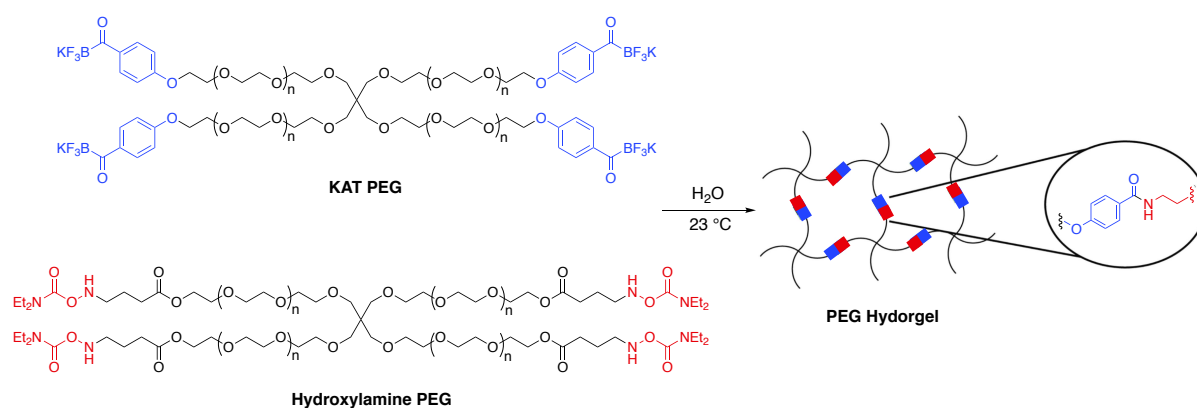


**Scheme 1.23** Chemoselective biotinylation, PEGylation, palmitoylation and incorporation of dyes into a 31-mer GLP1-analogue by KAT ligation.<sup>134</sup>

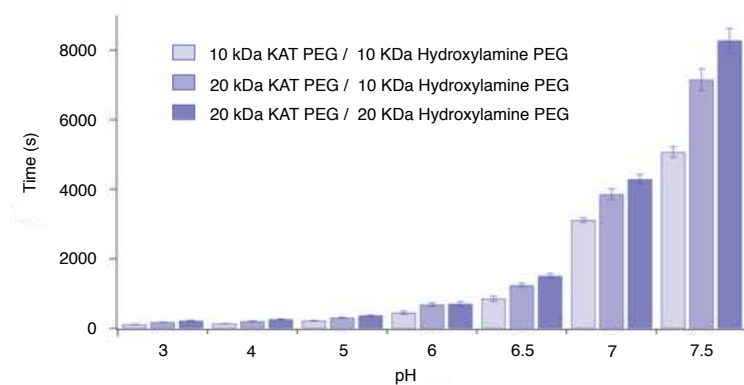
In 2015, a kinetic evaluation by BODE and SAITO revealed that the KAT ligation is strongly pH dependent. While fast ligation rates of over  $20 \text{ M}^{-1} \text{ s}^{-1}$  were observed under acidic conditions in the presence of oxalic acid, KAT ligation kinetics were found to be significantly decelerated at pH 5.1 exhibiting rates around  $0.39 \text{ M}^{-1} \text{ s}^{-1}$ .<sup>59</sup>

In the same year, BODE and MAZUNIN reported the synthesis of novel PEG-based hydrogels via chemoselective KAT ligation (Scheme 1.24, a).<sup>135</sup> Gelation kinetic studies by dynamic rheometry showed that the KAT ligation is indeed highly pH dependent over a broad pH range (pH 3 – 7.4) (Scheme 1.24, b). It was found that for a 4 wt% PEG hydrogel, at low acidic pHs (3 to 6) gelation proceeds rapidly within few minutes. At neutral and physiological pHs (7 and 7.4), however, the reaction is slower, forming a hydrogel in ca. 80 min.

a) Synthesis of PEG Hydrogels by KAT Ligation



b) Summarized Rheometry Kinetic Studies



**Scheme 1.24** a) Synthesis of PEG hydroxylamines developed by BODE and MAZUNIN. b) Summary of rheometry kinetic studies of three PEG systems.<sup>136</sup>

## 1.5 Concluding Remarks

Over the past decade, advances in chemoselective ligation reactions have transformed the fields of organic chemistry and chemical biology by facilitating the site-specific modification and labeling of proteins with small molecules and peptides. However, the covalent ligation of stoichiometric quantities of large molecules for applications such as protein-protein conjugation or the synthesis of oligomeric biomolecules remains one of the major contemporary challenges. Many established ligation reactions are hampered by slow reaction kinetics or instability of the produced unnatural linkages.

In 2012, BODE and MOLANDER have established a new bioorthogonal amide bond forming reaction – the KAT ligation – which comprises the conjugation of potassium acyltrifluoroborates and *O*-acylhydroxylamines. This chemoselective ligation reaction has great potential to fulfill all the requirements necessary to enable the equimolar conjugation of biomolecules at physiological pH. The reaction operates in water at room temperature, without the need for additional reagents or catalysts, forms stable and naturally occurring amide bond linkages and has been shown to produce only non-toxic byproducts. In addition, the KAT ligation displays fast reaction kinetics under acidic conditions and has successfully been applied in the PEGylation, lipidation and biotinylation of unprotected peptides proceeding with rate constants of up to  $20 \text{ M}^{-1} \text{ s}^{-1}$  at pH 3. However, recent studies have shown that the KAT ligation suffers from a significant decrease in reaction rates at elevated pH values (>pH 5), which up to date renders this ligation reaction inefficient for the equimolar conjugation of large biomolecules under physiological conditions.

## 1.6 References

- [1] For an excellent introduction into proteins and their related biological functions see: Murray, R. F.; Harper, H. W.; Granner, D. K.; Mayes, P. A.; Rodwell, V. W. Harper's Illustrated Biochemistry. Lange Medical Books/McGraw-Hill, New York, NY, USA, **2006**.
- [2] This figure has been adapted from the doctoral thesis of Niclas F. Rohrbacher, Synthesis of Cyclic Peptides and Proteins by  $\alpha$ -Ketoacid-Hydroxylamine Ligation. Diss. ETH No. 24342, **2017**. The picture of Collagen was taken from Lehninger Principles of Biochemistry, 3<sup>rd</sup> Edition, Worth Publishers, New York, NY, USA, **2003**. The picture of Hexokinase was taken from Pearson Edition, Inc., 2012. The picture of Insulin was taken from Protein Data Bank in Europe. The picture of IgG was taken from the National Library of Medicine. The picture of Myoglobin was taken from [www.chemden.in](http://www.chemden.in). The picture of Zincfinger was taken from [www.drkarafitzgerald.com](http://www.drkarafitzgerald.com).
- [3] For an excellent introduction into the structure of proteins see: Branden, C.; Tooze, J. Introduction to Protein Structure. Garland Pub, New York, NY, USA, **1999**.
- [4] This figure has been adapted from the doctoral thesis of Niclas F. Rohrbacher, Synthesis of Cyclic Peptides and Proteins by  $\alpha$ -Ketoacid-Hydroxylamine Ligation. Protein pictures were taken from Protein Data Bank in Europe.
- [5] Walsh, C. T. Posttranslational Modification of Proteins: Expanding Nature's Inventory. Roberts and Company, Greenwood Village, CO, USA, **2006**.
- [6] For detailed information on glycosylation see: Varki, A.; Cummings, R. D.; Esko, J. D.; Freeze, H. H.; Stanley, P.; Bertozzi, C. R.; Hart, G. W.; Etzler M. E. Essentials of Glycobiology, 2nd edition. Cold Spring Harbor, New York, NY, USA, **2009**.
- [7] Cozzone, A. J. Protein Phosphorylation in Prokaryotes. *Annu. Rev. Microbiol.* **1988**, *42*, 97–125.

- 
- [8] Glickman, M. H.; Ciechanover, A. The Ubiquitin-Proteasome Proteolytic Pathway: Destruction for the Sake of Construction. *Physiol. Rev.* **2002**, *82*, 373–428.
- [9] Mukhopadhyay, D; Riezman, H. Proteasome-Independent Functions of Ubiquitin in Endocytosis and Signaling. *Science.* **2007**, *315*, 201–205.
- [10] Schnell, J. D.; Hicke, L. Non-Traditional Functions of Ubiquitin and Ubiquitin-Binding Proteins. *J. Biol. Chem.* **2003**, *278*, 35857–35860.
- [11] Boyce, M.; Bertozzi, C. R. Bringing Chemistry to Life. *Nat. Methods* **2011**, *8*, 638-642.
- [12] Prescher, J. A.; Bertozzi, C. R. Chemistry in Living Systems. *Nat. Chem. Biol.* **2005**, *1*, 13–21.
- [13] Sunbul, M.; Yin, J. Site Specific Protein Labeling by Enzymatic Posttranslational Modification. *Org. Biomol. Chem.* **2009**, *7*, 3361–3371.
- [14] Chen, I.; Howarth, M.; Lin, W.; Ting, A. Y. Site-Specific Labeling of Cell Surface Proteins with Biophysical Probes Using Biotin Ligase. *Nat. Methods* **2005**, *2*, 99–104.
- [15] Jeger, S.; Zimmermann, K.; Blanc, A.; Grünberg, J.; Honer, M.; Hunziker, P.; Struthers, H.; Schibli, R. Site-Specific and Stoichiometric Modification of Antibodies by Bacterial Transglutaminase. *Angew. Chem. Int. Ed.* **2010**, *49*, 9995–9997.
- [16] For an excellent introduction into traditional approaches for selective chemical protein modification see the following review: Spicer, C. D.; Davis, B. G. Selective Chemical Protein Modification. *Nature Commun.* **2014**, *5*, 1–14.
- [17] For an overview of more recently developed strategies for selective chemical protein modification see the following review: Boutureira, O.; Bernardes, G. J. L. Advances in Chemical Protein Modification. *Chem. Rev.* **2015**, *115*, 2174–2195.

- [18] For selected examples of protein-polymer conjugation see: a) Roberts, M. J.; Bentley, M. D.; Harris, J. M. Chemistry for Peptide and Protein PEGylation. *Adv. Drug Delivery Rev.* **2002**, *54*, 459–476. b) Gauthier, M.; Klok, H. Peptide/Protein-Polymer Conjugates: Synthetic Strategies and Design Concepts. *Chem. Commun.* **2008**, 2591–2611. c) Alconcel, S. N. S.; Baas, A. S.; Maynard, H. D. FDA-Approved Poly(ethylene glycol)-Protein Conjugate Drugs. *Polym. Chem.* **2011**, *2*, 1442–1448. d) Dozier, J. K.; Distefano, M. D. Site-Specific PEGylation of Therapeutic Proteins. *Int. J. Mol. Sci.* **2015**, *16*, 25831–25864.
- [19] For selected examples of dimeric protein-protein conjugation see: a) Tao, L.; Kaddis, C. S.; Ogorzalek Loo, R. R.; Grover, G. N.; Loo, J. A.; Maynard, H. A. Synthetic Approach to Homodimeric Protein-Polymer Conjugates. *Chem. Commun.* **2009**, 2148–2150. b) Lorenzo, M. M.; Decker, C. G.; Kahveci, M. U.; Paluck, S. J.; Maynard, H. D. Homodimeric Protein-Polymer Conjugates via the Tetrazine-*trans*-Cyclooctene Ligation. *Macromolecules* **2016**, *49*, 30–37. c) ElSohly, A. M.; MacDonald, J. I.; Hentzen, N. B.; Aanei, I. L.; El Muslemay, K. M.; Francis, M. B. *ortho*-Methoxyphenols as Convenient Oxidative Bioconjugation Reagents with Application to Site-Selective Heterobifunctional Cross-Linkers. *J. Am. Chem. Soc.* **2017**, *139*, 3767–3773. d) Hudak, J. E.; Barfield, R. M.; de Hart, G. W.; Grob, P.; Nogales, E.; Bertozzi, C. R.; Rabuka, D. Synthesis of Heterobifunctional Protein Fusions Using Copper-Free Click Chemistry and the Aldehyde Tag. *Angew. Chem. Int. Ed.* **2012**, *51*, 4161–4165. e) Yang, Y.; Kluger, R. Efficient CuAAC Click Formation of Functional Hemoglobin *bis*-Tetramers. *Chem. Commun.* **2010**, *46*, 7557–7559. f) Hvasanov, D.; Nam, E. V.; Peterson, J. R.; Pornsaksit, D.; Wiedenmann, J.; Marquis, C. P.; Thordarson, P. One-Pot Synthesis of High Molecular Weight Synthetic Heteroprotein Dimers Driven by charge complementarity electrostatic interactions. *J. Org. Chem.* **2014**, *79*, 9594–9602.
- [20] a) Hemantha, H. P.; Brik, A. Non-Enzymatic Synthesis of Ubiquitin Chains: Where Chemistry Makes a Difference. *Bioorg. Med. Chem.* **2013**, *21*, 3411. (b) Kim, S.; Ko, W.; Sung, B. H.; Kim, S. C.; Lee, H. S. Direct Protein-Protein Conjugation by Genetically Introducing Bioorthogonal Functional Groups into Proteins. *Bioorg. Med. Chem.* **2016**, *24*, 5816.

- 
- [21] Hawker, C. J.; Wooley, K. L. The Convergence of Synthetic Organic and Polymer Chemistries. *Science* **2005**, *309*, 1200–1205.
- [22] Thordarson, P.; Le Droumaguet, B.; Velonia, K. Well-Defined Protein-Polymer Conjugates-Synthesis and Potential Applications. *Appl. Microbiol. Biotechnol.* **2006**, *73*, 243–254.
- [23] Lang, K.; Chin, J. W. Bioorthogonal Reactions for Labeling Proteins. *ACS Chem. Biol.* **2014**, *9*, 16–20.
- [24] Saito, F.; Noda, H.; Bode, J. W. Critical Evaluation of Rate Constants of Chemoselective Ligation Reactions for Stoichiometric Conjugations in Water. *ACS Chem. Biol.* **2015**, *10*, 1026–1033.
- [25] Picture of proteins were taken from Center for Cancer Research. Improving an Immunotoxin. *CCRconnections* **2011**, Vol. 5, No. 2.
- [26] For selected literature reports on bioorthogonal ligation reactions see: a) Borrmann, A.; van Hest, J. C. M. Bioorthogonal Chemistry in Living Organisms. *Chem. Sci.* **2014**, *5*, 2123–2123. b) Prescher, J. A.; Bertozzi, C. R.; Borrmann, A.; van Hest, J. C. M.; Shieh, P.; Sletten, E. M.; Ramil, C. P.; Lin, Q.; Patterson, D. M.; Nazarova, L. A. Orthogonal Bioorthogonal Chemistries. *Curr. Opin. Chem. Biol.* **2014**, *44*, 2123–2123. c) Ramil, C. P.; Lin, Q. Bioorthogonal Chemistry: Strategies and Recent Developments. *Chem. Comm.* **2013**, *49*, 11007–11022. d) Sletten, E. M.; Bertozzi, C. R. Bioorthogonal Reactions. *Acc. Chem. Res.* **2011**, *44*, 666–676. e) Sletten, E. M.; Bertozzi, C. R.: Bioorthogonal Chemistry: Fishing for Selectivity in a Sea of Functionality. *Angew. Chem. Int. Ed.* **2009**, *48*, 6974–6998.
- [27] Hang, H. C.; Yu, C.; Kato, D. L.; Bertozzi, C. R. A Metabolic Labeling Approach towards Proteomic Analysis of Mucin-Type O-Linked Glycosylation. *Proc. Natl. Acad. Sci. USA.* **2003**, *100*, 14846–14851.

- [28] Rideout, D.; Calogeropoulou, T.; Jaworski, J.; McCarthy, M. Synergism through Direct Covalent Bonding between Agents: A Strategy for Rational Design of Chemotherapeutic Combinations. *Biopolymers* **1990**, *29*, 247–262.
- [29] For an excellent perspective article on the topic see: Krall, N.; da Cruz, F. P.; Boutureira, O.; Bernardes, G. J. L. Site-Selective Protein-Modification Chemistry for Basic Biology and Drug Development. *Nature Chem.* **2016**, *8*, 103–113.
- [30] Bertozzi, C. R. A Decade of Bioorthogonal Chemistry. *Acc. Chem. Res.* **2011**, *44*, 651–653.
- [31] For an excellent review on bioorthogonal reactions and their application see: Zheng, M.; Zheng, L.; Zhang, P.; Li, J.; Zhang Y. Development of Bioorthogonal Reactions and Their Applications in Bioconjugation. *Molecules* **2015**, *20*, 3190–3205.
- [32] Krall, N.; da Cruz, F. P.; Boutureira, O.; Bernardes, G. J. L. Site-Selective Protein-Modification Chemistry for Basic Biology and Drug Development. *Nature Chem.* **2015**, 1–11.
- [33] Zheng, T.; Jiang, H.; Gros, M.; Soriano Del Amo, D.; Sundaram, S.; Lauvau, G. G.; Marlow, F.; Liu, Y.; Stanley, P.; Wu, P. Tracking *N*-Acetyllactosamine on Cell-Surface Glycans *in Vivo*. *Angew. Chem. Int. Ed.* **2011**, *50*, 4113–4118.
- [34] Saxon, E.; Bertozzi, C. R. Cell Surface Engineering by a Modified Staudinger Reaction. *Science* **2000**, *287*, 2007–2010.
- [35] Hudak, J. E.; Barfield, R. M.; de Hart, G. W.; Grob, P.; Nogales, E.; Bertozzi, C. R.; Rabuka, D. Synthesis of Heterobifunctional Protein Fusions Using Copper-Free Click Chemistry and the Aldehyde Tag. *Angew. Chem. Int. Ed.* **2012**, *51*, 4161–4165.



- 
- [36] McGinty, R. K.; Kim, J.; Chatterjee, C.; Roeder, R. G.; Muir, T. W. Chemically Ubiquitylated Histone H2B Stimulates hDot1L-Mediated Intranucleosomal Methylation. *Nature* **2008**, *453*, 812–816.
- [37] Agarwal, P.; Bertozzi, C. R. Site-Specific Antibody-Drug Conjugates: The Nexus of Bioorthogonal Chemistry, Protein Engineering, and Drug Development. *Bioconjug. Chem.* **2015**, *26*, 176–192.
- [38] Diamantis, N.; Banerji, U. Antibody-Drug Conjugates – An Emerging Class of Cancer Treatment. *Br. J. Cancer* **2016**, *144*, 362–367.
- [39] For an excellent overview of the *in vivo* application of bioorthogonal ligation reactions see: Gordon, C. G; Bertozzi, C. R. *In Vivo Applications of Bioorthogonal Chemistries*, in *Chemoselective and Bioorthogonal Ligation Reactions: Concepts and Applications*. Wiley-VCH Verlag GmbH & Co. KGaA, Weinheim, Germany, **2017**.
- [40] For an excellent overview of different bioorthogonal ligation reactions see: Gong, Y.; Pan, L. Recent Advances in Bioorthogonal Reactions For Site-Specific Protein Labeling and Engineering. *Tetrahedron Lett.* **2015**, *56*, 2123.
- [41] Best, M. D. Click Chemistry and Bioorthogonal Reactions: Unprecedented Selectivity in the Labeling of Biological Molecules. *Biochemistry* **2009**, *48*, 6571–6584.
- [42] Zhang, Z.; Smith, B. A. C.; Wang, L.; Brock, A.; Cho, C.; Schultz, P. G. A New Strategy for the Site-Specific Modification of Proteins *in Vivo*. *Biochemistry* **2003**, *42*, 6735–6746.
- [43] Sadamoto, R.; Niikura, K.; Ueda, T.; Monde, K.; Fukuhara, N.; Nishimura, S.-I. Control of Bacteria Adhesion by Cell-Wall Engineering. *J. Am. Chem. Soc.* **2004**, *126*, 3755–3761.
- [44] Zeng, Y.; Ramya, T. N.; Dirksen, A.; Dawson, P. E.; Paulson, J. C. High-Efficiency Labeling of Sialylated Glycoproteins on Living Cells. *Nat. Methods* **2009**, *6*, 207–209.

- [45] Jencks, W. P. Studies on the Mechanism of Oxime and Semicarbazone Formation. *J. Am. Chem. Soc.* **1959**, *81*, 475-481.
- [46] Cordes, E. H.; Jencks, W. P. Nucleophilic Catalysis of Semicarbazone Formation by Anilines. *J. Am. Chem. Soc.* **1962**, *84*, 826–831.
- [47] Cornish, V. W.; Hahn, K. M.; Schultz, P. G. Site-Specific Protein Modification Using a Ketone Handle. *J. Am. Chem. Soc.* **1996**, *118*, 8150–8151.
- [48] Sanders, J. K. Self-Assembly Using Dynamic Combinatorial Chemistry. *Philos. Trans. A* **2004**, *362*, 1239–1245.
- [49] Crisalli, P.; Kool, E. T. Water-Soluble Organocatalysts for Hydrazone and Oxime Formation. *J. Org. Chem.* **2013**, *78*, 1184–1189.
- [50] Crisalli, P.; Kool, E. T. Importance of *Ortho* Proton Donors in Catalysis of Hydrazone Formation. *Org. Lett.* **2013**, *15*, 1646–1649.
- [51] For a detailed review on the mechanism and catalysis of oxime and hydrazine ligation see: Kölmel, D. K.; Kool, E. T. Oximes and Hydrazones in Bioconjugation: Mechanism and Catalysis. *Chem. Rev.* **2017**, *117*, 10358–10376.
- [52] Kool, E. T.; Park, D.-H.; Crisalli, P. Fast Hydrazone Reactants: Electronic and Acid/Base Effects Strongly Influence Rate at Biological pH. *J. Am. Chem. Soc.* **2013**, *135*, 17663–17666.
- [53] Stockigt, J.; Antonchick, A. P.; Wu, F.; Waldmann, H. The Pictet-Spengler Reaction in Nature and in Organic Chemistry. *Angew. Chem. Int. Ed.* **2011**, *50*, 8538–8564.
- [54] Agarwal, P.; van der Weijden, J.; Sletten, E. M.; Rabuka, D.; Bertozzi, C. R. A Pictet-Spengler Ligation for Protein Chemical Modification. *Proc. Natl. Acad. Sci. USA.* **2013**, *110*, 46–51.

- [55] Gololobov, Y. G.; Zhmurova, I. N.; Kasukhin, L. F. Sixty Years of Staudinger Reaction. *Tetrahedron* **1981**, *37*, 437–472.
- [56] Nilsson, B. L.; Kiessling, L. L.; Raines, R. T. Staudinger Ligation: A Peptide from a Thioester and Azide. *Org. Lett.* **2000**, *2*, 1939–1941.
- [57] For two excellent reviews on Staudinger ligation see: a) Schilling, C. I.; Jung, N.; Biskup, M.; Schepers, U.; Bräse, S. Bioconjugation via Azide-Staudinger Ligation: An Overview. *Chem. Soc. Rev.* **2011**, *40*, 4840–4871. b) van Berkel, S. S.; van Eldijk, M. B.; van Hest, J. C. M. Staudinger Ligation as a Method for Bioconjugation. *Angew. Chem. Int. Ed.* **2011**, *50*, 8806–8827.
- [58] Lin, F. L.; Hoyt, H. M.; van Halbeek, H.; Bergman, R. G.; Bertozzi, C. R. Mechanistic Investigation of the Staudinger Ligation. *J. Am. Chem. Soc.* **2005**, *127*, 2686–2695.
- [59] Saito, F.; Noda, H.; Bode, J. W. Critical Evaluation and Rate Constants of Chemoselective Ligation Reactions for Stoichiometric Conjugations in Water. *ACS Chem. Biol.* **2015**, *10*, 1026–1033.
- [60] Saxon, E.; Armstrong, J. I.; Bertozzi, C. R. A "Traceless" Staudinger Ligation for the Chemoselective Synthesis of Amide Bonds. *Org. Lett.* **2000**, *2*, 2141–2143.
- [61] Nilsson, B. L.; Kiessling, L. L.; Raines, R. T. Staudinger Ligation: A Peptide from a Thioester and Azide. *Org. Lett.* **2000**, *2*, 1939–1941.
- [62] Soellner, M. B.; Nilsson, B. L.; Raines, R. T. Reaction Mechanism and Kinetics of the Traceless Staudinger Ligation. *J. Am. Chem. Soc.* **2006**, *128*, 8820–8828.
- [63] Rostovtsev, V. V.; Green, L. G.; Fokin, V. V.; Sharpless, K. B. A Stepwise Huisgen Cycloaddition Process: Copper(I)-Catalyzed Regioselective "Ligation" of Azides and Terminal Alkynes. *Angew. Chem. Int. Ed.* **2002**, *41*, 2596–2599.

- [64] Tornøe, C. W.; Christensen, C.; Meldal, M. Peptidotriazoles on Solid Phase: [1,2,3]-Triazoles by Regiospecific Copper(I)-Catalyzed 1,3-Dipolar Cycloadditions of Terminal Alkynes to Azides. *J. Org. Chem.* **2002**, *67*, 3057–3064.
- [65] For an excellent review on CuAAC see: Meldal, M.; Tornøe, C. W. Cu-Catalyzed Azide–Alkyne Cycloaddition. *Chem. Rev.* **2008**, *108*, 2952–3015.
- [66] Worrell, B. T.; Malik, J. A.; Fokin, V. V. Direct Evidence of a Dinuclear Copper Intermediate in Cu(I)-Catalyzed Azide–Alkyne Cycloadditions. *Science* **2013**, *340*, 457–460.
- [67] Wolbers, F.; ter Braak, P.; Le Gac, S.; Luttge, R.; Andersson, H.; Vermes, I.; van den Berg, A. Viability Study of HL60 Cells in Contact with Commonly Used Microchip Materials. *Electrophoresis* **2006**, *27*, 5073–5080.
- [68] Hong, V.; Steinmetz, N. F.; Manchester, M.; Finn, M. G. Labeling Live Cells by Copper-Catalyzed Alkyne–Azide Click Chemistry. *Bioconjugate Chem.* **2010**, *21*, 1912–1916.
- [69] Yang, M.; Li, J.; Chen, P. R. Transition Metal-Mediated Bioorthogonal Protein Chemistry in Living Cells. *Chem. Soc. Rev.* **2014**, *43*, 6511–6526.
- [70] Besanceney-Webler, C.; Jiang, H.; Zheng, T.; Feng, L.; Soriano del Amo, D.; Wang, W.; Klivansky, L. M.; Marlow, F. L.; Liu, Y.; Wu, P. Increasing the Efficacy of Bioorthogonal Click Reactions for Bioconjugation: A Comparative Study. *Angew. Chem. Int. Ed.* **2011**, *50*, 8051–8056.
- [71] Soriano Del Amo, D.; Wang, W.; Jiang, H.; Besanceney, C.; Yan, A. C.; Levy, M.; Liu, Y.; Marlow, F. L.; Wu, P. Biocompatible Copper(I) Catalysts for *in Vivo* Imaging of Glycans. *J. Am. Chem. Soc.* **2010**, *132*, 16893–16899.
- [72] Speers, A. E.; Adam, G. C.; Cravatt, B. F. Activity-Based Protein Profiling *In Vivo* Using a Copper(I)-Catalyzed Azide–Alkyne [3 + 2] Cycloaddition. *J. Am. Chem. Soc.* **2003**, *125*, 4686–4687.

- [73] Sieber, S. A.; Cravatt, B. F. Analytical Platforms for Activity-Based Protein Profiling – Exploiting the Versatility of Chemistry for Functional Proteomics. *Chem. Commun.* **2006**, 2311–2319.
- [74] Kennedy, D. C.; McKay, C. S.; Legault, M. C.; Danielson, D. C.; Blake, J. A.; Pegoraro, A. F.; Stolow, A.; Mester, Z.; Pezacki, J. P. Cellular Consequences of Copper Complexes Used to Catalyze Bioorthogonal Click Reactions *J. Am. Chem. Soc.* **2011**, *133*, 17993–18001.
- [75] Agard, N. J.; Prescher, J. A.; Bertozzi, C. R. A Strain-Promoted [3 + 2] Azide-Alkyne Cycloaddition for Covalent Modification of Biomolecules in Living Systems. *J. Am. Chem. Soc.* **2004**, *126*, 15046–15047.
- [76] Sletten, E. M.; Nakamura, H.; Jewett, J. C.; Bertozzi, C. R. Difluorobenzocyclooctyne: Synthesis, Reactivity, and Stabilization by Beta-Cyclodextrin. *J. Am. Chem. Soc.* **2010**, *132*, 11799–11805.
- [77] Gordon, C. G.; Mackey, J. L.; Jewett, J. C.; Sletten, E. M.; Houk, K. N.; Bertozzi, C. R. Reactivity of Biarylazacyclooctynones in Copper-Free Click Chemistry. *J. Am. Chem. Soc.* **2012**, *134*, 9199–1208.
- [78] de Almeida, G.; Sletten, E. M.; Nakamura, H.; Palaniappan, K. K.; Bertozzi, C. R. Thiacycloalkynes for Copper-Free Click Chemistry. *Angew. Chem. Int. Ed.* **2012**, *51*, 2443–2447.
- [79] Codelli, J. A.; Baskin, J. M.; Agard, N. J.; Bertozzi, C. R. Second-Generation Difluorinated Cyclooctynes for Copper-Free Click Chemistry. *J. Am. Chem. Soc.* **2008**, *130*, 11486–11493.
- [80] Baskin, J. M.; Prescher, J. A.; Laughlin, S. T.; Agard, N. J.; Chang, P. V.; Miller, I. A.; Lo, A.; Codelli, J. A.; Bertozzi, C. R. Copper-Free Click Chemistry for Dynamic *in Vivo* Imaging. *Proc. Natl. Acad. Sci. USA.* **2007**, *104*, 16793–16797.

- [81] Laughlin, S. T.; Baskin, J. M.; Amacher, S. L.; Bertozzi, C. R. *In Vivo* Imaging of Membrane-Associated Glycans in Developing Zebrafish. *Science* **2008**, *320*, 664–667.
- [82] Ning, X.; Guo, J.; Wolfert, M. A.; Boons, G.-J. Visualizing Metabolically Labeled Glycoconjugates of Living Cells by Copper-Free and Fast Huisgen Cycloadditions. *Angew. Chem. Int. Ed.* **2008**, *120*, 2285–2287.
- [83] Sletten, E. M.; Bertozzi, C. R. A Hydrophilic Azacyclooctyne for Cu-Free Click Chemistry. *Org. Lett.* **2008**, *10*, 3097–3099.
- [84] Blackman, M. L.; Royzen, M.; Fox, J. M. Tetrazine Ligation: Fast Bioconjugation Based on Inverse-Electron-Demand Diels-Alder Reactivity. *J. Am. Chem. Soc.* **2008**, *130*, 13518–13519.
- [85] Devaraj, N. K.; Weissleder, R.; Hilderbrand, S. A. Tetrazine-Based Cycloadditions: Application to Pretargeted Live Cell Imaging. *Bioconjugate Chem.* **2008**, *19*, 2297–2299.
- [86] Yang, J.; Šečkute, J.; Cole, C. M.; Devaraj, N. K. Live-Cell Imaging of Cyclopropene Tags with Fluorogenic Tetrazine Cycloadditions. *Angew. Chem. Int. Ed.* **2012**, *51*, 7476–7479.
- [87] Alge, D. L.; Azagarsamy, M. A.; Donohue, D. F.; Anseth, K. S. Synthetically Tractable Click Hydrogels for Three-Dimensional Cell Culture Formed Using Tetrazine-Norbornene Chemistry. *Biomacromolecules* **2013**, *14*, 949–953.
- [88] Chen, W.; Wang, D.; Dai, C.; Hamelberg, D.; Wang, B. Clicking 1,2,4,5-Tetrazine and Cyclooctynes with Tunable Reaction Rates. *Chem. Comm.* **2012**, *48*, 1736–1738.

- 
- [89] Kim, Y.; Ho, S. O.; Gassman, N. R.; Korlann, Y.; Landorf, E. V.; Collart, F. R.; Weiss, S. Efficient Site-Specific Labeling of Proteins via Cysteines. *Bioconjugate Chem.* **2008**, *19*, 786–791.
- [90] Nair, D. P.; Podgórski, M.; Chatani, S.; Gong, T.; Xi, W.; Fenoli, C. R.; Bowman, C. N. The Thiol-Michael Addition Click Reaction: A Powerful and Widely Used Tool in Materials Chemistry. *Chem. Mater.* **2014**, *26*, 724–744.
- [91] Schelte, P.; Boeckler, C.; Frisch, B.; and Schuber, F. Differential Reactivity of Maleimide and Bromoacetyl Functions with Thiols: Application to the Preparation of Liposomal Diepitope Constructs. *Bioconjugate Chem.* **2000**, *11*, 118–123.
- [92] Lainson, J. C.; Fuenmayor, M. F.; Johnston, S. A.; Diehnelt, C. W. Conjugation Approach to Produce a *Staphylococcus Aureus* Synbody with Activity in Serum. *Bioconjugate Chem.* **2015**, *26*, 2125–2132.
- [93] Palanki, M. S. S.; Bhat, A.; Lappe, R. W.; Liu, B.; Oates, B.; Rizzo, J.; Stankovic, N.; Bradshaw, C. Development of Novel Linkers to Conjugate Pharmacophores to a Carrier Antibody. *Bioorg. Med. Chem. Lett.* **2012**, *22*, 4249–4253.
- [94] Kalia, D.; Malekar, P. V.; Parthasarathy, M. Exocyclic Olefinic Maleimides: Synthesis and Application for Stable and Thiol-Selective Bioconjugation. *Angew. Chem. Int. Ed.* **2016**, *55*, 1432–1435.
- [95] Toda, N.; Asano, S.; Barbas, C. F. Rapid, Stable, Chemoselective Labeling of Thiols with Julia-Kocienski-Like Reagents: A Serum-Stable Alternative to Maleimide-Based Protein Conjugation. *Angew. Chem. Int. Ed.* **2013**, *52*, 12592–12596.
- [96] Johnson, E. C. B., and Kent, S. B. H. Insights into the Mechanism and Catalysis of the Native Chemical Ligation Reaction. *J. Am. Chem. Soc.* **2006**, *128*, 6640–6646.

- [97] Dawson, P. E.; Muir, T. W.; Clark-Lewis, I.; Kent, S. B. Synthesis of Proteins by Native Chemical Ligation. *Science* **1994**, *266*, 776–779.
- [98] Kochendoerfer, G. G.; Chen, S.-Y.; Mao, F.; Cressman, S.; Traviglia, S.; Shao, H.; Hunter, C. L.; Low, D. W.; Cagle, E. N.; Carnevali, M.; Gueriguian, V.; Keogh, P. J.; Porter, H.; Stratton, S. M.; Wiedeke, M. C.; Wilken, J.; Tang, J.; Levy, J. J.; Miranda, L. P.; Crnogorac, M. M.; Kalbag, S.; Botti, P.; Schindler-Horvat, J.; Savatski, L.; Adamson, J. W.; Kung, A.; Kent, S. B. H.; Bradburne, J. A. Design and Chemical Synthesis of a Homogeneous Polymer-Modified Erythropoiesis Protein. *Science*, **2003**, *299*, 884–887.
- [99] Wang, P.; Dong, S.; Brailsford, J. A.; Iyer, K.; Townsend, S. D.; Zhang, Q.; Hendrickson, R. C.; Shieh, J.H.; Moore, M. A. S.; Danishefsky, S. M. At Last: Erythropoietin as a Single Glycoform. *Science* **2012**, *51*, 11576–11584.
- [100] Torbeev, V. Y.; Kent, S. B. H. Convergent Chemical Synthesis and Crystal Structure of a 203 Amino Acid "Covalent Dimer" HIV-1 Protease Enzyme Molecule. *Angew. Chem. Int. Ed.* **2007**, *46*, 1667.
- [101] Wintermann, F.; Engelbrecht, S. Reconstitution of the Catalytic Core of F-ATPase ( $\alpha\beta$ )<sub>3</sub> $\gamma$  from *Escherichia Coli* Using Chemically Synthesized Subunit  $\gamma$ . *Angew. Chem. Int. Ed.* **2013**, *52*, 1309–1313.
- [102] Dirksen, A.; Meijer, E.; Adriaens, W.; Hackeng, T. M. Strategy for the Synthesis of Multivalent Peptide-Based Nonsymmetric Dendrimers by Native Chemical Ligation. *Chem. Commun.* **2006**, *15*, 1667–1669.
- [103] Paramonov, S. E.; Gauba, V.; Hartgerink, J. D. Synthesis of Collagen-Like Peptide Polymers by Native Chemical Ligation. *Macromolecules* **2005**, *38*, 7555–7561.



- [104] Bode, J. W.; Fox, R. M.; Baucom, K. D.: Chemoselective Amide Ligations by Decarboxylative Condensations of *N*-Alkylhydroxylamines and  $\alpha$ -Ketoacids. *Angew. Chem. Int. Ed.* **2006**, *45*, 1248–1252.
- [105] For an excellent summary of the utility of KAHA ligation and its application in protein synthesis see: Bode, J. W. Chemical Protein Synthesis with the  $\alpha$ -Ketoacid–Hydroxylamine Ligation. *Acc. Chem. Res.* **2017**, *50*, 2104–2115.
- [106] Wu, J.; J. Ruiz-Rodríguez; Comstock, J. M.; Dong, J. Z.; Bode, J. W.: Synthesis of Human GLP-1 (7–36) by Chemoselective  $\alpha$ -Ketoacid–Hydroxylamine Peptide Ligation of Unprotected Fragments. *Chem. Sci.* **2011**, *2*, 1976–1979.
- [107] For selected examples of site-specific protein modifications: a) Carrico, I. S. Chemoselective Modification of Proteins: Hitting the Target. *Chem. Soc. Rev.* **2008**, *37*, 1423–1431. b) Ducry, L.; Stump, B. Antibody-Drug Conjugates: Linking Cytotoxic Payloads to Monoclonal Antibodies. *Bioconjugate Chem.* **2010**, *21*, 5–13. c) Stephanopoulos, N.; Francis, M. B. Choosing an Effective Protein Bioconjugation Strategy. *Nat. Chem. Biol.* **2011**, *7*, 876–884.
- [108] Kim, S.; Ko, W.; Sung, B. H.; Kim, S. C.; Lee, H. S. Direct Protein-Protein Conjugation by Genetically Introducing Bioorthogonal Functional Groups into Proteins. *Bioorg. Med. Chem.* **2016**, *24*, 5816–5822.
- [109] Hutchins, B. M.; Kazane, S. A.; Staflin, K.; Forsyth, J. S.; Felding-Habermann, B.; Smider, V. V.; Schultz, P. G. Selective Formation of Covalent Protein Heterodimers with an Unnatural Amino Acid. *Chem. Biol.* **2011**, *18*, 299–303.
- [110] Hudak, J. E.; Barfield, R. M.; de Hart, G. W.; Grob, P.; Nogales, E.; Bertozzi, C. R.; Rabuka, D. Synthesis of Heterobifunctional Protein Fusions Using Copper-Free Click Chemistry and the Aldehyde Tag. *Angew. Chem. Int. Ed.* **2012**, *51*, 4161–4165.

- [111] Hamblett, K. J.; Senter, P. D.; Chace, D. F.; Sun, M. M. C.; Lenox, J.; Cervený, C. G.; Kissler, K. M.; Bernhardt, S. X.; Kopcha, A. K.; Zabinski, R. F.; Meyer, D. L.; Francisco, J. A. Effects of Drug Loading on the Antitumor Activity of a Monoclonal Antibody Drug Conjugate. *Clin. Cancer Res.* **2004**, *10*, 7063–7070.
- [112] Shen, B.-Q.; Xu, K.; Liu, L.; Raab, H.; Bhakta, S.; Kenrick, M.; Parsons-Reponte, K. L.; Tien, J.; Yu, S.-F.; Mai, E.; Li, D.; Tibbitts, J.; Baudys, J.; Saad, O. M.; Scales, S. J.; McDonald, P. J.; Hass, P. E.; Eigenbrot, C.; Nguyen, T.; Solis, W. A.; Fuji, R. N.; Flagella, K. M.; Patel, D.; Spencer, S. D.; Khawli, L. A.; Ebens, A.; Wong, W. L.; Vandlen, R.; Kaur, S.; Sliwkowski, M. X.; Scheller, R. H.; Polakis, P.; Junutula, J. R. Conjugation Site Modulates the *in Vivo* Stability and Therapeutic Activity of Antibody-Drug Conjugates. *Nat. Biotechnol.* **2012**, *30*, 184–189.
- [113] Pillow, T. H.; Tien, J.; Parsons-Reponte, K. L.; Bhakta, S.; Li, H.; Staben, L. R.; Li, G.; Chuh, J.; Fourie-O'Donohue, A.; Darwish, M.; Yip, V.; Liu, L.; Leipold, D. D.; Su, D.; Wu, E.; Spencer, S. D.; Shen, B.-Q.; Xu, K.; Kozak, K. R.; Raab, H.; Vandlen, R.; Lewis Phillips, G. D.; Scheller, R. H.; Polakis, P.; Sliwkowski, M. X.; Flygare, J. A.; Junutula, J. R. Site-Specific Trastuzumab Maytansinoid Antibody–Drug Conjugates with Improved Therapeutic Activity through Linker and Antibody Engineering. *J. Med. Chem.* **2014**, *57*, 7890–7899.
- [114] Alley, S. C.; Benjamin, D. R.; Jeffrey, S. C.; Okeley, N. M.; Meyer, D. L.; Sanderson, R. J.; Senter, P. D. Contribution of Linker Stability to the Activities of Anticancer Immunoconjugates. *Bioconjugate Chem.* **2008**, *19*, 759–765.
- [115] Dirksen, A.; Dawson, P. E. Rapid Oxime and Hydrazone Ligations with Aromatic Aldehydes for Biomolecular Labeling. *Bioconjugate Chem.* **2008**, *19*, 2543–2548.
- [116] Kalia, J.; Raines, R. T. Advances in Bioconjugation. *Curr. Org. Chem.* **2010**, *14*, 138–147.

- 
- [117] Saito, F.; Noda, H.; Bode, J. W. Critical Evaluation and Rate Constants of Chemoselective Ligation Reactions for Stoichiometric Conjugations in Water. *ACS Chem. Biol.* **2015**, *10*, 1026–1033.
- (118) Dumas, A. M.; Molander, G. A.; Bode, J. W. Amide-Forming Ligation of Acyltrifluoroborates and Hydroxylamines in Water. *Angew. Chem. Int. Ed.* **2012**, *51*, 5683–5686.
- [119] Molander, G. A.; Raushel, J.; Ellis, N. M. Synthesis of an Acyltrifluoroborate and its Fusion with Azides to Form Amides *J. Org. Chem.* **2010**, *75*, 4304–4306.
- [120] Dumas, A. M.; Bode, J. W. Synthesis of Acyltrifluoroborates. *Org. Lett.* **2012**, *14*, 2138–2141.
- [121] Katritzky, A. R.; Lang, H.; Wang, Z.; Zhang, Z.; Song, H. Benzotriazole-Mediated Conversions of Aromatic and Heteroaromatic Aldehydes to Functionalized Ketones. *J. Org. Chem.* **1995**, *60*, 7619–7624.
- [122] Katritzky, A. R.; Lang, H.; Wang, Z.; Lie, Z. Convenient Syntheses of Functionalized Dialkyl Ketones and Alkanoylsilanes: 1-(Benzotriazol-1-yl)-1-phenoxyalkanes as Alkanoyl Anion Equivalents. *J. Org. Chem.* **1996**, *61*, 7551–7557.
- [123] Erős, G.; Kushida, Y.; Bode, J. W. A Reagent for the One-Step Preparation of Potassium Acyltrifluoroborates (KATs) from Aryl- and Heteroarylhalides. *Angew. Chem. Int. Ed.* **2014**, *53*, 7604–7607.
- [124] For a selection of aromatic, heteroaromatic and alkyl KATs that are commercially available by SIGMA ALDRICH see:  
<https://www.sigmaaldrich.com/catalog/search?term=acyltrifluoroborates&interface=All&N=0&mode=match%20partialmax&lang=de&region=CH&focus=product>.

- [125] BODE KAT REAGENT is commercially available by SIGMA ALDRICH under the following CAS No.: 1622923-36-7.
- [126] Liu, S. M.; Mazunin, D.; Pattabiraman, V. R.; Bode, J. W. Synthesis of Bifunctional Potassium Acyltrifluoroborates. *Org. Lett.* **2016**, *18*, 5336–5339.
- [127] Taguchi, J.; Ikeda, T.; Takahashi, R.; Sasaki, I.; Ogasawara, Y.; Dairi, T.; Kato, N.; Yamamoto, Y.; Bode, J. W.; Ito, H. Synthesis of Acylborons by Ozonolysis of Alkenylboronates: Preparation of an Enantioenriched Amino Acid Acylboronate *Angew. Chem. Int. Ed.* **2017**, *56*, 13847–13815.
- [128] Scheme adapted from reference 127.
- [129] Phanstiel, O.; Wang, Q. X.; Powell, D. H.; Ospina, M. P.; Leeson, B. A. Synthesis of Secondary Amines via *N*-(Benzoyloxy)amines and Organoboranes *J. Org. Chem.* **1999**, *64*, 803–806.
- [130] Noda, H.; Erős, G.; Bode, J. W. Rapid Ligations with Equimolar Reactants in Water with the Potassium Acyltrifluoroborate (KAT) Amide Formation, *J. Am. Chem. Soc.* **2014**, *136*, 5611–5614.
- [131] Manandhar, B.; Ahn, J.-M. Glucagon-Like Peptide-1 (GLP-1) Analogs: Recent Advances, New Possibilities, and Therapeutic Implications. *J. Med. Chem.* **2015**, *58*, 1020–1037.
- [132] Montanya, E. A Comparison of Currently Available GLP-1 Receptor Agonists for the Treatment of Type 2 Diabetes. *Expert Opin. Pharmacother.* **2012**, *13*, 1451–1467.
- [133] Drucker, D. J.; Dritselis, A.; Kirkpatrick, P. Liraglutide. *Nat. Rev. Drug. Discov.* **2010**, *9*, 267–268.

- [134] Scheme has been adapted from the doctoral thesis of Hidetoshi Noda, Synthesis, Properties and Reactivities of Acylboronates in Amide Bond Forming Ligation with Hydroxylamines. Diss. ETH No. 22574, **2015**.
- [135] Mazunin, D.; Broguiere, N.; Zenobi-Wong, M.; Bode, J. W. Synthesis of Biocompatible PEG Hydrogels by pH-Sensitive Potassium Acyltrifluoroborate (KAT) Amide Ligations. *ACS Biomater. Sci. Eng.* **2015**, *1*, 456–462.
- [136] Scheme adapted from reference 135.



# ***Chapter 2***

---

***First Generation of Acyltrifluoroborates  
with Enhanced KAT Ligation Kinetics***

---

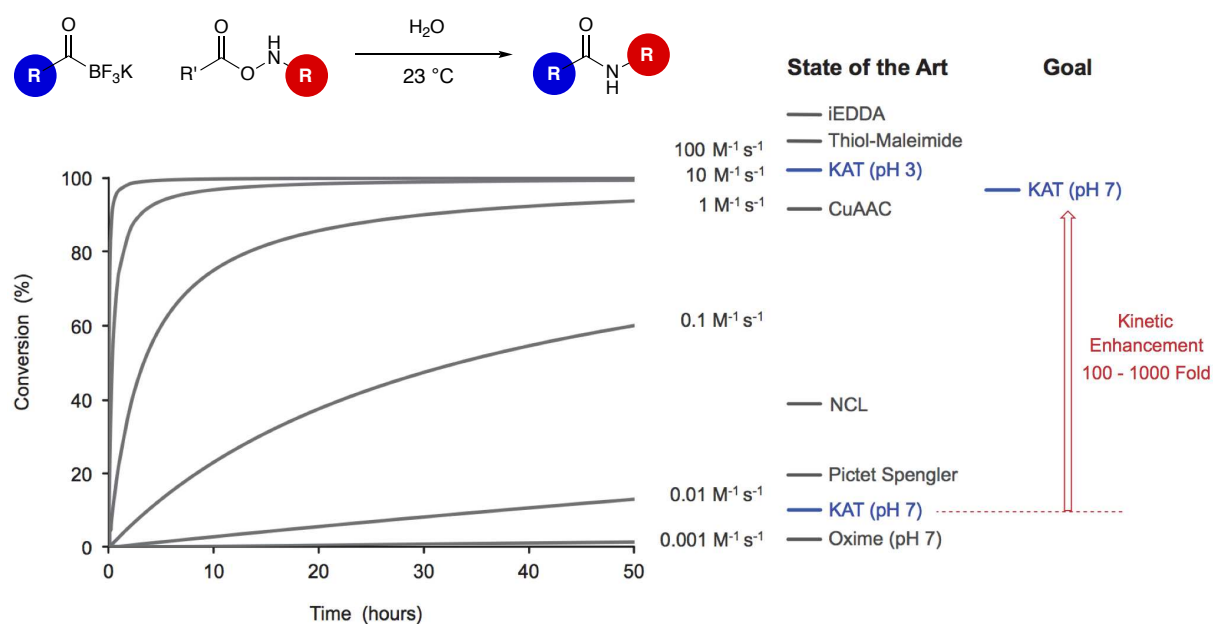




## 2 First Generation of Acyltrifluoroborates with Enhanced KAT Ligation Kinetics

### 2.1 Research Goal and Rationale

Despite the fact that the KAT ligation exhibits fast reaction rates under acidic conditions with rate constants of up to  $20 \text{ M}^{-1} \text{ s}^{-1}$ , its biological applications are hampered by slow ligation kinetics at elevated pH values. Preliminary kinetic studies have shown that the state-of-the-art KAT ligation displays rate constants on the order of  $10^{-3} \text{ M}^{-1} \text{ s}^{-1}$  at pH 7, which is comparable to reaction rates of the oxime and hydrazone ligation (Scheme 2.1). In this thesis, we aim to achieve enhanced KAT ligation kinetics by up to four orders of magnitude reaching reaction rates in the range of  $1 - 10 \text{ M}^{-1} \text{ s}^{-1}$  at neutral pH. The enhanced kinetics would render this ligation an effective bioorthogonal strategy for the covalent ligation of equimolar concentrations of two macromolecules to form stable bioconjugates.



**Scheme 2.1** Schematic representation of the current state-of-the-art KAT ligation rates and the aim of this thesis.

## 2.2 Strategies for the Improvement of KAT Ligation Kinetics

Several possible approaches can be considered to achieve enhanced KAT ligation kinetics at physiological pH:

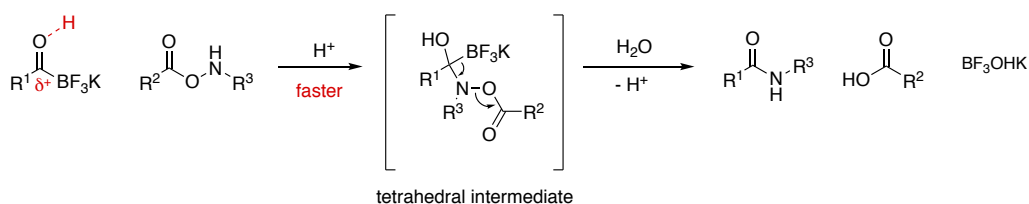
- 1) Fine-tuning of reaction conditions such as solvent, temperature etc.
- 2) Use of additives
- 3) Structural modification of the hydroxylamine
- 4) Structural modification of the KAT species

Optimization or fine-tuning of reaction conditions is limited since the reaction must be compatible with biological conditions. To avoid protein denaturation or degradation, biological reactions, including protein modifications and conjugations, are thus preferentially carried out in water at 23 – 37 °C and pH 6.8 – 7.4.<sup>137,138</sup> Furthermore, the use of additives, such as stoichiometric reagents or catalysts, is unfavorable due to introduction of unnecessary complexity and potential toxicological side effects.<sup>74</sup> In addition, modification of the hydroxylamine has already extensively been studied by BODE and coworkers in recent years resulting in the discovery of *N,N*-diethylcarbamoyl-hydroxylamine (**89**) as a superior ligation partner with the ideal balance between high reactivity and satisfying biostability (*cf.* Chapter 1.3.2). Consequently, we decided to focus our research on structural modifications of the acyltrifluoroborate species and examination of the corresponding underlying kinetic effects.

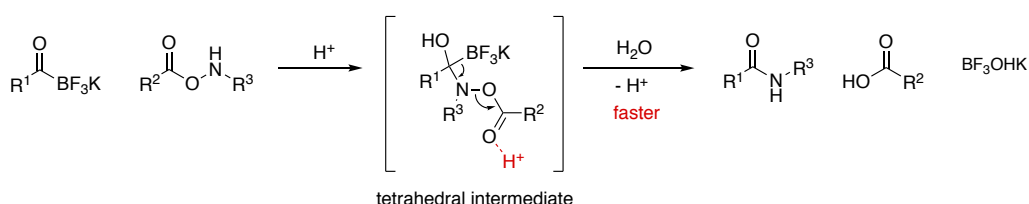
## 2.3 Design of Novel Acyltrifluoroborates

As the reaction rates of the KAT ligation significantly decelerate with increasing pH levels, we reasoned that the presence of acid plays an essential role in the ligation process. In fact, we surmised that the acidic environment might accelerate product formation by two distinct pathways shown in Scheme 2.2. On one hand, protonation of the acyl KAT moiety may lead to activation of the KAT group towards nucleophilic attack by hydroxylamine (Scheme 2.2, a). On the other hand, protonation of the acyl moiety of the hydroxylamine could lead to a facilitated breakdown of the tetrahedral ligation intermediate and thus substantially enhances the kinetic performance (Scheme 2.2, b).

a) Rate acceleration by protonation of the KAT moiety

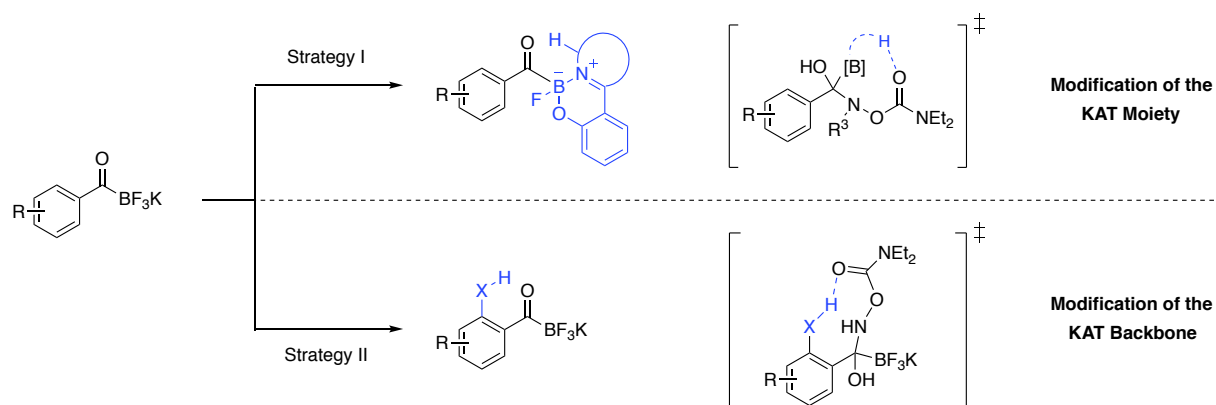


b) Rate acceleration by protonation of the carbonyl group of the hydroxylamine



**Scheme 2.2** Proposed rate acceleration of the KAT ligation in acidic environment.

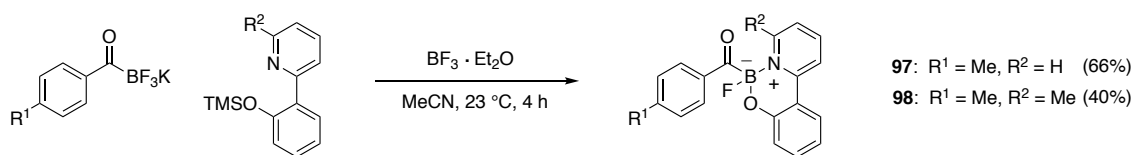
Inspired by this hypothesis, we intended to mimic the proposed rate enhancing function of the acidic environment by intramolecular proton transfer (Scheme 2.3). Hence, we envisioned the development of a novel generation of KATs with an incorporated proton donor moiety. This proton donor ought to be in close proximity to the carbonyl of the acylboronate, facilitating the formation of an intramolecular proton donor/acceptor pair, which might ultimately result in enhanced reaction rates. In Scheme 2.3 two possible synthetic strategies are shown that have been considered for the installation of such a proton donating group. The first strategy involves the modification of the KAT moiety by introduction of specially designed boronate ligands, whereas the second strategy suggests incorporation of the proton donor into the aryl backbone.



**Scheme 2.3** Synthetic strategies for preparation of KATs with incorporated proton donors including a proposed transition state of the tetrahedral intermediate. Strategy I: Modification of the KAT moiety with suitable boronate ligands. Strategy II: Alteration of the aryl backbone.

### 2.3.1 Strategy I – Modification of the KAT Moiety

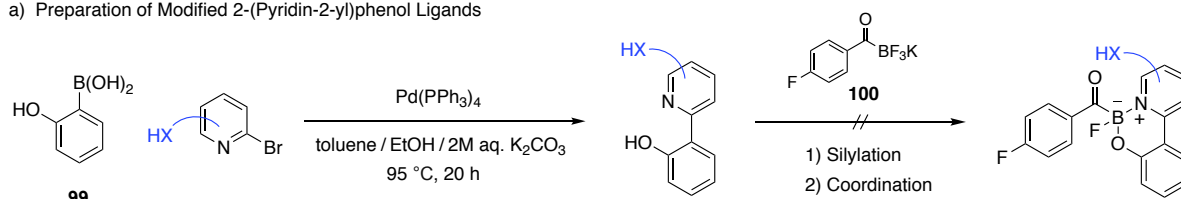
In 2015, BODE and NODA reported the synthesis of a variety of monofluoro acylboronates by treatment of KATs with different *in-situ* TMS-protected bidentate ligands in presence of boron trifluoro diethyl etherate. One class of bidentate ligands that have emerged as suitable candidates for the formation of stable monofluoro acylboronate complexes, such as **97** and **98**, are 2-(pyridin-2-yl)phenol ligands (Scheme 2.4, a).<sup>139,140</sup>



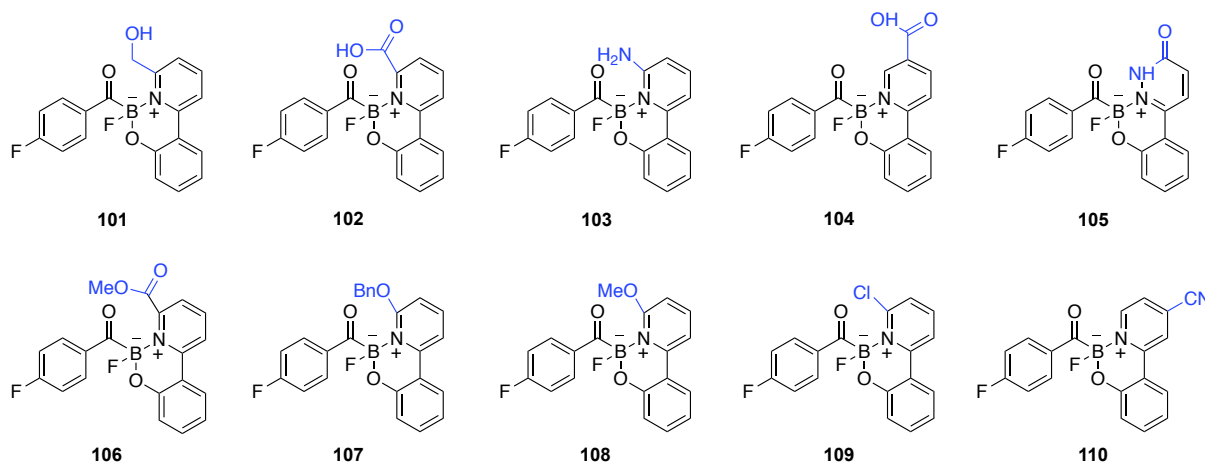
**Scheme 2.4** Synthesis of monofluoro acylboronates from bidentate 2-(pyridin-2-yl)phenol ligands reported by BODE and NODA in 2015.<sup>139</sup>

Based on these findings, we attempted the synthesis of a series of monofluoro acylboronates using 2-(pyridin-2-yl)phenol ligands with incorporated proton-donating moieties, such as alcohols, carboxylic acids or amines, which are in close proximity to the acyl group. In a first step, the modified 2-(pyridin-2-yl)phenol ligands were prepared via direct Suzuki cross-coupling between 2-hydroxyphenylboronic acid (**99**) and the appropriate 2-bromopyridines according to a modified procedure of IGLESIAS and SÁNCHEZ (Scheme 2.5, a).<sup>141</sup> In a second step, we tested whether our newly designed ligands with the incorporated proton donors form stable monofluoro acylboronate complexes with KAT **100** employing the standard coordination conditions developed by BODE and NODA. To our disappointment, the preparation of acylboronates **102–104** proved to be unsuccessful due to lack of coordination (Scheme 2.5, b). In a similar fashion, formation of acylboronate **105** using an analogous pyridazine ligand was met with failure. Consequently, we concluded that the presence of unprotected functional groups might be a potential reason for disrupted ligand coordination. As a result, we examined the coordination of ligands with masked protic groups, such as methyl esters and benzyl ethers. Even though traces of the desired acylboronates **106–108** were detected by mass spectrometry, isolation from the complex reaction mixtures

## a) Preparation of Modified 2-(Pyridin-2-yl)phenol Ligands



## b) Attempted Synthesis of Acylboronates with Incorporated Proton Donors



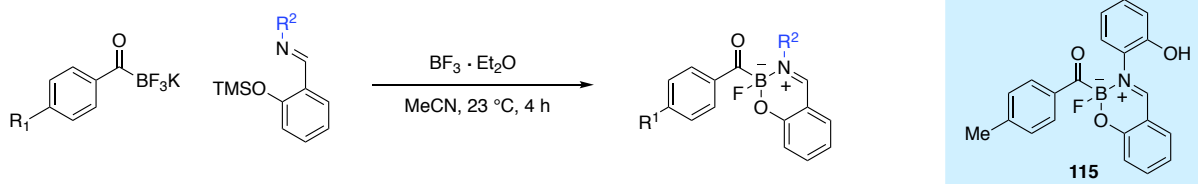
**Scheme 2.5** a) Preparation of 2-(pyridin-2-yl)phenol ligands with incorporated proton donors according to a modified procedure of IGLESIAS and SÁNCHEZ. b) Attempted acylboronate syntheses using 2-(pyridin-2-yl)phenol ligands with incorporated proton donor moieties.

was not achieved. We presumed that not only unprotected functional groups but also the increased steric demand of the ligands prevents successful complexation. To our surprise, further efforts toward the formation of chloro and cyano derivatives **109** and **110** were also ineffective, indicating that besides functional group tolerance and steric hindrance, electronic factors may also play a crucial role in ligand coordination.

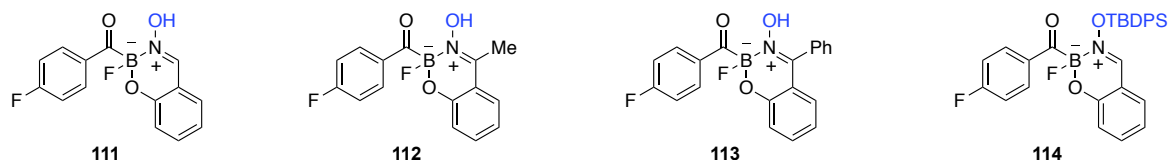
Given the fact that even small alterations in the design of 2-(pyridin-2-yl)phenol ligands were found to have a strongly limiting influence on acylboronate complex formation we decided to redirect our attention to the modification of alternative ligands. In the report by BODE and NODA, Schiff bases have also been described to form stable acylboronate complexes, as illustrated in Scheme 2.6, a.<sup>139</sup> To test our initial hypothesis that proton donors in close proximity to the acyl group may lead to enhanced ligation kinetics, we decorated different Schiff base ligands with protic *N*-hydroxyl substituents. Similar to what has been observed for the modified 2-(pyridin-2-yl)phenol ligands, Schiff bases with incorporated proton donating hydroxyl groups did not lead to the formation of stable acylboronate complexes **111**–**113**. Noteworthy, *tert*-butyl diphenyl silyl (TBDPS) protected ligand Schiff base failed to form the desired acylboronate complex **114**. Ultimately, phenol KAT **115** could

be isolated in 49 % yield according to the procedure reported by BODE and NODA. Disappointingly however, no improvement in ligation kinetics for **115** was observed when compared to standard aryl KATs. As a consequence of various difficulties in ligand coordination and unaltered kinetics of stable acylboronates we decided to abandon our initial strategy and continue with the modification of the aryl backbone.

a) Synthesis of Monofluoro Acylboronates Using Schiff Base Ligands



b) Attempted Synthesis of Acylboronates with Incorporated Proton Donors



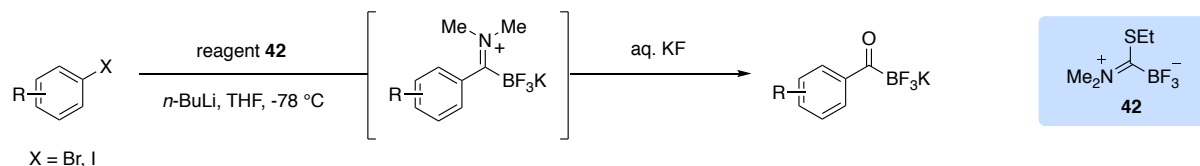
**Scheme 2.6** a) Synthesis of monofluoro acylboronates from bidentate Schiff base ligands reported by BODE and NODA in 2015. b) Attempted acylboronate synthesis using Schiff base ligands with incorporated proton donor moieties.

### 2.3.2 Strategy II – Modification of the KAT Backbone

Our second synthetic strategy that aimed at improved KAT ligation kinetics focused on the incorporation of proton donating groups into the KAT backbone. As aryl KATs were the most commonly employed acyltrifluoroborates at the outset of this thesis with respect to their robustness and ease of accessibility, they served as an ideal starting point for systematic structural modification. To mimic the rate enhancing function of the acidic environment, the proton donating groups should ideally be in close spatial proximity to the acyl group of the KAT. For this reason, we intended to install the proton donors at the *ortho*-position of the KAT moiety. Due to increased steric hindrance, the synthesis of KATs with *ortho*-substituents has proven to be difficult in the past. Besides a multitude of *para* and *meta*-substituted aryl KATs only a single *ortho*-substituted derivative, 2-toluyll KAT has been reported to the present day, with significantly reduced yields (Table 2.1, Entry 4).<sup>123</sup> To our disappointment, all attempts towards the installation of protected protic functionalities, such as ethyl ester (Table 2.1, Entry 5) or a benzyl ether (Table 2.1, Entry 6), at the *ortho*-position of the KAT moiety were

met with failure, due to difficulties in the final hydrolysis step. Other hydrolysis methods, such as the use of aq.  $\text{KHF}_2$  or aq. HF proved to be equally unsuccessful.

**Table 2.1** Synthetic comparison of KATs with *ortho*, *meta* and *para*-substitution.



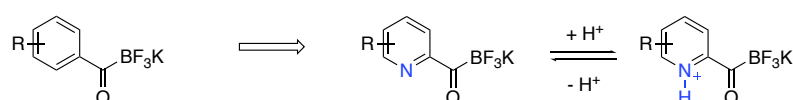
Entry	Substituent R	Yield (%) <sup>[a]</sup>
1	H	69
2	4-COOEt	74
3	3-COOEt	79
4	2-Me	12
5	2-COOEt	NP
6	2-OBn	NP

[a] Yields of isolated reaction products. NP = no product formation.

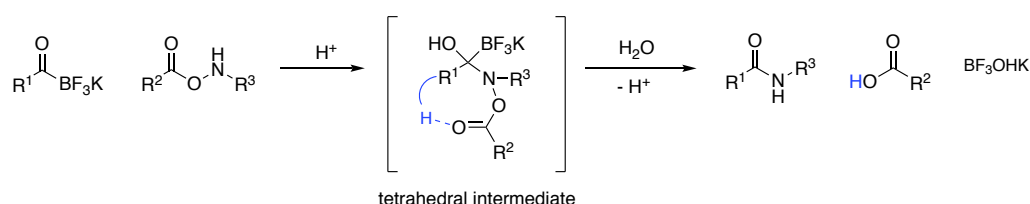
## 2.4 Pyridyl Acyltrifluoroborates

As the installation of proton donors into the aryl KAT backbone proved to be unfruitful, we subsequently decided to explore the incorporation of a Lewis-basic atom into the aryl moiety. We surmised that such a Lewis-basic functionality could be protonated *in-situ* under mildly acidic conditions and ultimately act as an intramolecular proton donor during the KAT ligation. Incorporation of a basic nitrogen atom into the aryl backbone led us to the pyridine scaffold (Scheme 2.7).

a) Incorporation of a Lewis-Basic Atom into the KAT Backbone



b) Attempted Kinetic Improvement via Intramolecular Proton Source

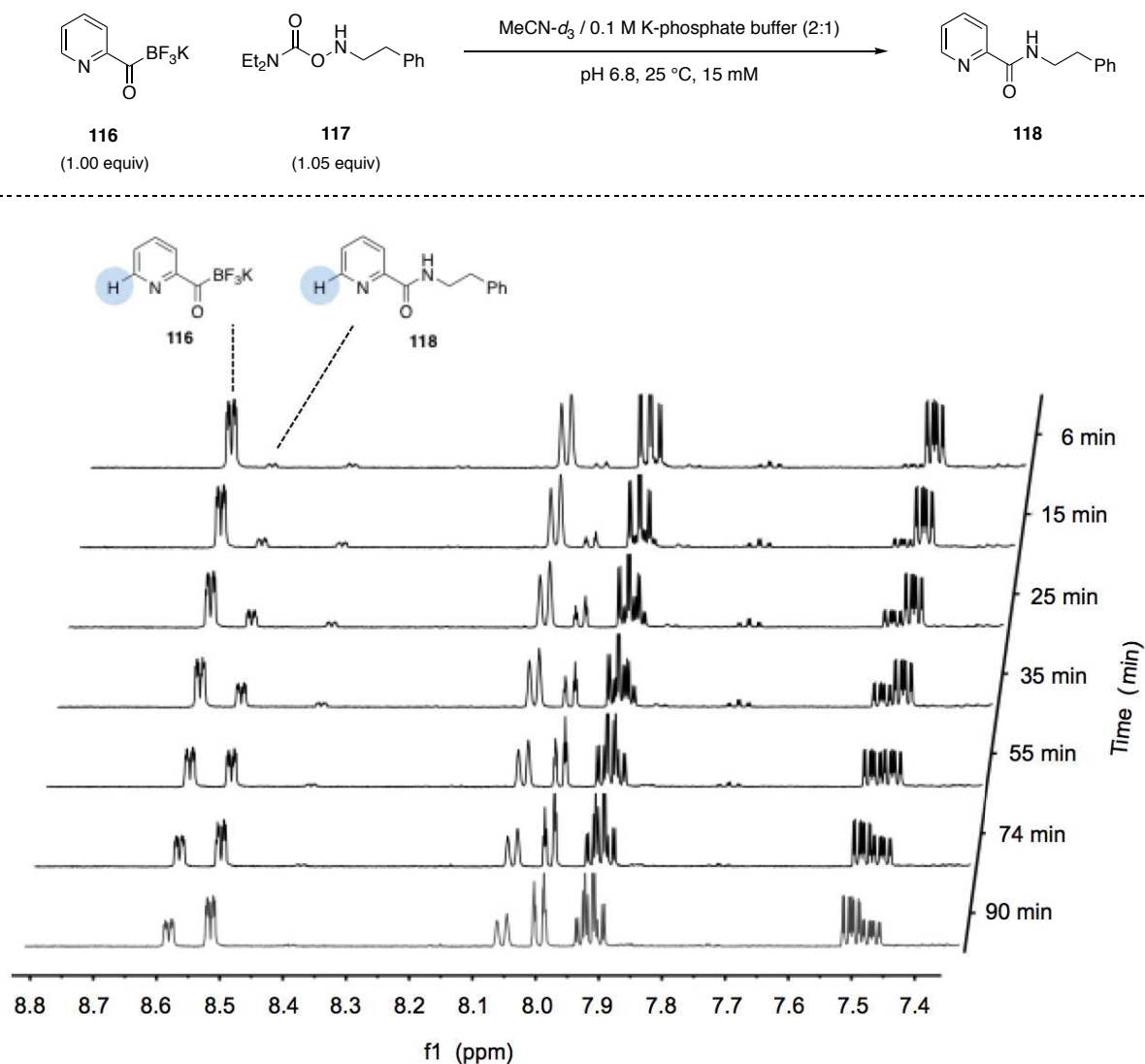


**Scheme 2.7** a) Incorporation of a Lewis-basic nitrogen atom into the aryl KAT backbone. b) Mechanistic hypothesis of the KAT ligation with an incorporated proton donor.

### 2.4.1 Initial Kinetic Investigations

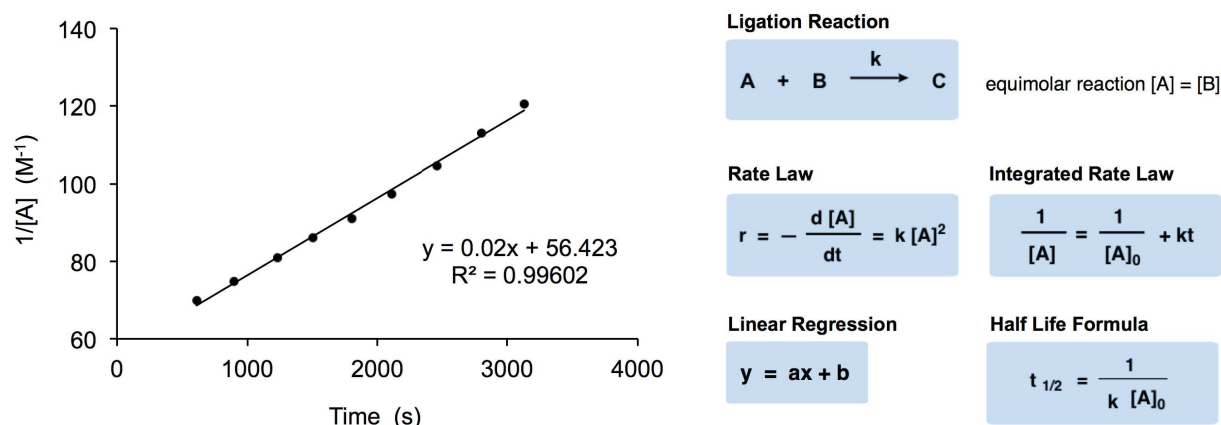
2-pyridyl KAT (**116**) was selected as a suitable candidate for initial kinetic studies. **116** was synthesized according to a previously established procedure by our group<sup>123</sup> and its kinetic performance was evaluated in the ligation reaction with *N,N*-diethylcarbamoylhydroxylamine **117**. As depicted in Scheme 2.8, kinetic measurements were carried out at room temperature with equimolar concentrations of the two reactants **116** and **117** (15 mM) in a solvent mixture of 2:1 MeCN-*d*<sub>3</sub> / 0.1 M deuterated aqueous potassium phosphate buffer at pH 6.8. Importantly, buffered solvent conditions were employed to compensate for possible pH changes during the ligation reaction, while MeCN-*d*<sub>3</sub> served as an organic cosolvent to promote the solubility of the small-molecule reactants. The reaction progress was monitored by non-invasive, real-time <sup>1</sup>H-NMR spectroscopy. Over time, consumption of starting material **116** and formation of product **118** and was observed. Due to its well separated resonances the proton signal at the 6-position of the pyridine ring (highlighted in blue) was chosen for integration.





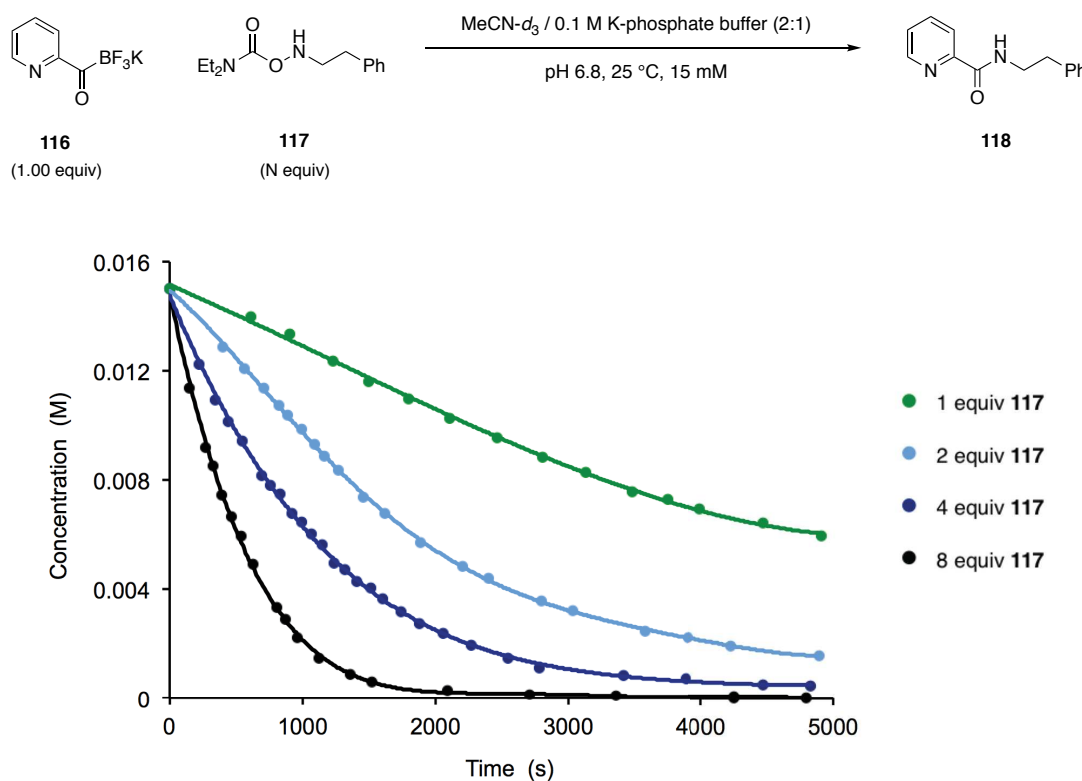
**Scheme 2.8** Kinetics of the KAT ligation between **116** and **117** were monitored by real-time  $^1\text{H-NMR}$  spectroscopy.

Reaction rates ( $k_{\text{obs}}$ ) were analyzed according to standard second-order kinetics plotting the reciprocal concentration of starting material **116**  $1/[\text{A}]$  in  $\text{M}^{-1}$  against the time in seconds (Scheme 2.9). By applying a linear fit, the reaction rate of the KAT ligation between **116** and **117** was determined as the slope  $a$  of the function and surprisingly found to be  $0.02 \text{ M}^{-1}\text{s}^{-1}$ . All kinetic measurements were performed at least three times to ensure the accuracy of each experiment. The rate constant of the reaction was determined as the average of the three measurements. To further verify the experimentally obtained rate constants the half-life formula of a second-order reaction was used. The half-life of the ligation reaction between **116** and **117** was measured to be  $t_{1/2} = 58 \text{ min}$  (3480 s). With the initial concentration of reactant **116** in hand ( $A_0 = 0.015 \text{ M}$ ), a rate constant of  $0.019 \text{ M}^{-1} \text{ s}^{-1}$  was calculated. This result is in excellent agreement with the previously obtained value of  $0.020 \text{ M}^{-1} \text{ s}^{-1}$ .



**Scheme 2.9** Second-order kinetic analysis of the KAT ligation between KAT **116** and hydroxylamine **117**.

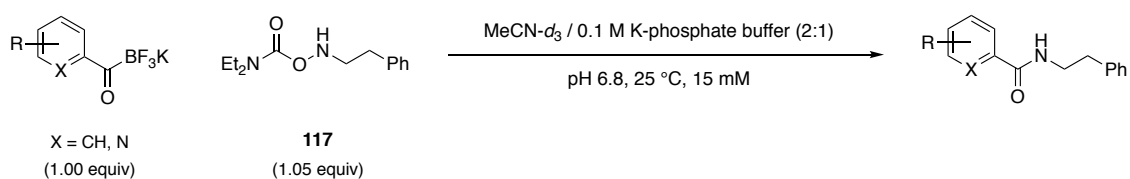
In a next step, we examined the reaction order of the KAT ligation between **116** and **117** to prove the validity of our kinetic method. A series of kinetic experiments starting from different initial concentrations of KAT **116** and hydroxylamine **117** was performed according to our previously established kinetic method (Scheme 2.10). As expected, the rate law of the KAT ligation was shown to be dependent on the concentration of both reactants. Overall, we confirmed that the KAT ligation displays second-order kinetics, first order in KAT **116** and first order in hydroxylamine **117**.



**Scheme 2.10** Reaction kinetics of the KAT Ligation with varying initial concentrations of hydroxylamine **117**.

To compare the kinetic performance of our newly designed 2-pyridyl KAT **116** with traditional aryl KATs, substrates **119–121** were selected for kinetic studies (Table 2.2). To our delight, 2-pyridyl KAT (**116**) ( $k_{\text{obs}} = 0.02 \text{ M}^{-1} \text{ s}^{-1}$ ) displayed enhanced reaction rates by up to 7 fold compared to aryl KATs **119–121** at pH 6.8. We further anticipated that electron deficient aryl KATs undergo faster ligation reactions compared to their electron-rich counterparts due to the increased electrophilicity of the acyltrifluoroborate carbonyl carbon making them more susceptible to nucleophilic attack by hydroxylamines. Although it has long been known that electron-withdrawing substituents can increase the reactivity of carbonyl substrates in ligation reactions, such as in the hydrazone formation,<sup>142</sup> it has later been found that this effect with a Hammett  $\rho$  value of 0.91 for the hydrazone formation at pH 1.75 is rather small.<sup>143</sup> Indeed, it was observed that electron-withdrawing aryl KAT **120** ligates slightly faster (20 % conversion after 74 min) than electron-rich derivative **119** (20 % conversion after 85 min). However, since the ligation kinetics of aryl KATs **119** and **120**

**Table 2.2** Kinetic comparison of 2-pyridyl KAT with traditional aryl KATs.



Entry	Substrate	Structure	$k_{\text{obs}} (\text{M}^{-1} \text{s}^{-1})$ <sup>[a]</sup>	$k_{\text{rel}}$ <sup>[b]</sup>
1	<b>119</b>		0.003	1.0
2	<b>120</b>		0.003	1.0
3	<b>121</b>		0.005	1.7
4	<b>116</b>		0.02	6.7

[a] Kinetic measurements were performed at equimolar concentrations (15 mM) of KAT and hydroxylamine **117** in MeCN- $d_3$  / 0.1 M deuterated potassium phosphate buffer (2:1, pH 6.8) at 25 °C. Kinetics were monitored by <sup>1</sup>H-NMR spectroscopy. The observed second-order rate constants  $k_{\text{obs}}$  were determined as the average of three measurements. [b]  $k_{\text{rel}}$  represents the relative rate constants with respect to 4-methoxyphenyl KAT **119** ( $k_{\text{obs}} = 0.003 \text{ M}^{-1} \text{ s}^{-1}$ ).

were extremely slow, the effect was not reflected in the rate constants, which in both cases were determined to be  $0.003 \text{ M}^{-1} \text{ s}^{-1}$ . In addition, 4-fluorophenyl KAT **121** was selected for kinetic studies since it is a convenient substrate for nucleophilic aromatic substitution ( $S_NAr$ ) and has previously been used as a platform for the functionalization of aryl KATs (i.e. PEGylation, installation of dyes or biotin etc.).<sup>130</sup> Even though **121** shows slightly enhanced kinetics compared to **119** and **120**, it still ligates four times slower than the superior pyridyl KAT **116**.

Besides traditional aryl KATs, 2-pyridyl KAT (**116**) was also shown to ligate faster than a selection of alkyl KATs **122**–**124** shown in Table 2.3. While sterically demanding secondary alkyl KAT **124** displayed even slower ligation kinetics than aryl KAT **119**, primary alkyl KATs **122** and **123** were found to be slightly faster with rate constants of 0.014 and 0.010, respectively.

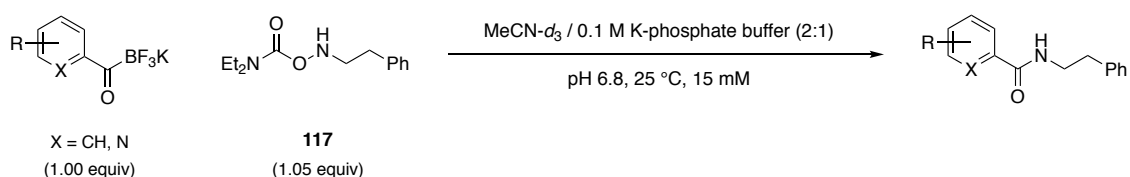
**Table 2.3** Kinetic comparison of 2-pyridyl KAT with different alkyl KATs

Entry	Substrate	Structure	$k_{\text{obs}} (\text{M}^{-1} \text{ s}^{-1})^{[a]}$	$k_{\text{rel}}^{[b]}$
1	<b>119</b>		0.003	1.0
2	<b>122</b>		0.014	4.7
3	<b>123</b>		0.010	3.3
4	<b>124</b>		0.0004	1.3
5	<b>116</b>		0.02	6.7

[a] Kinetic measurements were performed at equimolar concentrations (15 mM) of KAT and hydroxylamine **117** in  $\text{MeCN-d}_3$  / 0.1 M deuterated potassium phosphate buffer (2:1, pH 6.8) at 25 °C. Kinetics were monitored by  $^1\text{H-NMR}$  spectroscopy. The observed second-order rate constants  $k_{\text{obs}}$  were determined as the average of three measurements. [b]  $k_{\text{rel}}$  represents the relative rate constants with respect to 4-methoxyphenyl KAT **119** ( $k_{\text{obs}} = 0.003 \text{ M}^{-1} \text{ s}^{-1}$ ).

In an additional experiment, we examined the relative reactivity of different pyridyl KAT regioisomers in order to verify our hypothesis that the formation of an intramolecular proton acceptor/donor pair leads to the observed rate acceleration. The rate constants of the different pyridyl regioisomers **116**, **125** and **126** are shown in Table 2.4. Indeed, 2-pyridyl KAT **116** exhibits significantly improved ligation rates compared to regioisomers **125** and **126**, further substantiating our mechanistic rationale.

**Table 2.4** Kinetic comparison of 2-pyridyl KAT with pyridyl KAT regioisomers.



Entry	Substrate	Structure	$k_{\text{obs}}$ ( $\text{M}^{-1} \text{s}^{-1}$ ) <sup>[a]</sup>	$k_{\text{rel}}$ <sup>[b]</sup>
1	<b>119</b>		0.003	1.0
2	<b>116</b>		0.02	6.7
3	<b>125</b>		0.007	2.3
4	<b>126</b>		0.001	0.3

[a] Kinetic measurements were performed at equimolar concentrations (15 mM) of KAT and hydroxylamine **117** in MeCN- $d_3$  / 0.1 M deuterated potassium phosphate buffer (2:1, pH 6.8) at 25 °C. Kinetics were monitored by  $^1\text{H-NMR}$  spectroscopy. The observed second-order rate constants  $k_{\text{obs}}$  were determined as the average of three measurements. [b]  $k_{\text{rel}}$  represents the relative rate constants with respect to 4-methoxyphenyl KAT **119**.

As exemplified in Figure 2.1, it was shown that the farther away the KAT moiety was located from the pyridyl nitrogen the slower the ligation kinetics observed (**116** > **125** > **126**). If the KAT group is placed in the 4-position to the pyridyl nitrogen as in **126**, no rate enhancing effect could be observed. In fact, pyridyl KAT **126** displayed reaction rates that are slower than the ones of aryl KAT **119** or **120**. These experimental observations are consistent with our theory that the formation of a proton acceptor/donor pair is facilitated if the pyridyl nitrogen is in close proximity to the KAT functionality and impeded, if not

completely prevented, when the pyridyl nitrogen is at greater spatial distance. As a result, we demonstrated that the nitrogen in 2-position to the KAT moiety of **116** displays a key structural feature responsible for the kinetic enhancement of the KAT ligation and is not simply an artifact of the pyridyl KATs in general.

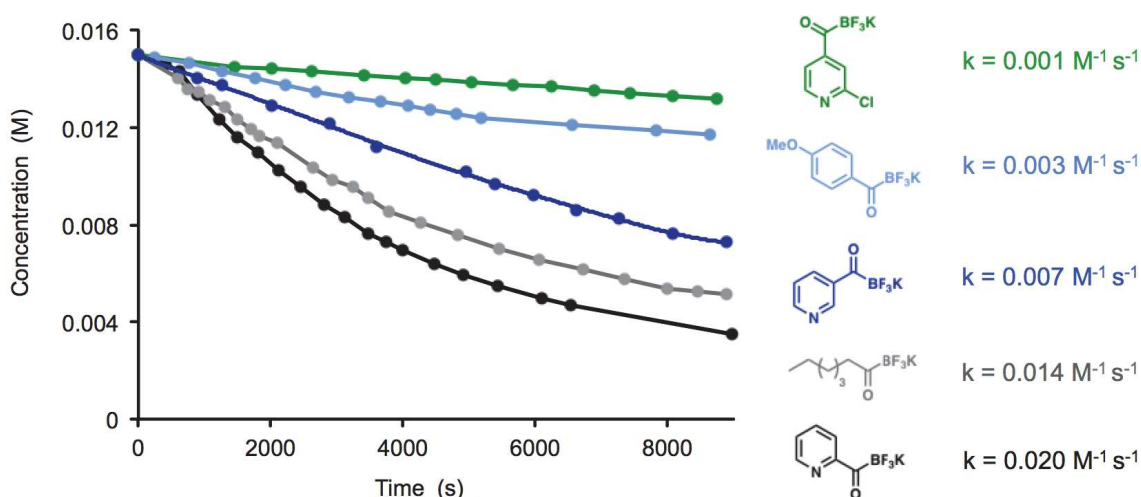
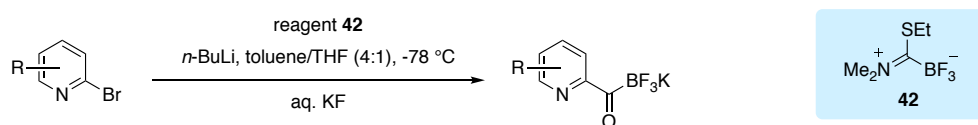


**Figure 2.1** Kinetic comparison of 2-pyridyl KAT with aryl KATs, alkyl KATs and pyridyl KAT regioisomers.

## 2.4.2 Substitution Effects

Encouraged by these remarkable results, we further investigated the influence of different substituents on 2-pyridyl KAT (**116**). For this purpose, a selection of 2-pyridyl KAT derivatives **127–136** were synthesized according to an improved procedure of the BODE group shown in Scheme 2.11.<sup>123</sup>

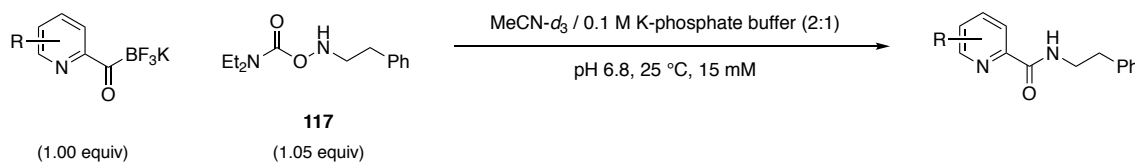


**Scheme 2.11** Improved synthetic procedure for the preparation of 2-pyridyl KATs.

Initially, we set out to evaluate a series of 2-pyridyl KAT derivatives **127–130** with different substituents in the 4-position (Table 2.5). The fluoro-derivative **130** with a rate constant of  $0.009 \text{ M}^{-1} \text{ s}^{-1}$  was found to be the slowest 2-methylphenyl KAT in this series, closely followed by the chloro-derivate **129** with a rate constant of  $0.011 \text{ M}^{-1} \text{ s}^{-1}$ . The measured rates for **129** and **130** might indicate that for 2-pyridyl KATs inductive effects are stronger than resonance effects. Even though **130** and **129** displayed reaction kinetics that

are slightly slower than unsubstituted 2-pyridyl KAT (**116**), they still ligate 3-4 times faster than aryl KAT **119**. By changing from electron-withdrawing substituents to an electron-donating methyl group, as shown for KAT **128**, a three-fold rate acceleration compared to the slowest 2-pyridyl KAT **130** of the series was achieved. Installation of an even more electron-donating group led us to 4-methoxy derivative **127**. Remarkably, **127** displayed the fastest ligation kinetics of all pyridyl KATs measured in this series with a rate constant of  $0.044 \text{ M}^{-1} \text{ s}^{-1}$ , which is twice as fast as unsubstituted 2-pyridyl KAT (**116**) and 15 times faster than standard aryl KAT **119**. Overall, this series of experiments shows that substituents in the 4-position

**Table 2.5** Effects of substituents in the 4-position of 2-pyridyl KAT.



Entry	Substrate	Structure	$k_{\text{obs}} (\text{M}^{-1} \text{s}^{-1})$ <sup>[a]</sup>	$k_{\text{rel}}$ <sup>[b]</sup>
1	<b>119</b>		0.003	1.0
2	<b>127</b>		0.044	15.0
3	<b>128</b>		0.030	10.0
4	<b>116</b>		0.02	6.7
5	<b>129</b>		0.011	3.7
6	<b>130</b>		0.009	3.0

<sup>[a]</sup> Kinetic measurements were performed at equimolar concentrations (15 mM) of KAT and hydroxylamine **117** in  $\text{MeCN-d}_3 / 0.1 \text{ M}$  deuterated potassium phosphate buffer (2:1, pH 6.8) at 25 °C. Kinetics were monitored by  $^1\text{H-NMR}$  spectroscopy. The observed second-order rate constants  $k_{\text{obs}}$  were determined as the average of three measurements. <sup>[b]</sup>  $k_{\text{rel}}$  represents the relative rate constants with respect to 4-methoxyphenyl KAT **119** ( $k_{\text{obs}} = 0.003 \text{ M}^{-1} \text{ s}^{-1}$ ).

of 2-pyridyl KAT (**116**) significantly affects the reaction rates. As illustrated in Figure 2.2, we report that in comparison to unsubstituted KAT **116** electron-donating substituents in the 4-position of 2-pyridyl KATs enhance the reaction rates, whereas electron-withdrawing substituents decelerate the reaction rates. Notably, it was observed that the more electron-donating the substituents in the 4-position of the 2-pyridyl KAT the faster the ligation kinetics and the more electron-withdrawing the substituents the slower the reactions kinetics (**127** > **128** > **116** > **129** > **130**). This general trend is in good compliance with our proposed hypothesis. By installing electron-donating substituents in the 4-position of **116** the basicity of the pyridyl nitrogen is increased. As a result, protonation and subsequent formation of a proton donor/acceptor pair is facilitated. This ultimately leads to enhanced reaction rates compared to unsubstituted pyridyl KAT **116**.

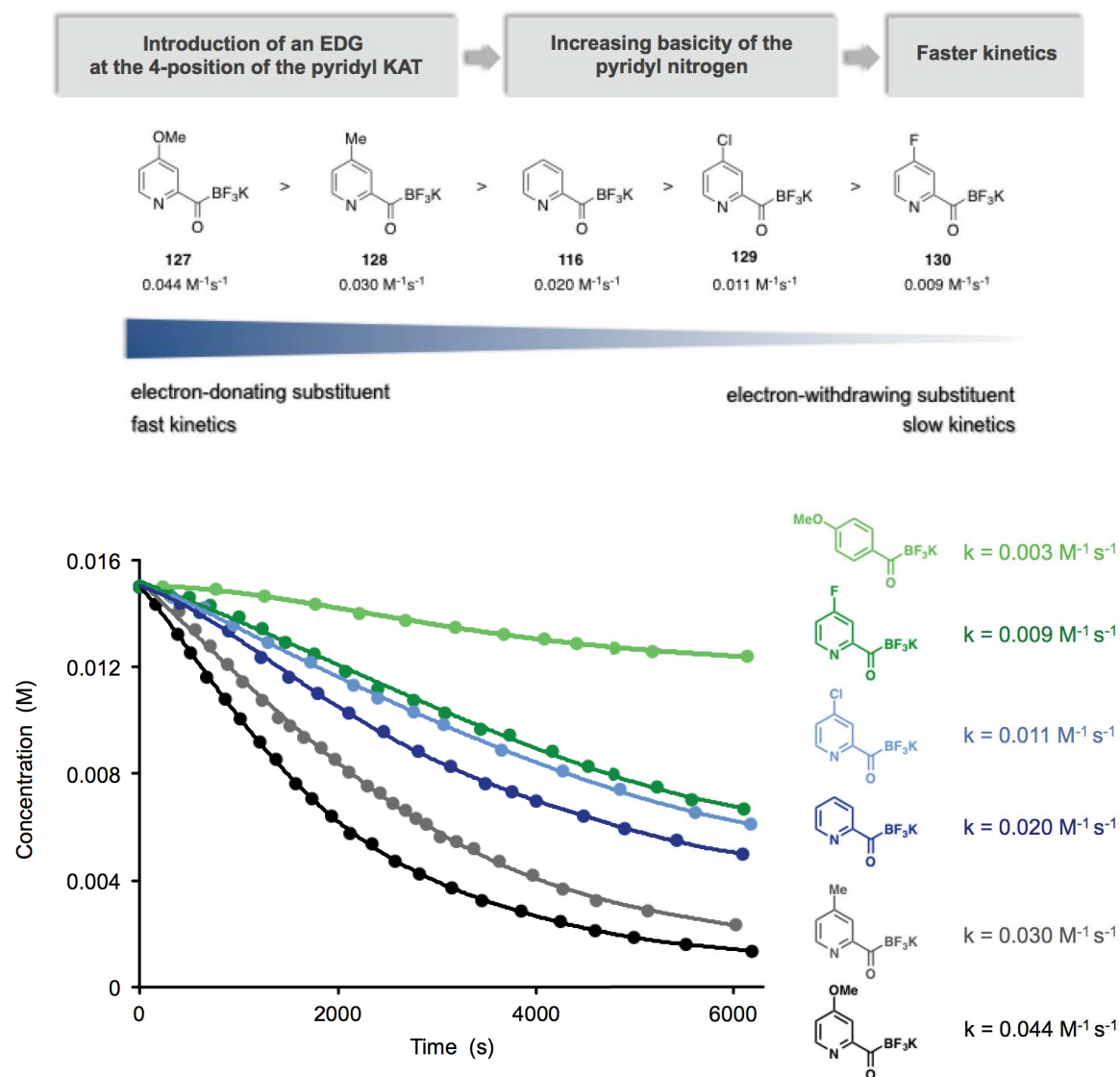


**Figure 2.2** Effects of substituents in the 4-position of 2-pyridyl KAT.



In order to quantify the observed substitution effects and give a correlation between the influence of substituents at the 4-position of 2-pyridyl KAT (**116**) and the corresponding reaction rates a Hammett plot<sup>144</sup> was generated (Figure 2.3). Interestingly, a concave, non-linear correlation was obtained, which indicates a change in reaction mechanism when going from electron-donating to electron-withdrawing substituents. Since the slope of the curve is increasing with decreasing  $\sigma$ -values, the data suggests that with electron-donating substituents a new reaction pathway is favored that is faster than the original reaction mechanism. In addition, the negative  $\rho$ -value indicates a positive charge building up during the reaction process. This finding correlates with our proposed hypothesis that upon protonation of the 2-pyridyl KAT species the pyridyl nitrogen can act as a proton acceptor/donor pair during the reaction process, thereby facilitating the breakdown of the tetrahedral ligation intermediate. If electron-donating substituents are incorporated in the 4-position of the 2-pyridyl KAT, the basicity of the pyridyl nitrogen is increased and consequently more protonated species is available. As a result, a larger number of molecules have the chance to undergo a facilitated elimination mechanism, which ultimately leads to enhanced ligation kinetics compared to 2-pyridyl KATs with electron-withdrawing substituents in the 4-position.

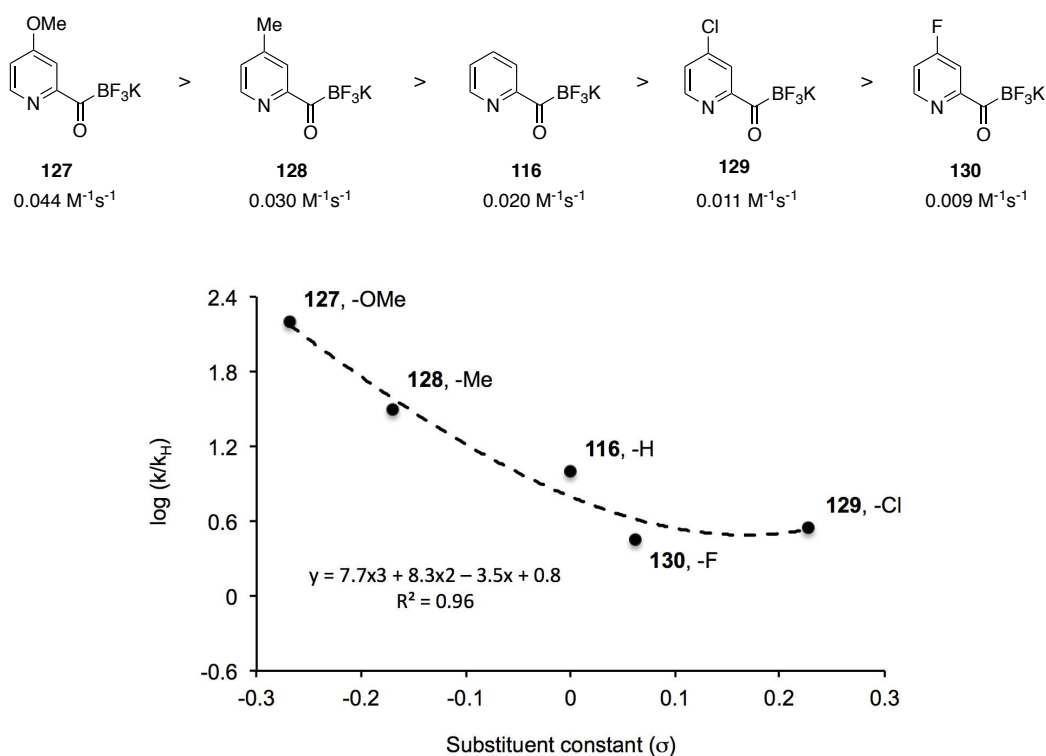
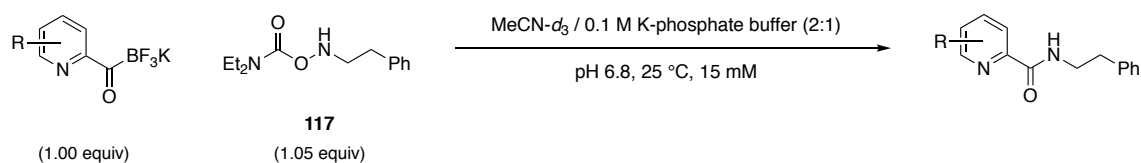


**Figure 2.3** Hammett plot for the KAT ligation of 2-pyridyl KAT derivatives. The dashed trend line shows a non-linear correlation with a  $R^2$  value of 0.96.

In a subsequent investigation, the ligation performance of 2-pyridyl KAT derivatives **131–136** with different substituents in the 5- and 6-position was studied. The results are illustrated in Table 2.6.

**Table 2.6** Comparison of substituents effects in the 5- and 6-position of 2-pyridyl KAT.



Entry	Substrate	Structure	$k_{\text{obs}}$ ( $\text{M}^{-1} \text{s}^{-1}$ ) <sup>[a]</sup>	$k_{\text{rel}}$ <sup>[b]</sup>
1	<b>127</b>		0.044	15.0
2	<b>131</b>		0.039	13.3
3	<b>132</b>		0.022	7.3
4	<b>129</b>		0.011	3.7
5	<b>133</b>		0.014	4.7
6	<b>134</b>		0.009	3.0
7	<b>130</b>		0.009	3.0
8	<b>135</b>		0.014	4.7
9	<b>136</b>		0.007	2.3

[a] Kinetic measurements were performed at equimolar concentrations (15 mM) of KAT and hydroxylamine **117** in  $\text{MeCN-}d_3 / 0.1 \text{ M}$  deuterated potassium phosphate buffer (2:1, pH 6.8) at 25 °C. Kinetics were monitored by  $^1\text{H-NMR}$  spectroscopy. The observed second-order rate constants  $k_{\text{obs}}$  were determined as the average of three measurements. [b]  $k_{\text{rel}}$  represents the relative rate constants with respect to 4-methoxyphenyl KAT **119**.

It was observed that all electron-withdrawing fluoro- and chloro-substituted derivatives **133–136** displayed slower reaction kinetics compared to unsubstituted pyridyl KAT **116**. In particular, we found that 5-substituted chloro-derivative **133** with a rate constant of  $0.014 \text{ M}^{-1} \text{ s}^{-1}$  displayed slightly enhanced ligation kinetics compared to 4- and 6-substituted derivatives **129** and **134** with rate constants of  $0.011 \text{ M}^{-1} \text{ s}^{-1}$  and  $0.009 \text{ M}^{-1} \text{ s}^{-1}$  respectively (Figure 2.4, a). The same trend was observed for fluoro-derivatives **135** and **136**. While for 5-substituted fluoro KAT **135** a rate constant of  $0.014 \text{ M}^{-1} \text{ s}^{-1}$  was measured, 4- and 6-substituted fluoro-species **130** and **136** showed only slow ligation rates with rate constants of  $0.009 \text{ M}^{-1} \text{ s}^{-1}$  and  $0.007 \text{ M}^{-1} \text{ s}^{-1}$  respectively (Figure 2.4,b).

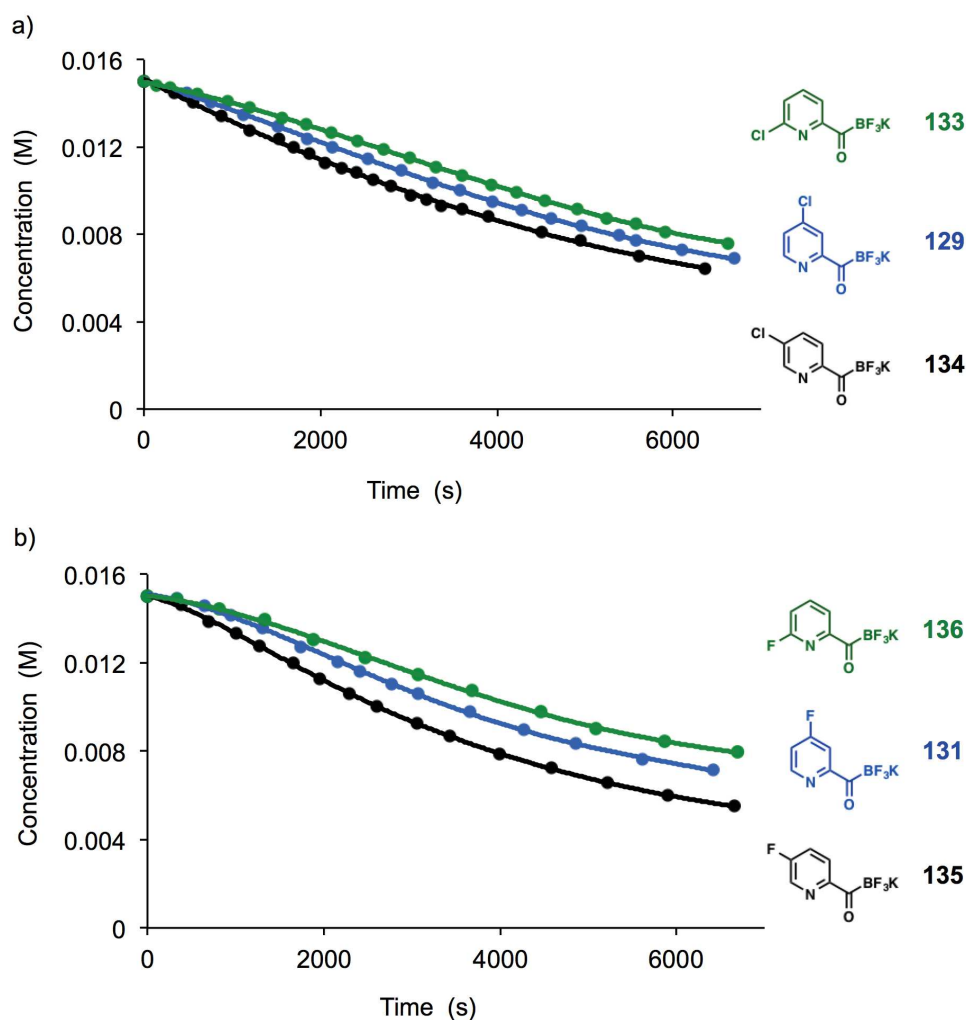


**Figure 2.4** Reaction kinetics of 4-, 5- and 6-substituted a) chloro KAT derivatives and b) fluoro KAT derivatives.

Our hypothesis was further supported upon investigation of the equivalent series of electron-donating methoxy substituents. As exemplified in Figure 2.5, 4-substituted methoxy derivative **127** displayed accelerated ligation kinetics compared to 5-methoxy analogue **131**. However, to our surprise, 6-substituted methoxy derivative **132** underwent significantly slower ligation reactions ( $k_{\text{obs}} = 0.022 \text{ M}^{-1} \text{ s}^{-1}$ ) compared to 5-substituted methoxy KAT **131** with a rate constant of  $0.044 \text{ M}^{-1} \text{ s}^{-1}$ . A possible explanation for this finding might be that once the pyridyl nitrogen of **131** is protonated during the course of the ligation, the oxygen of the methoxy group partially coordinates to this proton and competes with the rate enhancing proton acceptor/donor pair formation proposed for 2-pyridyl KATs.

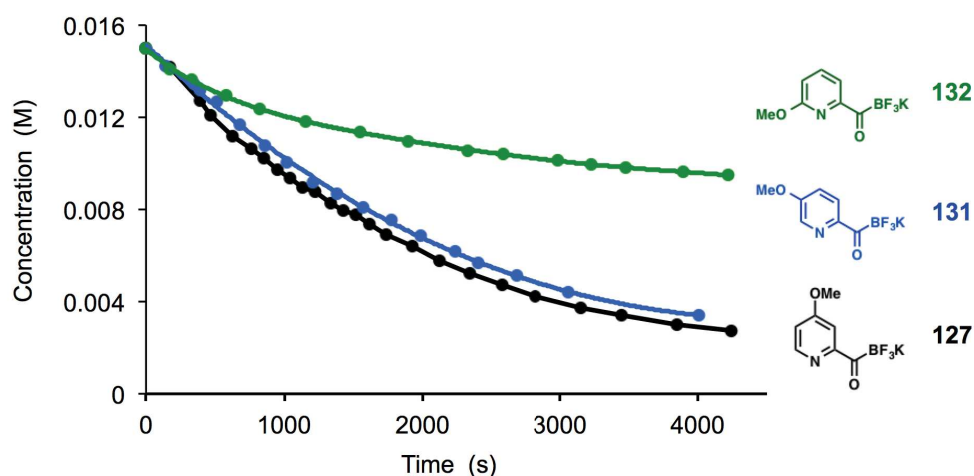


**Figure 2.5** Reaction kinetics of 4-, 5- and 6-substituted methoxy KAT derivatives.

In general, the observed reaction rates of 5- and 6-substituted 2-pyridyl KAT analogues **131–136** complemented our kinetic investigation of the series of 4-substituted 2-pyridyl KATs **127–130** and reinforced our hypothesis that the pyridyl nitrogen plays an important role in the reaction process. Our experimental findings were further supported by a recent report of Kool *et al.*, in which the ligation of hydrazines with a series of different aldehydes was examined. The authors claimed that 2-pyridylcarboxaldehyde showed improved ligation rates at physiological pH, however, no further mechanistic investigations were performed.<sup>52</sup>

### 2.4.3 Variable pH Kinetic Studies

We continued our kinetic investigations by measuring the pH profile of 2-pyridyl KAT (**116**) in comparison to reference aryl KAT **119**. Pursuant to our already established kinetic method, ligation reactions were performed with equimolar concentration of KAT and hydroxylamine reactants under buffered solvent conditions at different pH values ranging from pH 3.6 – 7.4. Notably, upon switching from neutral to more acidic pH a change in buffer was required. For pH values below pH 5.1, potassium acetate buffer was used instead of potassium phosphate buffer. Since the buffer capacity of acetate buffers is reduced between pH 3.6 – 3.9 more concentrated buffer solutions (0.2 M instead of 0.1 M) were employed and the ratio of MeCN-cosolvent was reduced in order to ensure a constant pH value throughout the course of the reaction. For pH 4.4 – 7.4, reaction rates were measured by  $^1\text{H-NMR}$  spectroscopy according to our previously established procedure (*cf.* Scheme 2.8). Below pH 4.4, KAT ligations were observed to be too rapid for NMR-timescale and were monitored at lower concentrations of 3.75 mM by changes in absorption using UV-Vis spectroscopy. As demonstrated in Figure 2.6, the variable pH measurements revealed that 2-pyridyl KAT (**116**) showed enhanced ligation kinetics with reference to aryl KAT **119** not only close to neutral pH (pH 6.8 – 7.4) but also at moderate and strongly acidic pH (pH 3.6 – 5.1). In general terms, it was observed that ligation rates for both **116** and **119** exponentially increase with acidic pH. While significant changes in ligation rates were observed at low pH (pH 3.6 – 5.1), only moderate changes in ligation rates were detected between pH 5.1 – 7.4. Furthermore, the turning point was evaluated to be around pH 5.1.

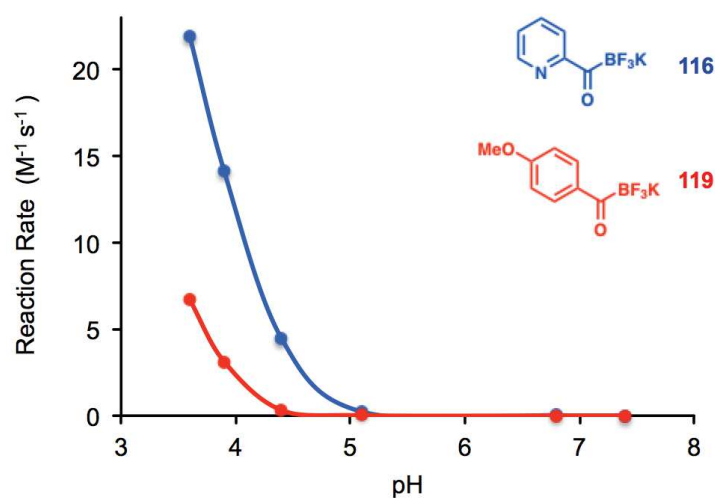
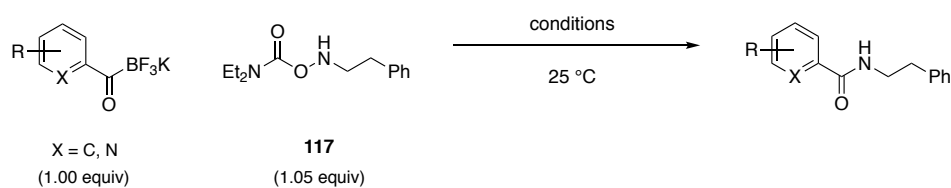


**Figure 2.6** Comparison of pH profiles of KAT **116** and **119**. Observed ligation rates were plotted against pH.

Interestingly, we found that the relative rate enhancement of 2-pyridyl KAT (**116**) with reference to aryl KAT **119** was larger at neutral to moderately acidic pH compared to strongly acidic pH. In fact, we observed that ligation rates of **116** compared to **119** were on average 10 times faster at range of pH 4.4 – 7.4, but only 5 times and 3 times faster at pH 3.9 and pH 3.6 respectively. This observation is in accordance to our proposal that the pyridyl nitrogen can act as an intramolecular proton acceptor/donor pair upon protonation, thus facilitating the breakdown of the tetrahedral intermediate and ultimately leading to accelerated reaction rates. As a matter of fact, only a small portion of **116** is present in its protonated form at pH 6.8 – 7.4, whereas at pH 4.4 – 5.1 a larger percentage of protonated pyridyl KAT **116-H<sup>+</sup>** is available. As a result, the difference in relative rates between **116** and **119** was observed to be larger at pH 4.4 – 5.1 than at pH 6.8 – 7.4. At more acidic pH

**Table 2.7** Variable pH kinetic measurements of 2-pyridyl KAT and 4-methoxyphenyl KAT



Entry	pH	<b>116</b>	<b>119</b>	$k_{\text{rel}}^{[b]}$
		$k_{\text{obs}} (\text{M}^{-1} \text{s}^{-1})^{[a]}$	$k_{\text{obs}} (\text{M}^{-1} \text{s}^{-1})^{[a]}$	
1	3.6	21.94	6.675	3.3
2	3.9	14.12	3.120	4.5
3	4.4	4.462	0.325	13.7
4	5.1	0.231	0.017	13.6
5	6.8	0.020	0.003	6.7
6	7.4	0.011	0.001	11.0

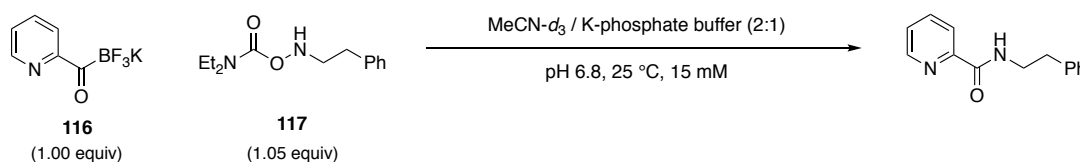
Conditions: [a] Kinetic experiments were performed at equimolar concentrations of KAT and hydroxylamine **117** under buffered solvent conditions at different pH values and 25 °C. For pH 4.4 – 7.4 kinetic measurements were performed at a concentration of 15 mM in MeCN-d<sub>3</sub> / 0.1 M deuterated potassium phosphate or acetate buffer (2:1). The reaction process was monitored by <sup>1</sup>H-NMR spectroscopy. For pH 3.6 – 3.9 kinetic measurements were performed at a concentration of 3.75 mM in MeCN / 0.2 M potassium acetate buffer (1:9). The reaction process was monitored by UV-Vis spectroscopy. In general, rate constants  $k_{\text{obs}}$  were evaluated by applying standard second-order kinetics. [b]  $k_{\text{rel}}$  represents the relative rate constants between 2-pyridyl KAT **116** and 4-methoxyphenyl KAT **119**.

(below pH 4.4) the difference in rates between **116** and **119** notably decreased. In fact, it was observed that the more acidic the pH, the smaller the rate difference between **116** and **119**. This change in relative ligation rates might be attributed to the fact that below pH 4.4 spontaneous intermolecular protonation of the carbonyl carbon at the carbamoyl moiety is triggered for both species **116** and **119** by acid present in the environment. For this reason, at strongly acidic pH, such as pH 3.6, the kinetic advantage of pyridyl KATs to form an intramolecular proton donor/acceptor pair becomes almost negligible and thus only a small difference in relative rates between **116** and **119** was observed.

#### 2.4.4 Specific Acid Catalysis vs. General Acid Catalysis

As the presence of acid plays a crucial role in the KAT ligation and significantly enhances the ligation kinetics we further evaluated whether the KAT ligation displays specific acid catalysis or general acid catalysis.<sup>145</sup> On this behalf, the ligation reaction was carried out under equimolar concentrations of KAT **116** and hydroxylamine **117** at constant pH (pH 6.8) using different potassium phosphate buffer concentrations ranging from 0.05 – 0.3 M (Table 2.8).

**Table 2.8** Kinetic measurements of 2-pyridyl KAT at variable potassium phosphate buffer concentrations



Entry	Buffer Concentration (M)	$k_{\text{obs}}$ ( $\text{M}^{-1} \text{s}^{-1}$ )
1	0.05	0.02
2	0.1	0.02
3	0.2	0.02
4	0.3	0.02

Kinetic measurements were performed at equimolar concentrations (15 mM) of KAT **116** and hydroxylamine **117** in MeCN- $d_3$  / deuterated potassium phosphate buffer (2:1, pH 6.8) at 25 °C and variable phosphate buffer concentrations (0.05 – 0.3 M). Kinetics were monitored by  $^1\text{H-NMR}$  spectroscopy and  $k_{\text{obs}}$  was determined by standard second order kinetics.

It was found that the buffer concentration has no effect on the rate of the ligation other than establish the pH of the reaction and thus suggesting that the KAT ligation proceeds via specific acid catalysis. This means that the reaction rate is dependent specifically on the concentration of hydronium ions ( $\text{H}_3\text{O}^+$ ). The rapid and reversible protonation of the KAT substrate is thus expected to occur prior to the rate-determining step (RDS) of the reaction.

## 2.5 Concluding Remarks

By systematic structural design we have developed a novel generation of potassium acyltrifluoroborates with enhanced overall ligation kinetics ranging from acidic to physiological pH. In this chapter, we demonstrated that 2-pyridyl KATs undergo faster ligation reactions with *O*-carbamoylhydroxylamines, by up to two orders of magnitude compared to commonly employed aryl or alkyl KATs. In addition, we have established a robust kinetic method for the quantitative evaluation of KAT ligation rates. With this suitable method in hand, we performed a detailed kinetic investigation of a series of potassium acyltrifluoroborates under aqueous conditions around physiological pH (pH 5.1 – 7.4). As a result, we revealed that the pyridyl nitrogen in the *ortho*-position to the potassium acyltrifluoroborate group displays a key structural feature responsible for kinetic enhancement. Furthermore, we found that substituents – especially in the 4-position of 2-pyridyl KAT – have a strong influence on the ligation kinetics. In addition, the KAT ligation shows significantly accelerated kinetics with decreasing pH. The KAT ligation was further shown to be independent of buffer concentration at constant pH which provides evidence that the reaction proceeds via specific acid catalysis. Variable pH kinetic studies revealed that the KAT ligation of 2-pyridyl KAT is faster compared to standard aryl KATs over the whole pH range measured (pH 3.6 – 7.4).



### 2.5.1 References

- [137] Jaremko, M.; Jaremko, U.; Kim, H.-Y.; Cho, M.-K.; Schwieters, C. D.; Giller, K.; Becker, S.; Zweckstetter, M. Cold Denaturation of a Protein Monitored at Atomic Resolution. *Nat. Chem. Biol.* **2013**, *9*, 264–270.
- [138] Herskovits, T. T.; Jaillet, H. Structural Stability and Solvent Denaturation of Myoglobin. *Science* **1969**, *163*, 282–285.
- [139] Noda, H.; Bode, J. W. Synthesis of Chemically and Configurationally Stable Monofluoro Acylboronates: Effect of Ligand Structure on their Formation, Properties, and Reactivities. *J. Am. Chem. Soc.* **2015**, *137*, 3958–3966.
- [140] Noda, H.; Bode, J. W. Synthesis and Reactivities of Monofluoro Acylboronates in Chemoselective Amide Bond Forming Ligation with Hydroxylamines. *Org. Biomol. Chem.* **2016**, *14*, 16–20.
- [141] del Pozo, C.; Debono, N.; Corma, A.; Iglesias, M.; Sánchez, F. Homogeneous versus Supported ONN Pincer-Type Gold and Palladium Complexes: Catalytic Activity. *ChemSusChem* **2009**, *2*, 650–657.
- [142] For examples in oxime ligation: Cordes, E. H.; Jencks, W. P. General Acid Catalysis of Semicarbazone Formation. *J. Am. Chem. Soc.* **1962**, *84*, 4319–4328.
- [143] Anderson, B. M.; Jencks, W. P. The Effect of Structure on Reactivity in Semicarbazone Formation. *J. Am. Chem. Soc.* **1960**, *82*, 1773–1777.
- [144] Hammett, L. P. The Effect of Structure upon the Reactions of Organic Compounds. Benzene Derivatives. *J. Am. Chem. Soc.* **1937**, *59*, 96–103.
- [145] For an excellent overview of specific and general acid catalysis see: Lowry, T. H.; Richardson, K. S. *Mechanism and Theory in Organic Chemistry*. Harper and Row, New York, NY, USA, **1981**.



# ***Chapter 3***

---

## ***Mechanistic Investigations of the KAT Ligation***

---

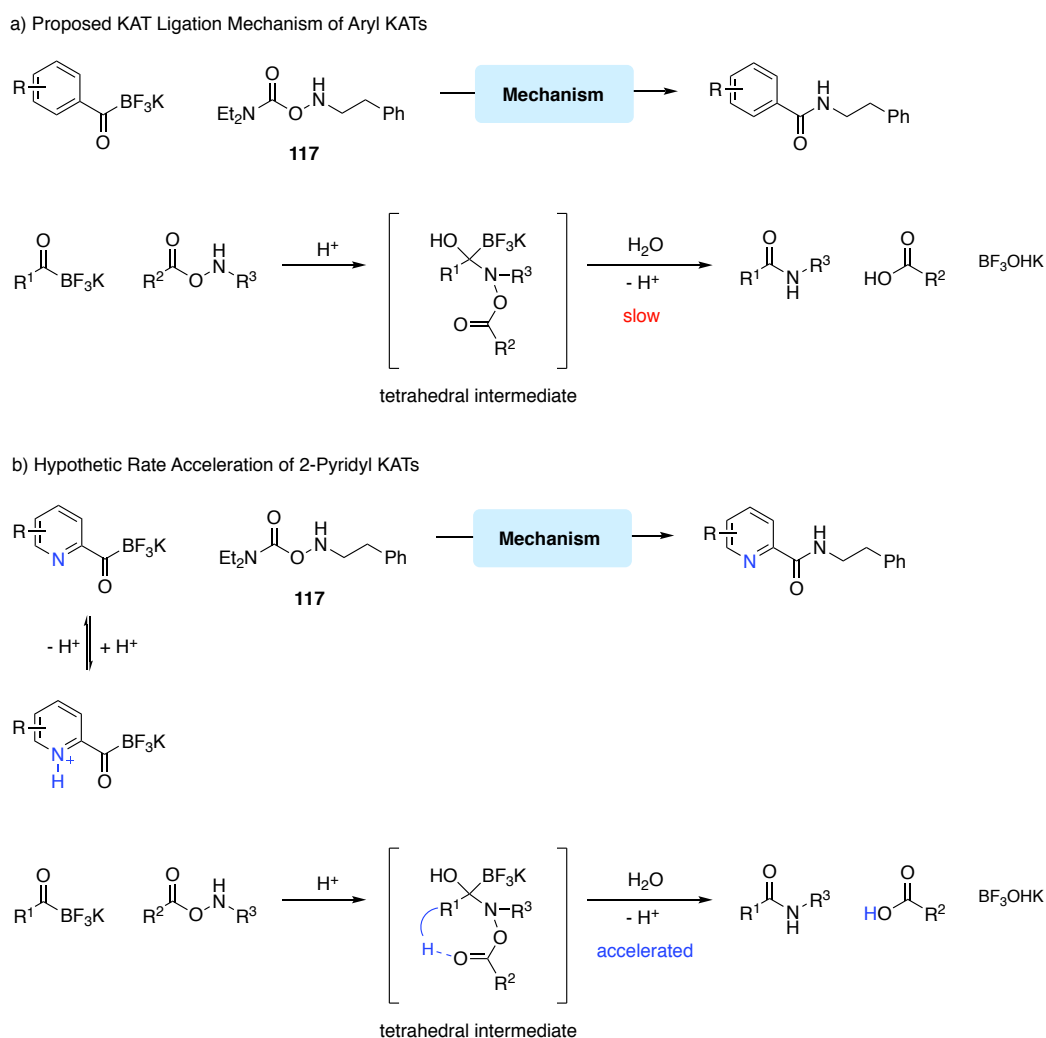
DFT calculations were performed by Erwin Lam independently and as parts of his Master thesis 'Theoretical Studies on the Ligation between Acylboronates and Hydroxylamines' in 2015 under the supervision of Prof. J. W. Bode at ETH Zurich and Prof. K. N. Houk at UCLA.



### 3 Mechanistic Investigations of the KAT Ligation

#### 3.1 Introductory Remarks

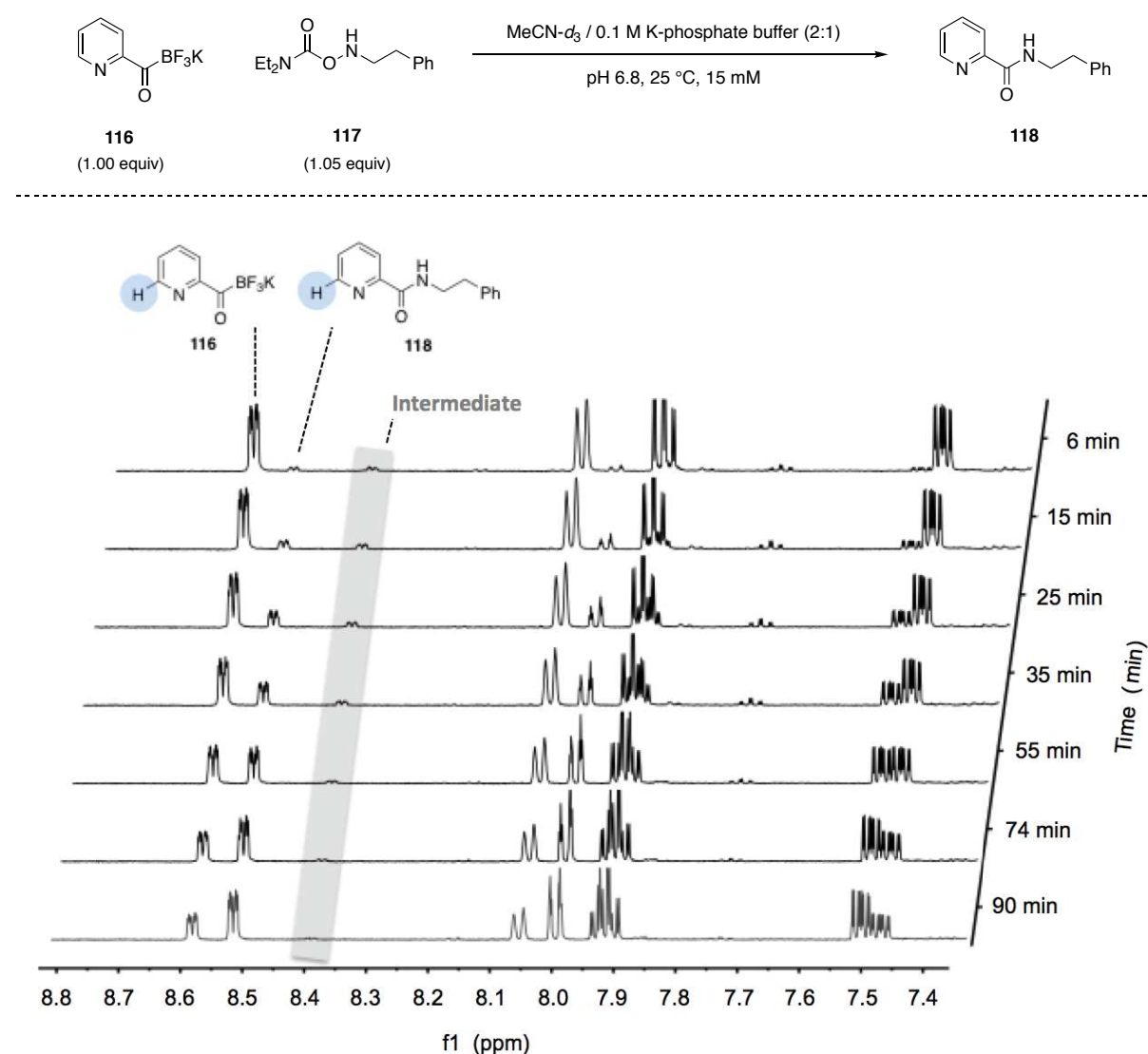
Having identified 2-pyridyl KATs as superior potassium acyltrifluoroborates in the KAT ligation reaction with hydroxylamines (*cf.* Chapter 2), we subsequently aimed to elucidate the underlying mechanistic pathway in order to fully understand why 2-pyridyl KATs undergo faster ligation reactions with hydroxylamines compared to aryl KATs (Scheme 3.1). We further intended to support or disprove our hypothesis that internal proton transfer of *in situ* protonated 2-pyridyl KAT leads to accelerated ligation kinetics (Scheme 3.1, b).



**Scheme 3.1** Proposed rate acceleration of 2-pyridyl KATs compared to aryl KATs in the KAT ligation reaction.

### 3.2 Reaction Profile of the KAT Ligation

Detailed analysis of the  $^1\text{H-NMR}$  spectra recorded for the KAT ligation between pyridyl KAT **116** and hydroxylamine **117** (*cf.* Scheme 2.8) revealed the presence of a third species in addition to **116** and **118** with characteristic peaks in the aromatic region between 7.4 – 8.6 ppm (Scheme 3.2). Interestingly, the observed species displayed the same multiplicities as the pyridyl protons of starting material **116** and amide product **118**, which led us to the assumption that the KAT ligation of **116** and **118** might involve a reaction intermediate.



**Scheme 3.2** Kinetic experiments were performed at equimolar concentrations (15 mM) of KAT **116** and hydroxylamine **117** in  $\text{MeCN-d}_3$  / 0.1 M deuterated potassium phosphate buffer (2:1, pH 6.8) at 25 °C. Kinetics of the KAT ligation were monitored by real-time  $^1\text{H-NMR}$  spectroscopy. Besides formation of product **118** and consumption of starting material **116**, the presence of an additional species, highlighted in grey, was observed.

Further valuable information was collected by monitoring the concentration changes of the three different species over time by  $^1\text{H-NMR}$  spectroscopy. The resulting reaction profile is shown in Figure 3.1. It was found that consumption of starting material KAT **116** proceeded at equal rates as formation of amide product **118**. However, to our surprise, it was noted that at the early stage of the ligation the observed kinetics showed a slight curvature and deviates from strict second-order behavior. The proposed reaction intermediate was detected at low concentrations (with a max. relative concentration of 7 % compared to **116** and **118** combined) at the beginning of the ligation reaction and was observed to slowly disappear over time as product **118** was formed.

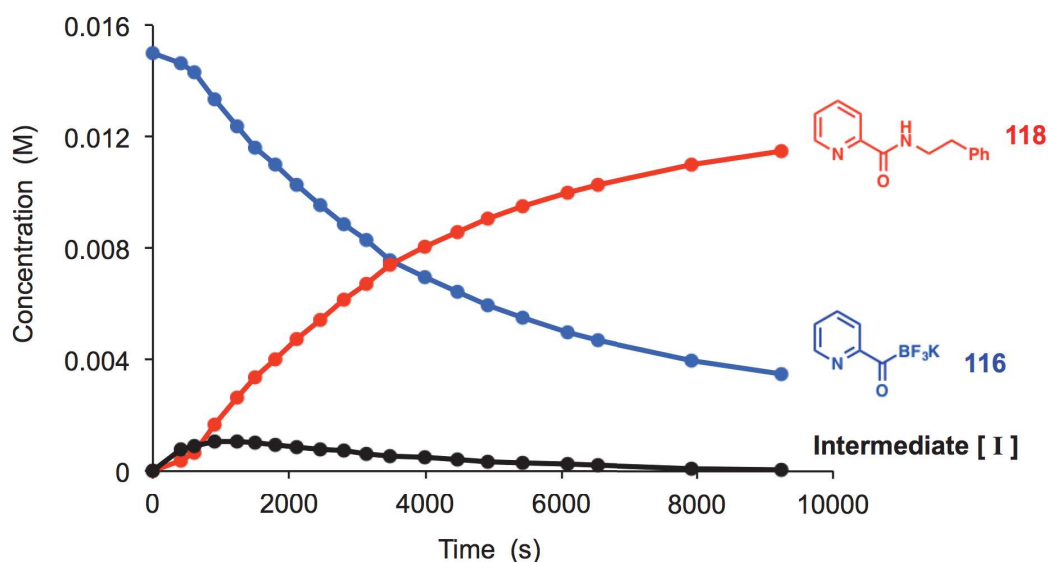
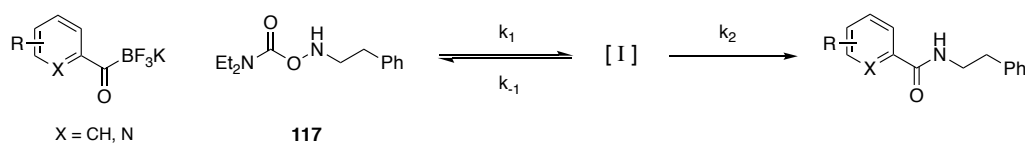


**Figure 3.1** Reaction profile of the KAT ligation between 2-pyridyl KAT **116** and hydroxylamine **117**.

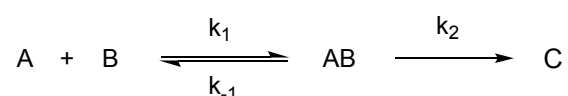
The observed reaction profile of the KAT ligation between 2-pyridyl KAT (**116**) and hydroxylamine **117** strongly indicates that the ligation proceeds by a rate-determining pre-equilibrium via reaction intermediate **[I]** involving the individual rate constants  $k_1$ ,  $k_{-1}$  and  $k_2$  as exemplified in Scheme 3.3.



**Scheme 3.3** Observed rate-determining pre-equilibrium of the KAT ligation between 2-pyridyl KAT **116** and hydroxylamine **117** proceeding via intermediate **[I]**.

Since reaction intermediate **[I]** did not accumulate during the ligation process but was observed to remain at low and steady concentration, individual rate  $k_2$  was assumed to be much smaller with regard to  $k_{-1}$  ( $k_2 \ll k_{-1}$ ). In order to verify this assumption, the individual rate constants  $k_1$ ,  $k_{-1}$  and  $k_2$  of the reaction between **116** and **117** were identified by numerical methods. The following system of ordinary differential equations was integrated on the basis of manually set initial conditions.

### Simplified Reaction Scheme



### Set of Ordinary Differential Equations

$$\frac{d[A]}{dt} = -k_1[A][B] + k_{-1}[AB]$$

$$\frac{d[B]}{dt} = -k_1[A][B] + k_{-1}[AB]$$

$$\frac{d[AB]}{dt} = k_1[A][B] - k_{-1}[AB] - k_2[AB]$$

$$\frac{d[C]}{dt} = k_2[AB]$$

### Mutually Set Initial Conditions

$$[A]_0 = 0.0143 \text{ M}$$

$$[B]_0 = 0.0150 \text{ M}$$

$$[AB]_0 = 9.15 \cdot 10^{-4} \text{ M}$$

$$[C]_0 = 6.75 \cdot 10^{-4} \text{ M}$$

The kinetic parameters were estimated by fitting the model equations to the experimentally obtained data. The generated cost function was minimized using a genetic algorithm. As a result, the following values for the individual rate constants  $k_1$ ,  $k_{-1}$  and  $k_2$  for the reaction between KAT **116** and hydroxylamine **117** were obtained:

$$k_1 = 4.76 \text{ M}^{-1} \text{ s}^{-1}$$

$$k_{-1} = 0.80 \text{ s}^{-1}$$

$$k_2 = 0.0036 \text{ s}^{-1}$$

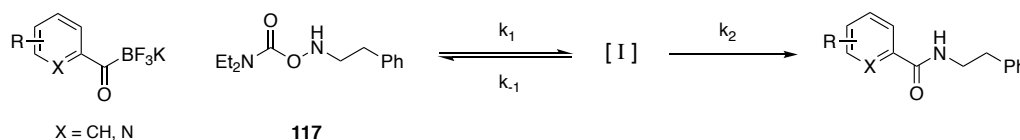
The obtained individual rate constants were subsequently tested in a kinetic simulation and to our satisfaction the reaction profile of **116** could be reproduced, thereby confirming the validity of our calculations.



The data revealed that the nucleophilic attack of hydroxylamine **117** to KAT **116** proceeds rapidly with a rate constant  $k_1$  of  $4.76 \text{ M}^{-1} \text{ s}^{-1}$ . The addition product **[I]** can either convert back to the two starting materials with an individual rate constant  $k_{-1}$  of  $0.80 \text{ s}^{-1}$  or react further to form the desired amide product **118**. The product formation step, which involves the breakdown of the addition intermediate **[I]** was identified to be the rate-determining step of the KAT ligation with an individual rate constant  $k_2$  of  $0.0036 \text{ s}^{-1}$ .

In light of these results, a similar rate-determining pre-equilibrium to **116** was observed for all tested KAT species **119–136**, including aryl KATs **119–121**.

**Table 3.1** Observed relative intermediate **[I]** concentration in KAT ligation reactions.

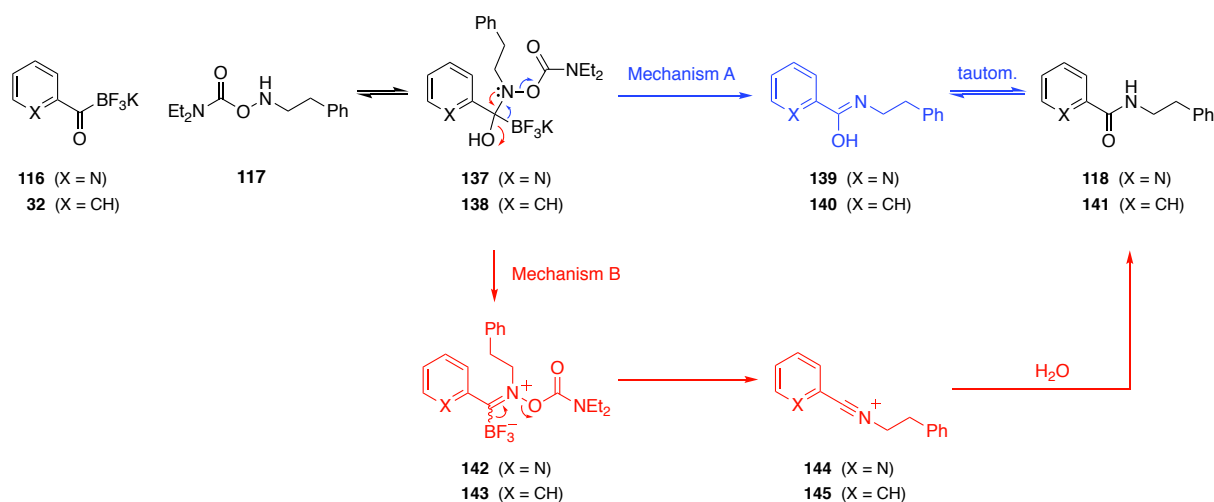


Entry	Substrate	Structure	Equiv of 117 <sup>[a]</sup>	Rel. Conc. of [I] (%) <sup>[b]</sup>
1	<b>116</b>		1	7
2	<b>119 – 121</b>		1	<1
3	<b>126</b>		1	<1
4	<b>127</b>		1	13
5	<b>116</b>		2	11
6	<b>116</b>		4	16
7	<b>116</b>		8	16

Ligation reactions were performed at equimolar concentrations (15 mM) of KAT and hydroxylamine **117** in MeCN- $d_3$  / 0.1 M deuterated potassium phosphate buffer (2:1, pH 6.8) at 25 °C. [a] Equivalent of hydroxylamine **117** were varied. [b] Relative intermediate concentrations **[I]** refer to the concentration of **[I]** with respect to **116** and **117** combined and were determined by integration. Only well separated resonances were used for integration.

### 3.3 Potential Mechanistic Pathways

On the basis of these interesting results, we further aimed to identify the nature of the observed reaction intermediate **[I]** and ultimately postulated a reasonable mechanism for the KAT ligation. As depicted in Scheme 3.4, two distinct mechanistic pathways can be envisioned for the KAT ligation between KAT (**116**, **32**) and hydroxylamine **117**.



**Scheme 3.4** Potential mechanistic pathways of the KAT ligation.

In both mechanisms initial nucleophilic attack of the hydroxylamine to the carbonyl carbon of the KAT leads to the formation of a tetrahedral addition intermediate (**137**, **138**). On one hand, this intermediate (**137**, **138**) can undergo concerted elimination to an imidic acid species (**139**, **140**), which could quickly tautomerize to the desired amide product (**118**, **141**) (Mechanism A). On the other hand, the tetrahedral addition intermediate (**137**, **138**) can convert into a nitron-like intermediate (**142**, **143**), which upon the formation of a nitrilium species (**144**, **145**) and addition of water also leads to formation of amide product (**118**, **141**) (Mechanism B). Since we expected the imidic acid (**139**, **140**) and nitrilium (**144**, **145**) intermediates to be short-lived species, we assumed that either the tetrahedral addition product (**137**, **138**) or the nitron-like species (**142**, **143**) might be the potentially observed reaction intermediate **[I]**. By performing  $^1\text{H-NMR}$  measurements with **116** in the presence of excess hydrochloric acid, we excluded that **[I]** is simply the protonated pyridyl KAT species **116-H<sup>+</sup>**. To our disappointment, all attempts to isolate or characterize the observed reaction intermediate **[I]** via 2D-NMR spectroscopy remained unsuccessful. In a further effort, we monitored the KAT ligation between **116** and **117** by high-resolution mass spectrometry (HR-MS). In addition to starting material KAT **116** and amide product **118**, a mass peak of  $m/z =$

406.1559 was detected in the negative mode that corresponds to the tetrahedral addition intermediate **137** minus exactly four protons. HR-MS/MS analysis (irradiation with 5 eV) confirmed that  $m/z$  406.1559 is a reaction intermediate and that the protons were subtracted from the carbamoyl moiety of **137**. In the positive mode, no correlations to potential reaction intermediates could be made. Even though mass analysis supports that the KAT ligation of **116** and **117** proceeds via intermediate **137**, it proved to be difficult to collect concluding experimental evidence. In the following, DFT calculations were performed to gain more insight into the KAT ligation mechanism and get a better understanding of why 2-pyridyl KATs exhibit faster ligation rates than aryl KATs.

### 3.4 DFT Calculations

Detailed density functional theory (DFT) studies were performed in order to 1) elucidate the lowest energy reaction pathway of the KAT ligation between potassium acyltrifluoroborates and hydroxylamines, 2) disclose the structure of the experimentally observed reaction intermediate **I** and 3) support or disprove our hypothesis why pyridyl KATs display accelerated ligation rates in comparison to aryl KATs.

DFT studies were conducted using Gaussian09 (d1).<sup>146</sup> Geometry optimization and transition state locations were performed employing the 6-31g(d)<sup>147</sup> basis set in combination with the B3LYP functional<sup>148</sup>. The nature of the observed geometry is confirmed by analyzing the vibrational frequencies at the same level of theory. In addition, transition states were confirmed by intrinsic reaction coordinates analysis (IRC).<sup>149</sup> Single point calculations were done by using the 6-311+g(d,p)<sup>150,151</sup> basis set with the M06-2X<sup>152</sup> function with additional PCM<sup>153,154</sup> solvation of water. 3D structures were generated by CYLview.<sup>155</sup>

As a basis for the DFT calculations and for reasons of simplification, a model system of the KAT ligation between KAT (**116**, **32**) and hydroxylamine **117** was employed. As outlined in Figure 3.2, KAT **116** and **32** were considered as negatively charged boronates **116'** and **32'** respectively without the presence of the potassium counterion. In the case of hydroxylamine **117**, the alkyl moiety was replaced by a methyl group and the diethylamine moiety was exchanged with a dimethylamine resulting in structure **117'**.

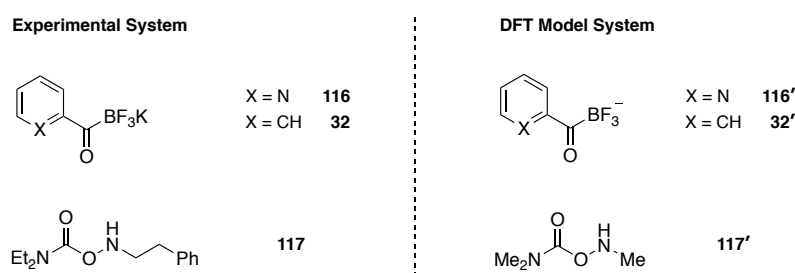


**Figure 3.2** Model system for DFT calculations.

With this model system in hand, the lowest energy conformers of the pyridyl, protonated pyridyl and aryl tetrahedral addition intermediates **137'**, **137'-H<sup>+</sup>** and **138'** were calculated first. As illustrated in Figure 3.3, it was found that for all three species the *anti* conformation is more stable with respect to the *gauche* conformation. In comparison to aryl intermediate **138'** with optimized free energies of 5.1 kcal mol<sup>-1</sup> for the *anti* and 5.7 kcal mol<sup>-1</sup> for the *gauche*

conformation, pyridyl intermediate **137'** showed additional stabilization (highlighted in blue) by hydrogen bonding between the pyridyl nitrogen and the newly formed hydroxyl group. In fact, relative free energies for **137'** were calculated to be  $-0.2 \text{ kcal mol}^{-1}$  for the *anti* and  $6.2 \text{ kcal mol}^{-1}$  for the *gauche* conformer. Remarkably, the *anti* conformation of **137'** is almost  $5 \text{ kcal mol}^{-1}$  more stable than the one of **138'**. The protonated pyridyl intermediate **137'-H<sup>+</sup>** was discovered to be even more stable with relative energies of  $-5.5 \text{ kcal mol}^{-1}$  and  $-2.5 \text{ kcal mol}^{-1}$  for *anti* and *gauche* conformation respectively. This extra stabilization effect, can be attributed to additional hydrogen bonding events, on one hand between the newly formed hydroxyl group and the trifluoroborate moiety and on the other hand, between the protonated pyridyl and the carbamoyl residue.

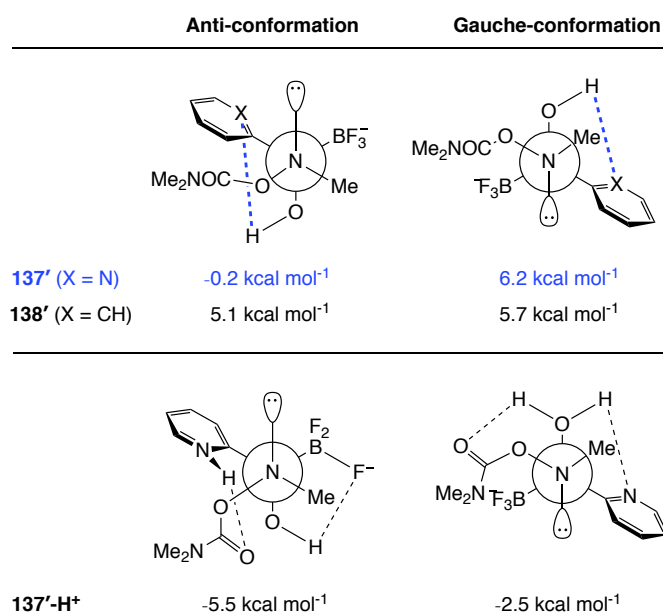


**Figure 3.3** Lowest-energy conformers of tetrahedral KAT ligation intermediate (**137**, **138**). Geometry optimizations were performed for two conformations, *anti* vs. *gauche*, using B3LYP/6-31g(d). Optimized structures are shown as Newman projections. Free energies are given in  $\text{kcal mol}^{-1}$  relative to the corresponding KAT and hydroxylamine starting materials.

In the following, ground and transition state energies of all intermediates and products were calculated for both potential mechanistic pathways depicted in Scheme 3.3 – the concerted elimination via a tetrahedral ligation intermediate (**137**, **138**) (Mechanism A) and the ligation via nitrene-like intermediate (**142**, **143**) (Mechanism B).

In the case of the ligation with pyridyl KAT **116'** two relevant transition states were found **137' TS-1** and **137' TS-2** that could potentially be involved in the concerted elimination of tetrahedral intermediate **137'** (Figure 3.4, black and blue reaction pathways).

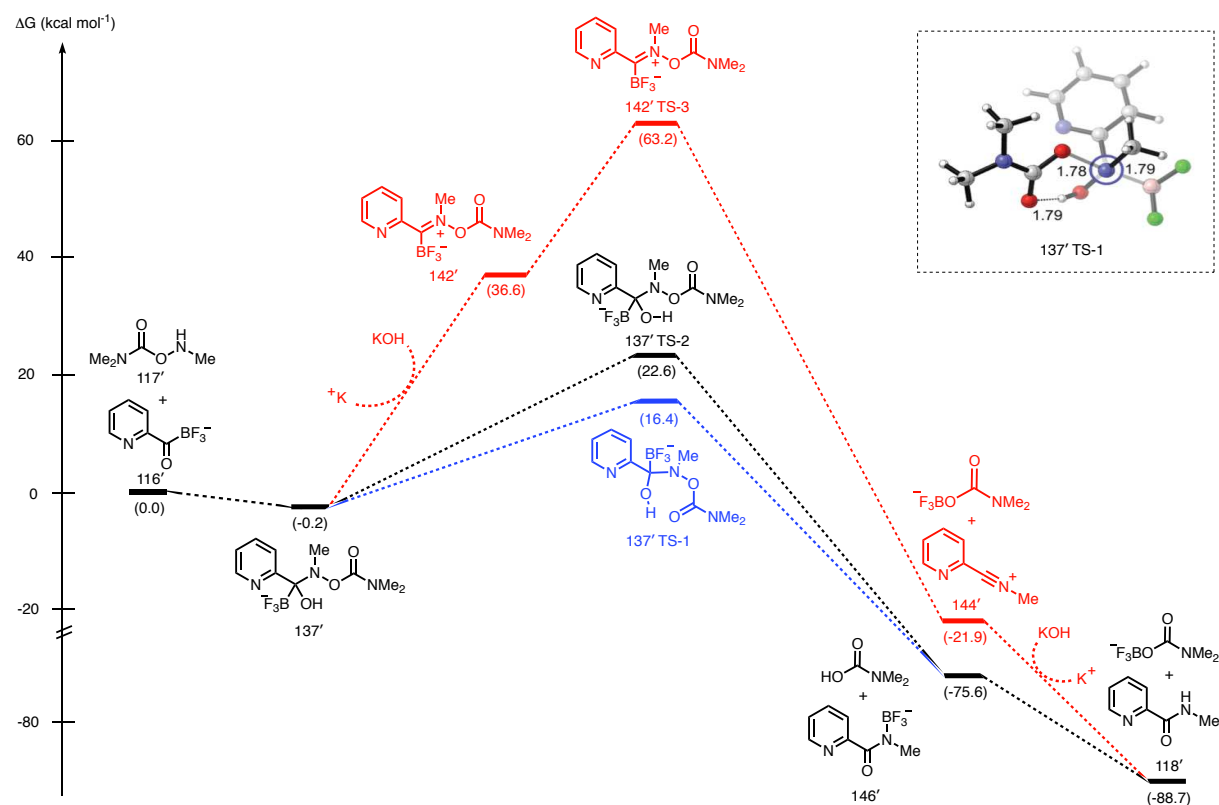


**Figure 3.4** Relative free energies for the KAT ligation of 2-pyridyl KAT **116'** were calculated using the B3LYP/6-31g(d) basis set. Free energies are given in parentheses in kcal mol<sup>-1</sup>, bond lengths in Å. Reaction pathways via nitrone-like intermediate **142'** are highlighted in red. Reaction pathways via a concerted elimination of tetrahedral intermediate **137'** are highlighted in black and blue respectively.

Both transition states **137' TS1** and **137' TS-2** were found to exhibit antiperiplanar geometry with relative free energies of 16.4 kcal mol<sup>-1</sup> and 22.6 kcal mol<sup>-1</sup> respectively. The obtained transition state energies **137' TS-1** and **137' TS-2** were shown to be feasible amide bond formation pathways at room temperature. In contrast, the lowest energy synperiplanar transition state displayed a relative free energy of 32.9 kcal mol<sup>-1</sup>, which is much higher in energy compared to the two transition states derived from the antiperiplanar conformations and was therefore not further considered. Similar to the ground state of **137'** also transition states were observed to preferentially adopt the energetically more stable antiperiplanar geometry.

The reason for the difference in energy of **137' TS1** and **137' TS-2** was observed to lie in the nature of the hydrogen bonding that occurs between the hydroxylamine moiety of **137'** and the carbamoyl leaving group (Figure 3.5). In transition state **137' TS-2** the hydroxyl group of **137'** formed a hydrogen bond to the carbamoyl oxygen (-NQC(=O)NMe<sub>2</sub>) leading to a five-

membered transition state. In contrast, **137'** **TS-1** shows hydrogen bonding between the hydroxyl group of **137'** and the carbonyl of the carbamoyl leaving group (-NOCONMe<sub>2</sub>) resulting in a seven-membered transition state, which was observed to be 6.2 kcal mol<sup>-1</sup> more favored compared to **137'** **TS-2**. In transition state **137'** **TS-2** the hydroxyl group of **137'** formed a hydrogen bond to the carbamoyl oxygen (-NOCONMe<sub>2</sub>) leading to a five-membered transition state. In contrast, **137'** **TS-1** shows hydrogen bonding between the hydroxyl group of **137'** and the carbonyl of the carbamoyl leaving group (-NOCONMe<sub>2</sub>) resulting in a seven-membered transition state, which was observed to be 6.2 kcal mol<sup>-1</sup> more favored compared to **137'** **TS-2**.

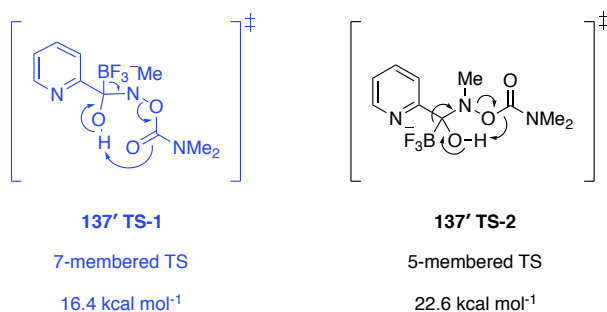
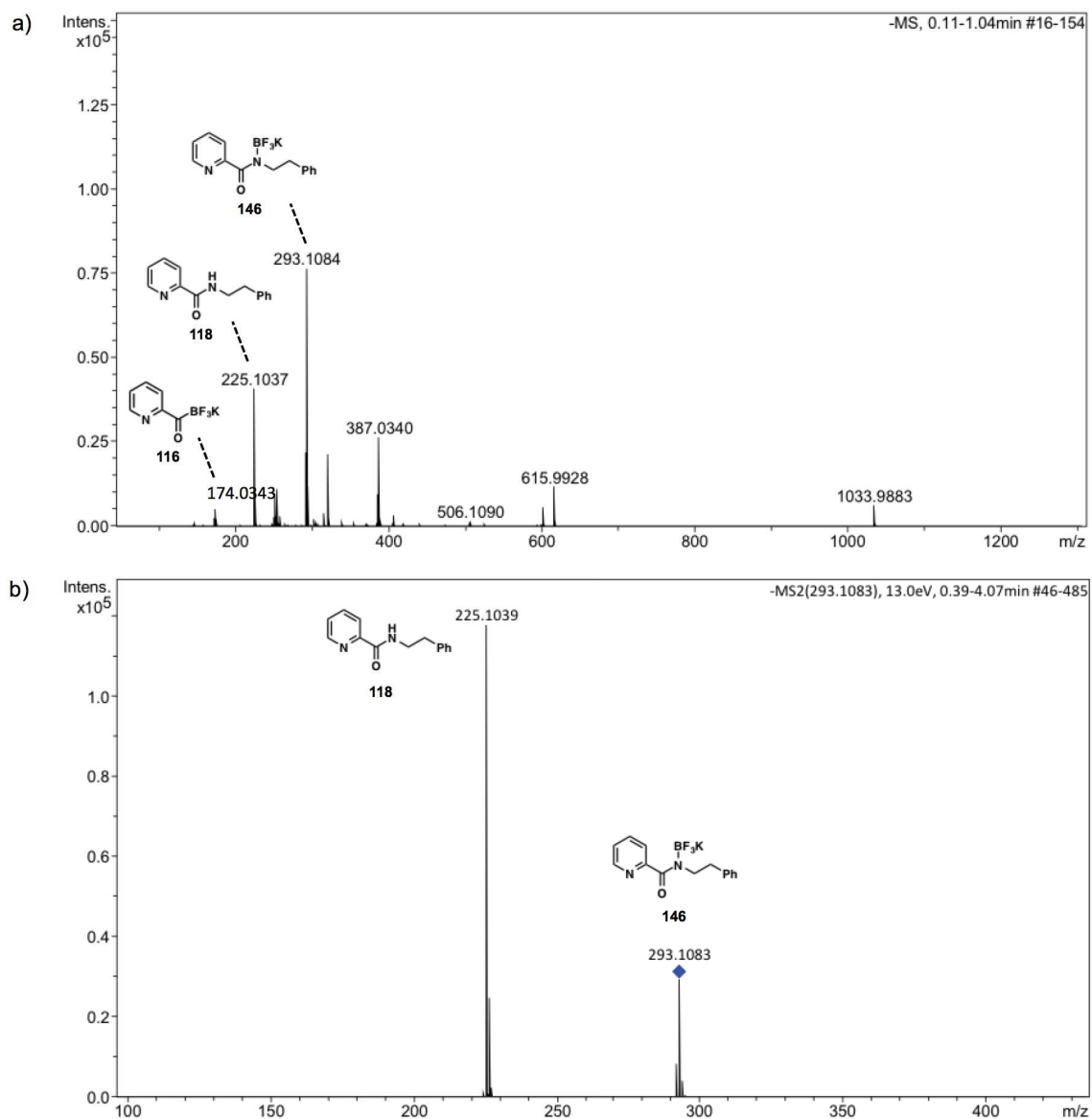
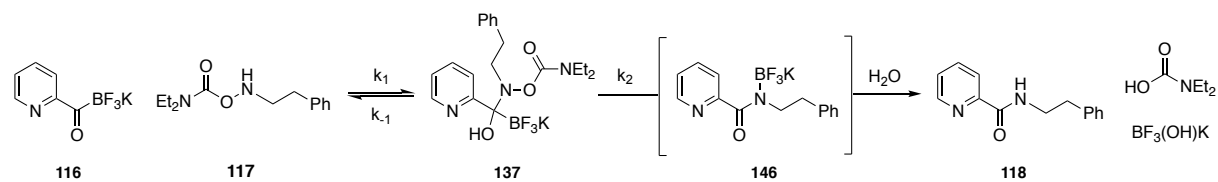


**Figure 3.5** Proposed transition states of protonated and non-protonated 2-pyridyl KAT. Geometry optimizations were performed using B3LYP/6-31g(d). Optimized geometries were confirmed by analysis of the vibrational frequencies. Transition states were confirmed by intrinsic reaction coordinates analysis (IRC).

To our surprise, concerted elimination of **137'** via **137'** **TS-1** or **137'** **TS-2** did not lead to tautomer **139** as described in Scheme 3.3, but rather a novel *N*-trifluoroboryl reaction intermediate **146'** was discovered, which was proposed to subsequently collapse to amide product **118'**. Indeed, the newly proposed reaction intermediate **146'** (*m/z* 293.1077) was detected by high-resolution mass analysis of the KAT ligation between **116** and **117** and confirmed as reaction intermediate by MS/MS (Scheme 3.5). Furthermore, it was observed that the ground state of nitron-like intermediate **142'** with a free energy of 36.6 kcal mol<sup>-1</sup> is 14 kcal mol<sup>-1</sup> higher in energy compared to the highest energy transition state **137'** **TS-2** for the concerted elimination of **137'** (Figure 3.4, red reaction pathway). Consequently, the transition state of **142'** (**142'**-**TS3** with a relative energy of 63.2 kcal mol<sup>-1</sup>) is 40.0 kcal mol<sup>-1</sup> higher in energy compared to **137'** **TS-2**. Overall, these energies indicate that the KAT ligation between 2-pyridyl KAT **116** and hydroxylamine **117** preferentially proceeds via a

concerted elimination pathway (Mechanism A) rather than via nitron-like intermediate **142'** (Mechanism B).



**Scheme 3.5** Kinetic experiments were performed at equimolar concentrations (15 mM) of KAT **116** and hydroxylamine **117** in MeCN / H<sub>2</sub>O (2:1) at 25 °C. a) Detection of N-borylated reaction intermediate during the KAT ligation between **116** and **117** by mass spectrometry. b) MS-MS Analysis for the validation of the ligation intermediate.



As illustrated in Figure 3.6, aryl KAT **32'** displayed a similar reaction profile to pyridyl KAT **116'**, however, all ground and transition states showed slightly increased relative free energies. It was found that the lowest energy pathway of **32'** proceeds by concerted elimination via a seven-membered transition state **138' TS-1** with a relative free energy of 19.1 kcal mol<sup>-1</sup>.

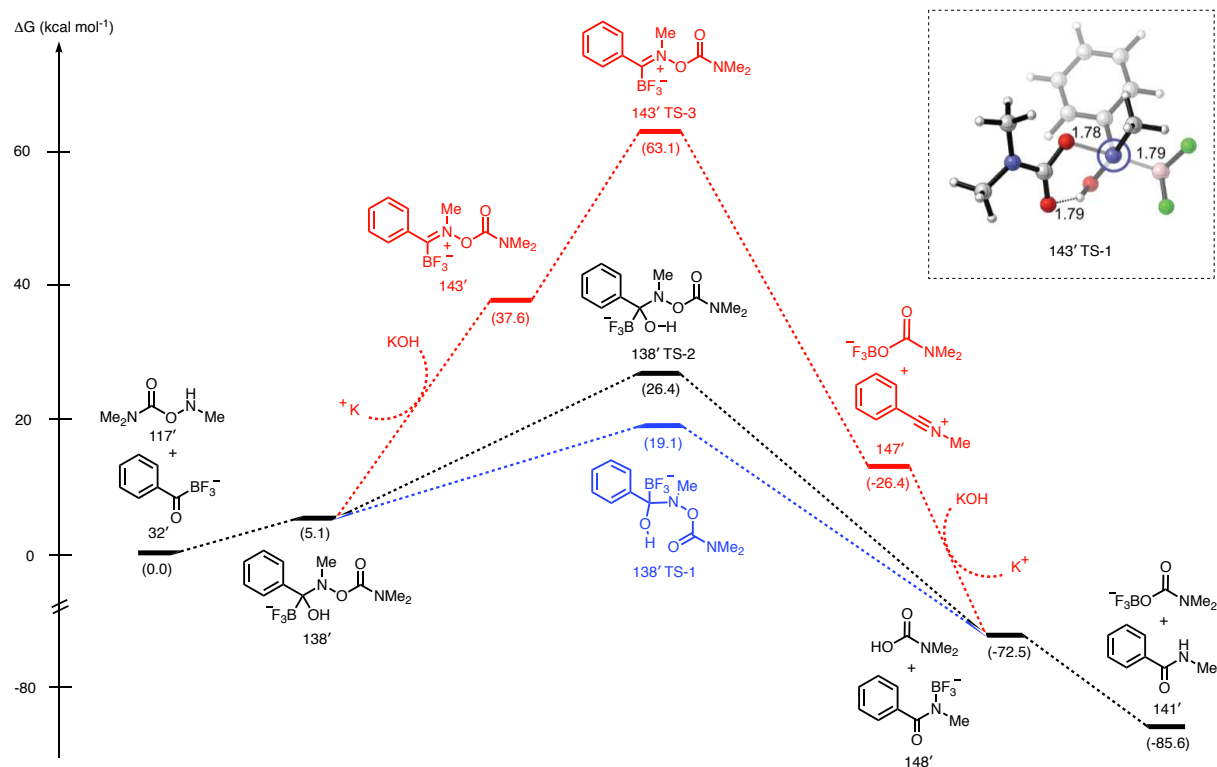


**Figure 3.6** Relative free energies for the KAT ligation of aryl KAT **32'** were calculated using the B3LYP/6-31g(d) basis set. Free energies are given in parentheses in kcal mol<sup>-1</sup>, bond lengths in Å. Reaction pathways via nitron-like intermediate **143'** are highlighted in red. Reaction pathways via a concerted elimination of tetrahedral intermediate **138'** are highlighted in black and blue respectively.

In light of this new mechanistic insight we further aimed to investigate the observed rate enhancement of pyridyl KATs *versus* aryl KATs. As illustrated in Figure 3.7, protonated pyridyl KAT **116'-H<sup>+</sup>** displays additional stabilization effects compared to non-protonated pyridyl KAT **116'**. This additional stabilization effect arises due to hydrogen bond formation between protonated pyridyl nitrogen and the carbonyl of the carbamoyl moiety and displays a relative free energy of 9.8 kcal mol<sup>-1</sup> (Figure 3.7, highlighted in green). In other words, the carbonyl oxygen of the carbamoyl group is properly aligned with the protonated pyridyl nitrogen to enable proton transfer (1.62 Å, Figure 3.7). In a set of basic calculations it was

found that the protonated carbamoyl moiety serves as an excellent leaving group in the concerted elimination of the tetrahedral intermediate, consequently facilitating product formation. Overall, these findings underline our hypothesis that the pyridyl nitrogen is able to act as a proton acceptor/donor pair via hydrogen-bonding during the course of the KAT ligation reaction, significantly accelerating the reaction rates of pyridyl KATs in comparison to aryl KATs.

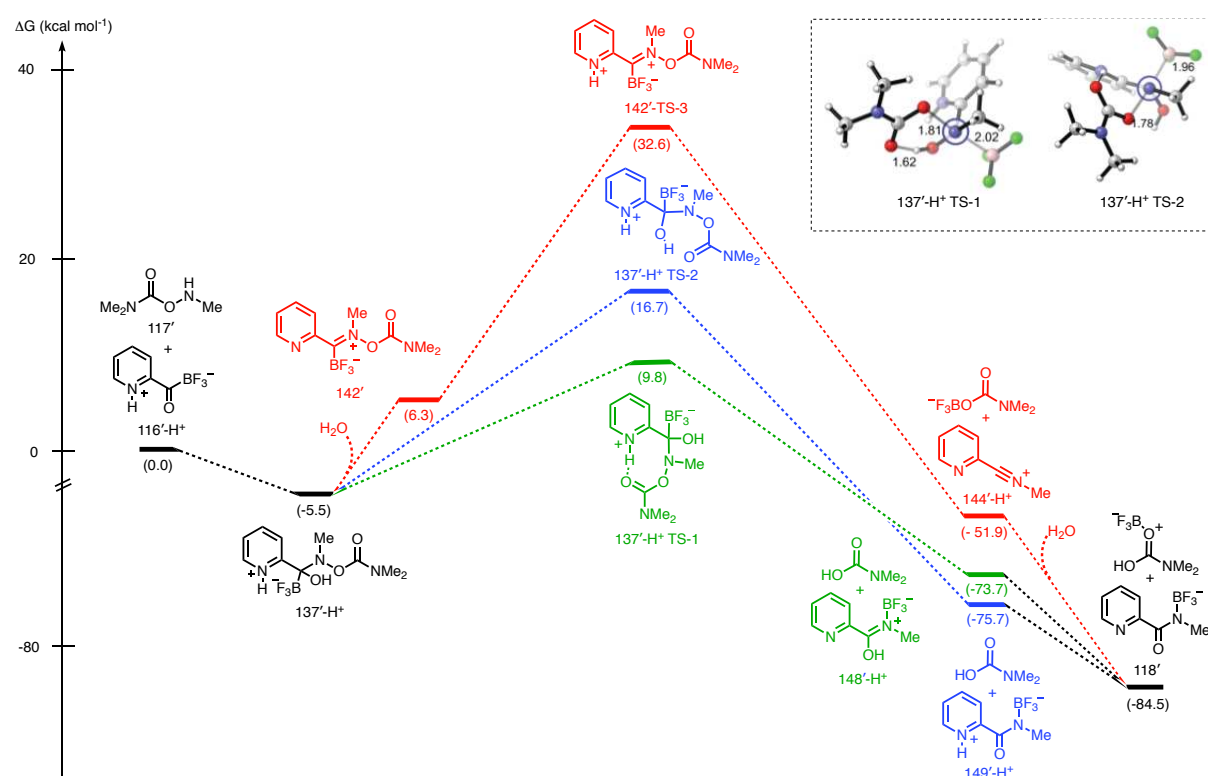
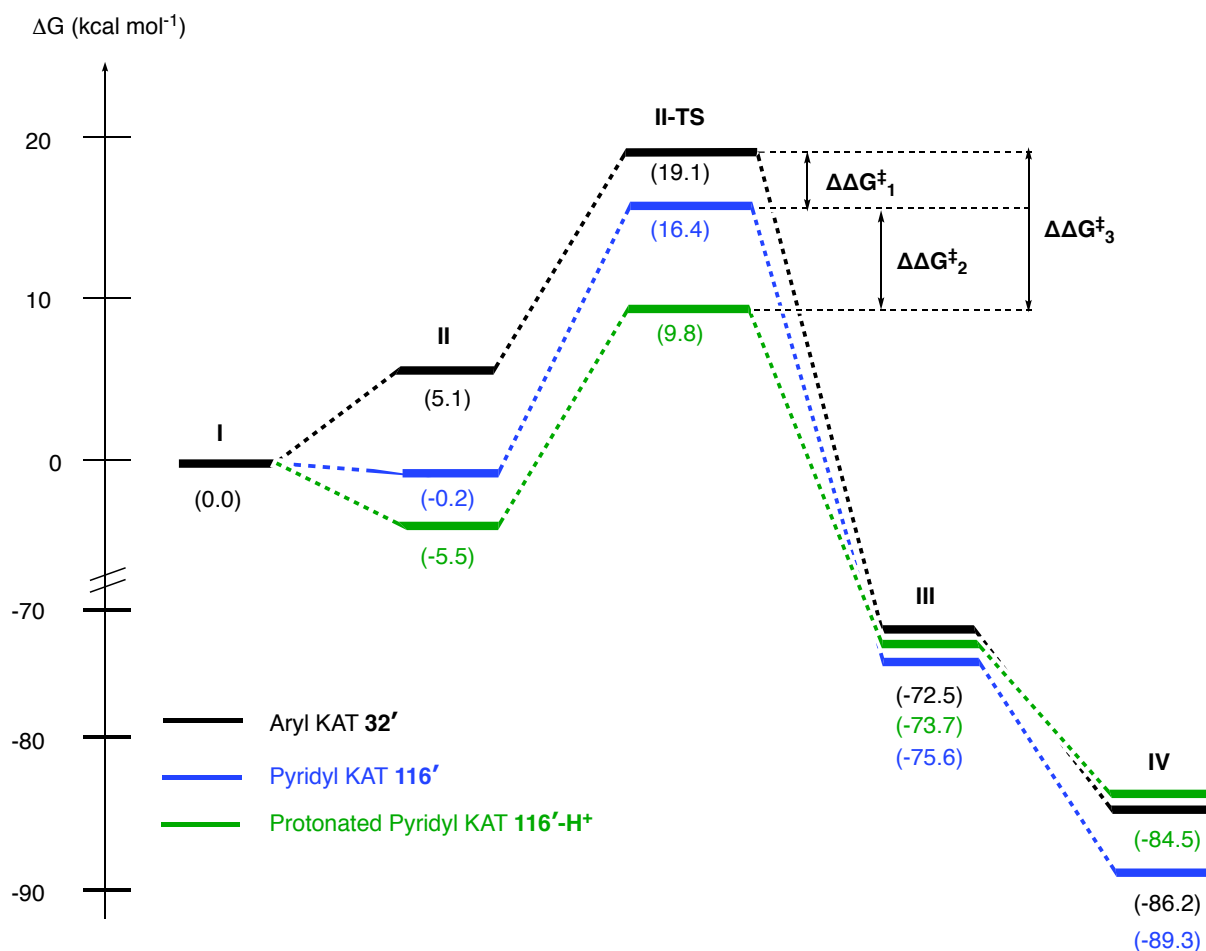
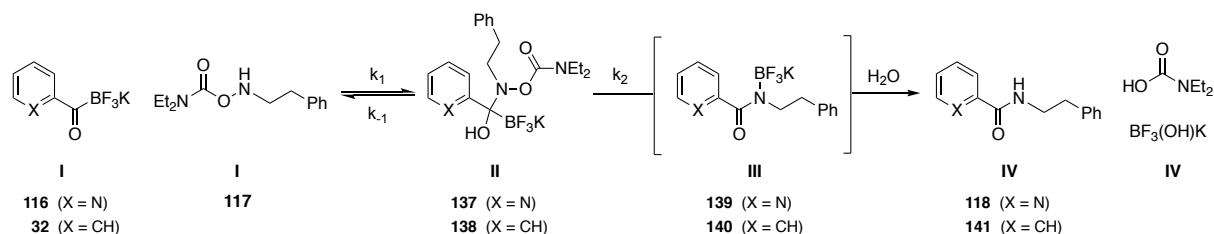


**Figure 3.7** Relative free energies for the KAT ligation of protonated 2-pyridyl-KAT **116'-H<sup>+</sup>** were calculated using the B3LYP/6-31g(d) basis set. Free energies are given in parentheses in kcal mol<sup>-1</sup>, bond lengths in Å. Reaction pathways via nitrone-like intermediate **142'** are highlighted in red. Reaction pathways via a concerted elimination tetrahedral intermediate **137'** are highlighted in green and blue respectively.

A comparison of the lowest energy pathways between the KAT ligation with structures **116'**, **116'-H<sup>+</sup>** and **32'** depicted in Scheme 3.5, showed that the transition state **138' TS-1** for aryl KAT **32'** is 2.5 kcal mol<sup>-1</sup> higher in energy than the lowest energy transition state **137' TS-1** for pyridyl KAT **116'** (Scheme 3.6, indicated by  $\Delta\Delta G^\ddagger_1$ ). Furthermore, it was discovered that the ligation via protonated pyridyl KAT **116'-H<sup>+</sup>** is the energetically most favorable reaction pathway with the overall lowest relative transitions state energy of 9.8 kcal mol<sup>-1</sup>. In fact, it was demonstrated that **116'-H<sup>+</sup> TS-1** is 6.6 kcal mol<sup>-1</sup> more stable than the lowest

energy transition state for non-protonated pyridyl KAT **116'-TS-1** with a relative energy of 16.4 kcal mol<sup>-1</sup> (Scheme 3.6, indicated by  $\Delta\Delta G^\ddagger_2$ ) and 9.3 kcal mol<sup>-1</sup> more stable than the lowest-energy transition state for aryl KAT **138'-TS-1** with an overall free energy barrier of 19.1 kcal mol<sup>-1</sup> (Scheme 3.6, indicated by  $\Delta\Delta G^\ddagger_3$ ).

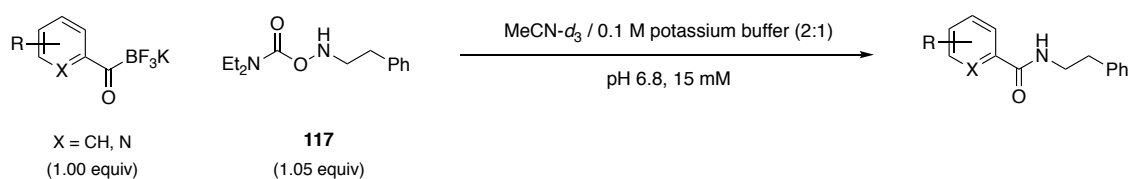


**Scheme 3.6** Comparison of the lowest energy pathways for non-protonated 2-pyridyl KAT **116'**, protonated 2-pyridyl KAT **116'-H<sup>+</sup>** and aryl KAT **32'**. Relative free energies were calculated using the B3LYP/6-31g(d) basis set. Free energies are given in parentheses in kcal mol<sup>-1</sup>. Transition states are confirmed by intrinsic reaction coordinates analysis (IRC).

### 3.5 Determination of Activation Parameters

A series of  $^1\text{H-NMR}$  experiments of KAT **116** and hydroxylamine **117** were performed at variable temperature (10 – 70 °C) according to the previously developed standard kinetic method (cf. 2.4.1) While at pH 6.8 the reaction rates of **116** gradually increased with increasing temperature, the ligation kinetics of **119** remained unaltered. At lower pH (pH 5.1), however, reaction rates of **119** were observed to be temperature dependent. Similar to pyridyl KAT **116** enhanced reaction rates were detected for aryl KAT **119** at higher temperature. A possible explanation for this unexpected finding might be that at pH 6.8 KAT ligation rates of **119** ( $k_{\text{obs}} = 0.003 \text{ M}^{-1} \text{ s}^{-1}$ ) were not rapid enough to observe distinct rate changes. With measured rate constants of **116** and **119** at pH 5.1 in hand, the enthalpy of activation  $\Delta H^\ddagger$ , entropy of activation  $\Delta S^\ddagger$  and the Gibbs free energy  $\Delta G^\ddagger$  were calculated according to the Eyring equation. The obtained values are presented in Table 3.2. The  $\Delta G^\ddagger$  of **116** with a value of  $18.28 \text{ kcal mol}^{-1}$  was observed to be slightly lower than the  $\Delta G^\ddagger$  of **119** with a value of  $19.81 \text{ kcal mol}^{-1}$ . The energy difference  $\Delta\Delta G^\ddagger_1$  for the KAT ligation of pyridyl KAT **116** versus aryl KAT **119** at pH 5.1 was determined to be  $1.53 \text{ kcal mol}^{-1}$ , which is in good accordance with the observed 13-fold rate difference of pyridyl KAT **116** ( $k_{\text{obs}}$  of  $0.23 \text{ M}^{-1} \text{ s}^{-1}$ ) and aryl KAT **119** ( $k_{\text{obs}} = 0.017 \text{ M}^{-1} \text{ s}^{-1}$ ) at the same pH. This experimentally obtained

**Table 3.2** Variable temperature NMR Study of the KAT ligation at pH 5.1.



Substrate	$\Delta H^\ddagger$ (kcal mol $^{-1}$ )	$\Delta S^\ddagger$ (cal mol $^{-1}$ K $^{-1}$ )	$\Delta G^\ddagger$ (kcal mol $^{-1}$ )
<b>116</b>	7.35	-37	18.28
<b>119</b>	2.20	-59	19.81

KAT ligations were performed at variable temperature (10 – 70 °C) Ligation reactions were performed at equimolar concentrations (15 mM) of KAT and hydroxylamine in MeCN- $d_3$  / 0.1 M deuterated potassium phosphate buffer (2:1, pH 5.1) at 25 °C. Reaction kinetics were monitored  $^1\text{H-NMR}$  spectroscopy. Enthalpy of activation  $\Delta H^\ddagger$ , entropy of activation  $\Delta S^\ddagger$  and the Gibbs free energy  $\Delta G^\ddagger$  were calculated according to the Eyring equation.

$\Delta\Delta G^\ddagger$  value was further supported by DFT calculations ( $\Delta\Delta G^\ddagger_{\text{calc}} = 2.7 \text{ kcal mol}^{-1}$ ). In addition, it was noted that the entropy of activation  $\Delta S^\ddagger$  for the KAT ligation of both **116** and **119** were extremely large with values ranging from  $-37$  to  $-59 \text{ cal mol}^{-1} \text{ K}^{-1}$ . Moreover, DFT-calculations presented in this chapter propose that the breakdown of the tetrahedral intermediate proceeds via a concerted elimination. Overall, these findings indicate that there is a large entropic penalty involved in the concerted elimination of the tetrahedral intermediate (**137**, **138**). As previously described for rate-determining pre-equilibrium reactions, this can be accounted to the many geometrical constraints that are accompanied with a concerted elimination.<sup>156</sup> Furthermore, the reverse step of  $k_{-1}$  is entropically favored over  $k_2$ , rendering the latter step rate-determining. This finding is in good accordance to our previously presented numerical calculations (cf. Chapter 3.2) indicating that the second step of the KAT ligation, which involves the breakdown of the tetrahedral intermediate, is rate-determining ( $k_2 = 0.0036 \text{ s}^{-1}$ ).

### 3.6 The Important Role of Acid in KAT Ligation Kinetics

Variable pH kinetic studies showed that the reaction rates of the KAT ligation are significantly accelerated with decreasing pH levels (cf. Chapter 2.4.3), which led us to the conclusion that the presence of acid plays an essential role in the ligation process. In the following, we revealed that the KAT ligation proceeds via specific acid catalysis meaning that the ligation kinetics are significantly accelerated with an increasing number of protons present in the reaction mixture. We therefore envisioned to mimic this specific acid catalysis by introduction of a proton donor in close proximity to the KAT moiety enabling intramolecular proton transfer. By incorporation of an *ortho*-pyridyl nitrogen into the aryl backbone of a standard phenyl KAT we uncovered 2-pyridyl KATs as a novel class of potassium acyltrifluoroborates with significantly enhanced ligation kinetics. Experimental and computational studies showed that the pyridyl nitrogen of 2-pyridyl KAT **116** can rapidly be protonated during the ligation process. Furthermore, it was found that this protonated pyridyl KAT **116'**- $\text{H}^+$  indeed facilitates product formation by intramolecular proton transfer via a different, lower energy transition state **137'-TS-1** in comparison to non-protonated pyridyl KAT **116'** and standard aryl KAT **119'**. It is important to note that there is no fundamental change in mechanism involved in this rate enhancement. The Lewis-basic pyridyl nitrogen simply acts as a proton sponge which brings the protons from the acidic environment in close proximity to the KAT substrate.

Consequently, at elevated pH the proportion of protonated pyridyl KAT is larger compared to protonated aryl KAT ultimately resulting in faster ligation kinetics.

### 3.7 Concluding Remarks

In this chapter we performed systematic mechanistic and computational studies of the KAT ligation with aryl and pyridyl KATs. Detailed analysis of the reaction profile by *in situ*  $^1\text{H-NMR}$  spectroscopy showed that the KAT ligation proceeds via a rate-determining pre-equilibrium in lieu of following standard second-order kinetics. The rate determining step of the ligation reaction was evaluated to be the breakdown of the tetrahedral intermediate with an individual rate constant  $k_2$  of  $0.0036\text{ s}^{-1}$ . Experimental and computational analysis of the KAT ligation process, including variable-temperature kinetic studies, high-resolution mass analysis of reaction intermediates and DFT transition state calculations provided additional in-depth mechanistic insight. As a result, we postulate that the ligation mechanism proceeds via nucleophilic attack of the hydroxylamine to the carbonyl carbon of the KAT resulting in a tetrahedral intermediate, which was observed at low concentrations by real-time NMR spectroscopy during the course of the ligation process. Concerted elimination of the tetrahedral intermediate further leads to a *N*-trifluoroboryl species, which is short-lived and rapidly collapses to the desired amide product. To our delight, the newly proposed *N*-trifluoroboryl species was confirmed by elaborate HR-MS and HR-MS/MS analysis of the KAT ligation between 2-pyridyl KAT **116** and hydroxylamine **117**. Furthermore, it was found that protonated-pyridyl KAT **116'-H<sup>+</sup>** displays additional stabilization effects during the KAT ligation reaction compared to aryl KAT. This additional stabilization effect arises due to hydrogen bond formation between protonated pyridyl nitrogen and the carbonyl of the carbamoyl moiety ( $1.62\text{ \AA}$ ) with a relative free energy value of  $9.8\text{ kcal mol}^{-1}$ . This implies that the carbonyl oxygen of the carbamoyl group is properly aligned with the protonated pyridyl nitrogen to enable proton transfer. Overall, these findings underline our hypothesis that the pyridyl nitrogen is able to act as a proton acceptor/donor pair via hydrogen-bonding during the course of the KAT ligation reaction, therefore significantly accelerating the reaction rates of pyridyl KATs in comparison to aryl KATs. This advanced mechanistic understanding paves the way for further structural fine-tuning of acyltrifluoroborates, which might lead to even faster reaction rates (*cf.* Chapter 5).

### 3.8 References

- [146] Frisch, M. J.; Trucks, G. W.; Schlegel, H. B.; Scuseria, G. E.; Robb, M. A.; Cheeseman, J. R.; Scalmani, G.; Barone, V.; Mennucci, B.; Petersson, G. A.; Nakatsuji, H.; Caricato, M.; Li, X.; Hratchian, H. P.; Izmaylov, A. F.; Bloino, J.; Zheng, G.; Sonnenberg, J. L.; Hada, M.; Ehara, M.; Toyota, K.; Fukuda, R.; Hasegawa, J.; Ishida, M.; Nakajima, T.; Honda, Y.; Kitao, O.; Nakai, H.; Vreven, T.; Montgomery, J. A.; Peralta, Jr., J. E.; Ogliaro, F.; Bearpark, M.; Heyd, J. J.; Brothers, E.; Kudin, K. N.; Staroverov, V. N.; Kobayashi, R.; Normand, J.; Raghavachari, K.; Rendell, A.; Burant, J. C.; Iyengar, S. S.; Tomasi, J.; Cossi, M.; Rega, N.; Millam, J. M.; Klene, M.; Knox, J. E.; Cross, J. B.; Bakken, V.; Adamo, C.; Jaramillo, J.; Gomperts, R.; Stratmann, R. E.; Yazyev, O.; Austin, A. J.; Cammi, R.; Pomelli, C.; Ochterski, J. W.; Martin, R. L.; Morokuma, K.; Zakrzewski, V. G.; Voth, G. A.; Salvador, P.; Dannenberg, J. J.; Dapprich, S.; Daniels, A. D.; Farkas, Ö.; Foresman, J. B.; Ortiz, J. V.; Cioslowski, J.; Fox, D. J. *Gaussian*, Inc., Wallingford CT, **2009**.
- [147] Hehre, W. J.; Ditchfield, R.; Pople, J. A. Self—Consistent Molecular Orbital Methods. XII. Further Extensions of Gaussian—Type Basis Sets for Use in Molecular Orbital Studies of Organic Molecules. *J. Chem. Phys.* **1972**, *56*, 2257–2261.
- [148] Stephens, P. J.; Devlin, F. J.; Chabalowski, C. F.; Frisch, M. J. Ab Initio Calculation of Vibrational Absorption and Circular Dichroism Spectra Using Density Functional Force Fields. *J. Phys. Chem.* **1994**, *98*, 11623–11627
- [149] Fukui, K. The Path of Chemical Reactions - The IRC Approach. *Acc. Chem. Res.*, **1981**, *14*, 363–368.
- [150] Krishnan, R.; Binkley, J. S.; Seeger, R.; Pople, J. A. Selfconsistent Molecular Orbital Methods. XX. A Basis Set for Correlated Wave Functions. *J. Chem. Phys.* **1980**, *72*, 650–654.
- [151] McLean, A. D.; Chandler, G. S. Contracted Gaussian Basis Sets for Molecular Calculations. I. Second Row Atoms, Z=11–18. *J. Chem. Phys.* **1980**, *72*, 5639–5648.

- [152] Zhao, Y.; Truhlar, D. G. The M06 Suite of Density Functionals for Main Group Thermochemistry, Thermochemical Kinetics, Noncovalent Interactions, Excited States, and Transition Elements: Two New Functionals and Systematic Testing of Four M06-Class Functionals and 12 Other Functionals. *Theoretical Chemistry Accounts* **2008**, *120*, 215–241.
- [153] Miertuš, S.; Scrocco, E.; Tomasi, J. Electrostatic Interaction of a Solute with a Continuum. A Direct Utilizaion of AB Initio Molecular potentials for the prevision of solvent effects. *Chemical Physics* **1981**, *55*, 117–129.
- [154] Miertuš, S.; Tomasi, J. Approximate Evaluations of the Electrostatic Free Energy and Internal Energy Changes in Solution Processes. *Chemical Physics* **1982**, *65*, 239–245.
- [155] CYLview, 1.0b; Legault, C. Y., Université de Sherbrooke, **2009**, (<http://www.cylview.org>)
- [156] Revell, L. E.; Williamson B. E. Why Are Some Reactions Slower at Higher Temperatures?. *J. Chem. Educ.* **2013**, *90*, 1024–1027.







# ***Chapter 4***

---

## ***Application of Pyridyl KATs in Radiolabeling***

---

The radiolabeling experiments were performed by Dr. Thomas Betzel, Dr. Aristeidis Chiotellis and Hazem Ahmed under the supervision of Prof. Simon M. Ametamey at the Center of Radiopharmaceutical Sciences at ETH Zurich. The model peptide and sf-GFP were prepared by Dr. Christopher J. White and Tz-Li Chen.



## 4 Application of Pyridyl KATs in Radiolabeling

### 4.1 Introduction

#### 4.1.1 General Remarks

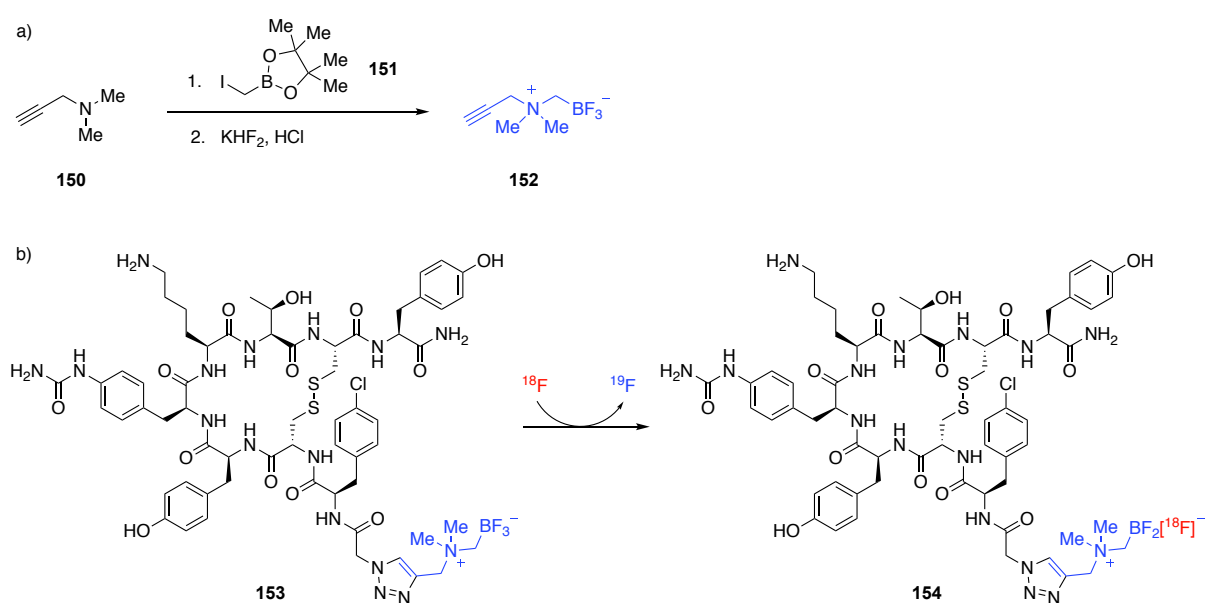
In modern medicine and research, non-invasive high resolution imaging techniques are amongst the most important diagnostic tools developed. While various imaging techniques have been already established in the 19<sup>th</sup> century, such as radiography with X-ray beams or sonography, it was only in the 1970s, when the successful journey of positron emission tomography (PET) and magnetic resonance imaging (MRI) began.<sup>157,158</sup> Importantly, in the last 20 years, MRI and PET have emerged as one of the most crucial diagnostic methods for the detection of various diseases such as cancer, Alzheimer's, multiple sclerosis and many more. A probable reason for the success of these two techniques lies in the significant advantages over other methods of diagnosis known in the state of the art. First, in contrast to many other techniques, both MRI and PET readily allow to not only take a single image, but to take various high resolution cross sections of the human organism. Therefore, physicians and researchers are able to investigate the topological structure of organs, tissue or bones in a non-invasive manner. Second, due to the vast technical advances in recent years, MRI and PET enable the recording of extremely high resolved images, such that even small alterations of organs can be visualized. Third, MRI employs radiation in the radiofrequency and does therefore not provide any harmful radiation exposure to the patient. Even though PET relies on radioactive decay processes, only a minute quantity of weakly radiant substances is employed. In addition, the physical half-life of these substances is usually short, i.e. in the range of minutes to days.<sup>159</sup> Furthermore, PET is especially useful for the discovery of tumors and metastases, as it exploits the significantly different metabolism of cancer cells as compared to healthy cells.

#### 4.1.2 Positron Emission Tomography

The positron emission tomography relies on a nuclear physical process.<sup>160</sup> At first, a radiopharmaceutical that is able to emit positrons, i.e.  $\beta^+$  rays is injected into the patient's blood system. A typical substance employed is radiolabeled glucose, for example a modified glucose molecule containing a radioactive fluoride group ( $^{18}\text{F}$ ). If a positron collides with an electron of the patient's organism, two high energy  $\gamma$  rays are emitted in opposite directions,

i.e. in an angle of  $180^\circ$  to each other, which are detected by one of the annular detectors of the PET device. A series of cross sectional images is then calculated based on the temporal and spatial distribution of the radioactive decay processes of the radioactive substance in the organism.

The most prominent nuclide is the fluorine isotope  $^{18}\text{F}$  with a physical half-life of almost two hours (109.8 min).<sup>161</sup> While this process is attractive due to the above mentioned advantages, the relatively short half-life time of the employed nuclides represents a major challenge, as the  $^{18}\text{F}$  nuclide first has to be prepared and introduced into a carrier substance, such as glucose. Therefore, chemical reactions for the introduction of  $^{18}\text{F}$  into such a carrier molecule need to possess relatively fast reaction rates. Otherwise, most of the  $^{18}\text{F}$  will already be decayed before it would even be delivered to the patient. As a consequence, various research groups focused on the development of late stage  $^{18}\text{F}$  fluorination techniques of suitable carrier molecules.<sup>162</sup> In 2014, PERRIN and co-workers published innovative zwitterionic organotrifluoroborate radiosynthons (AMBF<sub>3</sub>), which were successfully used in the bioconjugation to various clinically relevant peptides and a single example of a peptide inhibitor.<sup>163</sup> After formation of the complex peptide and enzyme bioconjugates using the radiosynthons, facile  $^{18}\text{F}$ -labeling was performed in a single step under aqueous conditions in <15 min via  $^{18}\text{F}$ - $^{19}\text{F}$  isotope exchange (IEX). Tracers were afforded without HPLC purification in good yields (20–40%) at high molar activity ( $\geq 3$  Ci/ $\mu\text{mol}$ ) and with a radiochemical purity of >98%. Subsequent PET imaging studies displayed good *in vivo* stability and tumor uptake.

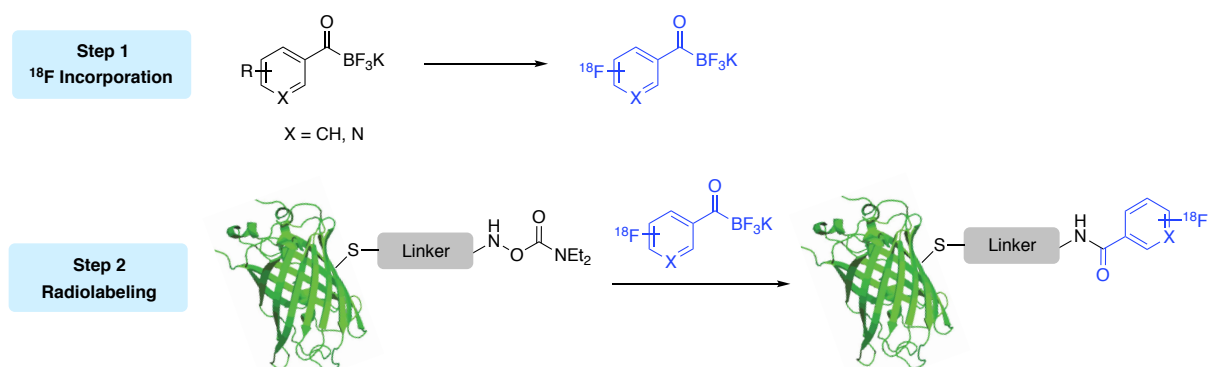


**Scheme 4.1** a) Synthesis of organotrifluoroborate radiosynthon (AMBF<sub>3</sub>). b)  $^{18}\text{F}$ -Radiolabeling of an AMBF<sub>3</sub>-LM3 bioconjugate via  $^{18}\text{F}$ - $^{19}\text{F}$  isotope exchange.

## 4.2 Project Goal and Rationale

Even though numerous strategies have been developed for the rapid introduction of  $^{18}\text{F}$  into small organic molecules, reliable methods for selective introduction of this nuclide into large biomolecules such as proteins and peptide are rare.<sup>164,165,166</sup> The biggest challenge for the development of such a method is the vast amount of unprotected functional groups present in biomolecules. Furthermore, the choice of suitable reaction conditions is extremely limited, as biological targets are sensitive towards increased temperatures and unfortunately to many organic reagents and organic solvents.

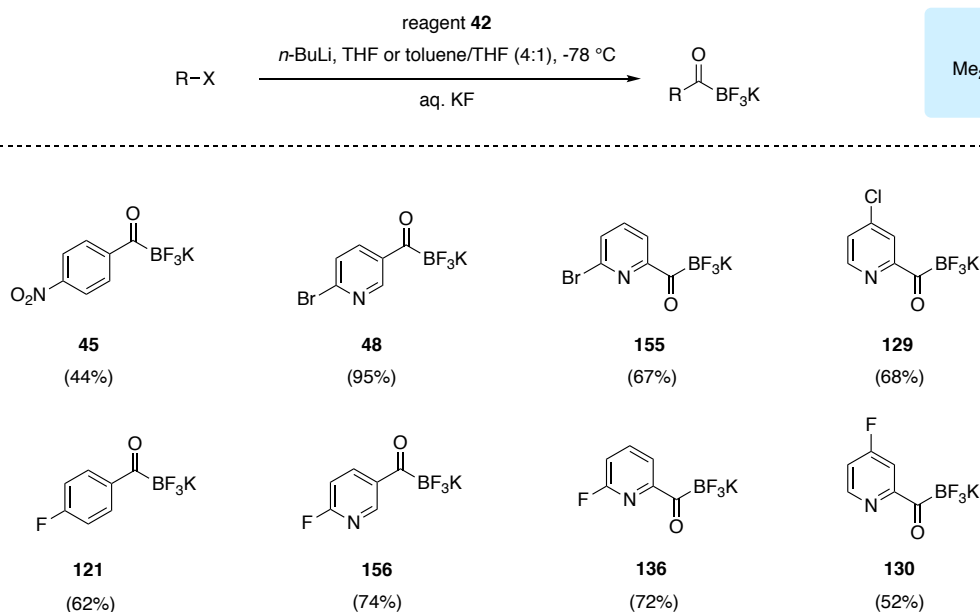
As such robust methodologies for the non-invasive study of large biomolecules in the mammalian body are highly desirable. To expand the scope of current indirect radiolabeling methodologies, we aimed to develop a novel radiofluorination strategy based on the KAT ligation (*cf.* Chapter 2). The KAT ligation was selected as it proceeds under mild reaction conditions without the need of toxic reagents or additional catalysts and has previously been shown to be compatible with biological environments.<sup>118,135</sup> Most importantly, the KAT ligation displays fast reaction kinetics under acidic conditions and moderate kinetics near neutral pH. Hence, we envisioned a two-step strategy for the  $^{18}\text{F}$  incorporation into biomolecules (Scheme 4.2). In a first step, the  $^{18}\text{F}$  radioisotope would be incorporated into the KAT backbone. In a subsequent second step,  $^{18}\text{F}$ -labeling of biomolecules was envisaged by ligating the resulting  $^{18}\text{F}$ -labeled KAT to a biomolecule of interest equipped with a hydroxylamine functionality using KAT ligation. Consequently, this approach does not require the development of a suitable biocompatible fluorination method and can thus rely on established, non-biocompatible nuclide introduction reactions for small molecules.



**Scheme 4.2** Attempted strategy for the  $^{18}\text{F}$ -labeling of proteins using KAT ligation.

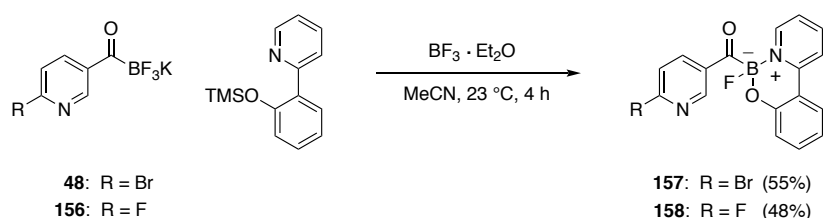
### 4.3 Synthesis of KATs for Radiolabeling

The synthesis of KAT precursors for radiolabeling was achieved by a previously established procedure of the BODE group or a slightly modified version.<sup>123</sup> The panel of synthesized KATs for radiolabeling is shown in Scheme 4.3. Beside the KAT precursors also the <sup>19</sup>F-substituted cold labeling products were prepared.



**Scheme 4.3** Synthesis of KAT precursors for <sup>18</sup>F-radiolabeling.

In addition to potassium acyltrifluorates also a potassium monofluoroborate precursor was synthesized according to a previously reported procedure by BODE and coworkers (Scheme 4.4).<sup>139</sup>

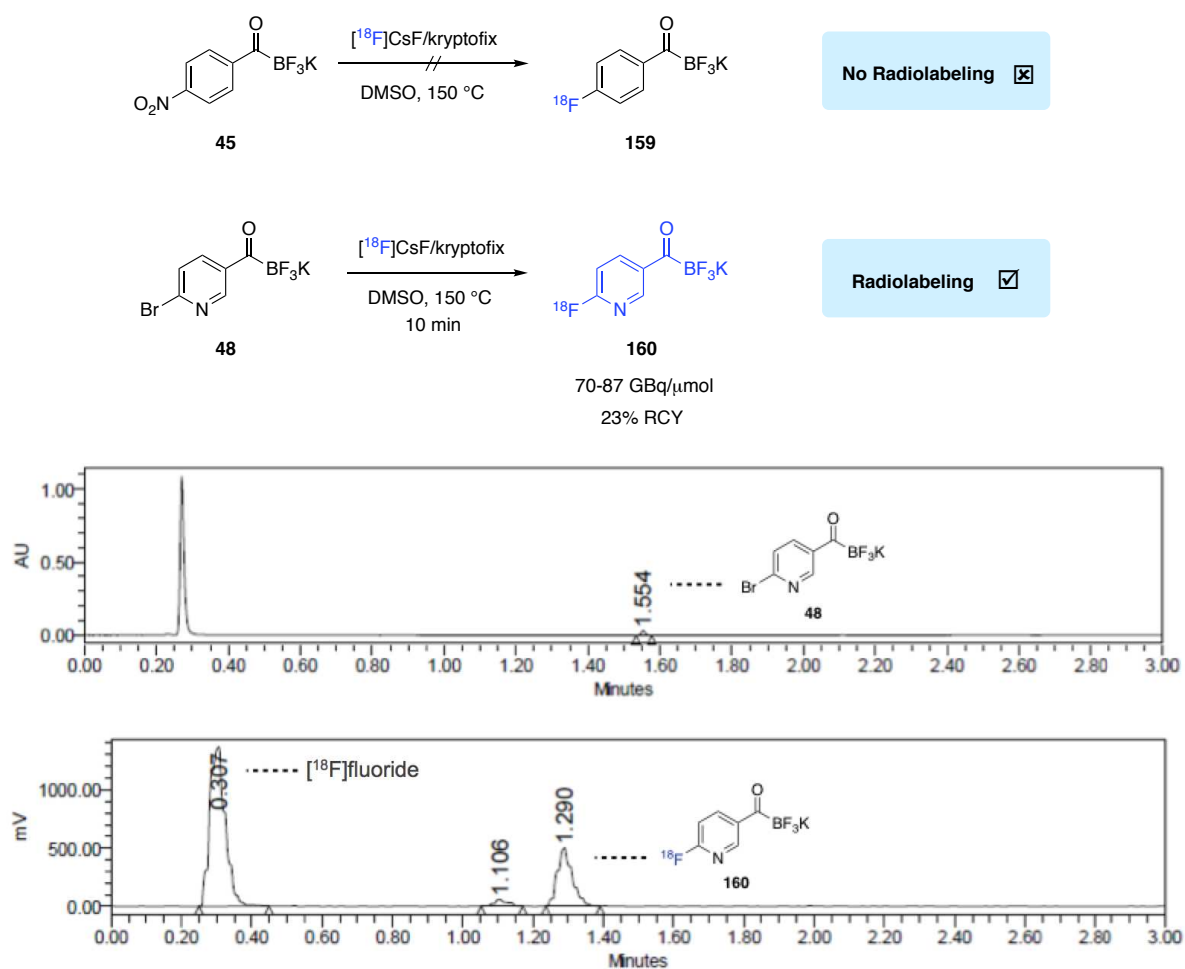


**Scheme 4.4** Synthesis of potassium monofluoroborate precursors for <sup>18</sup>F-radiolabeling.



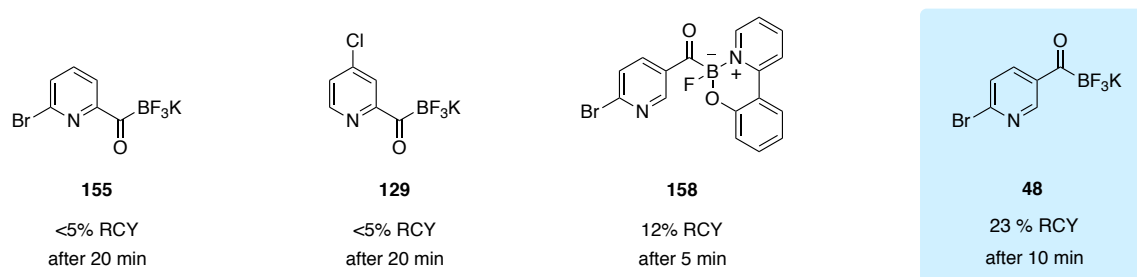
#### 4.4 Radiolabeling of KATs

In a preliminary study, the incorporation of fluorine-18 into different KATs species was investigated. While 4-nitrophenyl KAT **45** did not show any incorporation of fluorine-18, the more electron-deficient potassium 6-bromonicotinyltrifluoroborate (**48**) was identified as suitable candidate for radiolabeling. Rapid introduction of fluorine-18 into 6-bromonicotinyltrifluoroborate (**48**) was achieved in a single step by nucleophilic aromatic substitution using  $[^{18}\text{F}]\text{CsF}/\text{kryptofix}$  at 150 °C within only 10 minutes (Scheme 4.5). 6- $[^{18}\text{F}]$ fluoro-nicotinyltrifluoroborate **160** was obtained in  $23 \pm 3\%$  isolated radiochemical yield (RCY) with a radiochemical purity of  $>95\%$  and a molar activity of 70-87 GBq/ $\mu\text{mol}$ . The experiments were repeated at least twice for validation of the results. Yields and purity were determined by UPLC and purification of **160** was accomplished by semi-preparative HPLC (Scheme 4.5).<sup>167</sup> Importantly, it should be noted that no fluorine-18 incorporation into the KAT moiety was observed.



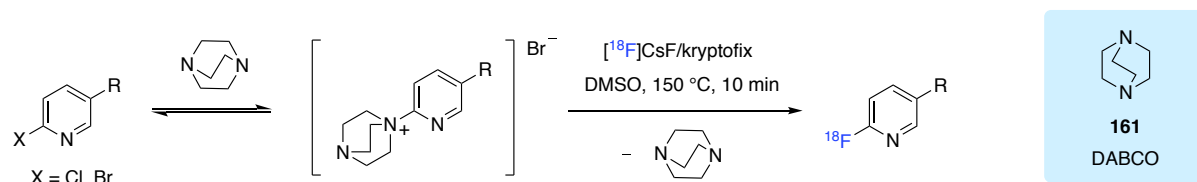
**Scheme 4.5** a)  $^{18}\text{F}$ -Labeling of aryl and aryl KATs via nucleophilic aromatic substitution. B) UPLC analysis of  $^{18}\text{F}$ -radiolabeling of potassium 6-bromonicotinyltrifluoroborate precursor **48**.

In a next step,  $^{18}\text{F}$ -labeling of alternative pyridyl acylboronate precursors was investigated according to the same procedure as described above (Scheme 4.6). In comparison to potassium 6-bromonicotinoyltrifluoroborate (**48**), 2-pyridyl KAT precursors **155** and **129** showed significantly decreased fluorine-18 incorporation with radiochemical yields of <5% after 20 min. Slightly better results, with fluorine-18 incorporation of 12%, were observed in the  $^{18}\text{F}$ -labeling of monofluoroboronate **158**. Nonetheless, all presented pyridyl acylborate precursors did not reach the isolated radiochemical yield of 23% observed for **48**.



**Scheme 4.6** Comparison of  $^{18}\text{F}$ -labeling of different KAT species.

In an effort to increase the radiochemical yields the use of additives was envisioned. In a recent report by PIKE and coworkers, cyclic tertiary amines, such as 1,4-diazabicyclo[2.2.2]octane (**161**) and quinuclidine, were discovered as effective additives for increased radiofluorination conversions of 5-substituted 2-halopyridines by more than 15%.<sup>168</sup> It was shown that these cyclic tertiary amines activate the substrates toward nucleophilic substitution via reversible formation of quaternary ammonium intermediates (Scheme 4.7).

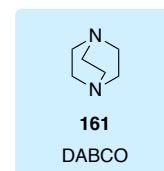
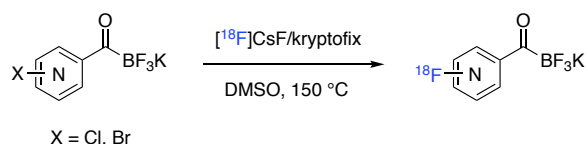


**Scheme 4.7** Proposed activating effect of tertiary amine bases, such as DABCO (**161**), in  $^{18}\text{F}$ -radiolabeling.

To our delight, addition of DABCO (**161**) resulted in increased radiolabeling conversions of previously tested precursors (Table 4.1). For bromopyridyl precursors **48** and **155** the isolated radiochemical yields significantly increased by up to 50-70%. In contrast, chloropyridyl precursor **129** showed only marginally improved fluorine-18 incorporation by 3-

5%. Addition of larger amounts of additive **161**, 200 mM instead of 140 mM, either impeded the reaction completely or reduced the radiochemical yields.

**Table 4.1** Addition of additives in the  $^{18}\text{F}$ -radiolabeling of KATs.



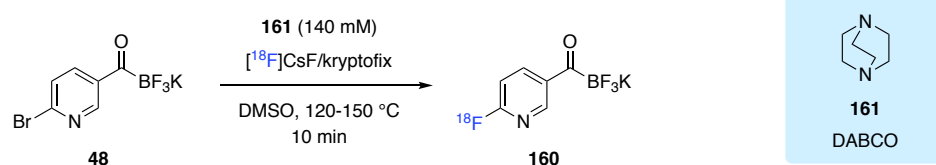
Entry	Precursor	Structure	Additive <sup>[a]</sup>	Reaction Time (min)	RCY (%) <sup>[b]</sup>
1	<b>48</b>		—	10	23
2	<b>48</b>		<b>161</b>	10	96
3	<b>155</b>		—	20	<5
4	<b>155</b>		<b>161</b>	20	54
5	<b>129</b>		—	20	<5
6	<b>129</b>		<b>161</b>	20	8

$^{18}\text{F}$ -Radiochemical labeling was performed with 1.0-1.5 mg precursor at 150 °C within 10-20 minutes. Excess of DABCO **161** (140 mM) was added. Each experiment was repeated at least twice. [b] Isolated radiochemical yields (RCY) are given as an average of three or more labeling experiments.

Potassium 6-bromonicotinoyltrifluoroborate (**48**) provided the highest isolated radiochemical yields of 96% under the improved reaction conditions using DABCO (**161**) as additive. As a result, **48** was selected for further radiolabeling studies. In the following, optimization of reaction parameters, such as fluoride salt, temperature and azeotropic drying, was performed (Table 4.2). In a first step, the fluoride salt  $^{18}\text{F}$ CsF was replaced with  $^{18}\text{F}$ TBAF in the hope that the higher solubility of  $^{18}\text{F}$ TBAF in DMSO would lead to improved radiochemical yields. Contrary to this expectation, labeling experiments with  $^{18}\text{F}$ TBAF as a

fluoride salt were found to be similar, if not slightly lower, in radiochemical yields compared to  $[^{18}\text{F}]\text{CsF}$ . In addition, it was shown that reduced temperatures from 150 °C to 120 °C in the radiolabelling experiments with either  $[^{18}\text{F}]\text{CsF}$  or  $[^{18}\text{F}]\text{TBAF}$  have almost no influence in radiochemical conversion. Further, it was discovered that with addition of DABCO (**161**) as an additive azeotropic drying with MeCN is not absolutely necessary in the  $^{18}\text{F}$ -labeling of pyridyl KAT **48**.

**Table 4.2** Optimization of radiofluorination parameters.

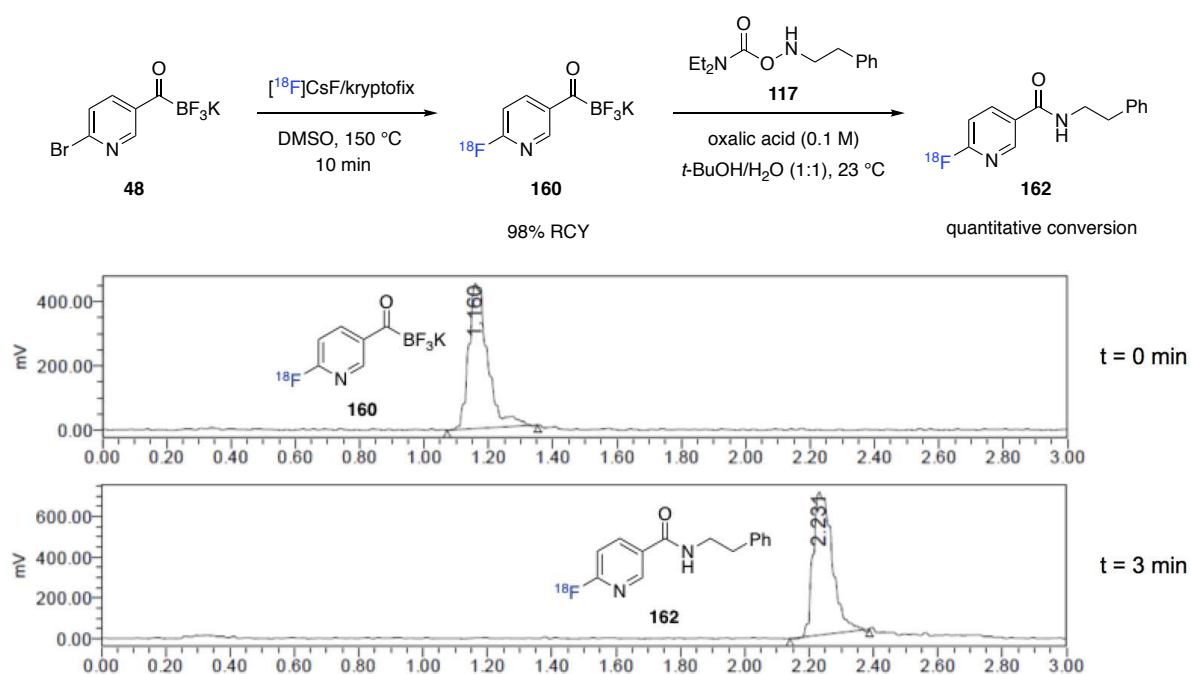


Entry	Precursor	Fluoride Salt	Temperature (°C)	Azeotropic Drying	RCY (%) <sup>[b]</sup>
1	<b>48</b>	$[^{18}\text{F}]\text{CsF}$	150	Yes	98
2	<b>48</b>	$[^{18}\text{F}]\text{CsF}$	120	Yes	95
3	<b>48</b>	$[^{18}\text{F}]\text{CsF}$	150	No	90
4	<b>48</b>	$[^{18}\text{F}]\text{TBAF}$	150	Yes	91
5	<b>48</b>	$[^{18}\text{F}]\text{TBAF}$	120	Yes	92
6	<b>48</b>	$[^{18}\text{F}]\text{TBAF}$	120	No	95

$^{18}\text{F}$ -Radiochemical labeling was performed with 1.0-1.2 mg precursor at 120 °C or 150 °C within 10 minutes. Excess of DABCO **161** (140 mM) was added. Each experiment was repeated at least once. [b] Isolated radiochemical yields (RCY) are given as an average of labeling experiments performed.

#### 4.5 KAT Ligation Using Radiolabeled Pyridyl KATs

In a subsequent investigation, it was examined if  $^{18}\text{F}$ -labeled potassium 6-bromonicotinoyltrifluoroborate (**160**) undergoes KAT ligation reaction with hydroxylamines. After incorporation of fluorine-18 and purification of the radiolabeled product **160** via semi-preparative HPLC, the HPLC solvent was rapidly evaporated at 90 °C for 10 min. The KAT ligation reaction was carried out by redissolving the residue in a mixture of *t*-BuOH/H<sub>2</sub>O 0.1 M oxalic acid (1:1) and addition of hydroxylamine **117**. The ligation reaction was monitored by UPLC at room temperature. At a hydroxylamine concentration of 1 mM the ligation reaction proceeded extremely fast and full conversion to ligation product **162** was observed after 3 minutes (Scheme 4.8).

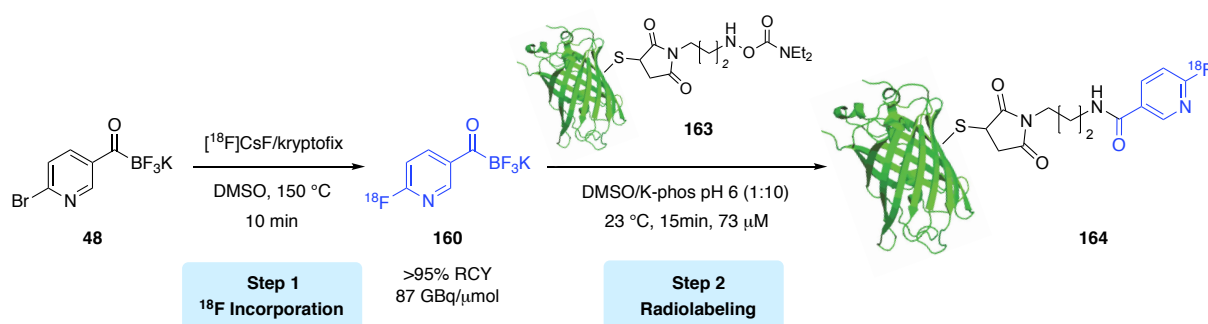


**Scheme 4.8** KAT ligation between  $^{18}\text{F}$ -labeled pyridyl KAT **160** and 0.1 mM hydroxylamine **117** at room temperature. Full conversion to the ligation product **162** was detected after 3 minutes.

The KAT ligation reaction was found to be concentration-dependent. Lower concentrations of hydroxylamine **117** (0.01 mM instead of 1 mM) resulted in slower ligation kinetics at room temperature. Nevertheless, full conversion of  $^{18}\text{F}$ -labeled pyridyl KAT **160** to amide product **162** was observed after 30 minutes. Noteworthy, the KAT ligation between  $^{18}\text{F}$ -labeled potassium 6-bromonicotinoyltrifluoroborate (**160**) and hydroxylamine **117** was also shown to proceed at room temperature in rat plasma.

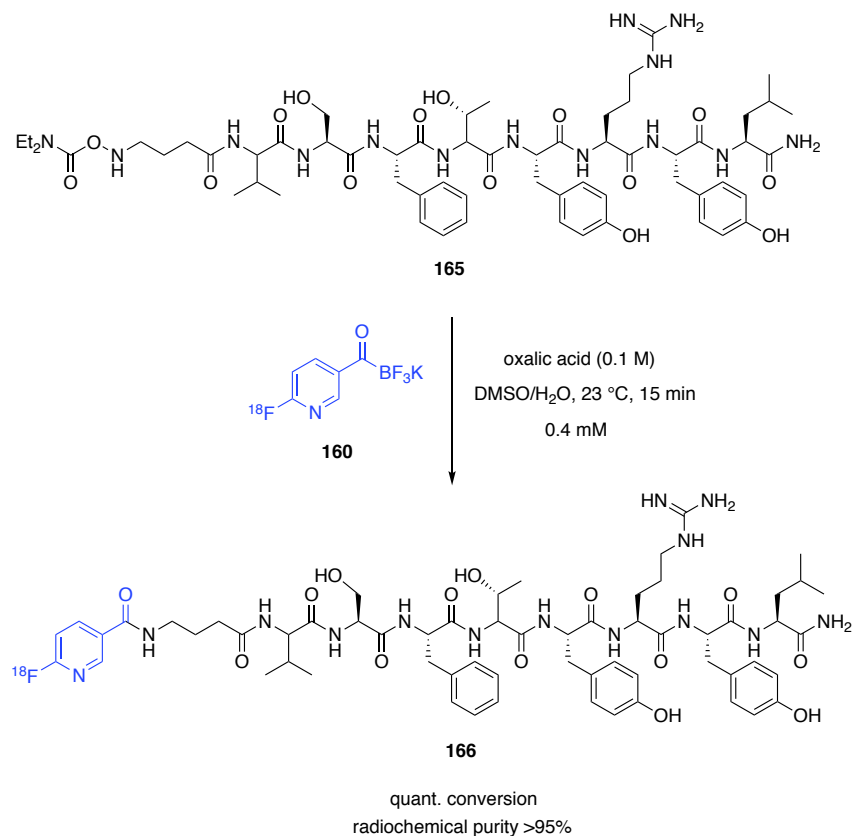
#### 4.6 Incorporation of Labeled Pyridyl KATs into Peptides and Proteins

As  $^{18}\text{F}$ -labeled KATs were shown to undergo rapid KAT ligation reaction with hydroxylamines (*cf.* Chapter 4.4), we attempted to exploit this unique bioorthogonal reactivity for the incorporation of  $^{18}\text{F}$ -labeled labeled potassium 6-bromonicotinoyltrifluoroborate (**160**) into peptides and proteins. A chemically modified superfolder green fluorescent protein (sfGFP) bearing a surface-exposed hydroxylamine was selected as a suitable target for  $^{18}\text{F}$ -labeling (Scheme 4.9). In an initial step, the  $^{18}\text{F}$ -labeled pyridyl species **160** was generated according to the previously described method (*cf.* Chapter 4.4). In a second step, the  $^{18}\text{F}$ -labeled pyridyl KAT **160** was incorporated into sfGFP **163** via KAT ligation with the surface exposed hydroxylamine moiety. It was found that a protein concentration of 73  $\mu\text{M}$  was required for quantitative conversion to  $^{18}\text{F}$ -labeled sfGFP **164** at room temperature within a reaction time of only 15 minutes.



**Scheme 4.9** Radiolabeling of chemically modified sfGFP **163** with  $^{18}\text{F}$ -labeled pyridyl KAT **160** by KAT ligation at room temperature.

In a similar fashion,  $^{18}\text{F}$ -labeling of model peptide **165** was achieved. A concentration of 0.4 mM of peptide **165** was required for quantitative conversion to  $^{18}\text{F}$ -labeled peptide **166** at room temperature within 15 minutes. To our delight,  $^{18}\text{F}$ -labeled peptide **166** was obtained in good radiochemical purity of >95% (Scheme 4.10).



**Scheme 4.10** Incorporation of fluorine-18 into model peptide **165** with  $^{18}\text{F}$ -labeled pyridyl KAT **160** by KAT ligation at room temperature.

#### 4.7 Concluding Remarks

Due to their increased ligation kinetics and superior electronic properties pyridyl KATs were found to be suitable candidates for radiolabeling. Rapid introduction of  $^{18}\text{F}$  into 6-fluoro-nicotinoyltrifluoroborate was achieved in a single step by nucleophilic aromatic substitution with  $[^{18}\text{F}]\text{CsF}/\text{kryptofix}$  at 150 °C within 10 minutes in good radiochemical purity of >95%. Radiochemical yields were significantly increased by addition of DABCO as a tertiary amine additive. Furthermore, it was shown that  $^{18}\text{F}$ -labeled 6-fluoro-nicotinoyltrifluoroborate is prone to undergo KAT ligation reactions with hydroxylamines in acidic aqueous media or rat plasma at room temperature. As a result,  $^{18}\text{F}$ -labeling of larger molecules, such as a model peptide and superfolder green fluorescent protein (sfGFP) bearing hydroxylamines was achieved by exploiting the unique reactivity of  $^{18}\text{F}$ -labeled 6-fluoro-nicotinoyltrifluoroborate.

## 4.8 References

- [157] Rich, D. A. A Brief History of Positron Emission Tomography. *Journal of Nuclear Medicine Technology* **1997**, *25*, 4–11.
- [158] Lauterbur, P. C. Image Formation by Induced Local Interactions: Examples Employing Nuclear Magnetic Resonance. *Nature*. **1973**, *242*, 190–191.
- [159] Jacobson, O.; Chen, X. PET Designated Fluoride-18 Production and Chemistry. *Curr. Top. Med. Chem.* **2010**, *10*, 1048–1059.
- [160] Bailey, D. L.; Townsend, D. W.; Valk, P.E; Maisey M. N. Positron Emission Tomography: Basic Science. Springer-Verlag Secaucus, NJ, USA, **2005**.
- [161] Tressaud, A.; Haufe, G. Fluorine and Health: Molecular Imaging, Biomedical Materials and Pharmaceuticals. Elsevier Science, Amsterdam, NLC, **2008**.
- [162] Jacobson, O.; Kiesewetter, D. O.; Chen, X. Fluorine-18 Radiochemistry, Labeling Strategies and Synthetic Routes. *Bioconjugate Chem.* **2015**, *26*, 1–18.
- [163] Liu, Z.; Pourghiasian, M.; Radtke, M. A.; Lau, J.; Pan, J.; Dias, G. M.; Yapp, D.; Lin, K.-S.; Bénard, F.; Perrin, D. M. *Angew. Chem. Int. Ed.* **2014**, *53*, 334. 11876–11880.
- [164] For selected examples of direct radiolabeling of biomolecules see: a) Becaud, J.; Mu, L.; Karamkam, M.; Schubiger, P. A.; Ametamey, S. M.; Graham, K.; Stellfeld, T.; Lehmann, L.; Borkowski, S.; Berndorff, D.; Dinkelborg, L.; Srinivasan, A.; Smits, R.; Kokschi, B. Direct One-Step <sup>18</sup>F-Labeling of Peptides via Nucleophilic Aromatic Substitution. *Bioconjugate Chem.* **2009**, *20*, 2254–2261. b) Hazari, P. P.; Schulz, J.; Vimont, D.; Chadha, N.; Allard, M.; Szlosek-Pinaud, M.; Fouquet, E.; Mishra, A. K. A New SiF-Dipropargyl Glycerol Scaffold as a Versatile Prosthetic Group to Design Dimeric Radioligands: Synthesis of the [(<sup>18</sup>F)BMPPSiF] Tracer to Image Serotonin Receptors. *ChemMedChem* **2014**, *9*, 337–349. c) Li, Y.; Liu, Z.; Lozada, J.; Wong, M.



- Q.; Lin, K. S.; Yapp, D.; Perrin, D. M. Single Step  $^{18}\text{F}$ -Labeling of Dimeric CycloRGD for Functional PET Imaging of Tumors in Mice. *Nucl. Med. Biol.* **2013**, *40*, 959–966.
- [165] For selected examples of indirect radiolabeling of biomolecules via the use of prosthetic groups see: a) Dialer, L. O.; Selivanova, S. V.; Muller, C. J.; Muller, A.; Stellfeld, T.; Graham, K.; Dinkelborg, L. M.; Kramer, S. D.; Schibli, R.; Reiher, M.; Ametamey, S. M. Studies Toward the Development of New Silicon-Containing Building Blocks for the Direct ( $^{18}\text{F}$ )-Labeling of Peptides. *J. Med. Chem.* **2013**, *56*, 7552–7563. b) Gao, Z.; Gouverneur, V.; Davis, B. G. Enhanced Aqueous Suzuki–Miyaura Coupling Allows Site-Specific Polypeptide  $^{18}\text{F}$ -Labeling. *J. Am. Chem. Soc.* **2013**, *135*, 13612–13615. c) Kiesewetter, D. O.; Jacobson, O.; Lang, L.; Chen, X. Automated Radiochemical Synthesis of [ $^{18}\text{F}$ ]FBEM: A Thiol Reactive Synthon for Radiofluorination of Peptides and Proteins. *Appl. Radiat. Isot.* **2011**, *69*, 410–414.
- [166] For selected examples of indirect radiolabeling of biomolecules via the use of bioorthogonal ligation reactions see: a) Ramenda, T.; Steinbach, J.; Wuest, F. 4- [ $^{18}\text{F}$ ]Fluoro-*N*-methyl-*N*-(propyl-2-yn-1-yl)benzenesulfonamide ([ $^{18}\text{F}$ ]F-SA): A Versatile Building Block for Labeling of Peptides, Proteins and Oligonucleotides with Fluorine-18 via Cu(I)-Mediated Click Chemistry. *Amino Acids* **2013**, *44*, 1167–1180. b) Carpenter, R. D.; Hausner, S. H.; Sutcliffe, J. L. Copper-Free Click for PET: Rapid 1,3-Dipolar Cycloadditions with a Fluorine-18 Cyclooctyne. *ACS Med. Chem. Lett.* **2011**, *2*, 885–889. c) Sachin, K.; Jadhav, V. H.; Kim, E. M.; Kim, H. L.; Lee, S. B.; Jeong, H. J.; Lim, S. T.; Sohn, M. H.; Kim, D. W. F-18 Labeling Protocol of Peptides Based on Chemically Orthogonal Strain-Promoted Cycloaddition under Physiologically Friendly Reaction Conditions. *Bioconjugate Chem.* **2012**, *23*, 1680–1686. d) Pretze, M.; Wuest, F.; Peppel, T.; Köckerling, M.; Mamat, C. The Traceless Staudinger Ligation with Fluorine-18: A Novel and Versatile Labeling Technique for the Synthesis of PET-Radiotracers. *Tetrahedron Lett.* **2010**, *51*, 6410–6414. e) Li, Z.; Cai, H.; Hassink, M.; Blackman, M. L.; Brown, R. C.; Conti, P. S.; Fox, J. M. Tetrazine-*trans*-Cyclooctene Ligation for the Rapid Construction of  $^{18}\text{F}$  Labeled Probes. *Chem. Commun.* **2010**, *46*, 8043–8045. f) Liu, S., Hassink, M.,

- Selvaraj, R.; Yap, L. P.; Park, R.; Wang, H.; Chen, X.; Fox, J. M.; Li, Z.; Conti, P. S. Efficient <sup>18</sup>F Labeling of Cysteine-Containing Peptides and Proteins Using Tetrazine-*trans*-Cyclooctene Ligation. *Mol. Imaging* **2013**, *12*, 121–128.
- [167] Chiotellis, A.; Betzel, T.; White, C. J.; Ahmed, A.; Schibli, R.; Bode, J.W.; Ametamey, S. M. A New Prosthetic Group for the Fluorine-18 Labelling of Small and Large Complex Biomolecules at Room Temperature. Poster Presentations. *Journal of Labelled Compounds and Radiopharmaceuticals* **2017**, *60*, 111–640.
- [168] Naumiec, G.; Cai, L.; Lu, S.; Pike, V. W. Quinuclidine and DABCO Enhance the Radiofluorinations of 5-Substituted 2-Halo-pyridines. *Eur. J. Org. Chem.* **2017**, 6593–6603.





# ***Chapter 5***

---

## ***Second Generation of Acyltrifluoroborates with Enhanced KAT Ligation Kinetics***

---

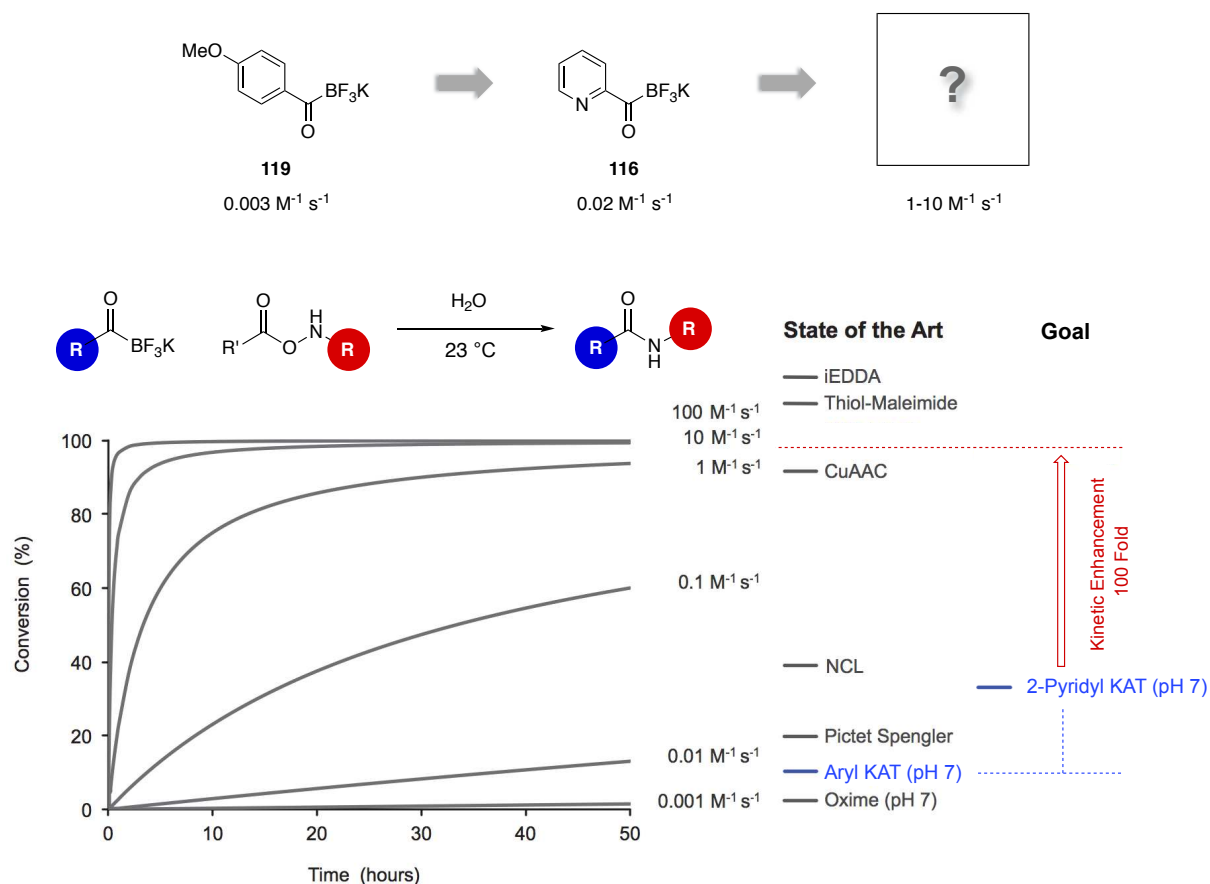
ESI Q-TOF mass experiments were performed in collaboration with Dr. Adrien H. Marchand from the group of Prof. Renato Zenobi at the Laboratory of Organic Chemistry at ETH Zurich.



## 5 Second Generation of Acyltrifluoroborates with Enhanced KAT Ligation Kinetics

### 5.1 Introductory Remarks

Despite the fact that 2-pyridyl KATs with maximum second-order rate constants of  $0.044 \text{ M}^{-1} \text{ s}^{-1}$  displayed enhanced ligation kinetics by up to 15-fold compared to state-of-the-art aryl KATs, the observed kinetic improvement did not reach our set goal of ligation kinetics between  $1 - 10 \text{ M}^{-1} \text{ s}^{-1}$  at pH 7 (Scheme 3.1). We thus continued our efforts to find a suitable KAT species with sufficiently enhanced ligation kinetics. According to the in-depth mechanistic insight gained earlier in this thesis (*cf.* Chapter 3), we surmised that slight changes in the spatial arrangement of the rate-enhancing heteroaryl-nitrogen atom and the KAT group might lead to a more effective proton transfer and thus result in further improved KAT ligation rates.

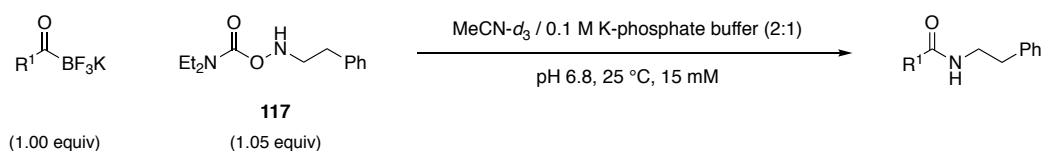


**Scheme 5.1** Schematic representation of the current state-of-the-art KAT ligation rates compared to 2-pyridyl KATs, the first generation of potassium acyltrifluoroborates with enhanced ligation rates, and the ultimate aim of this thesis.

## 5.2 From Pyridine to Other Heterocyclic Acyltrifluoroborates

In a first step, we evaluated the kinetics of recently reported amino acid derived KATs by the ITO and BODE group at pH 6.8 according to our previously developed  $^1\text{H-NMR}$  kinetic method (*cf.* Chapter 2.4.1).<sup>127</sup> We hoped that the secondary amino group in 3-position to the KAT moiety might lead to accelerated ligation rates via hydrogen bond donation. However, to our disappointment, glycine-derived KAT **167** and alanine-derived KAT **168** displayed decreased ligation rates compared to 2-pyridyl KAT **116** with measured second-order rate constants of  $0.005 \text{ M}^{-1} \text{ s}^{-1}$  and  $0.007 \text{ M}^{-1} \text{ s}^{-1}$  respectively (Table 5.1).

**Table 5.1** Kinetic comparison of 2-pyridyl KATs and amino acid derived KATs.



Entry	KAT	Structure	$k_{\text{obs}}$ [a]	$k_{\text{rel}}$ [b]
1	<b>116</b>		0.02	6.7
2	<b>167</b>		0.005	1.7
3	<b>168</b>		0.007	2.3

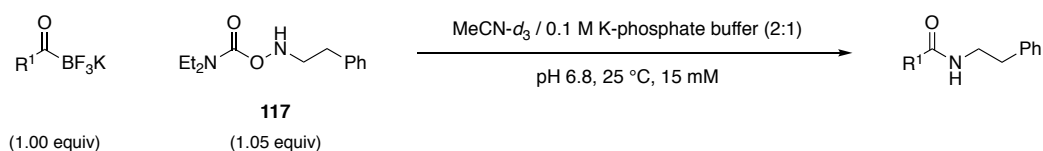
[a] Kinetic measurements were performed at equimolar concentrations (15 mM) of KAT and hydroxylamine **117** in  $\text{MeCN-d}_3$  / 0.1 M deuterated potassium phosphate buffer (2:1, pH 6.8) at 25 °C. Kinetics were monitored by  $^1\text{H-NMR}$  spectroscopy. The observed second-order rate constants  $k_{\text{obs}}$  were determined as the average of three measurements. [b]  $k_{\text{rel}}$  represents the relative rate constants with respect to 4-methoxyphenyl KAT **119** ( $k_{\text{obs}} = 0.003 \text{ M}^{-1} \text{ s}^{-1}$ ).

Based on the mechanistic analysis and the DFT calculation data (*cf.* Chapter 3) we further surmised that changing the angle between the KAT group and the nitrogen atom, which was found to be crucial in the ligation reaction, might lead to facilitated proton transfer during the reaction process. In the following, we synthesized a selection of different *N*-heterocyclic KATs and compared their kinetic performance (Table 5.2). Unfortunately, 2-(2-pyridyl)phenol KAT **169** and thiazole KAT **170** with ligation rates of  $0.008 \text{ M}^{-1} \text{ s}^{-1}$  and  $0.004$



$M^{-1} s^{-1}$ , respectively, did not show the desired rate improvement. However, to our surprise, 8-quinoline KAT **171** was discovered to undergo extremely fast ligation reactions at a concentration of 15 mM. Conversions to the desired amide product of >75% were detected after 3 minutes, indicating a rate constant of  $>2 M^{-1} s^{-1}$ . Yet, no accurate second-order rate constant could be determined by  $^1H$ -NMR spectroscopy as the reaction was too fast for NMR timescale. Even dilution of the sample concentration from 15 mM to 3.75 mM did not result in slow enough ligation kinetics for NMR timescale. Noteworthy, reaction concentrations lower than 3.75 mM did not result in sufficient signal to noise ratio for peak integration and were therefore not suitable for NMR kinetic analysis.

**Table 5.2** Kinetic comparison of 2-pyridyl KATs and other N-heterocyclic KAT species.

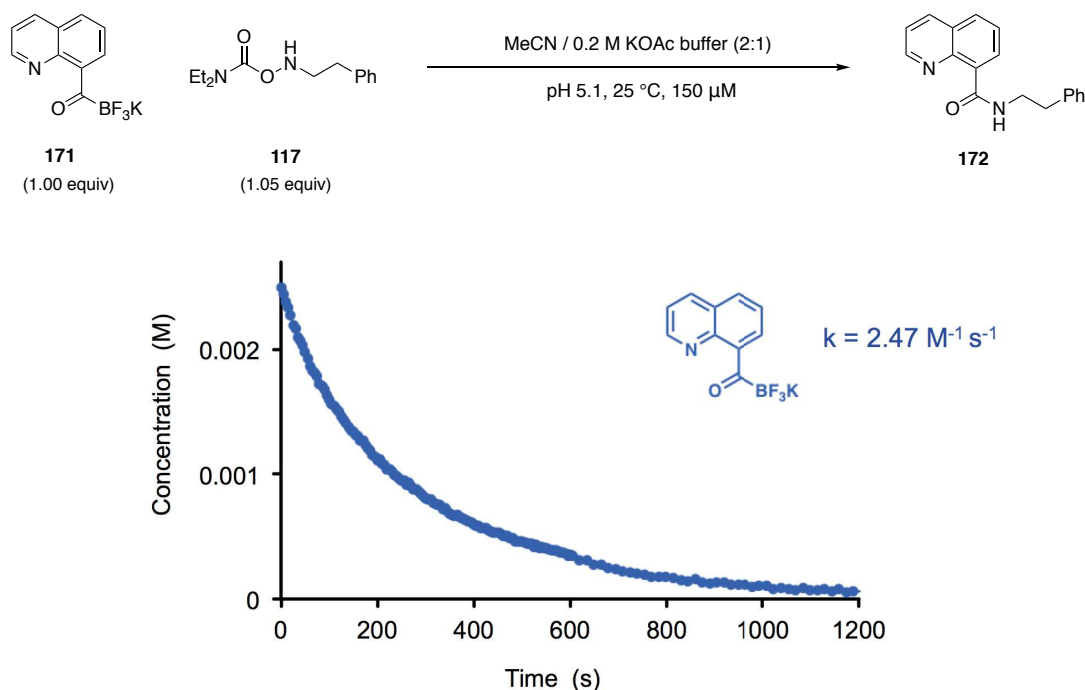


Entry	KAT	Structure	$k_{obs}$ <sup>[a]</sup>	$k_{rel}$ <sup>[b]</sup>
1	<b>116</b>		0.02	6.7
2	<b>169</b>		0.008	2.7
3	<b>170</b>		0.004	1.3
4	<b>171</b>		n.d. <sup>[c]</sup>	n.d.

*[a]* Kinetic measurements were performed at equimolar concentrations (15 mM) of KAT and hydroxylamine **117** in  $MeCN-d_3$  / 0.1 M deuterated potassium phosphate buffer (2:1, pH 6.8) at 25 °C. Kinetics were monitored by  $^1H$ -NMR spectroscopy. The observed second-order rate constants  $k_{obs}$  were determined as the average of three measurements. *[b]*  $k_{rel}$  represents the relative rate constants with respect to 4-methoxyphenyl KAT **119** ( $k_{obs} = 0.003 M^{-1} s^{-1}$ ). *[c]* Estimated rate constant. The ligation reaction was observed to be too fast for NMR timescale so that no accurate rate constant could be determined.

### 5.3 Kinetics of Quinoline KATs<sup>169</sup>

As the observed KAT ligation rate of 8-quinoline KAT **171** was too fast to be measured by NMR spectroscopy, an alternative kinetic method was required to determine the accurate second-order rate constant of 8-quinoline KAT **171**. UV/Vis spectroscopy was thereby selected as the method of choice. Real-time kinetic measurements were performed at an equimolar concentration of 2.5 mM of KAT **171** and hydroxylamine **117** in a solvent mixture of MeCN / 0.1 M potassium phosphate buffer (2:1) at room temperature and pH 6.8. To our delight, the second-order rate constant of **171** was determined to be  $2.45 \text{ M}^{-1} \text{ s}^{-1}$ , which is in good accordance to the estimated ligation rate of  $>2 \text{ M}^{-1} \text{ s}^{-1}$  by previously measured by  $^1\text{H}$ -NMR spectroscopy (Scheme 5.2).

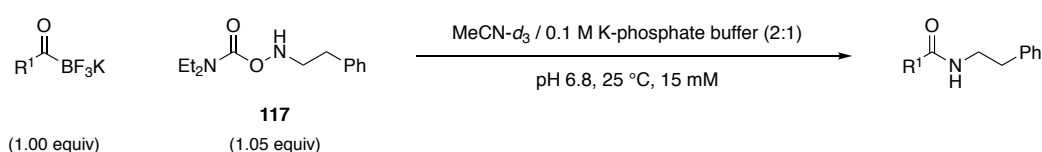


**Scheme 5.2** KAT ligation of equimolar concentrations (2.5 mM) of 8-quinoline KAT **171** and hydroxylamine **117** at room temperature monitored by UV/Vis spectroscopy. The second-order rate constant of the reaction was determined to be  $2.47 \text{ M}^{-1} \text{ s}^{-1}$  at pH 6.8.

With second-order rate constants of  $2.47 \text{ M}^{-1} \text{ s}^{-1}$  at pH 6.8, 8-quinoline KAT **171** represents by far the fastest acyltrifluoroborate species measured to date. With this outstanding discovery we ultimately achieved our goal of reaching KAT ligation kinetics between  $1 - 10 \text{ M}^{-1} \text{ s}^{-1}$  near neutral pH. As illustrated in Table 5.3, it was demonstrated that 8-quinoline KAT **171** displays improved ligation rates of  $>100$ -fold compared to previously disclosed 2-pyridyl KAT **116** (*cf.* Chapter 2.4,  $k_{\text{obs}} = 0.02 \text{ M}^{-1} \text{ s}^{-1}$ ) and  $>800$ -fold compared to

traditionally used aryl KATs, such as 4-methoxyphenyl KAT **119** ( $k_{\text{obs}} = 0.003 \text{ M}^{-1} \text{ s}^{-1}$ ). Furthermore, it was found that compared to quinoline KAT **171** structurally-related isoquinoline KAT **173** displayed significantly slower ligation kinetics (Table 5.2, Entry 4 – 5). Consequently, we concluded that the heteroaryl nitrogen of **171** in close proximity to the KAT moiety is a key structural feature responsible for the kinetic enhancement. This result is in good correlation to what has been observed for 2-pyridyl KATs in Chapter 2.4.1 (Table 5.3, Entry 2 – 3).

**Table 5.3** Kinetic comparison of 2-pyridyl KATs and other N-heterocyclic KAT species.

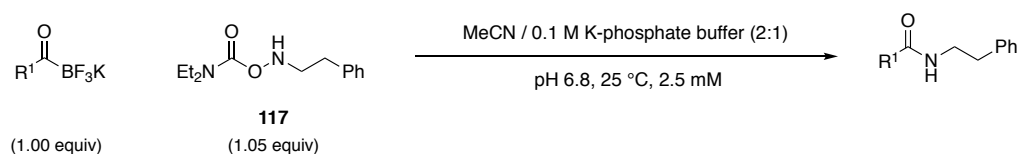


Entry	KAT	Structure	$k_{\text{obs}}$ <sup>[a]</sup>	$k_{\text{rel}}$ <sup>[b]</sup>
1	<b>119</b>		0.003	1
2	<b>116</b>		0.02	6.7
3	<b>125</b>		0.007	2.3
4	<b>171</b>		2.45 <sup>[c]</sup>	817
5	<b>173</b>		0.004	1.3

<sup>[a]</sup> Kinetic measurements were performed at equimolar concentrations (15 mM) of KAT and hydroxylamine **117** in MeCN- $d_3$  / 0.1 M deuterated potassium phosphate buffer (2:1, pH 6.8) at 25 °C. Kinetics were monitored by  $^1\text{H}$ -NMR spectroscopy. The observed second-order rate constants  $k_{\text{obs}}$  were determined as the average of three measurements. <sup>[b]</sup>  $k_{\text{rel}}$  represents the relative rate constants with respect to 4-methoxyphenyl KAT **119** ( $k_{\text{obs}} = 0.003 \text{ M}^{-1} \text{ s}^{-1}$ ). <sup>[c]</sup> This compound is an exception. Kinetic measurements were performed at equimolar concentrations (2.5 mM) of KAT and hydroxylamine in MeCN / 0.1 M potassium phosphate buffer (2:1, pH 6.8) at 25 °C. Kinetics were monitored by UV/Vis spectroscopy.

Subsequently, we investigated if 8-quinoline KAT **171** shows similar substitution effects as 2-pyridyl KAT **116**. In comparison to **171**, it was observed that 8-quinoline KAT **174** with an incorporated electron-donating methoxy-substituent displayed accelerated ligation rates with second-order rate constants of  $4.8 \text{ M}^{-1} \text{ s}^{-1}$  (Table 5.4, Entry 1 – 2). In contrary, 8-quinoline KAT **175** equipped with an electron-withdrawing chloro-substituent showed decelerated ligation rates with a rate constant of  $0.8 \text{ M}^{-1} \text{ s}^{-1}$  (Table 5.4, Entry 3).

**Table 5.4** Kinetic comparison of 2-pyridyl KATs and other N-heterocyclic KAT species.



Entry	KAT	Structure	$k_{\text{obs}}^{[a]}$	$k_{\text{rel}}^{[b]}$
1	<b>171</b>		2.45	818
2	<b>174</b>		4.80	1600
5	<b>175</b>		0.08	27

[a] Kinetic measurements were performed at equimolar concentrations (15 mM) of KAT and hydroxylamine **117** in  $\text{MeCN-d}_3$  / 0.1 M deuterated potassium phosphate buffer (2:1, pH 6.8) at 25 °C. Kinetics were monitored by  $^1\text{H-NMR}$  spectroscopy. The observed second-order rate constants  $k_{\text{obs}}$  were determined as the average of three measurements. [b]  $k_{\text{rel}}$  represents the relative rate constants with respect to 4-methoxyphenyl KAT **119** ( $k_{\text{obs}} = 0.003 \text{ M}^{-1} \text{ s}^{-1}$ ).

In Figure 5.1, a graphical illustration of the observed rate constant of Table 5.4 is shown. The finding that electron donating substituents in the 4-position lead to a rate increase, while electron-withdrawing substituents decelerate the ligation kinetics is in good agreement to the obtained results for 2-pyridyl KAT derivatives in Chapter 2.4.2. In conclusion, we assume that the basicity of the heteroaryl nitrogen is crucial for the kinetic performance, for both 2-pyridyl and 8-quinoline KAT ligation.

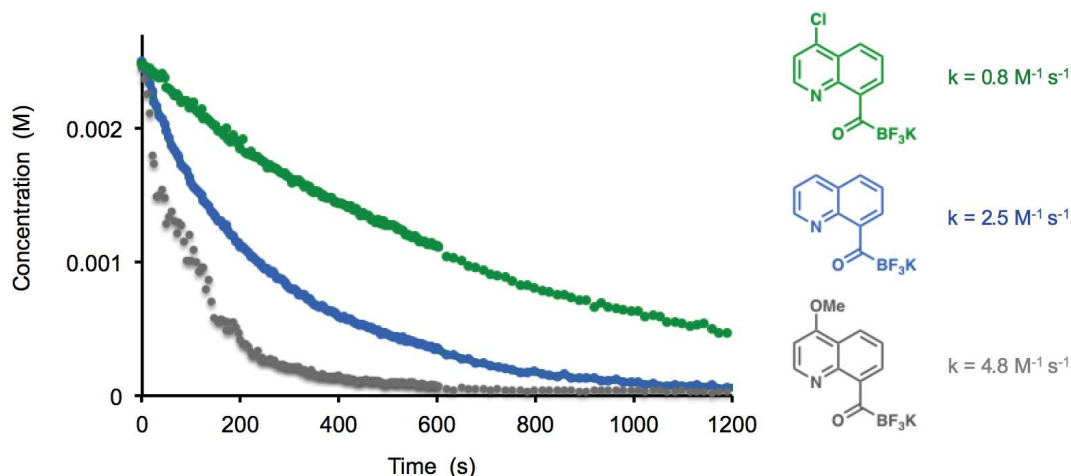


**Figure 5.1** Effect of substituents in the 4-position of 8-quinoline KAT.

In a next step, we examined the pH profile of 8-quinoline KATs between pH 3.6 – 7.4. It was found that the ligation kinetics of 8-quinoline KATs **171** were significantly faster than 2-pyridyl KAT **116** and 4-methoxyphenyl KAT **119** in this pH range (Figure 5.2). As expected, the ligation rates increased with more acidic pH. In fact, it was found that the lower the pH value is, the faster are the observed ligation reactions. As described in detail in Table 5.5, the difference in ligation rates of quinoline KAT **171** and pyridyl KAT **116** becomes smaller under acidic conditions between pH 3.6 – 4.4. This indicates that under acidic conditions the kinetic improvement based on the structural advantage of **171** over **116** disappears due to the excess of protons present in the environment. At pH of 3.6 both heterocyclic KATs **116** and **171** exhibit similar ligation rates with second-order rate constants between 21 – 23  $\text{M}^{-1} \text{s}^{-1}$ .

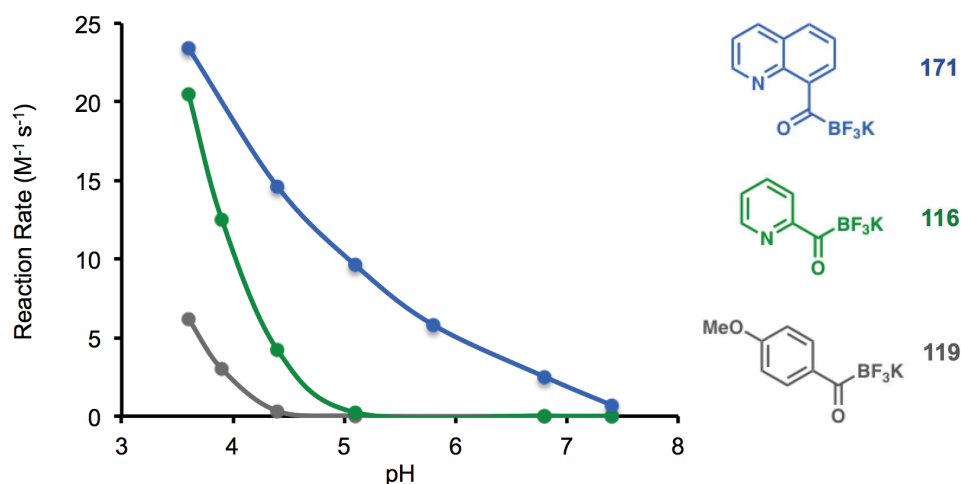


**Figure 5.2** Comparison of pH profiles of aryl KAT **119**, pyridyl KAT **116** and quinoline KAT **171** by UV/Vis spectroscopy.

**Table 5.5** Variable pH kinetic measurements of 4-methoxyphenyl KAT, 2-pyridyl KAT and 8-quinoline KAT.

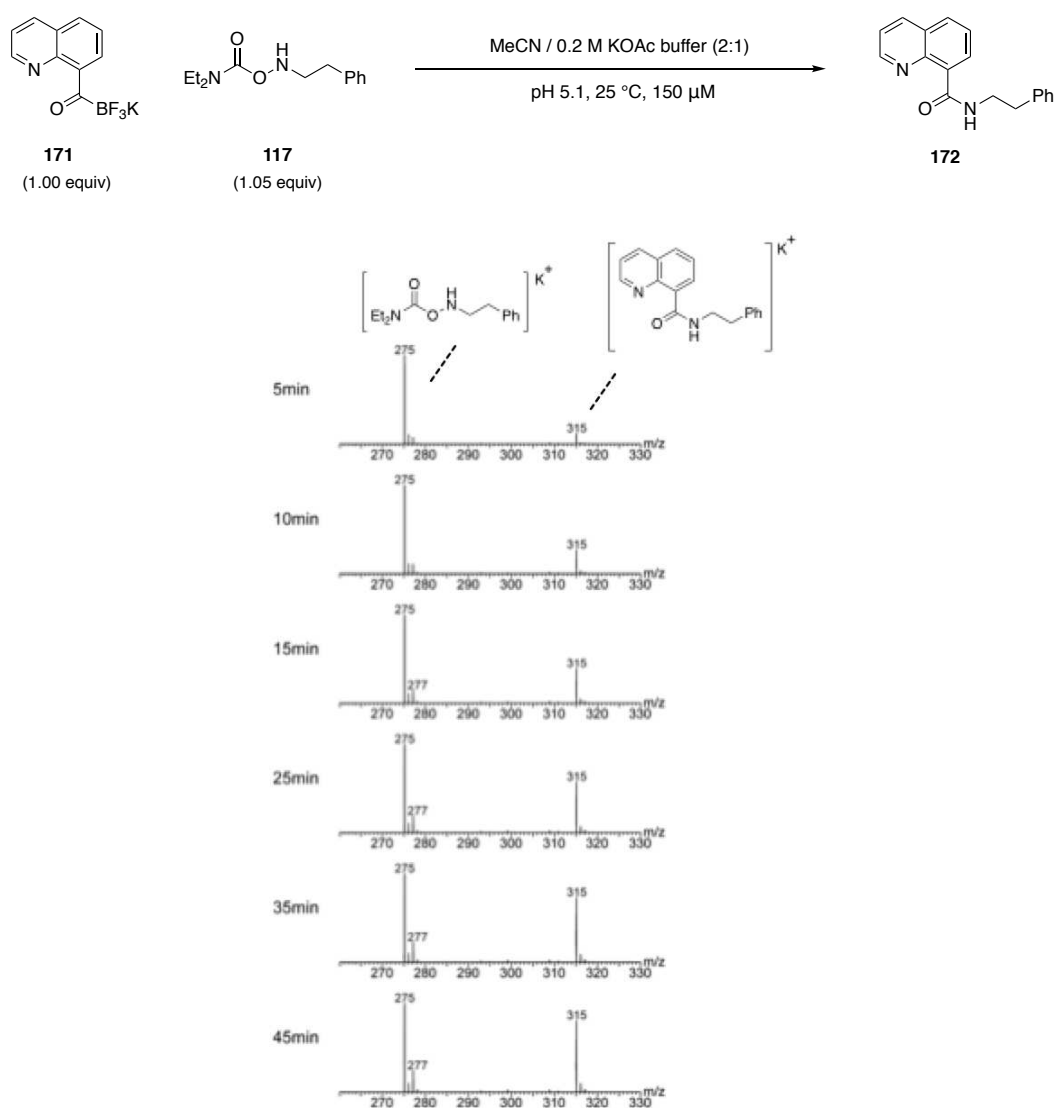
Entry	pH	$k_{\text{obs}}$ ( $\text{M}^{-1} \text{s}^{-1}$ ) <sup>[a]</sup>	$k_{\text{obs}}$ ( $\text{M}^{-1} \text{s}^{-1}$ ) <sup>[a]</sup>	$k_{\text{obs}}$ ( $\text{M}^{-1} \text{s}^{-1}$ ) <sup>[b]</sup>
1	3.6	6.7	21.9	23.4
2	3.9	3.1	14.1	–
3	4.4	0.3	4.5	14.6
4	5.1	0.017	0.231	9.6
5	5.8	–	–	5.8
6	6.8	0.003	0.020	2.5
7	7.4	0.001	0.011	0.7

Conditions: [a] Kinetic experiments were performed at equimolar concentrations of KAT and hydroxylamine **117** reactants under buffered solvent conditions at different pH values and 25 °C. For pH 4.4 – 7.4 kinetic measurements were performed at a concentration of 15 mM in MeCN- $d_3$  / 0.1 M deuterated potassium phosphate or acetate buffer (2:1). The reaction process was monitored by  $^1\text{H-NMR}$  spectroscopy. For pH 3.6 – 3.9 kinetic measurements were performed at a concentration of 3.75 mM in MeCN / 0.2 M potassium acetate buffer (1:9). Kinetic experiments were performed at equimolar (2.5 mM) concentrations of KAT and hydroxylamine reactants under buffered solvent conditions at different pH values in MeCN / 0.2 M potassium acetate buffer and 25 °C. Kinetics were monitored by UV/Vis spectroscopy.

Unlike for pyridyl KAT **116** and aryl KAT **119**, 8-quinoline KAT **171** did not show an exponential increase in ligation rates with decreasing pH, but rather a steady rate increase. Thus, no turning point was observed, at which the pH drastically increases or decreases.

Our results were further substantiated by additional kinetic measurements using ESI Q-TOF mass spectrometry (Scheme 5.3). Ligation reactions with 8-quinoline KAT **171** and hydroxylamine **117** were performed at an equimolar concentration of 150  $\mu\text{M}$  in a solvent mixture of MeCN / 0.2 M potassium acetate (pH 3.9 – 5.1) or phosphate buffer respectively (pH 5.8). Kinetics were measured in real-time by constant injection of the reaction sample

with a flow rate of 200  $\mu\text{L}$  using a syringe pump. All measurements were performed at least twice with satisfying reproducibility. Spectra were recorded in positive mode and the ligation was observed to proceed in a clean fashion. Product formation was monitored by increase of the corresponding mass peak  $[\mathbf{172} + \text{K}]^+$  at  $m/z = 315$ . Data analysis was performed by integration and fitting with exponential rise to maximum functions. In addition, the data was renormalized to the value of the plateau obtained from the fit for better comparison. The peak  $m/z$  275, corresponding to hydroxylamine plus  $\text{K}^+$ , remained unaltered during the reaction, presumably due to superior ionization compared to quinoline KAT **171** and amide species **172**. Starting material **171** was not observed in positive mode, only in negative mode and was therefore not considered in the subsequent measurements.



**Scheme 5.3** KAT ligation between 8-quinoline KAT **171** and hydroxylamine **117** at equimolar concentrations of 150  $\mu\text{M}$  in MeCN / 0.2 M KOAc buffer (2:1, pH 5.1) at 25 °C. The reaction was monitored by ESI Q-TOF mass spectrometry in positive mode.  $m/z = 275$  corresponds to  $[\mathbf{117} + \text{K}]^+$ ,  $m/z = 315$  corresponds to  $[\mathbf{172} + \text{K}]^+$ .

With this additional kinetic method in hand, the pH profile of 8-quinoline KAT **171** previously measured by UV/Vis spectroscopy could be confirmed (Figure 5.3).

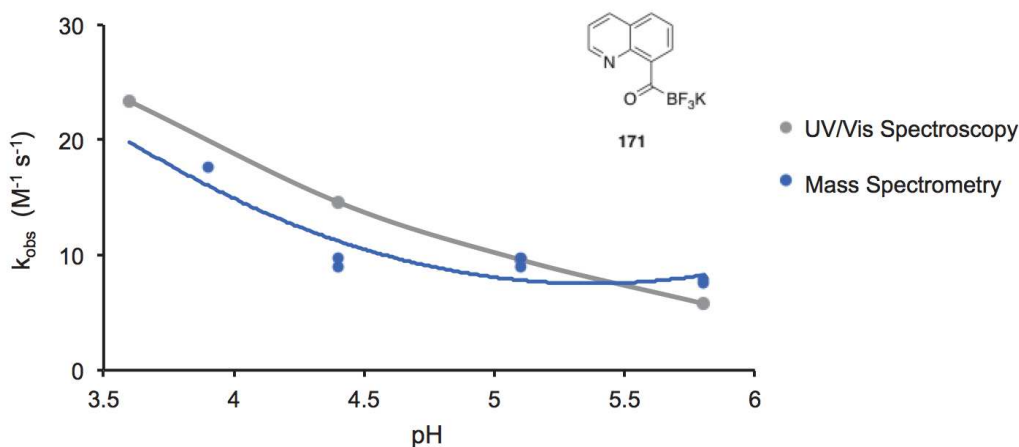


**Figure 5.3** pH Profile of quinoline KAT **171** monitored by ESI Q-TOF mass spectrometry (blue) and UV/Vis spectroscopy (grey).

Interestingly, during the ligation reaction no *N*-borylated intermediate was detected in negative mode. Preliminary DFT calculations propose that the activation barrier for both protonated and non-protonated quinoline KATs is 1.0 kcal mol<sup>-1</sup> lower compared to the activation barrier of the respective aryl KAT species. Furthermore, for protonated 8-quinoline KAT the ligation was suggested to proceed via a different transition state **177**. Compared to the transition state for protonated pyridyl KAT **137'-H<sup>+</sup>**, proton coordination to the nitrogen rather than the carbonyl of the hydroxylamine was observed.

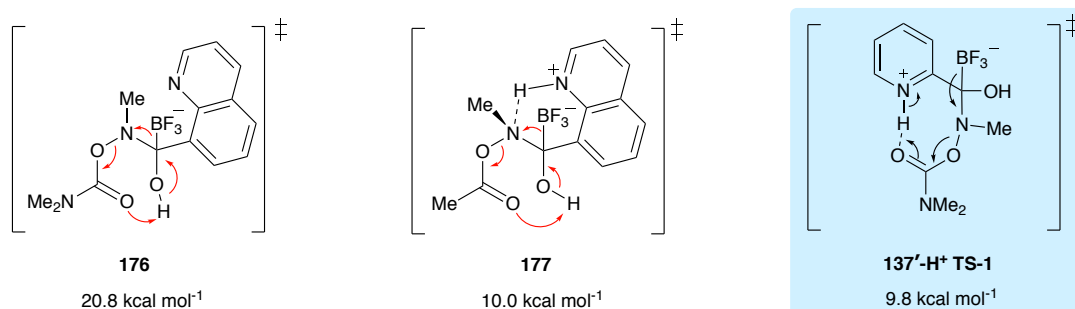
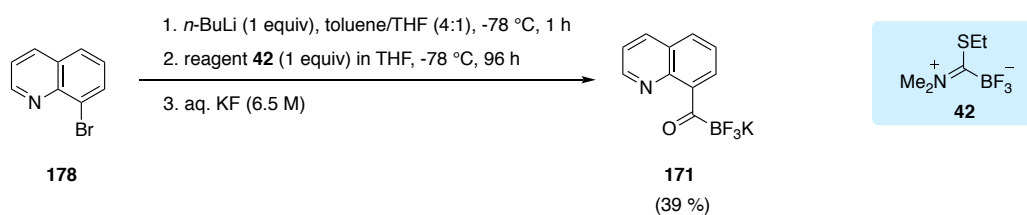


**Figure 5.4** Preliminary DFT calculation of non-protonated and protonated 8-quinoline KATs.



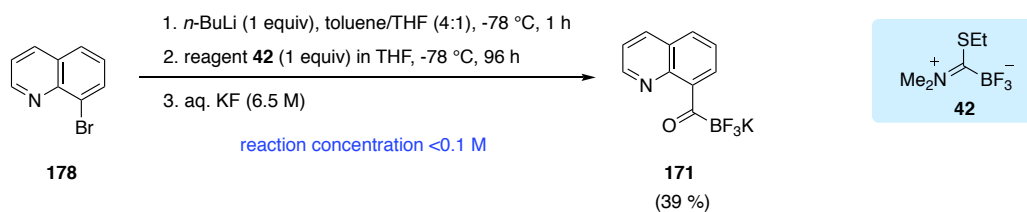
## 5.4 Synthesis and Functionalization of Quinoline KATs

Initial attempts on the preparation of 8-quinoline KAT **171** from 8-bromoquinoline **178** according to the standard synthetic procedure developed by BODE and ERŐS using the BODE KAT REAGENT **42** resulted in reaction yields <5 %. Even prelithiation of the 8-bromoquinoline starting material **178** did not result in improved yields (Scheme 5.4).



**Scheme 5.4** Unoptimized synthetic procedure for the preparation of 8-quinoline KAT **171** using BODE KAT REAGENT **42**.

To overcome these limitations extensive reaction optimization studies have been performed. In the beginning, the initial lithiation step was evaluated. We found that after treating bromoquinoline **178** with *n*-butyllithium for one hour at -78 °C followed by quenching with DMF, 8-quinolinecarbaldehyde was obtained in excellent yields >95% and satisfying purity. Having assured that the lithiation step proceeds as desired, we continued our efforts with screening various other reaction parameters, such as solvents, equivalents of BODE KAT REAGENT **42**, addition of additives, reaction temperature and time, quenching protocol, and reaction concentration. Evaluation of different solvents revealed that the reaction works better in a mixture of THF/toluene (1:4) resulting in increased yields of 11%. Furthermore, addition of two instead of one equivalent of reagent **42** did not affect the reaction outcome. Additives, such as TMEDA and DMPU led to marginally increased conversions of 17% and 15%, respectively. Interestingly, alteration of the reaction time and temperature disclosed that a combination of longer reaction times of up to 72 hours and lower temperatures of -60 °C instead of -78 °C increased the reaction yields to up to 21%. On the contrary, changing the quenching protocol from aq. KF (6.5 M) to aq. saturated  $\text{KHF}_2$  completely shut down the reaction and yielded no desired KAT product **171**. As the synthesis of KATs via BODE KAT REAGENT **42** usually requires concentrated reaction mixtures in the range of 0.2 – 0.3 M, we next envisioned to perform the synthesis under more dilute conditions. Dilution to less than 0.1 M finally led to satisfying reaction yields of up to 39%. Our optimized conditions for the synthesis of 8-quinoline KATs are depicted in Scheme 5.5.



**Scheme 5.5** Optimized synthetic procedure for the preparation of 8-quinoline KAT **171** using BODE KAT REAGENT **42**.

Having established an optimized procedure for the synthesis of quinoline KATs the following functionalized quinoline derivatives **174**, **175** and **179** were prepared as illustrated in Figure 5.5. Since 8-bromoquinoline precursors were found to be very expensive, these starting materials were independently prepared by Skraup synthesis.<sup>170,171,172</sup>

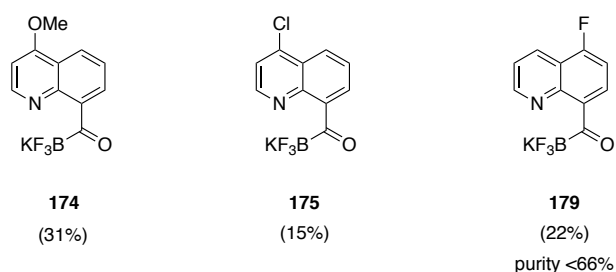
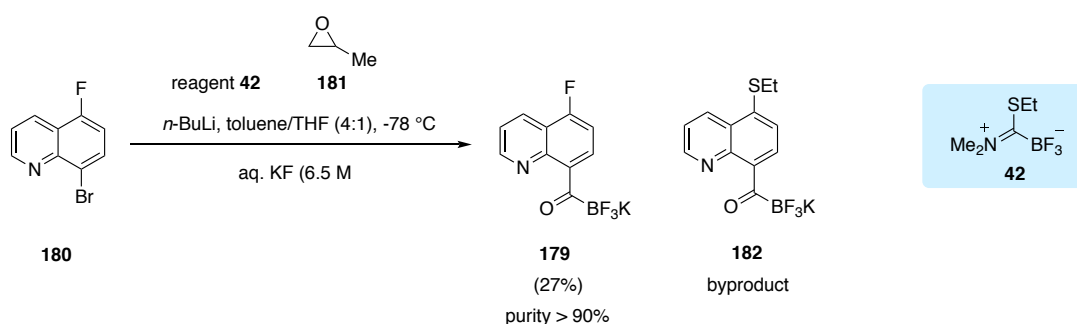


**Figure 5.5** A selection of 8-quinoline KAT derivatives prepared by the optimized synthetic procedure.

Interestingly, in the KAT synthesis of 5-fluoro-8-quinoline KAT **179** the formation of a byproduct (ca. 33%) was observed that could not be separated from the desired compound **179** resulting in poor overall purity. The byproduct could be identified as the thioethyl derivative **182**, formed by nucleophilic aromatic substitution of free thioethyl that is generated as a waste from BODE KAT REAGENT **42**. Addition of 2-methyloxirane **181** as a nucleophile scavenger prevented the undesired nucleophilic aromatic substitution by consuming the free thioethyl species (Scheme 5.6).



**Scheme 5.6** The use of 2-methyloxirane **181** as suitable scavenger towards the improved synthesis of 5-fluoro-8-quinoline KAT derivative **179**.

## 5.5 Concluding Remarks

The advanced mechanistic insight of the KAT ligation paved the way for further structural fine-tuning of potassium acyltrifluoroborates. In this chapter, we demonstrate that 8-quinoline KATs are superior potassium acyltrifluoroborate species with second-order rate constants of up to  $4.8 \text{ M}^{-1} \text{ s}^{-1}$  at pH 6.8. Hence, 8-quinoline KATs display a rate increase of >1000 fold compared to state-of-the-art aryl KATs (Figure 5.6). Similar to what has been observed for pyridyl KATs it was revealed that the quinoline nitrogen plays a crucial role in the kinetic enhancement.

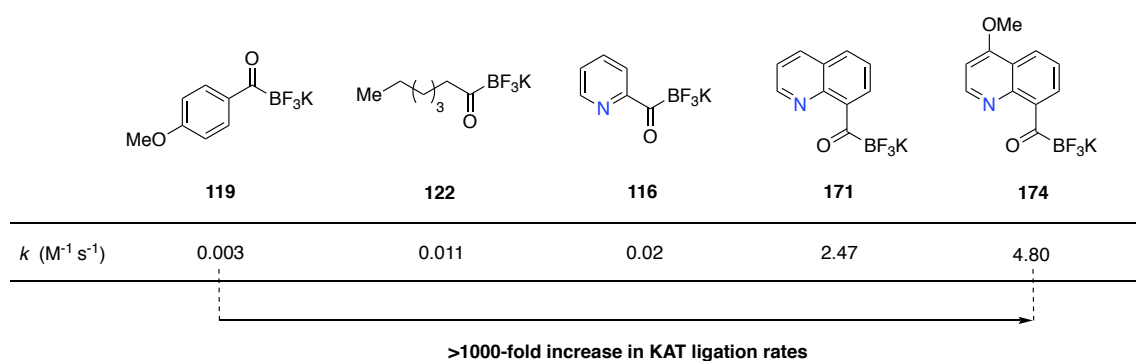


**Figure 5.6** Comparison of KAT ligation kinetics of different KAT species.

## 5.6 References

- [169] ESI Q-TOF mass experiments were performed in collaboration with Dr. Adrien H. Marchand from the group of Prof. Renato Zenobi at the Laboratory of Organic Chemistry at ETH Zurich.
- [170] Skraup, Z. H. Eine Synthese des Chinolins. *Berichte* **1980**, *13*, 2086–2087.
- [171] Manske, R. H. F. The Chemistry of Quinolines. *Chem. Rev.* **1942**, *30*, 113–144.
- [172] Manske, R. H. F.; Kulka, M. The Skraup Synthesis of Quinolines". *Org. React.* **1953**, *7*, 80–99.



# ***Chapter 6***

---

## ***Conclusion and Outlook***

---

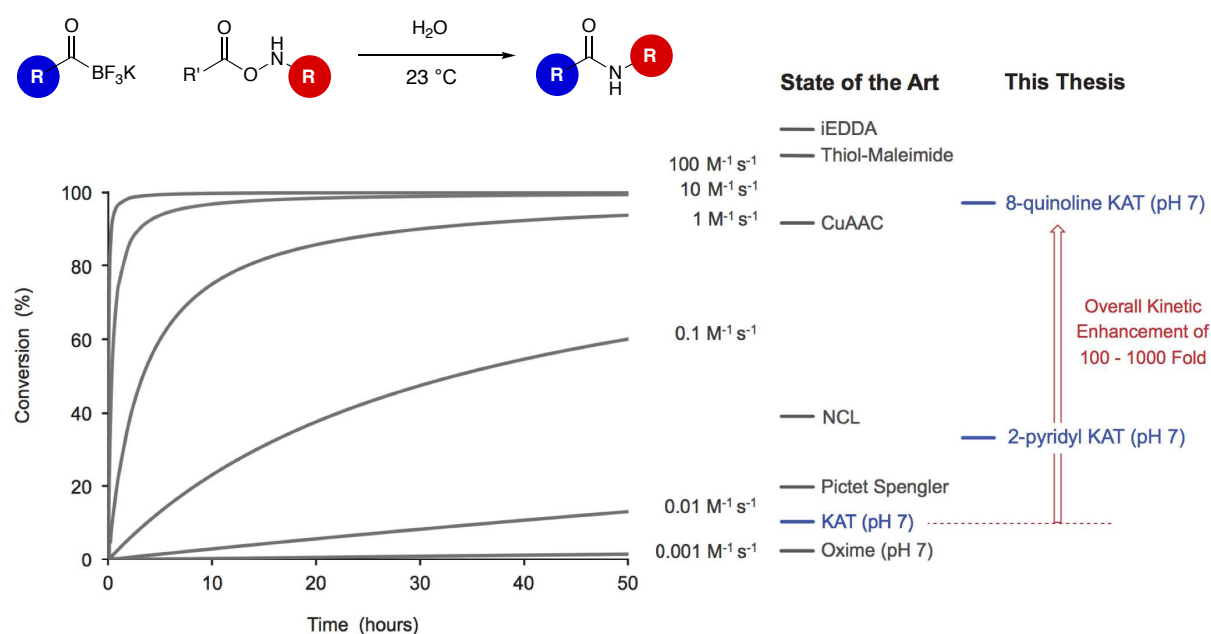


## 6 Conclusion and Outlook

### 6.1 Conclusion

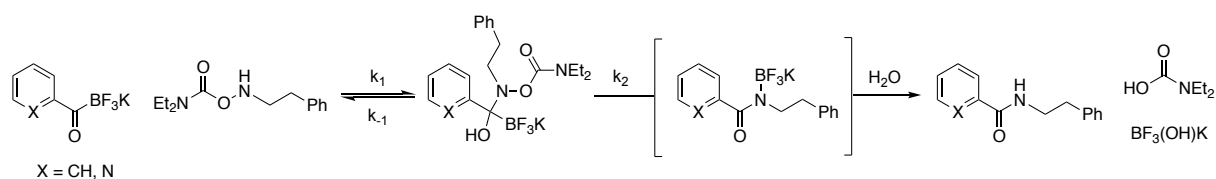
The KAT ligation developed by BODE and MOLANDER has recently emerged as a valuable tool for the chemoselective functionalization of small molecules and peptides. Despite many advantages, its broader use for biological applications has been hampered to date by slow ligation kinetics with second-order rate constants of  $0.001 \text{ M}^{-1} \text{ s}^{-1}$  under physiological conditions.

In this thesis, we present the development of two new classes of potassium acyltrifluoroborate species with enhanced ligation kinetics. In a first generation, we successfully showed that 2-pyridyl KATs undergo faster KAT ligation reactions by up to two orders of magnitude compared to state-of-the-art alkyl and aryl KATs reaching second-order rate constants between  $0.01 - 0.04 \text{ M}^{-1} \text{ s}^{-1}$  close to neutral pH. In a second generation, 8-quinoline KATs were discovered as superior potassium acyltrifluoroborates for KAT ligation with improved ligation kinetics by up to 1000-fold reaching reaction rates in the region of  $1 - 5 \text{ M}^{-1} \text{ s}^{-1}$  at neutral pH. The enhanced ligation rates bring the KAT ligation in the same kinetic range as other fast chemoselective ligation reactions, such as CuAAC (Scheme 6.1). This kinetic improvement renders the KAT ligation – for the first time ever – an effective bioorthogonal strategy for the covalent bioconjugation of equimolar concentrations of two macromolecules to form stable and naturally occurring amid-bond linkages.



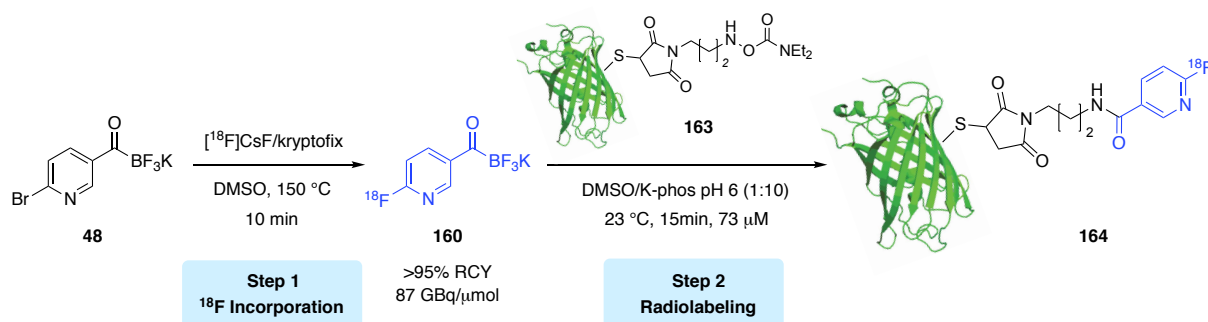
**Scheme 6.1** Schematic representation of the improved KAT ligation kinetics in this thesis.

Besides detailed kinetic studies, we performed thorough experimental and computational mechanistic investigations, which provided in-depth understanding of the KAT ligation mechanism. Noteworthy, we postulate that the KAT ligation proceeds via a rate-determining pre-equilibrium in lieu of following traditional second-order kinetics (Scheme 6.2). The rate-determining step of the ligation reaction was evaluated to be the concerted elimination of the tetrahedral addition intermediate. To our surprise, extensive DFT-calculations in combination with mass spectrometry analysis have led to the discovery of a novel *N*-trifluoroboryl ligation intermediate, which has never been proposed nor reported before.



**Scheme 6.2** Postulated KAT ligation mechanism for pyridyl and aryl KATs.

In another part of this thesis, pyridyl KATs have been identified as suitable candidates for radiolabeling. Rapid introduction of  $^{18}\text{F}$  into 6-fluoro-nicotinoyltrifluoroborate (**48**) was achieved in a single step by nucleophilic aromatic substitution in good radiochemical purity of >95%. Initially moderate radiochemical yields of 23% were significantly increased by addition of DABCO as a tertiary amine additive resulting in excellent radiochemical yields of >95%. As a proof of concept, it was shown that  $^{18}\text{F}$ -labeled potassium 6-fluoro-nicotinoyltrifluoroborate **160** undergoes KAT ligation reactions with hydroxylamines in acidic aqueous media and rat plasma at room temperature. As a result,  $^{18}\text{F}$ -labeling of larger model substrates, such as peptides and superfolder green fluorescent protein (sfGFP) **163** bearing hydroxylamines was achieved by a two-step strategy exploiting the KAT ligation (Scheme 6.3).



**Scheme 6.3** [ $^{18}\text{F}$ ]Radiofluorination of chemically modified sfGFP by KAT ligation at room temperature.

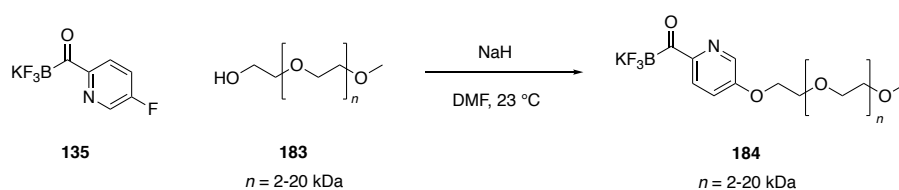


## 6.2 Outlook

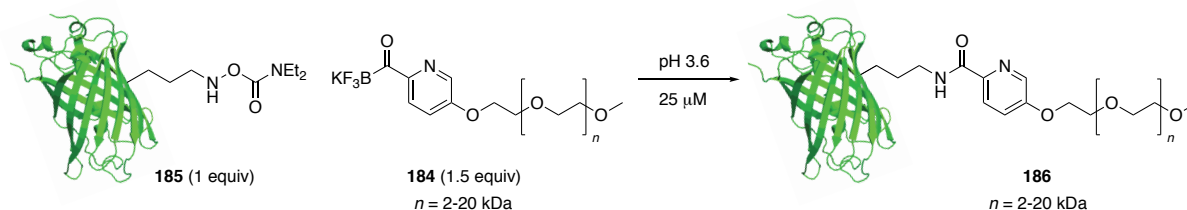
### 6.2.1 Application of Pyridyl KAT Ligation in Bioconjugation

Based on the improved ligation rates of 2-pyridyl KATs compared to their aryl counterparts presented in this thesis, BODE and coworkers have recently used 2-pyridyl KAT derivatives for the successful PEGylation and homodimerization of recombinant proteins close to equimolar conditions.<sup>173</sup> In a first step, the KAT moiety was incorporated into the termini of polyethylene glycol (PEG) chains of various sizes including 2, 5, 10 and 20 kDa mPEG **183** by aromatic nucleophilic substitution ( $S_NAr$ ) of 5-fluoropyridine-2-yl KAT **135** (Scheme 6.4, a). In second step, these PEGylated KAT reagents **184** were conjugated to the corresponding protein **185** equipped with a hydroxylamine via KAT ligation (Scheme 6.4, b). It was found that 2-pyridyl KAT derivatives exhibit superior conjugation rates compared to aryl KAT derivatives enabling the PEGylation of proteins with excellent conversions under aqueous acidic conditions. According to this two-step protocol four folded, recombinant proteins – sfGFP-(S147C), Ubc9-(C93A), T4L-(V131C) and HTP-(S261C) – equipped with a hydroxylamine could be PEGylated with 2–20 kDa 2-pyridyl mPEG KATs under aqueous, acidic conditions at micromolar concentrations (25  $\mu$ M) and near equimolar stoichiometry of the two coupling partners in excellent yields between 82–96%.

#### a) Synthesis of PEGylated KAT Reagents

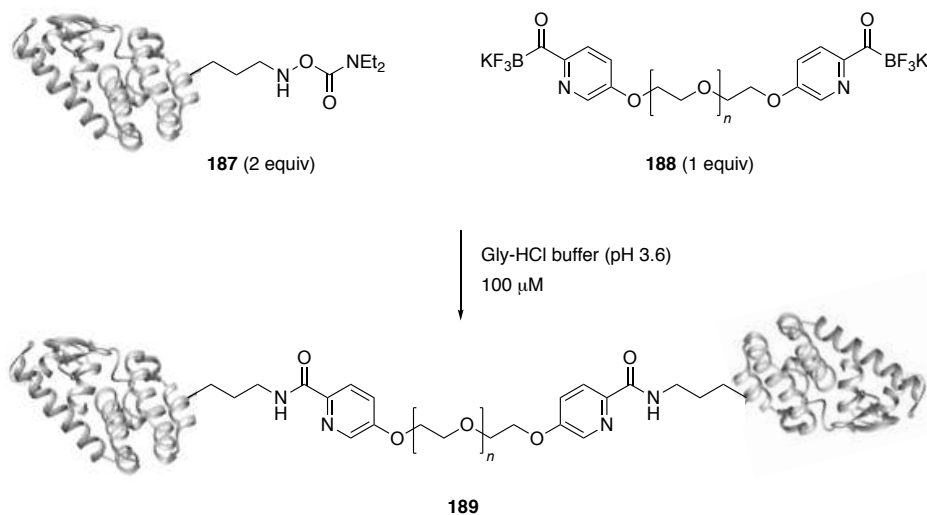


#### b) Site-Specific MonoPEGylation of sfGFP-(S147C) with PEGylated KAT Reagents



**Scheme 6.4** Site-specific monoPEGylation of proteins using a two-step protocol developed by BODE and coworkers.<sup>174</sup>

Furthermore, it was found that the use of *bis* 2-pyridyl PEG KAT reagent **188** enables the covalent homodimerization of proteins at a reaction concentration of 100  $\mu\text{M}$  in aqueous acidic Gly-HCl buffer (pH 3.6) with good conversion between 72–82% after 5 hours without any non-specific side-reactions (Scheme 6.5).



**Scheme 6.5** Homodimerization of proteins using a two-step protocol developed by BODE and coworkers.<sup>175</sup>

These results demonstrate that the 2-pyridyl KAT ligation developed in this thesis can successfully be applied to protein polymerization and conjugation at near-equimolar concentrations under dilute, aqueous acidic conditions.

## 6.2.2 Potential Applications of Quinoline KAT Ligation

The significantly enhanced ligation kinetics of 8-quinoline KATs compared to 2-pyridyl KATs might lead to PEGylated 8-quinoline KAT reagents that enable even faster bioconjugation reactions and ultimately allow clean and rapid protein-protein conjugation not only under aqueous acidic conditions (e.g. pH 3.6) but close to physiological conditions (pH 6 – 7) with equally satisfying conversions to what has been reported by BODE and coworkers.<sup>173</sup> Besides homodimeric protein-protein conjugates we envision that the enhanced ligation kinetics of 8-quinoline KATs may also facilitate the formation of more complex chimeric fusion architectures, such as protein oligomers. In addition, faster 8-quinoline KAT ligation might be of special advantage when manipulating proteins that do not tolerate acidic pH and must therefore be handled close to pH 7.

Furthermore, the superior ligation kinetics of 8-quinoline KATs might also be exploited in the field of radiolabeling. In the proof-of-concept study presented in this thesis (*cf.* Chapter 4)  $^{18}\text{F}$ -labeled 6-fluoro-nicotinoyltrifluoroborate was identified as a suitable substrate for the  $^{18}\text{F}$ -labeling of larger model substrates, such as peptides and superfolder green fluorescent protein (sfGFP) bearing hydroxylamines, via KAT ligation. The KAT ligation labeling reaction was shown to rapidly proceed in the presence of oxalic acid and full conversion was detected after a few minutes. However in the absence of oxalic acid, at elevated pH the labeling reaction did not proceed. For future *in vivo* PET imaging applications of the herein established two-step KAT ligation labeling strategy, enhanced ligation kinetics with rates of  $>1 \text{ M}^{-1} \text{ s}^{-1}$  are required. The quinoline KAT ligation developed in this thesis meets those requirements. Consequently, we envision the preparation of 8-quinoline KATs with handles for the incorporation of fluorine-18 by nucleophilic substitution. A selection of potential 8-quinoline KAT precursors **190–194** are presented in Figure 6.1.

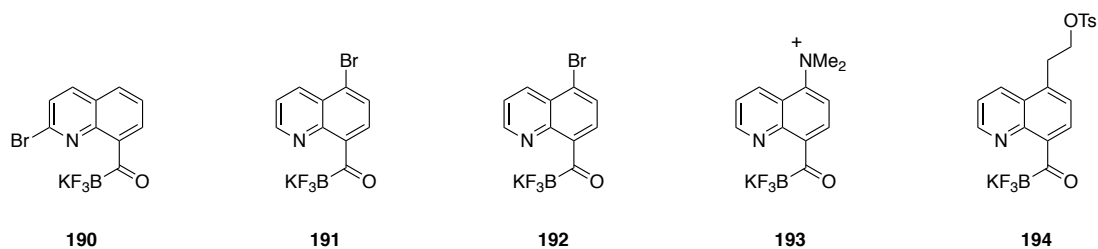


**Figure 6.1** Proposed 8-quinoline KAT derivatives as precursors for  $^{18}\text{F}$ -labeling.

### 6.3 References

- [173] White, C. J.; Bode, J. W. PEGylation and Dimerization of Expressed Proteins under Near Equimolar Conditions with Potassium 2-Pyridyl Acyltrifluoroborates. *ACS Cent. Sci.* **2018**, *4*, 197–206.
- [174] Scheme adapted from reference 173.
- [175] Scheme adapted from reference 173.



# ***Chapter 7***

---

***Experimental Procedures and  
Characterization Data***

---



## 7 Experimental Procedures and Characterization Data

### 7.1 General Methods

#### 7.1.1 Reactions and Purification

Unless otherwise stated, all reactions were performed in flame-dried glassware sealed with rubber septa under an inert atmosphere of dry nitrogen using standard Schlenk line techniques. The protecting gas was passed over a column of phosphorous pentoxide and supplied through a glass manifold. Reactions were stirred magnetically using Teflon-coated magnetic stir bars. Filtrations were performed using CHEMGLASS medium-fritted vacuum Buchner filter funnels (30 mL). The removal of solvents under reduced pressure was achieved by rotary evaporation with a water bath (temperature range of 40-50 °C). Thin layer chromatography (TLC) was performed on silica gel pre-coated aluminum sheets (MERCK SILICA GEL 60 F254) and visualized by fluorescence quenching under UV light or by staining (using *n*-butanolic ninhydrin<sup>176</sup> or aq. potassium permanganate<sup>177</sup> staining solutions). Flash column chromatography<sup>178</sup> was performed on SIGMA ALDRICH SILICA GEL (high purity grade, pore size 60 Å, 230–400 mesh) at 0.5–1.0 bar of air pressure.

#### 7.1.2 Chemicals and Solvents

All chemicals and solvents were purchased from ABCR, ACROS, COMBI-BLOCKS, FLUOROCHEM, FLUKA, MERCK, FISHER–SCIENTIFIC, TCI, SIGMA ALDRICH or STREM and were used as received from the commercial suppliers without further purification unless mentioned otherwise. (Ethylthio-trifluoroborate)-methane dimethyliminium (BODE KAT REAGENT, CAS: 1622923-36-7) **42**<sup>179</sup> and *O*-diethylcarbamoyl-*N*-phenethylhydroxylamine (**117**)<sup>180</sup> were synthesized according to previously established procedures by BODE group. Anhydrous THF and toluene were obtained from INERT PURESOLV MD5 solvent purification system under nitrogen (H<sub>2</sub>O content < 10 ppm, KARL–FISCHER titration).<sup>181</sup> Anhydrous DMF and DMSO were purchased by ACROS (extra dry, over molecular sieve, AcroSeal®, H<sub>2</sub>O content < 5 ppm). Deuterated solvents (D, 99.9 %) were purchased from CAMBRIDGE ISOTOPE LABORATORIES, INC., except for CDCl<sub>3</sub> (D, 99.8 %), which was obtained from ARMAR CHEMICALS.

### 7.1.3 Analytics

#### NMR Spectroscopy

$^1\text{H}$ -NMR spectroscopy was performed on a BRUKER DRX (500 MHz) or BRUKER AVANCE III (600 MHz with cryoprobe) spectrometer and the recorded spectra were referenced to the residual solvent signal as internal standard (acetone- $d_6$ : 2.05 ppm; DMSO- $d_6$ : 2.50 ppm).  $^{13}\text{C}$ -NMR spectroscopy was performed on a BRUKER DRX (126 MHz) or BRUKER AVANCE III (150 MHz) spectrometers and the recorded spectra are referenced to the solvent (acetone- $d_6$ : 29.84 ppm; DMSO- $d_6$ : 39.52 ppm);  $^{19}\text{F}$ -NMR spectroscopy was performed on a BRUKER DRX (470 MHz) spectrometer and the recorded spectra were referenced to an external standard of trifluoroacetic acid (−76.53 ppm).  $^{11}\text{B}$ -NMR spectra were recorded on a BRUKER DRX (160 MHz) spectrometer and referenced to an external sample of  $\text{BF}_3 \cdot \text{OEt}_2$  (0 ppm). All measurements were carried out at ambient temperature (22 °C) and chemical shifts are reported in ppm ( $\delta$ ). The data is reported as follows: chemical shift in ppm, multiplicity (s = singlet, d = doublet, t = triplet, q = quartet, sext = sextet, m = multiplet, dd = doublet of doublet, dt = doublet of triplet), coupling constant ( $J$ ) in Hz, and integration. In  $^{19}\text{F}$ -NMR and  $^{11}\text{B}$ -NMR, trifluoroborate multiplets are reported as the average of the observed signals. Service measurements were performed by the NMR service team of the LABORATORIUM FÜR ORGANISCHE CHEMIE at ETH ZURICH by MR. RENÉ ARNOLD, MR. REINER FRANKENSTEIN and MR. STEPHAN BURKHARDT under direction of DR. MARC-OLIVER EBERT.

**Mass spectrometry (MS)** analyses were performed as high resolution EI measurements on a WATERS MICROMASS AUTOSPEC ULTIMA at 70 eV, as high resolution ESI measurements on a BRUKER DIAGNOSTICS MAXIS (ESI-Qq-TOF-MS) instrument or as MALDI on a BRUKER SOLARIX (MALDI-FTICR-MS) instrument by the mass spectrometry service of the LABORATORIUM FÜR ORGANISCHE CHEMIE at ETH ZURICH by MR. LOUIS BERTSCHI, MR. OSWALD GRETER, MR. DANIEL WIRZ, DR. XIANGYANG ZHANG under direction of DR. BERTRAN GERRITS. The data is reported as follows:  $m/z$  (% relative intensity).

**LCMS analysis** was performed on a DIONEX ULTIMATE 3000 RSLC connected to a SURVEYOR MSQ PLUS mass spectrometer; a reversed-phase RESTEK PINNACLE II C18 (4.6 x 50 mm) column was used, running a gradient of 5 to 100% MeCN in  $\text{H}_2\text{O}$  over 6.5 min and 100% MeCN for 2.5 min.



**Melting points** were measured using a BÜCHI B-540 melting point apparatus using open glass capillaries and are uncorrected.

Infrared (IR) spectra were recorded on a PERKIN ELMER TWO FT-IR (UATR) as thin films. Absorption bands are given in wavenumbers ( $\text{cm}^{-1}$ ).

**UV-Vis spectra** were recorded on a THERMO SCIENTIFIC NANODROP 2000C spectrophotometer using a QS 1.000 quartz cell (path length 1 cm).

pH measurements were performed at room temperature (22 °C) using a HANNA HI 2210 bench pH meter. The pH meter was calibrated before every use with non-deuterated HANNA HI 7010 pH 10.01 ( $\pm 0.01$  at 25 °C) calibration buffer solution, HANNA HI 7007 pH 7.01 ( $\pm 0.01$  at 25 °C) calibration buffer solution and HANNA HI 7004 pH 4.01 ( $\pm 0.01$  at 25 °C) calibration buffer solution.

#### 7.1.4 Kinetic Measurements

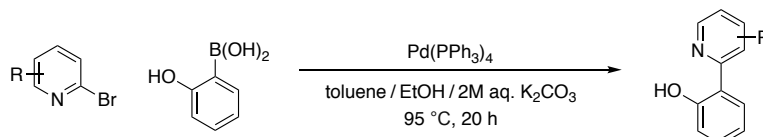
Kinetic measurements of the KAT ligation reaction were performed at equimolar concentration of potassium acyltrifluoroborate and the hydroxylamine. Unless stated otherwise, the kinetic measurements were carried out at room temperature and constant pH employing buffered solvent conditions. The reaction process was monitored by non-invasive real-time  $^1\text{H-NMR}$  spectroscopy on a BRUKER AVANCE III (500 MHz) spectrometer using unused DURAN economic NMR-tubes 178 x 4.95 mm (300 MHz), by UV-Vis spectrophotometry on a THERMO SCIENTIFIC NANODROP 2000C spectrophotometer using a QS 1.000 quartz cell (path length 1 cm) or by mass spectrometry on a SYNAPT G2S mass spectrometer in Q-TOF mode with constant sample injection. The collected data was analyzed with MICROSOFT EXCEL VERSION 14.6.9 or PRISM 6. To validate the accuracy of the measurements, all kinetic experiments were performed at least three times. The second-order rate constant of the reaction was determined as the average of the three measurements.

## 7.2 Experimental Procedures and Characterization Data

### 7.2.1 Ligand Synthesis

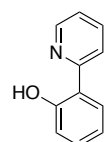
6-(2-Hydroxyphenyl)-pyridazine-3(2H)-one ligand **L105** was purchased by SIGMA ALDRICH.

#### General Procedure 1: Synthesis of 2-(pyridin-2-yl)phenol Ligands



The 2-(pyridin-2-yl)phenol ligands were prepared according to a slightly modified literature procedure.<sup>182</sup> An oven-dried Schlenk flask equipped with a stir bar was evacuated, degassed with nitrogen and charged with bromopyridine (4.25 mmol, 1.0 equiv), Pd(PPh<sub>3</sub>)<sub>4</sub> (98.2 mg, 0.09 mmol, 0.02 equiv), toluene (9.2 mL) and an aqueous solution of potassium carbonate (2 M, 5.10 mL, 10.2 mmol, 2.4 equiv). The solution was stirred at 23 °C for 15 min followed by the addition of 2-hydroxyphenylboronic acid (0.945 g, 6.8 mmol, 1.6 equiv) in EtOH (4.2 mL). The mixture was stirred for 20 h at 85 °C. After cooling to room temperature, H<sub>2</sub>O was added and the product was extracted using EtOAc (3 x 100 mL). The combined organic layers were washed with brine (50 mL) and H<sub>2</sub>O (50 mL) and filtered over a short plug of celite. The filtrate was dried over MgSO<sub>4</sub> and the volatiles were removed under reduced pressure. The residue was purified by column chromatography to afford the desired product in good to excellent yields.

#### 2-(Pyridin-2-yl)phenol (**L97**)



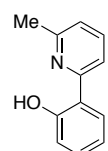
Prepared from 2-bromopyridine (672 mg) by general procedure 1. Purified by column chromatography (EtOAc/hexanes 1:10) and isolated as a yellow solid (599 mg, 3.50 mmol) in 82% yield. The spectral data of **L97** was in agreement with literature.<sup>183</sup>

**M.p.** 54 – 56 °C. **FT-IR** (neat, cm<sup>-1</sup>)  $\nu_{\max}$  = 2524 (br), 1585, 1561, 1503, 1473, 1430, 1392, 1303, 1266, 1244, 1223, 1170, 1153, 1119, 1098, 1058, 1043, 1022, 909, 857, 834, 794, 749, 725, 641, 627. **<sup>1</sup>H NMR** (400 MHz, acetone-*d*<sub>6</sub>)  $\delta$  14.14 (s, 1H), 8.62 (ddd, *J* = 5.0, 1.9,

1.0 Hz, 1H), 8.18 (dd,  $J = 8.3, 1.3$  Hz, 1H), 8.04 – 8.00 (m, 1H), 7.98 (dd,  $J = 7.9, 1.7$  Hz, 1H), 7.42 (ddt,  $J = 7.1, 5.1, 1.0$  Hz, 1H), 7.30 (ddd,  $J = 8.3, 7.2, 1.7$  Hz, 1H), 6.94 – 6.89 (m, 2H).

$^{13}\text{C}$  NMR (101 MHz, acetone- $d_6$ )  $\delta$  161.0, 158.7, 147.1, 147.0, 139.3, 132.2, 127.4, 122.9, 120.3, 119.5, 119.1. **HR-MS** (ESI) calcd for  $\text{C}_{11}\text{H}_9\text{NO}$   $[\text{M} + \text{H}]^+$  172.0757, found 172.0762.

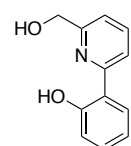
### 2-(6-Methylpyridin-2-yl)phenol (L98)



Prepared from 2-bromo-6-methylpyridine (731 mg) by general procedure 1. Purified by column chromatography (EtOAc/hexanes 1:10) and isolated as a colorless oil (575 mg, 3.10 mmol) in 73% yield. The spectral data of **L98** was in agreement with literature.<sup>184</sup>

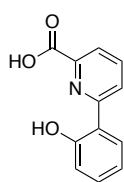
**FT-IR** (neat,  $\text{cm}^{-1}$ )  $\nu_{\text{max}}$  = 2617 (br), 1595, 1567, 1505, 1459, 1408, 1373, 1298, 1257, 1218, 1178, 1154, 1098, 1037, 873, 853, 823, 800, 750, 696, 633.  $^1\text{H}$  NMR (400 MHz, acetone- $d_6$ )  $\delta$  14.42 (s, 1H), 7.96 – 7.86 (m, 3H), 7.31 – 7.25 (m, 2H), 6.93 – 6.86 (m, 2H), 2.59 (s, 3H).  $^{13}\text{C}$  NMR (101 MHz, acetone- $d_6$ )  $\delta$  161.2, 158.2, 156.0, 139.5, 132.0, 127.4, 122.3, 119.7, 119.4, 119.0, 117.2, 23.8. **HR-MS** (ESI) calcd for  $\text{C}_{12}\text{H}_{12}\text{NO}$   $[\text{M} + \text{H}]^+$  186.0913, found 186.0911.

### 2-(6-(Hydroxymethyl)pyridin-2-yl)phenol (L101)



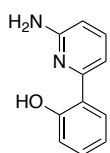
Prepared from 2-bromo-6-(hydroxymethyl)pyridine (799 mg) by general procedure 1. Purified by column chromatography (EtOAc/hexanes 1:2) and isolated as pale yellow crystals (719 mg, 3.57 mmol) in 84 % yield. The spectral data of **L101** was in agreement with literature.<sup>176</sup>

**M.p.** 54 – 56 °C. **FT-IR** (neat,  $\text{cm}^{-1}$ )  $\nu_{\text{max}}$  = 3391, 3048, 1585, 1495, 1460, 1434, 1406, 1300, 1242, 1208, 1175, 1067, 1045, 1002, 986, 854, 798, 747.  $^1\text{H}$  NMR (400 MHz,  $\text{CDCl}_3$ )  $\delta$  7.88 – 7.79 (m, 3H), 7.38 (dq,  $J = 7.4, 0.8$  Hz, 1H), 7.31 (ddd,  $J = 8.3, 7.2, 1.6$  Hz, 1H), 7.02 (dd,  $J = 8.3, 1.3$  Hz, 1H), 6.92 (ddd,  $J = 8.4, 7.2, 1.3$  Hz, 1H), 4.87 (s, 2H).  $^{13}\text{C}$  NMR (101 MHz,  $\text{CDCl}_3$ )  $\delta$  159.9, 157.5, 157.4, 138.7, 131.7, 126.5, 119.1, 119.0, 118.7, 118.6, 118.0, 65.3. **HR-MS** (ESI) calcd for  $\text{C}_{12}\text{H}_{12}\text{NO}_2$   $[\text{M} + \text{H}]^+$  202.0863, found 202.0866.

**6-(2-Hydroxyphenyl)picolinic acid (L102)**

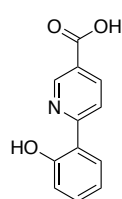
Prepared from 6-bromopicolinic acid<sup>185</sup> (859 mg) by a slight modification of general procedure 1. After the reaction mixture was cooled to room temperature, 1 M NaOH (100 mL) was added and the mixture was extracted CH<sub>2</sub>Cl<sub>2</sub> (3 x 100 mL). The aqueous layer was collected, filtered over celite and acidified to pH 3 with 6 M HCl. The yellow precipitate was filtered off and washed with H<sub>2</sub>O (2 x 50 mL). After drying under high vacuum the desired product was obtained as a pale yellow solid (466 mg, 2.17 mmol) in 51% yield. The spectral data of **L102** was in agreement with literature.<sup>186</sup>

**M.p.** 253 – 256 °C. **FT-IR** (neat, cm<sup>-1</sup>)  $\nu_{\max}$  = 2900 (br), 1698, 1587, 1500, 1481, 1463, 1427, 1407, 1331, 1270, 1232, 1162, 1092, 1002, 931, 918, 836, 822, 755, 737, 665. **<sup>1</sup>H NMR** (400 MHz, DMSO-*d*<sub>6</sub>)  $\delta$  14.11 (s, 1H), 13.76 (s, 1H), 8.45 (dd, *J* = 8.4, 0.9 Hz, 1H), 8.19 (t, 1H, *J* = 7.9 Hz), 8.09 (dd, *J* = 8.3, 1.7 Hz, 1H), 8.03 (dd, *J* = 7.6, 0.8 Hz, 1H), 7.35 (ddd, *J* = 8.6, 7.2, 1.6 Hz, 1H), 6.95 – 6.93 (m, 2H). **<sup>13</sup>C NMR** (101 MHz, DMSO-*d*<sub>6</sub>)  $\delta$  164.9, 159.3, 156.8, 144.7, 139.8, 131.9, 127.3, 123.0, 122.8, 118.9, 118.2, 118.2. **HR-MS** (ESI) calcd for C<sub>12</sub>H<sub>10</sub>NO<sub>3</sub> [M + H]<sup>+</sup> 216.0655, found 216.0657.

**2-(6-Aminopyridin-2-yl)phenol (L103)**

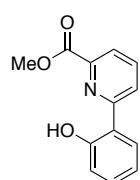
Prepared from methyl 6-bromopyridine-2-amine (735 mg) by general procedure 1. Purified by column chromatography (EtOAc/hexanes 1:5) and isolated as a yellow solid (627 mg, 3.37 mmol) in 79% yield.

**M.p.** 137 – 138 °C. **FT-IR** (neat, cm<sup>-1</sup>)  $\nu_{\max}$  = 1597, 1565, 1497, 1451, 1410, 1371, 1322, 1284, 1257, 1218, 1173, 1149, 1090, 1067, 994, 925, 820, 796, 756, 745, 706, 695. **<sup>1</sup>H NMR** (400 MHz, CDCl<sub>3</sub>)  $\delta$  14.09 (s, 1H), 7.75 (dd, *J* = 8.0, 1.7 Hz, 1H), 7.57 (t, *J* = 8.0 Hz, 1H), 7.27 – 7.23 (m, 2H), 6.98 (dd, *J* = 8.2, 1.3 Hz, 1H), 6.88 (ddd, *J* = 8.4, 7.2, 1.3 Hz, 1H), 6.44 (dd, *J* = 8.2, 0.7 Hz, 1H), 4.53 (s, 2H). **<sup>13</sup>C NMR** (101 MHz, CDCl<sub>3</sub>)  $\delta$  159.6, 156.2, 155.5, 139.5, 131.1, 126.6, 119.4, 118.9, 118.4, 109.3, 106.6. **HR-MS** (ESI) calcd for C<sub>11</sub>H<sub>11</sub>NO [M + H]<sup>+</sup> 187.0866, found 187.0870.

**6-(2-Hydroxyphenyl)nicotinic acid (L104)**

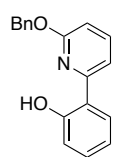
Prepared from 6-bromonicotinic acid (859 mg) by a slight modification of general procedure 1. After the reaction mixture was cooled to room temperature, 1 M NaOH (100 mL) was added and the mixture was extracted CH<sub>2</sub>Cl<sub>2</sub> (3 x 100 mL). The aqueous layer was collected, filtered over celite and acidified to pH 3 with 6 M HCl. The yellow precipitate was filtered off and washed with H<sub>2</sub>O (2 x 50 mL). After drying under *vacuo* the desired product was obtained as a bright yellow solid (558 mg, 2.59 mmol) in 61% yield.

**M.p.** 258 – 260 °C. **FT-IR** (neat, cm<sup>-1</sup>)  $\nu_{\max}$  = 2900 (br), 1680, 1588, 1558, 1504, 1485, 1416, 1374, 1300, 1273, 1227, 1148, 1137, 1019, 945, 927, 855, 839, 820, 749, 738, 727. **<sup>1</sup>H NMR** (400 MHz, methanol-*d*<sub>4</sub>)  $\delta$  9.12 (dd, *J* = 2.2, 0.9 Hz, 1H), 8.45 (dd, *J* = 8.6, 2.2 Hz, 1H), 8.16 (dd, *J* = 8.8, 0.9 Hz, 1H), 7.95 (dd, *J* = 8.7, 1.5 Hz, 1H), 7.36 – 7.31 (m, 1H), 6.96 – 6.92 (m, 2H). **<sup>13</sup>C NMR** (101 MHz, methanol-*d*<sub>4</sub>)  $\delta$  167.5, 162.2, 161.0, 148.9, 139.8, 133.4, 128.2, 125.6, 120.3, 120.1, 119.6, 119.2. **HR-MS** (ESI) calcd for C<sub>12</sub>H<sub>10</sub>NO<sub>3</sub> [M + H]<sup>+</sup> 216.0655, found 216.0660.

**Methyl 6-(2-hydroxyphenyl)picolinate (L106)**

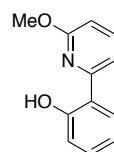
Prepared from methyl 6-bromopicolinate<sup>187</sup> (918 mg) by general procedure 1. Purified by column chromatography (EtOAc/hexanes 1:10) and isolated as a colorless solid (627 mg, 2.74 mmol) in 64% yield.

**M.p.** 86 – 87 °C. **FT-IR** (neat, cm<sup>-1</sup>)  $\nu_{\max}$  = 1720, 1595, 1463, 1436, 1409, 1333, 1227, 1138, 964, 849, 749, 734. **<sup>1</sup>H NMR** (400 MHz, DMSO-*d*<sub>6</sub>)  $\delta$  13.82 (s, 1H), 8.47 (dd, *J* = 8.4, 0.9 Hz, 1H), 8.20 (t, *J* = 7.9 Hz, 1H), 8.08 (dd, *J* = 8.5, 1.6 Hz, 1H), 8.05 (dd, *J* = 7.7, 0.9 Hz, 1H), 7.38 – 7.34 (m, 1H), 6.98 – 6.94 (m, 2H), 3.96 (s, 3H). **<sup>13</sup>C NMR** (101 MHz, DMSO-*d*<sub>6</sub>)  $\delta$  163.9, 159.1, 156.9, 143.7, 139.8, 132.0, 127.4, 123.6, 122.9, 119.0, 118.3, 118.1, 53.0. **HR-MS** (ESI) calcd for C<sub>13</sub>H<sub>12</sub>NO<sub>3</sub> [M + H]<sup>+</sup> 230.0812, found 230.0817.

**2-(6-(Benzyloxy)pyridin-2-yl)phenol (L107)**

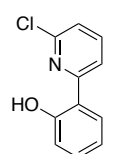
Prepared from methyl 2-(benzyloxy)-6-bromopyridine<sup>188</sup> (1.12 g) by general procedure 1. Purified by column chromatography (EtOAc/hexanes 1:15) and isolated as colorless crystals (838 mg, 3.02 mmol) in 71% yield.

**M.p.** 108 – 109 °C. **FT-IR** (neat,  $\text{cm}^{-1}$ )  $\nu_{\text{max}}$  = 1597, 1565, 1497, 1451, 1410, 1371, 1322, 1284, 1257, 1218, 1173, 1149, 1090, 1067, 994, 925, 820, 796, 756, 745, 706, 695. **<sup>1</sup>H NMR** (400 MHz,  $\text{CDCl}_3$ )  $\delta$  13.32 (s, 1H), 7.78 (d,  $J$  = 8.0, 1.7 Hz, 1H), 7.75 (t,  $J$  = 8.2 Hz, 1H), 7.51 – 7.34 (m, 6H), 7.31 (ddd,  $J$  = 8.2, 7.2, 1.6 Hz, 1H), 7.02 (dd,  $J$  = 8.3, 1.3 Hz, 1H), 6.93 (ddd,  $J$  = 8.3, 7.2, 1.3 Hz, 1H), 6.80 (dd,  $J$  = 8.3, 0.7 Hz, 1H), 5.39 (s, 2H). **<sup>13</sup>C NMR** (101 MHz,  $\text{CDCl}_3$ )  $\delta$  161.6, 158.9, 155.4, 140.5, 136.1, 131.5, 128.8, 128.4, 128.1, 126.8, 119.4, 118.4, 112.4, 109.4, 68.6. **HR-MS** (ESI) calcd for  $\text{C}_{18}\text{H}_{16}\text{NO}_2$   $[\text{M} + \text{H}]^+$  278.1176, found 278.1174.

**2-(6-Methoxypyridin-2-yl)phenol (L108)**

Prepared from 2-bromo-6-methoxypyridine<sup>189</sup> (799 mg) by general procedure 1. Purified by column chromatography (EtOAc/hexanes 1:10) and isolated as a colorless oil (522 mg, 2.59 mmol) in 61% yield.

**FT-IR** (neat,  $\text{cm}^{-1}$ )  $\nu_{\text{max}}$  = 1770, 1597, 1571, 1500, 1459, 1431, 1409, 1328, 1285, 1263, 1242, 1194, 1166, 1085, 1066, 1020, 998, 887, 807, 752, 632. **<sup>1</sup>H NMR** (400 MHz, acetone- $d_6$ )  $\delta$  13.26 (s, 1H), 7.94 – 7.88 (m, 2H), 7.70 (dt,  $J$  = 7.8, 0.6 Hz, 1H), 7.30 (ddd,  $J$  = 8.5, 7.1, 1.6 Hz, 1H), 6.94 – 6.88 (m, 2H), 6.83 (dd,  $J$  = 8.3, 0.7 Hz, 1H), 4.00 (s, 3H). **<sup>13</sup>C NMR** (101 MHz, Acetone)  $\delta$  163.1, 160.1, 156.1, 141.8, 132.1, 127.8, 120.0, 119.9, 118.9, 113.0, 109.4, 54.2. **HR-MS** (ESI) calcd for  $\text{C}_{12}\text{H}_{12}\text{NO}_2$   $[\text{M} + \text{H}]^+$  202.0863, found 202.0862.

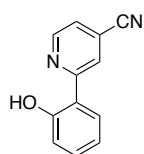
**2-(6-Chloropyridin-2-yl)phenol (L109)**

Prepared from 2-bromo-6-chloropyridine (818 mg) by general procedure 1. Purified by column chromatography (EtOAc/hexanes 1:15) and isolated as a colorless powder (629 mg, 3.06 mmol) in 72% yield.

**M.p.** 98 – 99 °C. **FT-IR** (neat,  $\text{cm}^{-1}$ )  $\nu_{\text{max}}$  = 1619, 1582, 1547, 1471, 1401, 1298, 1239, 1232, 1189, 1159, 1135, 1115, 1090, 1048, 997, 842, 799, 735, 675, 631. **<sup>1</sup>H NMR** (400 MHz,

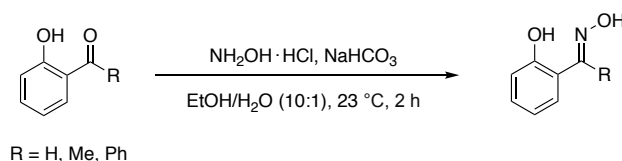
acetone- $d_6$ )  $\delta$  12.52 (s, 1H), 8.14 (dd,  $J$  = 8.1, 0.8 Hz, 1H), 8.05 (t,  $J$  = 8.0 Hz, 1H), 7.97 (dd,  $J$  = 8.0, 1.6 Hz, 1H), 7.49 (dd,  $J$  = 7.8, 0.8 Hz, 1H), 7.35 (ddd,  $J$  = 8.3, 7.2, 1.6 Hz, 1H), 6.98 – 6.93 (m, 2H).  $^{13}\text{C}$  NMR (101 MHz, Acetone)  $\delta$  160.1, 159.3, 148.5, 142.1, 133.0, 128.1, 123.0, 120.2, 119.4, 119.2, 119.2. **HR-MS** (ESI) calcd for  $\text{C}_{11}\text{H}_9\text{ClNO}$   $[\text{M} + \text{H}]^+$  206.0367, found 206.0364.

### 2-(2-Hydroxyphenyl)isonicotinonitrile (L110)

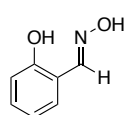


Prepared from 2-bromoisonicotinonitrile (778 mg) the general procedure 1. Purified by column chromatography (EtOAc/hexanes 1:10) and isolated as a bright yellow powder (458.6 mg, 2.34 mmol) in 55% yield.

**M.p.** 141 – 142 °C. **FT-IR** (neat,  $\text{cm}^{-1}$ )  $\nu_{\text{max}}$  = 1770, 1595, 1580, 1543, 1504, 1478, 1427, 1380, 1305, 1240, 1092, 860, 830, 777, 763, 725, 631.  $^1\text{H}$  NMR (400 MHz, acetone- $d_6$ )  $\delta$  13.32 (s, 1H), 8.88 (dd,  $J$  = 5.2, 1.0 Hz, 1H), 8.59 (d,  $J$  = 1.2 Hz, 1H), 8.10 (dd,  $J$  = 8.3, 1.6 Hz, 1H), 7.78 (dd,  $J$  = 5.2, 1.4 Hz, 1H), 7.38 (ddd,  $J$  = 8.3, 7.2, 1.6 Hz, 1H), 6.97 (dtd,  $J$  = 8.3, 3.6, 1.3 Hz, 2H).  $^{13}\text{C}$  NMR (101 MHz, acetone- $d_6$ )  $\delta$  160.9, 159.8, 148.6, 133.4, 128.1, 124.0, 123.3, 123.1, 120.1, 119.3, 117.2. **HR-MS** (ESI) calcd for  $\text{C}_{12}\text{H}_9\text{N}_2\text{O}$   $[\text{M} + \text{H}]^+$  197.0709, found 197.0713.

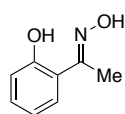
**General Procedure 2: Synthesis of Oxime Ligands**

The oxime ligands were prepared according to a slightly modified literature procedure.<sup>190</sup> To a stirred solution of the aldehyde (20 mmol, 1 equiv) in a mixture of EtOH (25 mL) and H<sub>2</sub>O (2.5 mL) was added NaHCO<sub>3</sub> (3.4 g, 40 mmol, 2 equiv) and hydroxylamine hydrochloride (2.1 g, 30 mmol, 1.5 equiv) at room temperature. After 2 h the mixture was concentrated, H<sub>2</sub>O was added and the mixture was extracted with EtOAc (3 x 150 mL). The combined organic layers were washed with brine, dried over MgSO<sub>4</sub> and concentrated.

**2-Hydroxybenzaldehyde oxime (L111)**

Prepared from 2-hydroxybenzaldehyde (2.4 g) by general procedure 2. Purified by column chromatography (EtOAc/hexanes 1:6) and isolated as colorless crystals (2.7 g, 19.7 mmol) in 98% yield. The spectral data of **L111** was in agreement with literature.<sup>191</sup>

**M.p.** 59 – 60 °C. **FT-IR** (neat, cm<sup>-1</sup>)  $\nu_{\text{max}}$  = 3375 (br), 1628, 1617, 1578, 1496, 1474, 1412, 1300, 1288, 1254, 1195, 1155, 990, 960, 900, 786, 766, 739, 720, 695, 647. **<sup>1</sup>H NMR** (400 MHz, acetone-*d*<sub>6</sub>)  $\delta$  10.63 (s, 1H), 10.06 (s, 1H), 8.36 (s, 1H), 7.36 – 7.34 (m, 1H), 7.27 (td, *J* = 7.9, 1.7 Hz, 1H), 6.91 (dd, *J* = 7.7, 7.0 Hz, 2H). **<sup>13</sup>C NMR** (101 MHz, acetone-*d*<sub>6</sub>)  $\delta$  158.3, 152.6, 131.5, 131.3, 120.3, 118.1, 117.1. **HR-MS** (EI) calcd for C<sub>7</sub>H<sub>7</sub>NO<sub>2</sub> [M] 137.0477, found 137.0479.

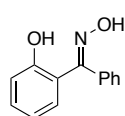
**2-Hydroxyacetophenone oxime (L112)**

Prepared from 2-hydroxyacetophenone (2.7 g) by general procedure 2. Purified by recrystallization in EtOAc/hexanes and isolated as pale yellow crystals (1.9 g, 12.6 mmol) in 63% yield. The spectral data of **L112** was in agreement with literature.<sup>192</sup>



**M.p.** 116 – 117 °C. **FT-IR** (neat,  $\text{cm}^{-1}$ )  $\nu_{\text{max}}$  = 3327, 1634, 1615, 1590, 1497, 1469, 1409, 1369, 1288, 1254, 1159, 1047, 1016, 944, 849, 835, 781, 746, 736, 643.  **$^1\text{H}$  NMR** (400 MHz,  $\text{DMSO-}d_6$ )  $\delta$  11.56 (s, 1H), 11.53 (s, 1H), 7.48 (dd,  $J$  = 7.6, 1.9 Hz, 0H), 7.23 (ddd,  $J$  = 8.1, 7.4, 1.7 Hz, 1H), 6.90 – 6.85 (m, 2H), 2.25 (s, 3H).  **$^{13}\text{C}$  NMR** (101 MHz,  $\text{DMSO-}d_6$ )  $\delta$  157.4, 157.1, 130.1, 127.9, 119.4, 118.9, 116.5, 11.1. **HR-MS** (EI) calcd for  $\text{C}_8\text{H}_9\text{NO}_2$  [M] 151.0633, found 151.0630.

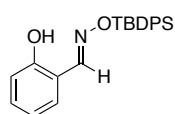
### 2-Hydroxybenzophenone oxime (L113)



Prepared from 2-hydroxybenzophenone (4.0 g) by general procedure 2. Purified by recrystallization in EtOAc/hexanes and isolated as colorless crystals (1.36 g, 6.4 mmol) in 32% yield. The spectral data of **L113** was in agreement with literature.<sup>193</sup>

**M.p.** 136 – 138 °C. **FT-IR** (neat,  $\text{cm}^{-1}$ )  $\nu_{\text{max}}$  = 3362, 1625, 1592, 1496, 1445, 1418, 1376, 1325, 1286, 1237, 1220, 1158, 1102, 1001, 933, 834, 770, 758, 687, 674, 659.  **$^1\text{H}$  NMR** (400 MHz, acetone- $d_6$ )  $\delta$  10.69 (s, 1H), 7.94 (s, 1H), 7.48 (dd,  $J$  = 7.4, 2.3 Hz, 2H), 7.36 – 7.29 (m, 4H), 7.05 (dd,  $J$  = 7.6, 1.8 Hz, 1H), 7.00 (dd,  $J$  = 8.2, 1.1 Hz, 1H), 6.94 (td,  $J$  = 7.4, 1.1 Hz, 1H).  **$^{13}\text{C}$  NMR** (101 MHz, acetone- $d_6$ )  $\delta$  155.9, 155.7, 137.8, 131.2, 131.0, 129.7, 128.9, 128.1, 122.4, 120.3, 117.6, 29.8. **HR-MS** (EI) calcd for  $\text{C}_{13}\text{H}_{11}\text{NO}_2$  [M] 213.0790, found 213.0784.

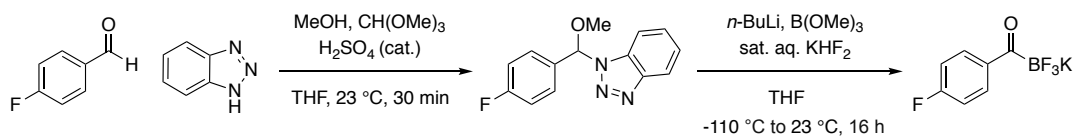
### 2-Hydroxybenzaldehyde O-(tert-butylidiphenylsilyl) oxime (L114)



Prepared from 2-hydroxybenzaldehyde (2.4 g) and *O*-(tert-butylidiphenylsilyl) hydroxylamine<sup>194</sup> (8.1 g) by general procedure 2. Purified by recrystallization in EtOAc/hexanes and isolated as colorless crystals (3.45 g, 9.2 mmol) in 46% yield.

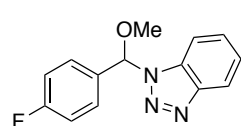
**M.p.** 62 – 64 °C. **FT-IR** (neat,  $\text{cm}^{-1}$ )  $\nu_{\text{max}}$  = 3021, 2955, 2857, 1620, 1609, 1589, 1573, 1491, 1471, 1427, 1392, 1348, 1262, 1196, 1156, 1116, 974, 922, 830, 820, 757, 839, 698, 613.  **$^1\text{H}$  NMR** (400 MHz,  $\text{CDCl}_3$ )  $\delta$  9.52 (s, 1H), 8.49 (s, 1H), 7.72 – 7.70 (m, 4H), 7.45 – 7.37 (m, 6H), 7.24 – 7.18 (m, 2H), 6.91 – 6.86 (m, 2H), 1.16 (s, 9H).  **$^{13}\text{C}$  NMR** (101 MHz,  $\text{CDCl}_3$ )  $\delta$  157.7, 156.9, 135.6, 132.4, 131.5, 131.0, 130.3, 128.0, 119.6, 116.9, 116.6, 27.2, 19.4. **HR-MS** (EI) calcd for  $\text{C}_{23}\text{H}_{25}\text{NO}_2\text{Si}$  [M] 375.1655, found 375.1656.

## 7.2.2 Synthesis of Potassium 4-Fluorobenzoyltrifluoroborate



The synthesis of potassium 4-fluorobenzoyltrifluoroborate (**100**) was performed according to a previously reported literature procedure by the BODE group.<sup>195</sup>

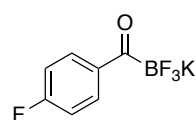
### 1-(Methoxy(4-fluorophenyl)methyl)-1H-benzotriazole (**S1**)



4-Fluorobenzaldehyde (5.00 g, 40 mmol, 1.0 equiv), benzotriazole (4.80 g, 40 mmol, 1.0 equiv), MeOH (3.26 mL, 81 mmol, 2.0 equiv), and trimethylorthoformate (13.2 mL, 121 mmol, 3.0 equiv) were dissolved in anhydrous THF (60 mL) at 23 °C. To this solution was added conc. H<sub>2</sub>SO<sub>4</sub> (12 drops), immediately resulting in the formation of a colorless precipitate. The mixture was stirred at 23 °C for 25 min, 1.0 g solid NaHCO<sub>3</sub> was added and the heterogeneous solution was concentrated to dryness. The resulting oil was dissolved in CH<sub>2</sub>Cl<sub>2</sub> (20 mL), filtered, concentrated and dried under high vacuum. The purity of acetal (10.3 g, 99% yield) was better than 95% and was used in the next step without further purification. The spectral data was in agreement to literature.<sup>195</sup>

<sup>1</sup>H NMR (300 MHz, dacetone-*d*<sub>6</sub>) 8.01-8.02 (m, 1H), 7.54-7.45 (m, 2H), 7.46-7.36 (m, 3H), 7.23-7.12 (m, 3H), 3.45 (s, 3H). <sup>19</sup>F NMR (282 MHz, acetone-*d*<sub>6</sub>) -114.5.

### Potassium 4-fluorobenzoyltrifluoroborate (**100**)



In a 500 mL flask, benzotriazole **S1** (10.0 g, 39 mmol, 1.05 equiv) was dissolved in dry THF (250 mL) at RT. The flask was placed in a dry ice/acetone bath which was cooled with liquid nitrogen to -110 °C and stirred for at least 15 min. *n*-Butyllithium (1.6 M in hexanes, 23 mL, 37 mmol, 1.0 equiv) was added slowly down the side of the flask over 10 min. The resulting deep green solution was stirred for 2 min following the end of *n*-butyllithium addition, and neat B(OMe)<sub>3</sub> (8.25 mL, 74 mmol, 2.0 equiv) was added slowly over 1 min directly into the solution. After 5-10 min of stirring the solution gradually turned red. The flask was kept in the dry ice/acetone bath for 1 h, which

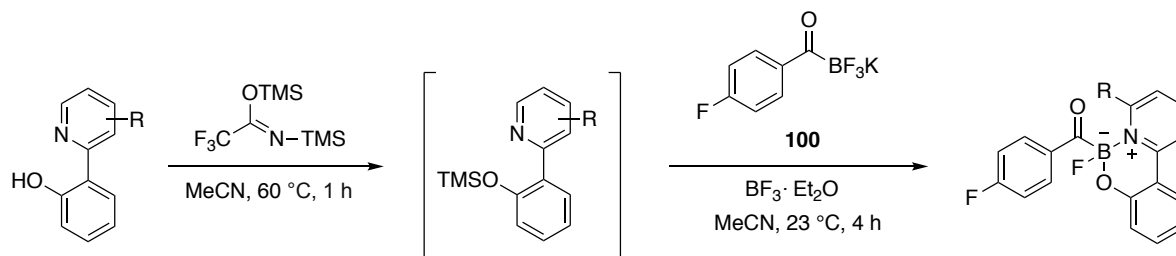
slowly warmed to  $-78\text{ }^{\circ}\text{C}$ , and then removed from the bath. Under vigorous stirring five portions of sat. aq.  $\text{KHF}_2$  were added (5 x 20 mL, 100 mL total). As the reaction warmed to room temperature a biphasic mixture consisting of a milky white aqueous layer and a yellow organic layer formed. The mixture was stirred for 16 h. The two layers were separated and the organic phase was evaporated until only water remained. The resulting yellow wet slurry was mixed with  $\text{Et}_2\text{O}$  (40 mL). After filtration, washing with additional  $\text{Et}_2\text{O}$  (4 x 30 mL) and drying under high vacuum, the product was afforded as a colorless solid (5.34 g) in 62% yield. The spectral data was in agreement with literature.<sup>195</sup>

**M.p.** decomposition  $>250\text{ }^{\circ}\text{C}$ . **FT-IR** (neat,  $\text{cm}^{-1}$ )  $\nu_{\text{max}}$  = 3013, 1637, 1580.  **$^1\text{H}$  NMR** (600 MHz,  $\text{DMSO-}d_6$ )  $\delta$  7.98 – 7.95 (m, 1H), 7.20 – 7.17 (m, 1H).  **$^{13}\text{C}$  NMR** (151 MHz,  $\text{DMSO}$ )  $\delta$  232.3 – 229.0 (m), 163.6 (d,  $J$  = 247.5 Hz), 138.0, 130.3 (dd,  $J$  = 8.9, 2.2 Hz), 114.5 (d,  $J$  = 21.2 Hz).  **$^{19}\text{F}$  NMR** (282 MHz,  $\text{acetone-}d_6$ )  $\delta$  -111.8 (1F), -144.7 (dd,  $J$  = 103.0, 50.2 Hz, 3F).  **$^{11}\text{B}$  NMR** (160 MHz,  $\text{DMSO-}d_6$ )  $\delta$  -1.14 (q,  $J$  = 53.5 Hz). **HR-MS** (EI) calcd for  $\text{C}_7\text{H}_4\text{BF}_4\text{O}_2$   $[\text{M} - \text{K}]^-$  191.0298, found 191.0297.

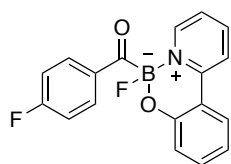
### 7.2.3 Synthesis of Potassium Monofluoroacylboronates

Potassium monofluoroacylboronate **115** and **158** were synthesized according to a previously reported literature procedure.<sup>196</sup>

#### General Procedure 3 for the Synthesis of Potassium Monofluoroacylboronates



Potassium monofluoroborate synthesis was performed according to a previously established procedure by the BODE group.<sup>196</sup> To a flame-dried 10 mL Schlenk flask equipped with a magnetic stir bar was added 2-(pyridin-2-yl)phenol ligand (1.0 mmol, 1.0 equiv). Anhydrous CH<sub>3</sub>CN (0.68 mL) and *N,O*-bis(trimethylsilyl) trifluoroacetamide (320  $\mu$ L, 1.20 mmol, 1.2 equiv) were added and the mixture was stirred for 1 h at 60 °C. After cooling to room temperature, all volatiles were removed carefully under vacuum and the residual pale yellow oil was additionally dried for 2 h under vacuum at 60 °C to give the TMS-capped ligand, which was used in the next step without further purification. A flame-dried 50 mL Schlenk flask equipped with a magnetic stir bar was charged with potassium 4-fluorobenzoyltrifluoroborate **100** (230 mg, 1.0 mmol, 1.0 equiv). A solution of the TMS-capped ligand in anhydrous CH<sub>3</sub>CN (6.0 + 2.0 + 2.0 mL) was added. To this suspension BF<sub>3</sub>·OEt<sub>2</sub> (123  $\mu$ L, 1.0 mmol, 1.0 equiv) was added dropwise. The mixture became homogeneous and was stirred for 4 h at 23 °C. The reaction mixture was carefully evaporated (temperature of water bath less than 30 °C). The crude material was purified by silica gel column chromatography (EtOAc/hexanes) to afford the desired product.

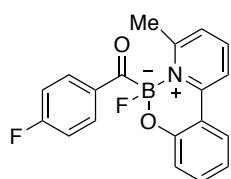
**4-Fluorophenyl monofluoroacylboronate from 2-(pyridin-2-yl)phenol ligand (S2)**

Prepared from 2-(pyridin-2-yl)phenol (171 mg) by general procedure 3.

Purified by silica gel column chromatography (EtOAc/hexanes 1:10) and isolated as a yellow solid (207 mg, 0.6 mmol) in 64% yield. The spectral

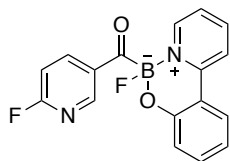
data of **S2** were in agreement with literature.<sup>196</sup>

**FT-IR** (neat,  $\text{cm}^{-1}$ )  $\nu_{\text{max}}$  = 3102, 3073, 1623, 1587, 1500, 1437, 1292, 1228, 1117, 1051, 958, 840. **<sup>1</sup>H NMR** (600 MHz,  $\text{CDCl}_3$ )  $\delta$  8.50 (ddd,  $J$  = 5.9, 1.7, 0.8 Hz, 1H), 8.25 – 8.21 (m, 2H), 8.16 (ddd,  $J$  = 8.4, 7.4, 1.7 Hz, 1H), 8.07 (dt,  $J$  = 8.5, 0.9 Hz, 1H), 7.76 – 7.74 (m, 1H), 7.57 (ddd,  $J$  = 7.3, 5.9, 1.3 Hz, 1H), 7.36 (ddd,  $J$  = 8.3, 7.2, 1.6 Hz, 1H), 7.13 – 7.10 (m, 2H), 7.03 (ddd,  $J$  = 8.3, 1.2, 0.4 Hz, 1H), 6.96 (ddd,  $J$  = 8.0, 7.2, 1.2 Hz, 1H). **<sup>13</sup>C NMR** (151 MHz,  $\text{CDCl}_3$ )  $\delta$  228.7 – 226.1 (m), 165.4 (d,  $J$  = 252.6 Hz), 155.1 (d,  $J$  = 5.2 Hz), 149.9, 142.6 (d,  $J$  = 6.3 Hz), 142.4, 136.4, 134.7, 131.3 (dd,  $J$  = 9.1, 2.3 Hz), 125.5, 122.9, 120.8, 120.5, 120.3, 116.6, 115.3 (d,  $J$  = 21.5 Hz). **<sup>19</sup>F NMR** (470 MHz,  $\text{CDCl}_3$ )  $\delta$  -107.2 (tt,  $J$  = 8.8, 5.7 Hz, 1F), -158.8 (d,  $J$  = 85.3 Hz, 3F). **<sup>11</sup>B NMR** (160 MHz,  $\text{CDCl}_3$ )  $\delta$  2.10 (d,  $J$  = 44.4 Hz). **HR-MS** (ESI) calcd for  $\text{C}_{18}\text{H}_{12}\text{BF}_2\text{NO}_2$  [ $\text{M} + \text{Na}$ ]<sup>+</sup> 346.0825, found 346.0820.

**4-Fluorophenyl monofluoroacylboronate from 2-(6-methylpyridin-2-yl)phenol ligand (S3)**

Prepared from 2-(6-methylpyridin-2-yl)phenol (186 mg) by general procedure 3. Purified by silica gel column chromatography (EtOAc/hexanes 1:10) and isolated as a yellow solid (115 mg, 0.3 mmol) in 34% yield.

**<sup>1</sup>H NMR** (300 MHz,  $\text{CDCl}_3$ )  $\delta$  8.28 – 8.22 (m, 2H), 8.10 (d,  $J$  = 8.2 Hz, 1H), 7.80 – 7.70 (m, 3H), 7.41 (ddd,  $J$  = 8.6, 7.2, 1.6 Hz, 1H), 7.165– 7.01 (m, 3H), 6.86 (dd,  $J$  = 8.5, 0.9 Hz, 1H), 3.82 (s, 3H). **<sup>19</sup>F NMR** (282 MHz,  $\text{CDCl}_3$ )  $\delta$  -108.4 (tt,  $J$  = 8.8, 5.8 Hz, 1F), -147.4 (brs, 3F). **HR-MS** (MALDI) calcd for  $\text{C}_{19}\text{H}_{14}\text{BF}_2\text{NO}_2$  [ $\text{M} + \text{Na}$ ]<sup>+</sup> 360.0978, found 360.0979.

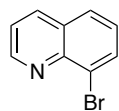
**2-fluoro-5-monofluoroboronate (158)**

Compound **158** was prepared from 2-(2-hydroxyphenyl)pyridine **L97** (171 mg, 1.00 mmol, 1.0 equiv) by general procedure 3. The crude material was directly purified by silica gel column chromatography (EtOAc/hexanes 1:5) to afford the desired product as a yellow solid (156 mg, 0.48 mmol, 48%).

**M.p.** 177.6 – 178.2 °C. **IR** (neat,  $\text{cm}^{-1}$ )  $\nu_{\text{max}}$  = 1639, 1622, 1607, 1578, 1560, 1500, 1482, 1456, 1433, 1367, 1292, 1228, 1170, 1140, 1112, 1075, 1054, 1018, 961, 843, 788, 756, 740, 620.  **$^1\text{H}$  NMR** (500 MHz,  $\text{CDCl}_3$ )  $\delta$  9.14 (d,  $J$  = 1.6 Hz, 1H), 8.50 (dd,  $J$  = 5.9, 0.9 Hz, 0H), 8.47 (td,  $J$  = 8.2, 2.4 Hz, 1H), 8.21 (ddd,  $J$  = 8.4, 7.5, 1.7 Hz, 1H), 8.11 (d,  $J$  = 8.6 Hz, 1H), 7.76 (dd,  $J$  = 8.1, 1.6 Hz, 1H), 7.60 (ddd,  $J$  = 7.3, 5.9, 1.3 Hz, 1H), 7.39 (ddd,  $J$  = 8.3, 7.2, 1.6 Hz, 1H), 7.04 (dd,  $J$  = 8.5, 0.9 Hz, 1H), 7.00 – 6.96 (m, 2H).  **$^{13}\text{C}$  NMR** (151 MHz,  $\text{CDCl}_3$ )  $\delta$  227.5 – 225.1 (m), 165.0 (d,  $J$  = 243.9 Hz), 154.7 (d,  $J$  = 5.2 Hz), 150.3 (dd,  $J$  = 15.9, 3.5 Hz), 149.8, 142.5, 142.4 (d,  $J$  = 6.3 Hz), 141.0 (d,  $J$  = 9.0 Hz), 134.8, 133.3, 125.4, 122.9, 120.9, 120.3, 120.3, 116.4, 109.3 (d,  $J$  = 37.2 Hz).  **$^{19}\text{F}$  NMR** (470 MHz,  $\text{CDCl}_3$ ):  $\delta$  -62.6 (dd,  $J$  = 7.8, 2.9 Hz), -159.6 (d,  $J$  = 70.6 Hz).  **$^{11}\text{B}$  NMR** (160 MHz,  $\text{CDCl}_3$ ):  $\delta$  1.84 (d,  $J$  = 48.1 Hz). **HR-MS** (ESI) calcd for  $\text{C}_{17}\text{H}_{11}\text{BF}_2\text{N}_2\text{NaO}_2$  [ $\text{M} + \text{Na}$ ] $^+$  347.0777, found 347.0783.

## 7.2.4 Synthesis of Bromoquinoline Precursors

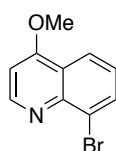
### 8-Bromoquinoline (178)



8-Bromoquinoline **178** was synthesized according to a previously reported literature procedure.<sup>197</sup> A 50 mL round bottom flask was charged with methanesulfonic acid (16 mL), 3-nitrobenzene sulfonic acid sodium salt (4.26 g, 18.9 mmol, 0.63 equiv) and FeSO<sub>4</sub>·7H<sub>2</sub>O (0.25 g, 0.9 mmol, 0.003 equiv). The mixture was heated to 125 °C before adding 2-bromoaniline (3.46 mL, 30 mmol, 1 equiv) and glycerol (4 x 2.21 mL, 60 mmol, 2 equiv). The mixture was stirred at 125 °C for 16 h. The dark brown mixture was cooled to room temperature and H<sub>2</sub>O was added slowly (20 mL). The mixture was transferred into a 500 mL Erlenmeyer flask with additional H<sub>2</sub>O and cooled to 0 °C using an ice-bath. The reaction mixture was basified to pH 14 by adding 2 M aq. NaOH solution and solid NaOH pallets. The mixture was extracted with Et<sub>2</sub>O (3 x 200 mL). The combined organic layers were washed with brine, dried over Na<sub>2</sub>SO<sub>4</sub>. The organic solvent was removed under reduced pressure to yield the desired product as a brown-yellow oil (4.75 g, 26.4 mmol, 88%).

The spectral data was in agreement with literature.<sup>198</sup> **FT-IR** (neat, cm<sup>-1</sup>)  $\nu_{\max}$  = 3051 (br), 3024 (br), 1607, 1594, 1489, 1456, 1381, 1306, 1203, 1062, 963, 819, 781, 755, 643. **<sup>1</sup>H NMR** (400 MHz, CDCl<sub>3</sub>)  $\delta$  9.03 (tt,  $J$  = 4.1, 1.7 Hz, 1H), 8.13 (ddd,  $J$  = 8.2, 3.4, 1.8 Hz, 1H), 8.03 (ddd,  $J$  = 7.7, 3.2, 1.5 Hz, 1H), 7.76 (ddd,  $J$  = 8.4, 3.5, 1.6 Hz, 1H), 7.44 (dtd,  $J$  = 8.0, 4.0, 1.5 Hz, 1H), 7.40 – 7.34 (m, 1H). **<sup>13</sup>C NMR** (101 MHz, CDCl<sub>3</sub>)  $\delta$  151.3, 145.3, 136.7, 133.3, 129.7, 127.9, 127.1, 124.8, 122.0. **HR-MS** (ESI) calcd for C<sub>9</sub>H<sub>7</sub>BrN [M + H]<sup>+</sup> 207.9756, found 207.9757.

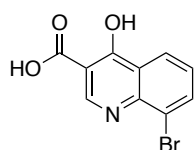
### 8-Bromo-4-methoxyquinoline (S4)



A 10 mL microwave vessel was charged with 8-bromo-4-chloroquinoline (**S7**) (200 mg, 1.23 mmol, 1 equiv), sodium methoxide (334.1 mg, 6.19 mmol, 5 equiv) and MeOH (2 mL). The vessel was sealed carefully and the suspension was heated to 95 °C for 12 h. The reaction mixture was cooled to room temperature, diluted with H<sub>2</sub>O (50 mL) and extracted with EtOAc (3 x 50 mL). The combined organic layers were dried over Na<sub>2</sub>SO<sub>4</sub> and concentrated under reduced pressure. The crude reaction mixture was purified by flash column chromatography (eluent: hexanes/EtOAc 2:1) to yield the desired product as colorless crystals (275 mg, 1.16 mmol) in 94 % yield.

**M.p.** 123 – 124 °C. **FT-IR** (neat,  $\text{cm}^{-1}$ )  $\nu_{\text{max}}$  = 3025, 2971, 1608, 1587, 1555, 1498, 1460, 1403, 1382, 1297, 1267, 1079, 994, 850, 825, 806, 779, 757.  **$^1\text{H NMR}$**  (400 MHz,  $\text{CDCl}_3$ )  $\delta$  8.89 (d,  $J$  = 5.2 Hz, 1H), 8.19 (dd,  $J$  = 8.3, 1.4 Hz, 1H), 8.03 (dd,  $J$  = 7.5, 1.4 Hz, 1H), 7.34 (dd,  $J$  = 8.3, 7.5 Hz, 1H), 6.81 (d,  $J$  = 5.2 Hz, 1H), 4.06 (s, 3H).  **$^{13}\text{C NMR}$**  (101 MHz,  $\text{CDCl}_3$ )  $\delta$  162.7, 152.3, 146.4, 133.7, 126.1, 124.3, 122.9, 121.9, 100.9, 56.2. **HR-MS** (ESI) calcd for  $\text{C}_{10}\text{H}_9\text{BrNO}$   $[\text{M} + \text{H}]^+$  237.9862, found 237.9863.

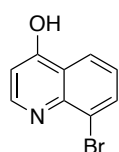
### 8-Bromo-3-carbethoxy-4-hydroxyquinoline (S5)



8-Bromo-3-carbethoxy-4-hydroxyquinoline **S5** was synthesized according to a slightly modified literature procedure.<sup>199</sup> A solution of 2-bromoaniline (1.58 mL, 14.62 mmol) and diethyl ethoxymethylenemalonate (2.9 mL, 14.62 mmol) was heated at 100 °C for 3 h. During the reaction, a stream of  $\text{N}_2$  was passed through the mixture to help removing the EtOH formed. Boiling diphenyl ether (10 mL) was added to the molten acrylate and the mixture was heated at reflux (290 °C) for 2 h in a tin bath. The mixture was cooled to room temperature and petroleum ether (100 mL) was added to the reaction mixture. The precipitated product was collected and washed with petroleum ether (2 x 100 mL). The product was used in the next step without further purification.

The spectral data was in agreement with literature.<sup>200</sup> **M.p** 284 – 285 °C. **FT-IR** (neat,  $\text{cm}^{-1}$ )  $\nu_{\text{max}}$  = 3060 (br), 1713, 1602, 1548, 1474, 1335, 1261, 1247, 1205, 1121, 936, 776.  **$^1\text{H NMR}$**  (400 MHz,  $\text{DMSO}-d_6$ )  $\delta$  12.66 (s, 1H), 8.68 (s, 1H), 8.33 (dd,  $J$  = 8.2, 1.3 Hz, 1H), 8.25 (dd,  $J$  = 7.7, 1.4 Hz, 1H), 7.56 – 7.52 (m, 1H), 3.56 (s, 4H).  **$^{13}\text{C NMR}$**  (101 MHz,  $\text{DMSO}$ )  $\delta$  178.2, 165.7, 145.9, 137.5, 137.1, 127.0, 126.3, 125.1, 112.7, 108.2. **HR-MS** (ESI) calcd for  $\text{C}_{10}\text{H}_5\text{BrNO}_3$   $[\text{M} + \text{H}]^+$  265.9458, found 265.9466.

### 8-Bromo-4-hydroxyquinoline (S6)



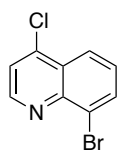
8-Bromo-4-hydroxyquinoline **S6** was synthesized according to a previously reported literature procedure.<sup>199</sup> **S5** was refluxed in 10% NaOH solution for 2 h until the solution became clear. The solution was cooled to room temperature and acidified with 1 M HCl solution. The precipitate was collected, washed with  $\text{H}_2\text{O}$  and dried at the high vacuum overnight. The subsequent decarboxylation was carried out by refluxing ether (290 °C) the crude carboxylic acid intermediate in diphenyl ether (50 mL) using a tin



bath until no gas formation was observed anymore. After cooling to room temperature, an equal volume of petroleum ether (50 mL) was added. The white precipitate was collected by vacuum filtration and washed with additional petroleum ether (2 x 50 mL). The product was used in the next step without further purification.

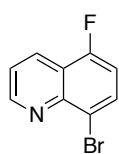
The spectral data was in agreement with literature.<sup>200</sup> **M.p.** 157 – 158 °C. **FT-IR** (neat,  $\text{cm}^{-1}$ )  $\nu_{\text{max}}$  = 3433 (br), 2996 (br), 1770, 1759, 1621, 1598, 1557, 1504, 1429, 1384, 1246, 1213, 1198, 1106, 1057, 823, 789, 743. **<sup>1</sup>H NMR** (400 MHz, methanol- $d_4$ )  $\delta$  8.25 (dd,  $J$  = 8.2, 1.3 Hz, 1H), 7.98 (dd,  $J$  = 7.6, 1.5 Hz, 2H), 7.37 – 7.26 (m, 1H), 6.36 (d,  $J$  = 7.4 Hz, 1H). **<sup>13</sup>C NMR** (101 MHz, methanol- $d_4$ )  $\delta$  180.4, 141.9, 139.2, 137.1, 128.2, 126.2, 125.7, 112.9, 110.5, 49.0. **HR-MS** (ESI) calcd for  $\text{C}_9\text{H}_7\text{BrNO}$  [ $\text{M} + \text{H}$ ]<sup>+</sup> 223.9707, found 223.9705.

### 8-Bromo-4-chloroquinoline (S7)



8-Bromo-4-hydroxyquinoline **S7** was synthesized according to a previously reported literature procedure.<sup>199</sup> 8-Bromo-4-hydroxyquinoline **S6** (500 mg, 2.2 mmol, 1.0 equiv) was refluxed in 4.5 mL of  $\text{POCl}_3$  for 3 h at 120 °C. The phosphorus oxychloride was removed under reduced pressure and the residue was poured onto ice water. The mixture was basified with  $\text{NH}_4\text{OH}$  and extracted with  $\text{CH}_2\text{Cl}_2$  (2 x 150 mL). The organic layers were combined, washed with brine and dried over  $\text{Na}_2\text{SO}_4$ . The crude was recrystallized from EtOH to yield the desired product as a colorless solid (497 mg, 2.1 mmol, 92 %).

The spectral data was in agreement with literature.<sup>200</sup> **M.p.** 133 – 134 °C. **FT-IR** (neat,  $\text{cm}^{-1}$ )  $\nu_{\text{max}}$  = 1064, 1584, 1483, 1452, 1371, 1282, 1193, 1077, 845, 804, 752, 731. **<sup>1</sup>H NMR** (400 MHz,  $\text{CDCl}_3$ )  $\delta$  8.92 (d,  $J$  = 4.7 Hz, 1H), 8.25 (dd,  $J$  = 8.5, 1.3 Hz, 1H), 8.13 (dd,  $J$  = 7.5, 1.3 Hz, 1H), 7.58 (d,  $J$  = 4.7 Hz, 1H), 7.51 (dd,  $J$  = 8.4, 7.5 Hz, 1H). **<sup>13</sup>C NMR** (101 MHz,  $\text{CDCl}_3$ )  $\delta$  150.7, 146.3, 143.3, 134.4, 128.1, 128.0, 125.4, 124.4, 122.2. **HR-MS** (ESI) calcd for  $\text{C}_9\text{H}_6\text{BrClN}$  [ $\text{M} + \text{H}$ ]<sup>+</sup> 241.9367, found 241.9369.

**8-Bromo-4-fluoroquinoline (180)**

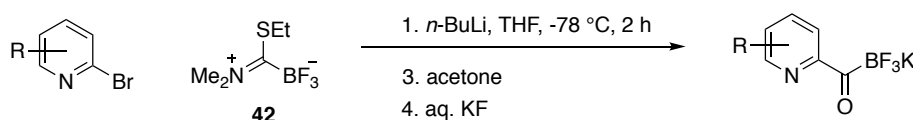
8-Bromo-4-hydroxyquinoline **S6** was synthesized according to a previously reported literature procedure.<sup>201</sup> To a mixture of 2-bromo-5-fluoroaniline (1.4 g, 7.4 mmol, 1 equiv), 3-nitrobenzene sulfonic acid sodium salt (2.6 g, 11.5 mmol, 1.6 equiv) and glycerol (1.4 g, 15.2 mmol, 2 equiv) was added dropwise aqueous sulfuric acid (70 %, 5 mL). The mixture was heated to 145 °C for 16 h. The mixture was cooled to room temperature, poured onto ice water and filtered through celite. The filtrate was neutralized with NaOH and extracted with CH<sub>2</sub>Cl<sub>2</sub> three times. The combined organic layers were dried over Na<sub>2</sub>SO<sub>4</sub> and concentrated under reduced pressure. The crude reaction mixture was purified by flash column chromatography (eluent 1 % MeOH in CH<sub>2</sub>Cl<sub>2</sub>) to yield the desired product **180** as a colorless crystalline solid (1.35 g, 6 mmol) in 81 % yield.

The spectral data was in agreement with literature.<sup>201</sup> **M.p.** 76 – 77 °C. **FT-IR** (neat, cm<sup>-1</sup>)  $\nu_{\max}$  = 2995, 1770, 1759, 1622, 1594, 1460, 1394, 1383, 1250, 1216, 1142, 1056, 1020, 937, 820, 804, 772, 622. **<sup>1</sup>H NMR** (400 MHz, CDCl<sub>3</sub>)  $\delta$  9.10 (dd, *J* = 4.2, 1.7 Hz, 1H), 8.46 (dd, *J* = 8.4, 1.7 Hz, 1H), 7.99 (dd, *J* = 8.3, 5.5 Hz, 1H), 7.55 (dd, *J* = 8.4, 4.3 Hz, 1H), 7.14 (dd, *J* = 9.1, 8.4 Hz, 1H). **<sup>13</sup>C NMR** (101 MHz, Chloroform-*d*)  $\delta$  157.51 (d, *J* = 256.4 Hz), 152.20, 145.69 (d, *J* = 3.2 Hz), 132.34 (d, *J* = 8.5 Hz), 130.12 (d, *J* = 4.7 Hz), 122.15 (d, *J* = 3.0 Hz), 120.52 (d, *J* = 17.1 Hz), 119.30 (d, *J* = 4.6 Hz), 111.12 (d, *J* = 20.8 Hz). **HR-MS** (ESI) calcd for C<sub>9</sub>H<sub>6</sub>BrFN [M + H]<sup>+</sup> 225.9662, found 225.9665.

## 7.2.5 Synthesis of Potassiumacyltrifluoroborates

Potassium 6-bromonicotinoyltrifluoroborate (**48**),<sup>179</sup> potassium 2-isonicotinoyltrifluoroborate (**116**),<sup>179</sup> potassium 4-anisoyltrifluoroborate (**119**),<sup>179</sup> potassium 4-cyanobenzoyltrifluoroborate (**120**),<sup>179</sup> potassium 4-fluorobenzoyltrifluoroborate (**121**),<sup>180</sup> potassium nonanoyltrifluoroborate (**122**),<sup>202</sup> potassium 5-hydroxypentanoyltrifluoroborate (**122**),<sup>202</sup> potassium nicotinoyltrifluoroborate (**125**),<sup>179</sup> potassium 2-chloroisonicotinoyltrifluoroborate (**126**)<sup>179</sup> and potassium 6-chloro-2-isonicotinoyltrifluoroborate (**134**)<sup>179</sup> were prepared according to previously established procedures by the BODE group. Glycine and alanine-derived KATs **167** and **168** were kindly provided by JUMPEI TAGUCHI in collaboration with the ITO group. (6-(2-hydroxyphenyl)-2-pyridyl KAT (**169**) was synthesized and provided by YI-CHUNG DZENG.

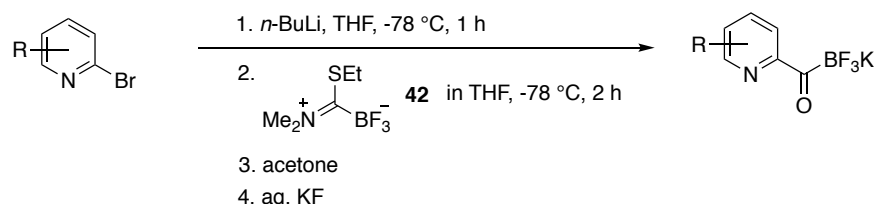
### General Procedure 4A: Synthesis of Pyridyl Acyltrifluoroborates without Pre-Lithiation



Potassium acyltrifluoroborates (KATs) were synthesized according to a slight modification of a previously reported procedure by the Bode group.<sup>179</sup> A flame-dried, 10 mL round-bottom flask equipped with magnetic stir bar and septum under inert nitrogen atmosphere was charged with pyridyl bromide (1.08 mmol, 1.00 equiv), (ethylthio-trifluoroborate)-methane dimethyliminium **42** (0.200 g, 1.08 mmol, 1.00 equiv) and a mixture of anhydrous toluene/THF (4:1, 4 mL). The mixture was cooled to -78 °C in a dry ice/acetone bath and *n*-butyllithium (1.6 M in hexanes, 675  $\mu$ L, 1.08 mmol, 1.00 equiv) was added dropwise over 30 min via syringe pump. After the mixture was stirred for 2 h at -78 °C, the residual *n*-butyllithium was quenched with acetone (80  $\mu$ L, 1.08 mmol, 1.00 equiv). Ten minutes after the addition of acetone, an aqueous KF solution (6.5 M, 0.5 mL, 3.24 mmol, 3.00 equiv) was added at -78 °C. The flask was removed from the dry ice/acetone bath and the mixture was stirred for 1 h at room temperature. To the resulting heterogeneous mixture was added  $\text{CH}_2\text{Cl}_2$  (5 mL). The mixture was filtered and washed with additional  $\text{CH}_2\text{Cl}_2$  (3x20 mL) and acetone (2x10 mL). The remaining filter cake was washed with DMF (50 mL) until the filtrate was colorless. The

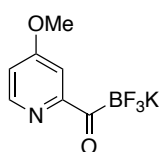
DMF was removed under reduced pressure at 50 – 60 °C to yield the desired KAT as a colorless or yellow solid.

#### General Procedure 4B: Synthesis of Pyridyl Acyltrifluoroborates via Pre-Lithiation



A flame-dried, 10-mL round-bottom flask equipped with magnetic stir bar and septum under inert nitrogen atmosphere was charged with pyridyl bromide (1.08 mmol, 1.00 equiv) and a mixture of anhydrous toluene/THF (4:1, 4 mL). The mixture was cooled to -78 °C in a dry ice/acetone bath and *n*-butyllithium (1.6 M in hexanes, 675  $\mu\text{L}$ , 1.08 mmol, 1.00 equiv) was added dropwise over 30 min via syringe pump. After the mixture was stirred for one h at -78 °C, a solution of (ethylthio-trifluoroborate)-methane dimethyliminium **42** (200 mg, 1.08 mmol, 1.00 equiv) in anhydrous THF (1.0 mL) was added dropwise over 30 min via syringe pump. After the mixture was stirred for 2 h at -78 °C, the residual *n*-butyllithium was quenched with acetone (80  $\mu\text{L}$ , 1.08 mmol, 1.00 equiv). Ten minutes after the addition of acetone, an aqueous KF solution (6.5 M, 0.5 mL, 3.24 mmol, 3.00 equiv) was added at -78 °C. The flask was removed from the dry ice/acetone bath and the mixture was stirred for 1 h at room temperature. To the resulting heterogeneous mixture was added  $\text{CH}_2\text{Cl}_2$  (5 mL). The mixture was filtered and washed with additional  $\text{CH}_2\text{Cl}_2$  (3x20 mL) and acetone (2x10 mL). The remaining filter cake was washed with DMF (50 mL) until the filtrate was colorless. The DMF was removed under reduced pressure at 50 – 60 °C to yield the desired KAT as colorless or yellow solid.

#### Potassium 4-methoxy-2-isonicotinoyltrifluoroborate (**127**)

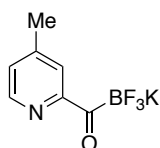


Prepared from 2-bromo-4-methoxypyridine (203 mg) by general procedure 4B and isolated as yellow solid (150 mg, 0.62 mmol) in 57% yield.

**M.p.** decomposition >170 °C. **IR** (neat,  $\text{cm}^{-1}$ )  $\nu_{\text{max}}$  = 1660, 1584, 1565, 1481, 1468, 1301, 1285, 1200, 1174, 1098, 1071, 1033, 1003, 946, 801, 754, 627.  **$^1\text{H-NMR}$**  (500

MHz, DMSO- $d_6$ ): 8.41 (dd,  $J = 5.6, 0.5$  Hz, 1H), 7.37 (d,  $J = 2.7$  Hz, 1H), 6.98 (dd,  $J = 5.6, 2.7$  Hz, 1H), 3.82 (s, 3H).  $^{13}\text{C-NMR}$  (150 MHz, DMSO- $d_6$ ):  $\delta$  234.9 – 231.5 (brs), 165.7, 159.6 (brs), 150.3, 110.7, 108.8 (q,  $J = 2.5$  Hz), 55.3.  $^{19}\text{F-NMR}$  (470 MHz, DMSO- $d_6$ ):  $\delta$  -142.6 (q,  $J = 94.7, 38.4$  Hz).  $^{11}\text{B-NMR}$  (160 MHz, DMSO- $d_6$ ):  $\delta$  -1.23 (q, 49.2, 43.0 Hz). **HR-MS** (ESI) calcd for  $\text{C}_7\text{H}_6\text{BF}_3\text{NO}_2$  [M – K] $^-$  204.0450, found 204.0445.

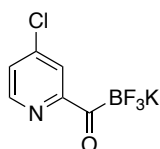
### Potassium 4-methyl-2-isonicotinoyltrifluoroborate (128)



Prepared from 2-bromo-4-methylpyridine (186 mg) by general procedure 4A and isolated as yellow solid (154 mg, 0.68 mmol) in 63% yield.

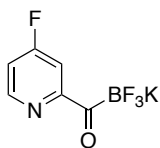
**M.p.** decomposition  $>170$  °C. **IR** (neat,  $\text{cm}^{-1}$ )  $\nu_{\text{max}} = 2915, 2981, 1661, 1597, 1085, 1037, 1037, 997, 935, 828, 806, 756, 685, 630$ .  $^1\text{H-NMR}$  (500 MHz, DMSO- $d_6$ ):  $\delta$  8.43 (d,  $J = 4.7$  Hz, 1H), 7.67 (s, 1H), 7.21 (d,  $J = 4.6$  Hz, 1H), 2.34 (s, 3H).  $^{13}\text{C-NMR}$  (150 MHz, DMSO- $d_6$ ):  $\delta$  235.7 – 232.1 (brs), 157.7 (brs), 148.7, 146.9, 125.6, 123.5, 20.6.  $^{19}\text{F-NMR}$  (470 MHz, DMSO- $d_6$ ):  $\delta$  -142.5 – -142.6 (m).  $^{11}\text{B-NMR}$  (160 MHz, DMSO- $d_6$ ):  $\delta$  -1.19 (q,  $J = 49.7, 42.5$  Hz). **HR-MS** (ESI) calcd for  $\text{C}_7\text{H}_6\text{BF}_3\text{NO}$  [M – K] $^-$  188.0501, found 188.0498.

### Potassium 4-chloro-2-isonicotinoyltrifluoroborate (129)



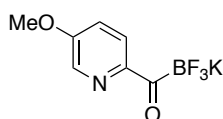
Prepared from 2-bromo-4-chloropyridine (208 mg) by general procedure 4A and isolated as yellow solid (182 mg, 0.73 mmol) in 68% yield

**M.p.** decomposition  $>175$  °C. **IR** (neat,  $\text{cm}^{-1}$ )  $\nu_{\text{max}} = 2988, 2902, 1658, 1567, 1551, 1227, 1075, 1037, 1000, 917, 837, 747, 697, 686, 628$ .  $^1\text{H-NMR}$  (600 MHz, DMSO- $d_6$ ):  $\delta$  8.60 (dd,  $J = 5.2, 0.6$  Hz, 1H), 7.85 (d,  $J = 2.0$  Hz, 1H), 7.58 (dd,  $J = 5.2, 2.2$  Hz, 1H).  $^{13}\text{C-NMR}$  (150 MHz, DMSO- $d_6$ ):  $\delta$  234.3 – 230.0 (brs), 159.1 (brs), 150.7, 143.3, 124.9, 122.8 (q,  $J = 2.9$  Hz).  $^{19}\text{F-NMR}$  (470 MHz, DMSO- $d_6$ ):  $\delta$  -142.9 (q,  $J = 55.5, 36.5$  Hz).  $^{11}\text{B-NMR}$  (160 MHz, DMSO- $d_6$ ):  $\delta$  -1.28 (q,  $J = 47.9, 45.7$  Hz). **HR-MS** (ESI) calcd for  $\text{C}_6\text{H}_3\text{BClF}_3\text{NO}$  [M – K] $^-$  207.9955, found 207.9956.

**Potassium 4-fluoro-2-isonicotinoyltrifluoroborate (130)**

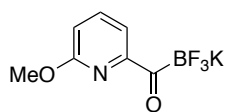
Prepared from 2-bromo-4-fluoropyridine (190 mg) by a slight modification of general procedure 4B. After general procedure 1 was applied, the isolated pale yellow solid was resuspended in THF and a solution of concentrated aqueous  $\text{KHF}_2$  (0.5 mL) was added. The mixture was stirred for 2 h at room temperature. The solvents were removed under reduced pressure and the water residue was lyophilized. The crude material was washed with DMF (3 x 10 mL). The combined DMF filtrates were evaporated to dryness under reduced pressure at 50 – 60 °C to yield the desired product as yellow solid (130 mg, 0.56 mmol, 52 %).

**M.p.** decomposition >180 °C. **IR** (neat,  $\text{cm}^{-1}$ )  $\nu_{\text{max}}$  = 1662, 1577, 1178, 1033, 997, 953, 822, 752, 630.  **$^1\text{H-NMR}$**  (500 MHz,  $\text{DMSO-}d_6$ ):  $\delta$  8.64 (dd,  $J$  = 8.8, 5.5 Hz, 1H), 7.58 (dd,  $J$  = 10.1, 2.6 Hz, 1H), 7.34 (ddd,  $J$  = 8.8, 5.5, 2.7 Hz, 1H).  **$^{13}\text{C-NMR}$**  (150 MHz,  $\text{DMSO-}d_6$ ):  $\delta$  234.0 – 230.2 (m), 168.5 (d,  $J$  = 260.2 Hz), 161.4, 151.8 (d,  $J$  = 5.9 Hz), 112.4 (d,  $J$  = 16.0 Hz), 109.8 (dq,  $J$  = 15.8, 2.8 Hz).  **$^{19}\text{F-NMR}$**  (470 MHz,  $\text{DMSO-}d_6$ ):  $\delta$  -103.8 (s, 1F), -142.8 (q,  $J$  = 53.8, 44.6 Hz, 3F).  **$^{11}\text{B-NMR}$**  (160 MHz,  $\text{DMSO-}d_6$ ):  $\delta$  -1.29 (q,  $J$  = 51.1, 50.5 Hz). **HR-MS** (ESI) calcd for  $\text{C}_6\text{H}_3\text{BF}_4\text{NO}$  [ $\text{M} - \text{K}$ ] $^-$  192.0250, found 192.0253.

**Potassium 5-methoxy-2-isonicotinoyltrifluoroborate (131)**

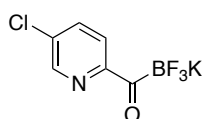
Prepared from 2-bromo-5-methoxypyridine (203 mg) the general procedure 4B and isolated as yellow solid (155 mg, 0.64 mmol) in 59% yield

**M.p.** decomposition >160 °C. **IR** (neat,  $\text{cm}^{-1}$ )  $\nu_{\text{max}}$  = 3467, 1649, 1579, 1255, 1092, 1027, 987, 893, 757, 713, 674, 599.  **$^1\text{H-NMR}$**  (600 MHz,  $\text{DMSO-}d_6$ ):  $\delta$  8.30 (d,  $J$  = 2.8 Hz, 1H), 7.94 (d,  $J$  = 8.6 Hz, 1H), 7.42 (dd,  $J$  = 8.6, 2.9 Hz, 1H), 3.86 (s, 2H).  **$^{13}\text{C-NMR}$**  (150 MHz,  $\text{DMSO-}d_6$ ):  $\delta$  232.9 – 230.0 (m), 156.2, 150.8 (brs), 137.04, 124.7 (q,  $J$  = 2.7 Hz), 119.4, 55.6.  **$^{19}\text{F-NMR}$**  (470 MHz,  $\text{DMSO-}d_6$ ):  $\delta$  -142.3 – -142.4 (m).  **$^{11}\text{B-NMR}$**  (160 MHz,  $\text{DMSO-}d_6$ ):  $\delta$  -1.10 (brs). **HR-MS** (ESI) calcd for  $\text{C}_7\text{H}_6\text{BF}_3\text{NO}_2$  [ $\text{M} - \text{K}$ ] $^-$  204.0450, found 204.0452.

**Potassium 6-methoxy-2-isonicotinoyltrifluoroborate (132)**

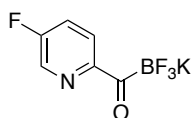
Prepared from 2-bromo-6-methoxypyridine (203 mg) the general procedure 4B and isolated as yellow solid (121 mg, 0.50 mmol) in 46% yield.

**M.p.** 176-177 °C. **IR** (neat,  $\text{cm}^{-1}$ )  $\nu_{\text{max}}$  = 1651, 1576, 1462, 1434, 1292, 1008, 910, 824, 804, 740, 633.  **$^1\text{H-NMR}$**  (600 MHz,  $\text{DMSO-}d_6$ ):  $\delta$  7.77 (dd,  $J$  = 8.2, 7.2 Hz, 1H), 7.62 (d,  $J$  = 7.2 Hz, 1H), 6.84 (dd,  $J$  = 8.2, 0.8 Hz, 1H), 3.85 (s, 2H).  **$^{13}\text{C-NMR}$**  (150 MHz,  $\text{DMSO-}d_6$ ):  $\delta$  234.9 – 231.4 (m), 162.9, 155.4 (brs), 139.2, 118.0 (q,  $J$  = 3.1 Hz), 112.2, 52.8.  **$^{19}\text{F-NMR}$**  (470 MHz,  $\text{DMSO-}d_6$ ):  $\delta$  -142.4 – -142.6 (m).  **$^{11}\text{B-NMR}$**  (160 MHz,  $\text{DMSO-}d_6$ ):  $\delta$  -1.23 (q,  $J$  = 52.3, 46.8 Hz). **HR-MS** (ESI) calcd for  $\text{C}_7\text{H}_6\text{BF}_3\text{NO}_2$  [ $\text{M} - \text{K}$ ] $^-$  204.0450, found 204.0451.

**Potassium 5-chloro-2-isonicotinoyltrifluoroborate (133)**

Prepared from 2-bromo-5-chloropyridine (208 mg) the general procedure 4A and isolated as yellow solid (166 mg, 0.67 mmol) in 62% yield

**M.p.** decomposition >180 °C. **IR** (neat,  $\text{cm}^{-1}$ )  $\nu_{\text{max}}$  = 1659, 1568, 1097, 1038, 998, 891, 668, 644, 570.  **$^1\text{H-NMR}$**  (500 MHz,  $\text{DMSO-}d_6$ ):  $\delta$  8.63 (dd,  $J$  = 2.5, 0.7 Hz, 1H), 7.98 (dd,  $J$  = 8.4, 2.5 Hz, 1H), 7.88 (d,  $J$  = 8.4 Hz, 1H).  **$^{13}\text{C-NMR}$**  (150 MHz,  $\text{DMSO-}d_6$ ):  $\delta$  234.2 – 230.4 (m), 156.0 (brs), 147.5, 136.1, 132.0, 124.2 (q,  $J$  = 2.8 Hz).  **$^{19}\text{F-NMR}$**  (470 MHz,  $\text{DMSO-}d_6$ ):  $\delta$  -142.9 (dd,  $J$  = 99.8, 45.3 Hz).  **$^{11}\text{B-NMR}$**  (160 MHz,  $\text{DMSO-}d_6$ ):  $\delta$  -1.25 (q,  $J$  = 49.2, 42.4 Hz). **HR-MS** (ESI) calcd for  $\text{C}_6\text{H}_3\text{BClF}_3\text{NO}$  [ $\text{M} - \text{K}$ ] $^-$  207.9955, found 207.9953.

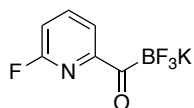
**Potassium 5-fluoro-2-isonicotinoyltrifluoroborate (135)**

Prepared from 2-bromo-5-fluoropyridine (190 mg) the general procedure 4B and isolated as pale yellow solid (228 mg, 0.68 mmol) in 91% yield.

**M.p.** decomposition >180 °C. **IR** (neat,  $\text{cm}^{-1}$ )  $\nu_{\text{max}}$  = 1657, 1587, 1578, 1476, 1291, 1220, 1126, 1078, 1039, 1020, 997, 925, 882, 843, 762, 664.  **$^1\text{H-NMR}$**  (600 MHz,  $\text{DMSO-}d_6$ ):  $\delta$  8.56 (dt,  $J$  = 2.9 Hz, 0.5 Hz, 1H), 7.96 (dd,  $J$  = 8.7 Hz, 4.9 Hz, 1H), 7.75 (td,  $J$  = 8.8 Hz, 2.9 Hz, 1H).  **$^{13}\text{C-NMR}$**  (150 MHz,  $\text{DMSO-}d_6$ ):  $\delta$  233.3 – 229.5 (m), 159.5 (d,  $J$  = 257.2 Hz), 154.5, 137.1 (d,  $J$  = 23.2 Hz), 124.8 (dd,  $J$  = 4.7, 2.4 Hz), 123.0 (d,  $J$  = 18.0 Hz).  **$^{19}\text{F-NMR}$**  (470 MHz,

DMSO- $d_6$ ):  $\delta$  -124.7 (1F), -142.7 – -142.9 (m, 3F).  $^{11}\text{B-NMR}$  (160 MHz, DMSO- $d_6$ ):  $\delta$  -1.19 (q,  $J$  = 48.6 Hz). **HR-MS** (ESI) calcd for  $\text{C}_6\text{H}_3\text{BF}_4\text{NO}$  [ $\text{M} - \text{K}$ ] $^-$  192.0250, found 192.0253.

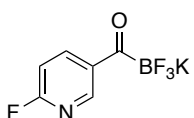
### Potassium 6-fluoro-2-isonicotinoyltrifluoroborate (136)



Prepared from 2-bromo-6-fluoropyridine (190 mg) the general procedure 4B and isolated as yellow solid (180 mg, 0.78 mmol) in 72% yield.

**M.p.** decomposition  $>180$  °C. **IR** (neat,  $\text{cm}^{-1}$ )  $\nu_{\text{max}}$  = 1660, 1595, 1570, 1449, 1308, 1270, 1259, 1106, 1034, 990, 955, 844, 819, 741, 711, 633.  $^1\text{H-NMR}$  (600 MHz, DMSO- $d_6$ ):  $\delta$  8.07 (td,  $J$  = 8.3, 7.3 Hz, 1H), 7.89 (dd,  $J$  = 7.3, 2.8 Hz, 1H), 7.21 (ddd,  $J$  = 8.1, 3.1, 0.7 Hz, 1H).  $^{13}\text{C-NMR}$  (150 MHz, DMSO- $d_6$ ):  $\delta$  232.8 – 229.7 (m), 162.5 (d,  $J$  = 236.0 Hz), 155.8 (brs), 142.5 (d,  $J$  = 7.3 Hz), 121.7 (p,  $J$  = 3.0 Hz), 111.1 (d,  $J$  = 38.7 Hz).  $^{19}\text{F-NMR}$  (470 MHz, DMSO- $d_6$ ):  $\delta$  -67.4 (1F), -142.9 (dd,  $J$  = 98.7, 45.1 Hz, 3F).  $^{11}\text{B-NMR}$  (160 MHz, DMSO- $d_6$ ):  $\delta$  -1.31 (q,  $J$  = 51.1, 50.3 Hz). **HR-MS** (ESI) calcd for  $\text{C}_6\text{H}_3\text{BF}_4\text{NO}$  [ $\text{M} - \text{K}$ ] $^-$  192.0250, found 192.0245.

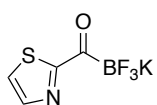
### Potassium 2-fluoronicotinoyltrifluoroborate (156)



Prepared from 5-bromo-2-fluoropyridine (190 mg) the general procedure 4A and isolated as pale yellow solid (185 mg, 0.80 mmol) in 74% yield.

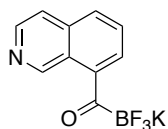
**M.p.** decomposition  $>190$  °C. **IR** (neat,  $\text{cm}^{-1}$ )  $\nu_{\text{max}}$  = 3173 (br.), 1633, 1579, 1478, 1373, 1315, 1255, 1227, 1082, 1009, 991, 886, 845, 752, 692, 615.  $^1\text{H NMR}$  (600 MHz, acetone- $d_6$ ):  $\delta$  8.90 (d,  $J$  = 2.3 Hz, 1H), 8.42 (td,  $J$  = 8.4, 2.3 Hz, 1H), 7.06 (ddd,  $J$  = 8.4, 2.7, 0.7 Hz, 1H).  $^{13}\text{C NMR}$  (151 MHz, acetone- $d_6$ ):  $\delta$  233.9 – 231.2 (m), 166.1, 164.5, 150.5 (dq,  $J$  = 16.1, 3.1 Hz), 141.7 (d,  $J$  = 7.0 Hz), 135.8, 109.5 (d,  $J$  = 37.8 Hz).  $^{19}\text{F NMR}$  (470 MHz, acetone- $d_6$ ):  $\delta$  -67.0 (d, 8.2 Hz, 1H), -145.7 (dd,  $J$  = 100.6, 49.4 Hz, 3H).  $^{11}\text{B NMR}$  (160 MHz, acetone- $d_6$ ):  $\delta$  -1.01 (q,  $J$  = 50.6 Hz). **HR-MS** (ESI) calc'd for  $\text{C}_6\text{H}_3\text{BF}_4\text{NO}$  [ $\text{M} - \text{K}$ ] $^-$  192.0250, found 192.0254.



**Potassium (2-thiazolyl)methanotrifluoroborate (168)**

Prepared from 2-bromothiophene (260 mg) the general procedure 4A and isolated as a pale brown solid (90 mg, 0.41 mmol) in 38% yield.

**M.p.** decomposition >240 °C. **FT-IR** (neat,  $\text{cm}^{-1}$ )  $\nu_{\text{max}}$  = 1649, 1480, 1388, 1241, 1155, 1075, 1002, 886, 818, 752, 733, 707, 635, 607.  **$^1\text{H}$  NMR** (600 MHz,  $\text{DMSO-}d_6$ )  $\delta$  7.96 (d,  $J$  = 3.0 Hz, 1H), 7.85 (d,  $J$  = 3.0 Hz, 1H).  **$^{13}\text{C}$  NMR** (150 MHz,  $\text{DMSO-}d_6$ )  $\delta$  213.3 – 206.0 (brs), 144.22, 123.76, 39.52.  **$^{19}\text{F}$  NMR** (470 MHz,  $\text{DMSO-}d_6$ )  $\delta$  -144.28 (dd,  $J$  = 95.3, 45.2 Hz).  **$^{11}\text{B}$  NMR** (160 MHz,  $\text{DMSO-}d_6$ )  $\delta$  -1.40 (q,  $J$  = 48.7 Hz). **HR-MS** (ESI) calcd for  $\text{C}_4\text{H}_3\text{BF}_3\text{N}_2\text{S}$  [ $\text{M} - \text{K}$ ] $^-$  179.0068, found 179.0061.

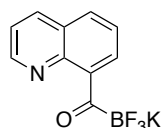
**Potassium (isoquinoline-8-yl)methanotrifluoroborate (173)**

Prepared from 8-bromoisoquinoline (225 mg) by general procedure 4A and isolated as a pale brown solid (34 mg, 0.13 mmol) in 12% yield.

**M.p.** decomposition >186 °C. **FT-IR** (neat,  $\text{cm}^{-1}$ )  $\nu_{\text{max}}$  = 1620, 1596, 1490, 1441, 1384, 1212, 1172, 1139, 1002, 900, 843, 804, 780, 756, 713, 620.  **$^1\text{H}$  NMR** (500 MHz,  $\text{DMSO-}d_6$ )  $\delta$  9.70 (s, 1H), 8.46 (d,  $J$  = 5.6 Hz, 1H), 8.09 (d,  $J$  = 7.1 Hz, 1H), 7.96 (dt,  $J$  = 8.4, 1.1 Hz, 1H), 7.81 (dd,  $J$  = 5.6, 1.0 Hz, 1H), 7.78 (dd,  $J$  = 8.2, 7.1 Hz, 1H).  **$^{13}\text{C}$  NMR** (151 MHz,  $\text{DMSO-}d_6$ )  $\delta$  150.74, 142.23, 141.81, 135.39, 129.56, 128.76, 128.03, 124.57, 120.51, ipso-carbon could not be detected.  **$^{19}\text{F}$  NMR** (470 MHz,  $\text{DMSO-}d_6$ )  $\delta$  -143.05 (dd,  $J$  = 100.5, 44.4 Hz).  **$^{11}\text{B}$  NMR** (160 MHz,  $\text{DMSO-}d_6$ )  $\delta$  -1.38 (q,  $J$  = 53.7, 52.4 Hz). **HR-MS** (ESI) calcd for  $\text{C}_{10}\text{H}_6\text{BF}_3\text{NO}$  [ $\text{M} - \text{K}$ ] $^-$  224.0502, found 224.0497.

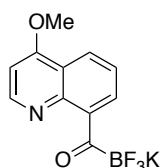
**General Procedure 5: Synthesis of 8-Quinoline Acyltrifluoroborates**

A flame-dried, 50-mL round-bottom flask equipped with magnetic stir bar and septum under inert N<sub>2</sub>-atmosphere, was charged with and anhydrous THF/toluene (4:1, 12 mL). The mixture was cooled to -78 °C in a dry ice/acetone bath and *n*-butyllithium (1.6 M in hexanes, 675 µL, 1.08 mmol, 1.00 equiv) was added dropwise over 30 min via syringe pump. After the mixture was stirred for 1 h at -78 °C, a solution of (ethylthio-trifluoroborate)-methane dimethyliminium **42** (0.200 g, 1.08 mmol, 1.00 equiv) in anhydrous THF (1 mL) was added dropwise over 30 min via syringe pump. After the mixture was stirred for 96 h at -78 °C, the residual *n*-butyllithium was quenched with acetone (80 µL, 1.08 mmol, 1.00 equiv). 10 min after the addition of acetone, an aqueous KF solution (6.5 M, 0.5 mL, 3.24 mmol, 3.00 equiv) was added at -78 °C. The flask was removed from the dry ice/acetone bath and the mixture was stirred for 2 h at room temperature. To the resulting heterogeneous mixture CH<sub>2</sub>Cl<sub>2</sub> (5 mL) was added. The mixture was filtered and washed with additional CH<sub>2</sub>Cl<sub>2</sub> (3 x 20 mL) and acetone (3 x 5 mL). The remaining filter cake was washed with DMF (50 mL) until the filtrate was colorless. The DMF was removed under reduced pressure at 50 – 60 °C to yield the desired KAT.

**Potassium (quinoline-8-yl)methanonetrifluoroborate (171)**

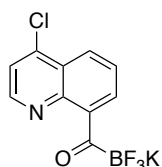
Prepared from 8-bromoquinoline (225 mg) by general procedure 5 and isolated as a yellow solid (111 mg, 0.42 mmol) in 39% yield.

**M.p.** decomposition >190 °C. **FT-IR** (neat, cm<sup>-1</sup>)  $\nu_{\max}$  = 1770, 1759, 1646, 1598, 1568, 1493, 1383, 1247, 1126, 1102, 1061, 1012, 1003, 986, 920, 890, 830, 813, 791, 771, 763, 706, 640, 612. **<sup>1</sup>H NMR** (600 MHz, DMSO-*d*<sub>6</sub>)  $\delta$  8.80 (dd, *J* = 4.1, 1.9 Hz, 1H), 8.30 (dd, *J* = 8.3, 1.9 Hz, 1H), 7.86 (dd, *J* = 6.5, 3.2 Hz, 1H), 7.54 – 7.51 (m, 2H), 7.46 (dd, *J* = 8.2, 4.1 Hz, 1H). **<sup>13</sup>C NMR** (150 MHz, DMSO-*d*<sub>6</sub>)  $\delta$  243.4 – 239.5 (brs), 149.6, 147.1, 144.9, 135.7, 127.8, 127.3, 125.6, 125.4, 120.9. **<sup>19</sup>F NMR** (470 MHz, DMSO-*d*<sub>6</sub>): -144.8 – -145.0 (m). **<sup>11</sup>B NMR** (160 MHz, DMSO-*d*<sub>6</sub>):  $\delta$  -1.56 (q, *J* = 54.4, 53.9 Hz). **HR-MS** (ESI) calcd for C<sub>10</sub>H<sub>6</sub>BF<sub>3</sub>NO [M – K]<sup>-</sup> 224.0502, found 224.0505.

**Potassium (4-methoxyquinoline-8-yl)methanonetrifluoroborate (174)**

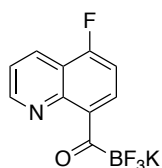
Prepared from 8-bromoquinoline (257 mg) by the general procedure 5 and isolated as a pale brown solid (98 mg, 0.33 mmol) in 31% yield.

**M.p.** decomposition >220 °C. **FT-IR** (neat,  $\text{cm}^{-1}$ )  $\nu_{\text{max}}$  = 1647, 1611, 1596, 1570, 1502, 1464, 1411, 1308, 1276, 1247, 1221, 1205, 1160, 1111, 1081, 1025, 992, 926, 904, 856, 816, 770, 750, 716, 670, 652, 612.  **$^1\text{H}$  NMR** (600 MHz,  $\text{DMSO-}d_6$ )  $\delta$  8.63 (d,  $J$  = 5.1 Hz, 1H), 8.05 – 8.02 (m, 1H), 7.48 – 7.45 (m, 2H), 6.96 (d,  $J$  = 5.1 Hz, 1H), 4.02 (s, 3H).  **$^{13}\text{C}$  NMR** (150 MHz,  $\text{DMSO-}d_6$ )  $\delta$  242.9 – 239.1 (brs), 161.1, 150.5, 147.1, 145.72, 125.5, 124.7, 120.5, 120.4, 100.5, 55.9.  **$^{19}\text{F}$  NMR** (470 MHz,  $\text{DMSO-}d_6$ ): -144.8 – -145.0 (m).  **$^{11}\text{B}$  NMR** (160 MHz,  $\text{DMSO-}d_6$ ):  $\delta$  -1.47 – -1.79 (m). **HR-MS** (ESI) calcd for  $\text{C}_{11}\text{H}_8\text{BF}_3\text{NO}_2$   $[\text{M} - \text{K}]^-$  254.0608, found 254.0606.

**Potassium (4-chloroquinoline-8-yl)methanonetrifluoroborate (175)**

Prepared from 8-bromoquinoline (260 mg) by a slight modification of general procedure 5. Due to insolubility of the starting material in toluene, anhydrous THF/toluene (1:1, 12 mL) was used as a solvent mixture instead of anhydrous THF/toluene (4:1, 12 mL). The desired product was **175** isolated as a pale brown solid (48 mg, 0.16 mmol) in 15% yield.

**M.p.** decomposition >210 °C. **FT-IR** (neat,  $\text{cm}^{-1}$ )  $\nu_{\text{max}}$  = 1648, 1621, 1599, 1567, 1495, 1409, 1395, 1219, 1106, 1072, 1050, 1000, 981, 805, 851, 835, 787, 712, 645, 626, 579.  **$^1\text{H}$  NMR** (500 MHz,  $\text{DMSO-}d_6$ )  $\delta$  8.91 (dd,  $J$  = 4.1, 1.7 Hz, 1H), 8.53 (dd,  $J$  = 8.6, 1.7 Hz, 1H), 7.73 (d,  $J$  = 7.7 Hz, 1H), 7.64 (dd,  $J$  = 8.6, 4.1 Hz, 1H), 7.52 (dd,  $J$  = 7.7, 0.6 Hz, 1H).  **$^{13}\text{C}$  NMR** (150 MHz,  $\text{DMSO}$ )  $\delta$  215.8 – 206.5 (brs), 150.5, 146.7, 145.6, 131.7, 128.9, 125.9, 125.5, 125.2, 122.2.  **$^{19}\text{F}$  NMR** (470 MHz,  $\text{DMSO-}d_6$ ): -145.0 – -145.2 (m).  **$^{11}\text{B}$  NMR** (160 MHz,  $\text{DMSO-}d_6$ ):  $\delta$  -1.57 (dd,  $J$  = 98.9, 40.8 Hz). **HR-MS** (ESI) calcd for  $\text{C}_{10}\text{H}_5\text{BClF}_3\text{NO}$   $[\text{M} - \text{K}]^-$  258.0112, found 258.0108.

**Potassium (quinoline-8-yl)methanonetrifluoroborate (179)**

Prepared from 8-bromoquinoline (244 mg) by a slight modification of the general procedure 5. After the mixture was stirred for 96 h at  $-78\text{ }^{\circ}\text{C}$ , the residual *n*-butyllithium was quenched with acetone (80  $\mu\text{L}$ , 1.08 mmol, 1.00 equiv). Ten minutes after the addition of acetone, an aqueous KF solution (6.5 M, 0.5 mL, 3.24 mmol, 3.00 equiv) and 2-methyloxirane (1.13 mL, 16.2 mmol, 15 equiv) as thioethyl scavenger were added slowly at  $-78\text{ }^{\circ}\text{C}$ . The flask was removed from the dry ice/acetone bath and the mixture was stirred for 2 h at room temperature. To the resulting heterogeneous mixture  $\text{CH}_2\text{Cl}_2$  (5 mL) was added. The mixture was filtered and washed with additional  $\text{CH}_2\text{Cl}_2$  (3 x 20 mL) and acetone (3 x 5 mL). The remaining filter cake was washed with DMF (50 mL) until the filtrate was colorless. The DMF filtrate was concentrated under vacuo to yield the desired product **179** as a pale yellow solid (82 mg, 0.29 mmol) in 27% yield.

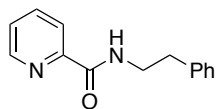
**M.p.** decomposition  $>220\text{ }^{\circ}\text{C}$ . **FT-IR** (neat,  $\text{cm}^{-1}$ )  $\nu_{\text{max}}$  = 1648, 1620, 1599, 1567, 1495, 1409, 1395, 1219, 1204, 1106, 1071, 1050, 1023, 1001, 981, 850, 834, 805, 787, 712, 627, 579.  **$^1\text{H}$  NMR** (500 MHz,  $\text{DMSO}-d_6$ )  $\delta$  8.90 (dd,  $J$  = 4.2, 1.8 Hz, 1H), 8.44 (dd,  $J$  = 8.4, 1.8 Hz, 1H), 7.63 – 7.55 (m, 2H), 7.37 (dd,  $J$  = 10.1, 8.0 Hz, 1H).  **$^{13}\text{C}$  NMR** (150 MHz,  $\text{DMSO}-d_6$ )  $\delta$  225.0 – 221.7 (brs), 156.2 (d,  $J$  = 252.8 Hz), 150.7, 145.6 (d,  $J$  = 2.6 Hz), 143.4, 128.3 (d,  $J$  = 4.9 Hz), 125.9 (dd,  $J$  = 9.1, 2.1 Hz), 121.4 (d,  $J$  = 2.8 Hz), 117.9 (d,  $J$  = 15.7 Hz), 109.2 (d,  $J$  = 18.8 Hz).  **$^{19}\text{F}$  NMR** (470 MHz,  $\text{DMSO}-d_6$ )  $\delta$  -123.3 (dd,  $J$  = 10.1, 6.4 Hz), -144.8 (d,  $J$  = 82.3 Hz).  **$^{11}\text{B}$  NMR** (160 MHz,  $\text{DMSO}-d_6$ )  $\delta$  -1.56 (q,  $J$  = 52.4, 51.9 Hz). **HR-MS** (ESI) calcd for  $\text{C}_{10}\text{H}_5\text{BF}_4\text{NO} [\text{M} - \text{K}]^-$  242.0408, found 242.0404.

**7.2.6 Purification of Pyridyl Acyltrifluoroborates**

Prior to kinetic measurements the crude pyridyl acyltrifluoroborates obtained by general procedure 1 were additionally purified. For this purpose, crude reaction product 1 was suspended in acetone. The suspension was sonicated, centrifuged and the supernatant was decanted. The sequence of steps was repeated twice with acetone and once with  $\text{CH}_2\text{Cl}_2$  for each compound. The residual solid was dried under high vacuum at room temperature and used for further ligation reactions.

### 7.2.7 Synthesis of Amide Ligation Products

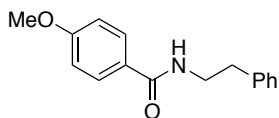
#### *N*-(2-Phenethyl)-2-picolinamide (**118**)



Prepared by the KAT ligation between **116** (3.83 mg, 0.018 mmol, 1.00 equiv) and **117** (4.47 mg, 0.02 mmol, 1.05 equiv) in MeCN/0.1 M aq. potassium buffer (2:1, 1.2 mL, total concentration 15 mM). After full conversion was indicated by  $^1\text{H-NMR}$  EtOAc (5 mL) was added and the mixture was extracted with  $\text{H}_2\text{O}$  (2 x 5 mL), dried over  $\text{Na}_2\text{SO}_4$  and concentrated under reduced pressure. The crude material was purified by flash column chromatography (EtOAc/hexanes 1:4) to yield the desired product as pale yellow oil (3.79 mg, 0.017 mmol, 93%).

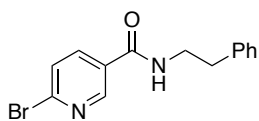
The spectral data was in agreement with literature.<sup>203</sup>  $^1\text{H-NMR}$  (400 MHz,  $\text{CDCl}_3$ ):  $\delta$  7.36-7.16 (m, 10H), 5.43 (br s, 1H), 3.55 (q,  $J = 6.9$  Hz, 2H), 2.84 (t,  $J = 6.9$  Hz, 2H), 2.65 (t,  $J = 7.5$  Hz, 2H), 2.15 (t,  $J = 7.2$  Hz, 2H), 1.97 (p,  $J = 7.5$  Hz, 2H).  $^{13}\text{C-NMR}$  (100 MHz,  $\text{CDCl}_3$ )  $\delta$  172.6, 141.5, 138.9, 128.8, 128.7, 128.5, 128.4, 126.5, 125.9, 40.5, 35.9, 35.7, 35.1, 27.1.

#### *N*-(2-Phenylethyl)-4-methoxybenzamide (**S8**).



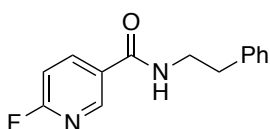
Prepared by the KAT ligation between **119** (4.36 mg, 0.018 mmol, 1.00 equiv) and **117** (4.47 mg, 18.9 mmol, 1.05 equiv) in MeCN/0.1 M aq. potassium buffer (2:1, 1.2 mL, total concentration 15 mM). After full conversion was indicated by  $^1\text{H-NMR}$  EtOAc (5 mL) was added and the mixture was extracted with  $\text{H}_2\text{O}$  (2 x 5 mL), dried over  $\text{Na}_2\text{SO}_4$  and concentrated under reduced pressure. The crude material was purified by flash column chromatography (EtOAc/hexanes 1:4) to yield the desired product as pale yellow oil (4.14 mg, 0.016 mmol, 90%).

The spectral data was in agreement with literature.<sup>204</sup>  $^1\text{H-NMR}$  (400 MHz,  $\text{CDCl}_3$ ):  $\delta$  7.69 (d,  $J = 8.8$  Hz, 2H), 7.35 (t,  $J = 7.7$  Hz, 2H), 7.27 (t,  $J = 7.3$  Hz, 3H), 6.92 (d,  $J = 8.8$  Hz, 2H), 6.13 (br, 1H), 3.86 (s, 3H), 3.73 (q,  $J = 6.6$  Hz, 2H), 2.95 (t,  $J = 6.9$  Hz, 2H).  $^{13}\text{C-NMR}$  (100 MHz,  $\text{CDCl}_3$ ):  $\delta$  167.0, 162.1, 139.0, 128.8, 128.7, 128.6, 126.9, 126.6, 113.7, 55.4, 41.1, 35.8.

**N-(2-Phenethyl)-2-bromo-3-picolinamide (S9)**

To a solution of **48** (20.0 mg, 0.07 mmol, 1.00 equiv) and **117** (17.0 mg, 0.07 mmol, 1.05 equiv) in *t*-BuOH/H<sub>2</sub>O (1:1, 2.0 mL) 1 drop of oxalic acid (0.1 M) was added. The reaction was stirred at 23 °C for 2 h. After full conversion was indicated by TLC, EtOAc was added and the mixture was extracted with H<sub>2</sub>O, dried over Na<sub>2</sub>SO<sub>4</sub> and concentrated under reduced pressure. The crude material was purified by flash column chromatography (EtOAc/hexanes 1:4) to yield the desired product as a pale yellow oil (19.0 mg, 0.06 mmol, 91%).

**M.p.** 138.9 – 139.5 °C. **IR** (neat, cm<sup>-1</sup>)  $\nu_{\max}$  = 3332, 2929, 2883, 1634, 1603, 1579, 1557, 1533, 1453, 1356, 1309, 1276, 1237, 1197, 1158, 1086, 1015, 864, 839, 752, 701, 646, 571 . **<sup>1</sup>H NMR** (600 MHz, acetone-*d*<sub>6</sub>)  $\delta$  8.78 (dd, *J* = 2.5, 0.8 Hz, 1H), 8.10 (dd, *J* = 8.2, 2.5 Hz, 1H), 8.06 (brs, 1H), 7.70 (dd, *J* = 8.2, 0.7 Hz, 1H), 7.30 – 7.25 (m, 4H), 7.21 – 7.19 (m, 1H), 3.66 – 3.62 (m, 2H), 2.93 (t, 7.4 Hz, 2H). **<sup>13</sup>C NMR** (150 MHz, acetone-*d*<sub>6</sub>)  $\delta$  164.9, 149.9, 145.0, 140.4, 138.7, 131.1, 129.6, 129.3, 128.8, 127.1, 42.2, 36.3. **HR-MS** (ESI) calc'd for C<sub>14</sub>H<sub>14</sub>BrN<sub>2</sub>O [M + H]<sup>+</sup> 305.0284, found 305.0274.

**N-(2-Phenethyl)-2-fluoro-3-picolinamide (S10)**

To a solution of **S5** (20.0 mg, 0.09 mmol, 1.00 equiv) and **177** (21.5 mg, 0.09 mmol, 1.05 equiv) in *t*-BuOH/H<sub>2</sub>O (1:1, 2.0 mL) 1 drop of oxalic acid (0.1 M) was added. The reaction was stirred at 23 °C for 2 h. After full conversion was indicated by TLC, EtOAc was added and the mixture was extracted with H<sub>2</sub>O, dried over Na<sub>2</sub>SO<sub>4</sub> and concentrated under reduced pressure. The crude material was purified by flash column chromatography (EtOAc/hexanes 1:3) to yield the desired product as a pale yellow oil (19.7 mg, 0.08 mmol, 93 %).

**M.p.** 97.5 – 98.3 °C. **IR** (neat, cm<sup>-1</sup>)  $\nu_{\max}$  = 3292, 3063, 3028, 2924, 2853, 1634, 1594, 1540, 1475, 1880, 1322, 1295, 1259, 1025, 881, 845, 776, 743, 696, 625, 599. **<sup>1</sup>H NMR** (600 MHz, CDCl<sub>3</sub>)  $\delta$  8.47 (dt, *J* = 2.6, 0.8 Hz, 1H), 8.17 (ddd, *J* = 8.5, 7.5, 2.5 Hz, 1H), 7.36 – 7.32 (m, 2H), 7.28 – 7.22 (m, 3H), 6.99 (ddd, *J* = 8.5, 2.9, 0.7 Hz, 1H), 6.07 (brs, 1H), 3.74 (td, *J* = 6.9, 5.8 Hz, 2H), 2.95 (t, *J* = 6.9 Hz, 2H). **<sup>13</sup>C NMR** (150 MHz, CDCl<sub>3</sub>)  $\delta$  165.9, 164.53, 164.3, 146.5 (d, *J* = 16.0 Hz), 140.9 (d, *J* = 8.8 Hz), 138.6, 129.0 (d, *J* = 15.0 Hz), 128.8 (d, *J* = 4.6

Hz), 127.0, 109.9 (d,  $J = 37.4$  Hz), 41.3, 35.7.  **$^{19}\text{F}$  NMR** (470 MHz,  $\text{CDCl}_3$ ):  $\delta$  -63.4 (d,  $J = 4.5$  Hz). **HR-MS** (ESI) calc'd for  $\text{C}_{14}\text{H}_{14}\text{FN}_2\text{O}$   $[\text{M} + \text{H}]^+$  245.1085, found 245.1091.

## 7.2.8 Radiolabeling Experiments

### Procedure using [<sup>18</sup>F]TBAF as a fluoride source

0.8 mL of TBAHCO<sub>3</sub> (933 mg of TBAOH in 20 mL of MeOH and bubbling CO<sub>2</sub>) was used followed by evaporation at 110 °C for 5 min (no azeotropic drying is needed). The mixture was cooled for 2 min by a stream of N<sub>2</sub>. After cooling 4.69 mg of DABCO dissolved in 0.15 ml DMSO and 1 mg of precursor dissolved in 0.15 DMSO was added. The reaction was heated for 10 min at 120 °C. The mixture was cooled for 5 min by a stream of nitrogen. Subsequently, the reaction mixture was diluted for the HPLC injection and analyzed by HPLC. Radiochemical yields above 90% were obtained.

### Procedure using [<sup>18</sup>F]CsF as a fluoride source

2 mL of 2.8 mg Cs<sub>2</sub>CO<sub>3</sub> in 0.6 mL H<sub>2</sub>O and 10 mg of kryptofix in 1.4 mL of MeCN were mixed followed by evaporate for 6.5 min at 110 °C (no azeotropic drying is needed). The mixture was cooled for 2 min by a stream of N<sub>2</sub> before addition of ~ 4.69 mg of DABCO dissolved in 2% aqueous DMSO (0.15 mL) and ~ 1 mg of precursor dissolved in 2% aqueous DMSO (0.15 mL). The mixture was heated for 10 min at 150 °C. Subsequently, the mixture was cooled down for 5 min by a stream of nitrogen. The mixture was diluted and injected into the HPLC. Radiochemical yields between 80–85% were obtained.



### 7.3 Kinetic Procedures and Data

#### Solvent Mixtures and pH

Unless otherwise stated, MeCN- $d_3$  / 0.1 M deuterated potassium phosphate buffer (2:1, pH 6.8 or 7.4), MeCN- $d_3$  / 0.1 M deuterated potassium acetate buffer (2:1, pH 4.4 or 5.1) or MeCN / 0.2 M aq. potassium acetate buffer (1:9, pH 3.6 or pH 3.9) were used as solvent mixtures for the kinetic measurements. MeCN- $d_3$  served as organic co-solvent to promote the solubility of the small-molecule reactants. Buffered solvent conditions were employed to compensate for possible pH changes. To avoid the exchange of potassium counterions of the KAT in solution we deliberately decided to use potassium buffers in lieu of sodium buffers. This considerably simplified the kinetic measurements as it allowed us to monitor a single acyltrifluoroborate species. Upon mixing the aqueous buffer solutions with acetonitrile, the final pH was adjusted using 0.10 M solutions of DCl in  $D_2O$ . The pH of the reaction mixture was measured at the beginning and end of each kinetic measurement to ensure that the pH remained constant during the reaction process. Since the kinetic measurements were performed in a deuterated instead of a non-deuterated solvent mixture the displayed pH value pH(D) was converted into the real pH for non-deuterated solutions pH(H), according to the following formula reported by Krężel and Bal.<sup>205</sup>

$$\text{pH(H)} = 0.9291 \cdot \text{pH(D)} + 0.421$$

#### Preparation of Deuterated and Non-Deuterated Aqueous Buffer Solutions

For the kinetic measurements two types of deuterated buffer solutions were used, deuterated potassium acetate buffers (pH 3.6, pH 4.4 and pH 5.1) and deuterated potassium phosphate buffers (pH 6.8 and pH 7.4).

#### Deuterated Aqueous Potassium Phosphate Buffer (0.1 M, pH 6.8 and pH 7.4)

Deuterated aq. potassium phosphate buffer solution was prepared according to Sørensen's phosphate buffer table (buffer range pH 5.8 – 8.0).<sup>206</sup>

Stock solution A (0.1 M):  $K_2HPO_4$  (0.174 g) was diluted with  $D_2O$  to 10 mL.

Stock solution B (0.1 M):  $KH_2PO_4$  (0.136 g) was diluted with  $D_2O$  to 10 mL.

For the preparation of 10 mL deuterated aq. potassium phosphate buffer, stock solution A and B were mixed according to the table below.

pH value	Stock A [mL]	Stock B [mL]
6.8	5.0	5.0
7.4	2.0	8.0

#### Deuterated Aqueous Potassium Acetate Buffer (0.1 M, pH 4.4 and 5.1)

Deuterated aq. acetate buffer solution was prepared according to Pearse's method (pH range 3.6 – 5.6).

Stock solution A (0.2 M): glacial acetic acid (0.116 mL) was diluted with D<sub>2</sub>O to 10 mL.

Stock solution B (0.2 M): potassium acetate (KOAc, 0.196 g) was diluted with D<sub>2</sub>O to 10 mL.

For the preparation of 0.1 M deuterated aq. potassium acetate buffer stock solutions A and B were mixed according to the following table and diluted with D<sub>2</sub>O to 10 mL.

pH value	Stock A [mL]	Stock B [mL]
4.4	3.1	1.9
5.1	1.3	3.7

#### Non-deuterated aqueous potassium acetate buffers (0.2 M, pH 3.6 and pH 3.9)

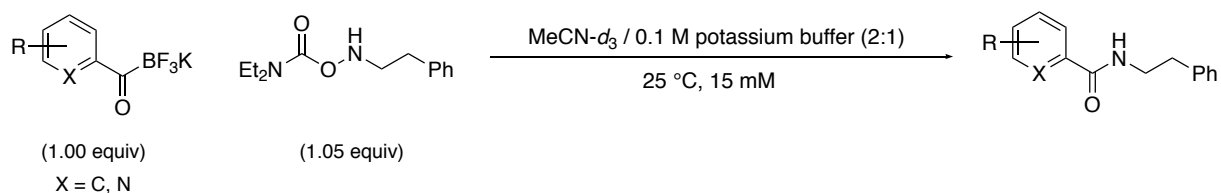
Deuterated acetate buffer solution was prepared according to Pearse's method (pH range 3.6 – 5.6).<sup>207</sup>

Stock solution A (0.2 M): glacial acetic acid (0.116 mL) was diluted with H<sub>2</sub>O to 10 mL.

Stock solution B (0.2 M): potassium acetate (KOAc, 0.196 g) was diluted with H<sub>2</sub>O to 10 mL.

For the preparation of 0.2 M deuterated potassium acetate buffer, stock solution A and B were mixed according to the following buffer table without further dilution.

pH value	Stock A [mL]	Stock B [mL]
3.6	4.6	0.4
3.9	4.2	0.8

**General Procedure 6:  $^1\text{H-NMR}$  Kinetic Studies of the KAT Ligation (pH 4.4 – 7.4)**

Reactions were performed under second-order conditions with equimolar concentrations of the two reactants. A solution of KAT (0.009 mmol, 1.00 equiv) and hydroxylamine (0.009 mmol, 1.05 equiv) in  $\text{MeCN-}d_3$  / 0.1 M deuterated aq. potassium buffer (2:1, 0.6 mL, total concentration 15 mM) was transferred into an NMR-tube. The reaction was carried out at room temperature (25 °C) and constant pH (pH 4.4, 5.1, 6.8 or 7.4) without magnetic stirring. The reaction process was followed by real-time  $^1\text{H-NMR}$  spectroscopy. With a reactant concentration of 15 mM sufficient signal to noise ratio was achieved within a standard measurement period of 16 scans. The reaction mixture was locked to an external  $\text{H}_2\text{O} / \text{D}_2\text{O}$  (9:1, containing 2 mM sucrose and 0.5 mM DSS) solvent sample. Before the automatic shim (topshim) was performed, 3D-strychnine shimming parameters were pre-loaded. During the measurements sample rotation (rotation frequency of sample: 20 Hz, MASR 42 kHz) was switched on. Unless stated otherwise,  $^1\text{H-NMR}$  spectra were recorded with 16 scans and standard parameters (pulse/flip angle: 30 °, acquisition time aq: 5 sec, relaxation delay d1: 0.01 sec). Time points were taken after half of the scans (16 scans / 2 = 8 scans).

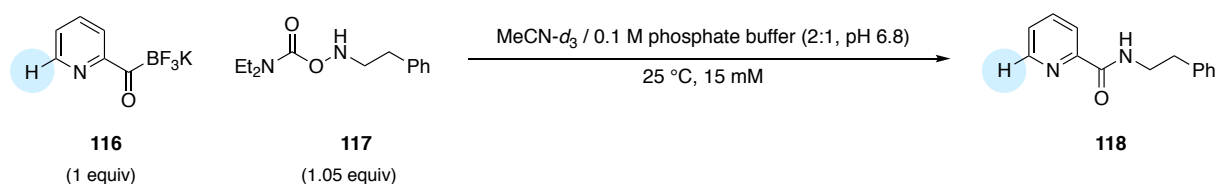
$^1\text{H-NMR}$  spectra were analyzed by *Topspin*. Spectra were referenced to  $\text{MeCN-}d_3$  (1.94 ppm) and only well-separated resonances were used for integration. Based on the integration of the starting material and product the reaction conversion at a given time was determined and converted into the corresponding starting material concentration of KAT (given the fact that the initial concentration  $A_0$  is known). Reaction rates were determined applying standard second-order kinetics by plotting the reciprocal concentration of the starting material at a given time  $[\text{A}]^{-1}$  in  $\text{M}^{-1}$  against the time in seconds. By applying a linear fit ( $y = ax + b$ ) the rate of the reaction  $k$  was determined as the slope of the graph  $a$  and was given in  $\text{M}^{-1} \text{s}^{-1}$ . Linear fits were only performed with data points up to max. 40 % reaction conversion. All kinetic measurements were performed at least three times. The rate constant of the reaction was determined as the average of the three measurements.

The obtained rate constants were further verified using the half-life method. By definition, the half-life of a reaction  $t_{1/2}$  is the time it takes until half of the starting material is consumed. If  $t_{1/2}$  and  $A_0$  is known, the rate of a second-order reaction can be determined via the following formula.

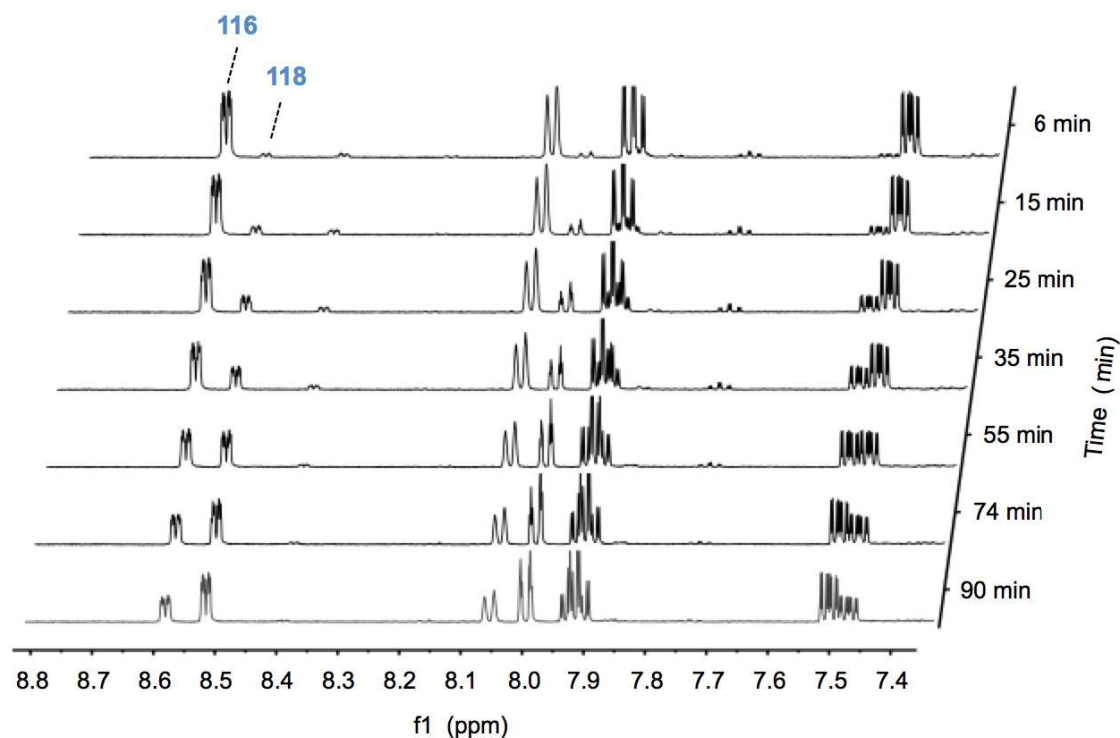
$$k = \frac{1}{t_{1/2} \cdot A_0}$$

In general, the experimentally measured rate constants were in good agreement with the calculated rate constants via the  $t_{1/2}$ -formula.

Example of a kinetic measurement:



The reaction between **116** and **117** was monitored by  $^1\text{H-NMR}$  spectroscopy. Integration of the recorded spectra allowed us to monitor the consumption of KAT starting material **116** and formation of amide product **118**. Due to its well-separated resonances the proton signal at the 6-position of the pyridyl ring was chosen for integration.



Based on integration of **116** and **118** the reaction conversion at a given time  $t$  was calculated (**116** + **118** = 100 %) and converted into the corresponding starting material concentration of **116** at a given time  $t$  (given the fact that the initial starting material concentration  $A_0 = 15 \text{ mM}$  is known).

Conversion [%]	Conc. 116 [M]	1/Conc. 116 [M <sup>-1</sup> ]	Time [s]
4.5	0.014325	69.80802792	610
11	0.01335	74.90636704	900
17.6	0.01236	80.90614887	1230
22.5	0.011625	86.02150538	1500
26.7	0.010995	90.95043201	1800
31.5	0.010275	97.32360097	2110
36.2	0.00957	104.4932079	2460
41	0.00885	112.9943503	2805
44.7	0.008295	120.5545509	3130
46	0.0081	123.4567901	3130
48.7	0.007695	129.9545159	3300
49.5	0.007575	132.0132013	3480
51.3	0.007305	136.8925394	3750
53.6	0.00696	143.6781609	3995
57.2	0.00642	155.7632399	4440
60.4	0.00594	168.3501684	4910
63.4	0.00549	182.1493625	5400

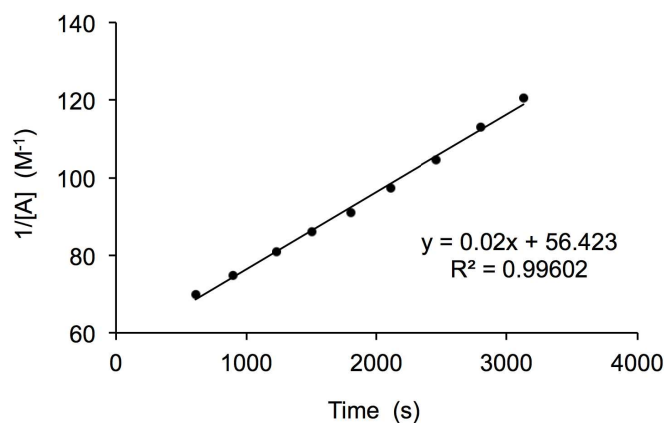
Reaction rates were determined by applying standard second-order kinetics. Since the reaction was performed with equimolar concentrations of the starting materials  $[A] = [B]$ , the observed rate of the reaction  $r$  can be expressed by the following differential equation.

$$r = -\frac{d[A]}{dt} = k$$

The integrated second order rate law can be derived as follows.

$$\frac{1}{[A]} = \frac{1}{[A]_0} + kt$$

By plotting the reciprocal concentration of the starting material at a given time  $1/[A]$  in  $M^{-1}$  against the time in seconds and applying a linear fit ( $y = ax + b$ ), the rate of the reaction  $k$  was determined as the slope  $a$  of the graph and was given in  $M^{-1} s^{-1}$ . Linear fits were only performed with data points up to max. 40 % reaction conversion.

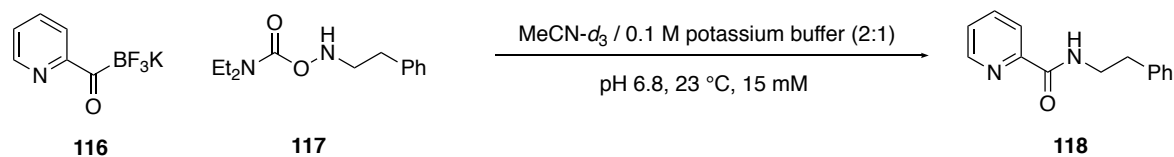


The reaction rate of the KAT ligation between **116** and **117** was found to be  $k = a = 0.02 M^{-1} s^{-1}$ . The experimentally obtained rate constant was further verified by the half-life method using the standard second-order half-life formula given below.

$$t_{1/2} = \frac{1}{k[A_0]}$$

The half-life of the reaction was  $t_{1/2} = 58$  min (3480 s) and the initial concentration of the starting material was 0.015 M. By applying the half-life formula a rate constant of  $0.019 M^{-1} s^{-1}$  could be calculated, which is in good agreement with the experimentally obtained value ( $0.020 M^{-1} s^{-1}$ ).

### Determining the Reaction Order of the KAT Ligation



A series of amide-bond forming ligation experiments of KAT **116** and hydroxylamine **117** in MeCN- $d_3$  / 0.1 M deuterated potassium phosphate buffer (2:1, pH 6.8) were performed at room temperature (25 °C) according to general procedure 6. For determining the reaction order different initial concentrations of the reactants were employed as shown in the tables below (1 equiv. = 15 mM).

Varying the equivalents of **116** (while keeping the concentration of **117** constant)

Entry	Equivalents 116	Equivalents 117	Kinetics $k$ [ $\text{M}^{-1}\text{s}^{-1}$ ]
1	0.5	1.0	0.04
2	1.0	1.0	0.02
3	2.0	1.0	0.04

Varying the equivalents of **117** (while keeping the concentration of **116** constant)

Entry	Equivalents 116	Equivalents 117	Kinetics $k$ [ $\text{M}^{-1}\text{s}^{-1}$ ]
1	1.0	0.5	0.04
2	1.0	1.0	0.02
3	1.0	2.0	0.04
4	1.0	4.0	0.08
5	1.0	8.0	0.15

### Substituent Effects – Hammett Plot

The kinetic performance of a series of 2-pyridyl KATs **127-130** with different substituents was evaluated and compared to unsubstituted 2-pyridyl KAT **116**. A Hammett plot was generated to give a measure for how strong substituent changes affect the KAT ligation of 2-pyridyl KATs. The Hammett plot was created on the basis of the standard Hammett equation,<sup>208</sup> which describes a linear free energy relationship (LFER) between substituent effects and reaction rates (or equilibrium constants).

$$\log \frac{k}{k_H} = \sigma \rho$$

where,

$k$  = reaction rate

$k_H$  = reference reaction rate of the unsubstituted compound

$\sigma$  = substituent constant

$\rho$  = reaction constant (also known as sensitivity constant)

The substituent constant  $\sigma$  is a measure of the total electronic influence by a certain substituent X, relative to no substituent. Substituent constants  $\sigma$  were referenced to the dissociation of benzoic acid in water at 25 °C ( $\rho = 1$ ).

Substituent constants  $\sigma$  relative to the dissociation of benzoic acid in water at 25 °C.

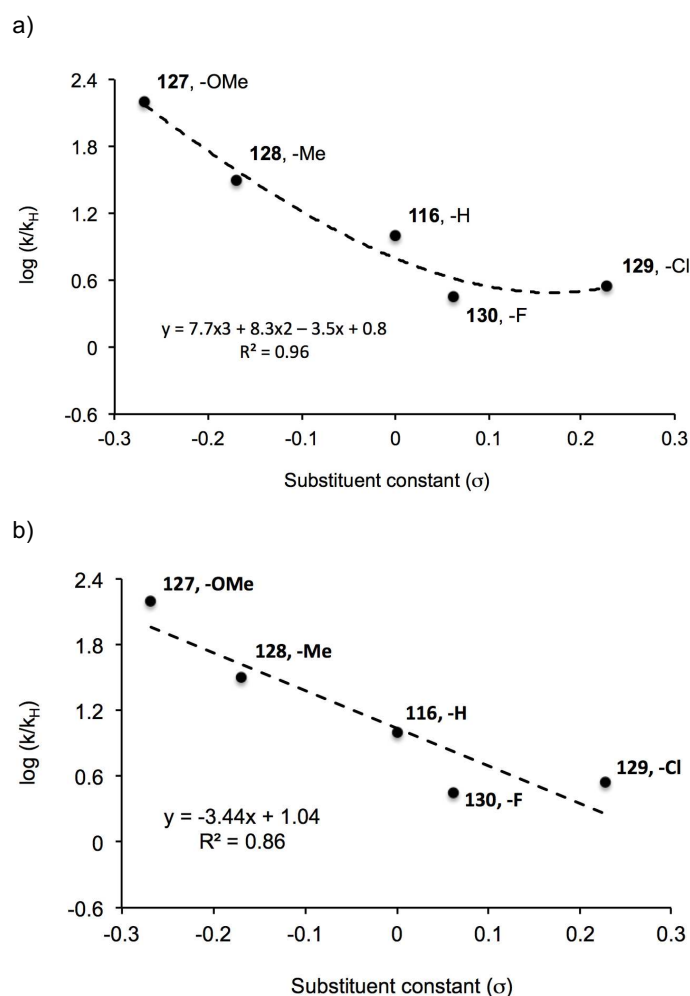
Substituent	Para Substituent Constant $\sigma$
OMe	-0.27
Me	-0.17
H	0
Cl	0.23
F	0.06



Substituents in 4-position of **116**: Calculation for  $k/k_H$  with  $k_H = 0.02 \text{ M}^{-1} \text{ s}^{-1}$

Substrate	Substituent	Reaction rate $k$ [ $\text{M}^{-1} \text{ s}^{-1}$ ]	$k/k_H$
<b>127</b>	OMe	0.044	2.2
<b>128</b>	Me	0.030	1.5
<b>116</b>	H	0.020	1
<b>129</b>	Cl	0.011	0.55
<b>130</b>	F	0.009	0.45

$k/k_H$  versus the reference substituent constants  $\sigma$  was plotted. A linear (Scheme a) and a non-linear polynomial fit (Scheme b) was applied. Since the  $R^2$  value for the polynomial fit was much better than for the linear fit, the correlation of substituent effects and reaction rates in the KAT ligation of 2-pyridyl KATs with different substituents in the 4-position was determined to be non-linear. Taking the linear fit into account, reaction constant  $\rho$  was determined to be -3.44.



### Variable Temperature (vT) NMR Studies

A series of amide-bond forming ligation experiments between KAT and hydroxylamine **117** in MeCN- $d_3$  / 0.1 M deuterated potassium buffer (2:1, pH 5.1 or 6.8) were performed at variable temperatures (10 – 70 °C) according to the general procedure 6. All kinetic measurements were performed at least three times. The rate constant of the reaction was determined as the average of the three measurements. The reaction enthalpy ( $\Delta H$ ), entropy ( $\Delta S$ ) and the Gibbs free energy ( $\Delta G$ ) could be calculated using the Eyring equation.

The general form of the Eyring equation is

$$k = \frac{k_B T}{h} e^{\frac{\Delta G^\ddagger}{RT}}$$

where,

$k$  = rate ( $M^{-1} s^{-1}$ )

$T$  = temperature (K)

$\Delta G^\ddagger$  = Gibbs energy of activation

$k_B$  = Boltzmann's constant

$h$  = Planck's constant

$R$  = universal gas constant

According to the second law of thermodynamics ( $\Delta G = \Delta H - T \Delta S$ ) the equation above can also be written as follows.

$$k = \frac{k_B T}{h} e^{\frac{\Delta S^\ddagger}{R}} e^{\frac{\Delta H^\ddagger}{RT}}$$

where  $\Delta H^\ddagger$  is the enthalpy of activation and  $\Delta S^\ddagger$  is the entropy of activation.

The linear form of the equation is:

$$\ln \frac{k}{T} = \frac{-\Delta H^\ddagger}{R} \cdot \frac{1}{T} + \ln \frac{k_B}{h} + \frac{\Delta S^\ddagger}{R}$$

By plotting  $\ln(k/T)$  versus the reciprocal of the temperature ( $1/T$ ) a linear fit can be applied ( $y = ax + b$ ), where the  $\Delta H^\ddagger$  can be derived from the slope ( $a = -\Delta H^\ddagger/R$ ) and  $\Delta S^\ddagger$  form the intercept ( $b = \ln(k_B/h) + \Delta S^\ddagger/R$ ).

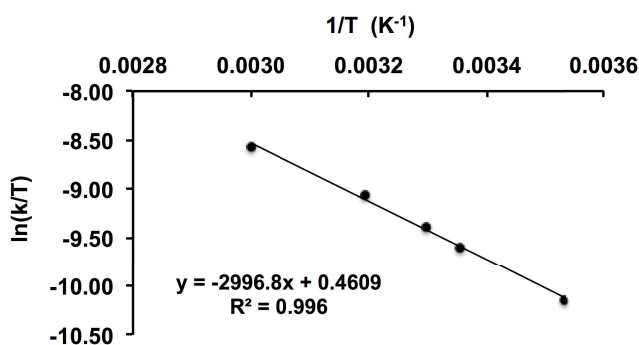
### Temperature Studies between 116 and 117 (pH 6.8)

Experimental data collected by variable-temperature  $^1\text{H-NMR}$  spectroscopy

Temperature T (°C)	Temperature T (K)	Rate k ( $\text{M}^{-1}\text{s}^{-1}$ )
60	333.16	0.063
40	313.16	0.036
30	303.16	0.025
25	298.16	0.020
10	283.16	0.011

By plotting  $\ln(k/T)$  versus the reciprocal of the temperature ( $1/T$ ) a linear fit ( $y = ax + b$ ) could be applied, where the  $\Delta H^\ddagger$  can be derived from the slope ( $a = -\Delta H^\ddagger/R$ ) and  $\Delta S^\ddagger$  form the intercept ( $b = \ln(k_B/h) + \Delta S^\ddagger/R$ ).

$\ln(k/T)$	$1/T$ ( $\text{K}^{-1}$ )
-8.57	0.00300
-9.06	0.00319
-9.40	0.00330
-9.60	0.00335
-10.15	0.00353



The following values for  $\Delta H^\ddagger$ ,  $\Delta S^\ddagger$  and  $\Delta G^\ddagger$  of **116** were obtained (pH 6.8).

$$\Delta H^\ddagger = 5.95 \text{ kcal mol}^{-1}$$

$$\Delta S^\ddagger = -46 \text{ cal mol}^{-1} \text{ K}^{-1}$$

$$\Delta G^\ddagger = 19.76 \text{ kcal mol}^{-1}$$

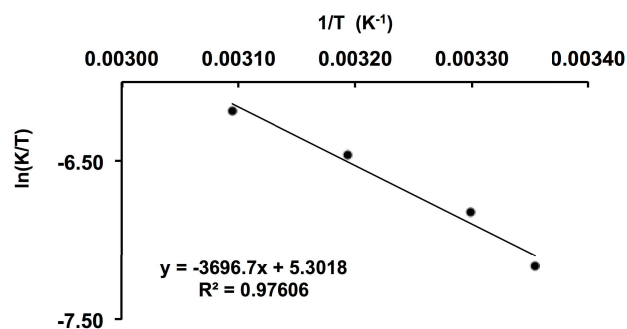
**Temperature Studies between 116 and 117 (pH 5.1)**

Experimental data collected by variable-temperature  $^1\text{H-NMR}$  spectroscopy

Temperature T (°C)	Temperature T (K)	Rate k ( $\text{M}^{-1}\text{s}^{-1}$ )
50	323.16	0.67
40	313.16	0.49
30	303.16	0.33
25	298.16	0.23

By plotting  $\ln(k/T)$  versus the reciprocal of the temperature ( $1/T$ ) a linear fit ( $y = ax + b$ ) could be applied, where the  $\Delta H^\ddagger$  can be derived from the slope ( $a = -\Delta H^\ddagger/R$ ) and  $\Delta S^\ddagger$  form the intercept ( $b = \ln(k_B/h) + \Delta S^\ddagger/R$ ).

$\ln(k/T)$	$1/T$
-6.18	0.00309
-6.46	0.00319
-6.82	0.00330
-7.17	0.00335



The following values for  $\Delta H^\ddagger$ ,  $\Delta S^\ddagger$  and  $\Delta G^\ddagger$  of **119** were obtained (pH 5.1).

$$\Delta H^\ddagger = 7.35 \text{ kcal mol}^{-1}$$

$$\Delta S^\ddagger = -37 \text{ cal mol}^{-1} \text{ K}^{-1}$$

$$\Delta G^\ddagger = 18.28 \text{ kcal mol}^{-1}$$

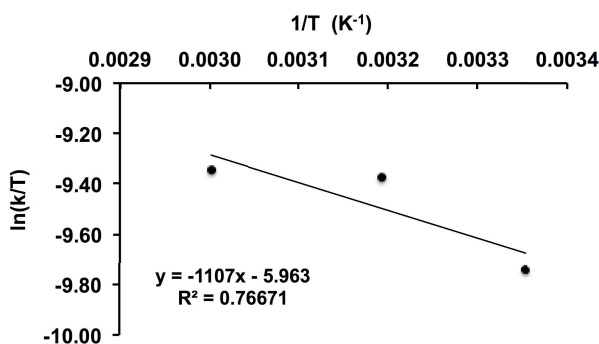
**Temperature Studies between 119 and 117 (pH 5.1)**

Experimental data collected by variable-temperature  $^1\text{H-NMR}$  spectroscopy

Temperature T (°C)	Temperature T (K)	Rate k ( $\text{M}^{-1}\text{s}^{-1}$ )
60	333.16	0.29
40	313.16	0.27
25	298.16	0.018

By plotting  $\ln(k/T)$  versus the reciprocal of the temperature ( $1/T$ ) a linear fit ( $y = ax + b$ ) could be applied, where the  $\Delta H^\ddagger$  can be derived from the slope ( $a = -\Delta H^\ddagger/R$ ) and  $\Delta S^\ddagger$  from the intercept ( $b = \ln(k_B/h) + \Delta S^\ddagger/R$ ).

$\ln(k/T)$	$1/T$ ( $K^{-1}$ )
-9.34221	0.00300
-9.37356	0.00319
-9.74318	0.00335



The following values for  $\Delta H^\ddagger$ ,  $\Delta S^\ddagger$  and  $\Delta G^\ddagger$  of **119** were obtained (pH 5.1).

$$\Delta H^\ddagger = 2.20 \text{ kcal mol}^{-1}$$

$$\Delta S^\ddagger = -59 \text{ cal mol}^{-1} K^{-1}$$

$$\Delta G^\ddagger = 19.81 \text{ kcal mol}^{-1}$$

### Comparison of $\Delta G^\ddagger$ of the KAT Ligation with Pyridyl KATs versus Phenyl KATs

For the investigation of  $\Delta\Delta G^\ddagger$  of the KAT ligation with pyridyl KAT **117** versus phenyl KAT **119** the Eyring equation was applied.

$$\Delta G^\ddagger = -RT \ln \frac{kh}{k_B T}$$

where the reaction rates  $k$  were measured at 25 °C at pH 5.1.

	$k$ ( $M^{-1} s^{-1}$ )	$\Delta G^\ddagger$ ( $kcal mol^{-1}$ )
<b>116</b>	0.231	19.84
<b>119</b>	0.017	18.32
$\Delta\Delta G^\ddagger$		1.52

$\Delta\Delta G^\ddagger$  was determined to be 1.52  $kcal M^{-1}$ , which is in good agreement with the observed 10-fold rate enhancement of the KAT ligation with **116** compared to **119**.

### Determining Molar Absorptivities

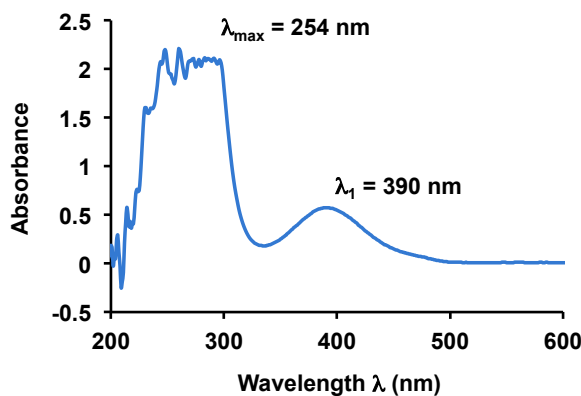
To determine the molar absorptivity of **116**, **119**, **118** and **S8** a series of solutions in MeCN / 0.2 M aq. potassium acetate buffer (1:9, pH 3.6 and pH 3.9) was prepared for each compound (concentrations from 1.88 – 15 mM). The absorbance was measured and plotted against the corresponding concentrations [M]. By applying a linear fit ( $y = ax + b$ ), the respective extinction coefficients ( $\epsilon$ ) were determined as the slope of the graph ( $a$ ) and given in  $M^{-1}cm^{-1}$ .

In the following table extinction coefficients of compound **116**, **119**, **118** and **S8** are listed.

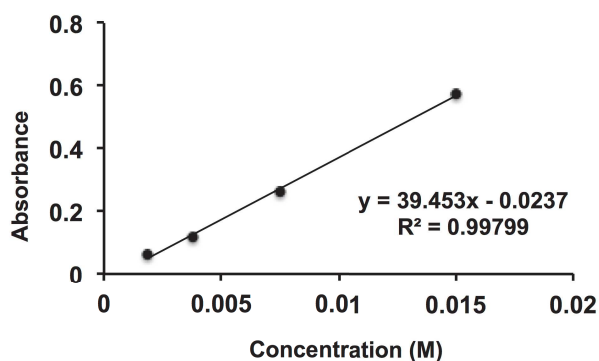
Entry	Compound	pH	Wavelength $\lambda$ (nm)	Extinction Coeff. $\epsilon$ [ $M^{-1}cm^{-1}$ ]
1	<b>116</b>	3.9	390	34.2
		3.6	390	39.4
2	<b>119</b>	3.9	355	81.2
		3.6	355	128.4
3	<b>118</b>	3.9	390	19.6
		3.6	390	27.1
4	<b>S8</b>	3.9	355	45.7
		3.6	355	87.4

Example: Determining the molar absorptivity of **116** (pH 3.6)

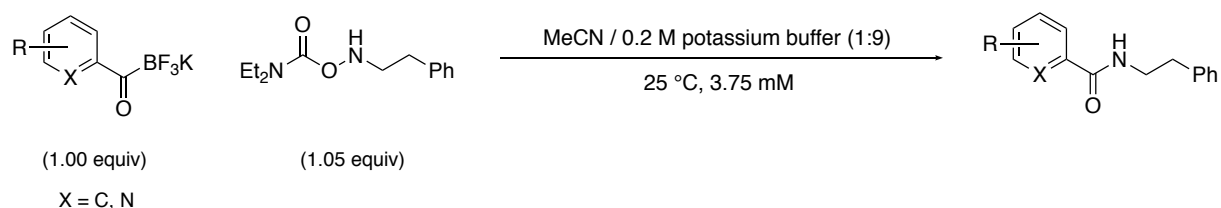
Absorbance spectrum of **116** in MeCN / 0.2 M aq. potassium acetate buffer (1:9, pH 3.6) at a concentration of 15 mM.



Absorbances at 390 nm were measured at different concentrations (3.75 – 15 mM). By plotting the measured absorbances against the corresponding molar concentrations and by applying a linear fit ( $y = ax + b$ ), the extinction coefficients ( $\epsilon$ ) were obtained as the slope of the graph (a). In this example, the extinction coefficient was found to be  $39.4 \text{ M}^{-1} \text{ cm}^{-1}$ .



#### General Procedure 7: UV-Vis Kinetic Studies of the KAT Ligation (pH 3.6 – 3.9)



Reactions were performed under second-order conditions with equimolar concentrations of the reactants (3.75 mM) in quartz cells (path length 1 cm, total volume ~2 mL) without magnetic stirring. All solutions were pre-equilibrated at room temperature (25 °C). Prior to the measurement a background spectrum of KAT in MeCN / 0.2 M aq. potassium acetate buffer (1:9, 3.75 mM, 1.0 mL) was recorded and saved. For the measurement a quartz cell was charged with a stock solution of KAT in MeCN / 0.2 M aq. potassium acetate buffer (1:9, 7.5 mM, 0.5 mL, 1.00 equiv). The reaction was initiated by adding a stock solution of hydroxylamine in MeCN / 0.2 M aq. potassium buffer (1:9, 7.88 mM, 0.5 mL, 1.05 equiv). Absorbance spectra were recorded repeatedly at 5 – 10 second intervals at room temperature (25 °C) and constant pH (pH 3.6 or 3.9). For each pair of reactants the wavelength of maximal change was monitored. Slower reactions, such as **119** at pH 3.9 were measured at slightly higher equimolar concentrations of the reactants (7.5 mM).

Concentrations of KAT were calculated by the molar absorptivities of both starting material KAT and amide product, applying the following equation derived from Lambert Beer's law:

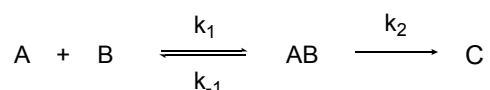
$$c_1 = \frac{A_t - (\epsilon_3 c_0)}{\epsilon_1 - \epsilon_3}$$

Where  $A_t$  is the total absorbance value measured,  $c_0$  is the initial concentration and  $\epsilon_1$  and  $\epsilon_3$  are the extinction coefficients of KAT and amide product respectively.



### Analysis of Individual Reaction Rate Constants

Based on  $^1\text{H-NMR}$  kinetic studies it was shown that the KAT ligation proceeds via a rate-determining pre-equilibrium, which can be simplified by the following sequential reaction scheme.



The individual rate equations for this reaction were derived as follows:

$$\frac{d[\text{A}]}{dt} = -k_1[\text{A}][\text{B}] + k_{-1}[\text{AB}]$$

$$\frac{d[\text{B}]}{dt} = -k_1[\text{A}][\text{B}] + k_{-1}[\text{AB}]$$

$$\frac{d[\text{AB}]}{dt} = k_1[\text{A}][\text{B}] - k_{-1}[\text{AB}] - k_2[\text{AB}]$$

$$\frac{d[\text{C}]}{dt} = k_2[\text{AB}]$$

The system of ordinary differential equations (ODE) was integrated using the following initial concentrations, which correspond to the initial time  $t_0 = 610$  s.

$$[\text{A}]_0 = 0.0143 \text{ M}$$

$$[\text{B}]_0 = 0.0150 \text{ M}$$

$$[\text{AB}]_0 = 9.15 \cdot 10^{-4} \text{ M}$$

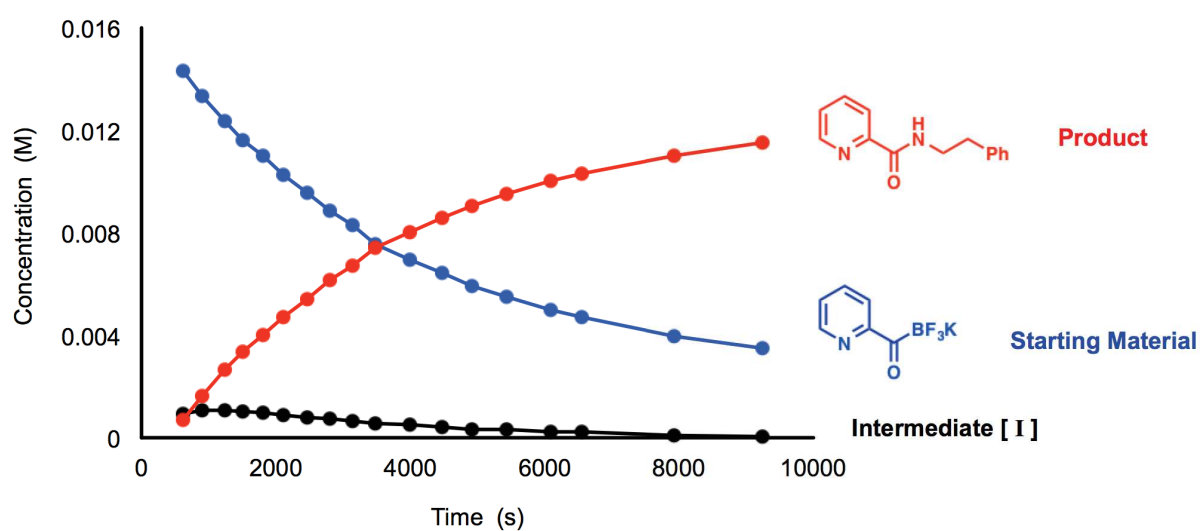
$$[\text{C}]_0 = 6.75 \cdot 10^{-4} \text{ M}$$

The kinetic parameters were estimated by fitting the model equations to the experimental data. The cost function (sum of errors between experimental and calculated data) is minimized using a genetic algorithm (GA function of Matlab). The following individual rate constants were obtained:

$$k_1 = 4.76 \text{ M}^{-1}\text{s}^{-1}$$

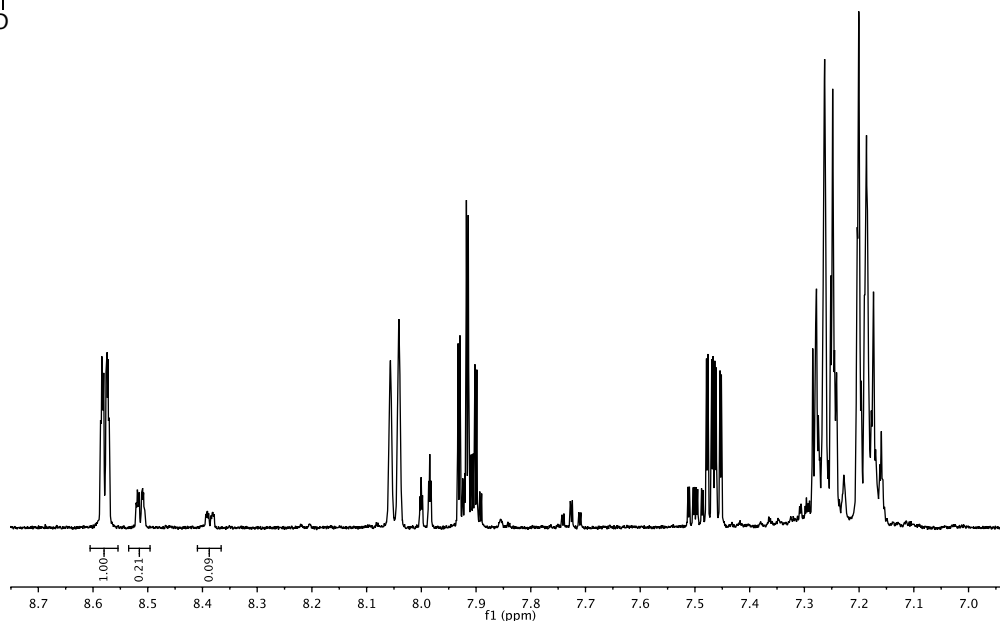
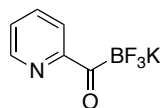
$$k_{-1} = 0.80 \text{ s}^{-1}$$

$$k_2 = 0.00359 \text{ s}^{-1}$$

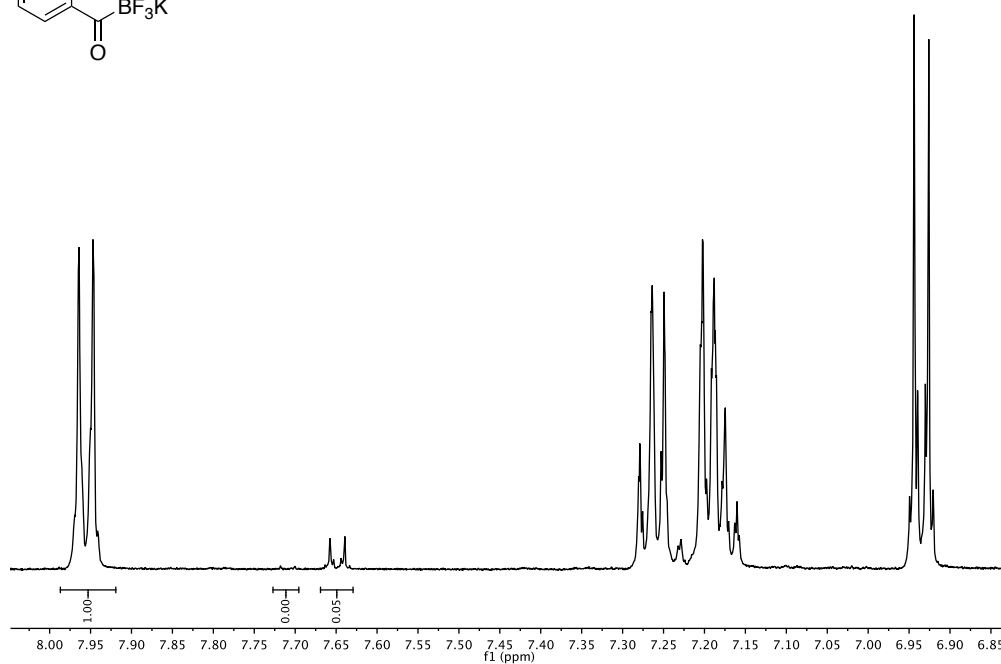
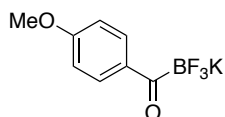


**KAT Ligation – Analysis of the Relative Intermediate Concentration**

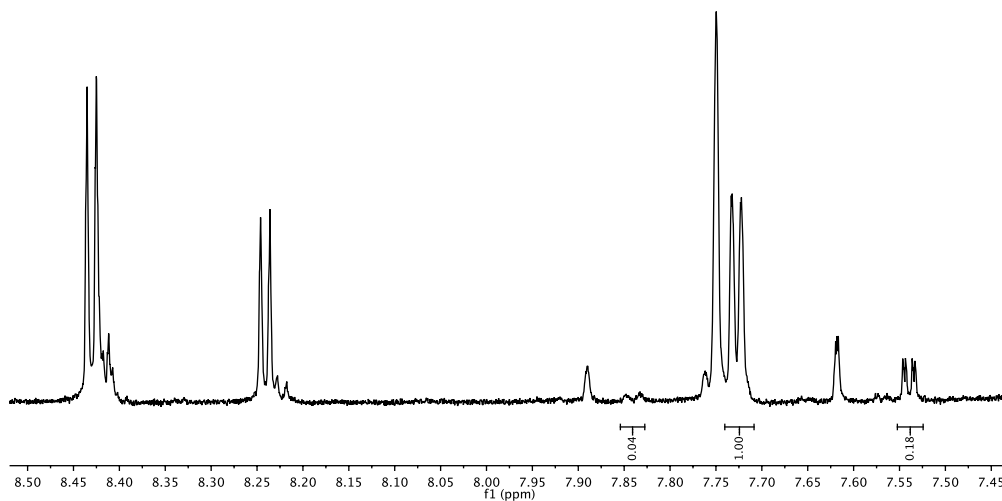
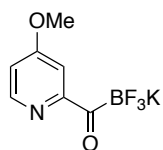
Observed relative intermediate concentration of **116** (1 equiv of **117**) = 7%



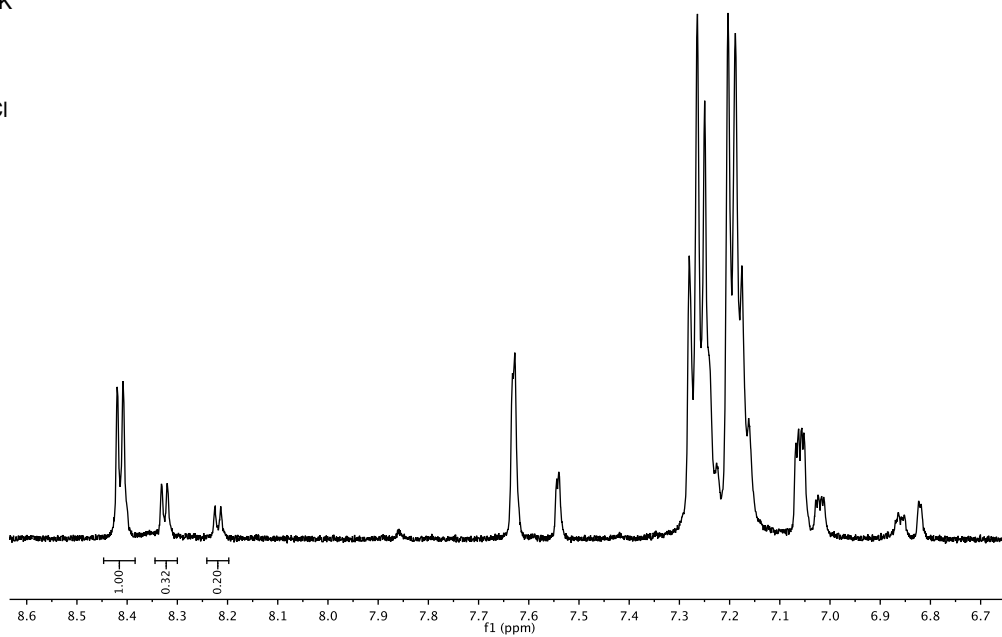
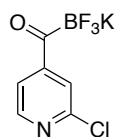
Observed relative intermediate concentration of **119** (1 equiv of **117**) = <1%



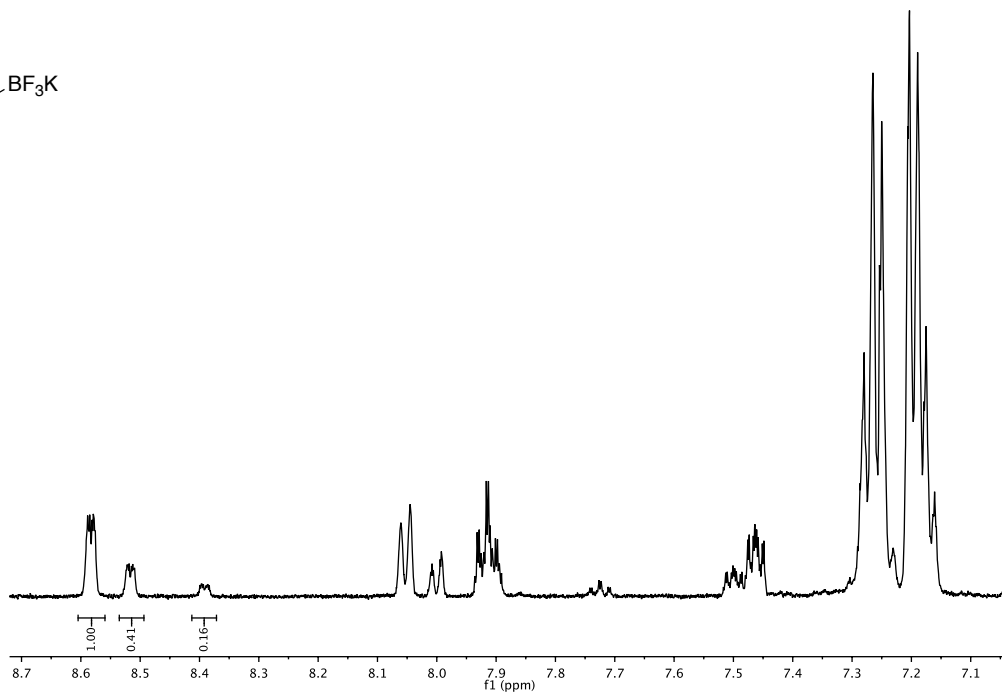
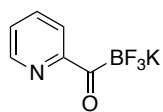
Observed relative intermediate concentration of **1f27** (1 equiv of **117**) = 3%



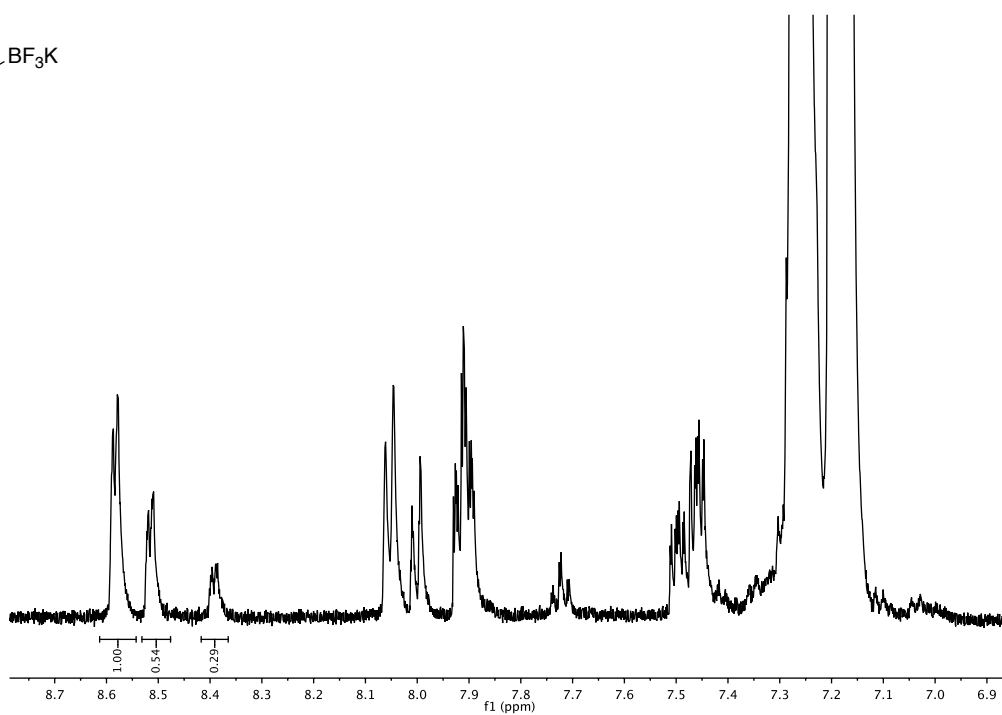
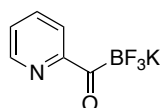
Observed relative intermediate concentration of **126** (1 equiv of **117**) = 13%



Observed relative intermediate concentration of **116** (2 equiv of **117**) = 11%



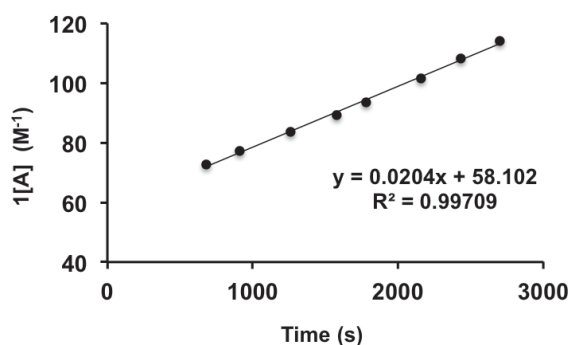
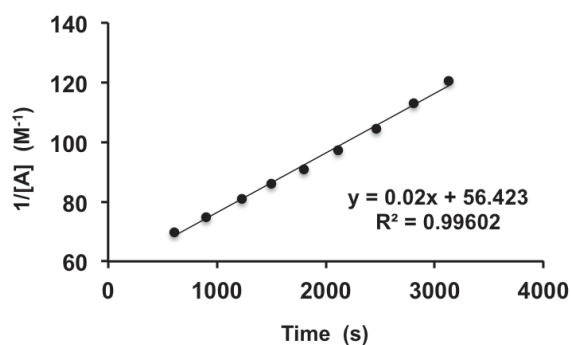
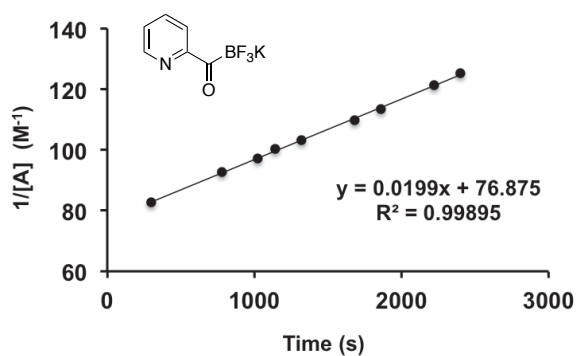
Observed relative intermediate concentration of **116** (4 and 8 equiv of **117**) = 16%



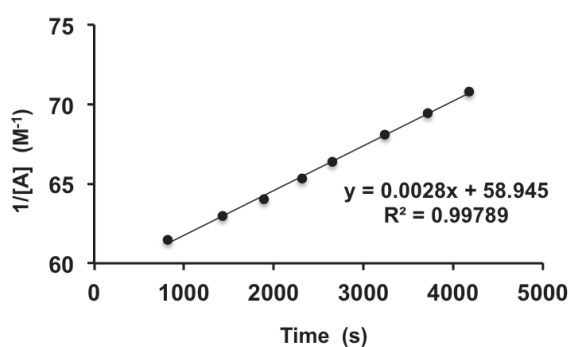
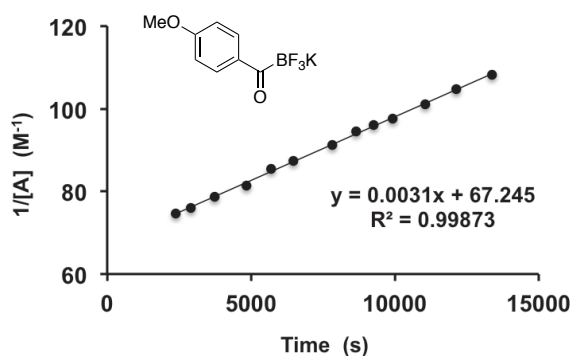
## Rate Constants of KATs by $^1\text{H-NMR}$ Kinetic Studies

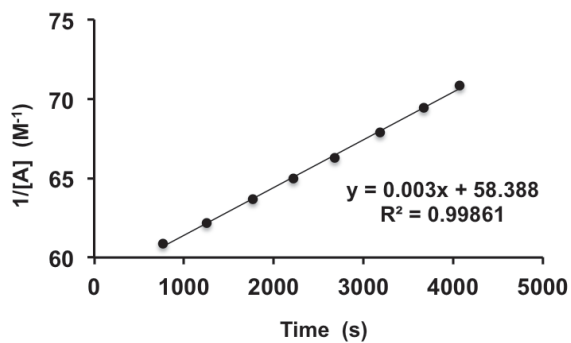
Unless otherwise stated, KAT ligation reactions between KAT and hydroxylamine **117** were carried out at equimolar concentration (15 mM) in  $\text{MeCN-}d_3$  / 0.1 M deuterated potassium phosphate buffer (2:1, pH 6.8) at room temperature (25 °C) according to general procedure 6.

### Kinetic Data of **116**

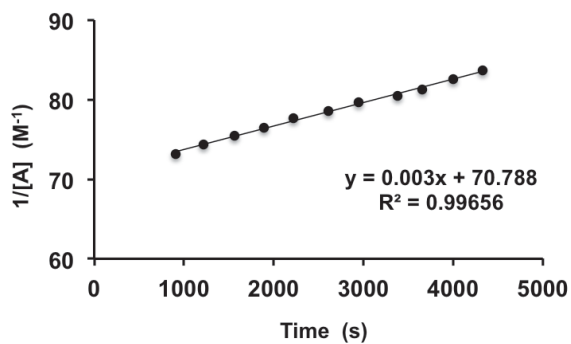
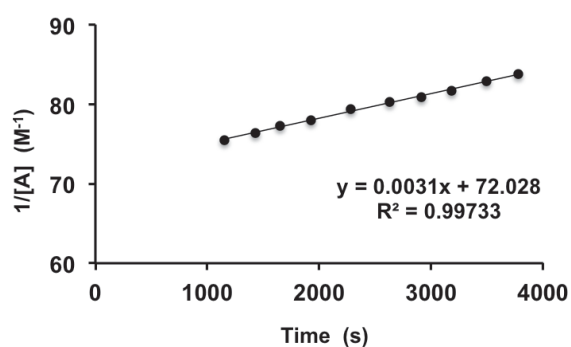
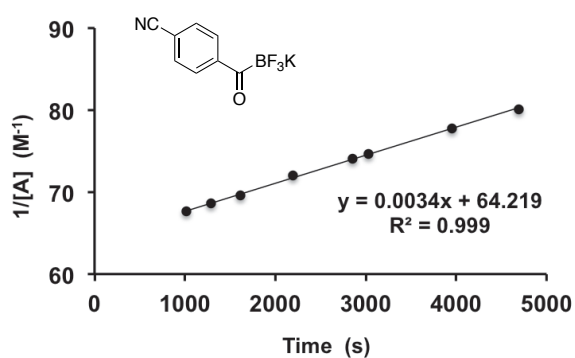


### Kinetic Data of **119**

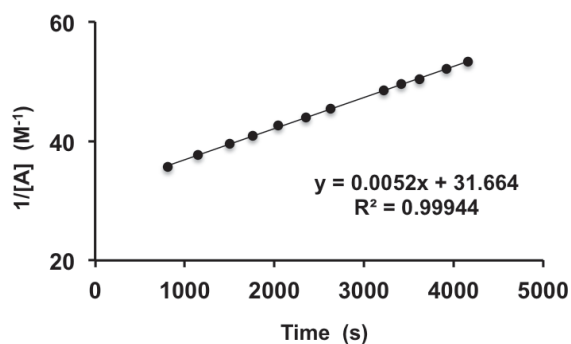
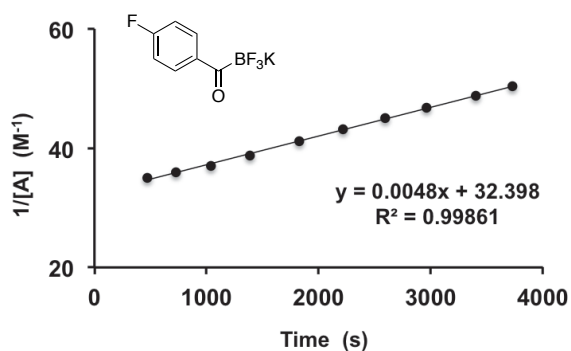


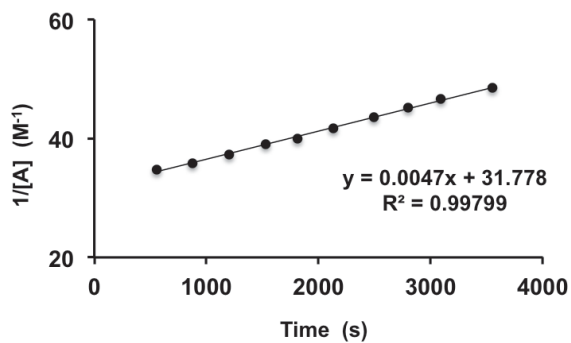


## Kinetic Data of 120

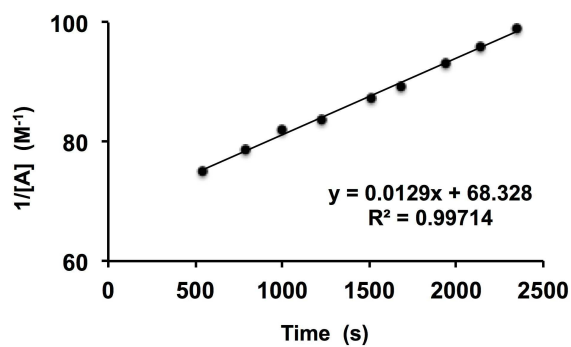
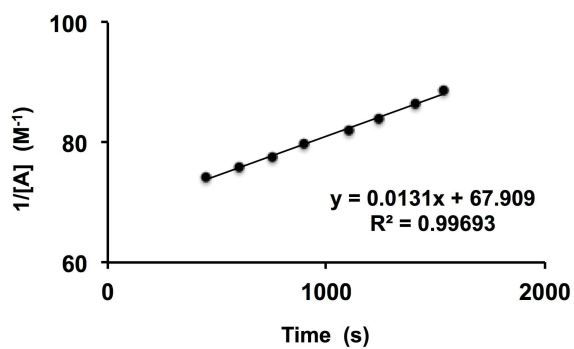
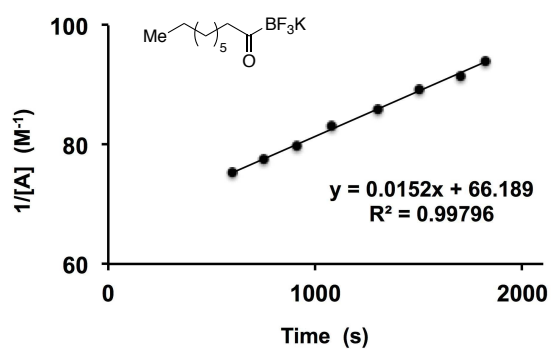


## Kinetic Data of 121 (modification of the general procedure 6: reaction conc. 30 mM)

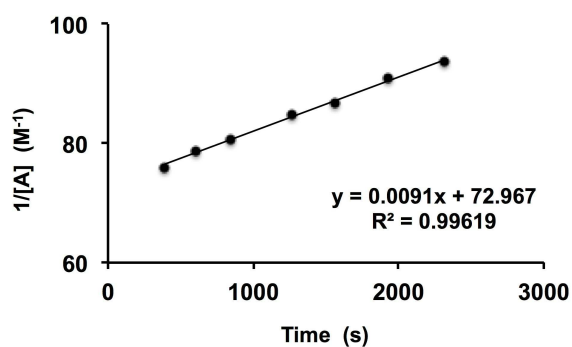
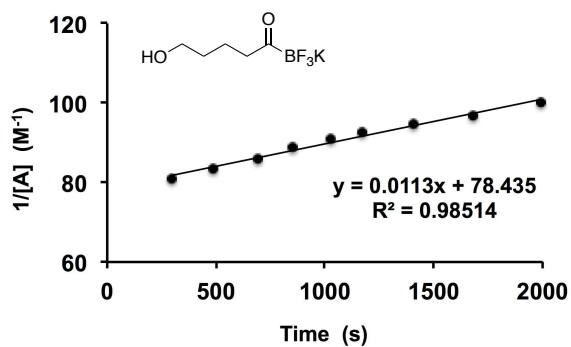




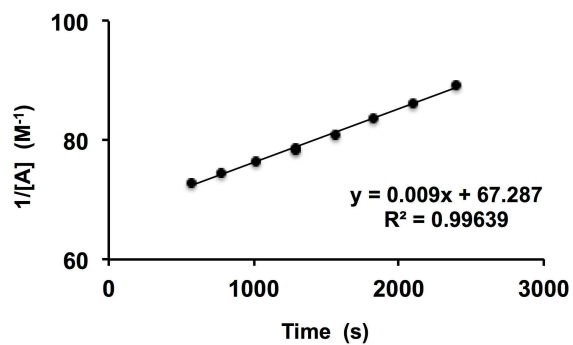
## Kinetic Data of 122



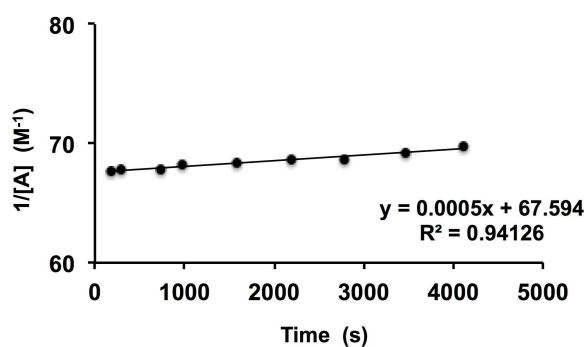
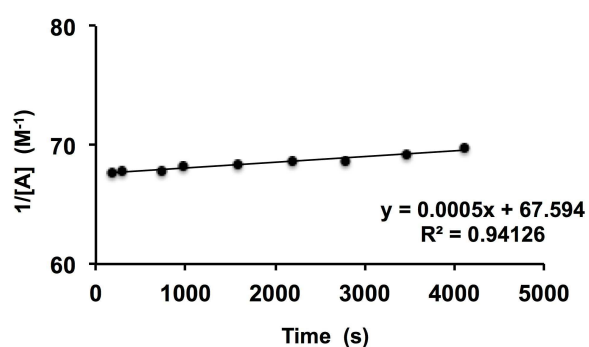
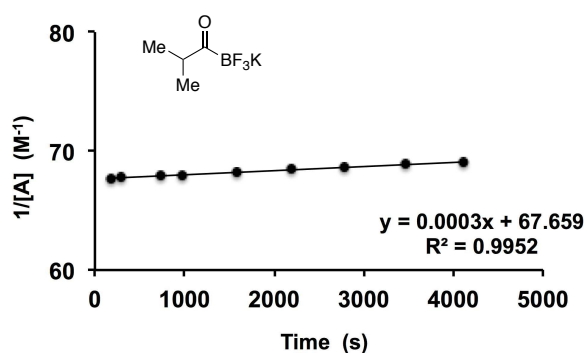
## Kinetic Data of 123



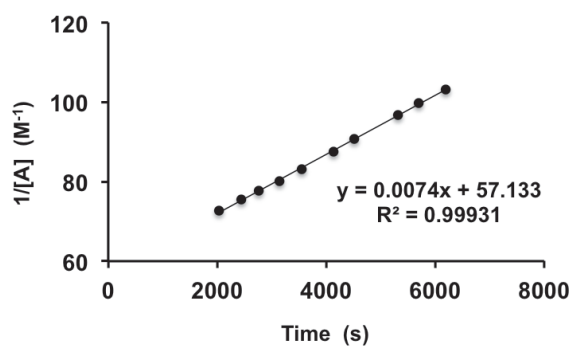
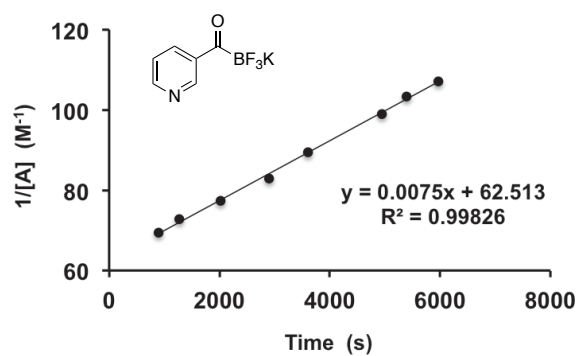


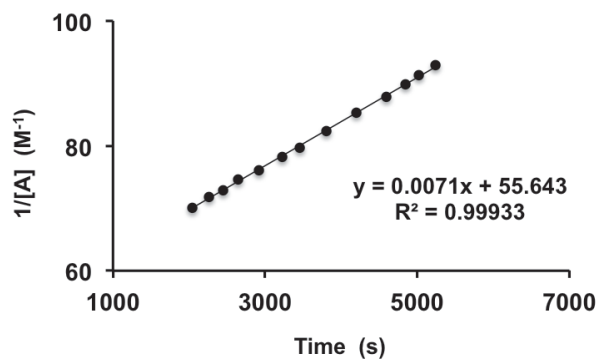
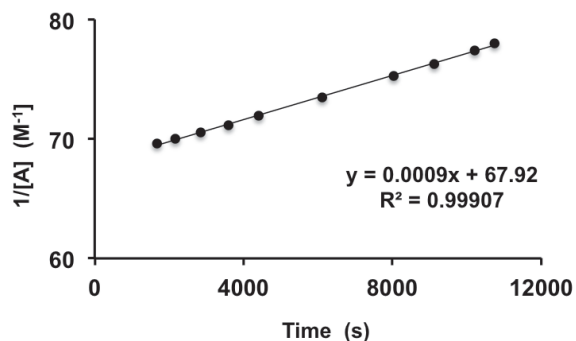
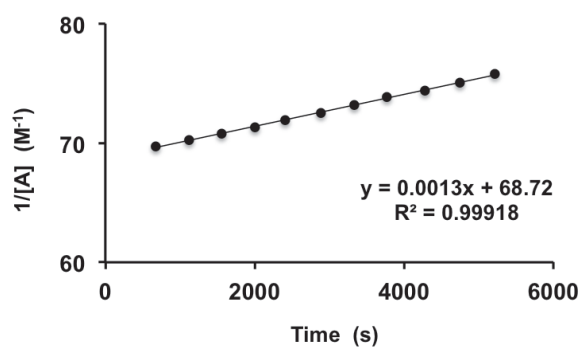
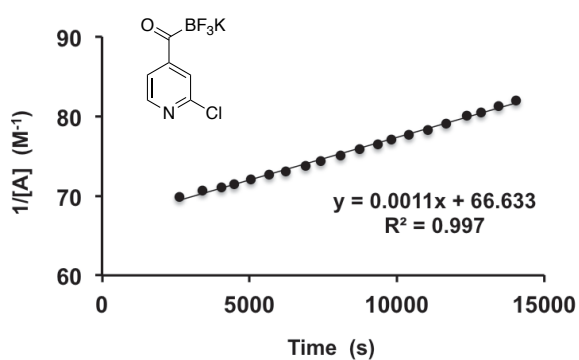
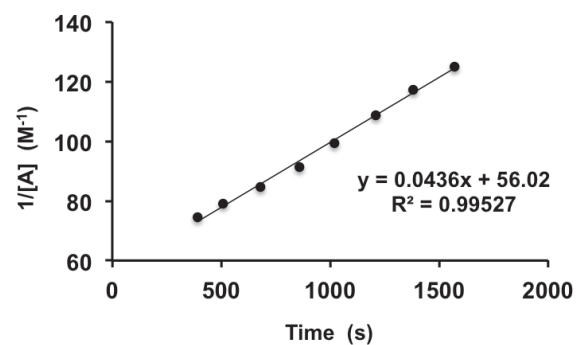
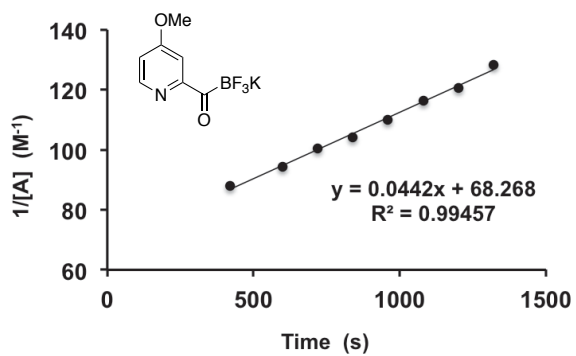


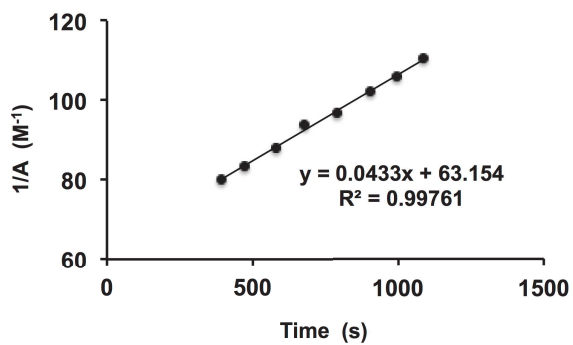
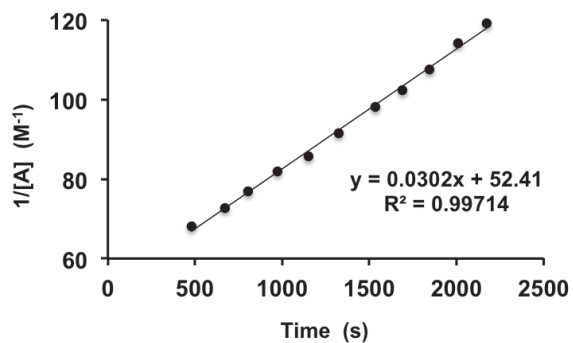
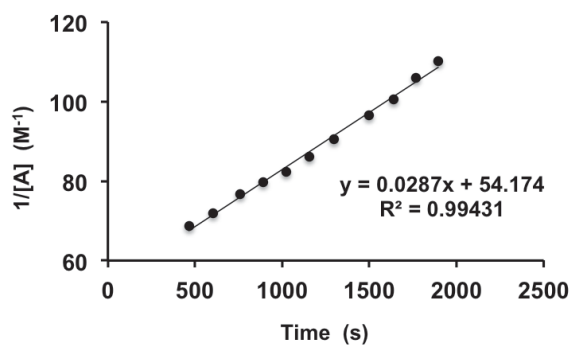
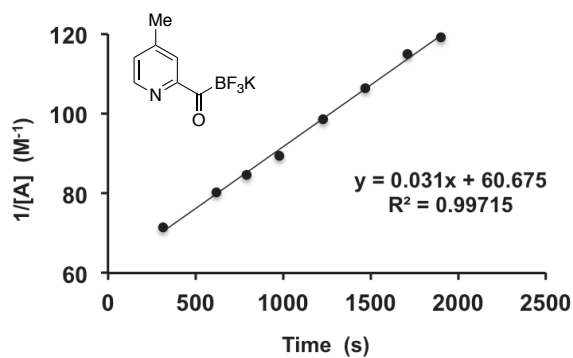
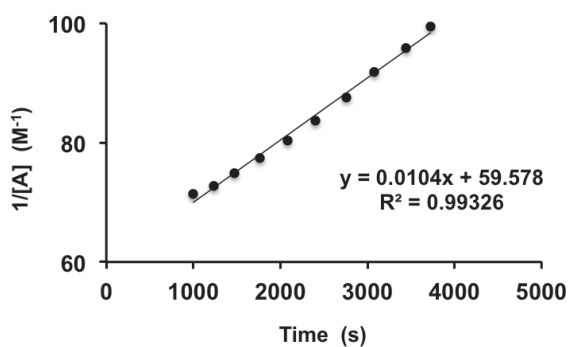
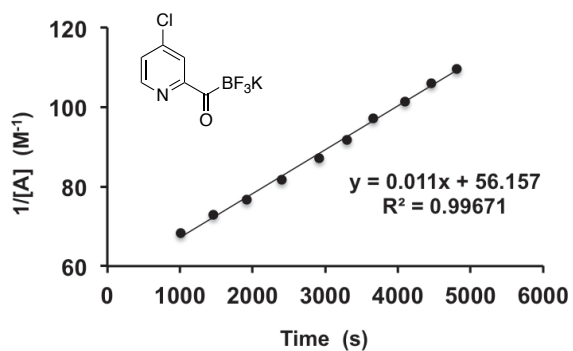
## Kinetic Data of 124

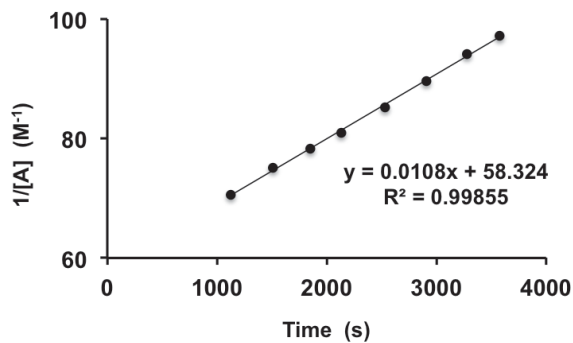


## Kinetic Data of 125

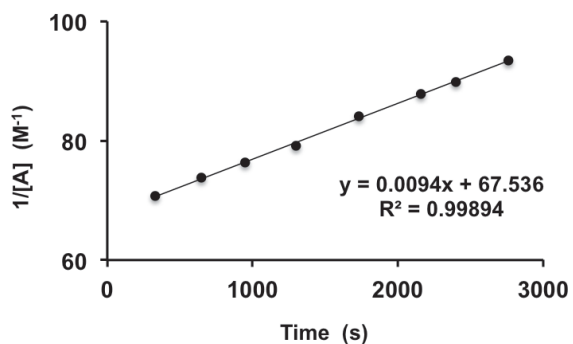
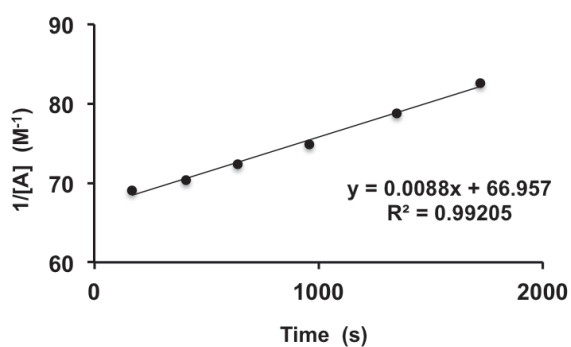
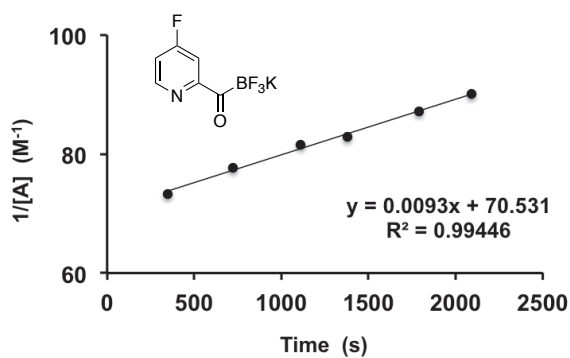


Kinetic Data of **126**Kinetic Data of **127**

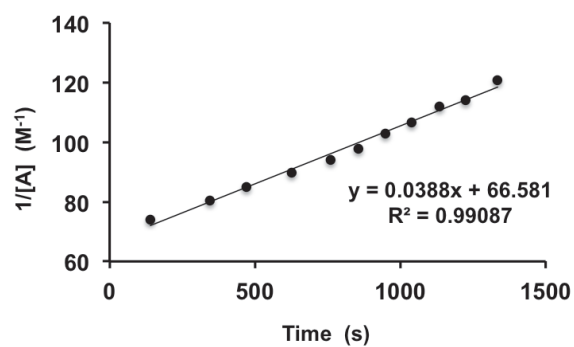
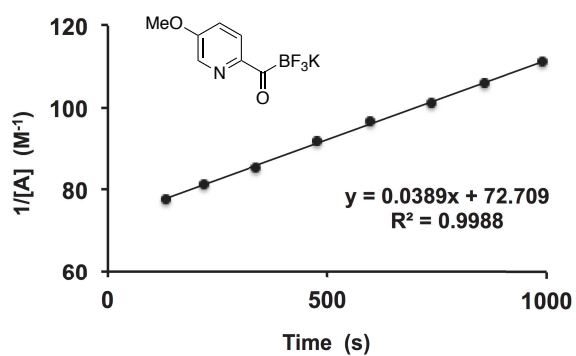
Kinetic Data of **128**Kinetic Data of **129**

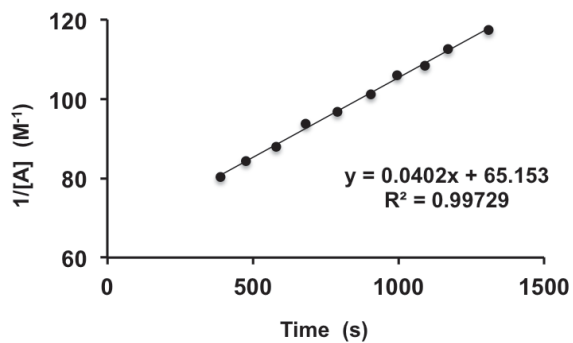
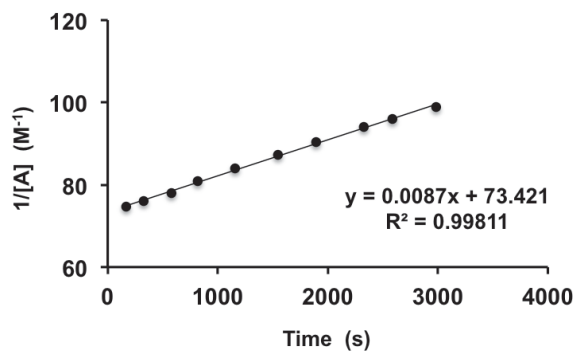
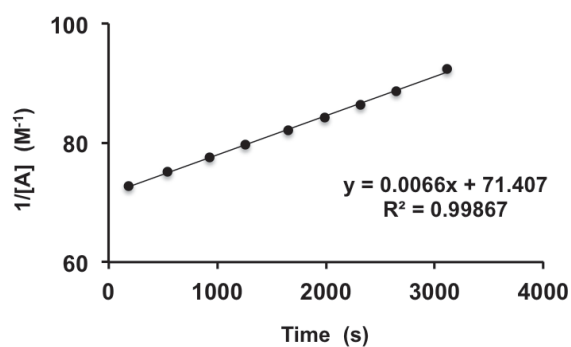
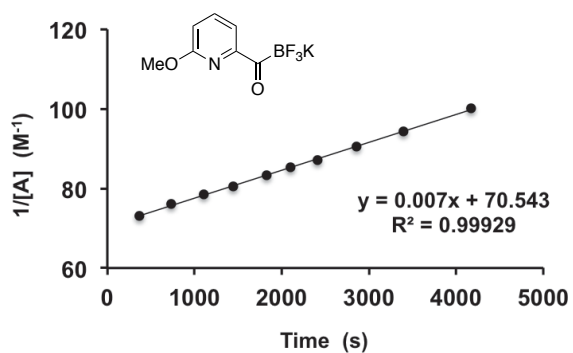
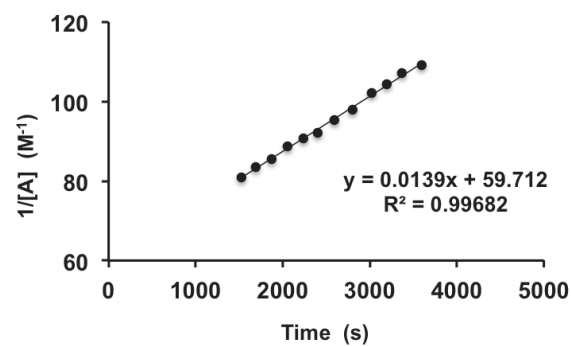
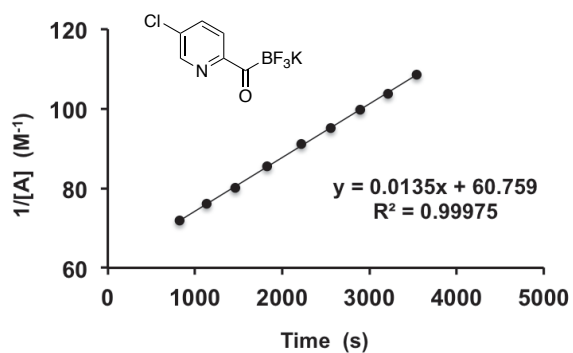


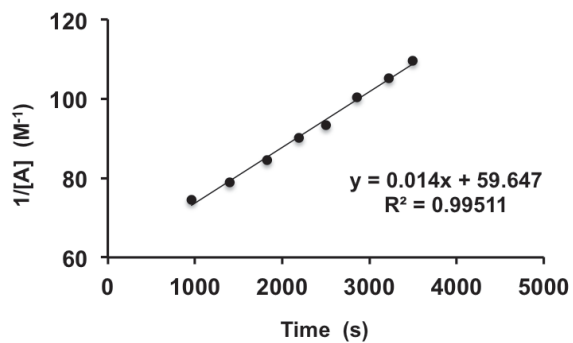
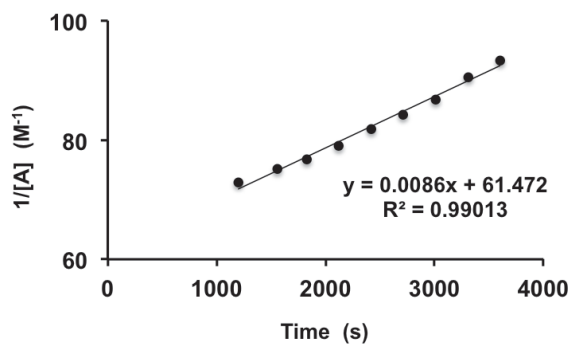
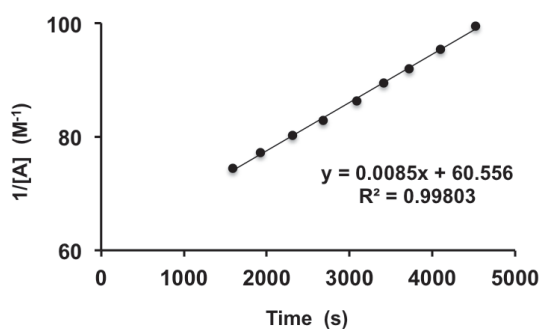
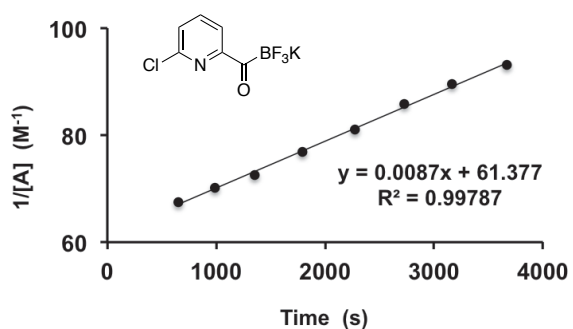
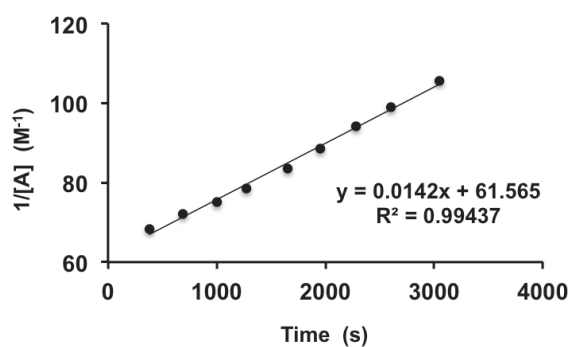
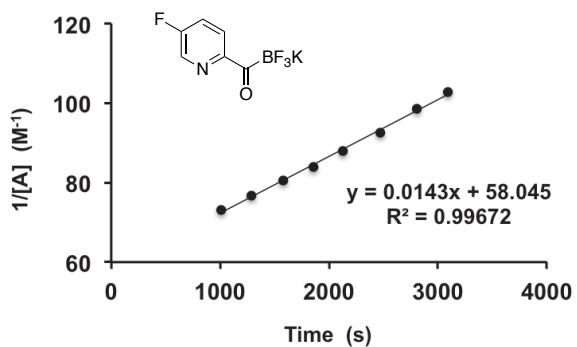
## Kinetic Data of 130

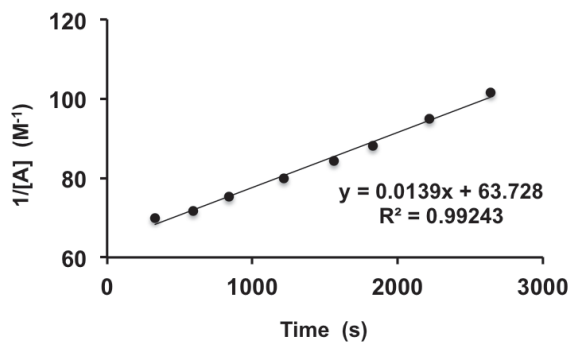
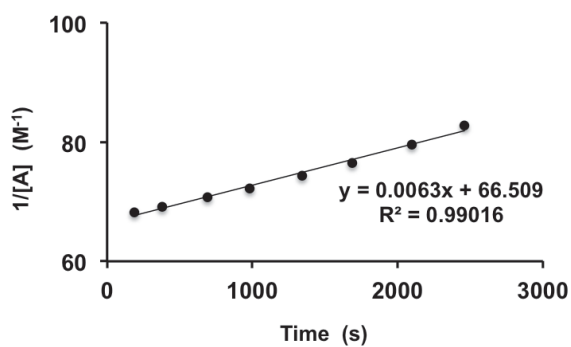
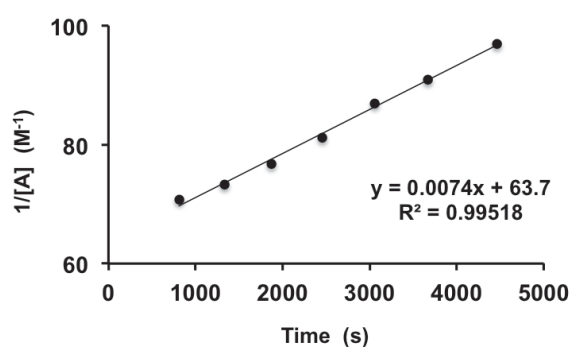
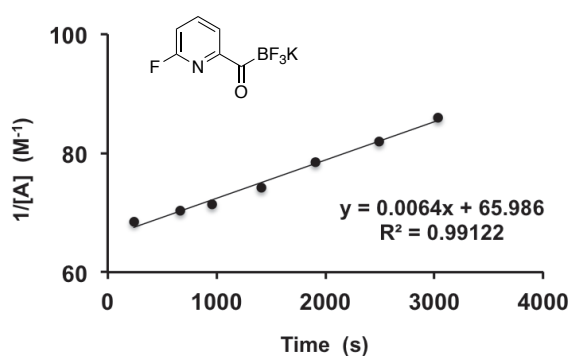
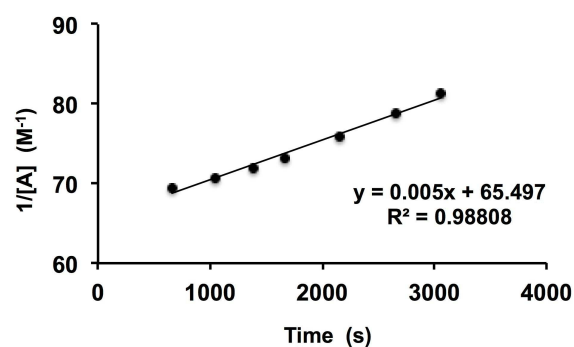
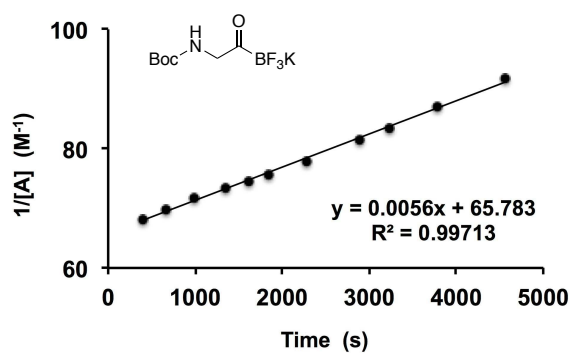


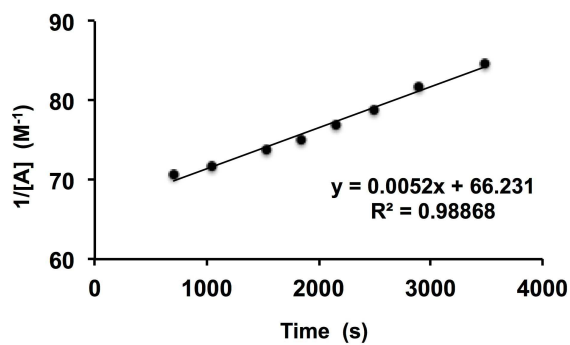
## Kinetic Data of 131



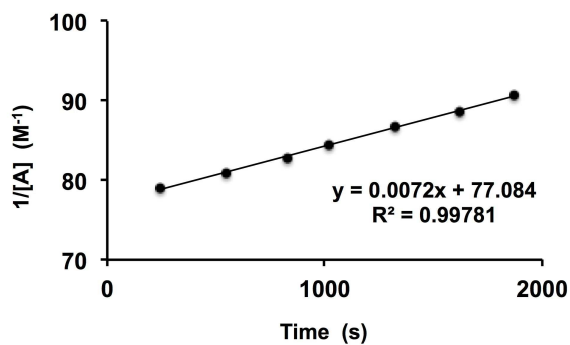
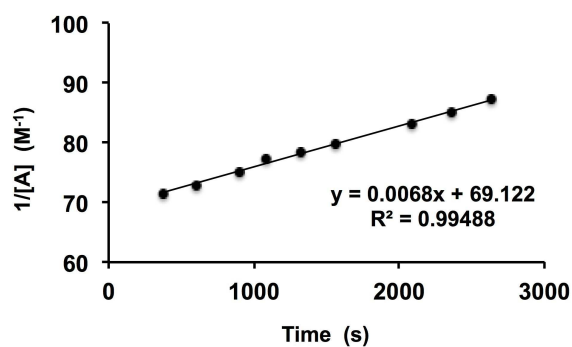
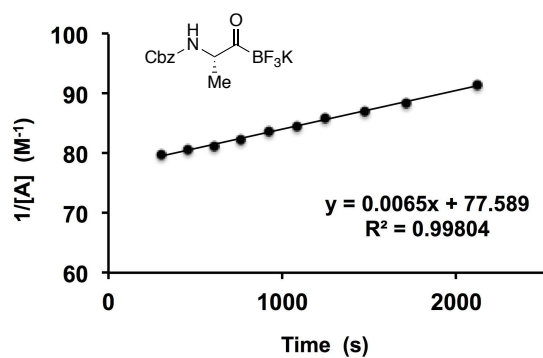
Kinetic Data of **132**Kinetic Data of **133**

Kinetic Data of **134**Kinetic Data of **135**

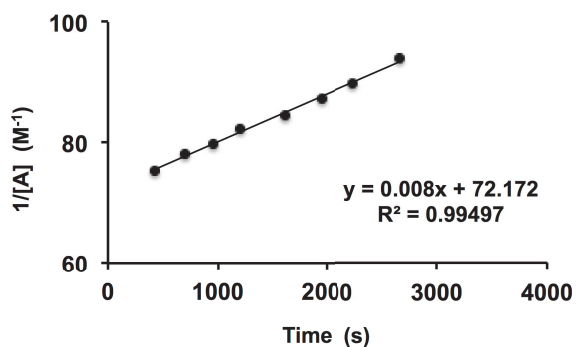
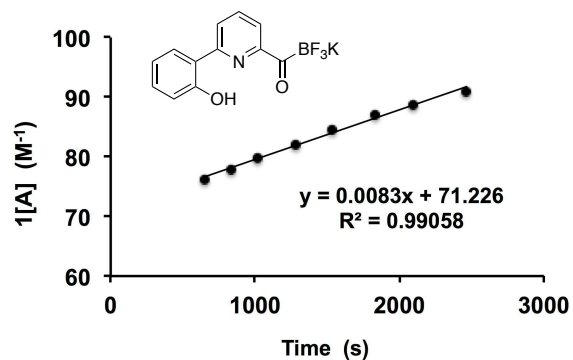
Kinetic Data of **136**Kinetic Data of **167**



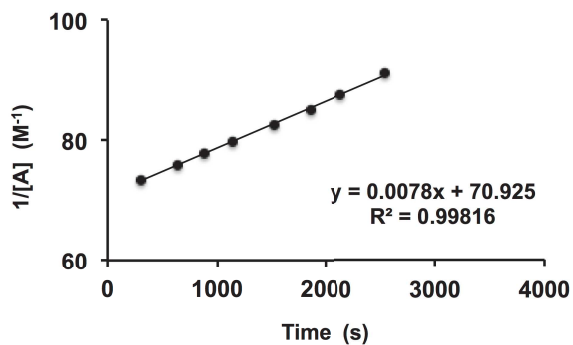
## Kinetic Data of 168



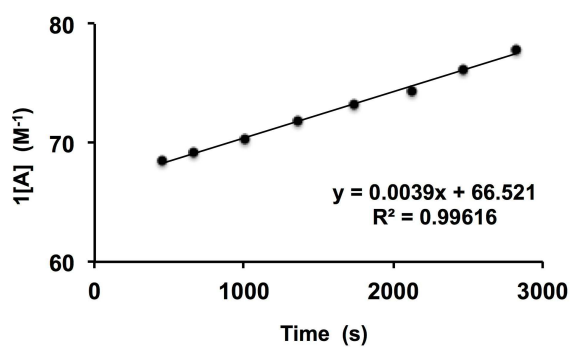
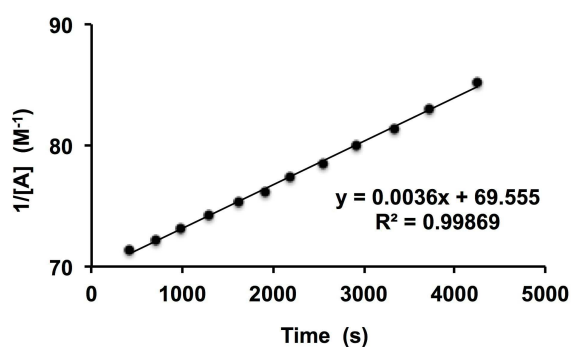
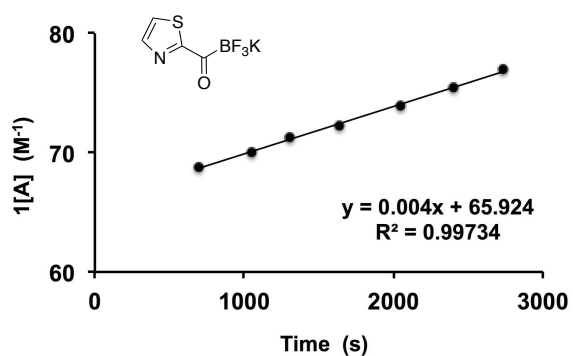
## Kinetic Data of 169



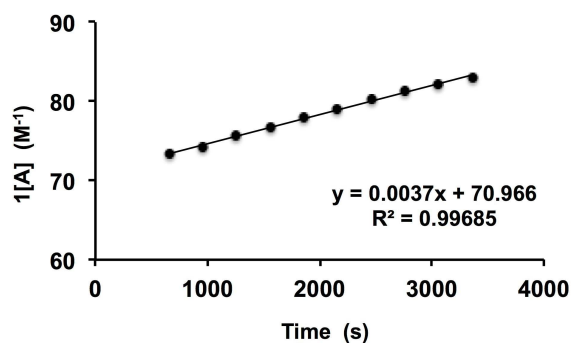
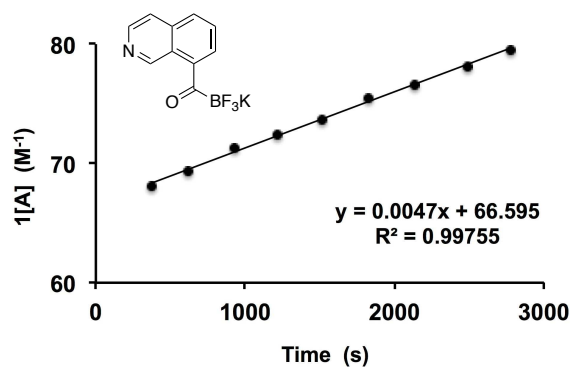


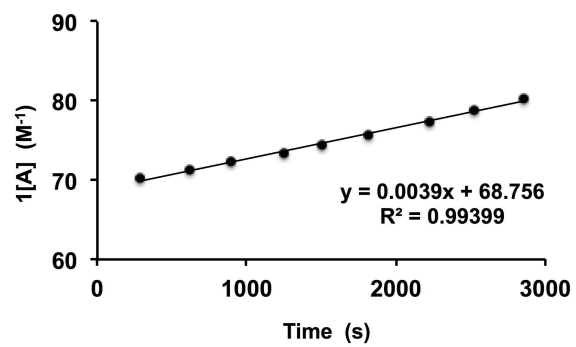


## Kinetic Data of 170



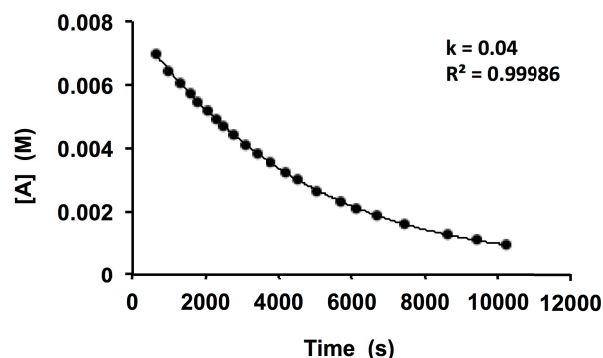
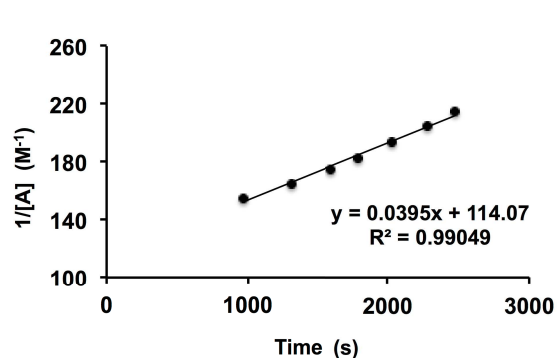
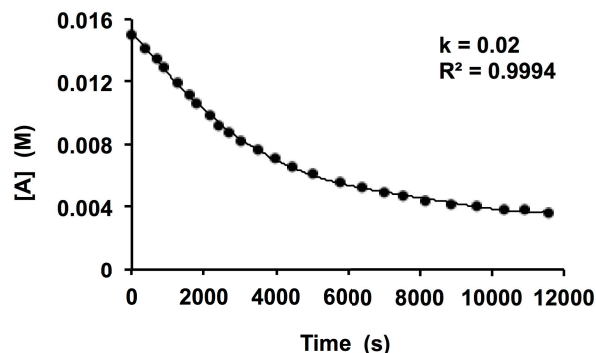
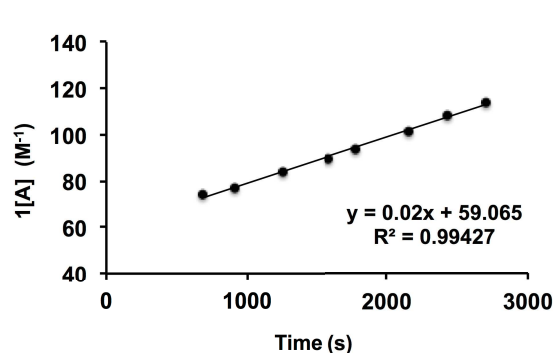
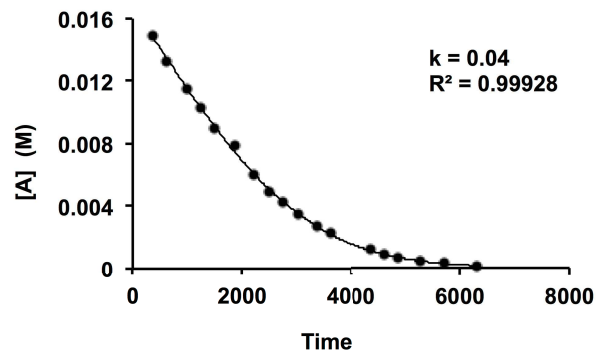
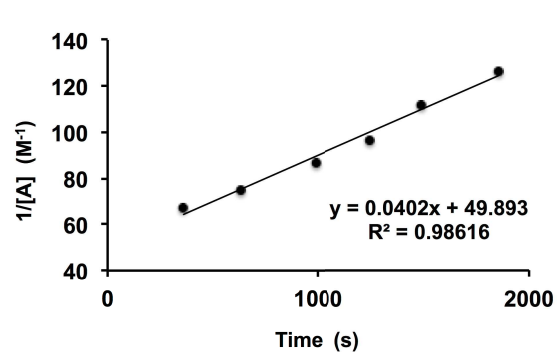
## Kinetic Data of 173

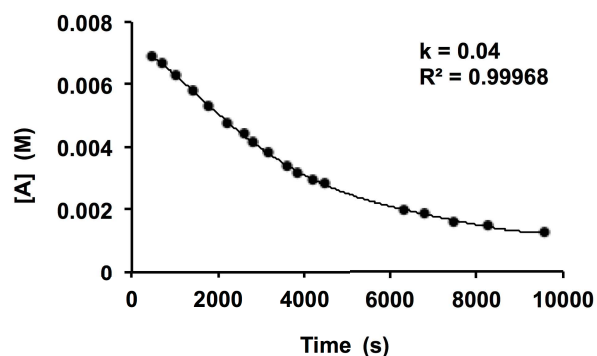
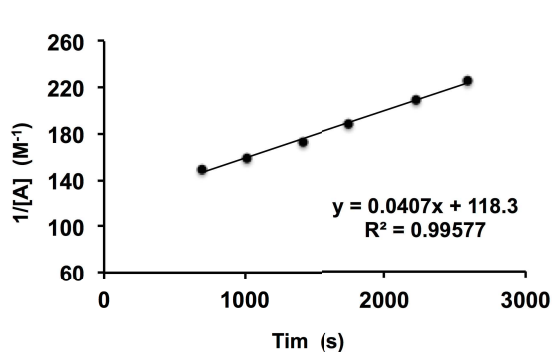
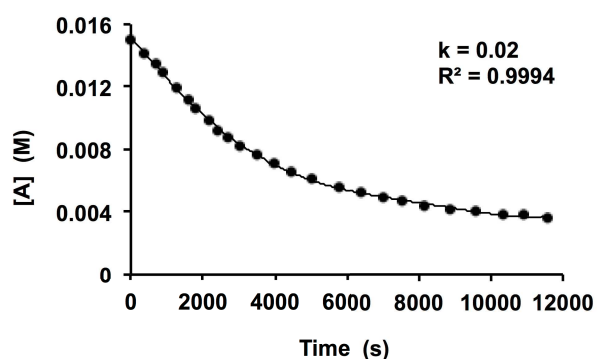
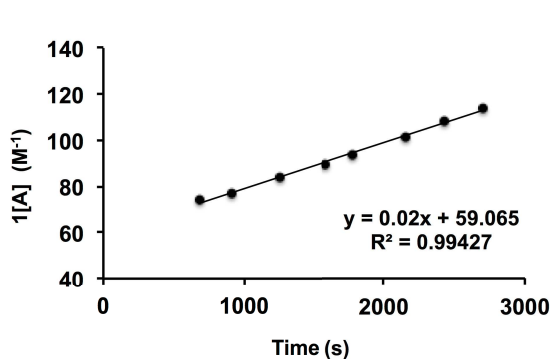
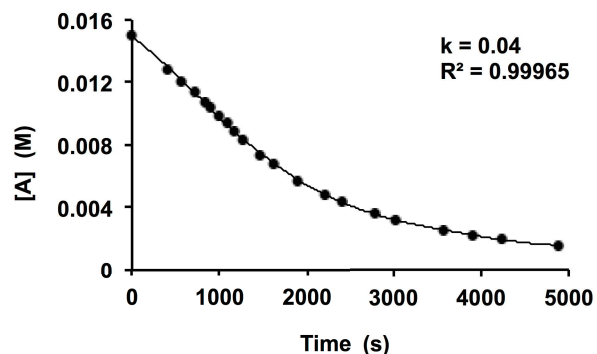
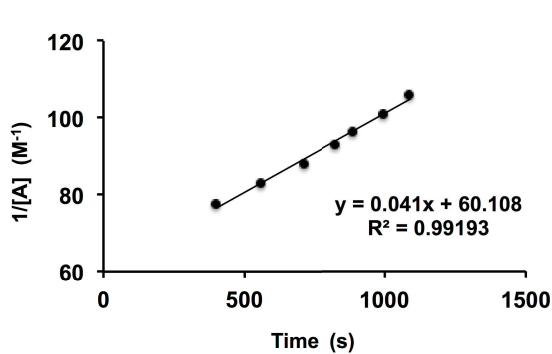
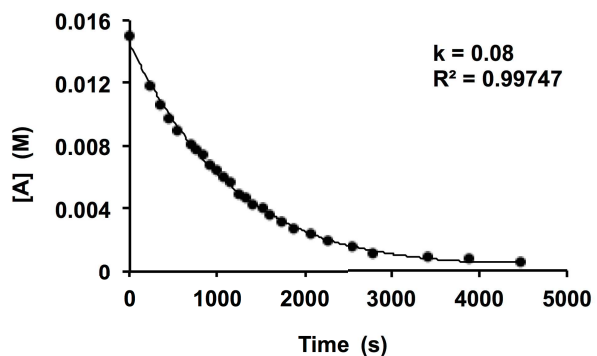
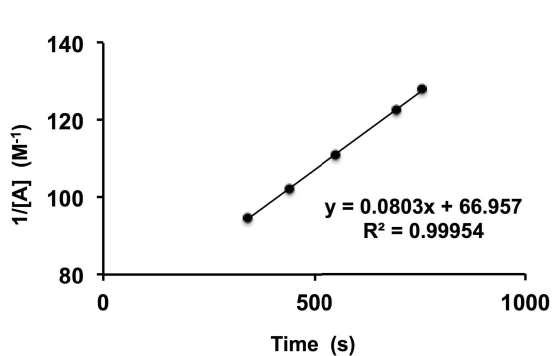




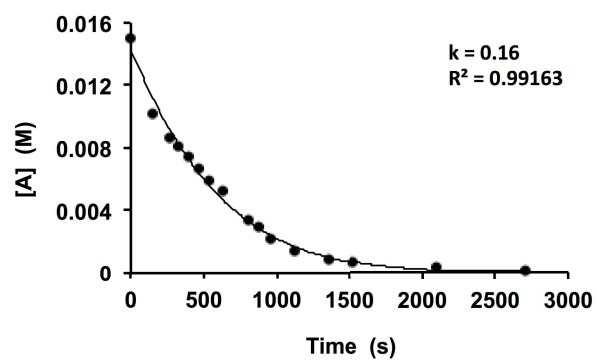
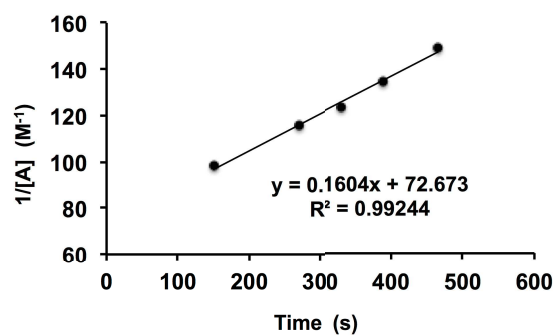
**KAT Ligation – Determination of the Reaction Order by <sup>1</sup>H-NMR Kinetic Studies**

Unless otherwise stated, KAT ligation reaction between **116** and **117** were carried out in MeCN-*d*<sub>3</sub> / 0.1 M deuterated potassium phosphate buffer (2:1, pH 6.8) at room temperature (25 °C) according to general procedure 6. Different initial concentrations of the reactants were employed (1 equiv = 15 mM).

**Kinetic Data of **116** (0.5 equiv) and **117** (1.0 equiv)****Kinetic Data of **116** (1.0 equiv) and **117** (1.0 equiv)****Kinetic Data of **116** (2.0 equiv) and **117** (1.0 equiv)**

Kinetic Data of **116** (1.0 equiv) and **117** (0.5 equiv)Kinetic Data of **116** (1.0 equiv) and **117** (1.0 equiv)Kinetic Data of **116** (1.0 equiv) and **117** (2.0 equiv)Kinetic Data of **116** (1.0 equiv) and **117** (4.0 equiv)

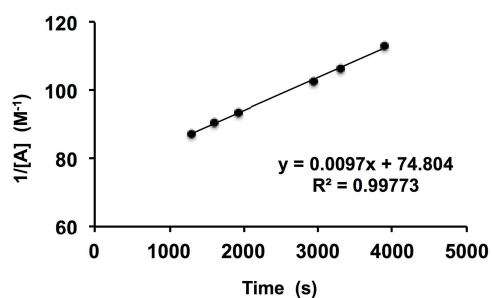
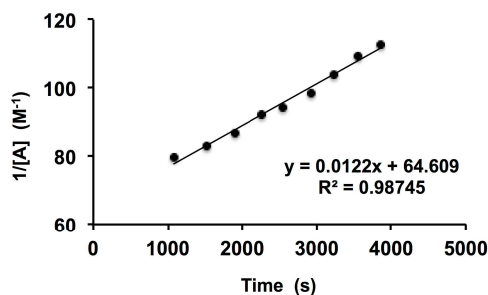
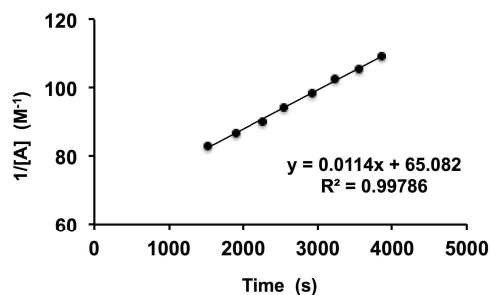
Kinetic Data of **116** (1.0 equiv) and **117** (8.0 equiv)



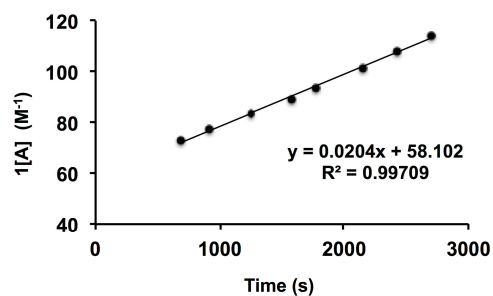
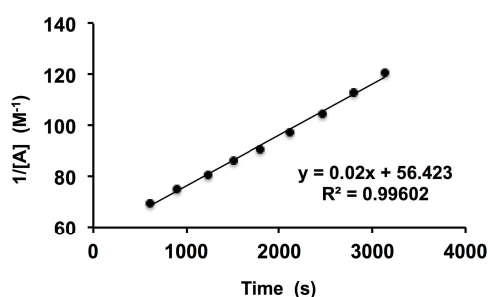
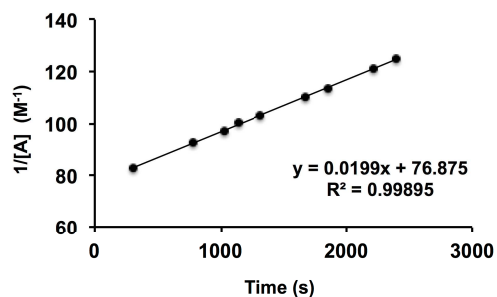
## Variable Temperature Kinetic Studies of the KAT Ligation by $^1\text{H-NMR}$ Spectroscopy

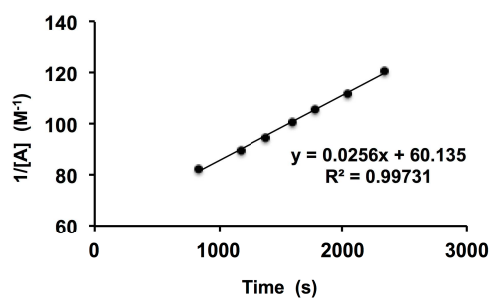
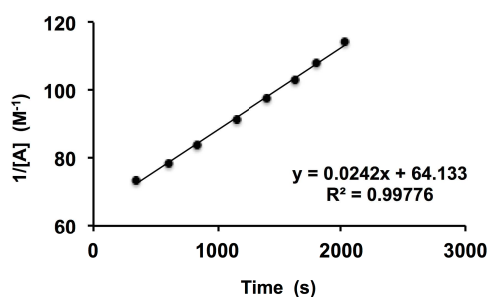
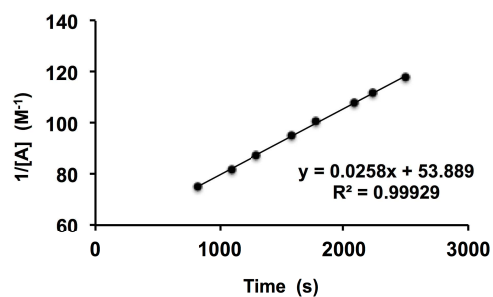
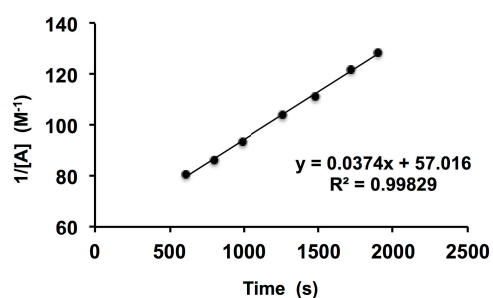
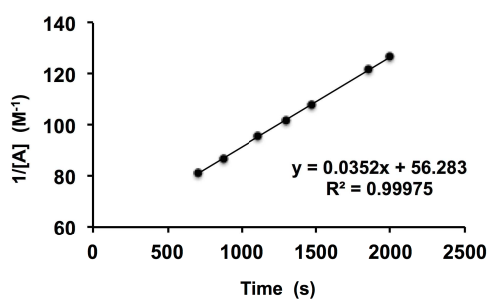
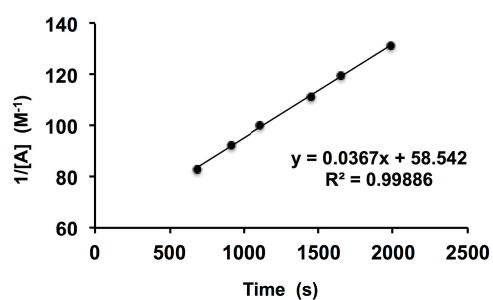
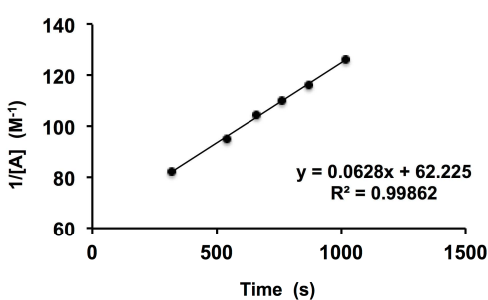
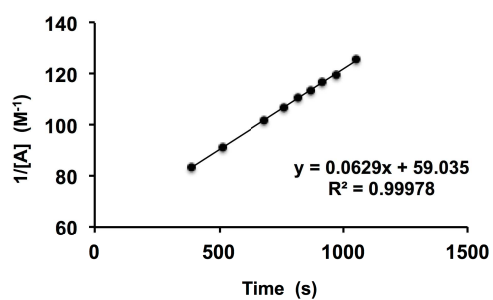
Unless otherwise stated, KAT ligation reaction between KAT and hydroxylamine **117** were carried out at equimolar concentration (15 mM) in  $\text{MeCN-}d_3$  / 0.1 M deuterated potassium phosphate buffer (2:1, pH 5.1 or 6.8) at variable temperature (10 °C – 70 °C).

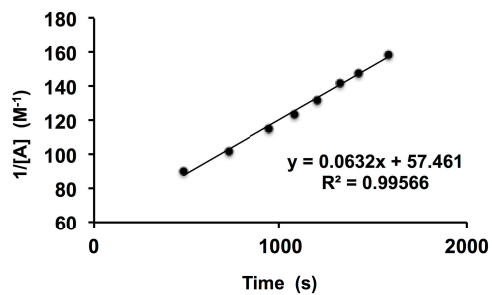
### Kinetic Data of **116** (15 mM, pH 6.8, 10 °C)



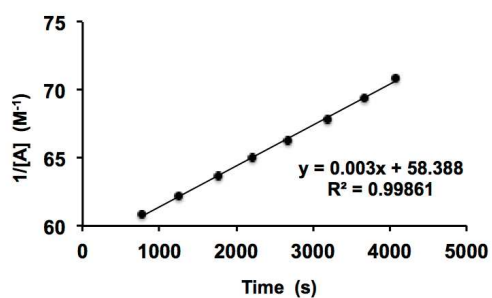
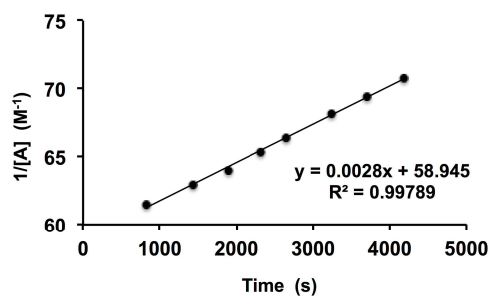
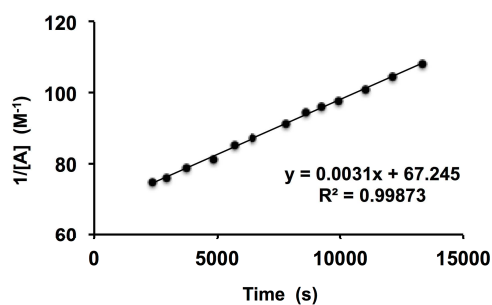
### Kinetic Data of **116** (15 mM, pH 6.8, 25 °C)



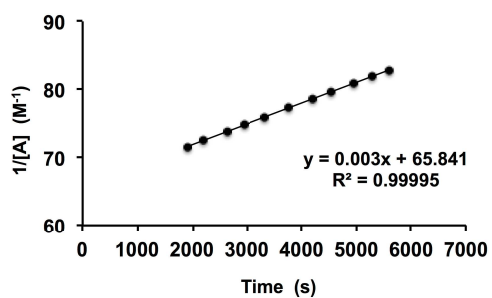
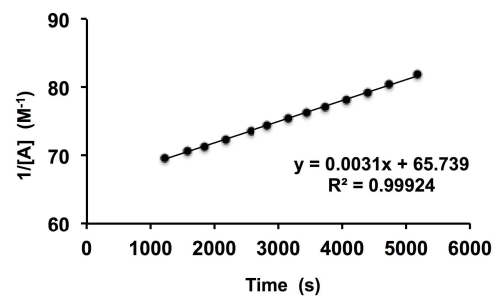
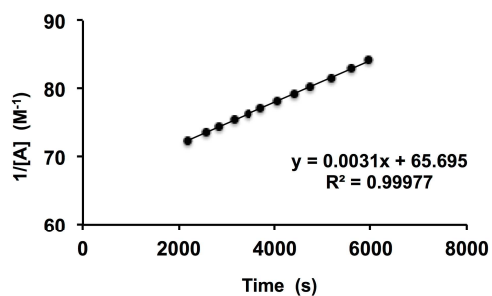
Kinetic Data of **116** (15 mM, pH 6.8, 30 °C)Kinetic Data of **116** (15 mM, pH 6.8, 40 °C)Kinetic Data of **116** (15 mM, pH 6.8, 60 °C)



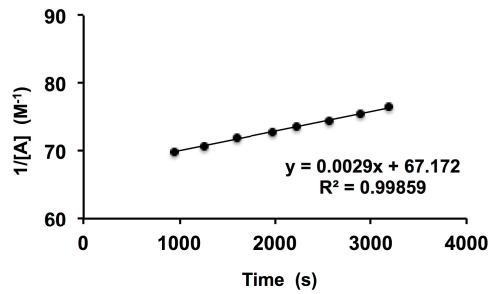
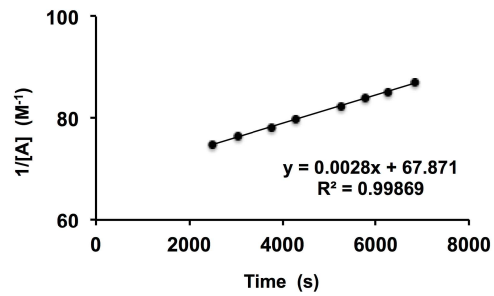
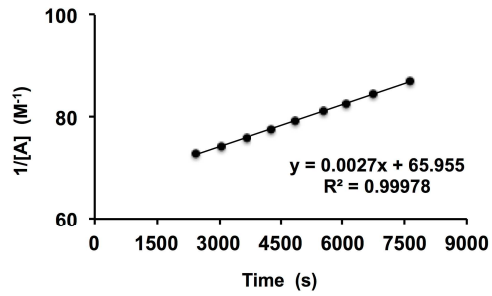
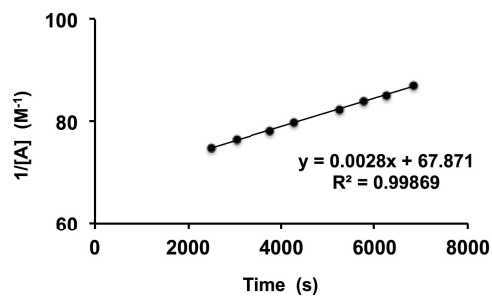
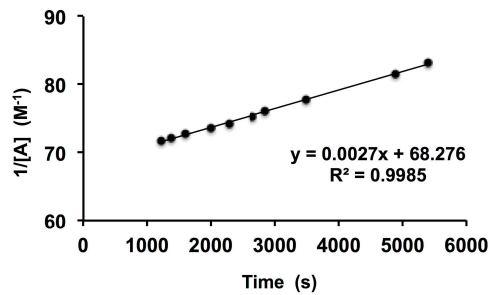
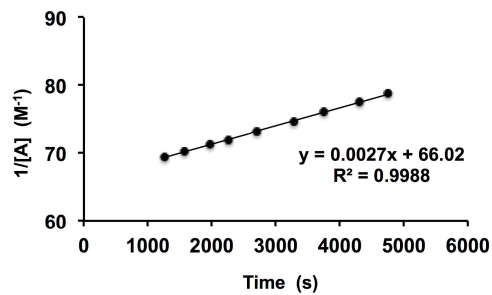
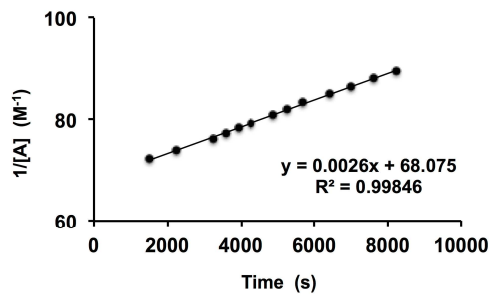
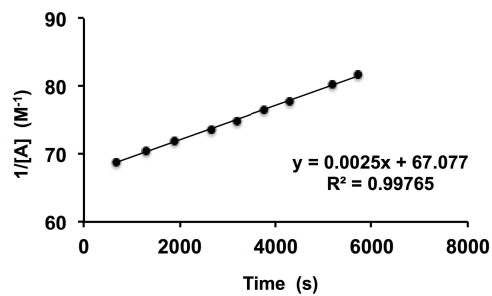
Kinetic Data of 119 (15 mM, pH 6.8, 25 °C)

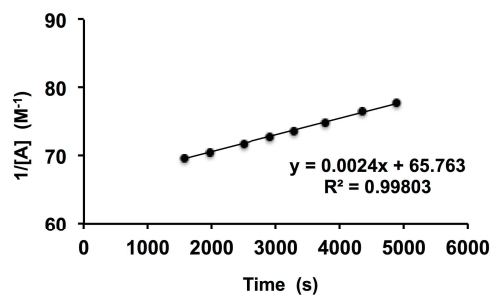
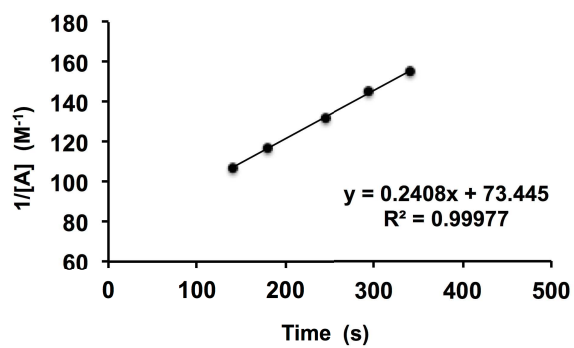
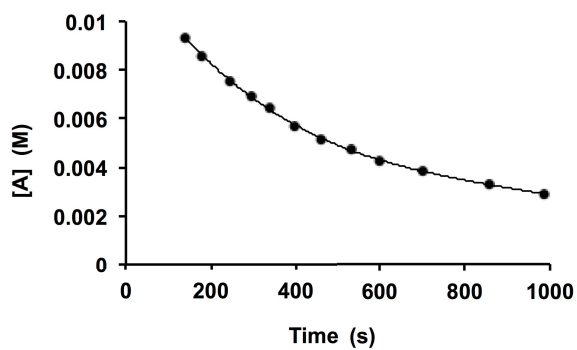
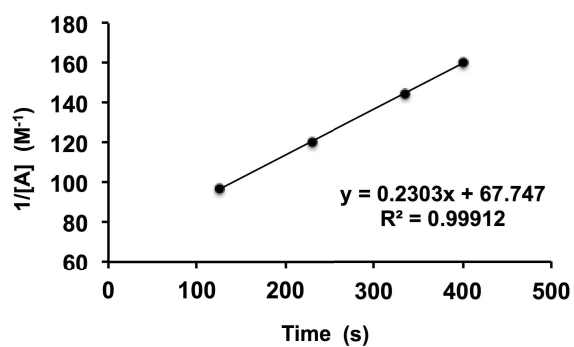
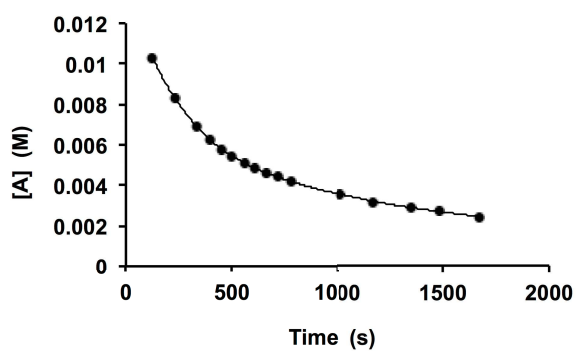
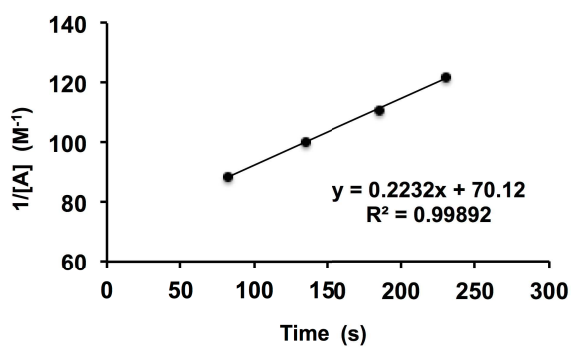
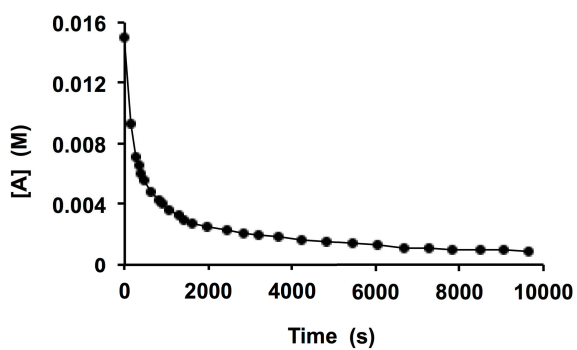


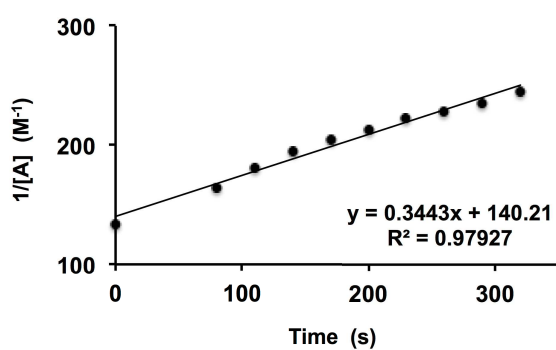
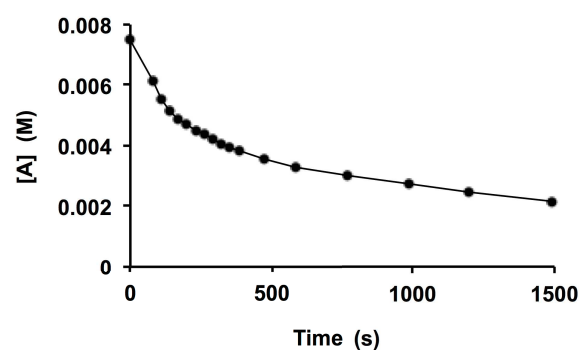
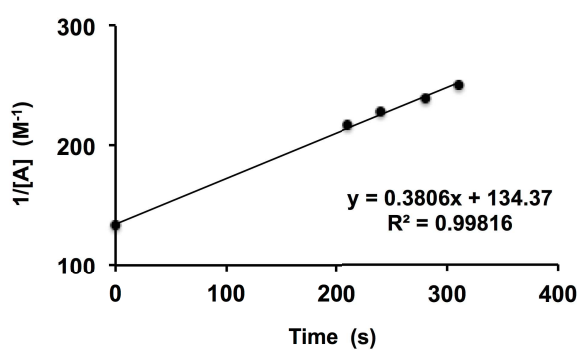
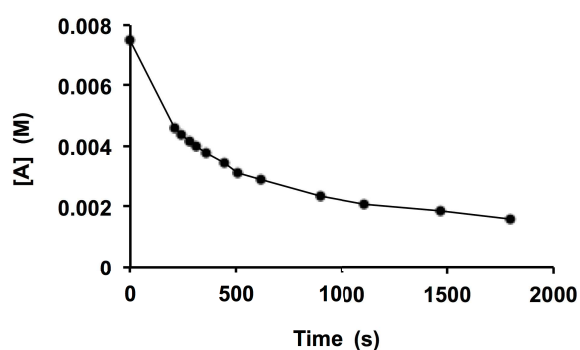
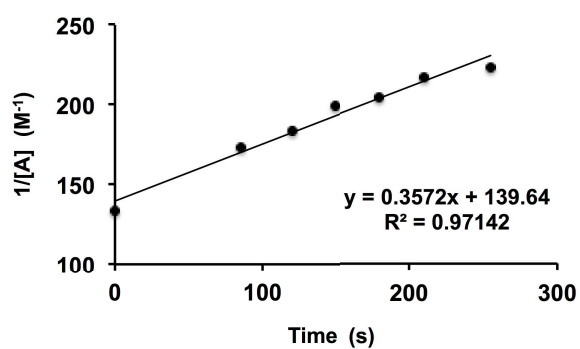
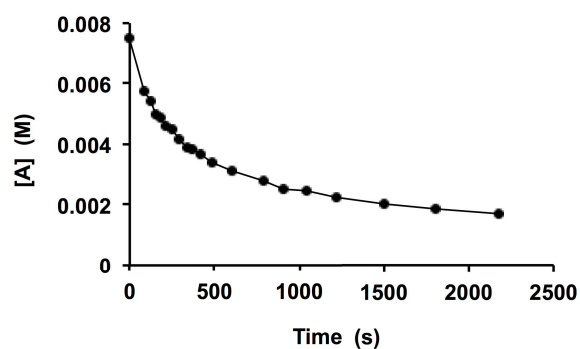
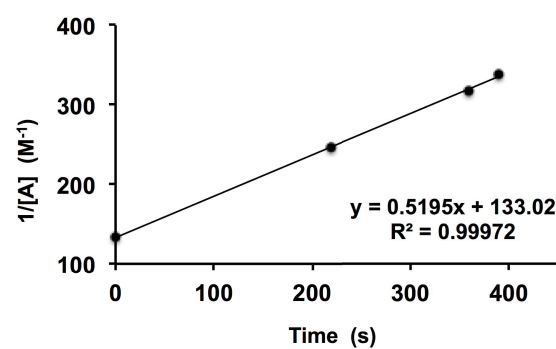
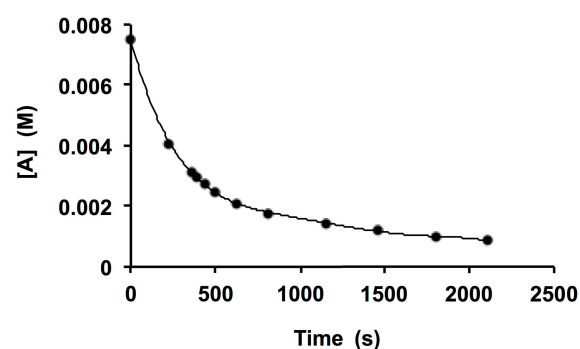
Kinetic Data of 119 (15 mM, pH 6.8, 30 °C)

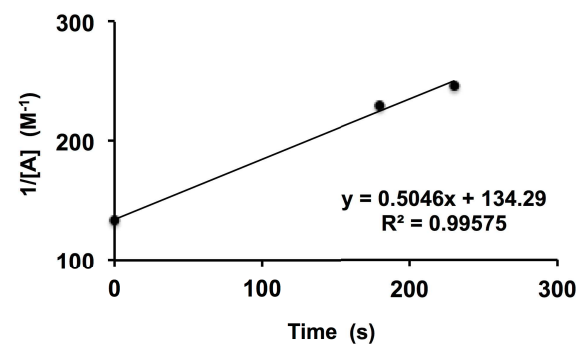
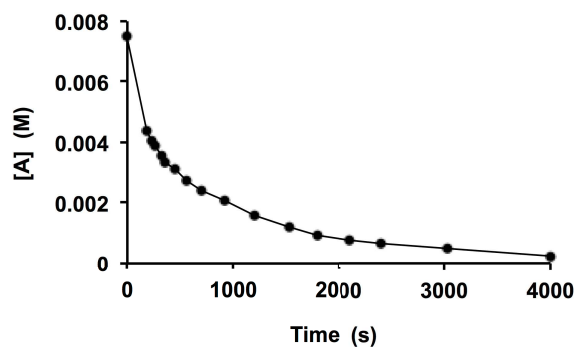
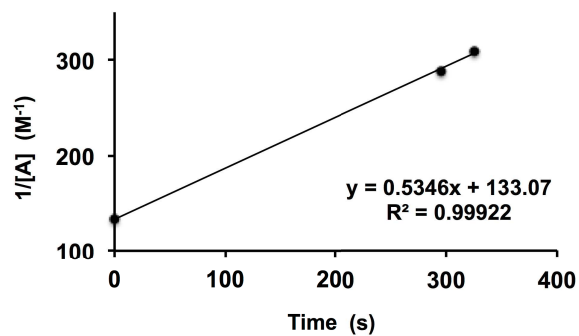
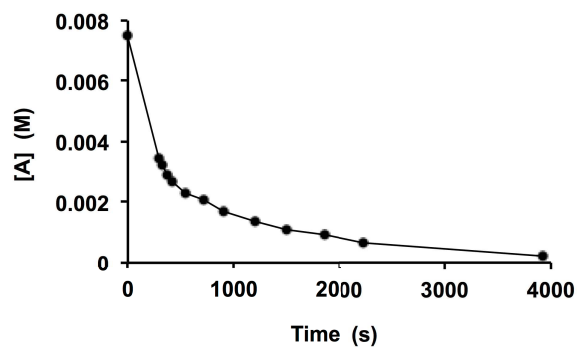
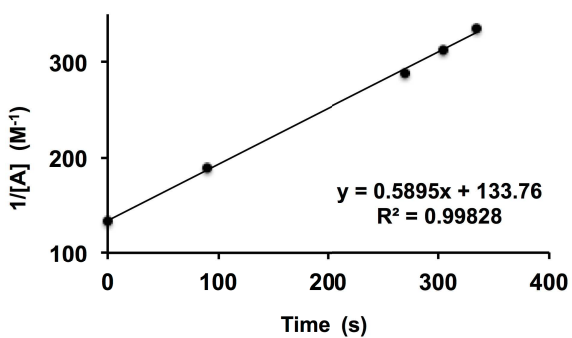
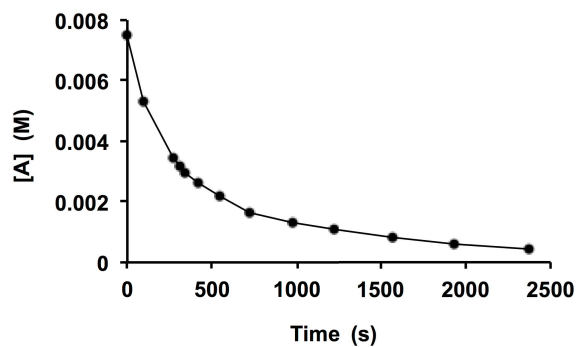
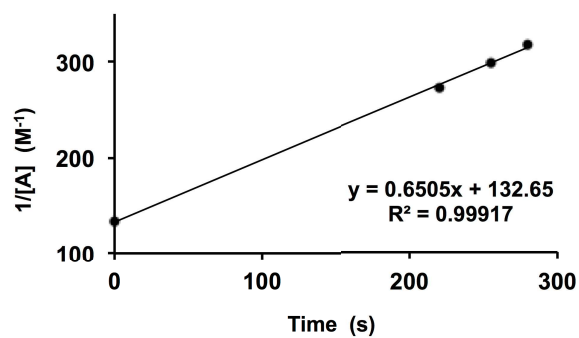
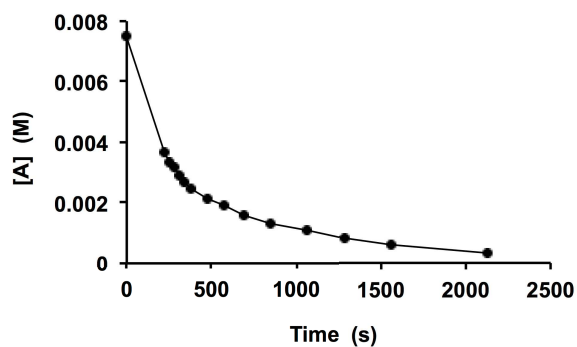


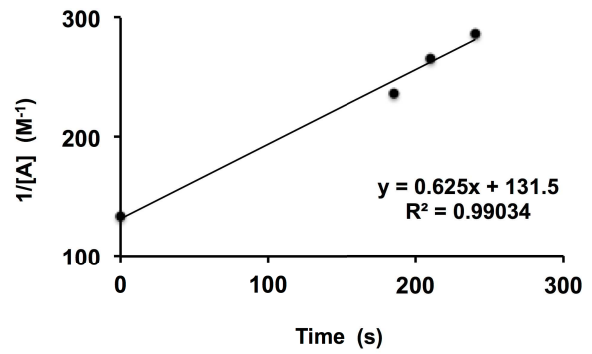
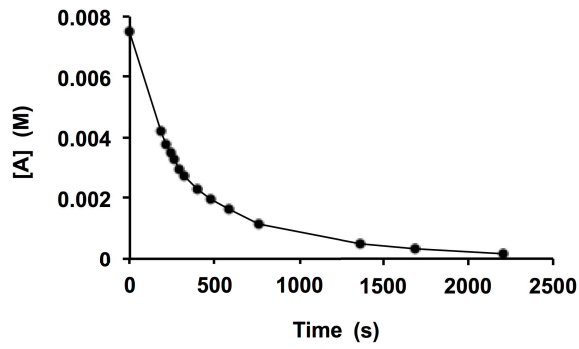
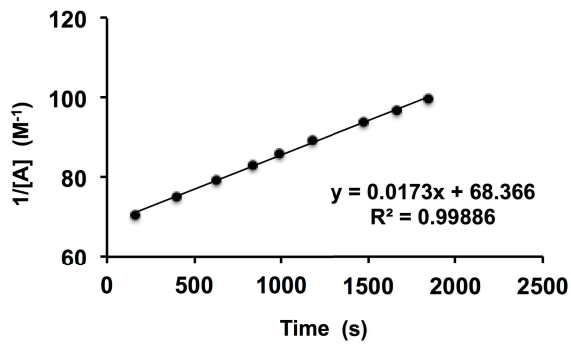
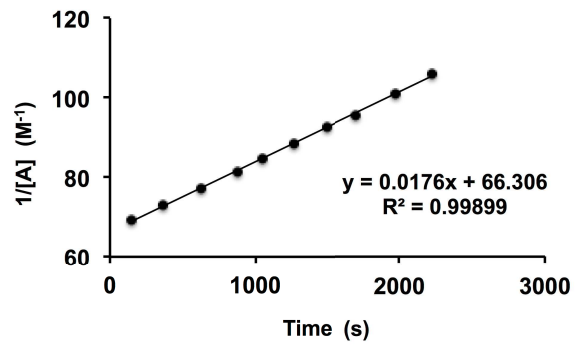
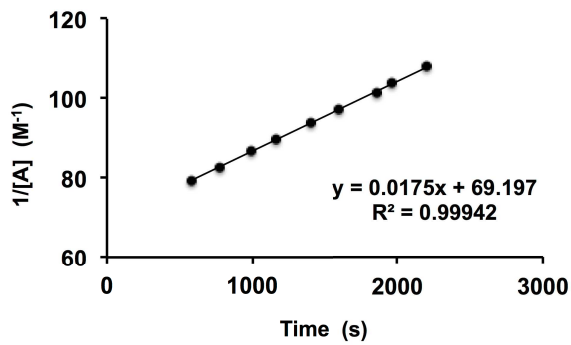
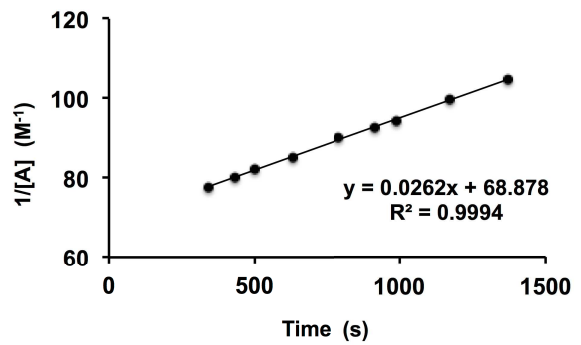
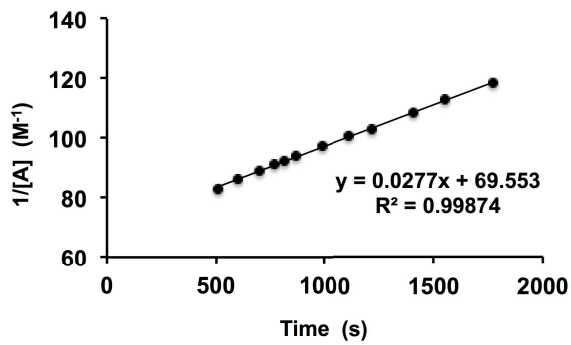


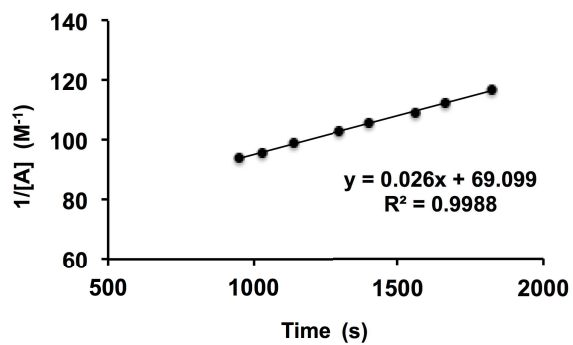
Kinetic Data of **119** (15 mM, pH 6.8, 40 °C)Kinetic Data of **119** (15 mM, pH 6.8, 60 °C)Kinetic Data of **119** (15 mM, pH 6.8, 70 °C)

Kinetic Data of **116** (15 mM, pH 5.1, 25 °C)

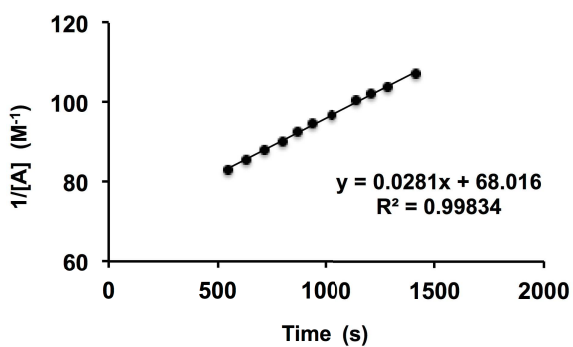
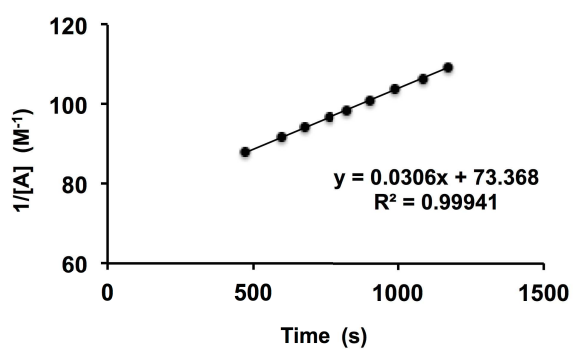
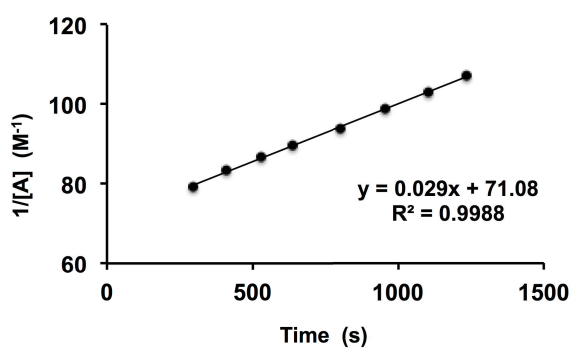
Kinetic Data of **116** (7.5 mM, pH 5.1, 30 °C)Kinetic Data of **116** (7.5 mM, pH 5.1, 40 °C)

Kinetic Data of **116** (7.5 mM, pH 5.1, 50 °C)

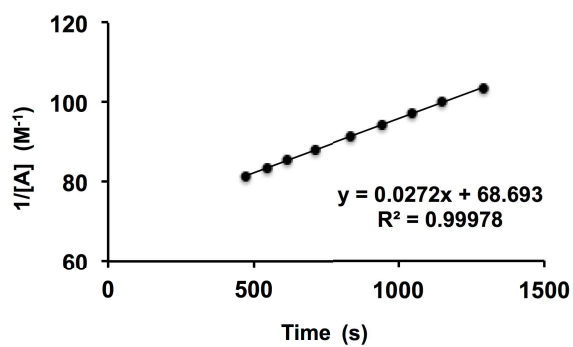
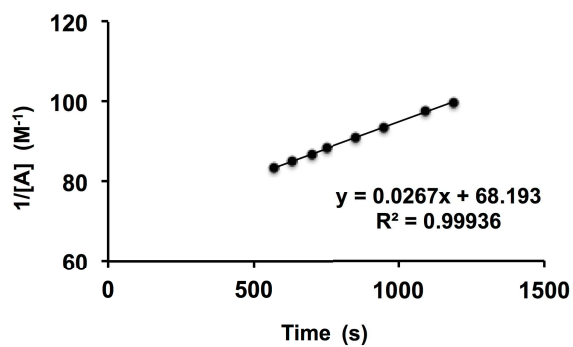
Kinetic Data of **119** (15 mM, pH 5.1, 25 °C)Kinetic Data of **119** (15 mM, pH 5.1, 40 °C)

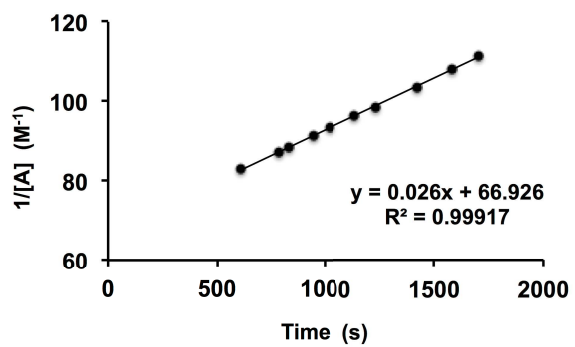


Kinetic Data of 119 (15 mM, pH 5.1, 60 °C)



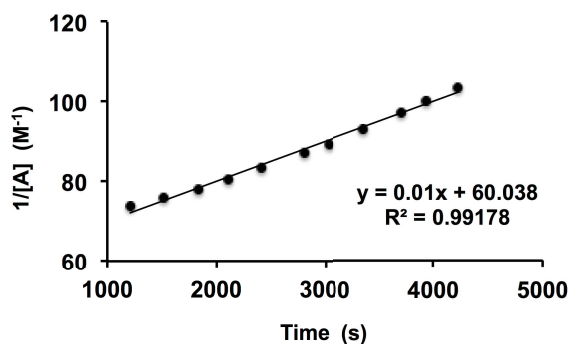
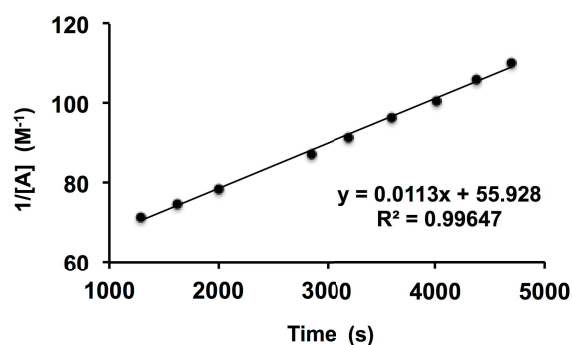
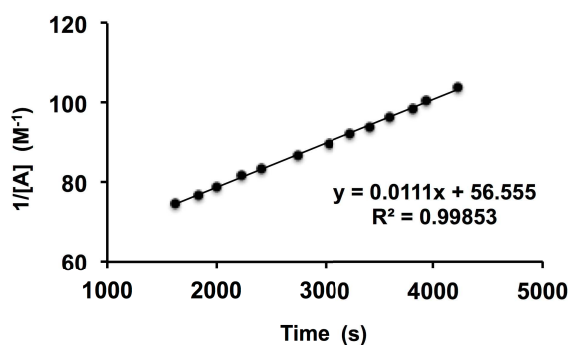
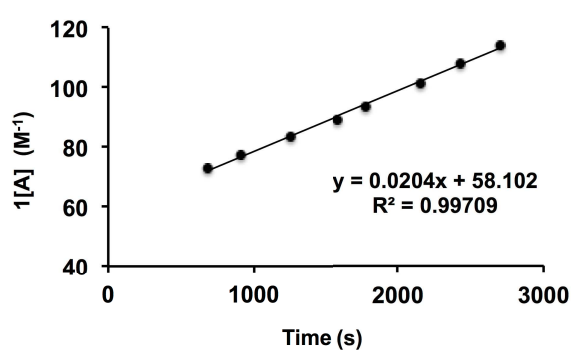
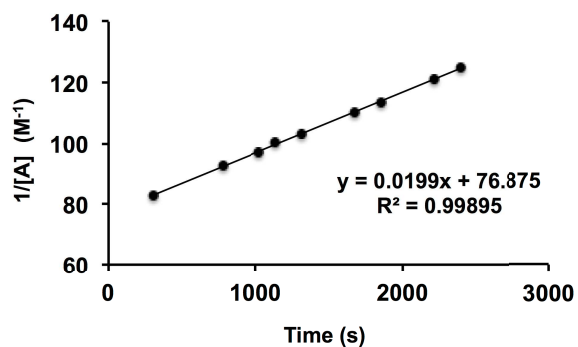
Kinetic Data of 119 (15 mM, pH 5.1, 70 °C)



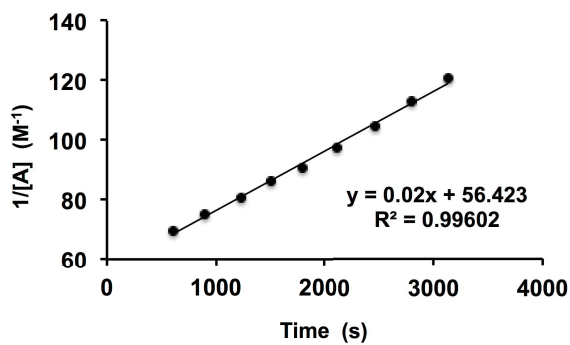


**Variable pH Kinetic Studies of the KAT Ligation by <sup>1</sup>H-NMR Spectroscopy (pH 4.4 – 7.4)**

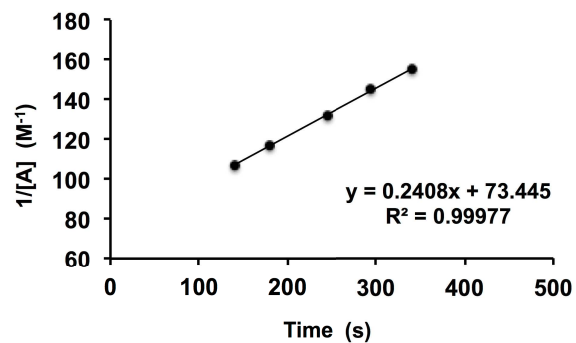
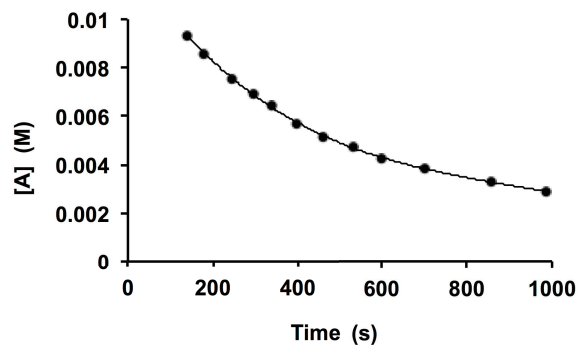
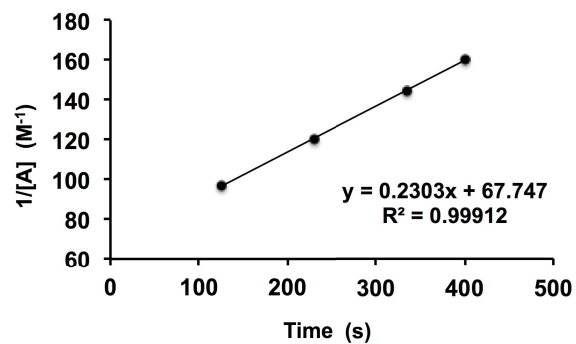
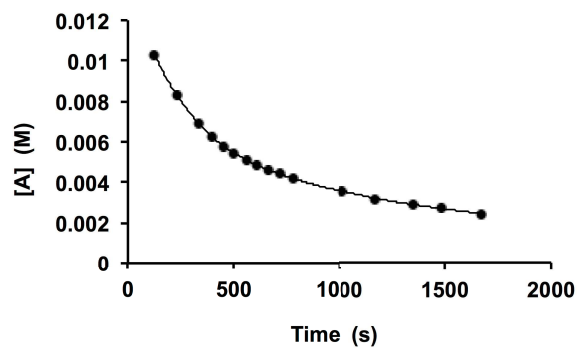
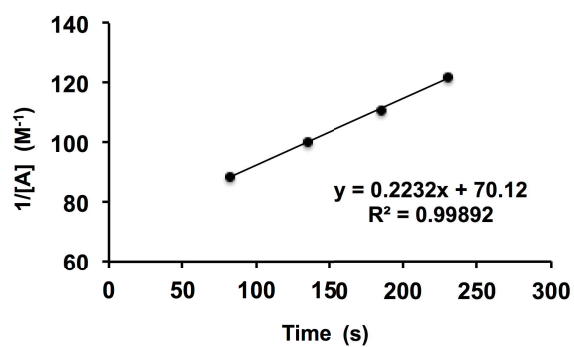
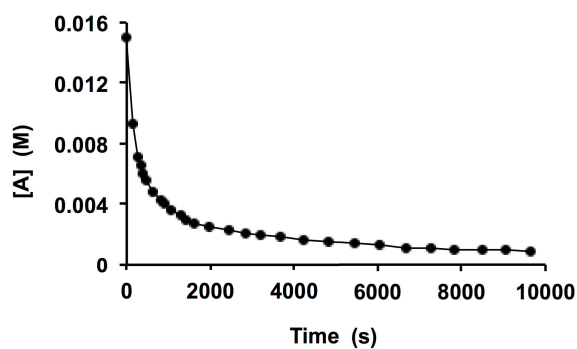
Unless otherwise stated, KAT ligation reaction between KAT and hydroxylamine **117** were carried out at equimolar concentration (15 mM) in MeCN-*d*<sub>3</sub> / 0.1 M deuterated potassium phosphate buffer (2:1) at room temperature (25 °C) and at variable pH (pH 4.4, 5.1, 6.8, 7.4) according to general procedure 6.

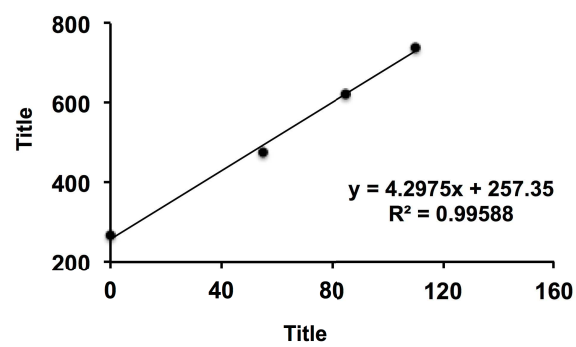
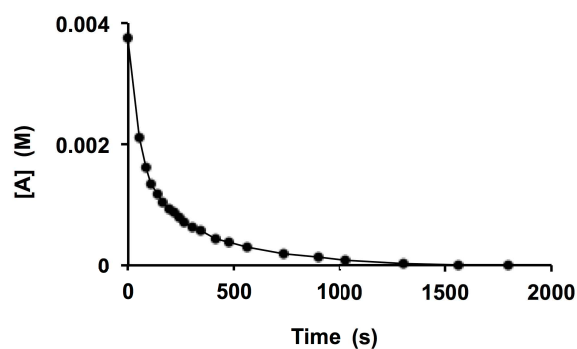
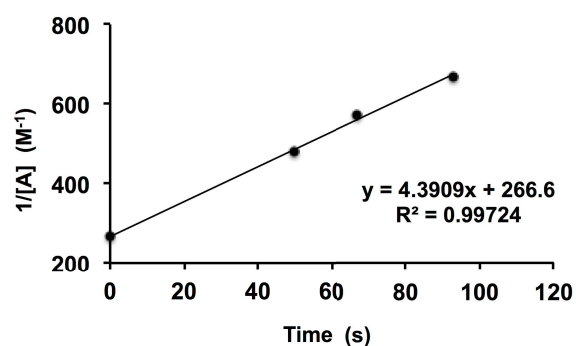
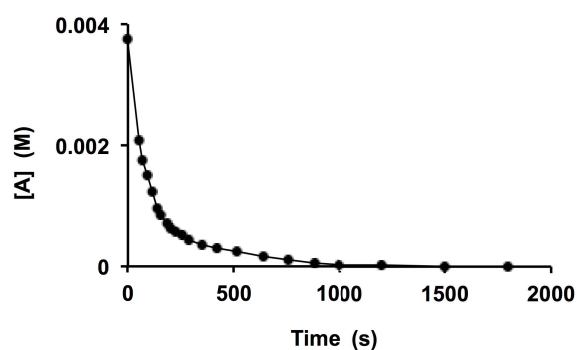
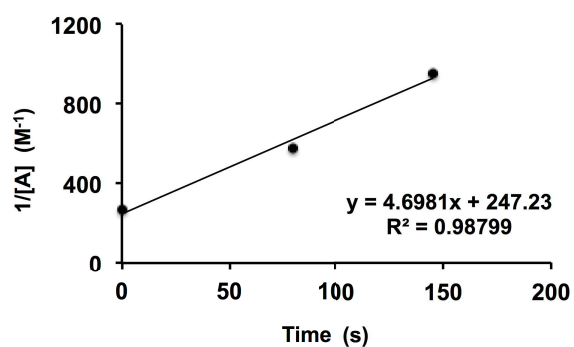
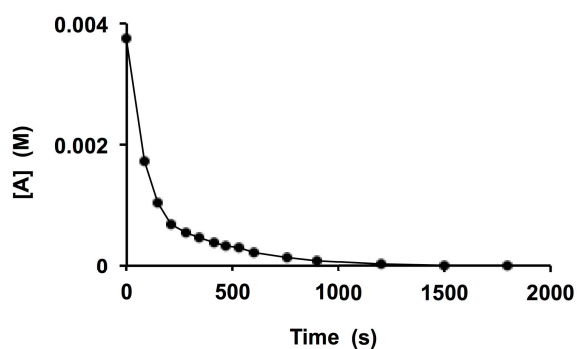
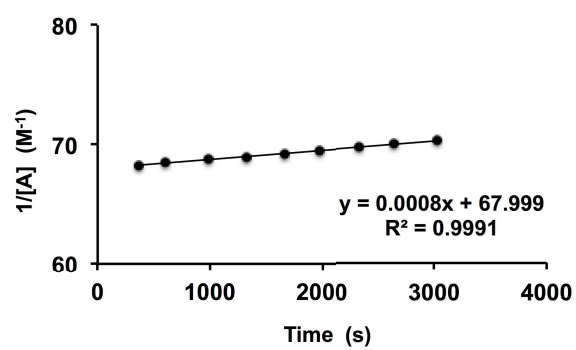
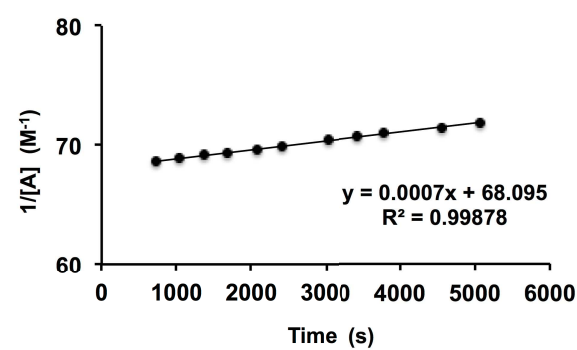
**Kinetic Data of **116** (15 mM, pH 7.4, 25 °C)****Kinetic Data of **116** (15 mM, pH 6.8, 25 °C)**

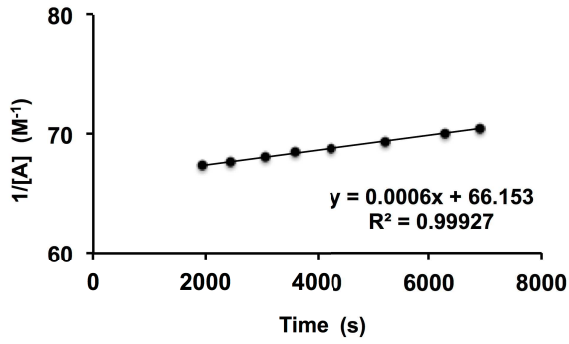




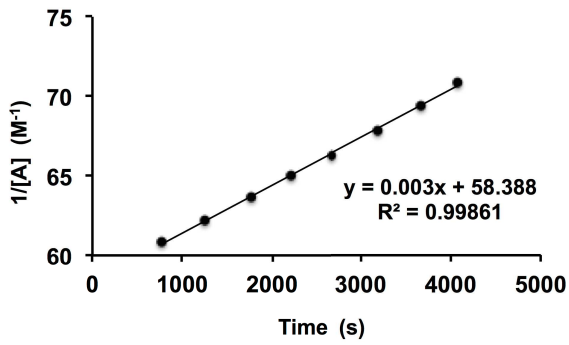
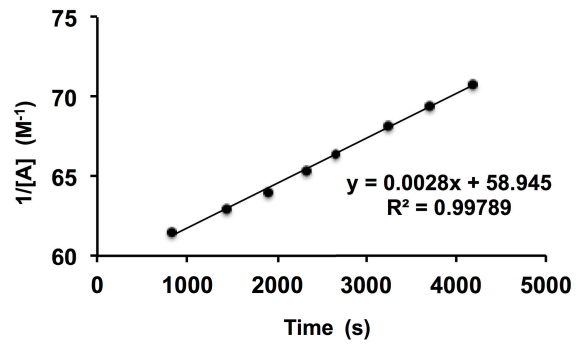
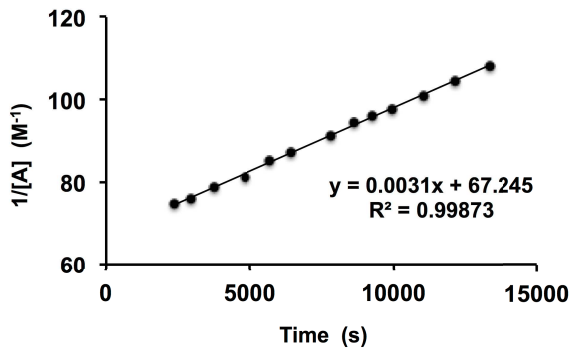
Kinetic Data of **116** (15 mM, pH 5.1, 25 °C)



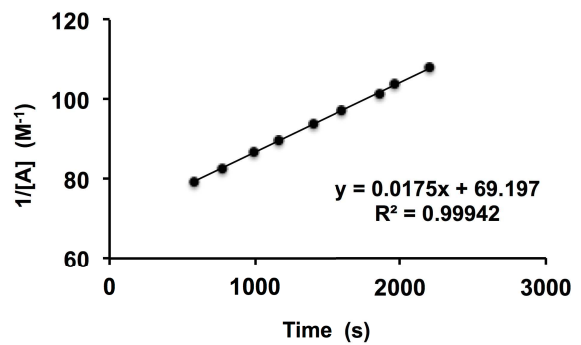
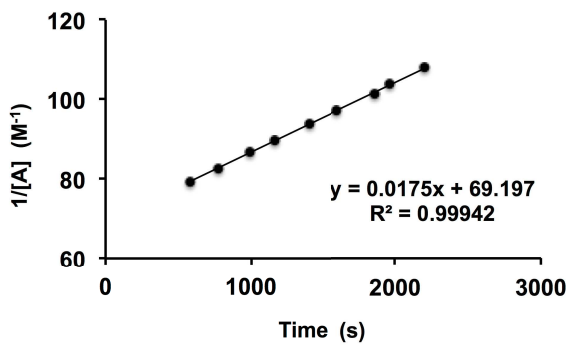
Kinetic Data of **116** (3.75 mM, pH 4.4, 25 °C)Kinetic Data of **119** (15 mM, pH 7.4, 25 °C)

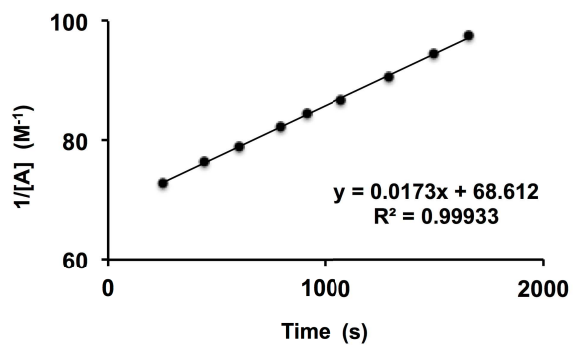


Kinetic Data of 119 (15 mM, pH 6.8, 25 °C)

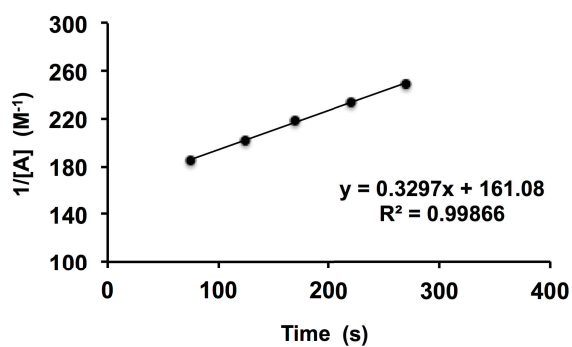
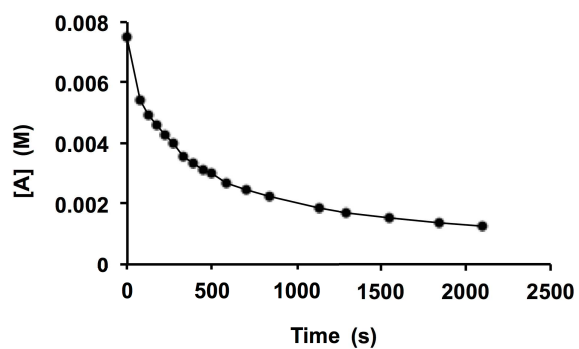
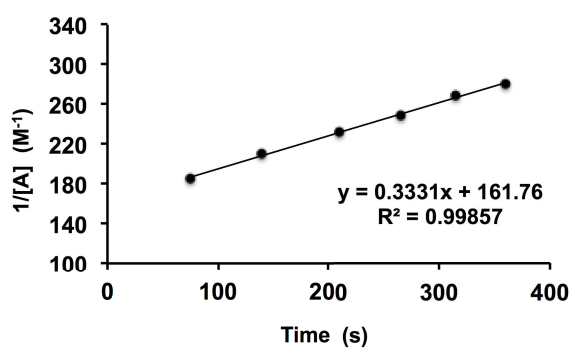
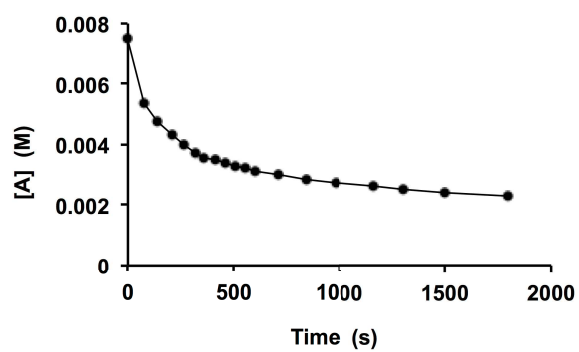
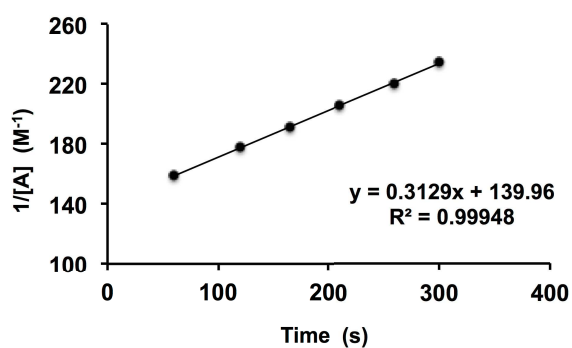
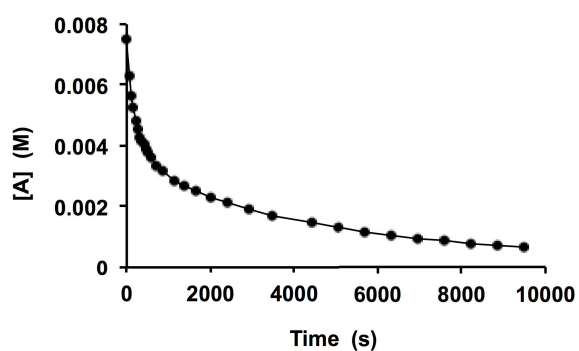


Kinetic Data of 119 (15 mM, pH 5.1, 25 °C)





Kinetic Data of **119** (7.5 mM, pH 4.4, 25 °C)

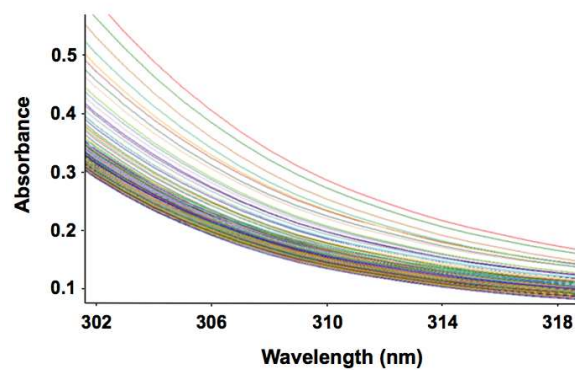
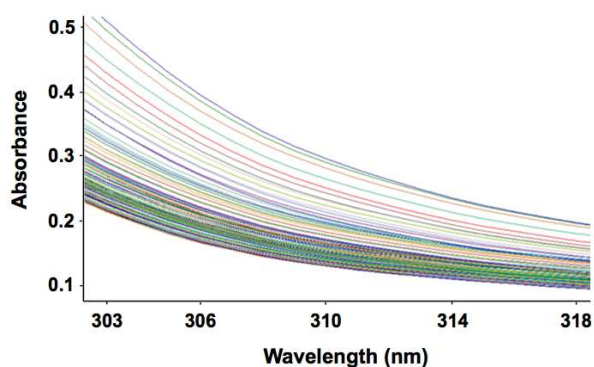
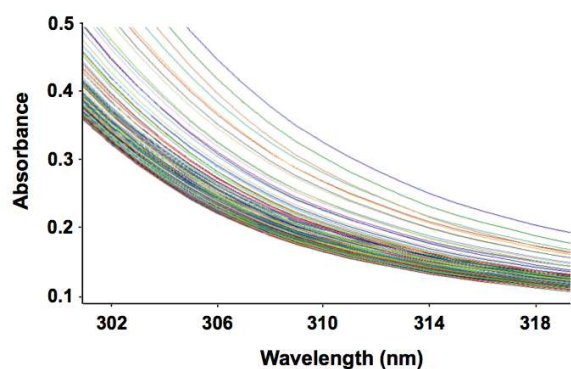


## Variable pH Kinetic Studies of the KAT Ligation by UV-Vis Spectrophotometry (pH 3.6 – 3.9)

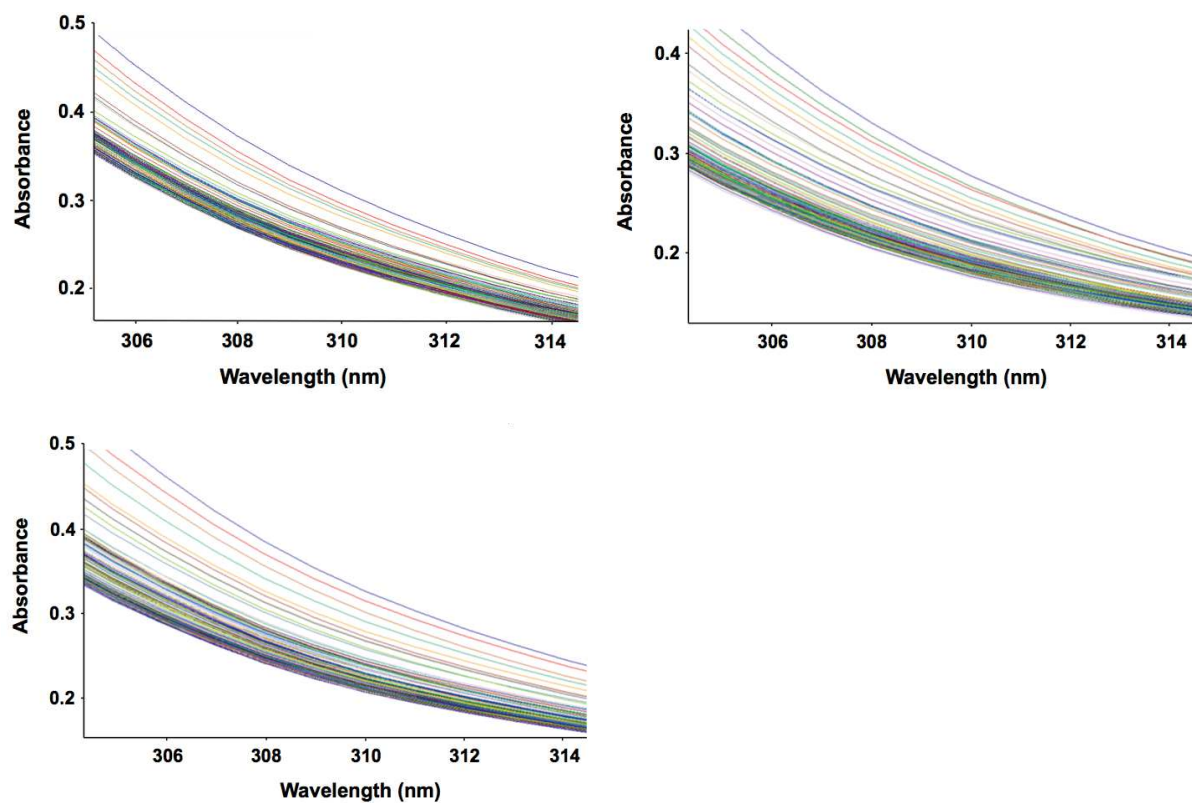
Unless otherwise stated, KAT ligation reactions between KAT and hydroxylamine **117** were carried out at equimolar concentration (3.75 mM) in MeCN / 0.2 M deuterated potassium acetate buffer (1:9) at room temperature and at variable pH (pH 3.6 or 3.9) according to general procedure 7.

### 1) Time-dependent UV-Vis Spectral Changes

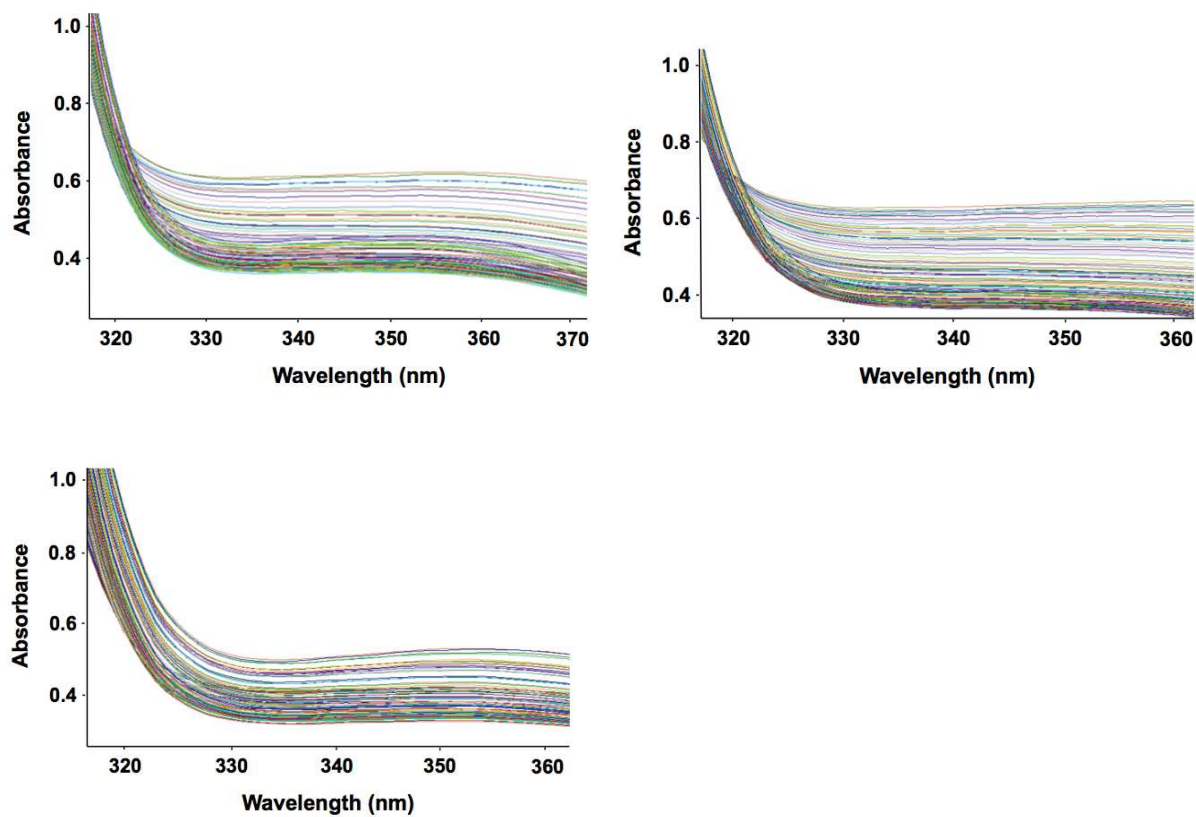
Kinetic Data of **116** (3.75 mM, pH 3.6, 25 °C) recorded at 310 nm



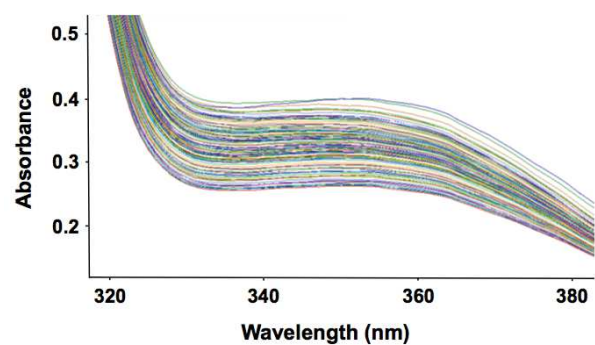
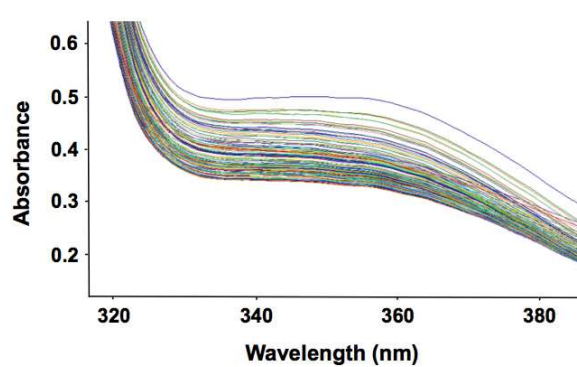
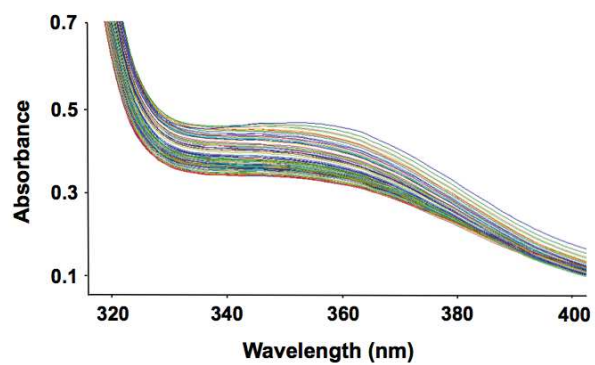
Kinetic Data of **116** (3.75 mM, pH 3.6, 25 °C) recorded at 310 nm



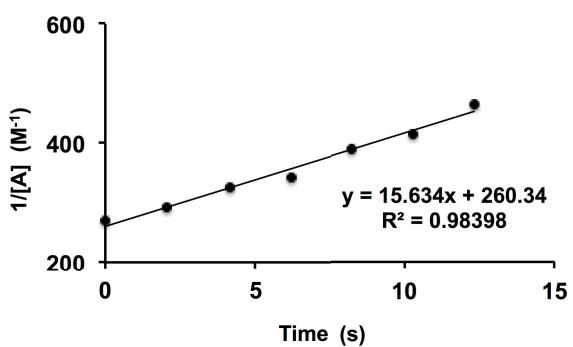
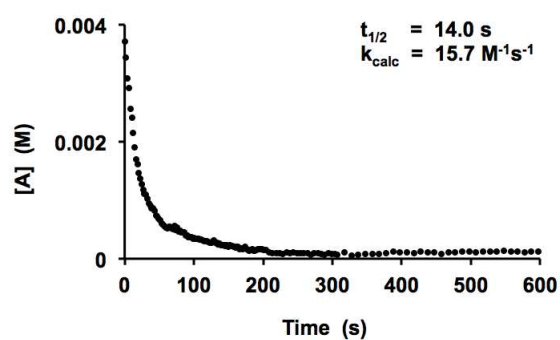
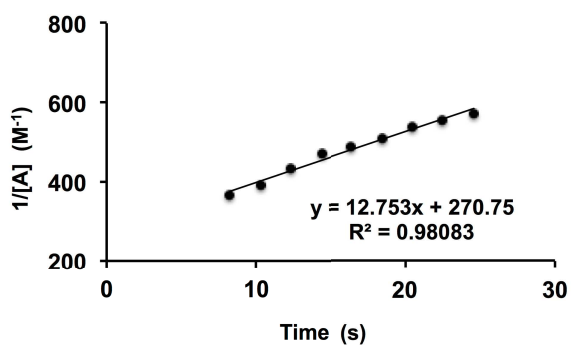
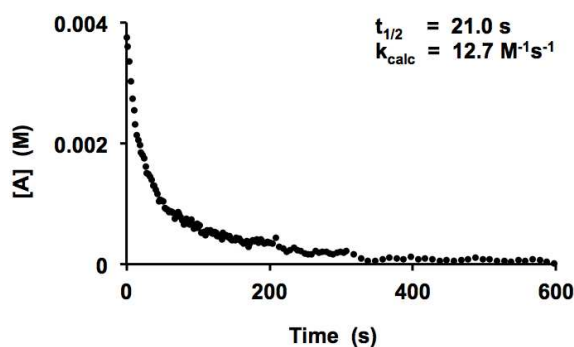
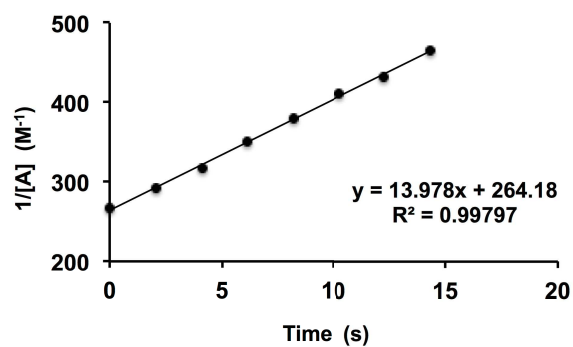
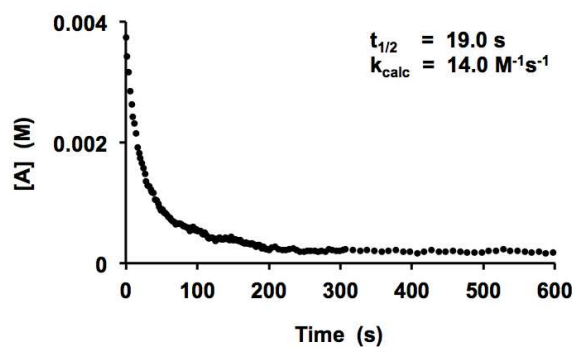
Kinetic Data of **119** (7.50 mM, pH 3.9, 25 °C) recorded at 355 nm



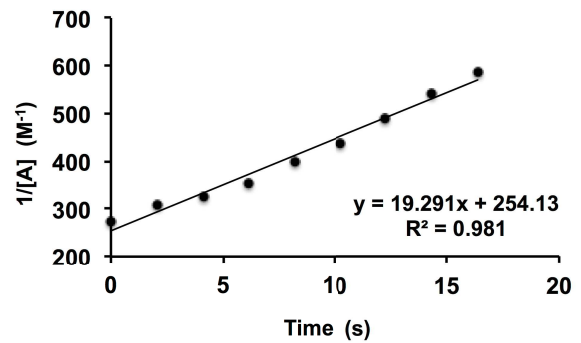
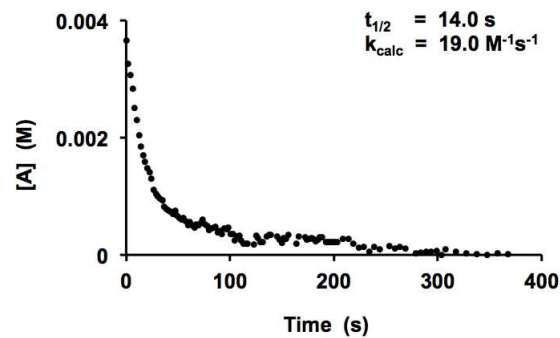
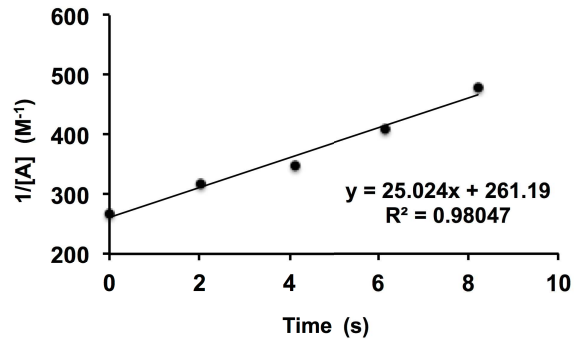
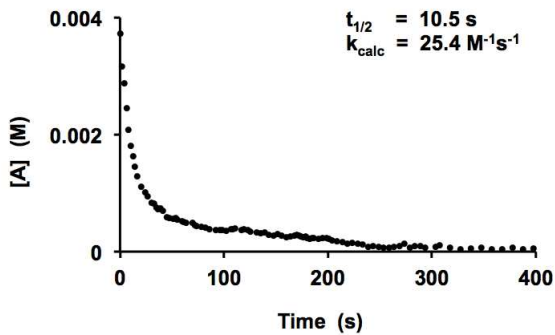
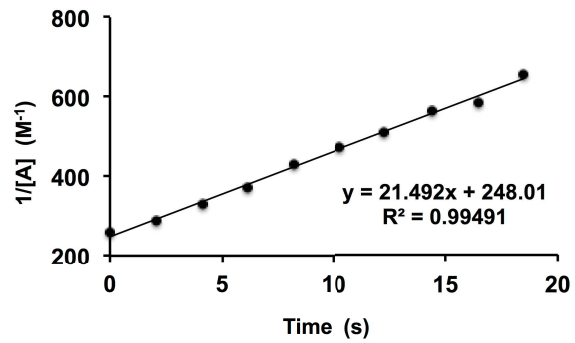
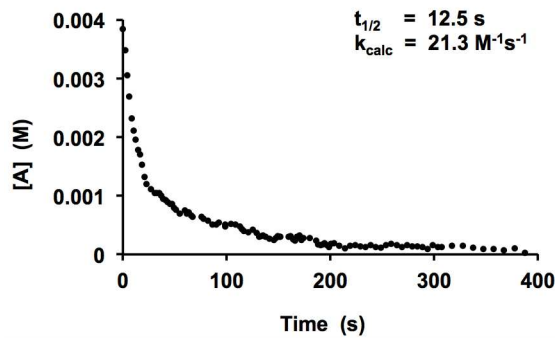
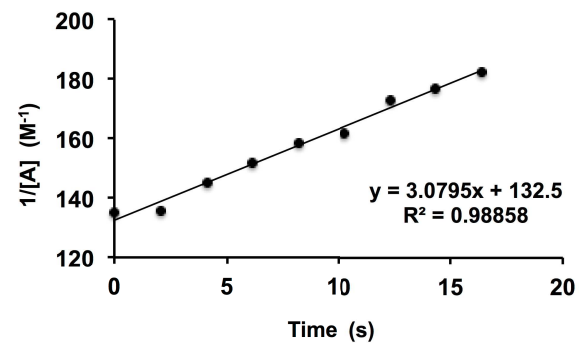
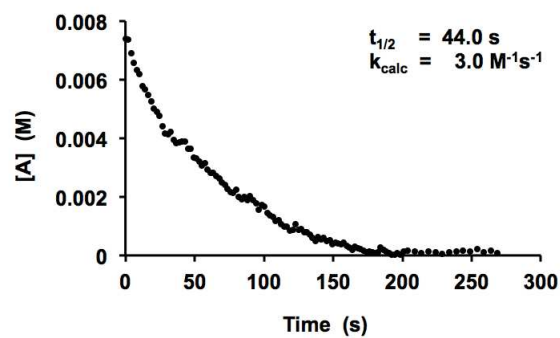
Kinetic Data of **119** (3.75 mM, pH 3.6, 25 °C) recorded at 355 nm

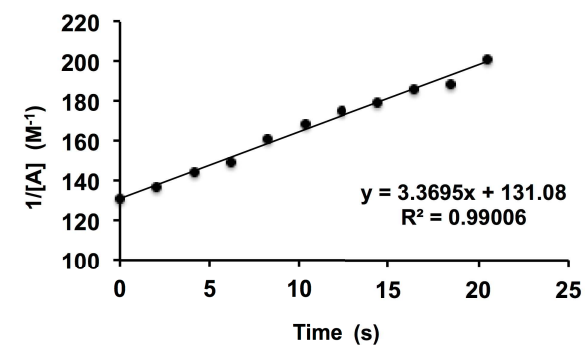
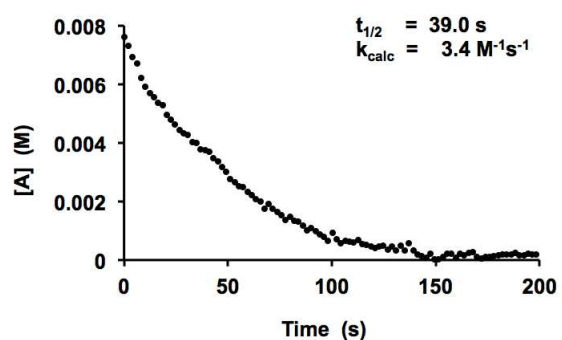
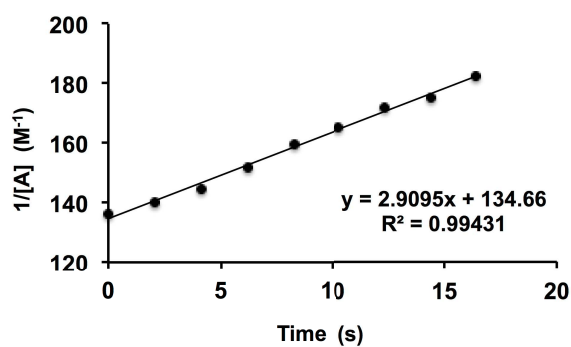
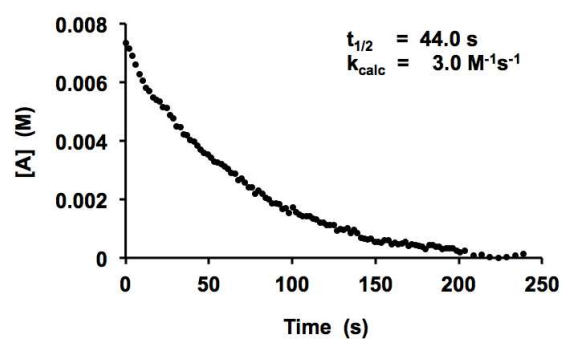


## 2) Kinetic Plots of Time-Dependent Absorbance Changes and Linear Fits

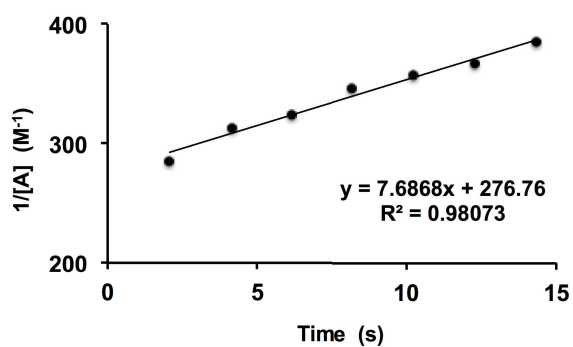
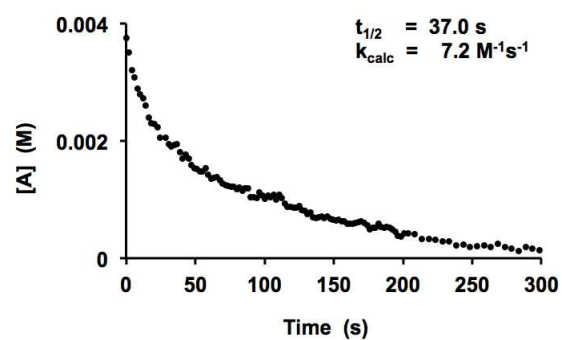
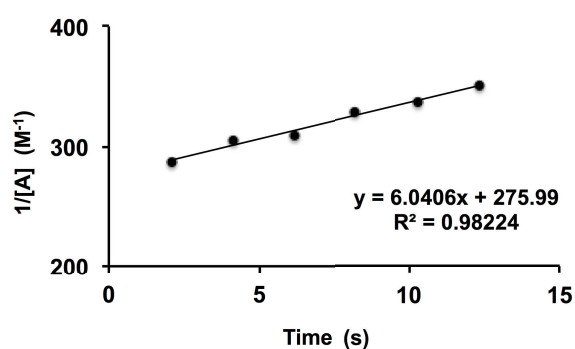
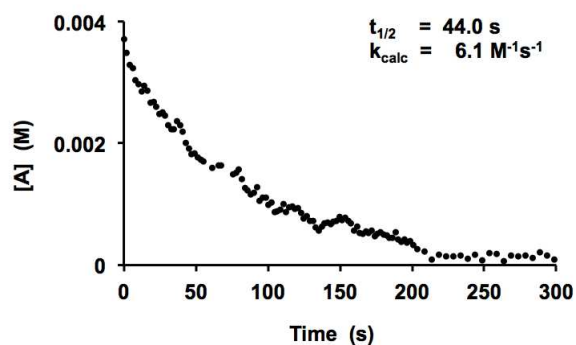
Kinetic Data of **116** (3.75 mM, pH 3.9, 25 °C) recorded at 310 nm

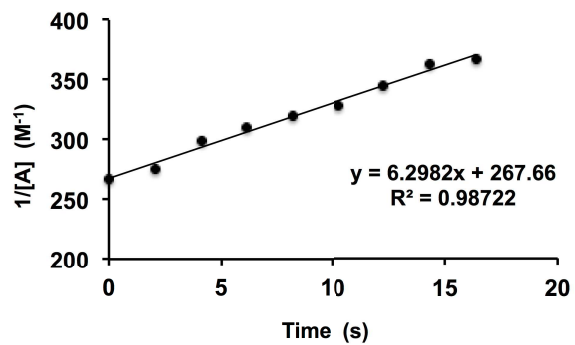
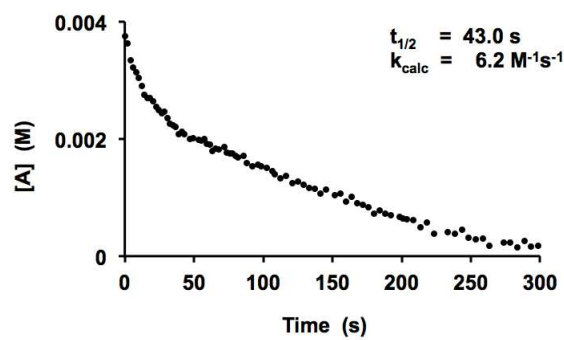


Kinetic Data of **116** (3.75 mM, pH 3.6, 25 °C) recorded at 310 nmKinetic Data of **119** (7.5 mM, pH 3.9, 25 °C) recorded at 355 nm



Kinetic Data of **119** (3.75 mM, pH 3.6, 25 °C) recorded at 355 nm

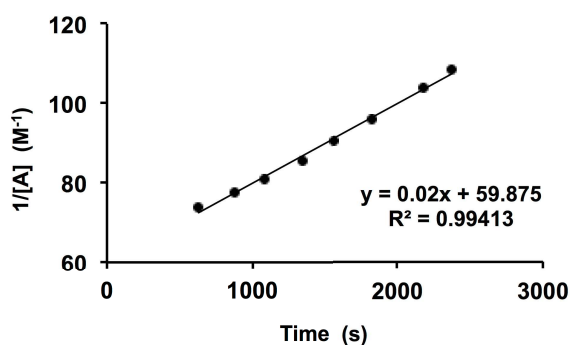




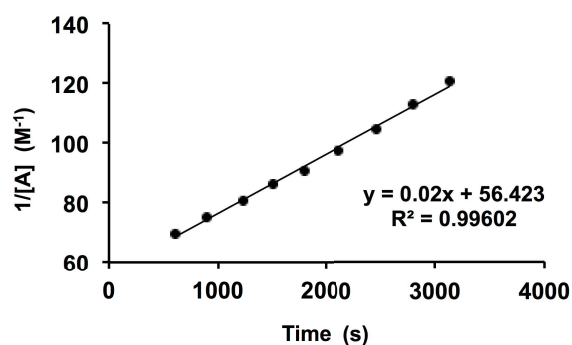
### Kinetic Measurements of the KAT Ligation at Variable Buffer Concentrations

To verify whether the KAT ligation proceeds via specific acid catalysis or general acid catalysis a series of kinetic experiments were conducted at constant pH but variable buffer concentrations. Unless otherwise stated, KAT ligation reactions between 2-pyridyl KAT **116** and hydroxylamine **117** were carried out at equimolar concentration (15 mM) and room temperature (25 °C) in a solvent mixture of MeCN- $d_3$  / deuterated potassium phosphate buffer (2:1, pH 6.8) at variable potassium phosphate buffer concentrations (0.05 – 0.3 M) according to general procedure 6.

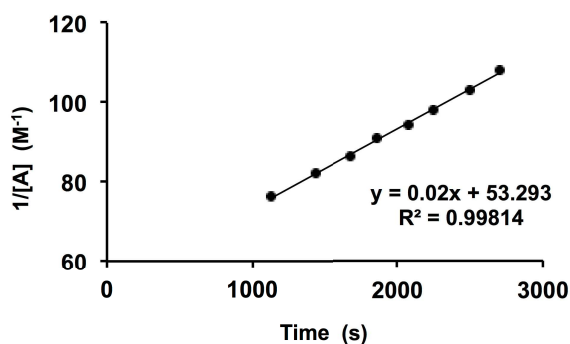
buffer concentration 0.05 M



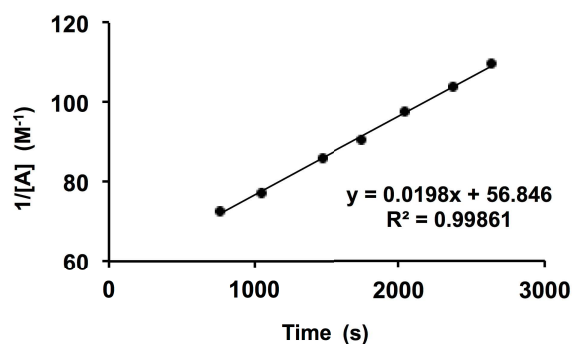
buffer concentration 0.1 M



buffer concentration 0.2 M



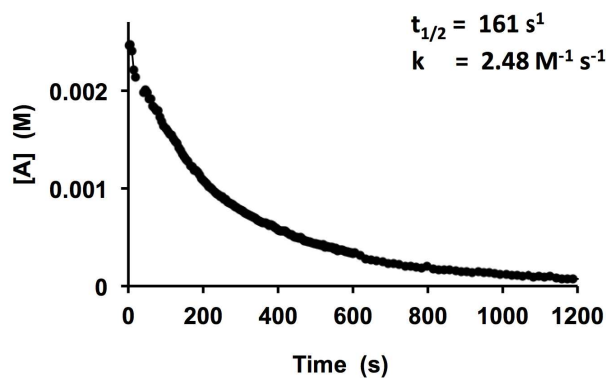
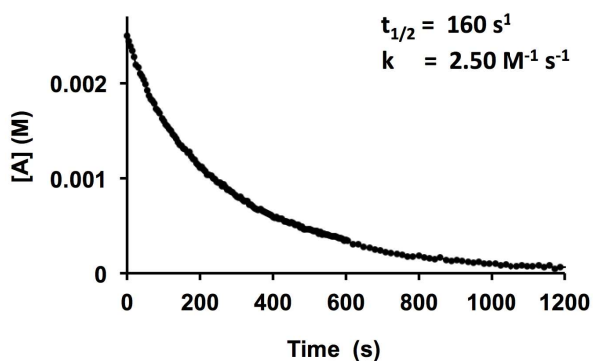
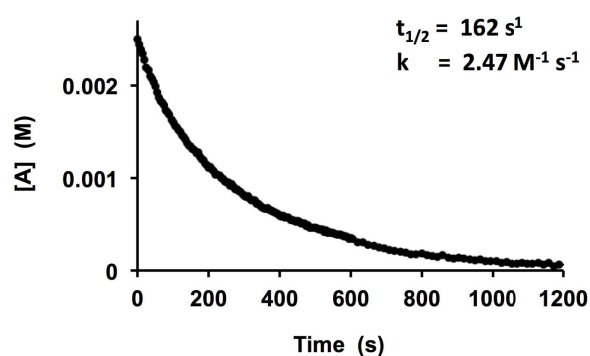
buffer concentration 0.3 M



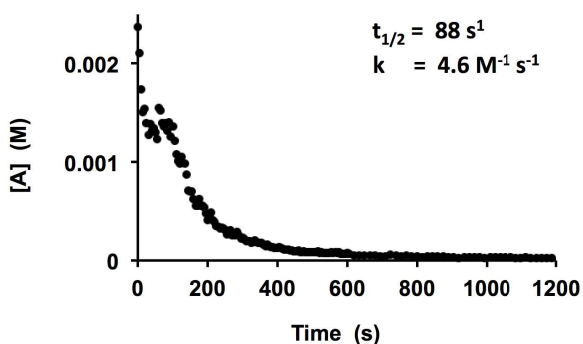
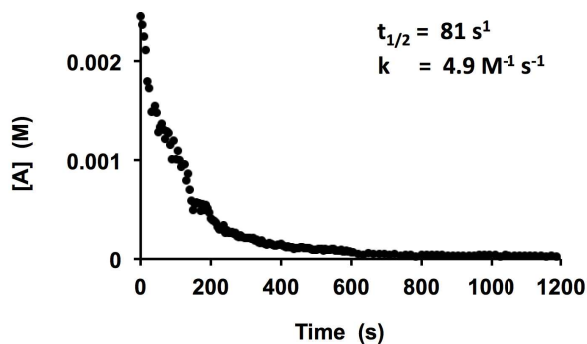
### Rate Constants of 8-Quinoline KATs by UV/Vis Spectrophotometry

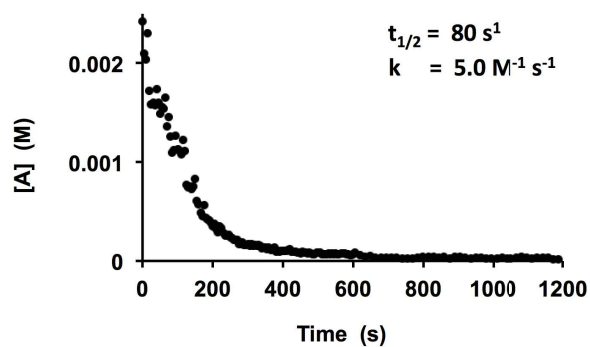
Unless otherwise stated, KAT ligation reactions between the respective 8-quinoline KAT and hydroxylamine **117** were carried out at equimolar concentration (2.5 mM) and room temperature (25 °C) in a solvent mixture of MeCN / 0.2 M potassium phosphate buffer (2:1, pH 6.8) according to general procedure 7.

Kinetic Data of **171** (2.5 mM, pH 6.8, 25 °C)

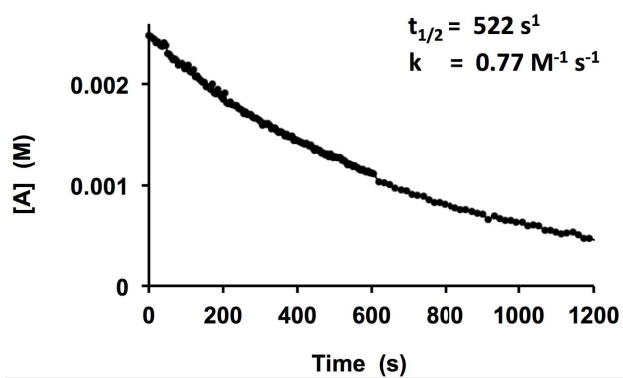
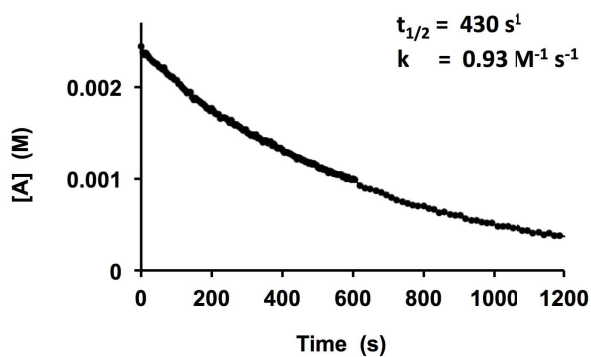
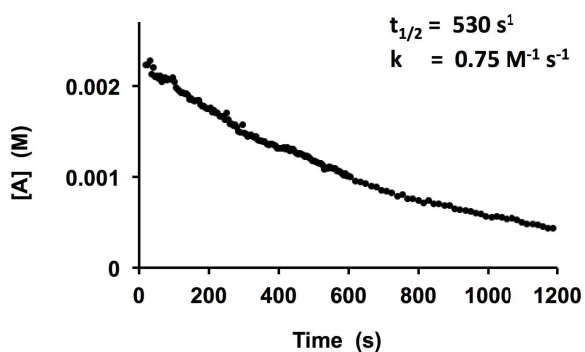


Kinetic Data of **174** (2.5 mM, pH 6.8, 25 °C)





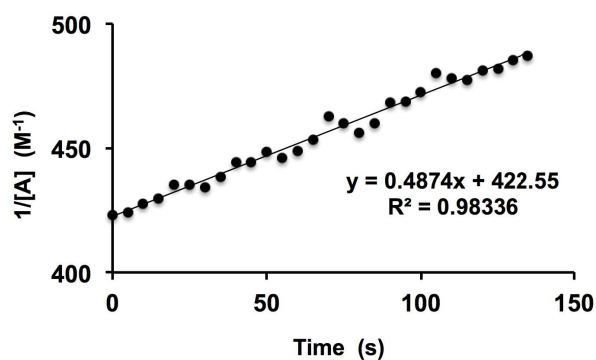
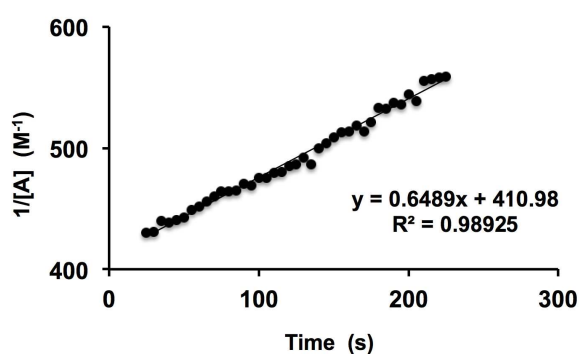
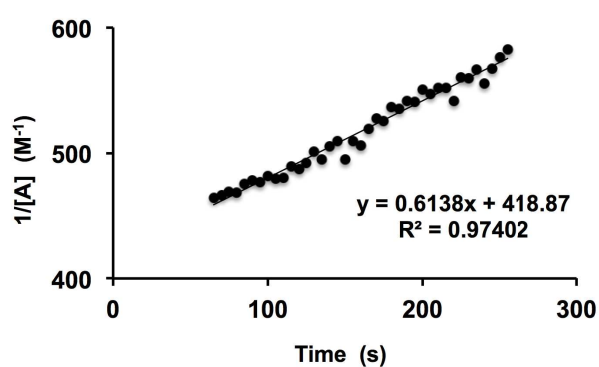
Kinetic Data of 175 (2.5 mM, pH 6.8, 25 °C)



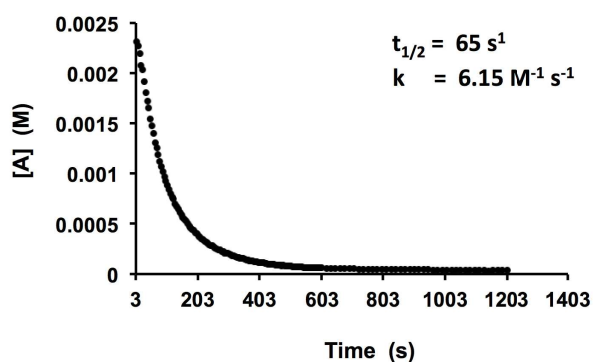
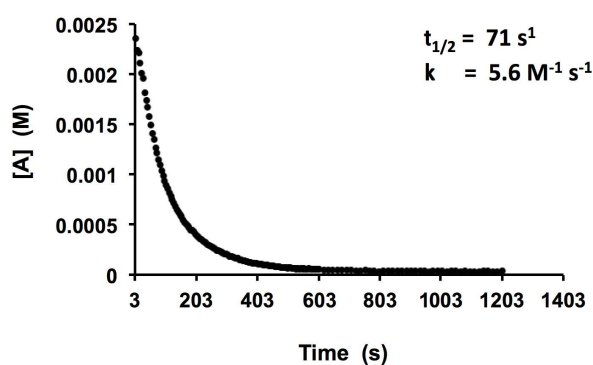
## Variable pH Kinetic Studies of the Quinoline KAT Ligation by UV-Vis Spectrophotometry

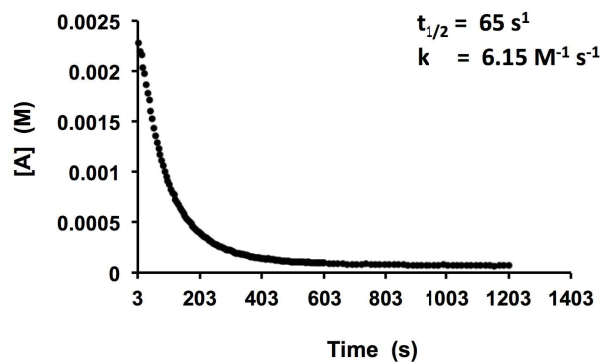
Unless otherwise stated, the KAT ligation reaction between 8-quinoline KAT **171** and hydroxylamine **117** were carried out at equimolar concentration (2.5 mM) and room temperature (25 °C) in a solvent mixture of MeCN / 0.2 M potassium buffer (2:1) at variable pH (pH 5.8 – 3.9) according to general procedure 7.

### Kinetic Data of **171** (2.5 mM, pH 7.4, 25 °C)

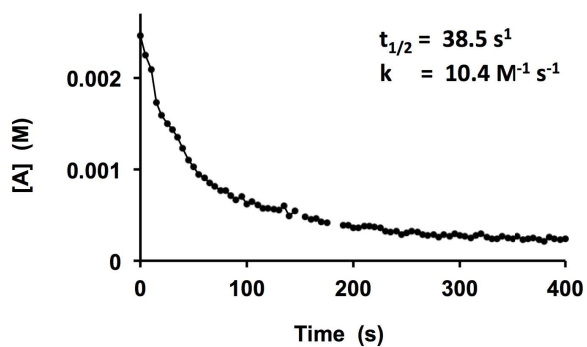
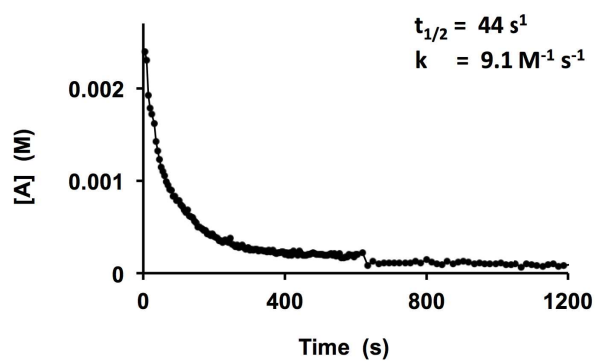
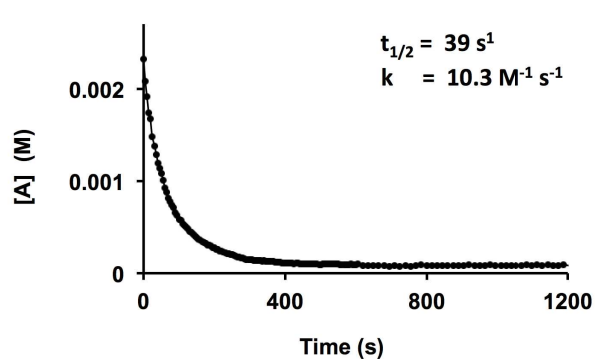


### Kinetic Data of **171** (2.5 mM, pH 5.8, 25 °C)

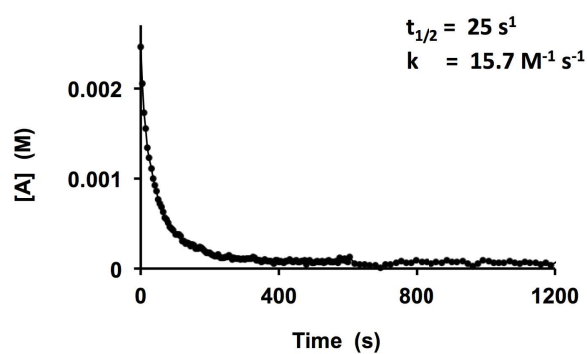
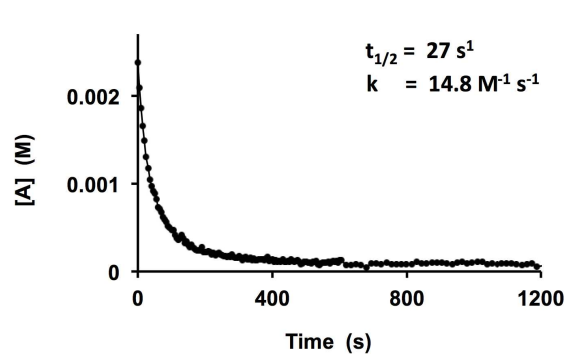




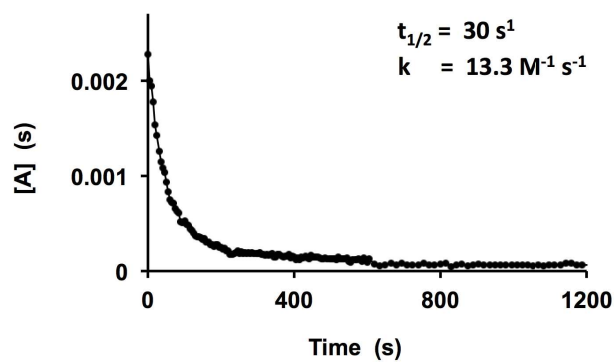
Kinetic Data of 171 (2.5 mM, pH 5.1, 25 °C)



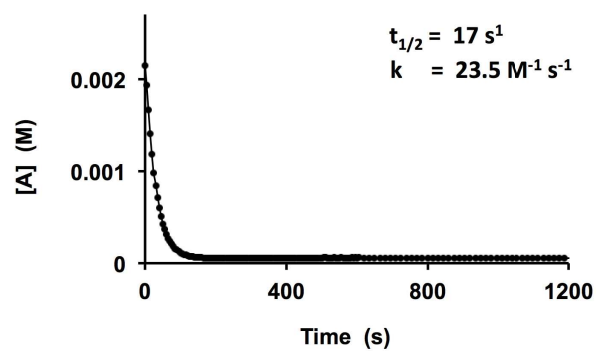
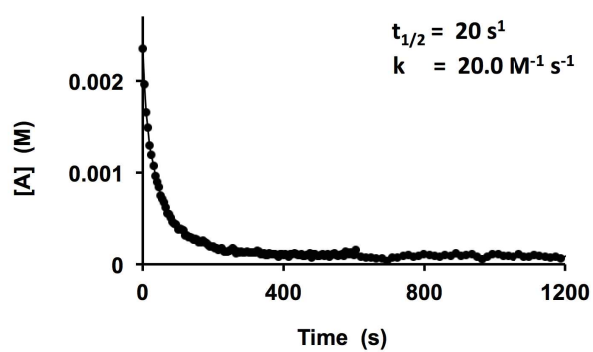
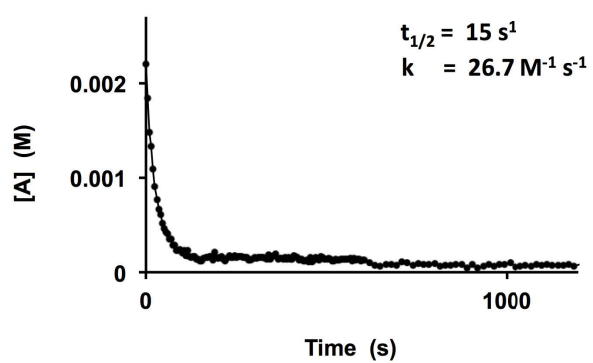
Kinetic Data of 171 (2.5 mM, pH 4.4, 25 °C)







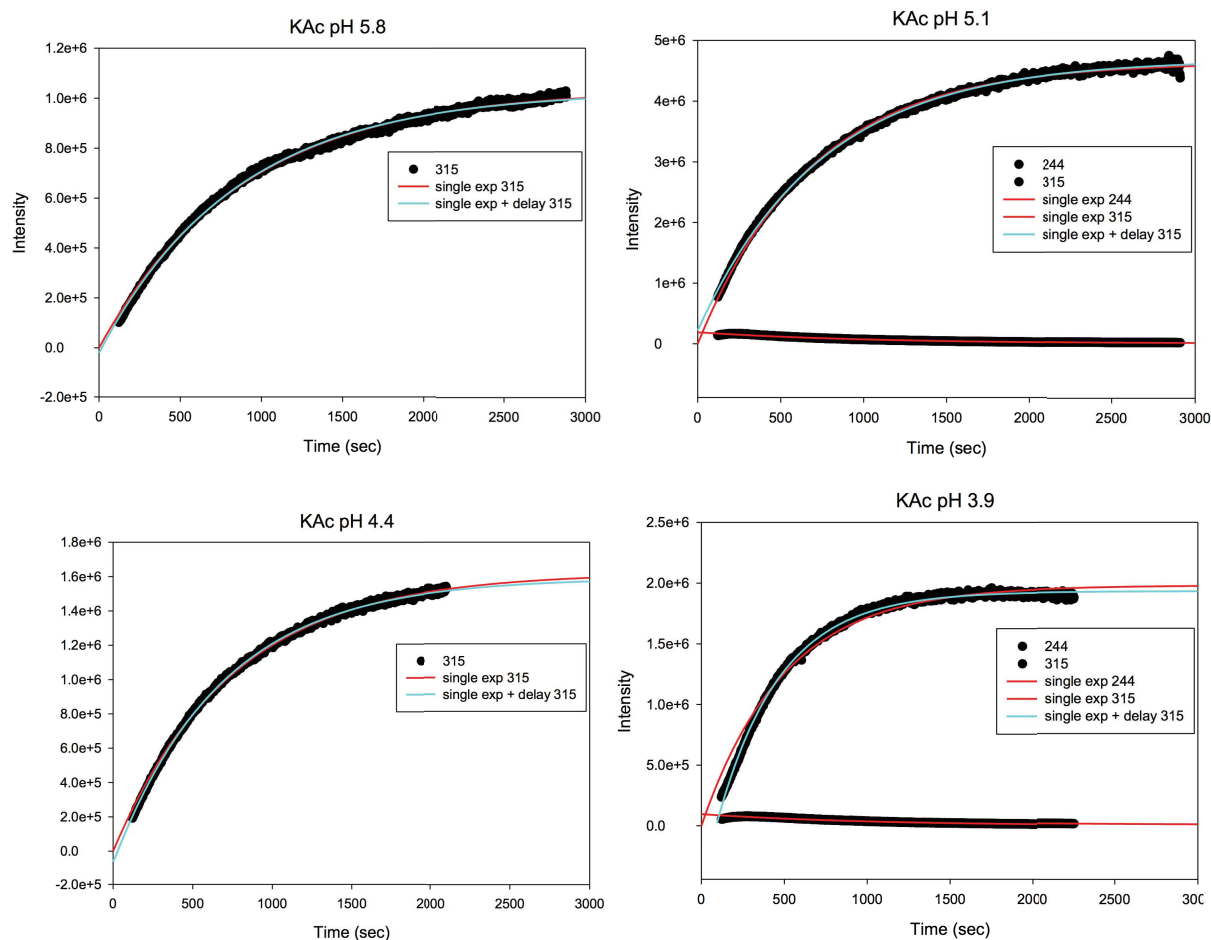
Kinetic Data of 171 (2.5 mM, pH 3.6, 25 °C)



## Variable pH Kinetic Studies of the Quinoline KAT Ligation by Mass Spectrometry

Unless otherwise stated, the KAT ligation reaction between 8-quinoline KAT **171** and hydroxylamine **117** were carried out at equimolar concentration (150  $\mu\text{M}$ ) and room temperature (25  $^{\circ}\text{C}$ ) in a solvent mixture of MeCN / 0.2 M potassium acetate buffer (2:1) at variable pH (pH 5.8 – 3.9). All mass spectra were obtained in positive mode on a SYNAPT G2S mass in Q-TOF mode (ion mobility disabled). The sample was constantly injected using a Chemyx Fusion 400 syringe pump at a flow rate of 200  $\mu\text{L}/\text{h}$ . Ions were generated using the commercially available normal ESI source. The capillary voltage was 1.5 kV and the cone temperature was set to 40  $^{\circ}\text{C}$ . The Trap CE voltage was set to 4 V. The instrument was calibrated with CsI from 50 to 1000  $m/z$  prior to the experiments. One spectrum per 1.1 seconds was recorded.

Product formation was monitored by following the mass peak at  $m/z=315$ , corresponding to the product plus a potassium ion [**169** + K] $^{+}$ . The peak was integrated and fitted with a standard “exponential rise to maximum” function  $fx = y_0 + a (1-\exp(-bx))$ . For better comparison the data was normalized to the value of the plateau obtained from the fit (the “ $a$ ” parameter).



## Mass Analysis of the KAT Ligation of **116** and **117**

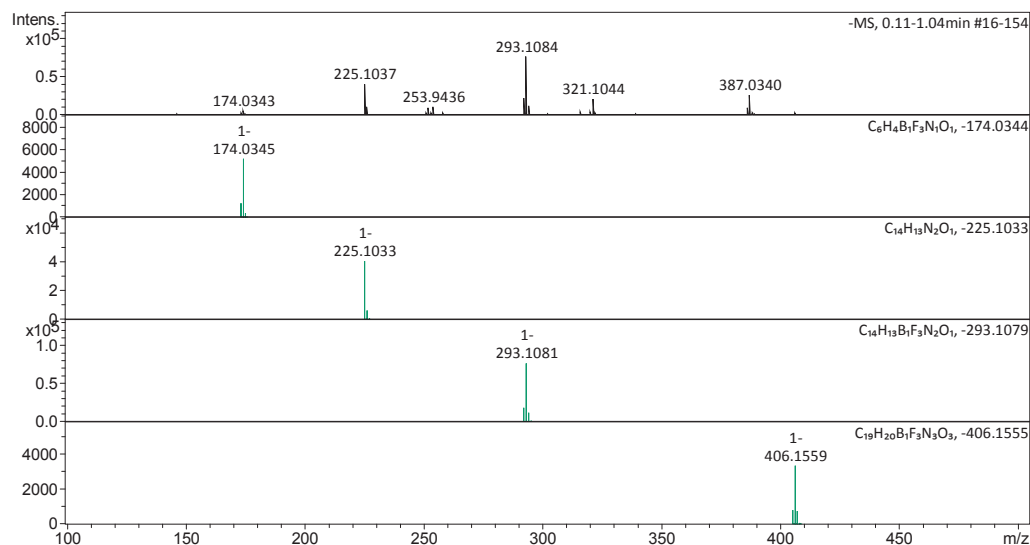
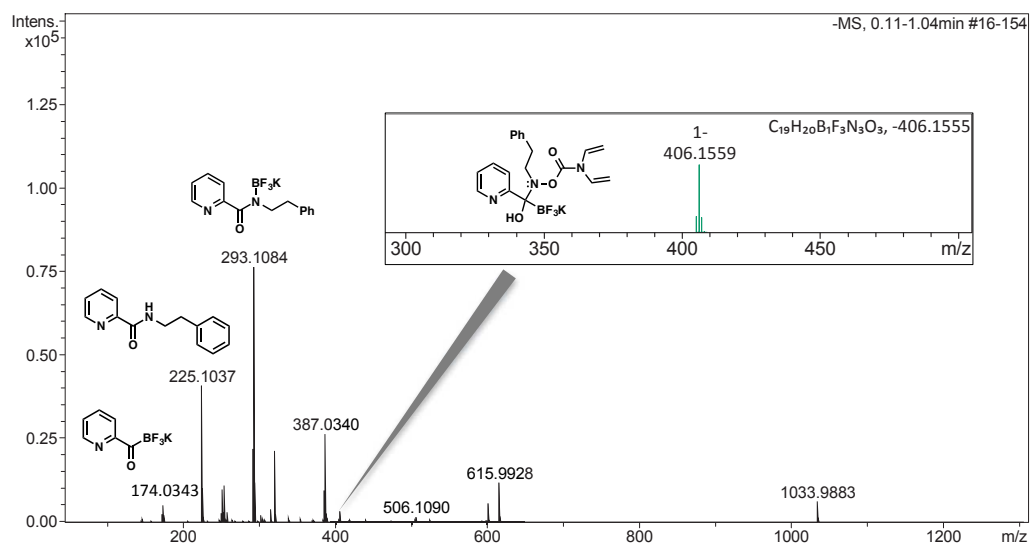
A series of amide-bond forming ligation experiments between **116** (1.92 mg, 0.009 mmol, 1.00 equiv) and **117** (2.23 mg, 0.0095 mmol, 1.05 equiv) in MeCN/H<sub>2</sub>O (2:1, 15 mM) were performed at 25 °C and monitored by high-resolution mass spectrometry (ESI negative). Reaction intermediates were identified by high-resolution tandem mass spectrometry (MS/MS).

HI-RES Mass Analysis  
ESI negative

Calibrant: ESI Tunemix  
Injection Volume: 20 µL

### Acquisition Parameter

Method:	ETH_HyStar_HPLC_QTOF_Neg_LowMass_Loop-AS.m	Acquisition Date:	01.11.2016 10:07:44
File Name:	D:\Data\max299xx\MAX29996.d	Operator:	Louis Bertschi
Source Type	ESI	Ion Polarity	Negative
Focus	Active	Set Capillary	4500 V
Scan Begin	50 m/z	Set End Plate Offset	-500 V
Scan End	1300 m/z	Set Collision Cell RF	430.0 Vpp
		Set Nebulizer	1.6 Bar
		Set Dry Heater	200 °C
		Set Dry Gas	8.0 l/min
		Set Divert Valve	Source



## Evaluation Spectra / Validation Formula:

#	Ion Formula	Adduct	m/z	z	Meas. m/z	mSigma	N-Rule	err [mDa]	err [ppm]
1	C6H4BF3NO	M	174.0345	1-	174.0343	207.4	ok	-0.2	-1.0
1	C14H13N2O	M-H	225.1033	1-	225.1037	49.5	ok	-0.3	-1.5
1	C14H13BF3N2O	M-H	293.1081	1-	293.1084	24.1	ok	0.3	1.0
1	C19H20BF3N3O3	M	406.1559	1-	406.1558	36.0	ok	0.1	0.2

## Calibration Info:

Date: 01.11.2016 10:43:11  
Polarity: Negative  
Calibration spectrum: -MS, 0.11-1.04min #16-154: Scan  
Reference mass list: ESI: Tunemix (neg) ESI-TOF  
Calibration mode: Quadratic

Reference m/z	Resulting m/z	Intensity	Error [ppm]
112.9856	112.9855	32	-0.627
301.9981	301.9985	2241	1.086
431.9823			
556.0019			
601.9790	601.9785	5665	-0.724
615.9946			
1033.9881	1033.9883	6210	0.173
1333.9689			
1633.9498			
1933.9306			
2233.9115			
2533.8923			
2833.8731			

Standard deviation: 1.582

## Mass List:

#	m/z	Res.	S/N	I %	FWHM
1	146.0396	31444	1614.3	1.3	0.0046
2	173.0377	22760	3774.9	3.2	0.0076
3	174.0343	24323	8160.3	6.8	0.0072
4	175.0383	38623	3435.6	2.9	0.0045
5	225.1037	33793	58239.7	53.3	0.0067
6	225.9501	30015	1096.0	1.0	0.0075
7	226.1069	29411	14308.2	13.1	0.0077
8	227.1106	28265	1337.2	1.2	0.0080
9	250.9497	36923	4014.0	3.7	0.0068
10	251.9456	29037	13849.3	12.7	0.0087
11	252.9478	27216	4226.2	3.9	0.0093
12	253.9436	36241	15699.9	14.4	0.0070
13	257.9967	30787	4210.3	3.9	0.0084
14	258.0936	25033	1189.9	1.1	0.0103
15	264.9344	29009	1111.6	1.0	0.0091
16	292.1124	39864	31330.2	28.7	0.0073
17	293.1084	37089	109352.5	100.0	0.0079
18	294.1121	29455	16979.0	15.5	0.0100
19	301.9985	36419	3247.7	2.9	0.0083
20	303.0147	26973	1273.6	1.1	0.0112
21	305.0137	31466	1373.2	1.2	0.0097
22	316.0142	41021	5700.5	5.1	0.0077
23	320.1083	32988	6033.4	5.4	0.0097
24	321.1044	42002	31737.6	28.1	0.0076
25	322.1080	28248	3483.4	3.1	0.0114
26	339.2335	31948	1854.2	1.6	0.0106
27	355.0871	27524	1279.9	1.1	0.0129
28	385.0415	25860	1242.9	1.0	0.0149
29	386.0378	30722	14887.9	12.5	0.0126
30	387.0340	40151	40946.7	34.4	0.0096
31	388.0372	27469	4386.8	3.7	0.0141
32	389.0334	26154	1850.1	1.5	0.0149
33	406.1558	33581	5347.9	4.4	0.0121
34	506.1090	27987	2665.4	2.0	0.0181
35	525.2301	31534	1395.9	1.0	0.0167
36	601.9785	61374	10424.1	7.4	0.0098
37	615.9928	59453	22050.9	15.6	0.0104
38	616.9999	45027	3256.2	2.3	0.0137
39	1033.9883	71293	14492.7	8.1	0.0145
40	1034.9928	43325	2289.9	1.3	0.0239

#	m/z	Res.	S/N	I %	FWHM
1	173.0380	24184		24.4	0.0072
2	174.0345	24323		100.0	0.0072
3	175.0374	24463		6.8	0.0072
4	176.0397	24603		0.4	0.0072

#	m/z	Res.	S/N	I %	FWHM
1	225.1033	33792		100.0	0.0067
2	226.1064	33943		16.0	0.0067
3	227.1092	34094		1.4	0.0067

#	m/z	Res.	S/N	I %	FWHM
1	292.1115	36963		23.9	0.0079
2	293.1081	37089		100.0	0.0079
3	294.1111	37216		15.7	0.0079
4	295.1137	37342		1.4	0.0079

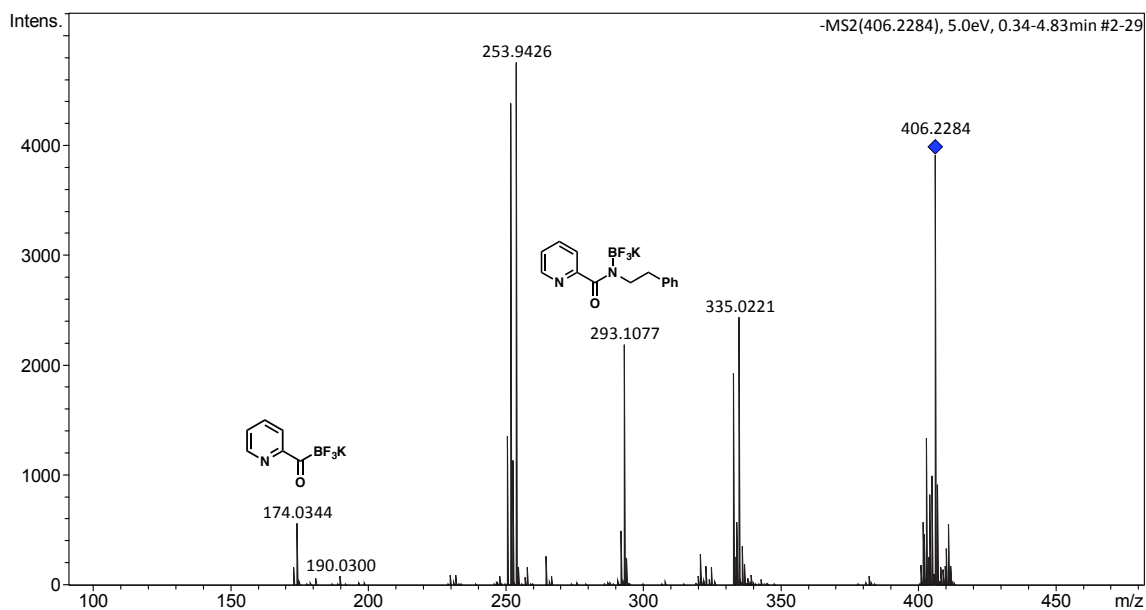
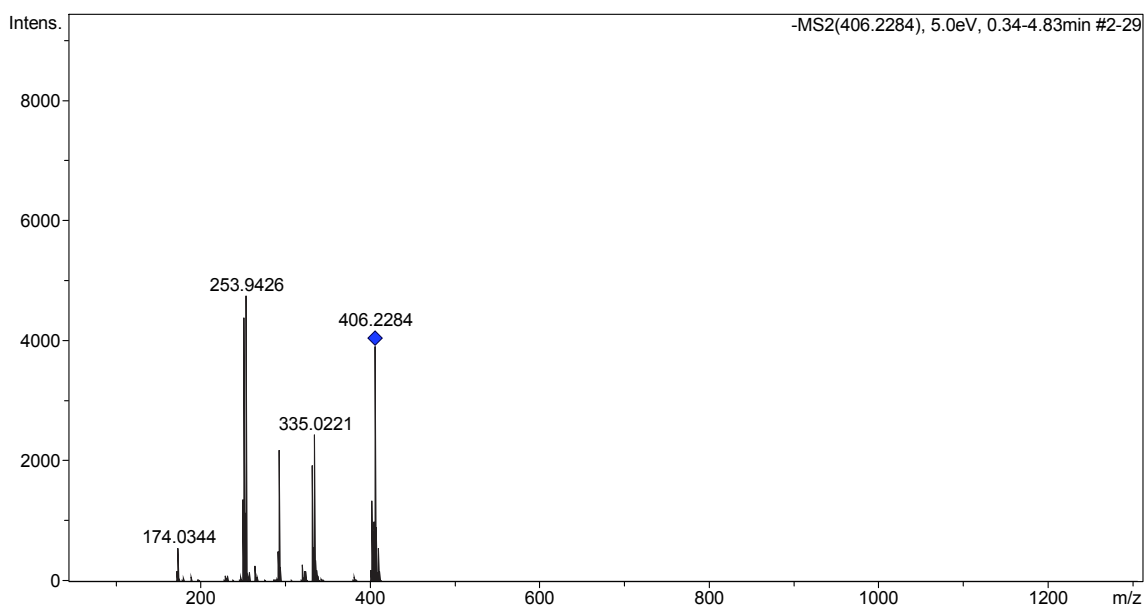
#	m/z	Res.	S/N	I %	FWHM
1	405.1592	33499		23.6	0.0121
2	406.1559	33581		100.0	0.0121
3	407.1588	33664		21.5	0.0121
4	408.1612	33747		2.8	0.0121
5	409.1643	33830		0.3	0.0121

HI-RES MS/MS (isolation of peak m/z 406)  
ESI negative  
Fragmentation Method: CID

Calibrant: Na Formate  
Injection Volume: 5  $\mu$ L/min (syringe pump)

**Acquisition Parameter**

Method:	ETH_HyStar_HPLC_QTOF_NEG_LowMass_Loop-AS.m	Acquisition Date:	13.02.2017 10:34:21		
File Name:	D:\Data\max312xx\MAX31246e.d	Operator:	Louis Bertschli		
Source Type	ESI	Ion Polarity	Negative	Set Nebulizer	0.4 Bar
Focus	Active	Set Capillary	4500 V	Set Dry Heater	200 °C
Scan Begin	50 m/z	Set End Plate Offset	-500 V	Set Dry Gas	4.0 l/min
Scan End	1300 m/z	Set Collision Cell RF	430.0 Vpp	Set Divert Valve	Source



**Calibration Info:**

Date: 13.02.2017 10:41:42  
Polarity: Negative  
Calibration spectrum: -MS, 0.34-5.53min #2-42: Scan  
Reference mass list: ESI: Na Formate (neg)  
Calibration mode: Enhanced Quadratic

Reference m/z	Resulting m/z	Intensity	Error [ppm]
112.9856	112.9856	33	0.007
180.9731	180.9731	416	0.058
248.9605	248.9604	3446	-0.290
316.9479	316.9480	3267	0.286
384.9353	384.9354	1629	0.075
452.9227	452.9228	815	0.054
520.9102	520.9099	436	-0.533
588.8976	588.8979	252	0.449
656.8850	656.8849	118	-0.107

Standard deviation: 0.379

**Mass List:**

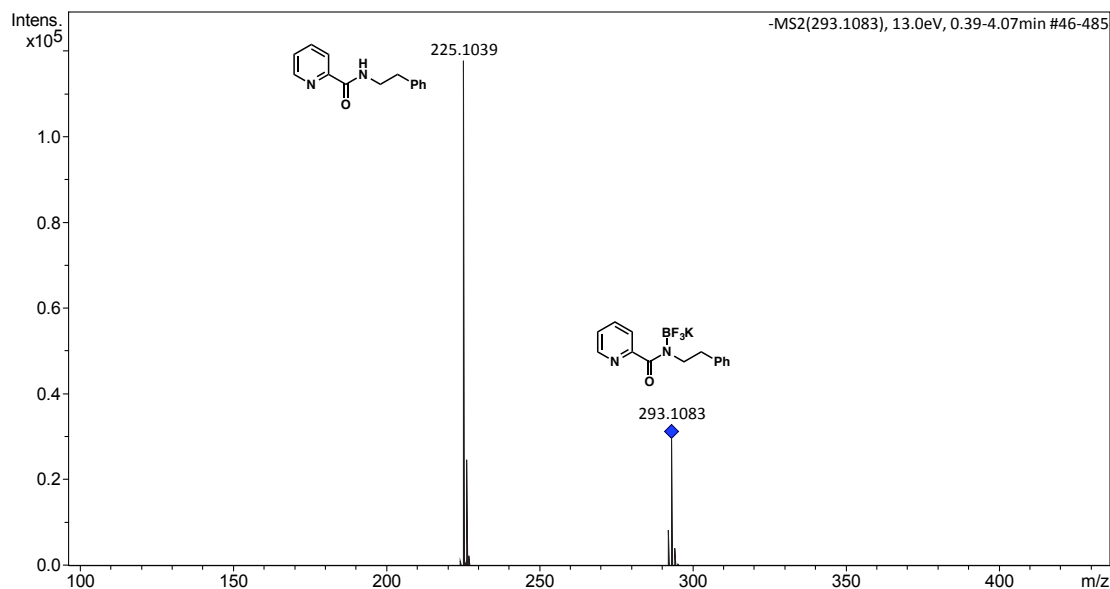
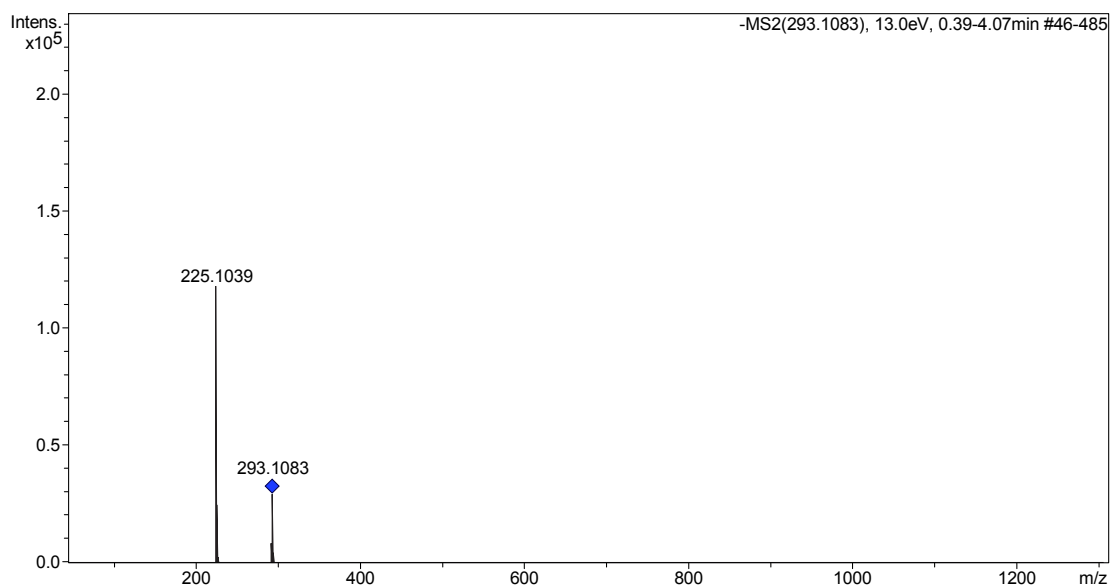
#	m/z	Res.	S/N	I %	FWHM
1	174.0344	23563	241.4	11.8	0.0074
2	250.9484	28697	543.3	28.5	0.0087
3	251.9446	27082	1753.6	92.2	0.0093
4	252.9464	24934	455.4	24.0	0.0101
5	253.9426	37378	1899.4	100.0	0.0068
6	254.9454	18909	66.4	3.5	0.0135
7	264.9337	22757	105.9	5.6	0.0116
8	291.9165	25690	67.7	3.6	0.0114
9	292.1114	24310	192.0	10.3	0.0120
10	293.1077	31889	856.0	46.1	0.0092
11	294.1111	23727	96.6	5.2	0.0124
12	321.1031	26241	109.9	6.0	0.0122
13	323.0544	24524	66.7	3.6	0.0132
14	332.9381	26659	740.5	40.6	0.0125
15	333.9421	24913	96.6	5.3	0.0134
16	334.0255	29591	218.8	12.0	0.0113
17	334.1347	23841	113.0	6.2	0.0140
18	334.9375	24465	168.1	9.2	0.0137
19	335.0221	26729	934.2	51.3	0.0125
20	336.0253	23245	133.7	7.3	0.0145
21	337.0215	22680	72.9	4.0	0.0149
22	400.9431	22617	70.1	3.9	0.0177
23	402.0312	23658	212.0	12.0	0.0170
24	402.1393	20730	173.0	9.8	0.0194
25	403.0274	22843	494.5	28.1	0.0176
26	403.2164	22905	64.6	3.7	0.0176
27	404.0364	12578	94.7	5.4	0.0321
28	404.2132	25389	305.9	17.4	0.0159
29	404.3307	22875	69.4	3.9	0.0177
30	405.0395	21025	178.4	10.1	0.0193
31	405.1560	21992	312.9	17.8	0.0184
32	405.2302	23387	366.0	20.8	0.0173
33	406.1534	26928	1048.5	59.8	0.0151
34	406.2284	25829	1443.0	82.4	0.0157
35	407.1573	22192	228.1	13.1	0.0183
36	407.2324	21209	333.9	19.2	0.0192
37	409.9939	26749	60.9	3.6	0.0153
38	410.1852	16163	118.9	7.0	0.0254
39	410.9900	21874	195.4	11.6	0.0188
40	411.9933	28786	61.8	3.7	0.0143

HI-RES MS/MS (isolation of peak m/z 293)  
ESI negative  
Fragmentation Method: CID

Calibrant: Na Formate  
Injection Volume: 5  $\mu$ L/min (syringe pump)

**Acquisition Parameter**

Method:	ETH_HyStar_HPLC_QTOF_NEG_LowMass_Loop-AS.m	Acquisition Date:	13.02.2017 10:15:33		
File Name:	D:\Data\max312xx\MAX31246d.d	Operator:	Louis Bertschi		
Source Type	ESI	Ion Polarity	Negative	Set Nebulizer	0.4 Bar
Focus	Active	Set Capillary	4500 V	Set Dry Heater	200 °C
Scan Begin	50 m/z	Set End Plate Offset	-500 V	Set Dry Gas	4.0 l/min
Scan End	1300 m/z	Set Collision Cell RF	430.0 Vpp	Set Divert Valve	Source



**Calibration Info:**

Date: 13.02.2017 10:23:39  
Polarity: Negative  
Calibration spectrum: -MS, 0.26-4.80min #31-573: Scan  
Reference mass list: ESI: Na Formate (neg)  
Calibration mode: Enhanced Quadratic

Reference m/z	Resulting m/z	Intensity	Error [ppm]
112.9856	112.9856	18	0.040
180.9731			
248.9605	248.9604	1936	-0.282
316.9479	316.9479	2961	0.145
384.9353	384.9354	1477	0.257
452.9227	452.9229	837	0.238
520.9102	520.9099	384	-0.568
588.8976	588.8976	219	0.039
656.8850	656.8851	93	0.131
724.8724			
792.8599			
860.8473			
928.8347			
996.8221			
1064.8096			
1132.7970			
1200.7844			
1268.7718			
1336.7593			
1404.7467			
1472.7341			

Standard deviation: 0.389

**Mass List:**

#	m/z	Res.	S/N	I %	FWHM
1	121.0406	30966	125.0	0.1	0.0039
2	146.0622	17387	10.7	0.0	0.0084
3	173.0389	21914	26.2	0.0	0.0079
4	174.0355	23092	112.3	0.1	0.0075
5	187.0666	19828	8.5	0.0	0.0094
6	188.0625	20883	33.0	0.0	0.0090
7	196.0780	22122	56.7	0.1	0.0089
8	220.1478	18102	9.3	0.0	0.0122
9	221.1557	20113	20.9	0.0	0.0110
10	224.1204	27527	689.8	0.8	0.0081
11	224.6457	6026	13.1	0.0	0.0373
12	224.6580	18079	12.2	0.0	0.0124
13	224.6759	54240	11.1	0.0	0.0041
14	224.6964	54241	11.2	0.0	0.0041
15	224.7166	21221	12.5	0.0	0.0106
16	224.7243	18082	12.4	0.0	0.0124
17	224.7526	6028	13.3	0.0	0.0373
18	225.1039	37102	85633.2	100.0	0.0061
19	225.2584	16921	10.5	0.0	0.0133
20	225.3230	29261	837.9	1.0	0.0077
21	225.4575	41450	741.2	0.9	0.0054
22	225.6577	34731	152.2	0.2	0.0065
23	225.7946	42597	228.5	0.3	0.0053
24	225.9727	17636	36.5	0.0	0.0128
25	226.1067	30623	17923.2	21.0	0.0074
26	226.4654	16742	30.9	0.0	0.0135
27	226.7935	22955	17.0	0.0	0.0099
28	227.1103	26549	1706.8	2.0	0.0086
29	228.1129	19902	27.9	0.0	0.0115
30	236.1063	23423	37.4	0.0	0.0101
31	272.1190	22478	23.9	0.0	0.0121
32	291.1285	22853	55.6	0.1	0.0127
33	292.1128	34944	5608.6	7.0	0.0084
34	293.1083	30086	20687.6	25.0	0.0097
35	294.1119	28184	2982.0	3.4	0.0104
36	295.1152	20809	163.6	0.2	0.0142



## 7.4 References

- [176] Sherman, J.; Fried, B. *Handbook of Thin-Layer Chromatography*. Third Edition, Marcel Dekker, New York, USA, **2003**.
- [177] Jork, H.; Funk, W.; Fischer, W.; Wimmer, H. *Thin-Layer Chromatography Reagents and Detection Methods*. Volume 1a, Physical and Chemical Detection Methods: Fundamentals Reagents I, VHC, Weinheim, Germany, **1990**.
- [178] Still, W. C.; Kahn, M.; Mitra, A. J. Rapid Chromatographic Technique for Preparative Separations with Moderate Resolutions. *J. Org. Chem.* **1978**, *43*, 2923–2925.
- [179] Erős, G.; Kushida, Y.; Bode J. W. A Reagent for the One-Step Preparation of Potassium Acyltrifluoroborates (KATs) from Aryl- and Heteroarylhalides. *Angew. Chem. Int. Ed.* **2014**, *53*, 7604–7607.
- [180] Noda, H.; Erős, G.; Bode J. W. Rapid Ligations with Equimolar Reactants in Water with the Potassium Acyltrifluoroborate (KAT) Amide Formation. *J. Chem. Am. Soc.* **2014**, *136*, 5611–5614.
- [181] Pangborn, A. B.; Giardello, M. A.; Grubbs, R. H.; Rosen, R. K.; Timmers, F. J. Safe and Convenient Procedure for Solvent Purification. *Organometallics* **1996**, *15*, 1518–1520.
- [182] del Pozo, C.; Debono, N.; Corma, A.; Iglesias, M.; Sánchez, F. Homogeneous versus Supported ONN Pincer-Type Gold and Palladium Complexes: Catalytic Activity. *ChemSusChem* **2009**, *2*, 650–657.
- [183] Tanaka, H.; Tokito, S.; Taga, Y.; Okada, A. Novel Metal-Chelate Emitting Materials Based on Polycyclic Aromatic Ligands for Electroluminescent Devices. *J. Mater. Chem.* **1998**, *8*, 1999–2003.

- [184] Nelson, J. T.; Davis, R.  $^1\text{H}$  and  $^{13}\text{C}$  NMR Spectra of Fifteen Substituted Isoquinolines. *Magnetic Resonance in Chemistry* **1991**, *29*, 513–517.
- [185] Meier, P.; Legraverant, S.; Müller, S.; Schaub, J. Synthesis of Formylphenylpyridinecarboxylic Acids Using Suzuki–Miyaura Coupling Reactions. *Synthesis* **2003**, *4*, 551–554.
- [186] M Couchman, S. M.; Jeffery, J. C.; Thornton, P.; Ward, M. D. Co-ordination Chemistry of 6-(2-hydroxyphenyl)pyridine-2-carboxylic acid: A Terdentate Ligand with a Mixed Phenolate/Pyridyl/Carboxylate Donor Set. *J. Chem. Soc., Dalton Trans.* **1998**, 1163–1170.
- [187] Methyl 6-bromopicolinate was synthesized according to the following literature procedure with slight modifications: Pissarnitski, D. M.; Josien, H. B.; Smith, E. M.; Clader, J. W.; Asberom, T.; Guo, T.; Hobbs, D. W. Novel Gamma Secretase Inhibitors. US 2004/0171614 A1, **2004**.
- [188] Doyle, A. A.; Parsons, S.; Solan, G. A.; Winpenny, R. E. P. Pentanuclear Copper(II) Complexes with the Novel 6-(Phenylethynyl)-2-yridonate Ligand: Synthesis, Structures and Magnetic Properties. *J. Chem. Soc., Dalton Trans.* **1997**, 2131–2138.
- [189] 2-Bromo-6-methoxypyridine was synthesized according to the following literature procedure: Testaferri, L.; Tiecco, M.; Tingoli, M.; Bartoli, D.; Massoli, A. The Reactions of some Halogenated Pyridines with Methoxide and Methanethiolate Ions in Dimethylformamide. *Tetrahedron* **1985**, *41*, 1373–1384.
- [190] Zhu, J.; Ye, Y.; Ning, M.; Mándi, A.; Feng, Y.; Zou, Q.; Kurtán, T.; Leng, Y.; Shen, J. Design, Synthesis, and Structure–Activity Relationships of 3,4,5-Trisubstituted 4,5-Dihydro-1,2,4-oxadiazoles as TGR5 Agonists. *ChemMedChem* **2013**, *8*, 1210–1223.

- [191] Puerto Galvis, C. E.; Kouznetsov, V. V. Regio- and Stereoselective Synthesis of Spirooxindole 1'-nitro Pyrrolizidines with Five Concurrent Stereocenters under Aqueous Medium and their Bioprospection using the Zebrafish (*Danio rerio*) Embryo Model. *Org. Biomol. Chem.*, **2013**, 11, 7372–7386.
- [192] Dawson, D. M.; Ke, Z.; Mack, F. M.; Doyle, R. A.; Bignami, G. P. M.; Smellie, I. A.; Bühl, M.; Ashbrook, S. E. Calculation and Experimental Measurement of Paramagnetic NMR Parameters of Phenolic Oximate Cu(II) Complexes. *Chem. Commun.* **2017**, 53, 10512–10515.
- [193] Kopczyński, T.; Krzyżanowska, E.; & Olszanowski, A. Synthesis and Spectral Data of (E) and (Z) Oximes of 2-Hydroxybenzophenone Derivatives. *J. prakt. Chem.* **1989**, 331, 486–492.
- [194] O-(*tert*-butyldiphenylsilyl) hydroxylamine was synthesized according to the following literature procedure: Stewart, A. O.; & Martin, J. G. Synthesis of (1-Aryl-1-alkylethyl)alkoxyamines. *J. Org. Chem.* **1989**, 54, 1221–1223.
- [195] Noda, H., Erős, G.; Bode, J. W. Rapid Ligations with Equimolar Reactants in Water with the Potassium Acyltrifluoroborate (KAT) Amide Formation, *J. Am. Chem. Soc.* **2014**, 136, 5611–5614.
- [196] Noda, H.; Bode, J. W. Synthesis of Chemically and Configurationally Stable Monofluoro Acylboronates: Effect of Ligand Structure on their Formation, Properties, and Reactivities. *J. Am. Chem. Soc.* **2015**, 137, 3958.
- [197] Chang, Y.-C.; Chang, W.-C.; Hu, C.-Y.; Hong, F.-E. Alkyl(quinoline-8-yl)phosphine Oxides as Hemilabile Preligands for Palladium-Catalyzed Reactions. *Organometallics* **2014**, 33, 3523–3534.

- [198] Dreis, A. M.; Douglas, C. J. Catalytic Carbon–Carbon  $\sigma$  Bond Activation: An Intramolecular Carbo-Acylation Reaction with Acylquinolines. *J. Am. Chem. Soc.* **2009**, *131*, 412–413.
- [199] Lin, A. J.; Loo, T. L. Synthesis and Antitumor Activity of Halogen-Substituted 4-(3,3-Dimethyl-1-triazeno)quinolines. *J. Med. Chem.* **1978**, *21*, 268–272.
- [200] WO 2013118071 A1, Bicyclic Compounds As mPGES-1 Inhibitors, **2013**.
- [201] WO 2006135839 A2, Piperazine-Piperidine Antagonists and Agonists of the 5-HT<sub>1A</sub> Receptor, **2006**.
- [202] Dumas, A. M.; Bode, J. W. Synthesis of Acyltrifluoroborates. *Org. Lett.* **2012**, *14*, 2138–2141.
- [203] Morimoto, H.; Fujiwara, R.; Shimizu, Y.; Morisaki, K.; Ohshima, T. Lanthanum(III) Triflate Catalyzed Direct Amidation of Esters. *Org. Lett.* **2014**, *16*, 2018–2021.
- [204] Gualtierotti, J. B.; Schumacher, X.; Fontaine, P.; Masson, G.; Wang, Q.; Zhu, Amidation of Aldehydes and Alcohols via  $\alpha$ -Iminonitriles and a Sequential Oxidative Three-component Strecker Reaction/Thio-Michael Addition/Alumina-promoted Hydrolysis to Access  $\alpha$ -Mercaptoamides from Aldehydes, Amines and Thiols. *J. Chem. Eur. J.* **2012**, *18*, 14812–14819.
- [205] Krężel, A.; Bal, W. A formula for Correlating pK<sub>a</sub> Values Determined in D<sub>2</sub>O and H<sub>2</sub>O. *J. Inorg. Biochem.* **2004**, *98*, 161–166.
- [206] a) Sørensen, S. P. L. *Biochem. Z.* **1990**, *21*, 131. b) Sørensen, S. P. L. *Biochem. Z.* **1909**, *22*, 352. c) Gomori, G. *Methods Enzymol.* **1955**, *1*, 138.

- [207] Pearse, A. G. E. *Histochemistry: Theoretical and Applied : Preparative and Optical Technology Vol 1*, Churchill, Livingstone, London, UK, **1980**.
- [208] Hammett, L. P. The Effect of Structure upon the Reactions of Organic Compounds. Benzene Derivatives. *J. Am. Chem. Soc.* **1937**, 59, 96–103.



# ***Chapter 8***

---

***Spectroscopic Data  
and DFT Calculations***

---



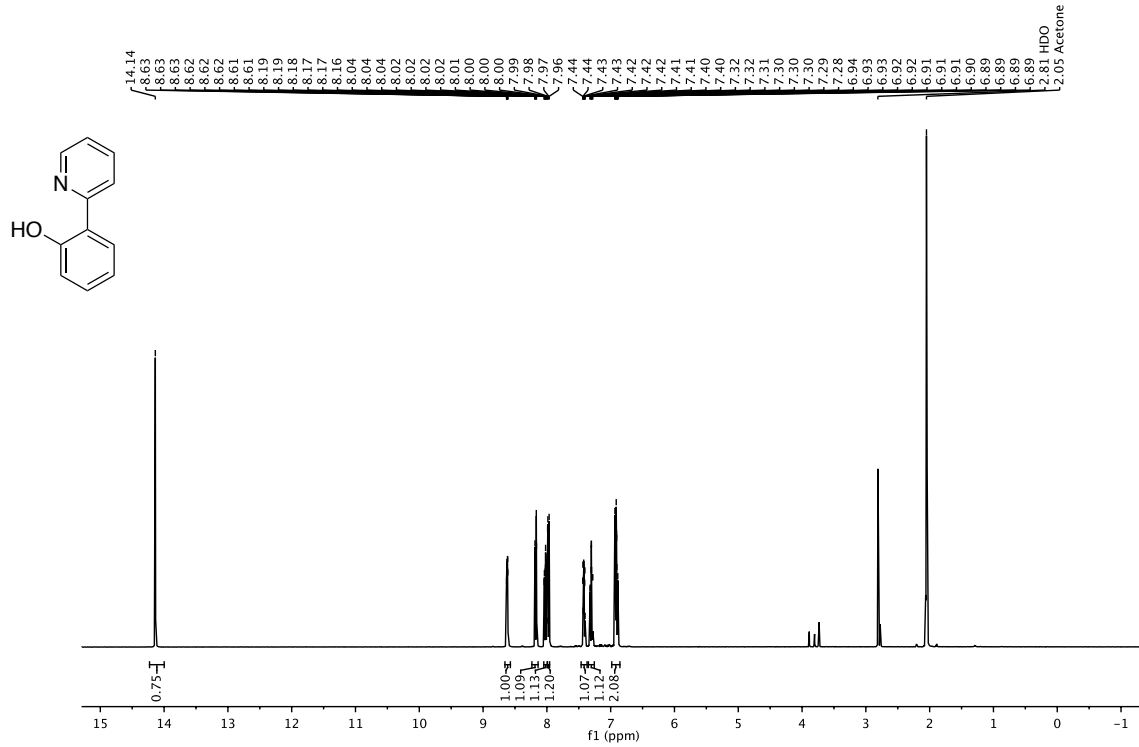


## 8 Spectroscopic Data and DFT Calculations

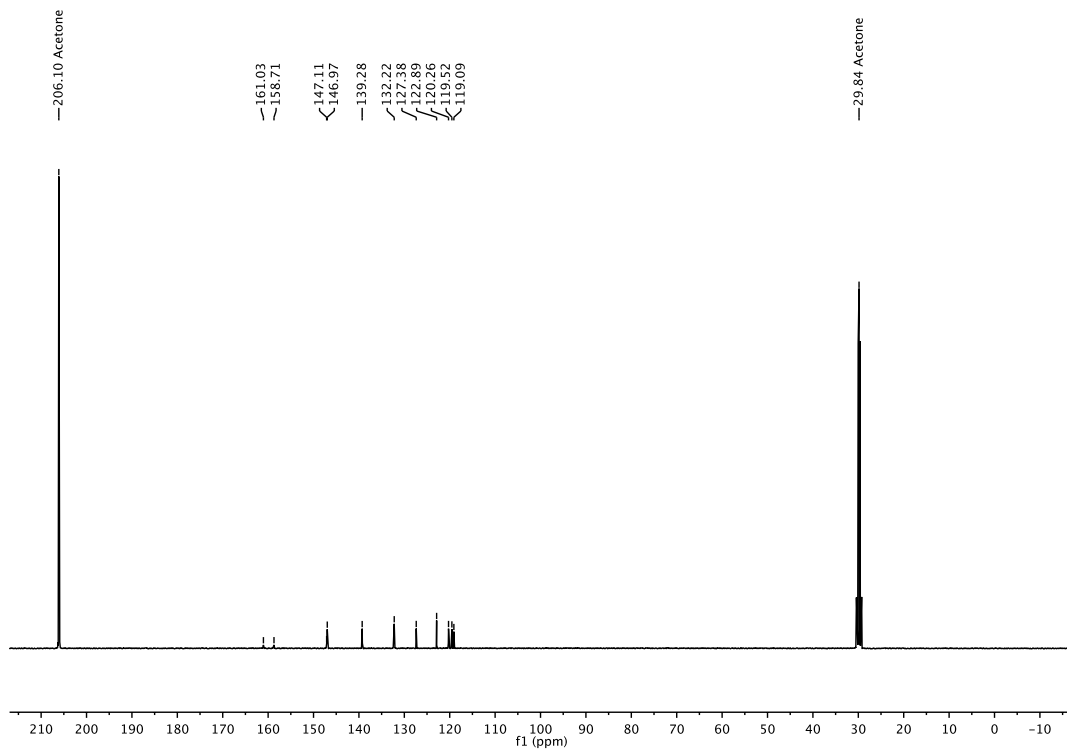
### 8.1 NMR Spectroscopic Data

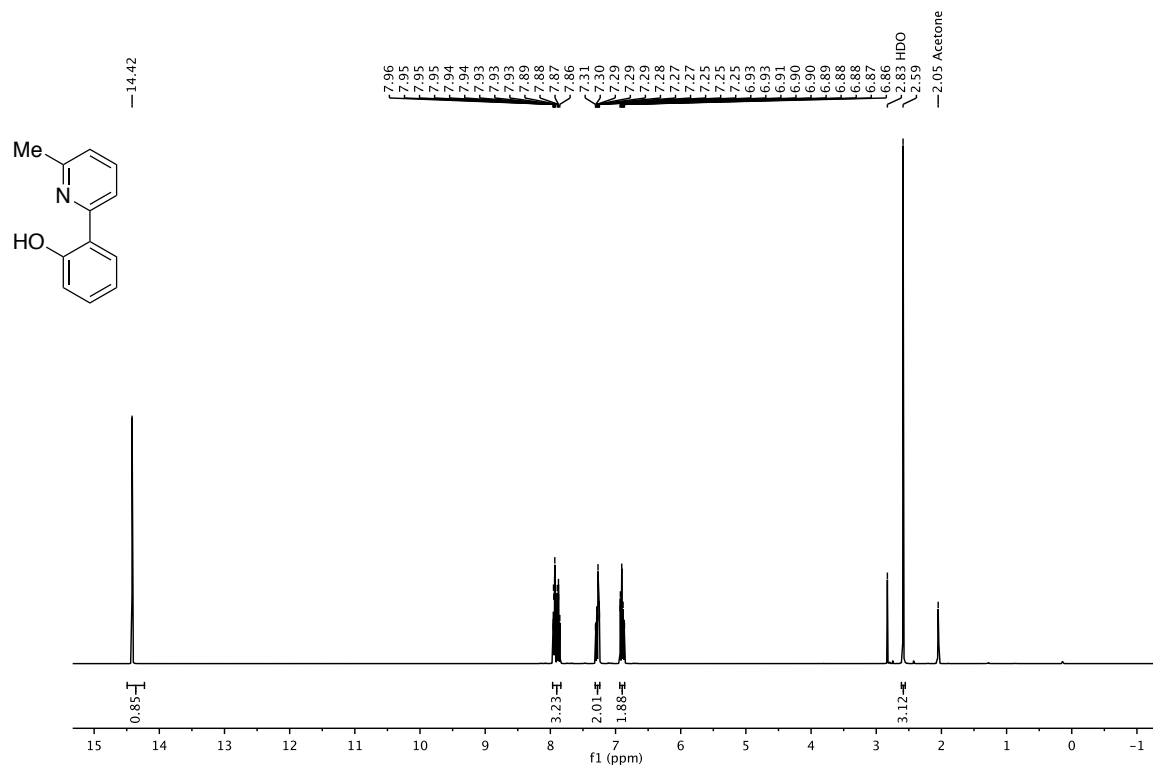
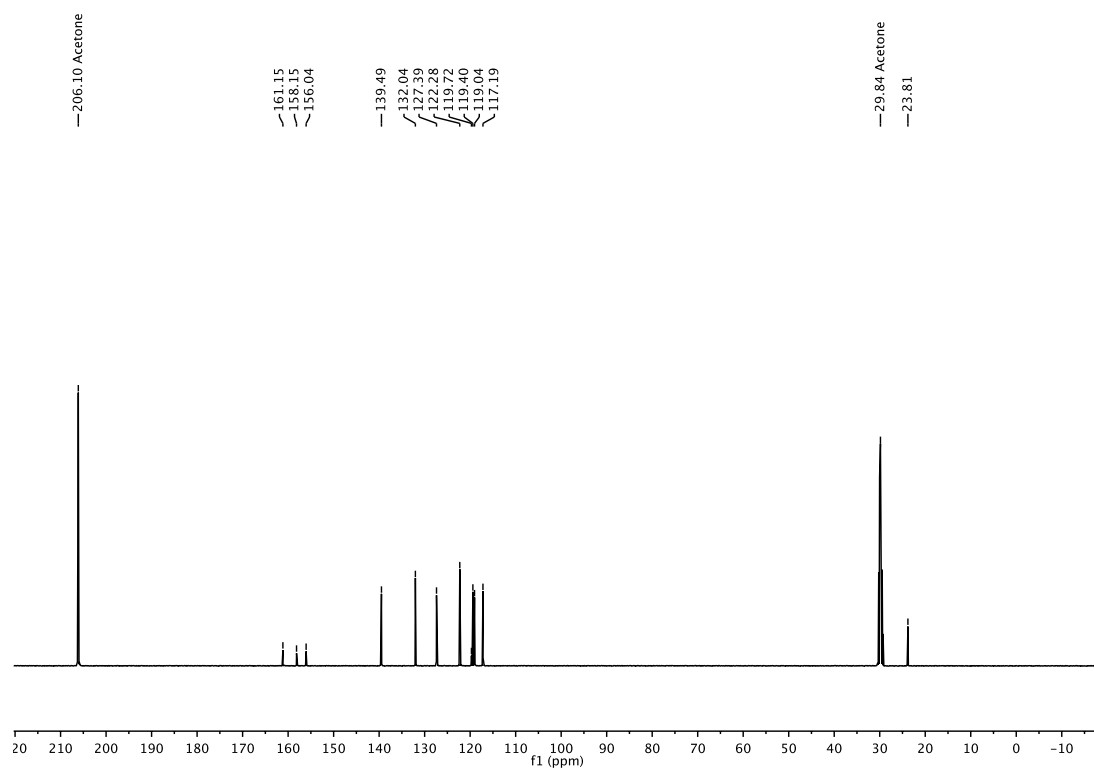
#### 2-(Pyridin-2-yl)phenol (L97)

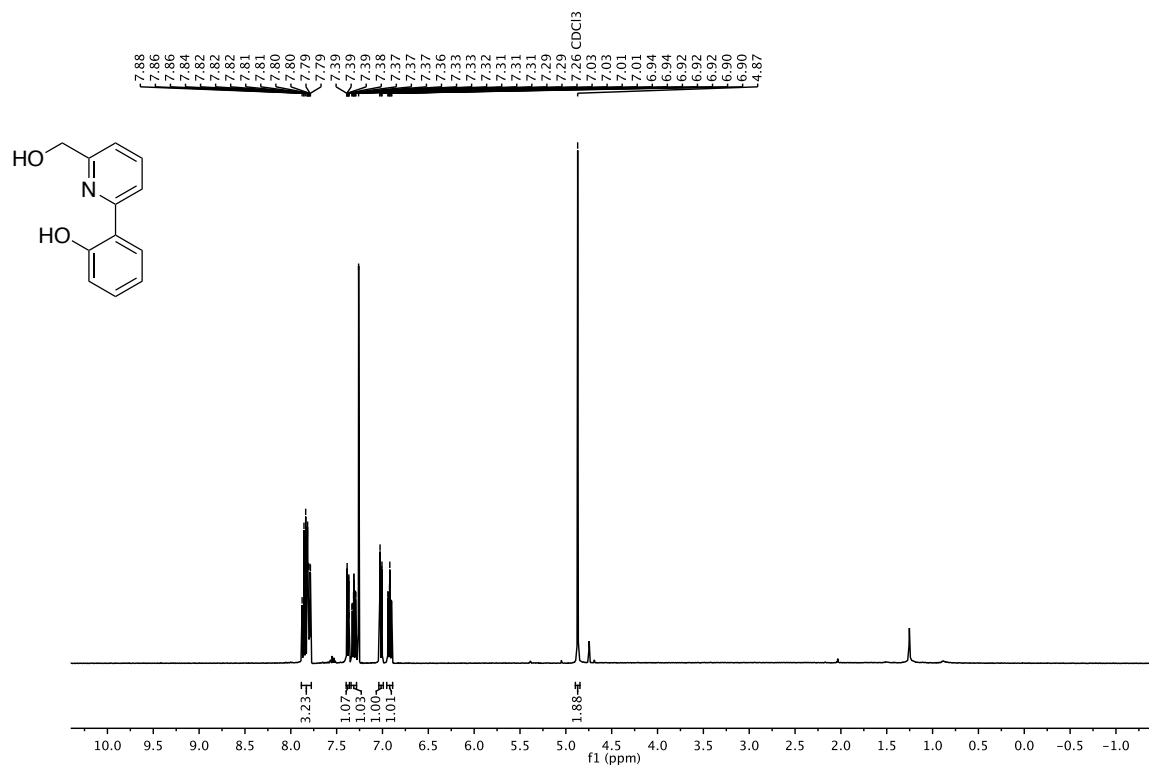
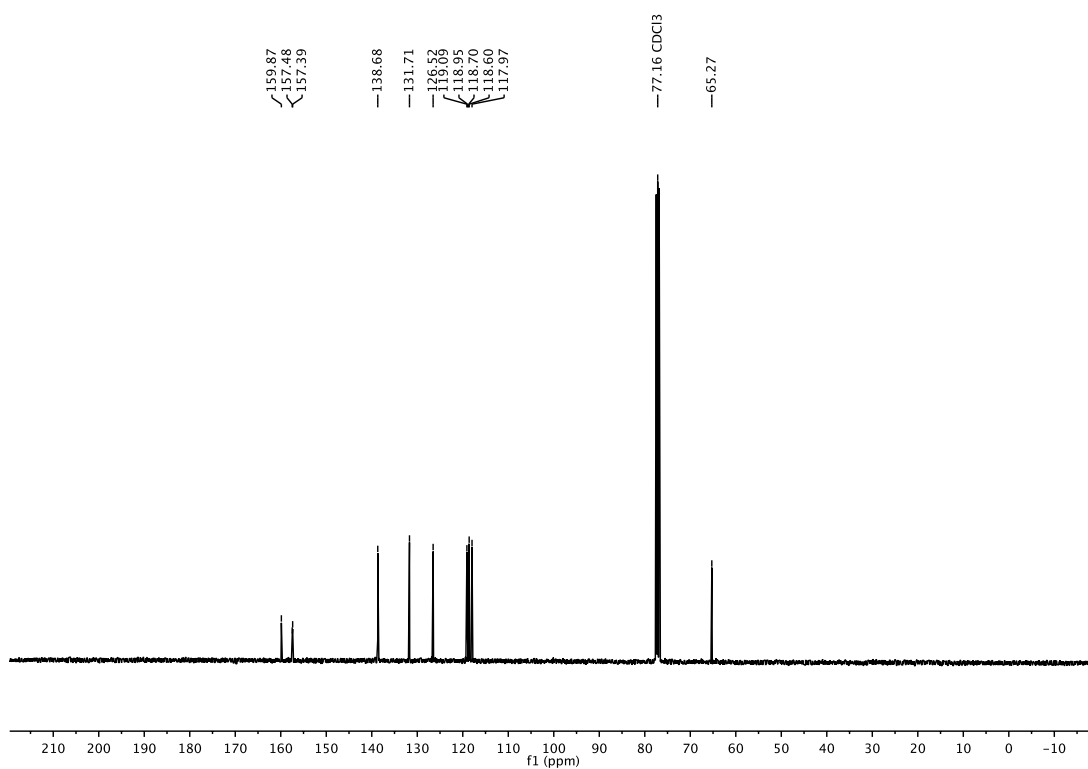
#### $^1\text{H-NMR}$ (400 MHz, acetone- $d_6$ )

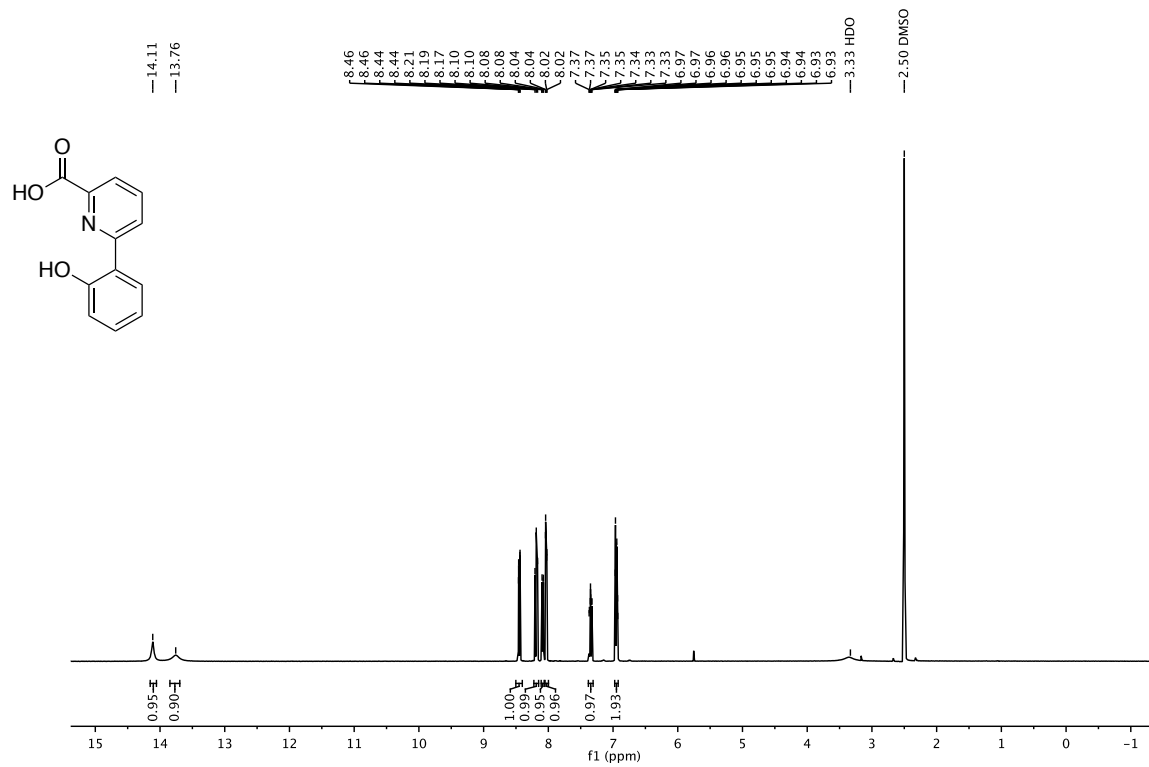
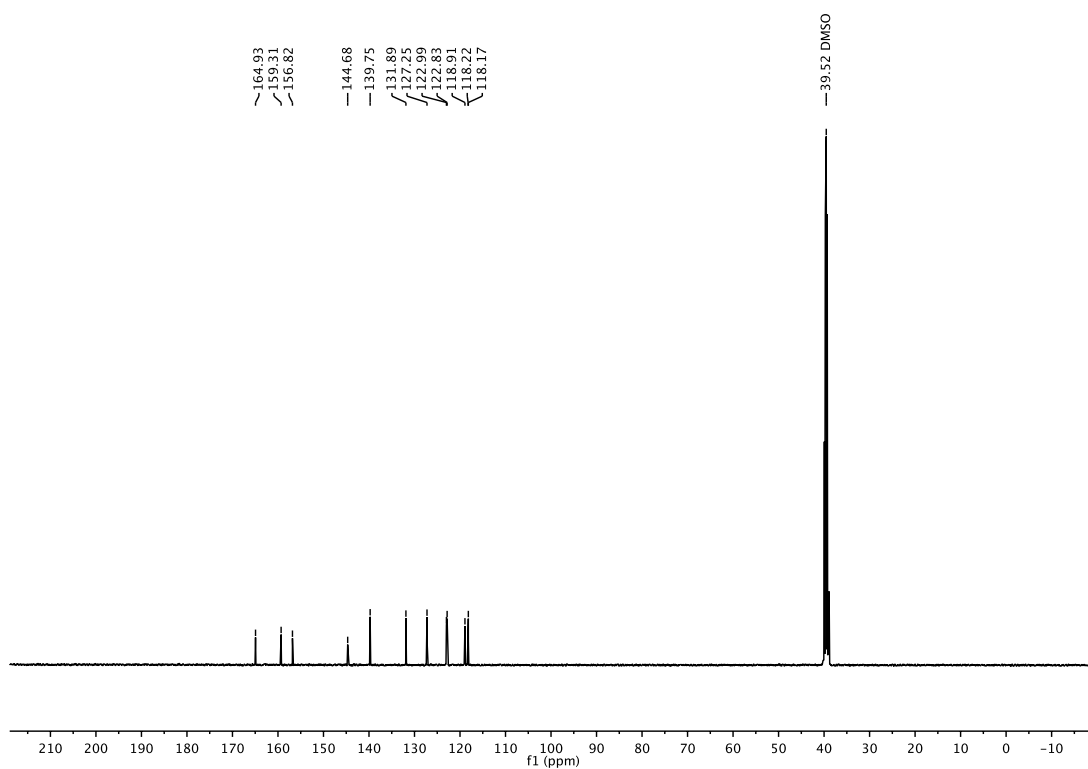


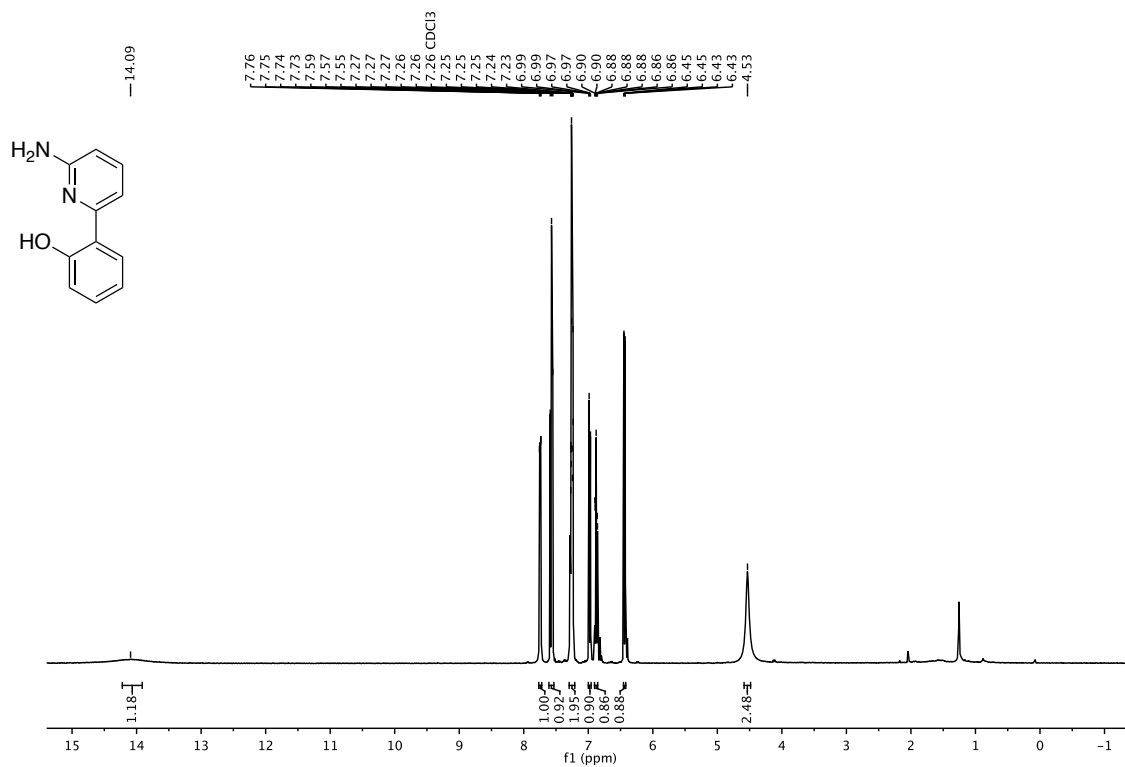
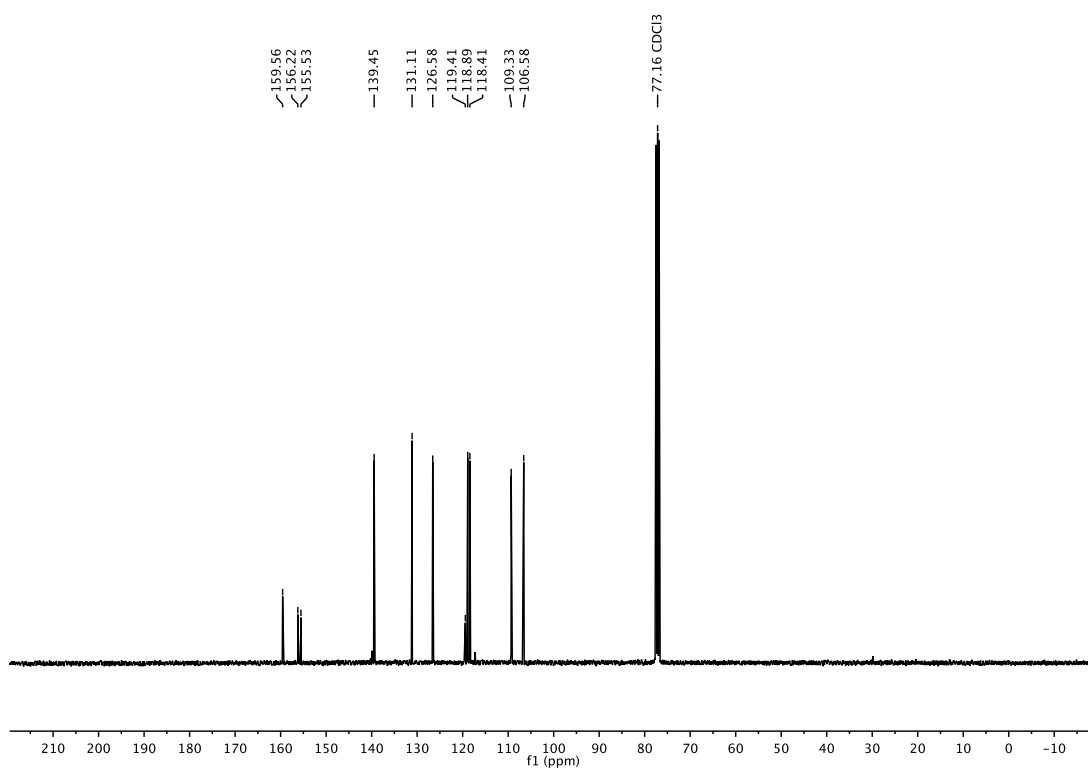
#### $^{13}\text{C-NMR}$ (101 MHz, acetone- $d_6$ )

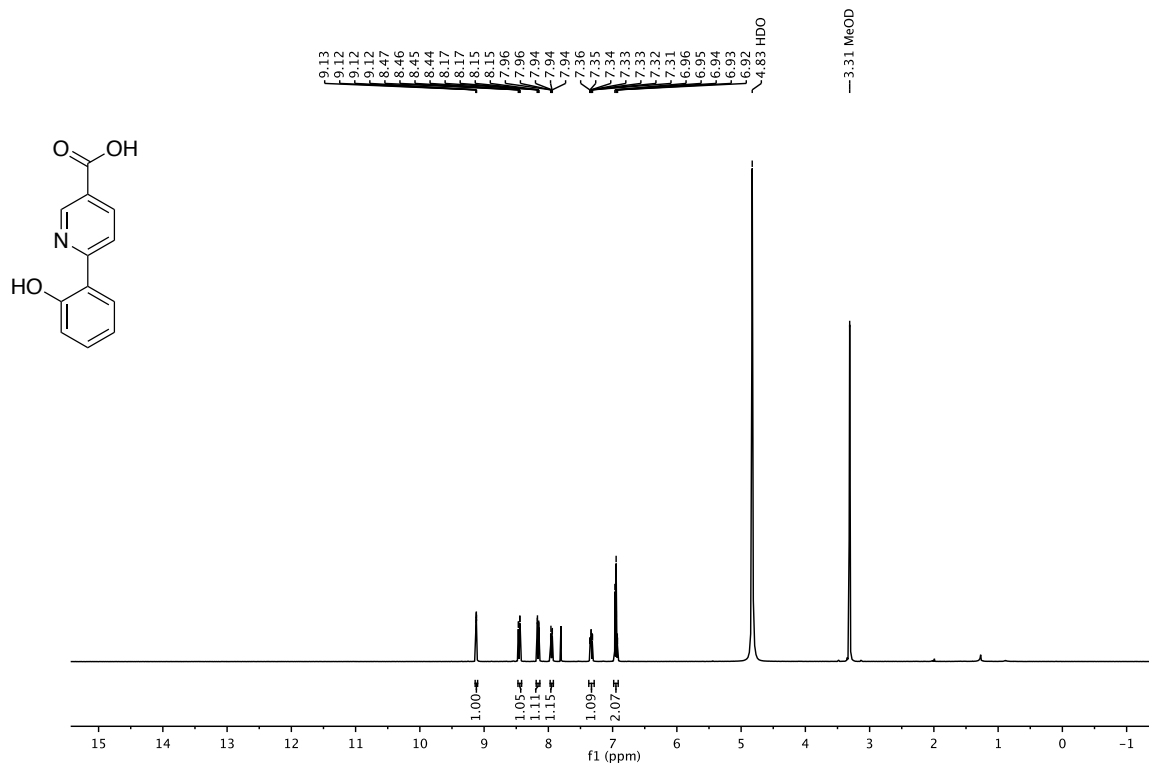
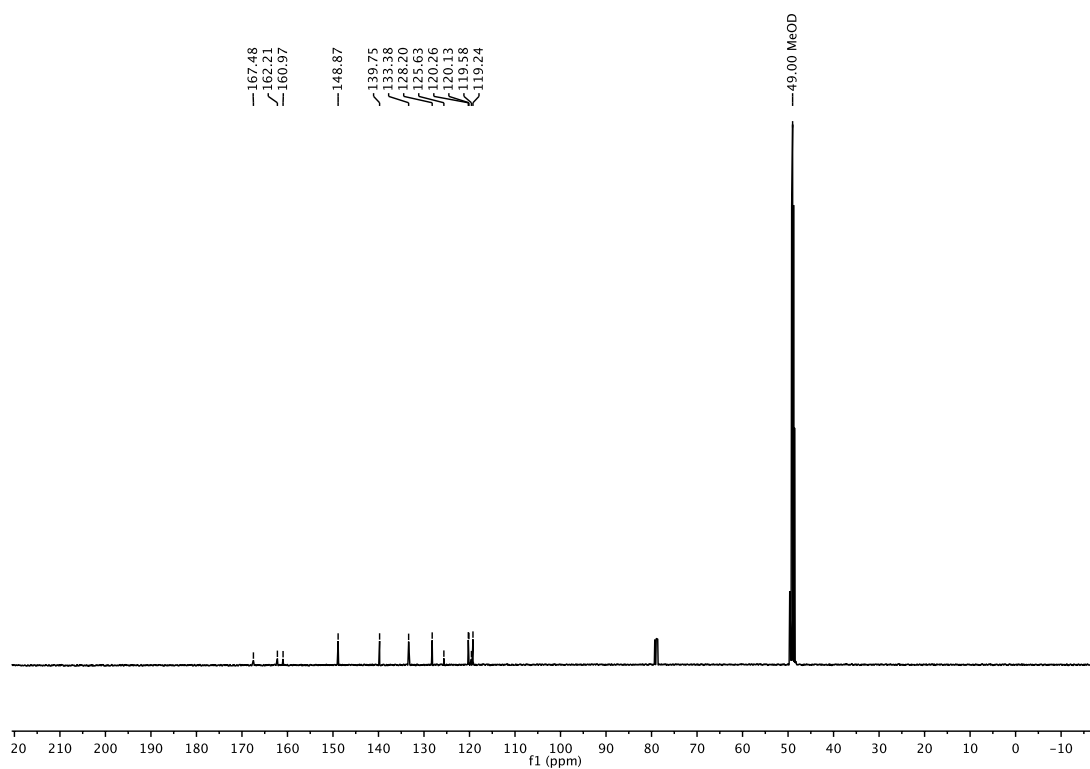


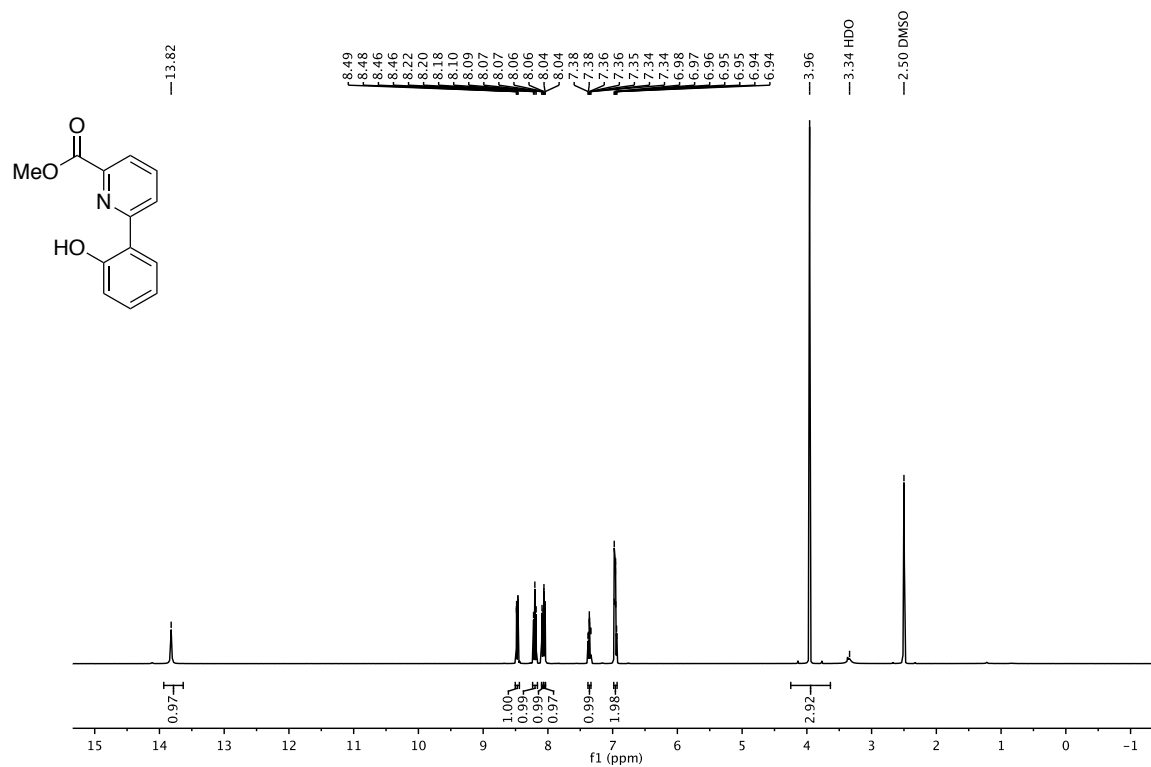
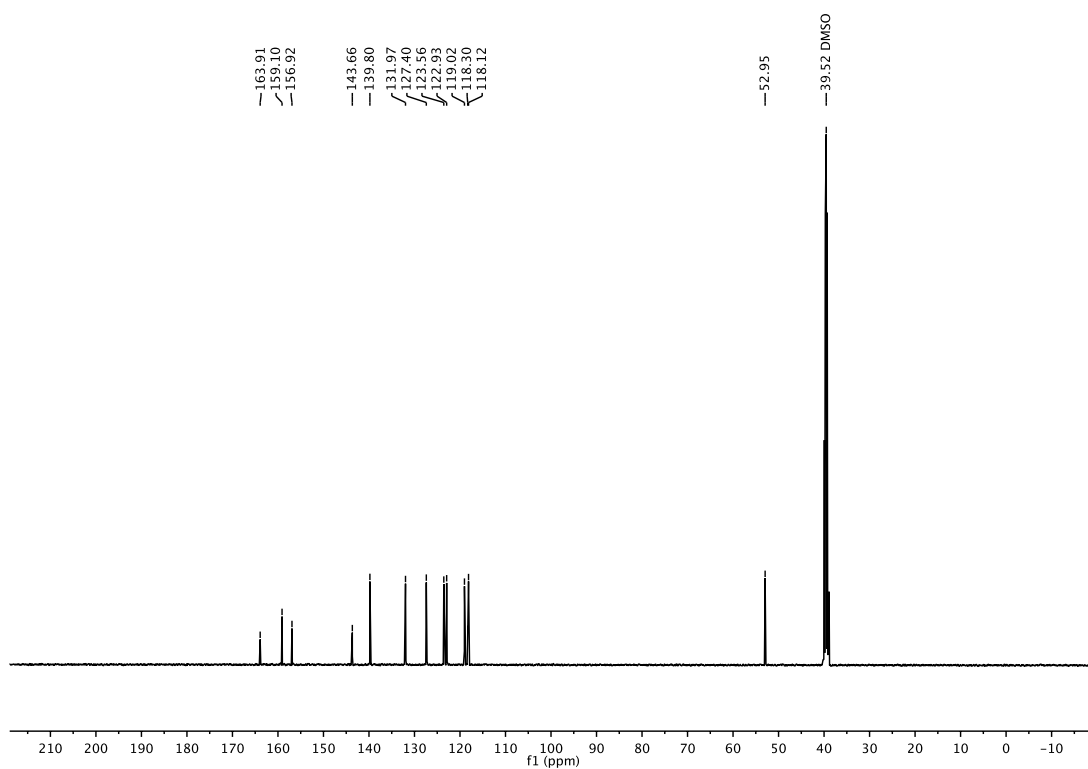
**2-(6-Methylpyridin-2-yl)phenol (L98)****<sup>1</sup>H-NMR (400 MHz, acetone-*d*<sub>6</sub>)****<sup>13</sup>C-NMR (101 MHz, acetone-*d*<sub>6</sub>)**

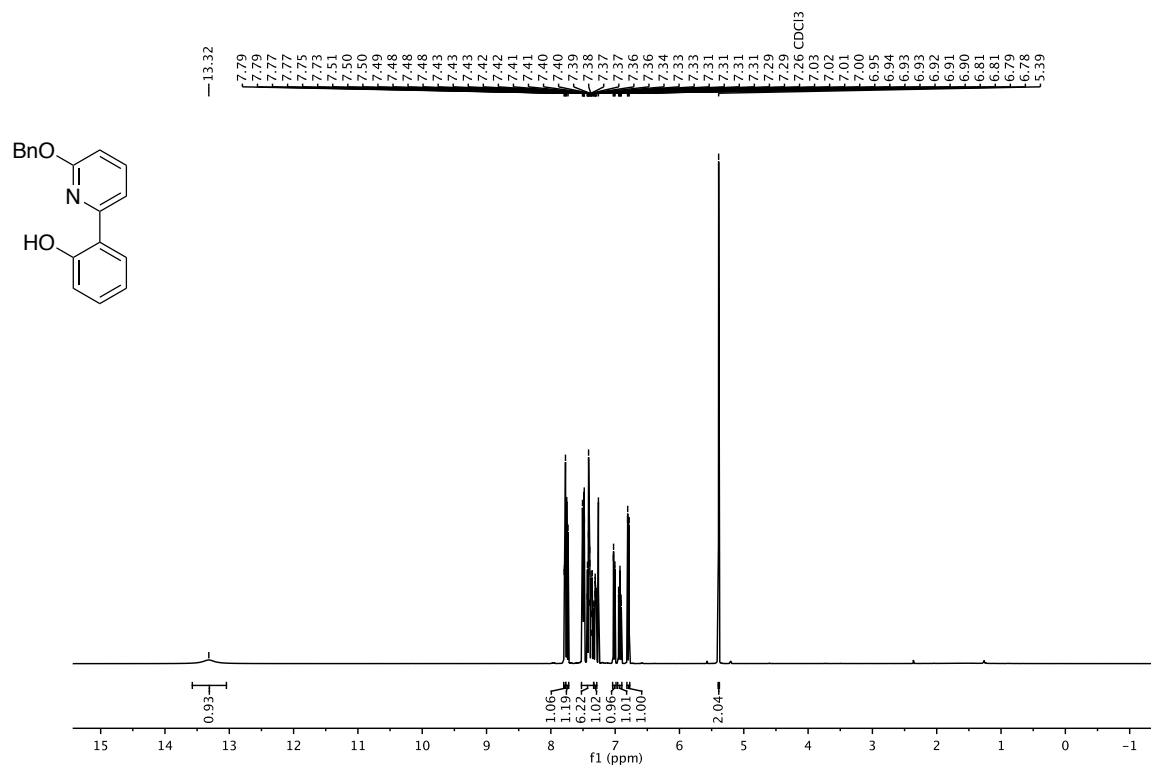
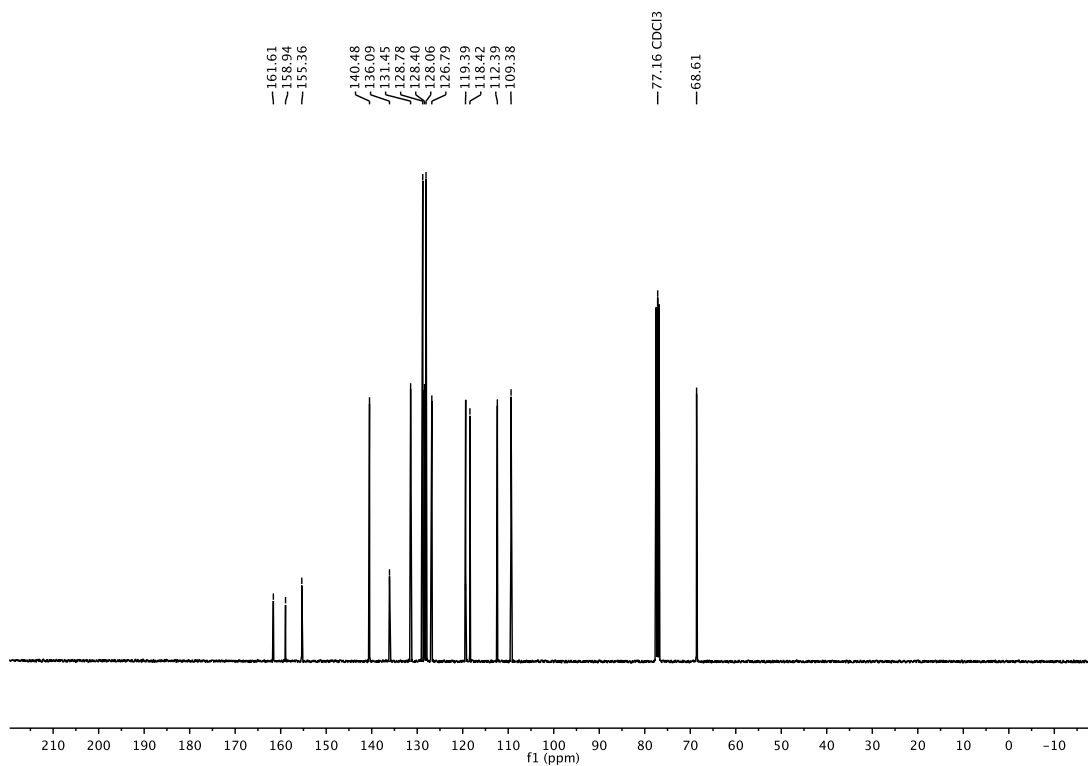
**2-(6-(Hydroxymethyl)pyridin-2-yl)phenol (L101)****<sup>1</sup>H-NMR (400 MHz, CDCl<sub>3</sub>)****<sup>13</sup>C-NMR (101 MHz, CDCl<sub>3</sub>)**

**6-(2-Hydroxyphenyl)picolinic acid (L102)****<sup>1</sup>H-NMR (400 MHz, DMSO-*d*<sub>6</sub>)****<sup>13</sup>C-NMR (101 MHz, DMSO-*d*<sub>6</sub>)**

**2-(6-Aminopyridin-2-yl)phenol (L103)****<sup>1</sup>H-NMR (400 MHz, CDCl<sub>3</sub>)****<sup>13</sup>C-NMR (101 MHz, CDCl<sub>3</sub>)**

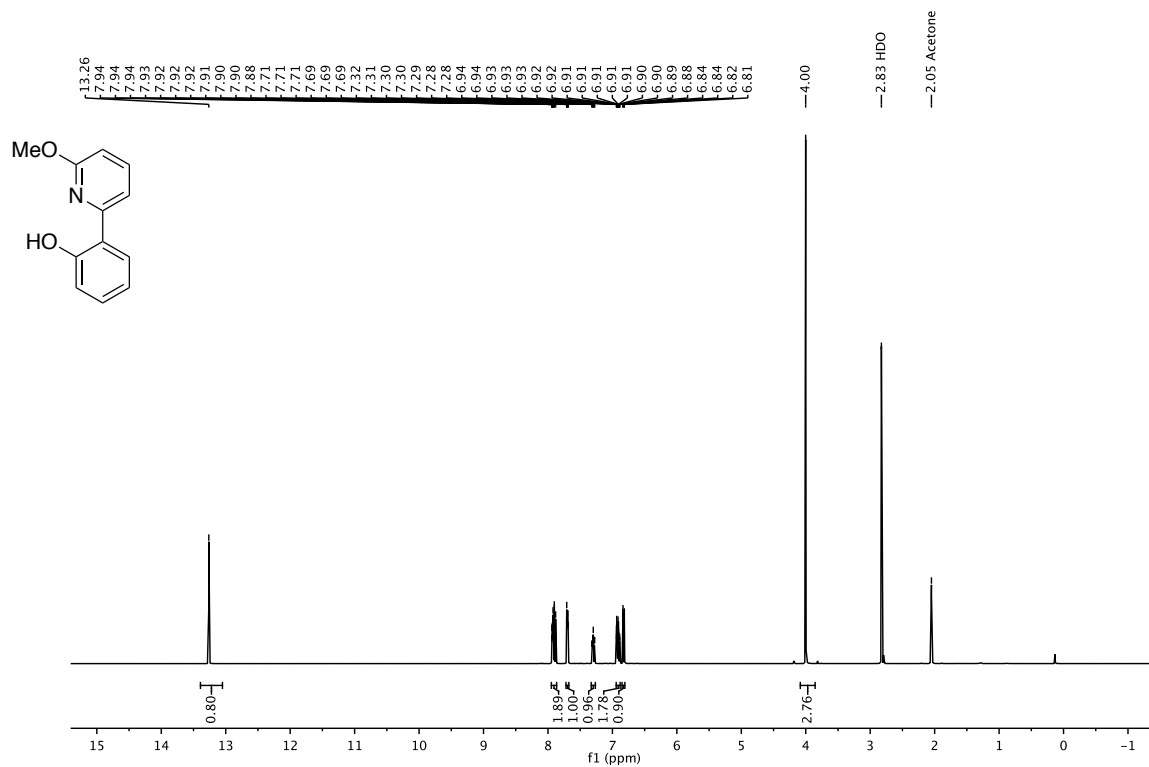
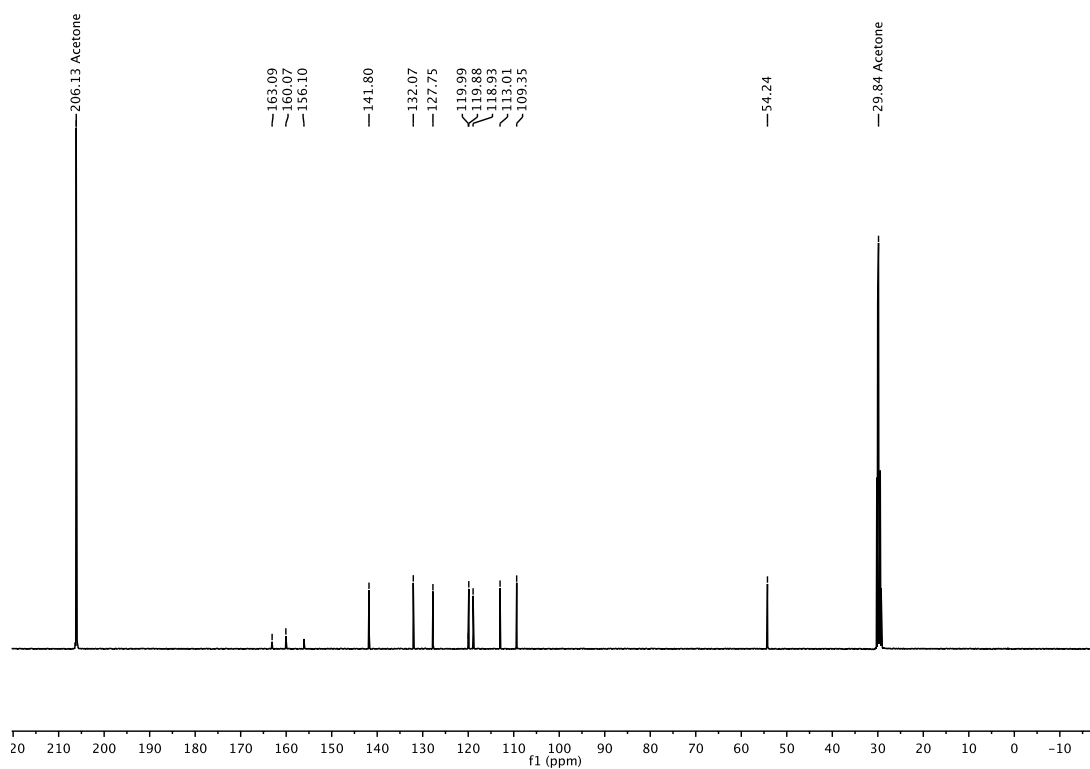
**6-(2-Hydroxyphenyl)nicotinic acid (L104)****<sup>1</sup>H-NMR (400 MHz, methanol-*d*<sub>4</sub>)****<sup>13</sup>C-NMR (101 MHz, methanol-*d*<sub>4</sub>)**

**Methyl 6-(2-hydroxyphenyl)picolinate (L106)****<sup>1</sup>H-NMR (400 MHz, DMSO-*d*<sub>6</sub>)****<sup>13</sup>C-NMR (101 MHz, DMSO-*d*<sub>6</sub>)**

**2-(6-(Benzyloxy)pyridin-2-yl)phenol (L107)****<sup>1</sup>H-NMR (400 MHz, CDCl<sub>3</sub>)****<sup>13</sup>C-NMR (101 MHz, CDCl<sub>3</sub>)**

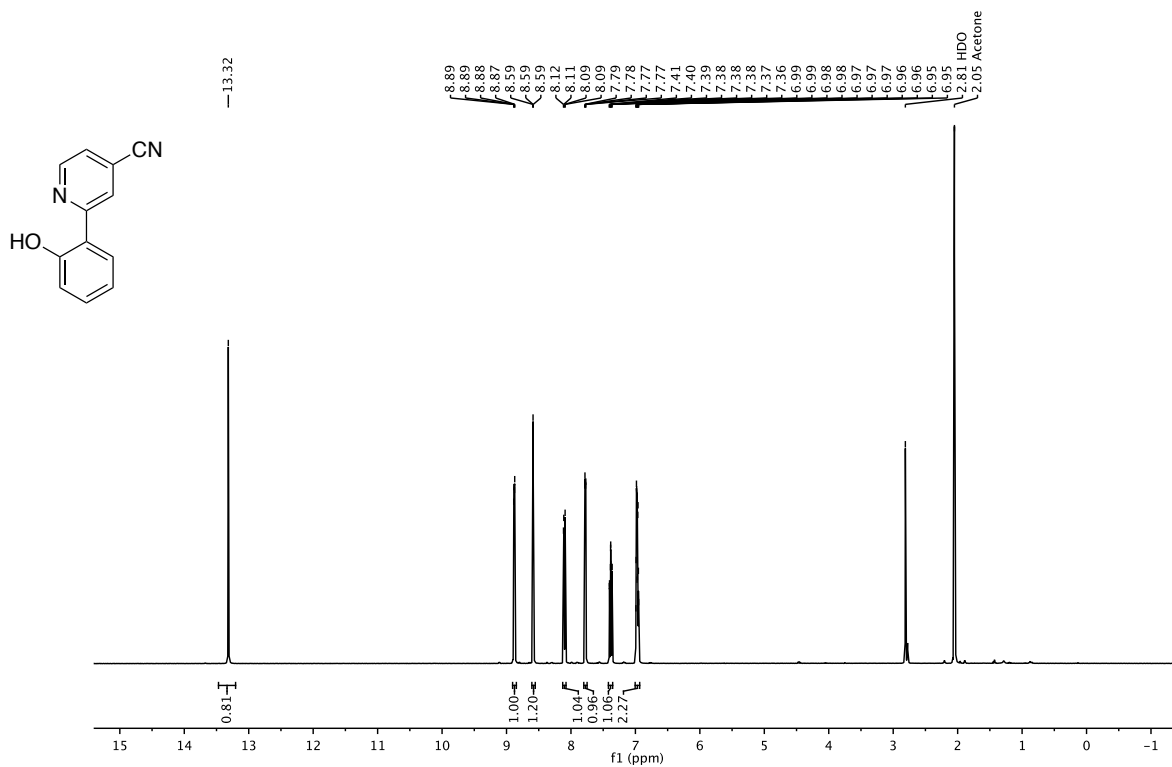
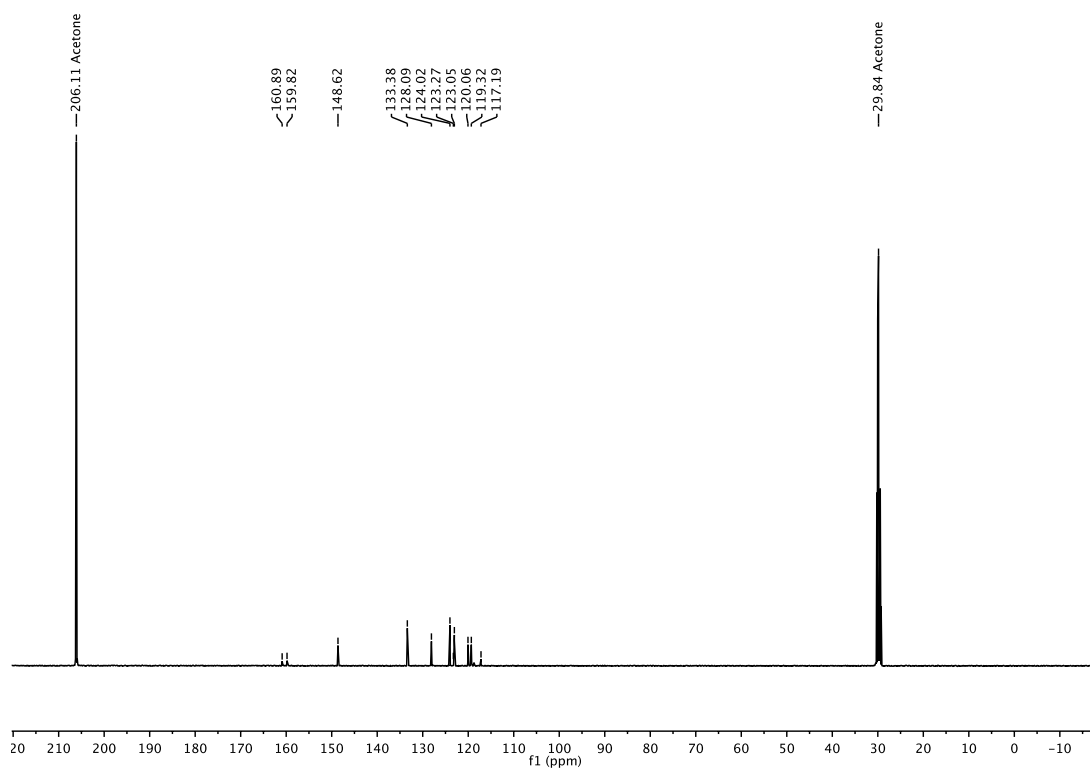


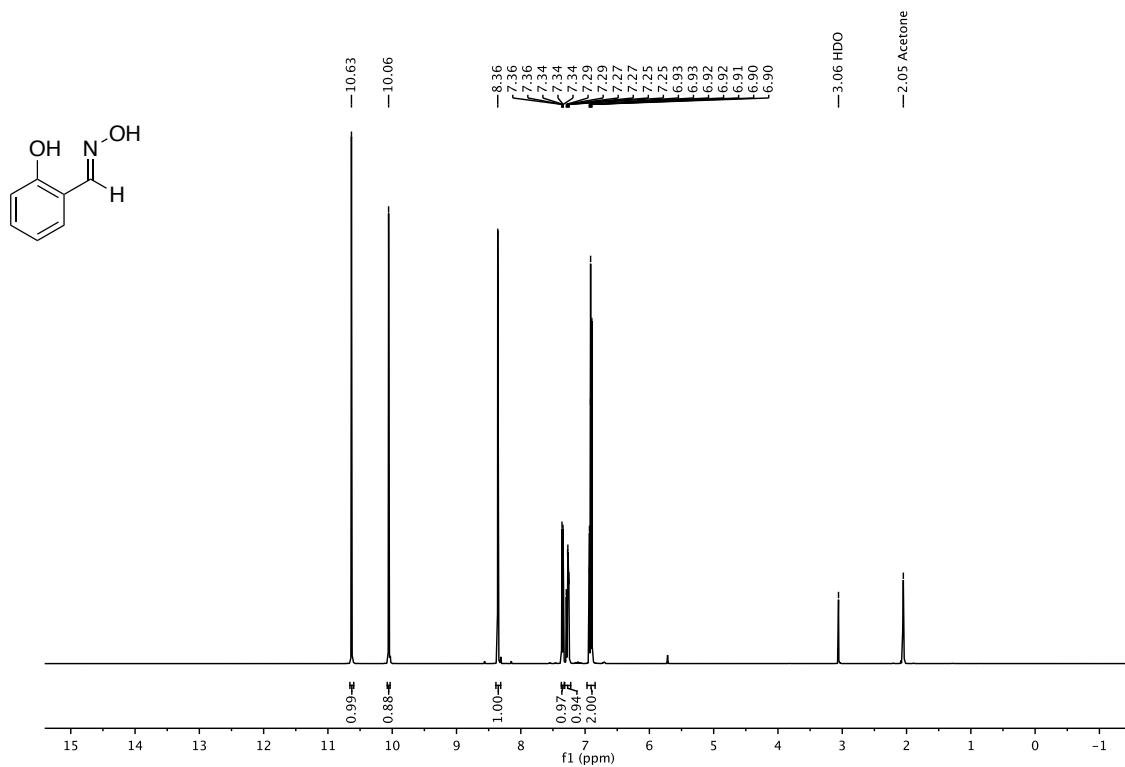
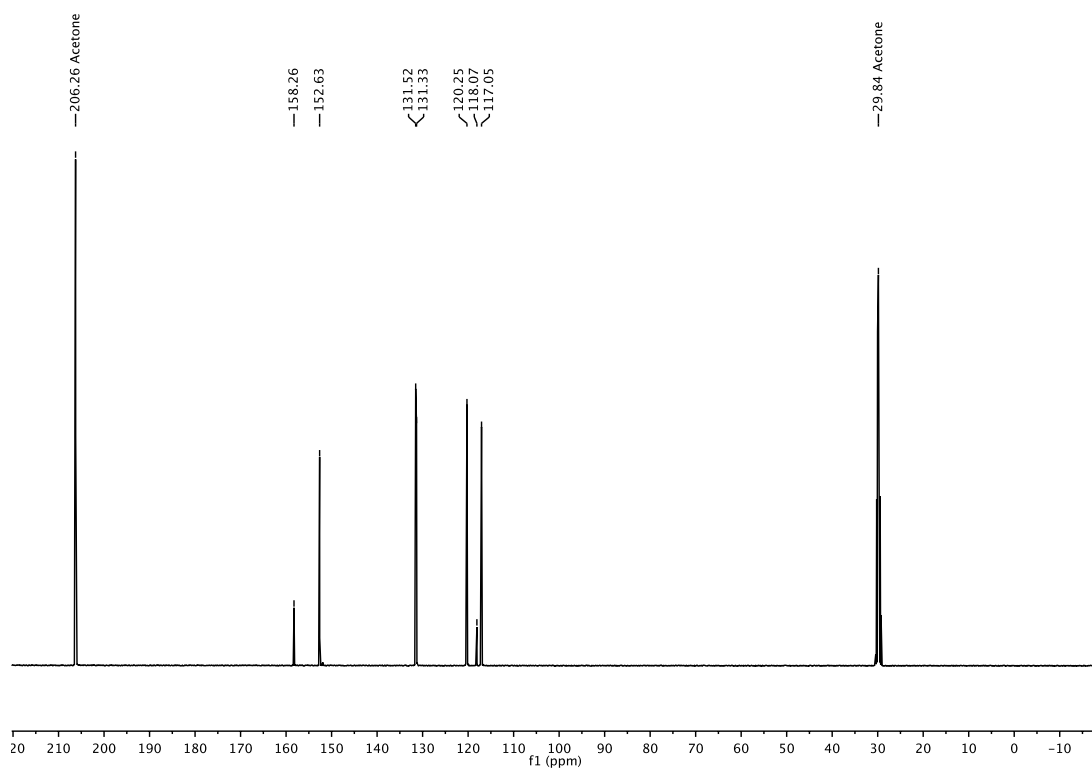
## 2-(6-Methoxypyridin-2-yl)phenol (L108)

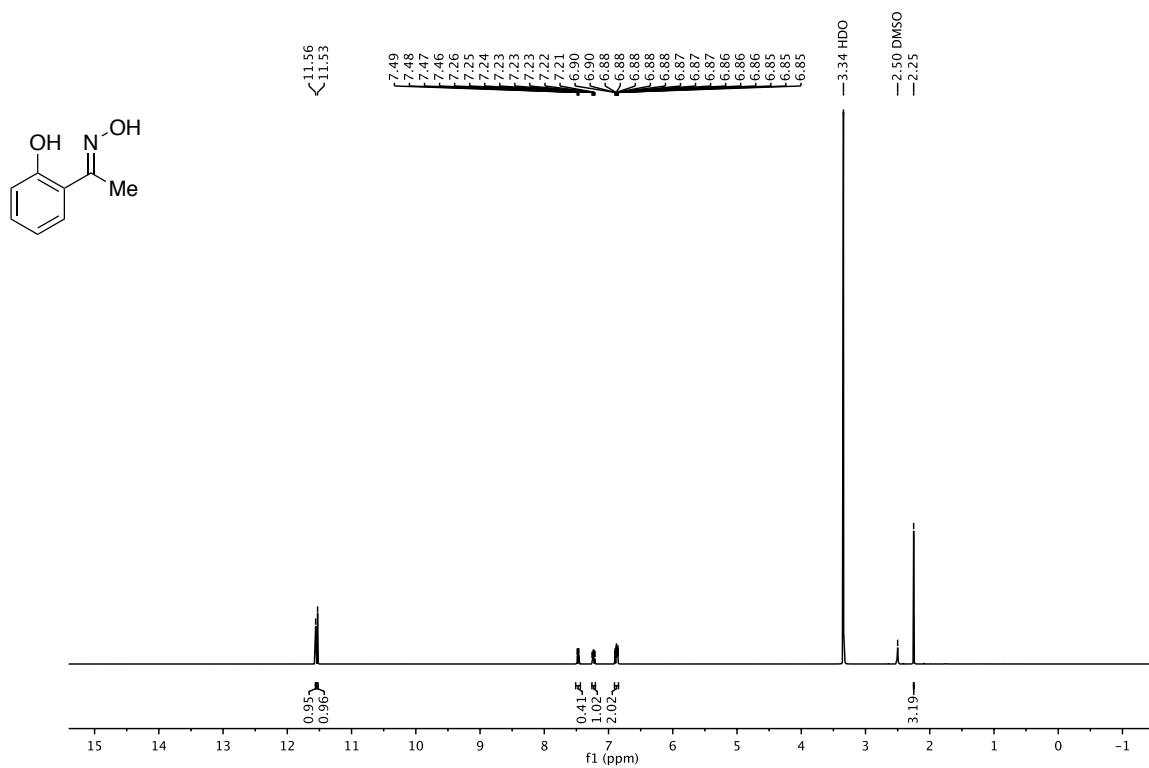
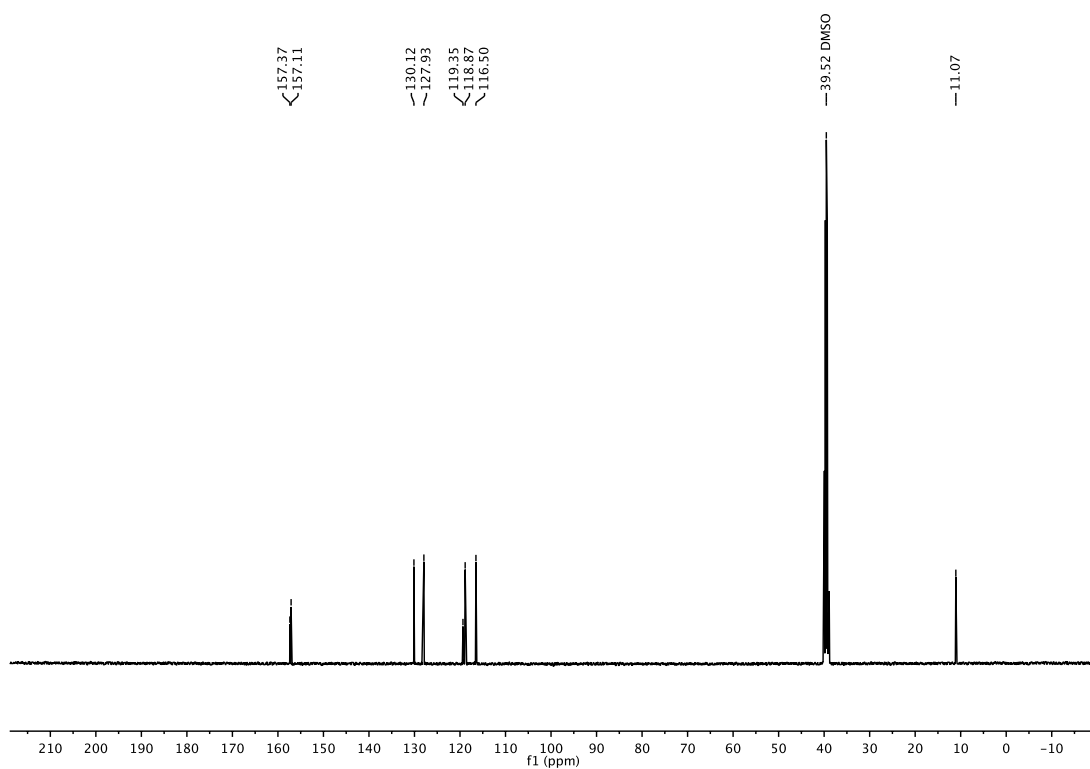
 $^1\text{H-NMR}$  (400 MHz, acetone- $d_6$ ) $^{13}\text{C-NMR}$  (101 MHz, acetone- $d_6$ )

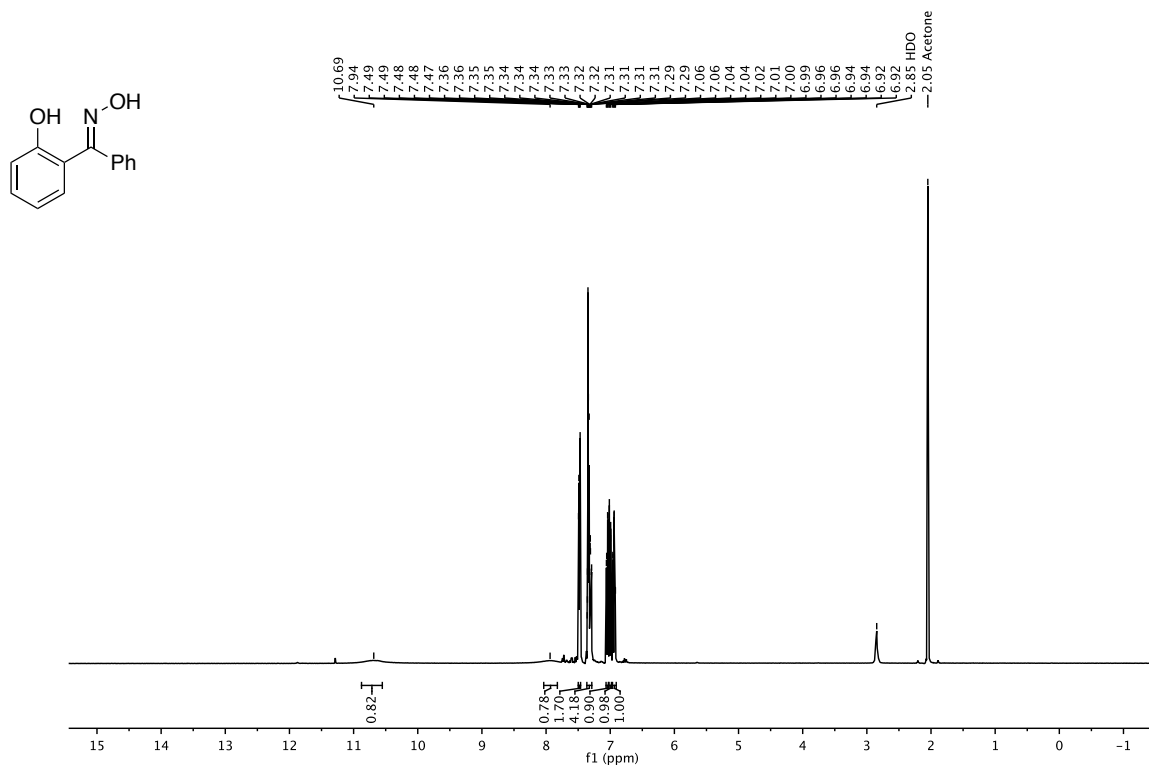
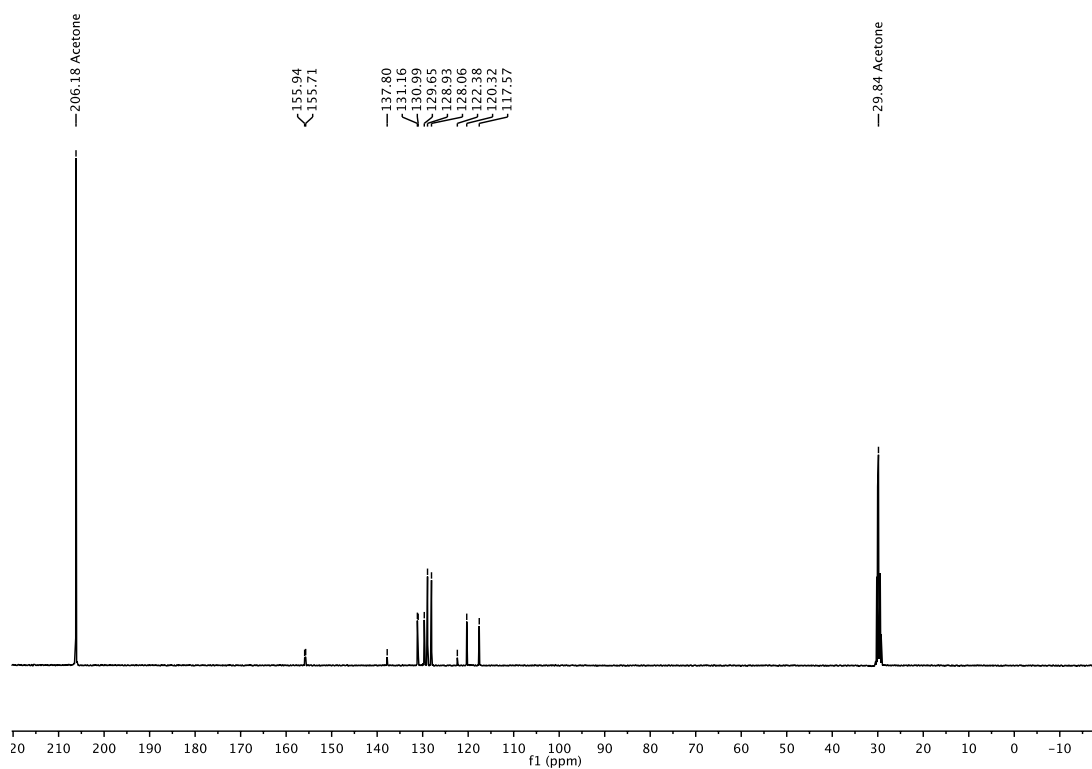


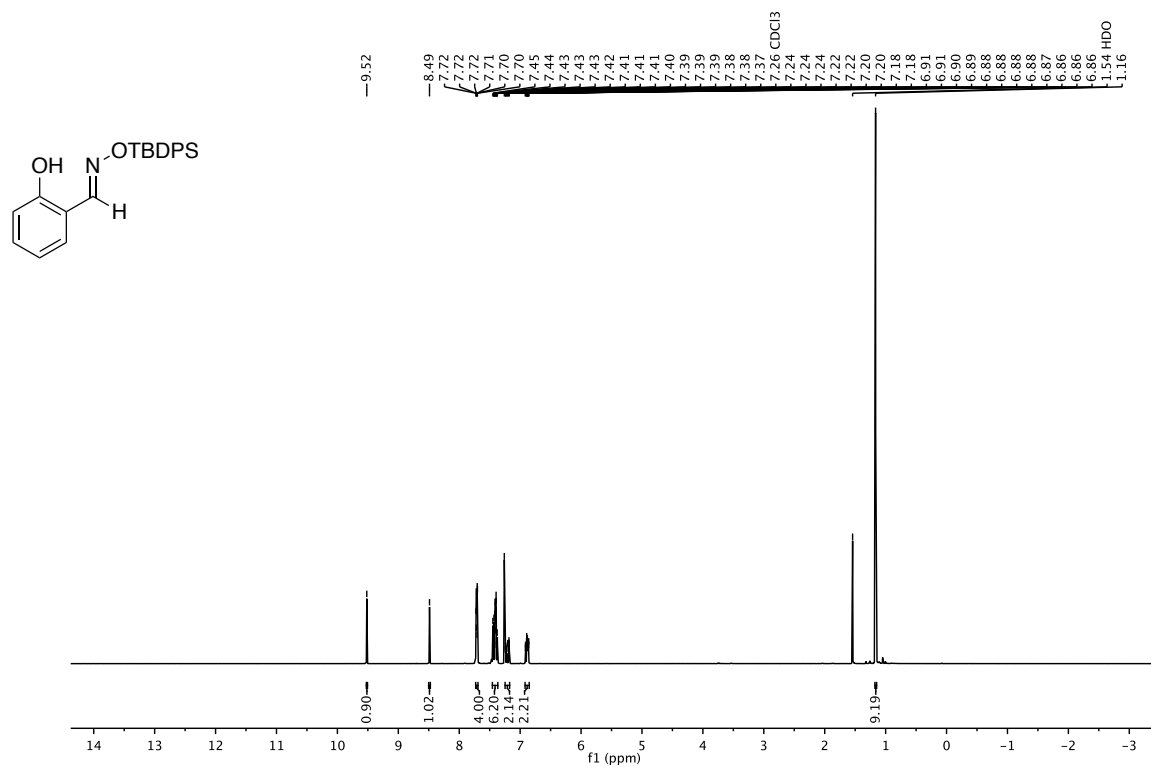
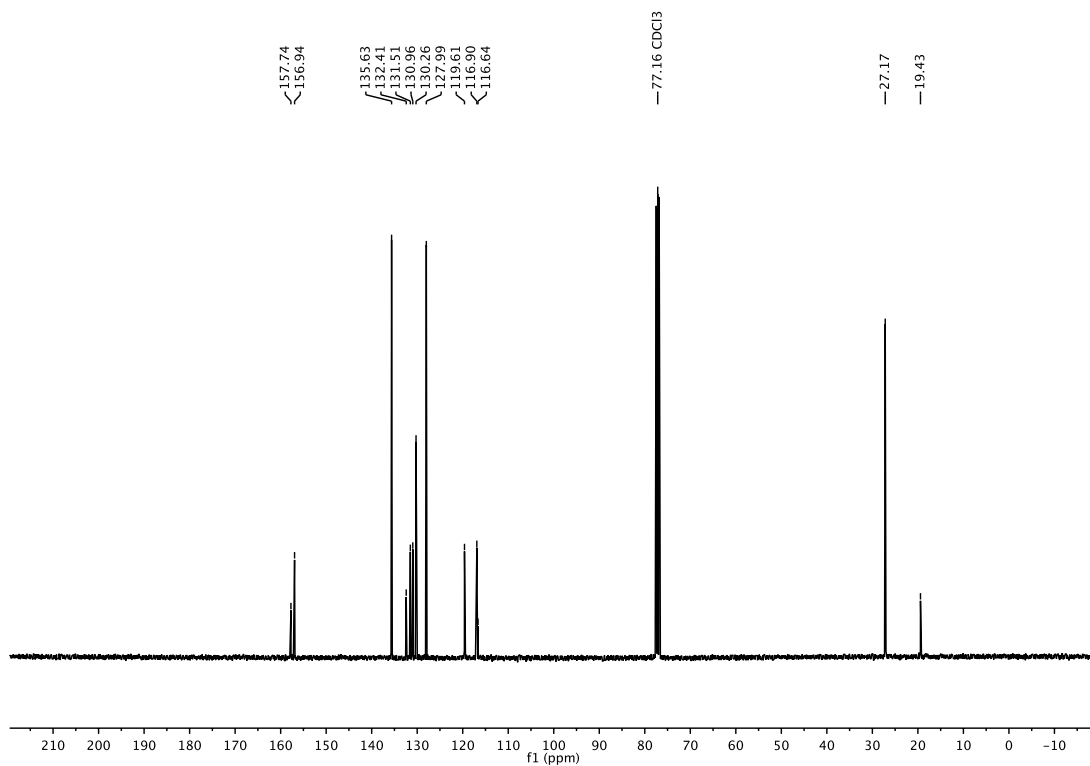
## 2-(2-Hydroxyphenyl)isonicotinonitrile (L110)

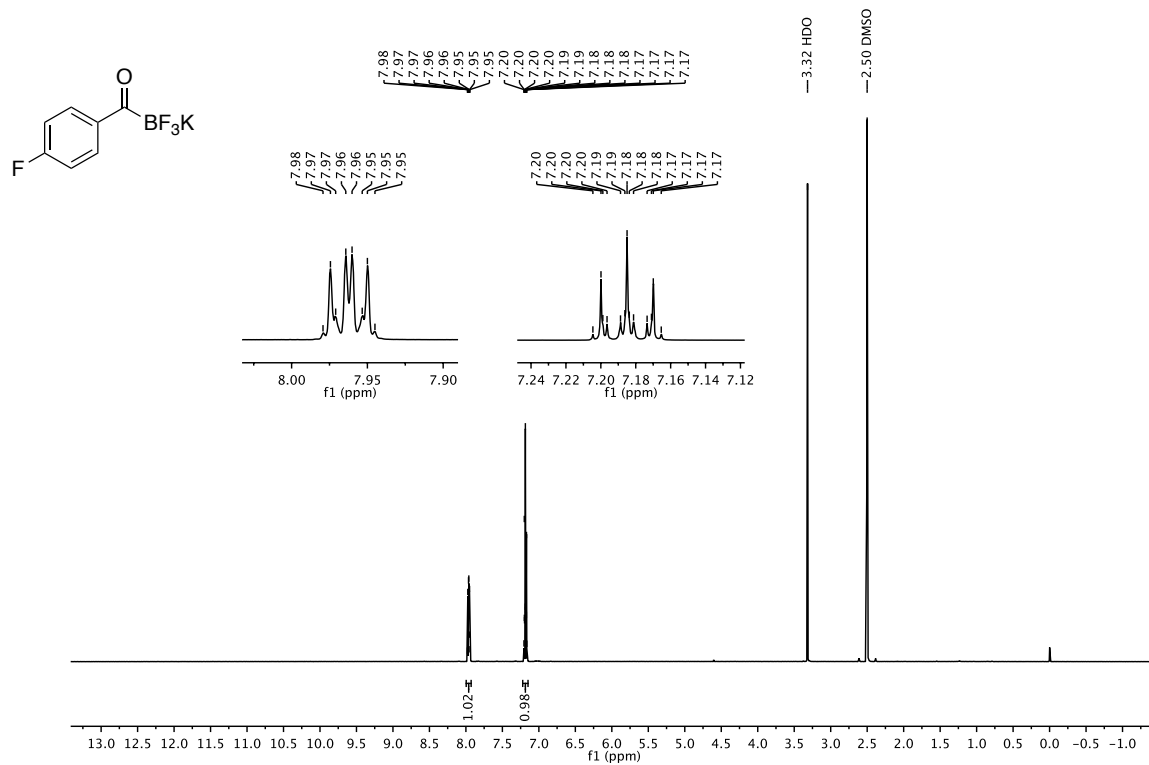
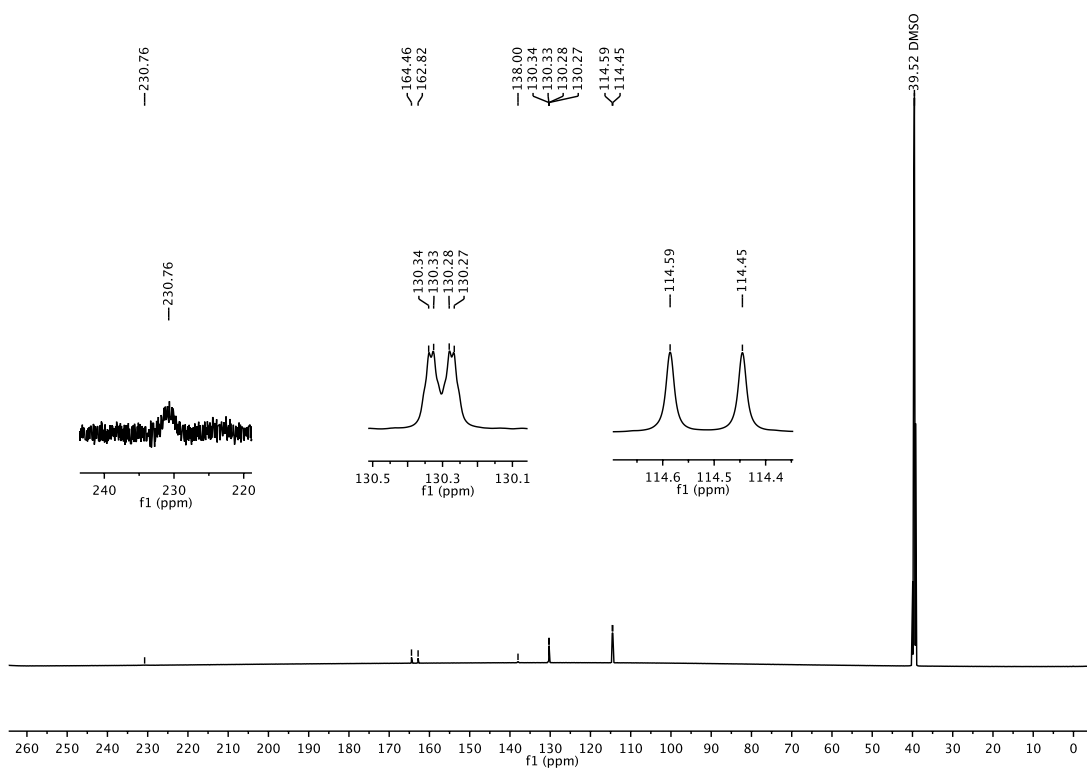
 $^1\text{H-NMR}$  (400 MHz, acetone- $d_6$ ) $^{13}\text{C-NMR}$  (101 MHz, acetone- $d_6$ )

**2-Hydroxybenzaldehyde oxime (L111)****<sup>1</sup>H-NMR (400 MHz, acetone-d<sub>6</sub>)****<sup>13</sup>C-NMR (101 MHz, acetone-d<sub>6</sub>)**

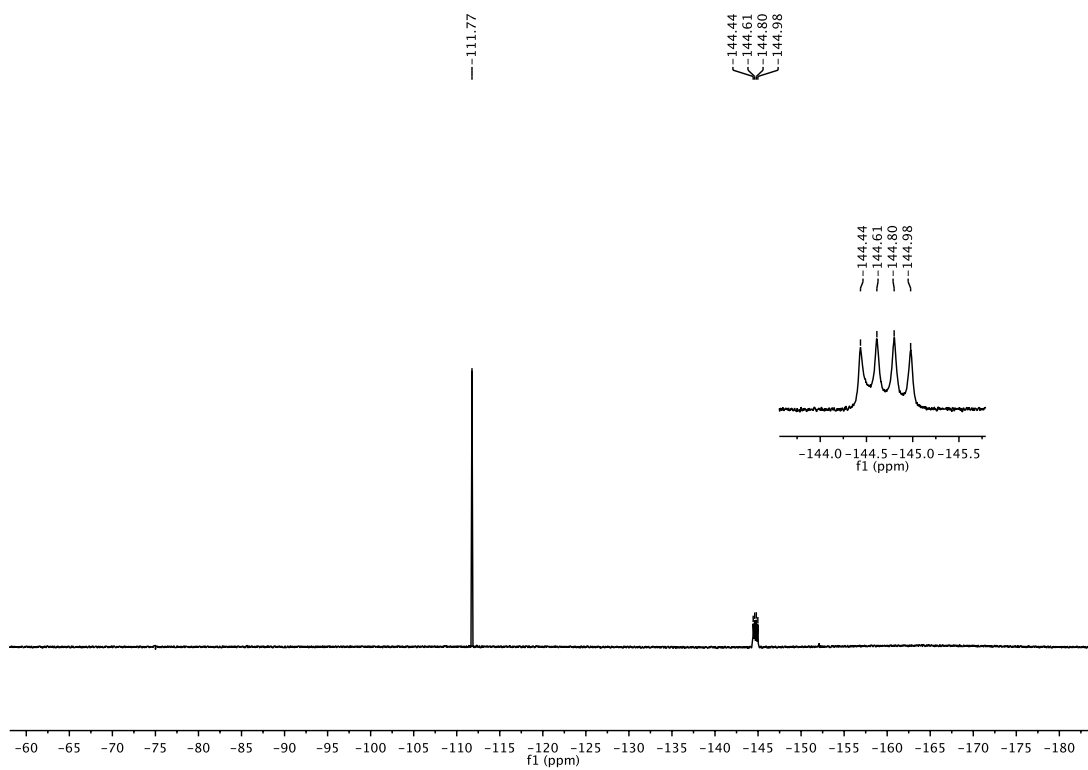
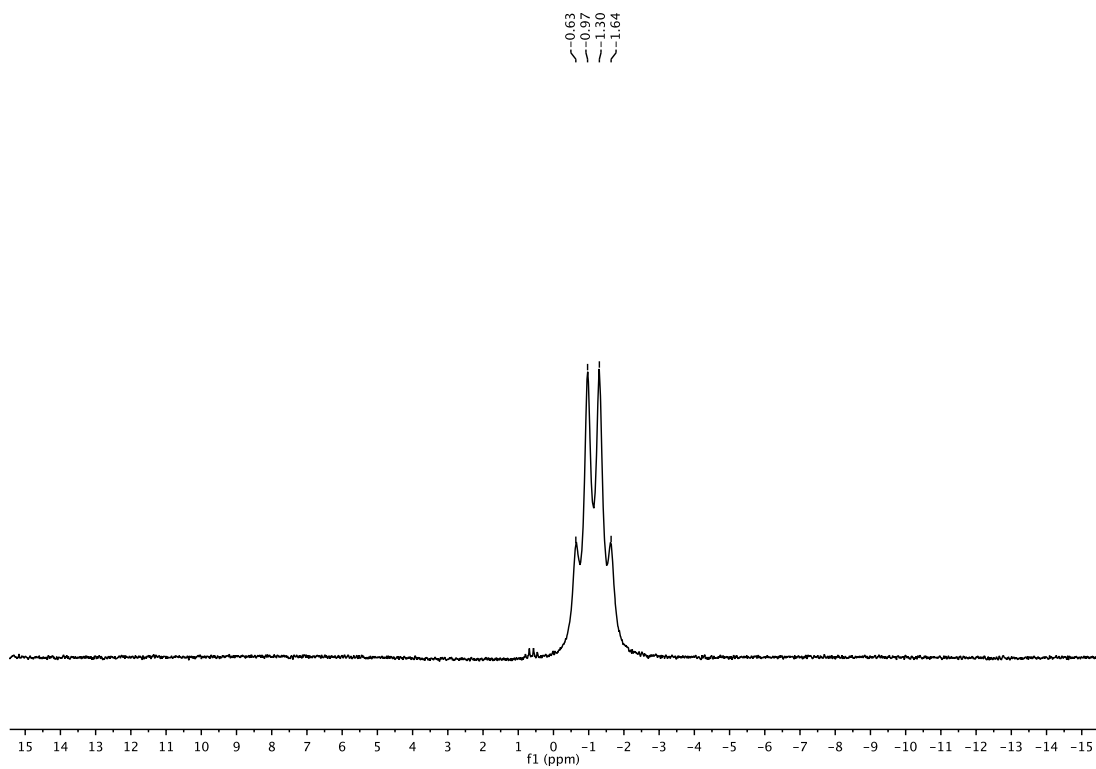
**2-Hydroxyacetophenone oxime (L112)****<sup>1</sup>H-NMR (400 MHz, DMSO-*d*<sub>6</sub>)****<sup>13</sup>C-NMR (101 MHz, DMSO-*d*<sub>6</sub>)**

**2-Hydroxybenzophenone oxime (L113)****<sup>1</sup>H-NMR (400 MHz, acetone-*d*<sub>6</sub>)****<sup>13</sup>C-NMR (101 MHz, acetone-*d*<sub>6</sub>)**

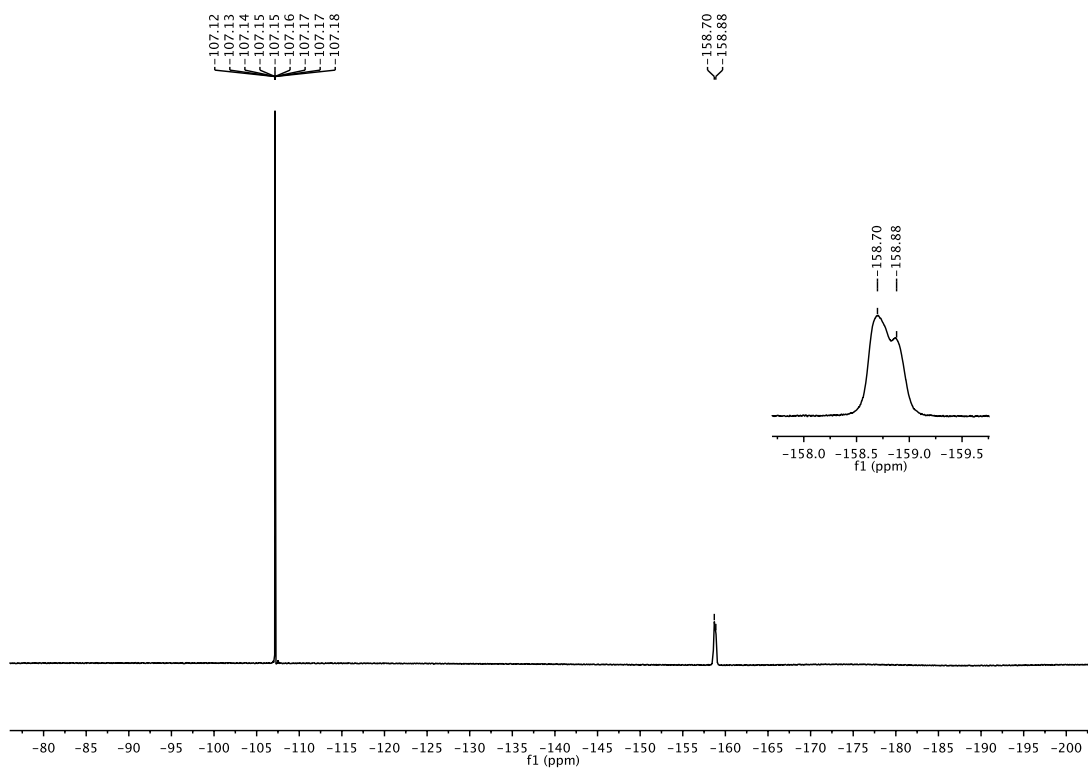
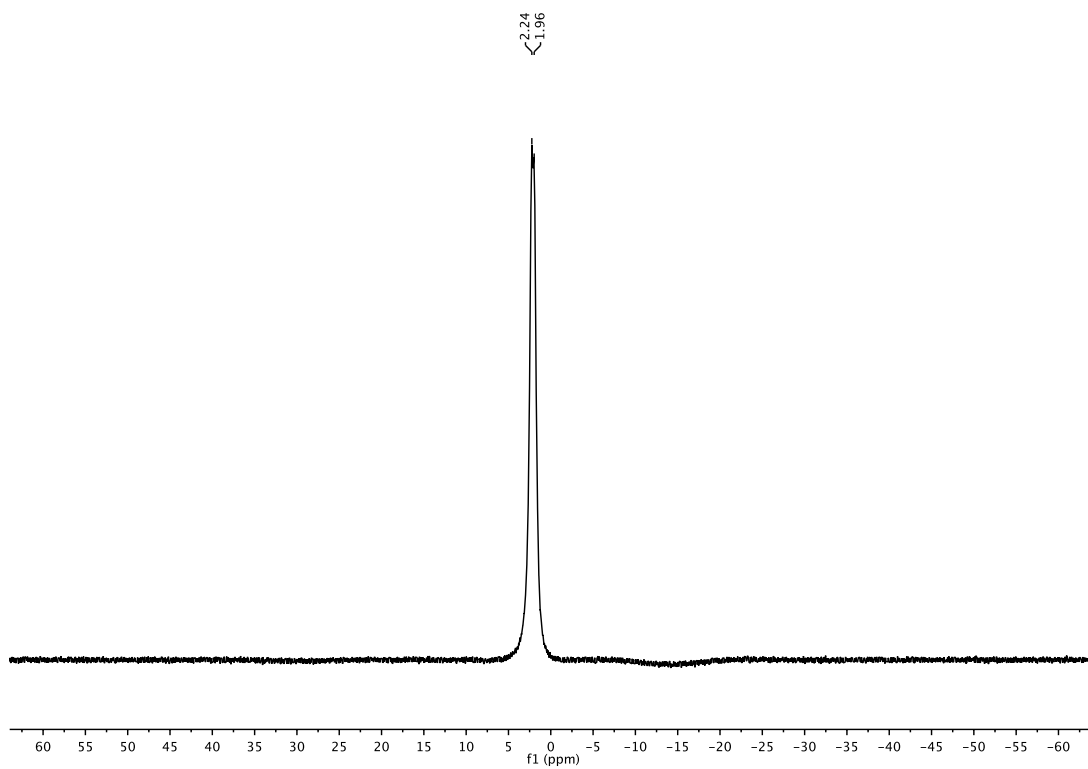
**2-Hydroxybenzaldehyde O-(*tert*-butyldiphenylsilyl) oxime (L114)****<sup>1</sup>H-NMR (400 MHz, CDCl<sub>3</sub>)****<sup>13</sup>C-NMR (101 MHz, CDCl<sub>3</sub>)**

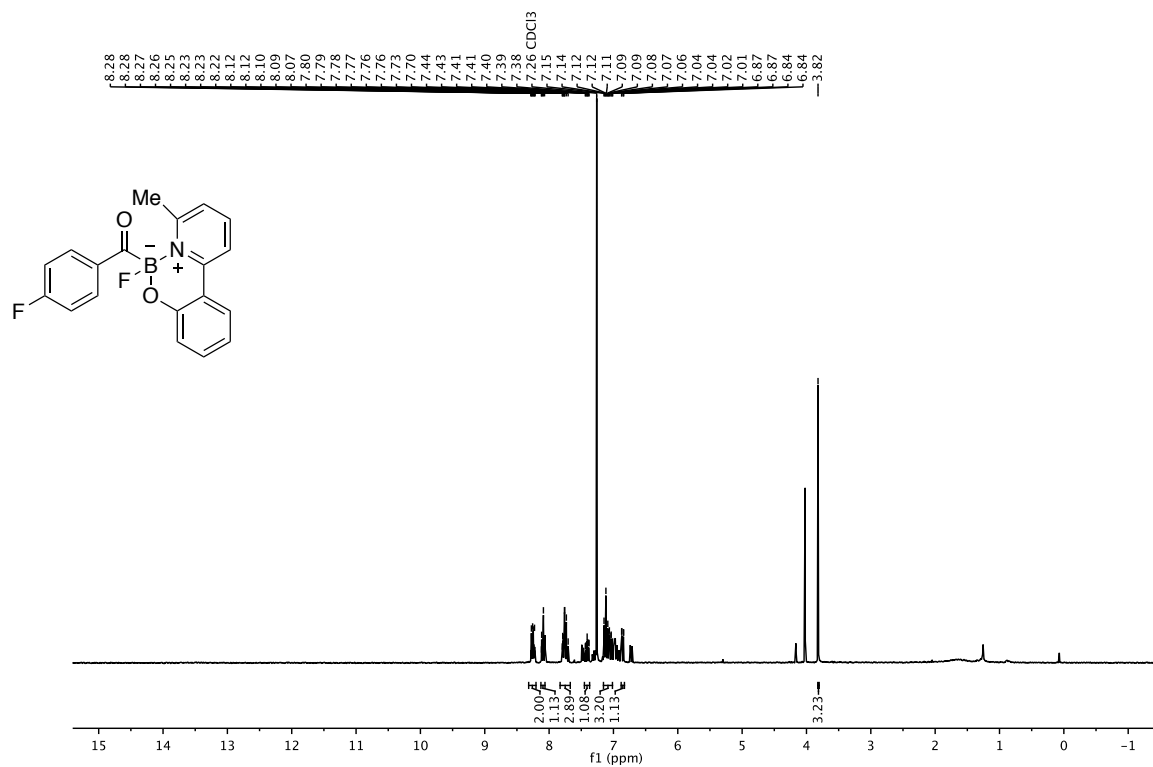
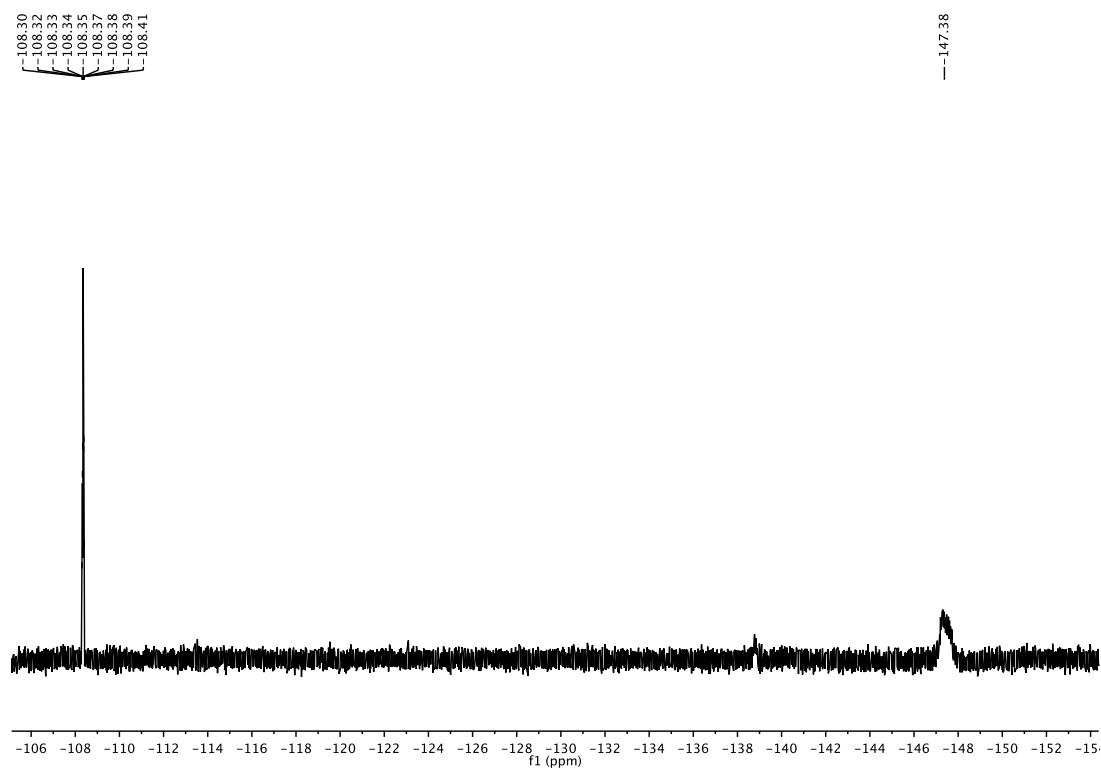
**Potassium 4-fluorobenzoyltrifluoroborate (100)****<sup>1</sup>H-NMR (600 MHz, DMSO-*d*<sub>6</sub>)****<sup>13</sup>C-NMR (151 MHz, DMSO-*d*<sub>6</sub>)**



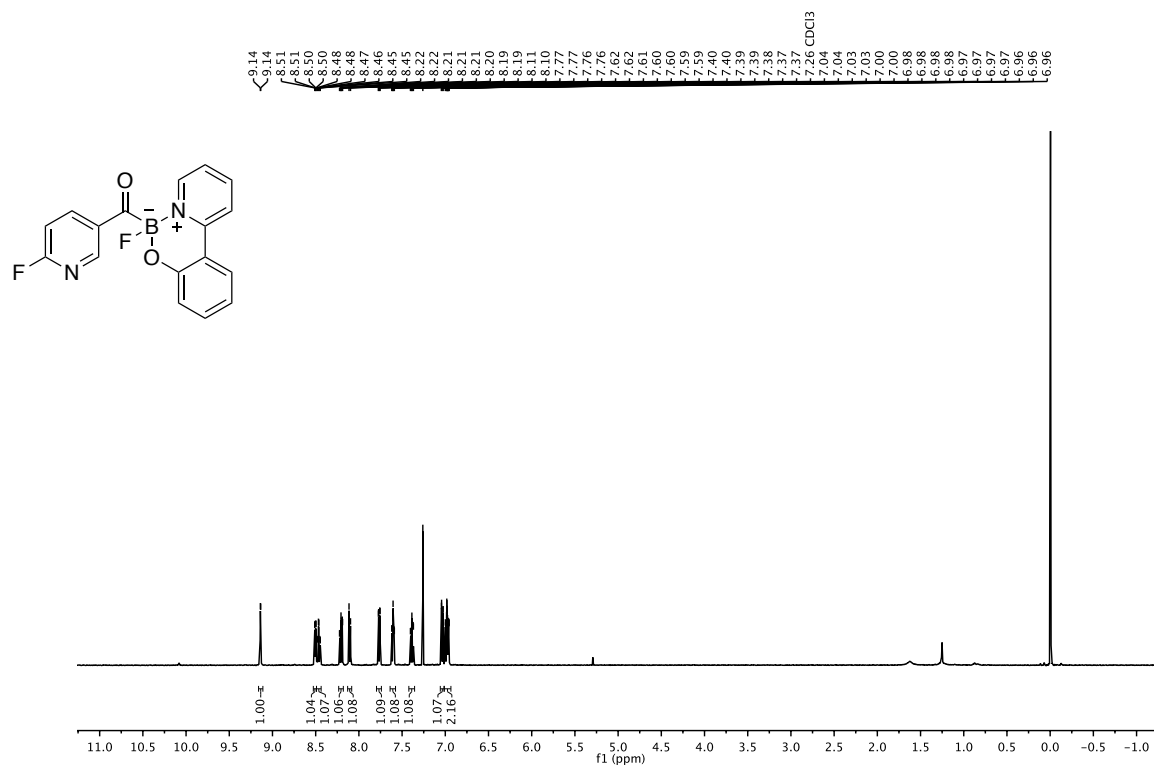
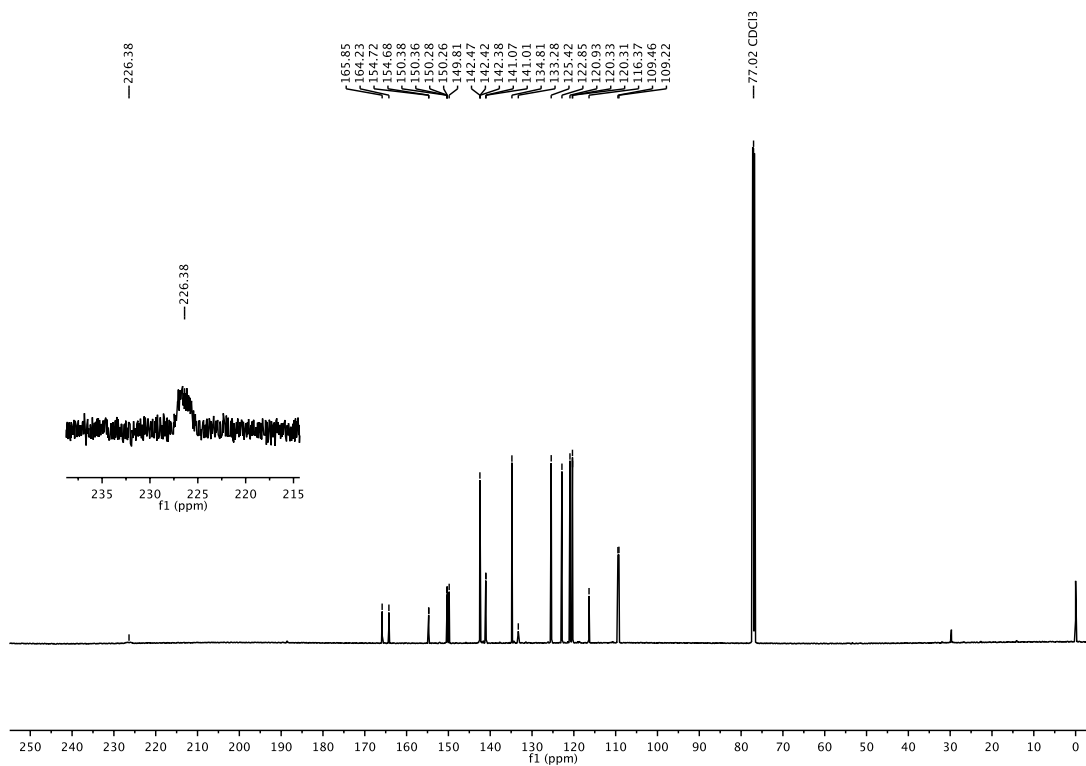
**$^{19}\text{F}$ -NMR (282 MHz, acetone- $d_6$ )** **$^{11}\text{B}$ -NMR (160 MHz, DMSO- $d_6$ )**

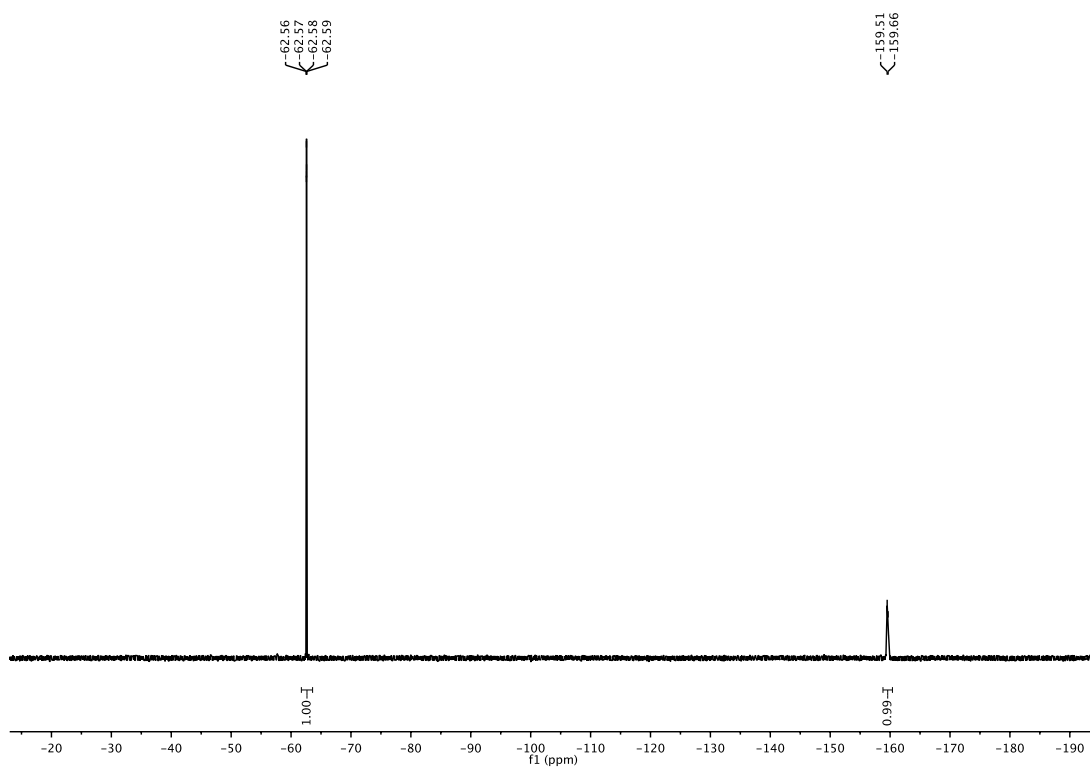
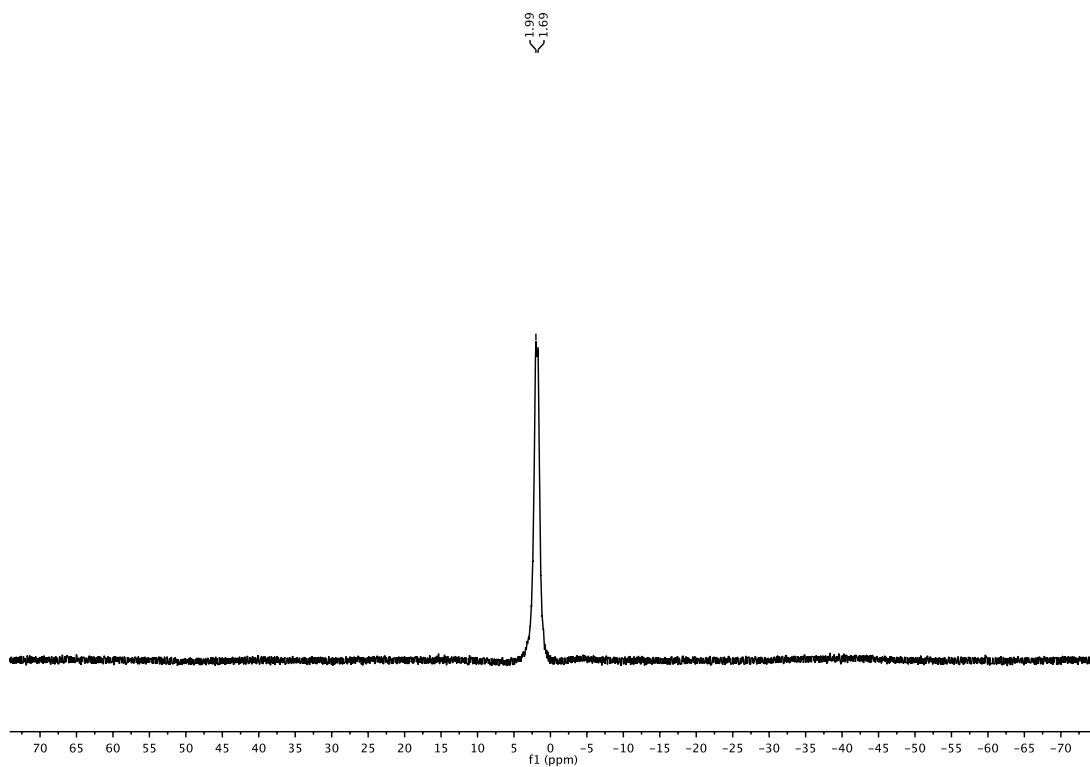


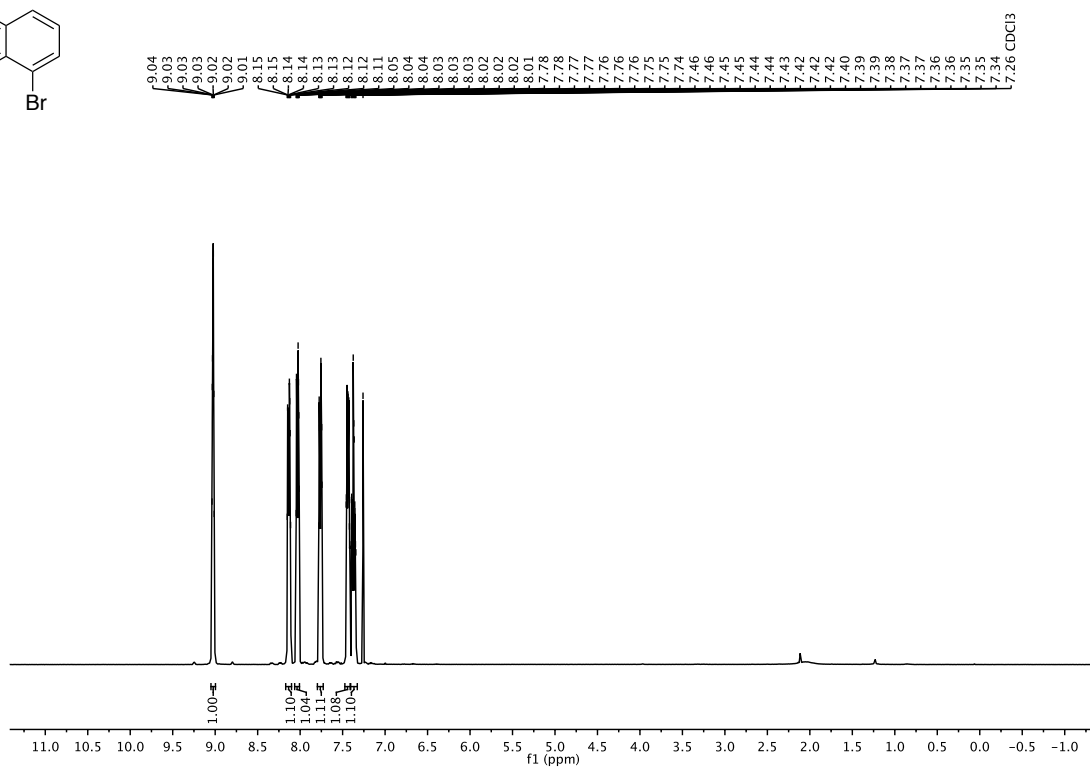
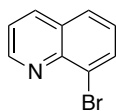
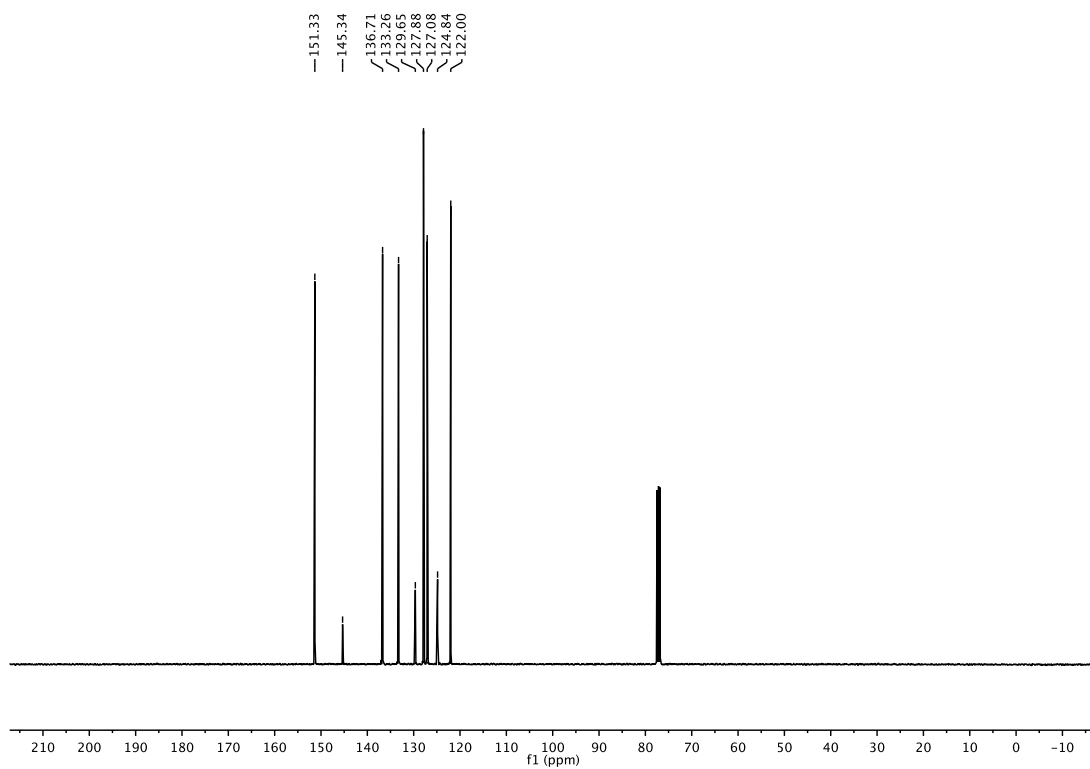
**$^{19}\text{F}$ -NMR (470 MHz,  $\text{CDCl}_3$ )** **$^{11}\text{B}$ -NMR (160 MHz,  $\text{CDCl}_3$ )**

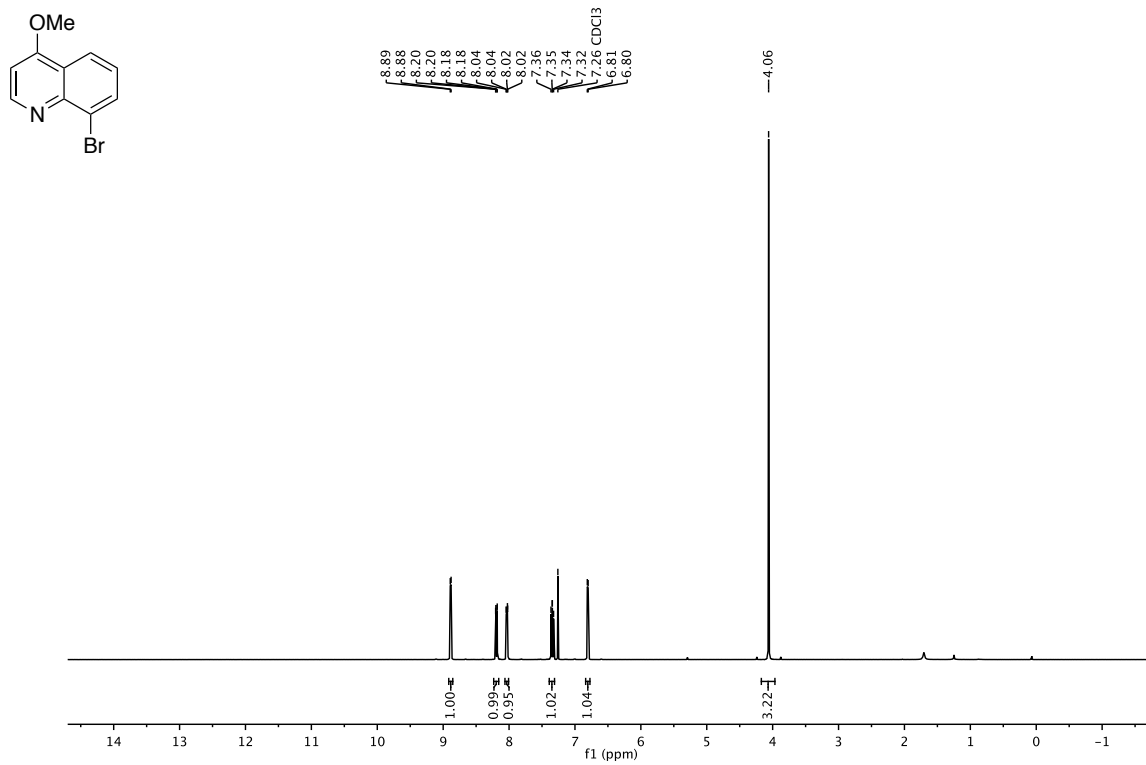
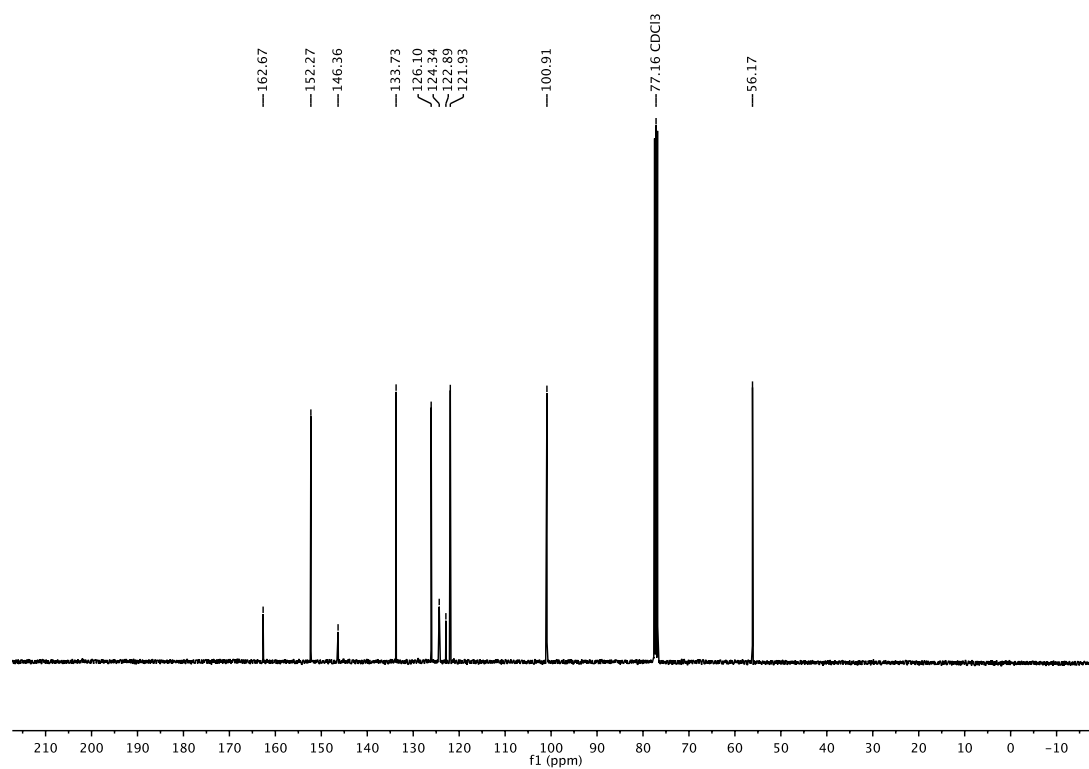
**4-Fluorophenyl monofluoroboronate from 2-(6-methylpyridin-2-yl)phenol ligand (S3)** **$^1\text{H-NMR}$  (300 MHz,  $\text{CDCl}_3$ )** **$^{19}\text{F-NMR}$  (470 MHz,  $\text{CDCl}_3$ )**

## 2-fluoro-5-monofluoroboronate (158)

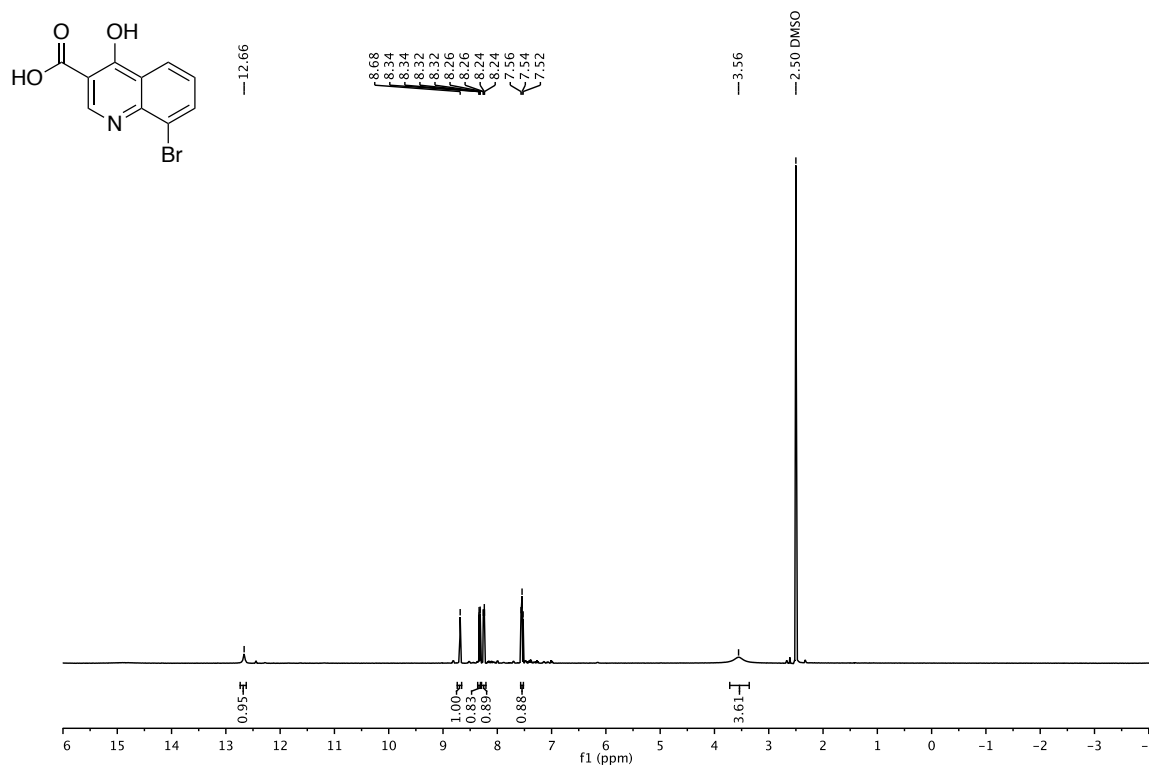
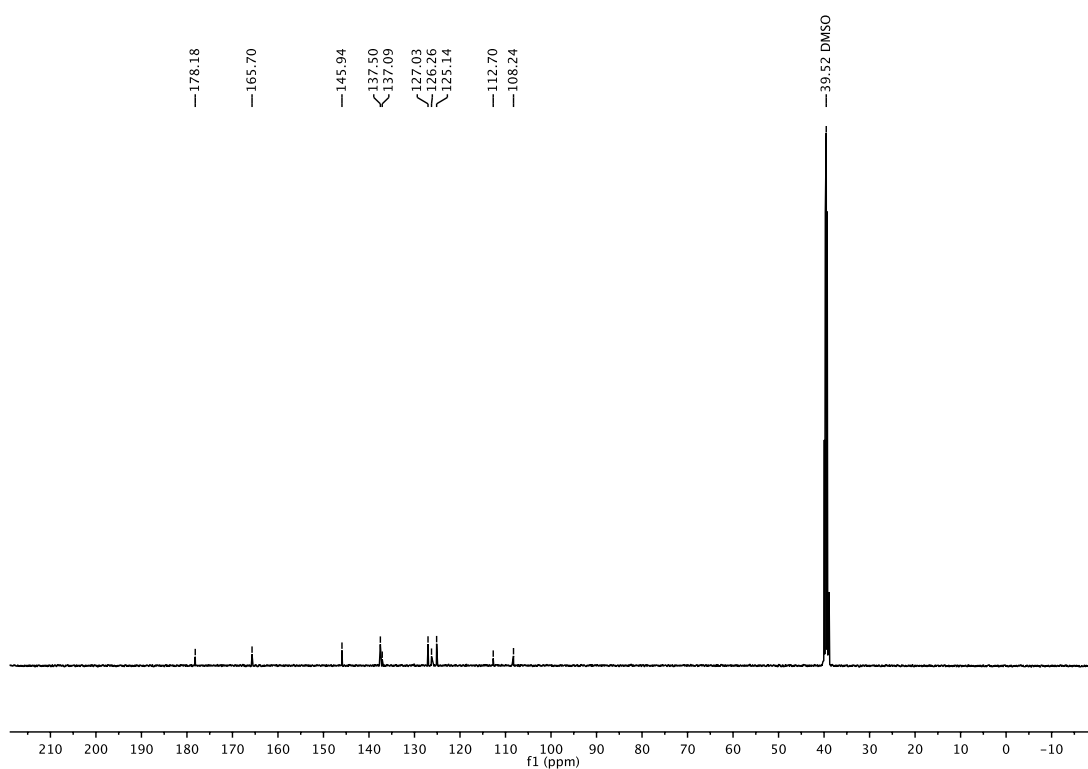
 $^1\text{H-NMR}$  (600 MHz,  $\text{CDCl}_3$ ) $^{13}\text{C-NMR}$  (150 MHz,  $\text{CDCl}_3$ )

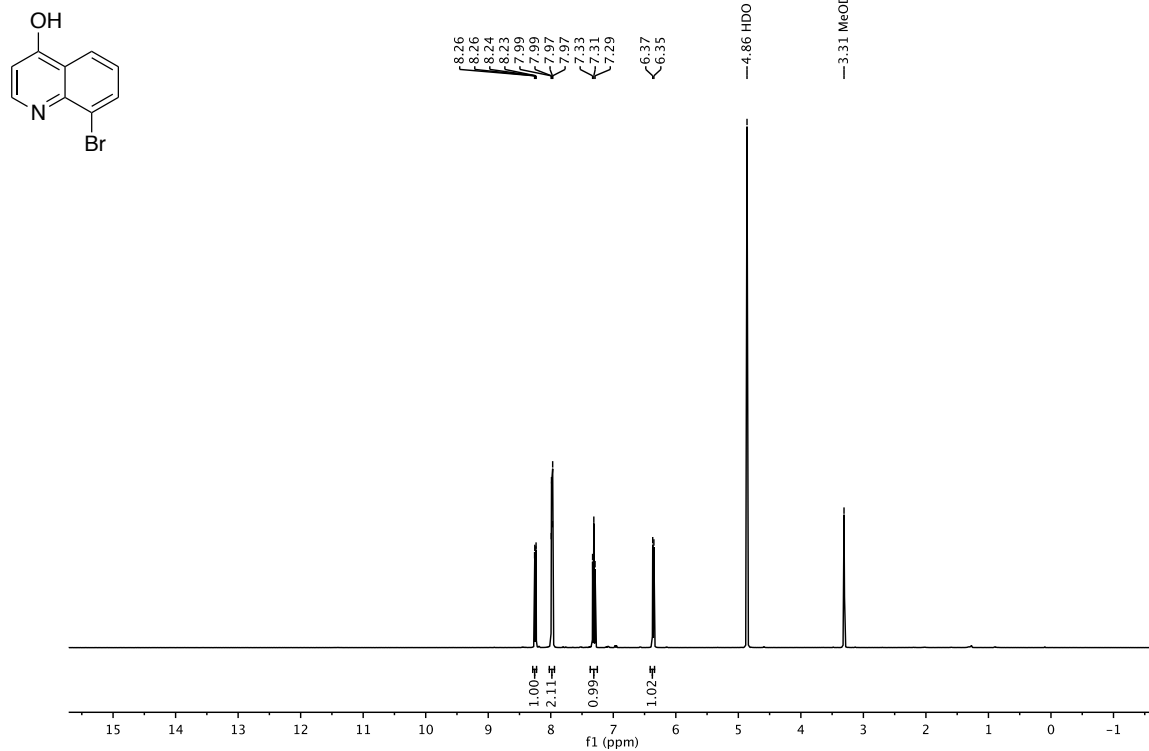
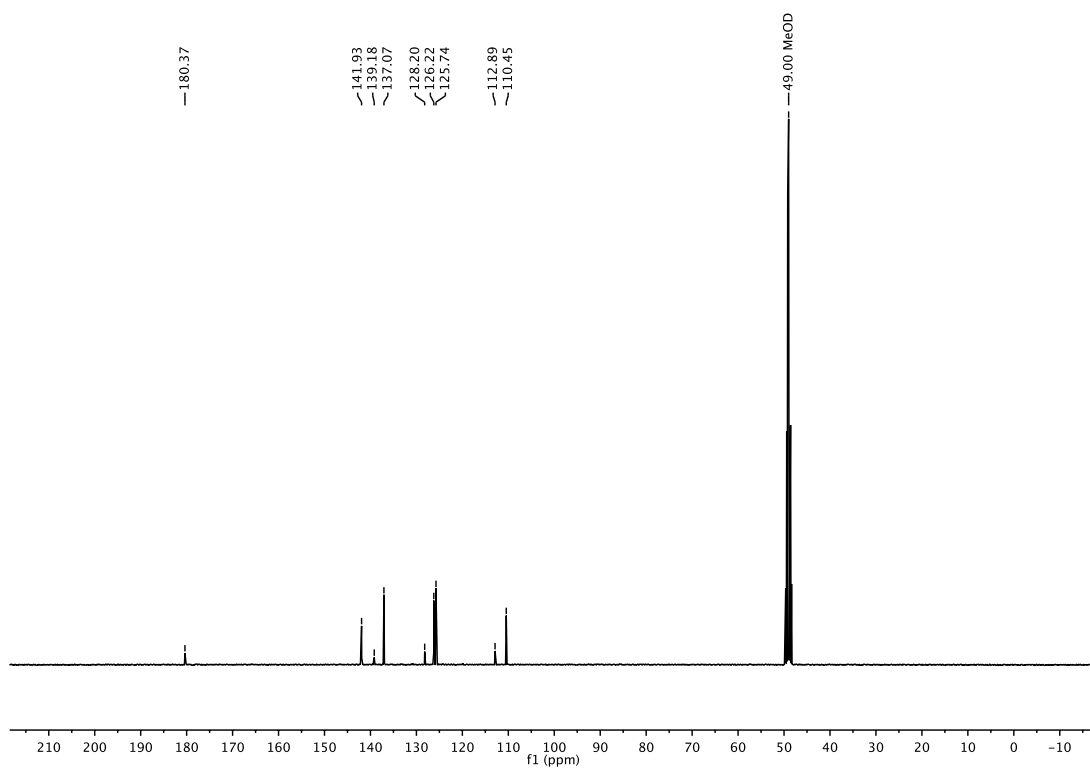
**$^{19}\text{F}$ -NMR (470 MHz,  $\text{CDCl}_3$ )** **$^{11}\text{B}$ -NMR (600 MHz,  $\text{CDCl}_3$ )**

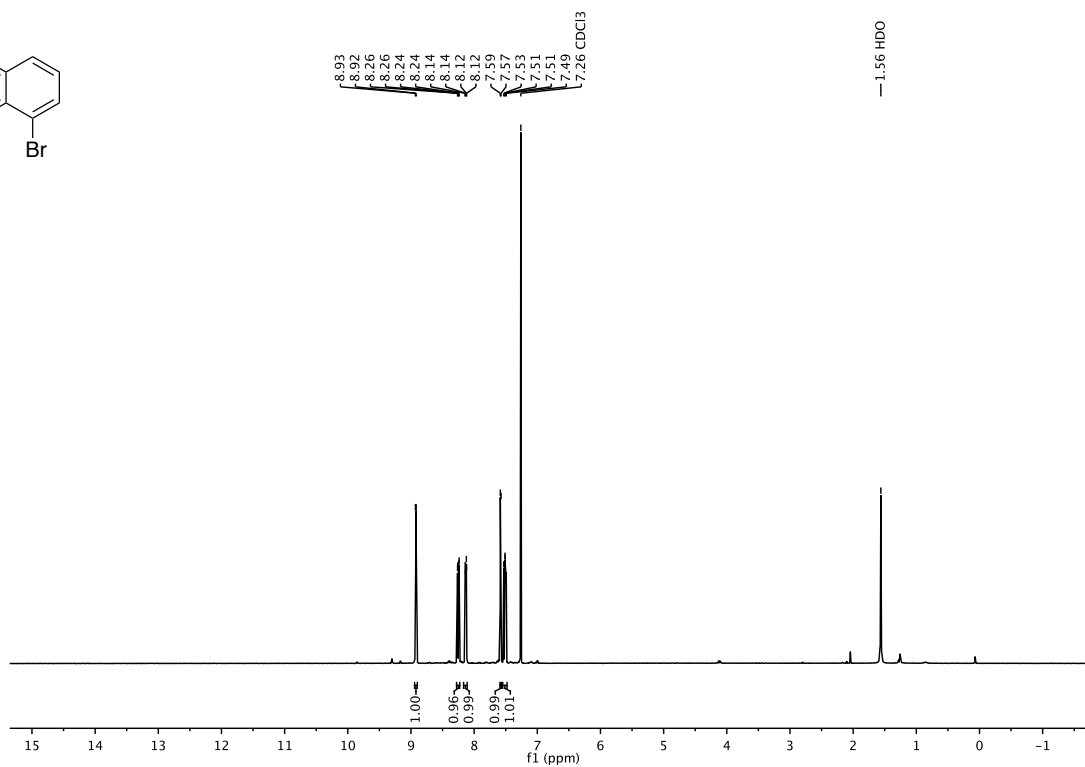
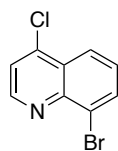
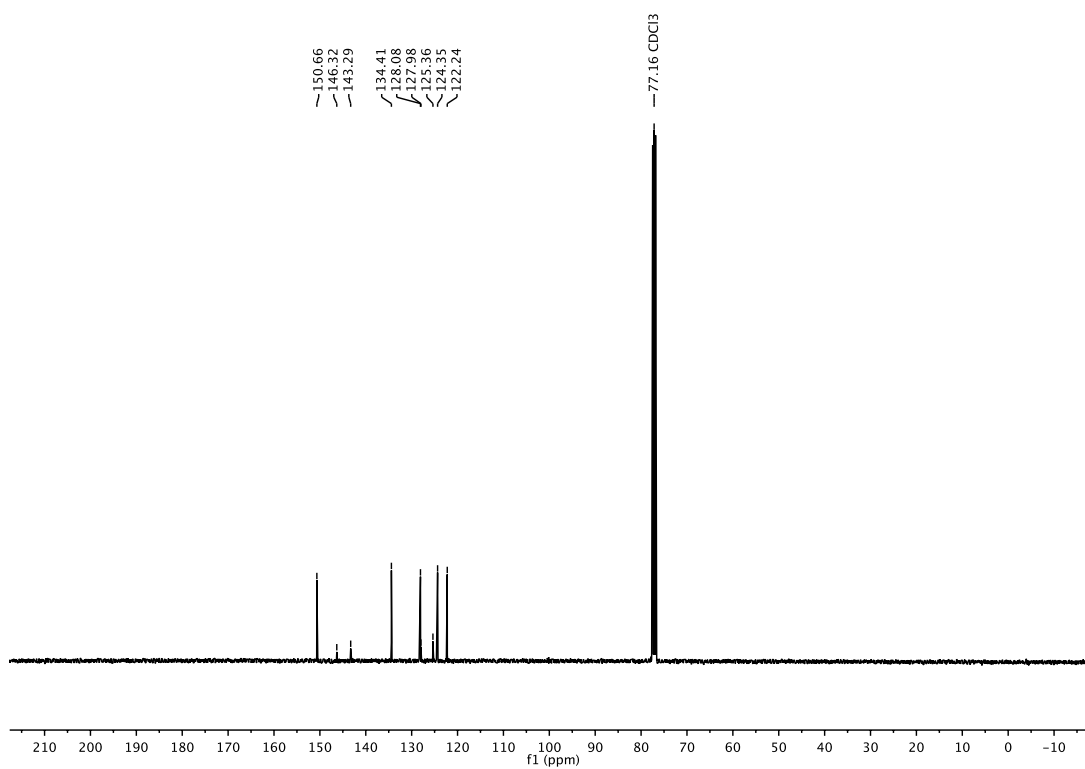
**8-Bromoquinoline (178)****<sup>1</sup>H-NMR (400 MHz, CDCl<sub>3</sub>)****<sup>13</sup>C-NMR (101 MHz, CDCl<sub>3</sub>)**

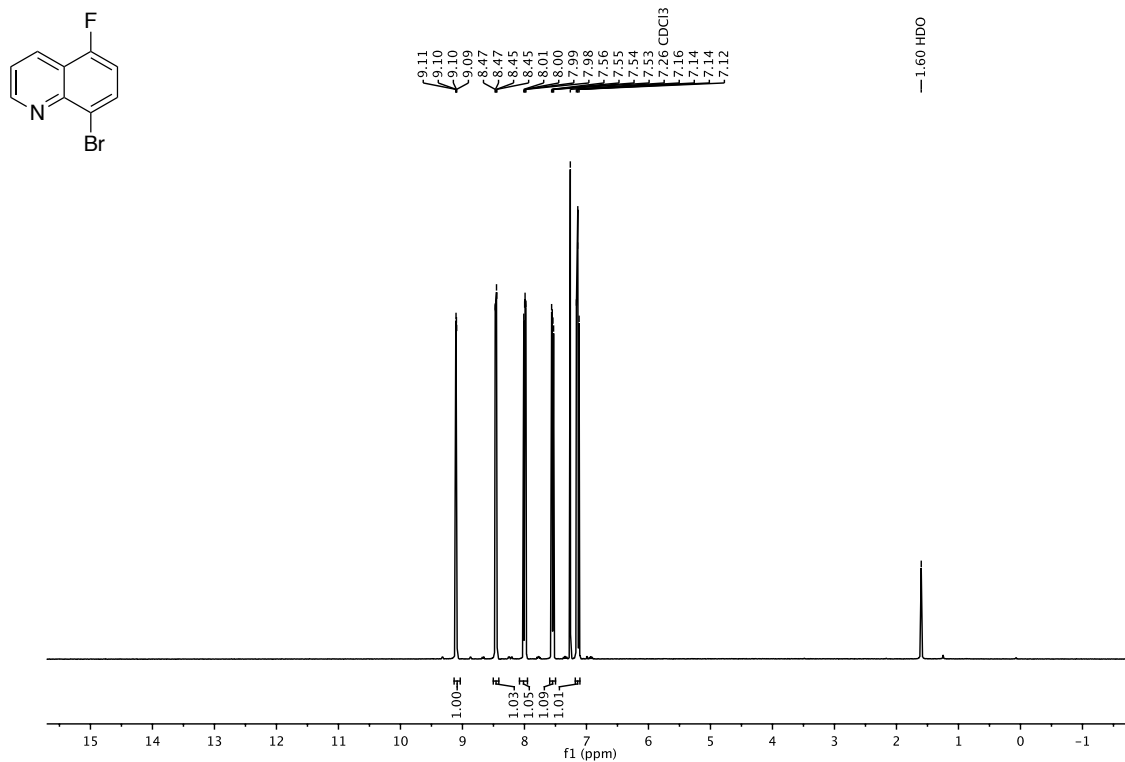
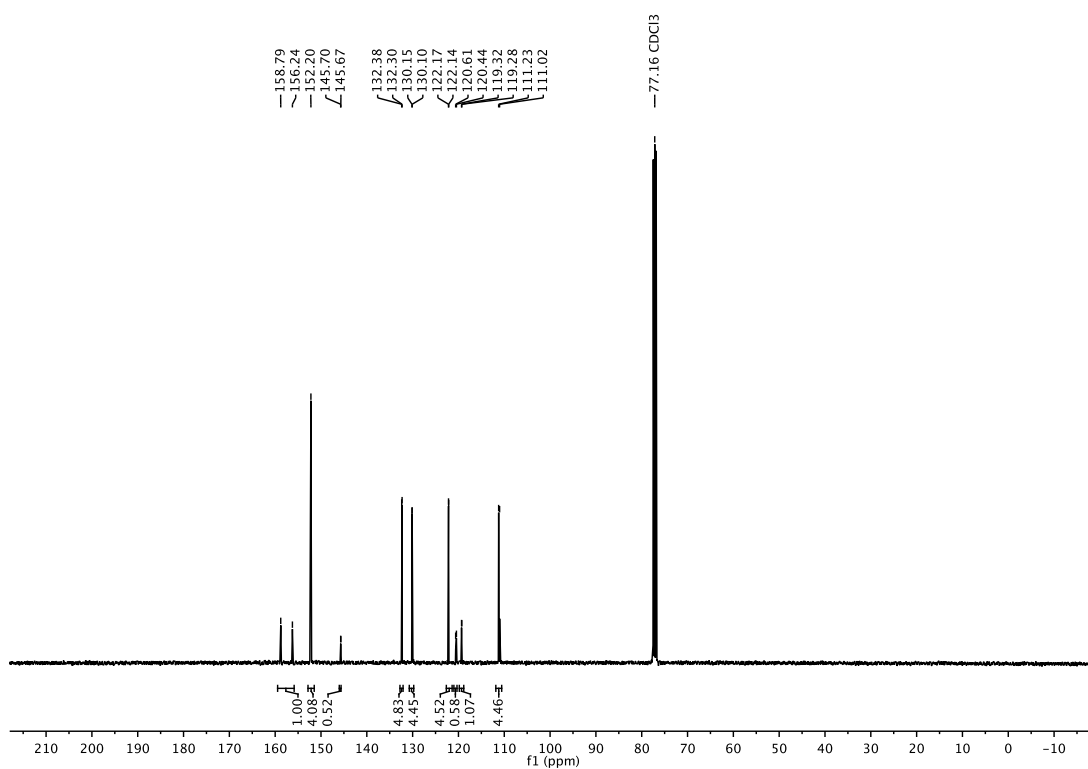
**8-Bromo-4-methoxyquinoline (S4)****<sup>1</sup>H-NMR (400 MHz, CDCl<sub>3</sub>)****<sup>13</sup>C-NMR (101 MHz, CDCl<sub>3</sub>)**



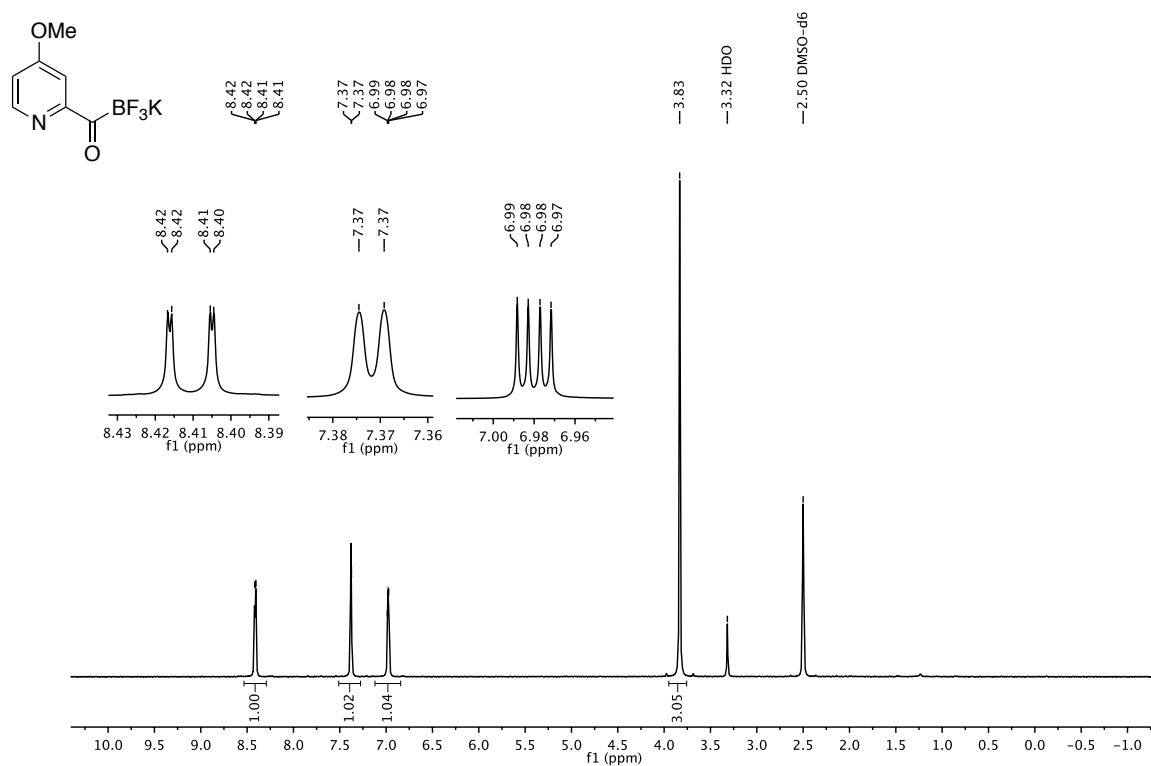
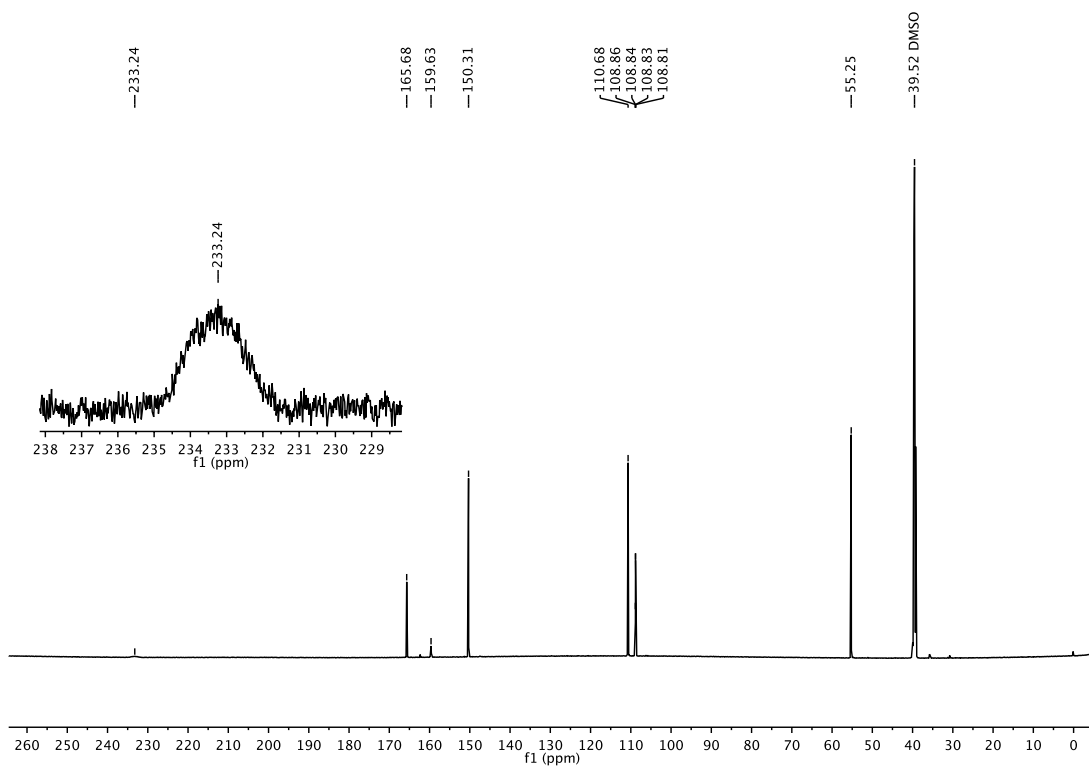
**8-Bromo-3-carbethoxy-4-hydroxyquinoline (S5)** **$^1\text{H-NMR}$  (500 MHz,  $\text{CDCl}_3$ )** **$^{13}\text{C-NMR}$  (101 MHz,  $\text{DMSO-}d_6$ )**

**8-Bromo-4-hydroxyquinoline (S6)****<sup>1</sup>H-NMR (400 MHz, methanol-*d*<sub>4</sub>)****<sup>13</sup>C-NMR (101 MHz, methanol-*d*<sub>4</sub>)**

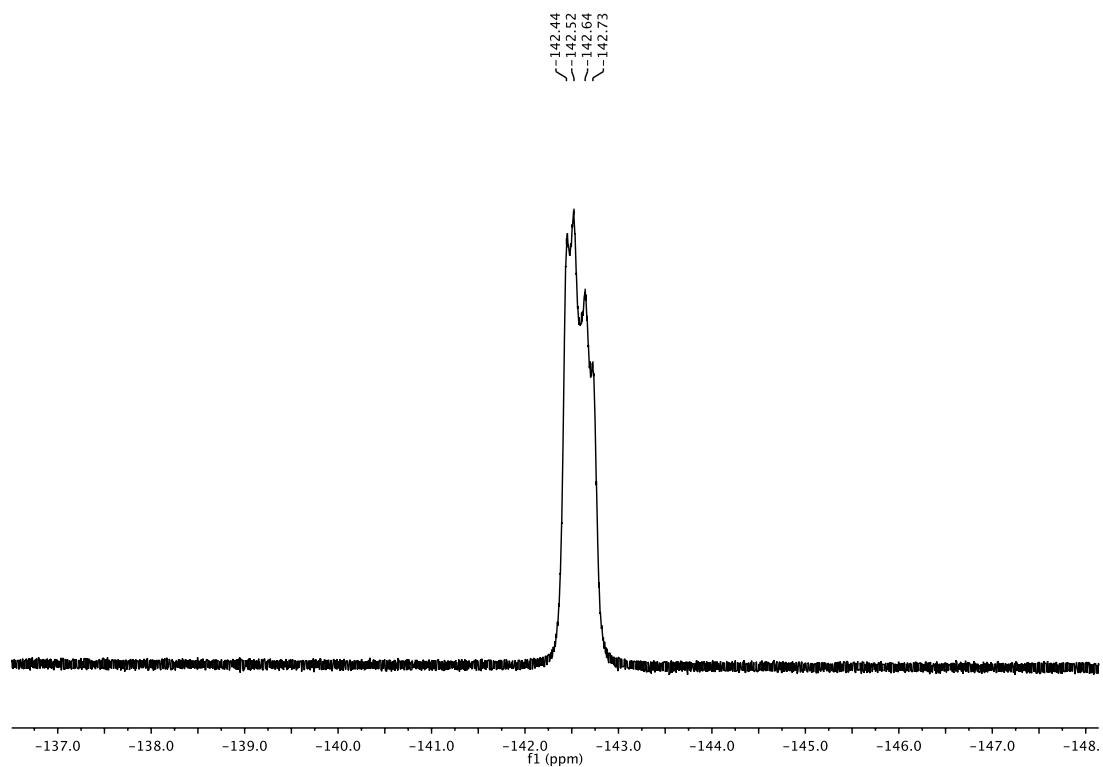
**8-Bromo-4-chloroquinoline (S7)****<sup>1</sup>H-NMR (400 MHz, CDCl<sub>3</sub>)****<sup>13</sup>C-NMR (101 MHz, CDCl<sub>3</sub>)**

**8-Bromo-5-fluoroquinoline (180)****<sup>1</sup>H-NMR (400 MHz, CDCl<sub>3</sub>)****<sup>13</sup>C-NMR (400 MHz, CDCl<sub>3</sub>)**

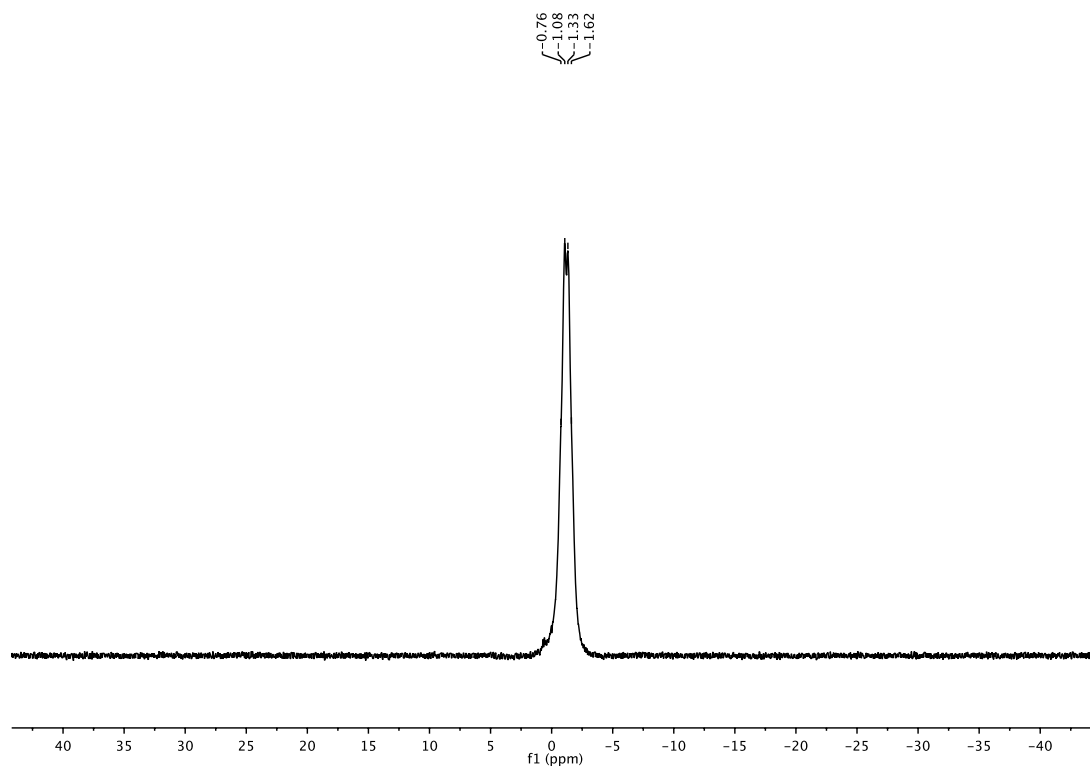
## Potassium 4-methoxy-2-isonicotinoyltrifluoroborate (127)

 $^1\text{H-NMR}$  (500 MHz,  $\text{DMSO-d}_6$ ) $^{13}\text{C-NMR}$  (150 MHz,  $\text{DMSO-d}_6$ )

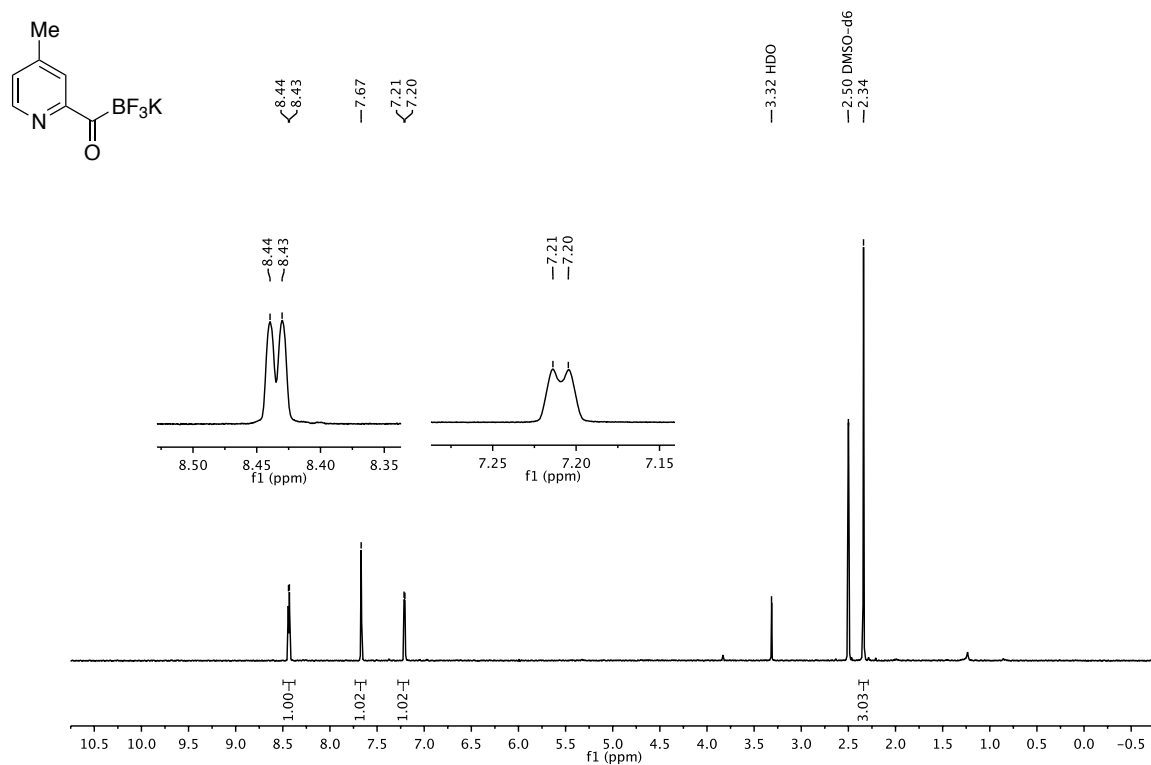
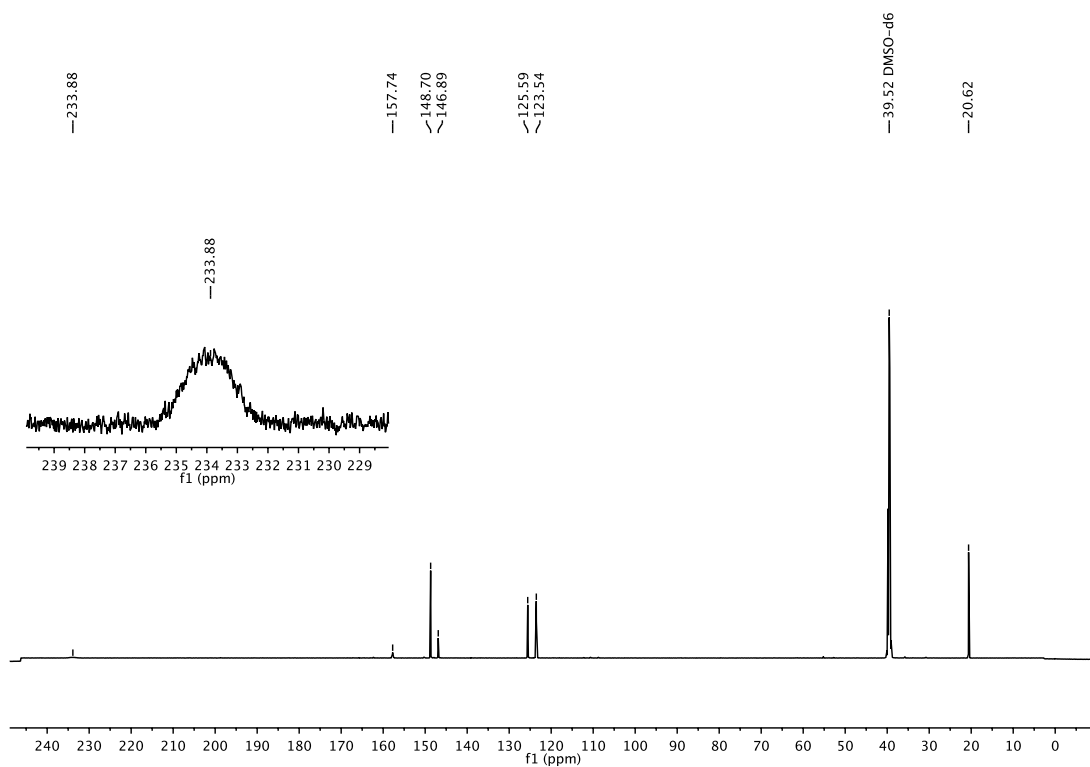
<sup>19</sup>F-NMR (470 MHz, DMSO-d<sub>6</sub>)



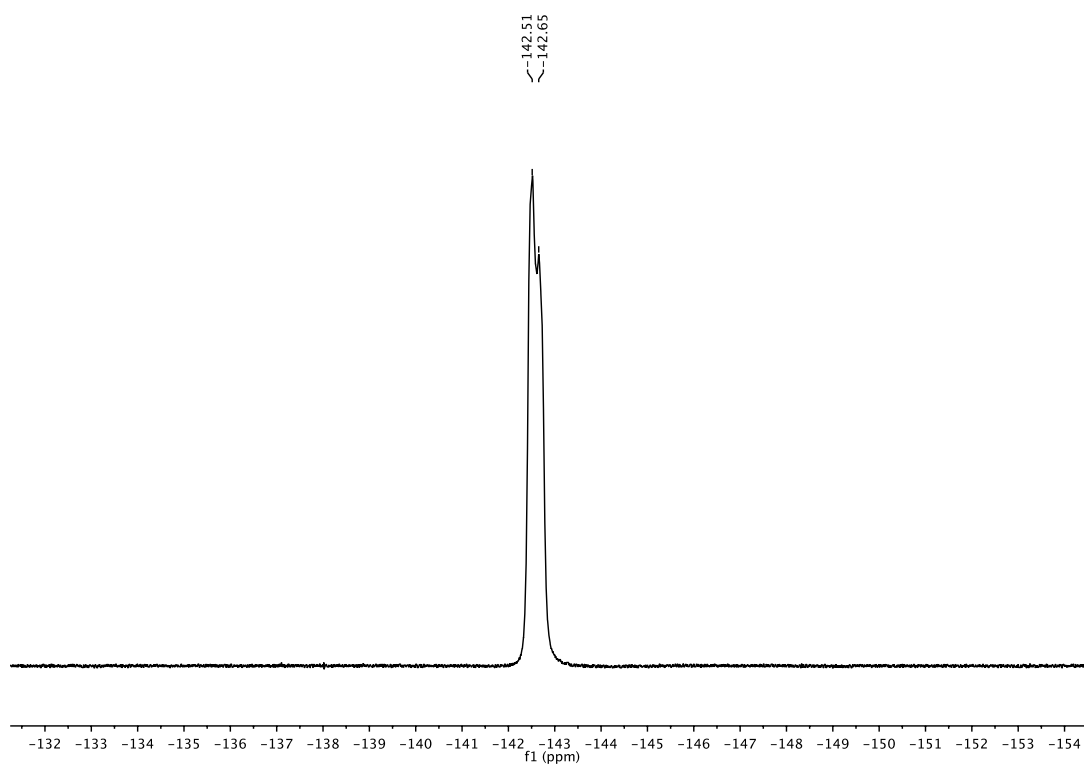
<sup>11</sup>B-NMR (160 MHz, DMSO-d<sub>6</sub>)



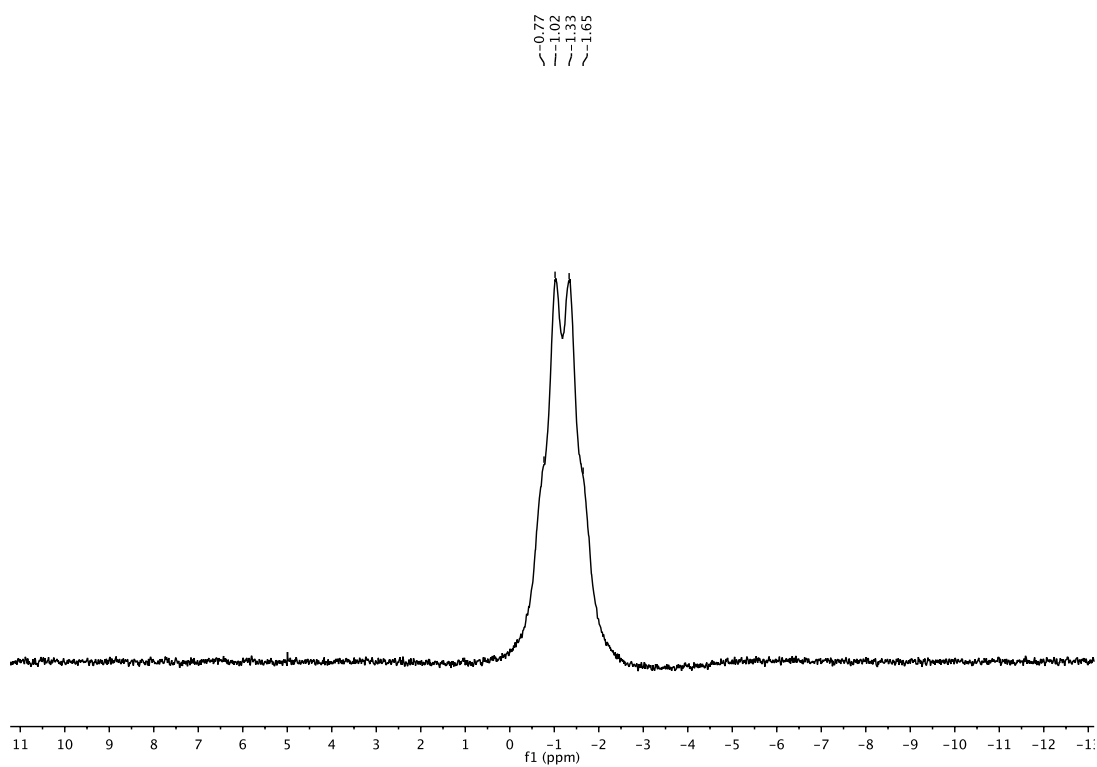
## Potassium 4-methyl-2-isonicotinoyltrifluoroborate (128)

 $^1\text{H-NMR}$  (500 MHz,  $\text{DMSO-d}_6$ ) $^{13}\text{C-NMR}$  (150 MHz,  $\text{DMSO-d}_6$ )

<sup>19</sup>F-NMR (470 MHz, DMSO-d<sub>6</sub>)

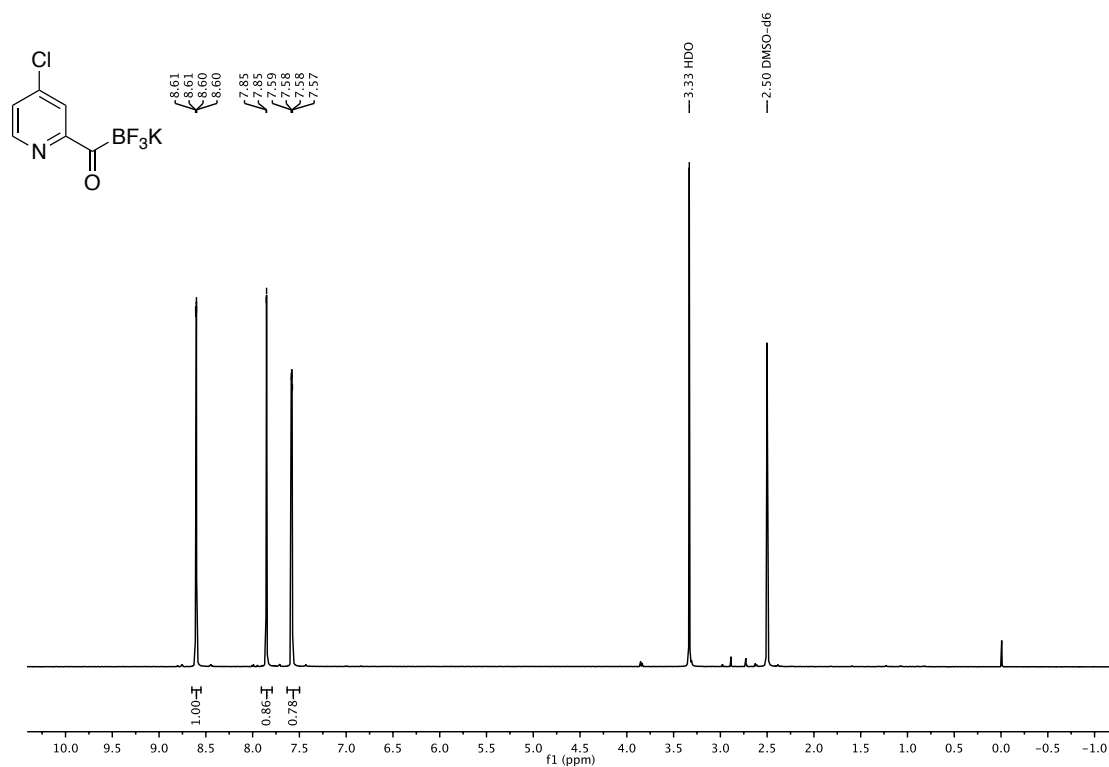
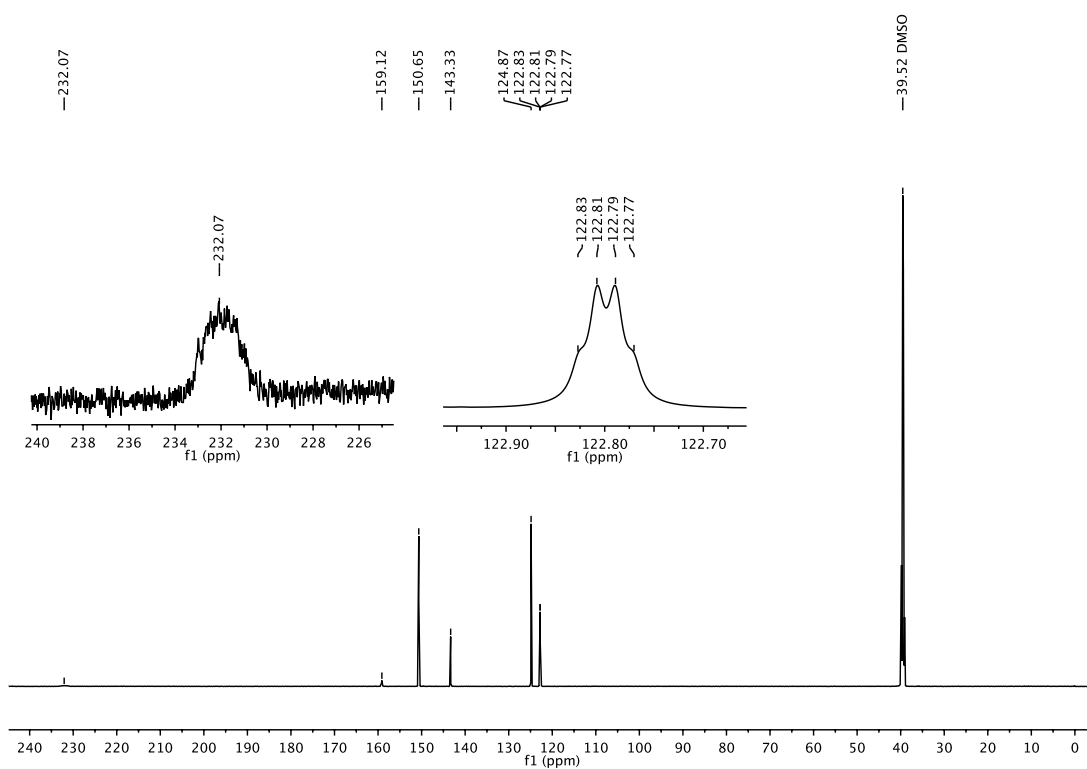


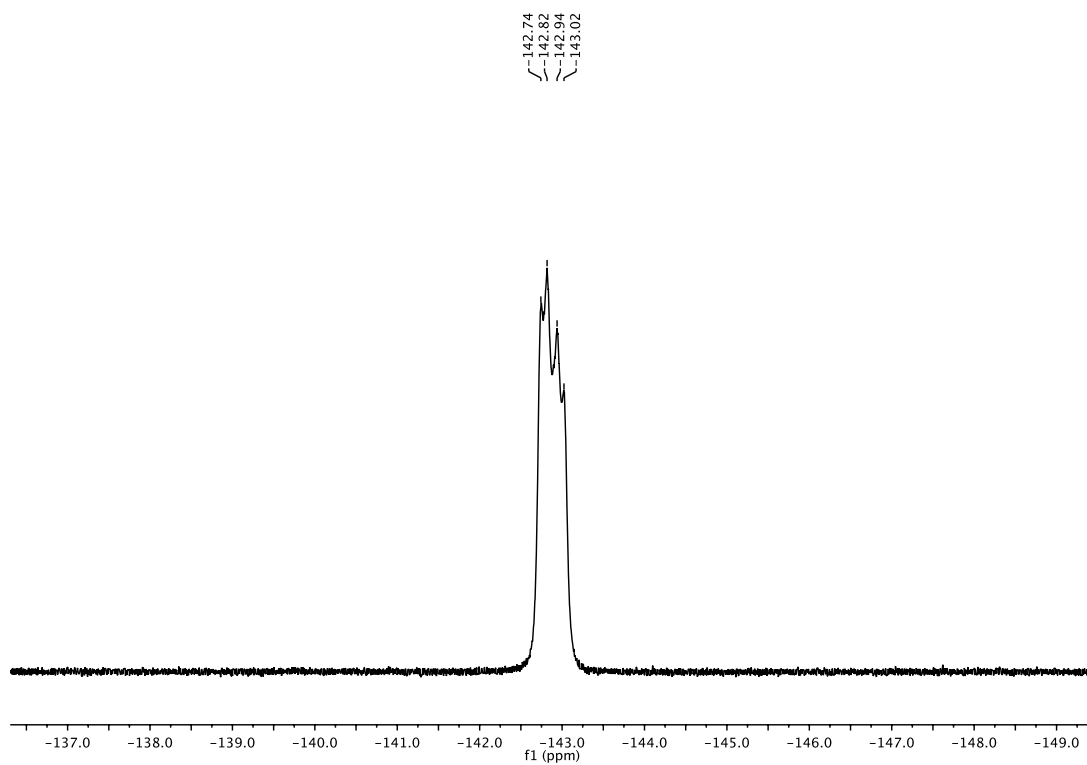
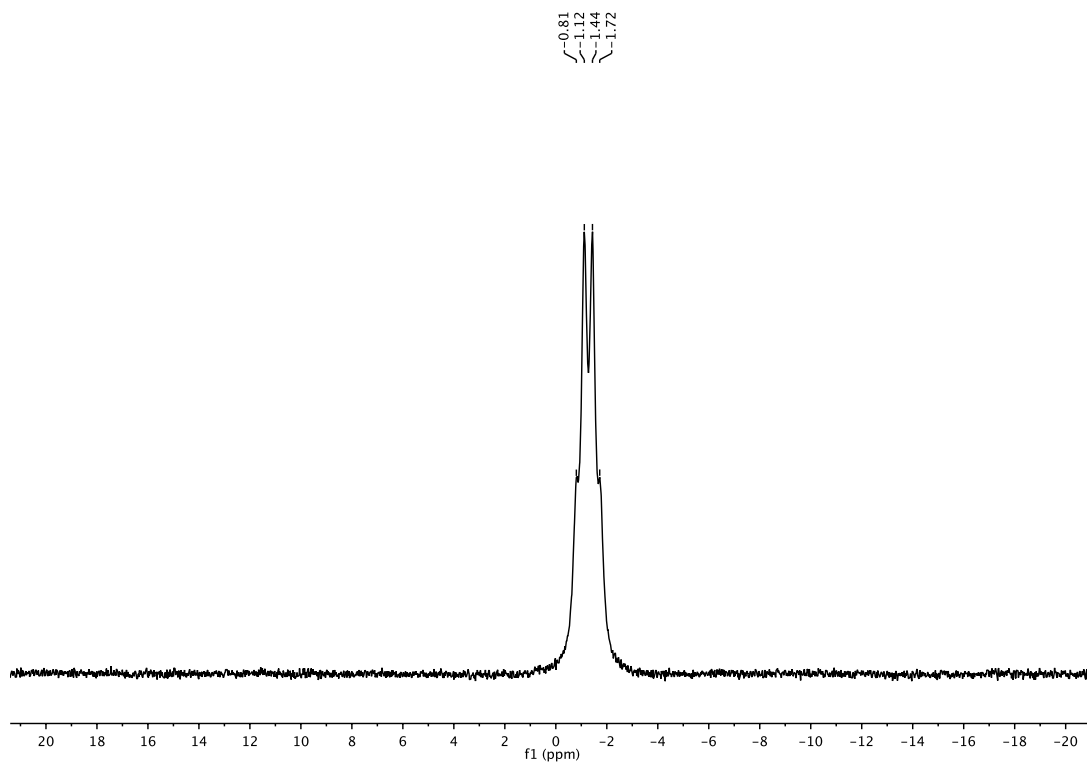
<sup>11</sup>B-NMR (160 MHz, DMSO-d<sub>6</sub>)



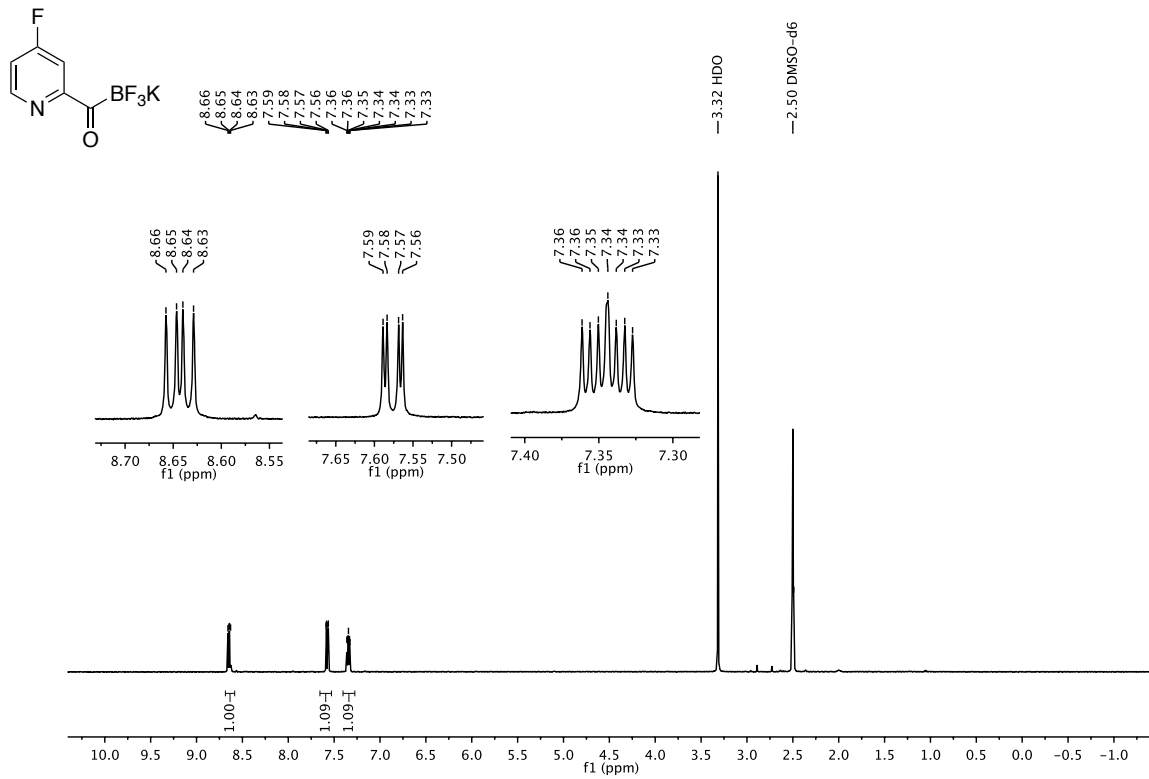
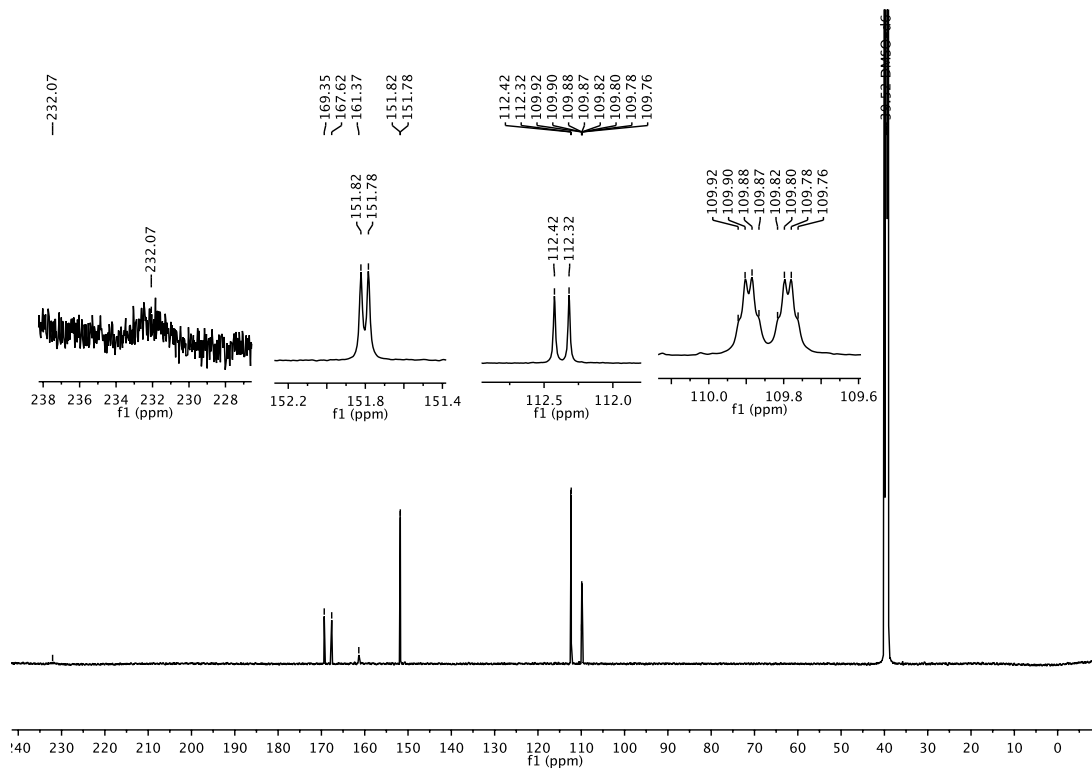


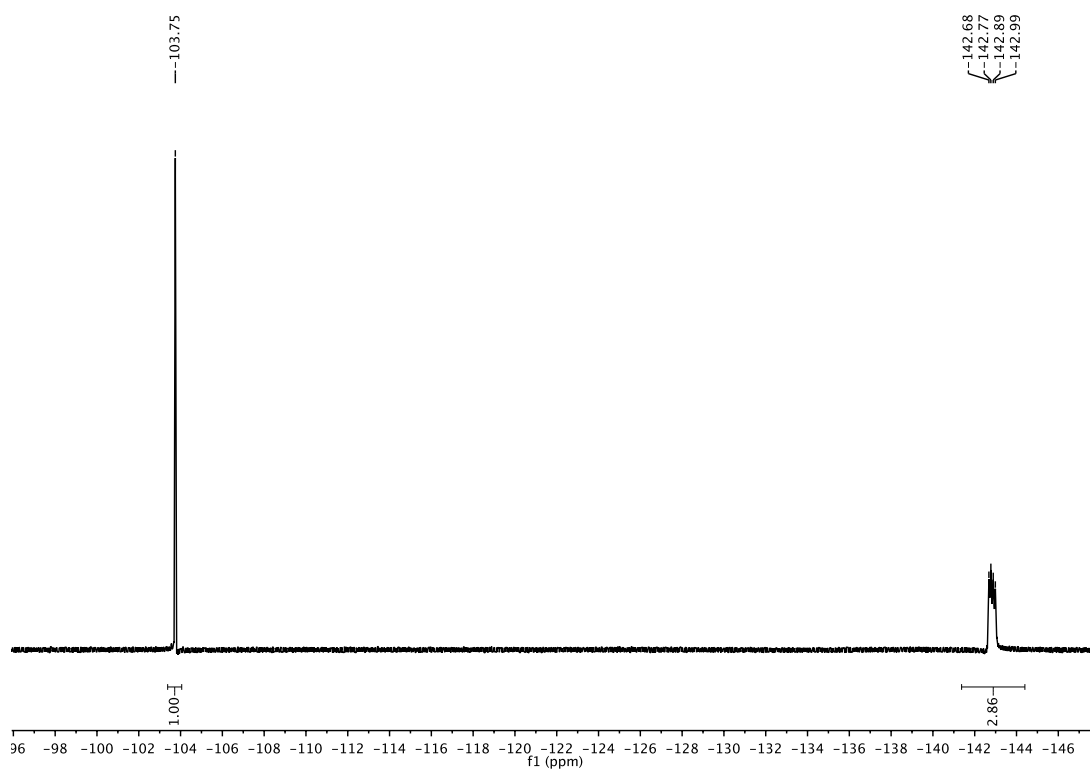
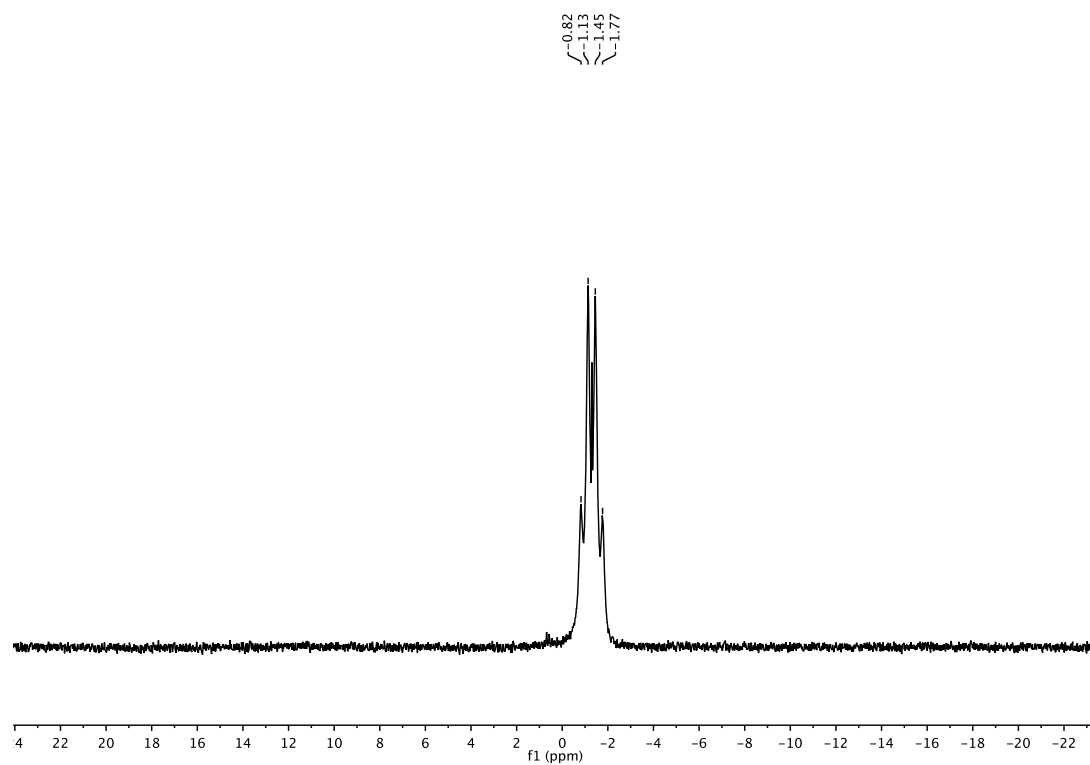
## Potassium 4-chloro-2-isonicotinoyltrifluoroborate (129)

 $^1\text{H-NMR}$  (600 MHz,  $\text{DMSO-d}_6$ ) $^{13}\text{C-NMR}$  (150 MHz,  $\text{DMSO-d}_6$ )

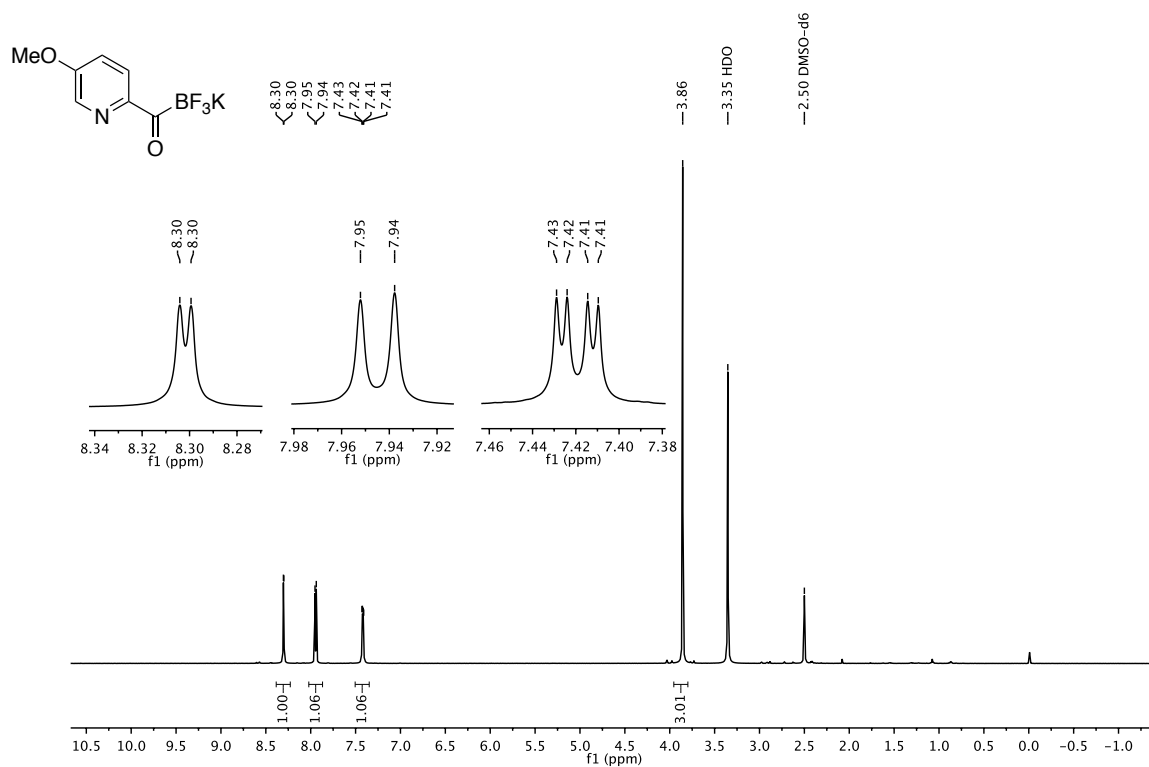
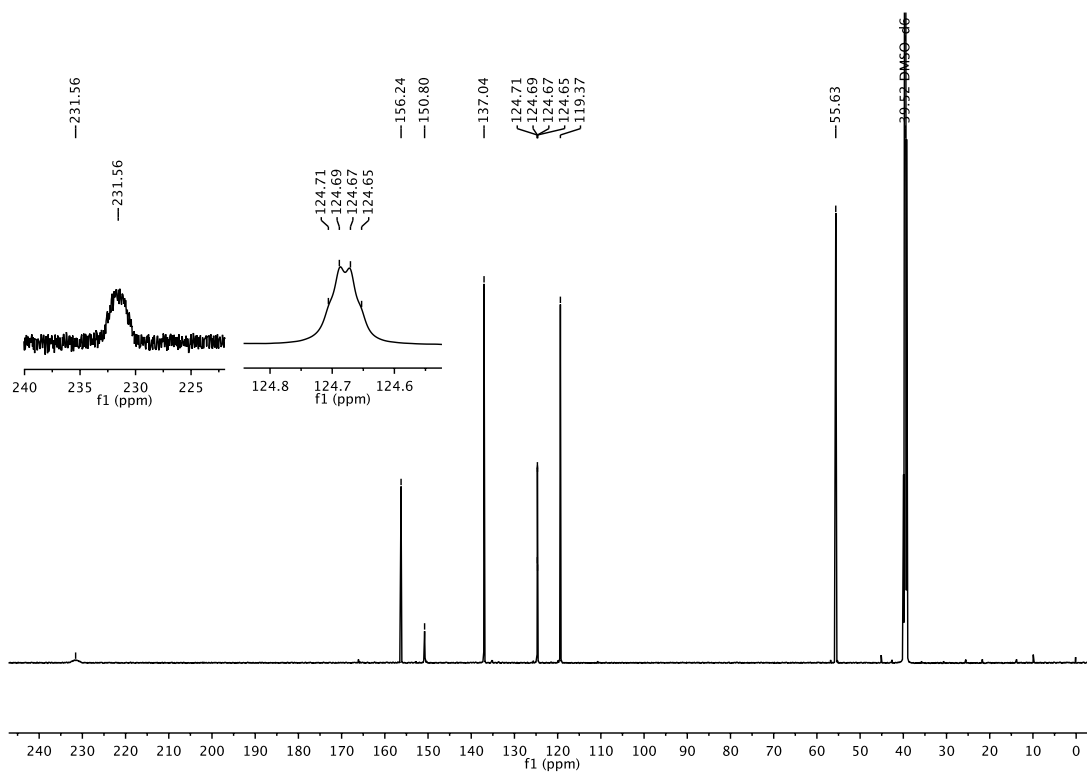
**$^{19}\text{F}$ -NMR (470 MHz,  $\text{DMSO-}d_6$ )** **$^{11}\text{B}$ -NMR (160 MHz,  $\text{DMSO-}d_6$ )**

## Potassium 4-fluoro-2-isonicotinoyltrifluoroborate (130)

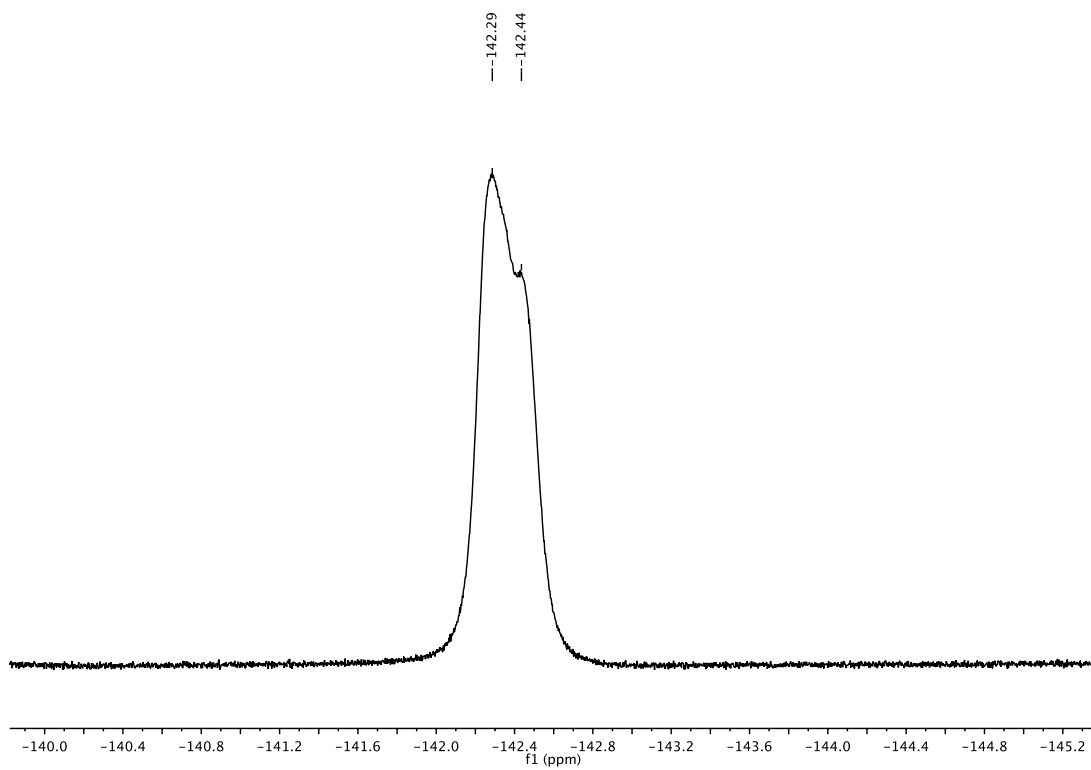
 $^1\text{H-NMR}$  (600 MHz,  $\text{DMSO-d}_6$ ) $^{13}\text{C-NMR}$  (150 MHz,  $\text{DMSO-d}_6$ )

**$^{19}\text{F}$ -NMR (470 MHz,  $\text{DMSO-}d_6$ )** **$^{11}\text{B}$ -NMR (160 MHz,  $\text{DMSO-}d_6$ )**

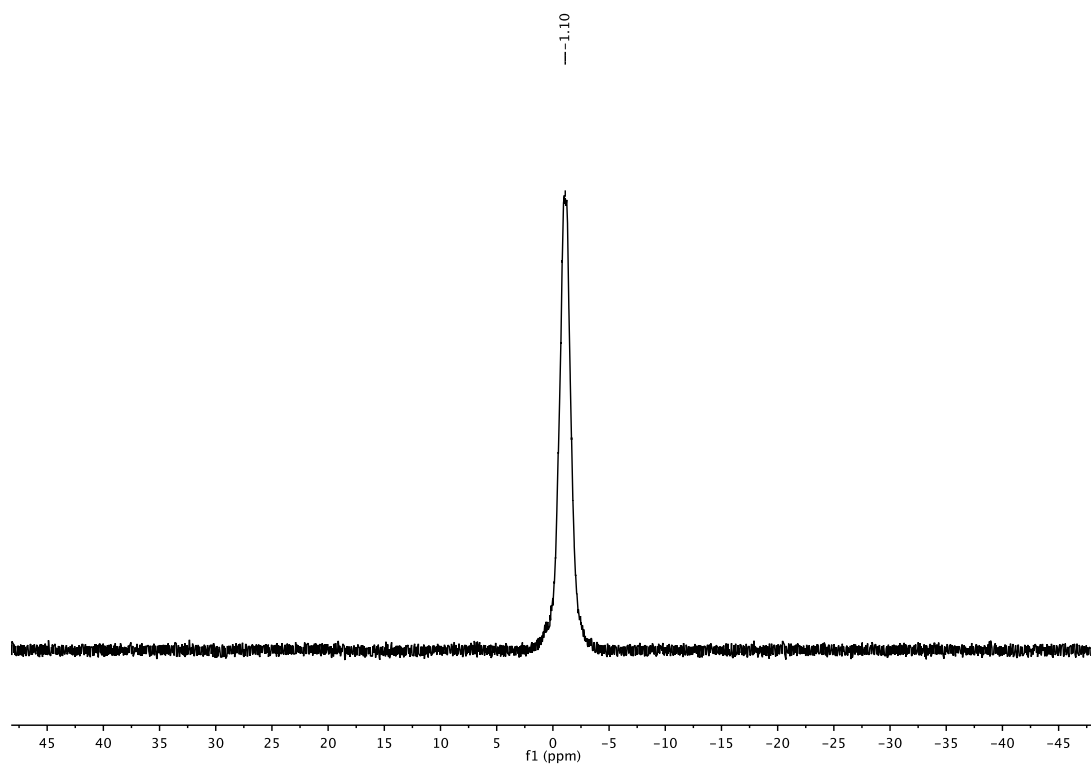
## Potassium 5-methoxy-2-isonicotinoyltrifluoroborate (131)

 $^1\text{H-NMR}$  (600 MHz,  $\text{DMSO-d}_6$ ) $^{13}\text{C-NMR}$  (150 MHz,  $\text{DMSO-d}_6$ )

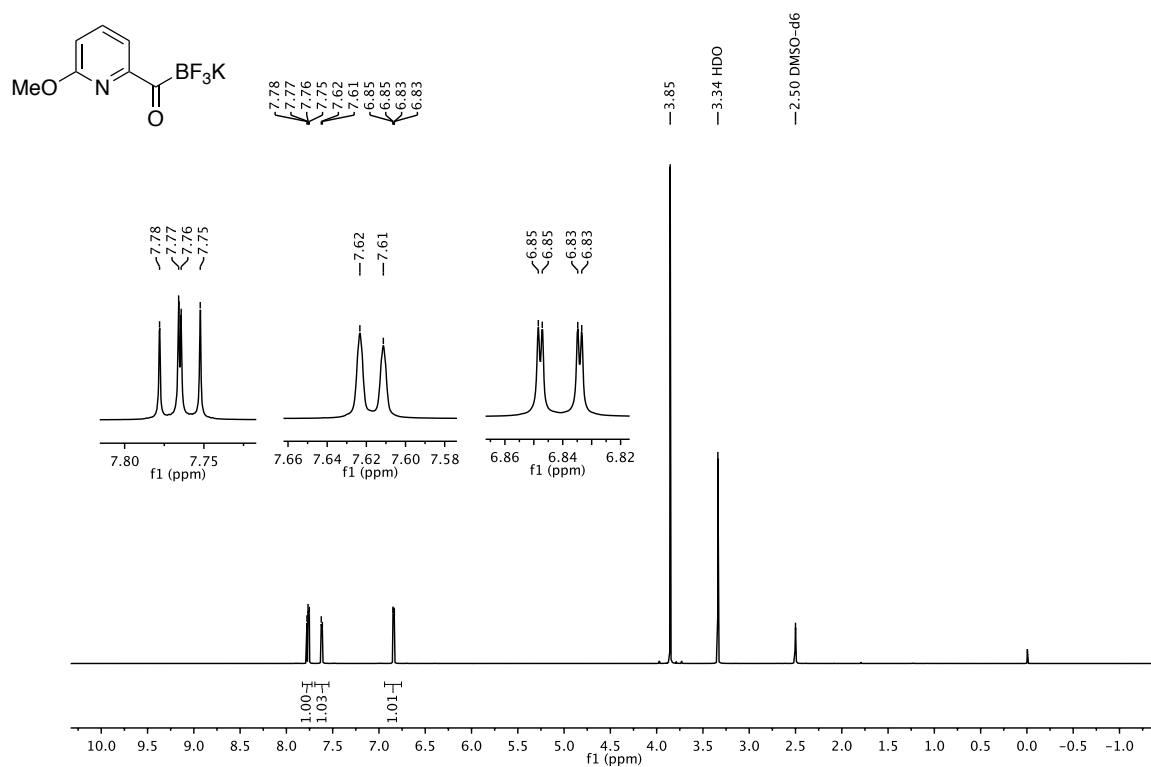
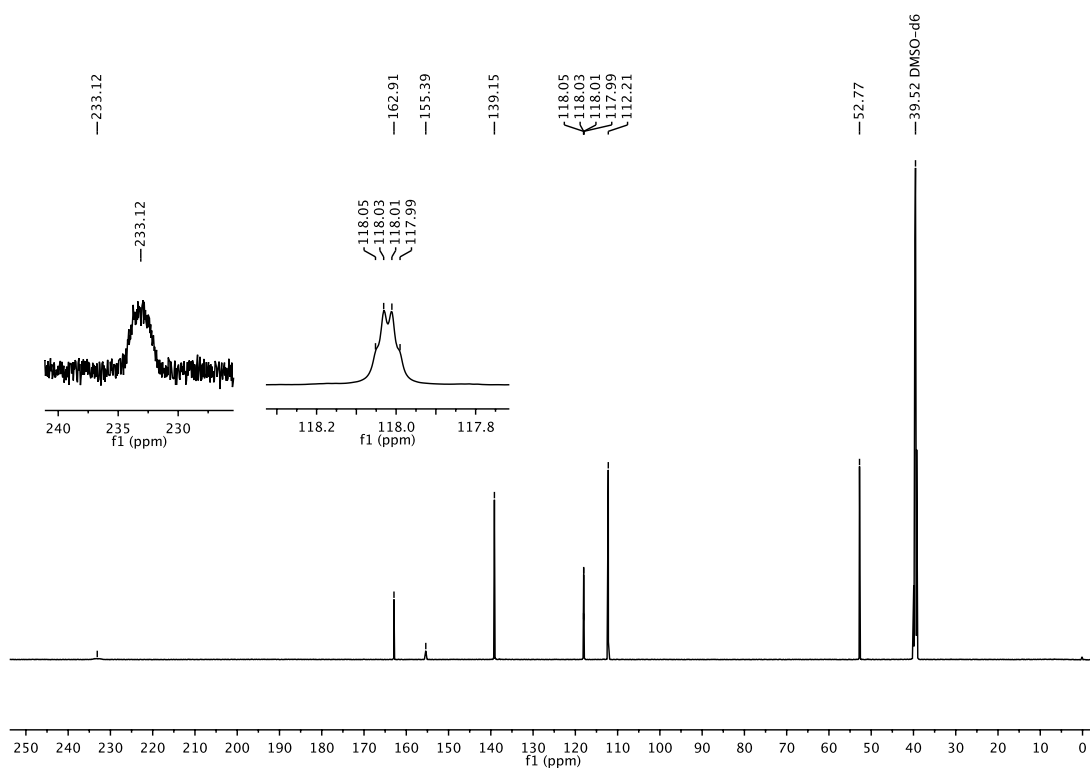
**$^{19}\text{F}$ -NMR (470 MHz,  $\text{DMSO-}d_6$ )**



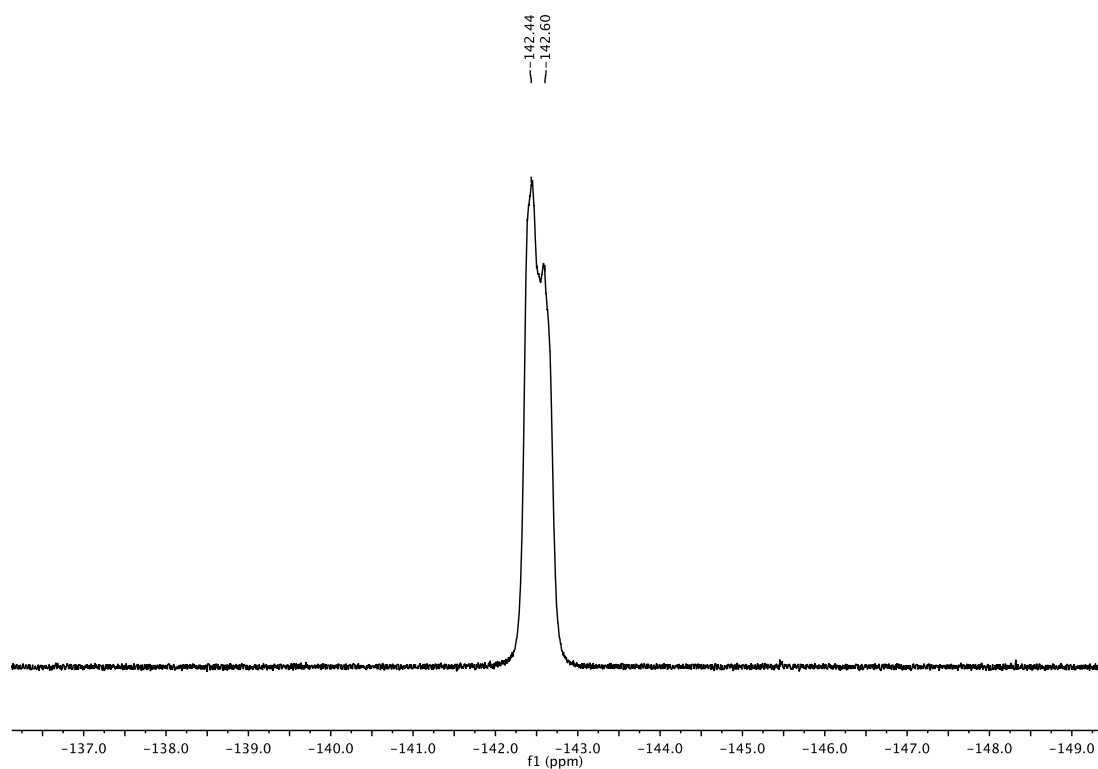
**$^{11}\text{B}$ -NMR (160 MHz,  $\text{DMSO-}d_6$ )**



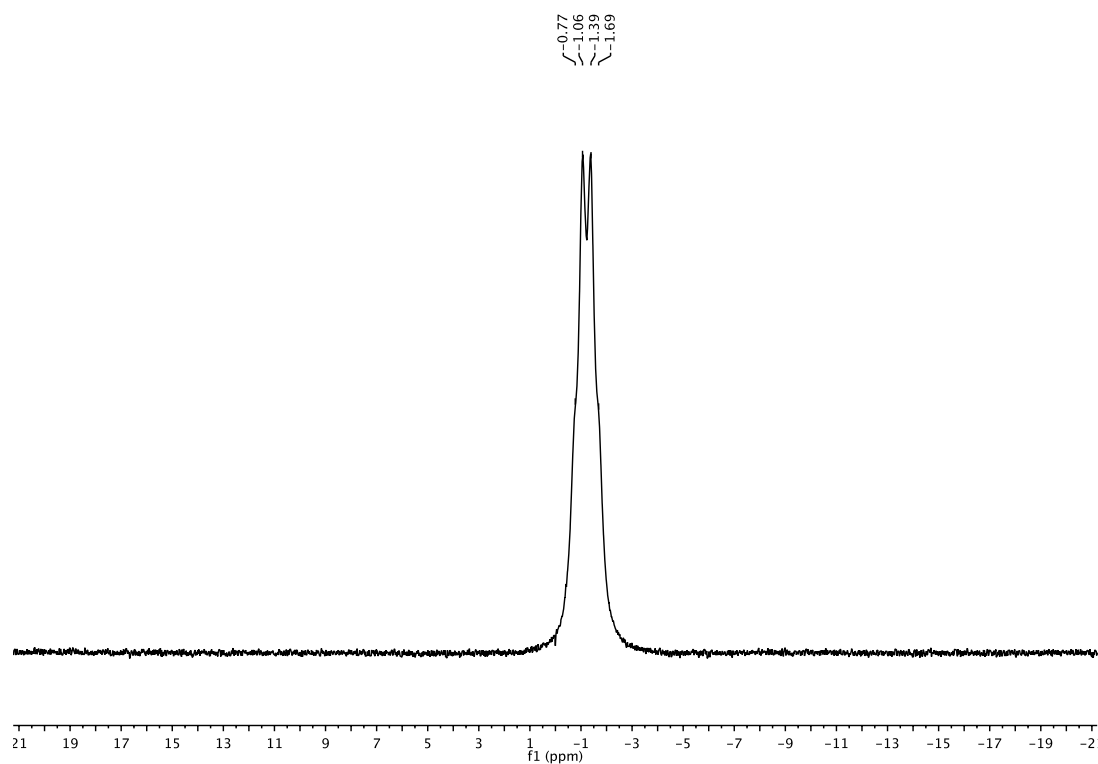
## Potassium 6-methoxy-2-isonicotinoyltrifluoroborate (132)

 $^1\text{H-NMR}$  (600 MHz,  $\text{DMSO-d}_6$ ) $^{13}\text{C-NMR}$  (150 MHz,  $\text{DMSO-d}_6$ )

**$^{19}\text{F}$ -NMR (470 MHz,  $\text{DMSO-}d_6$ )**

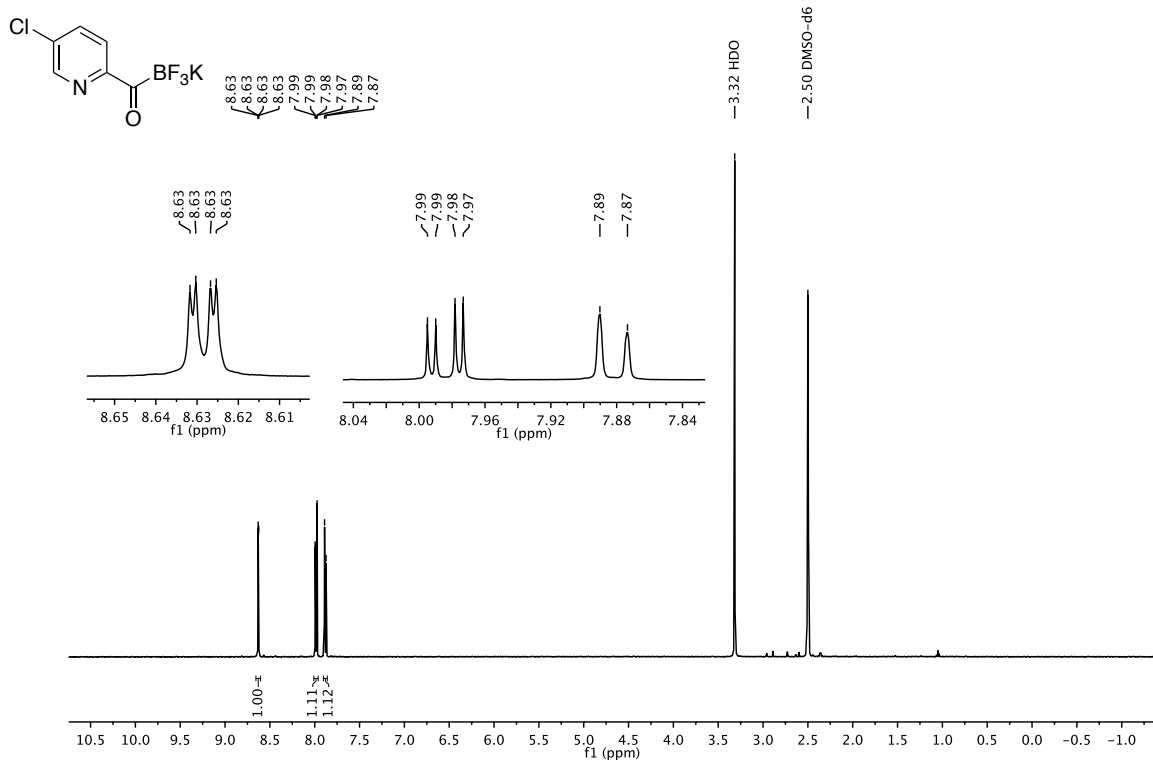
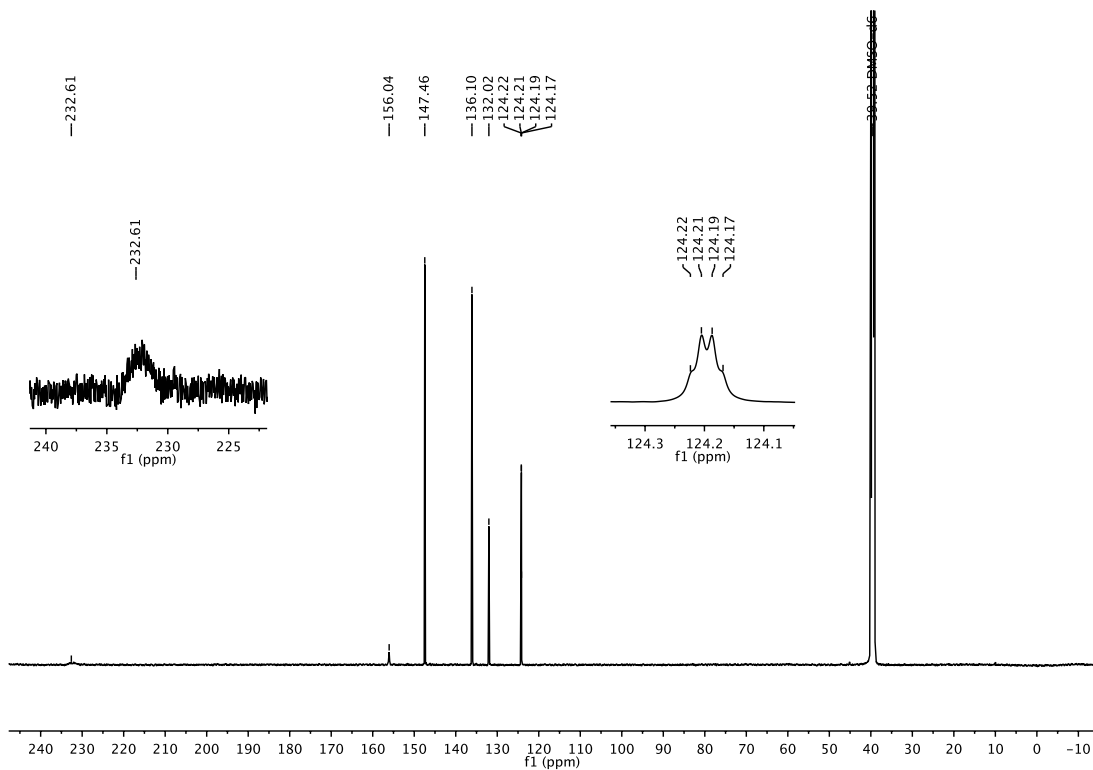


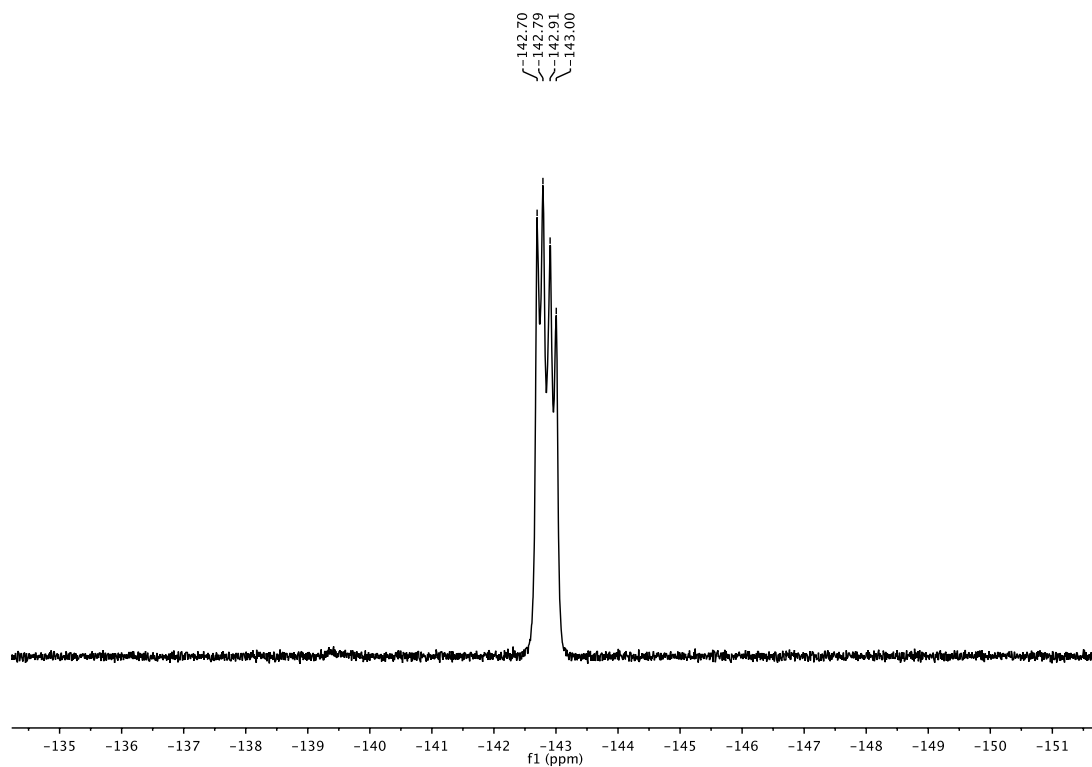
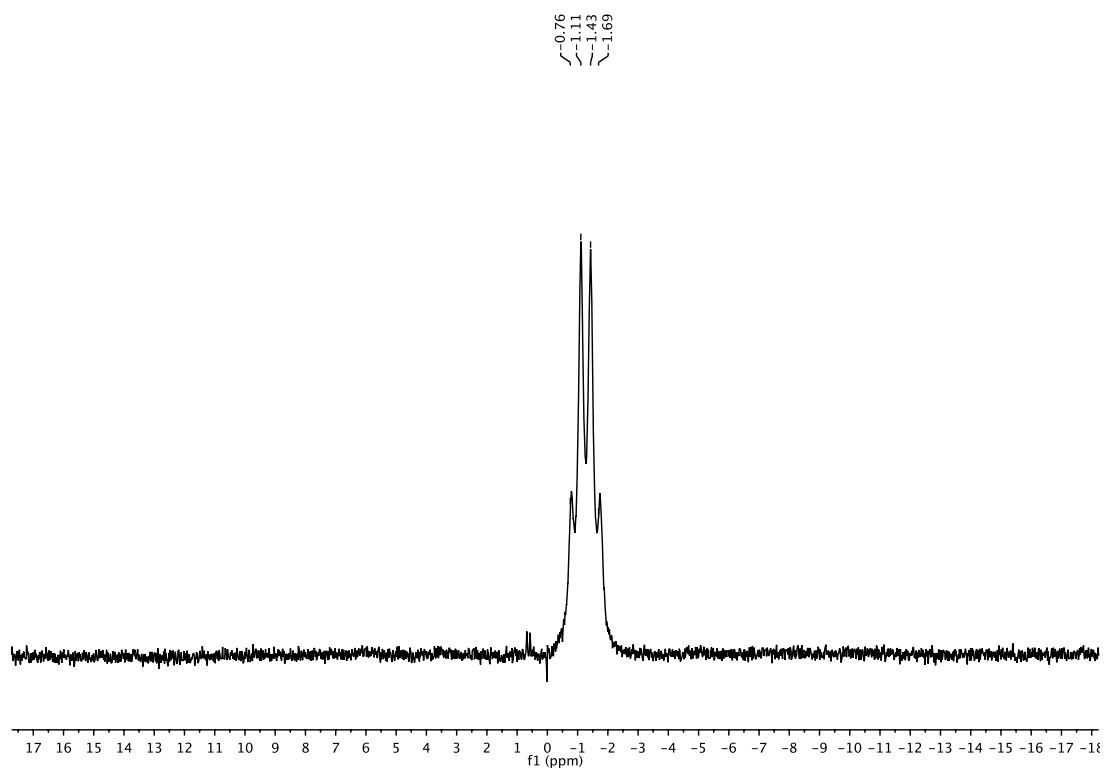
**$^{11}\text{B}$ -NMR (160 MHz,  $\text{DMSO-}d_6$ )**



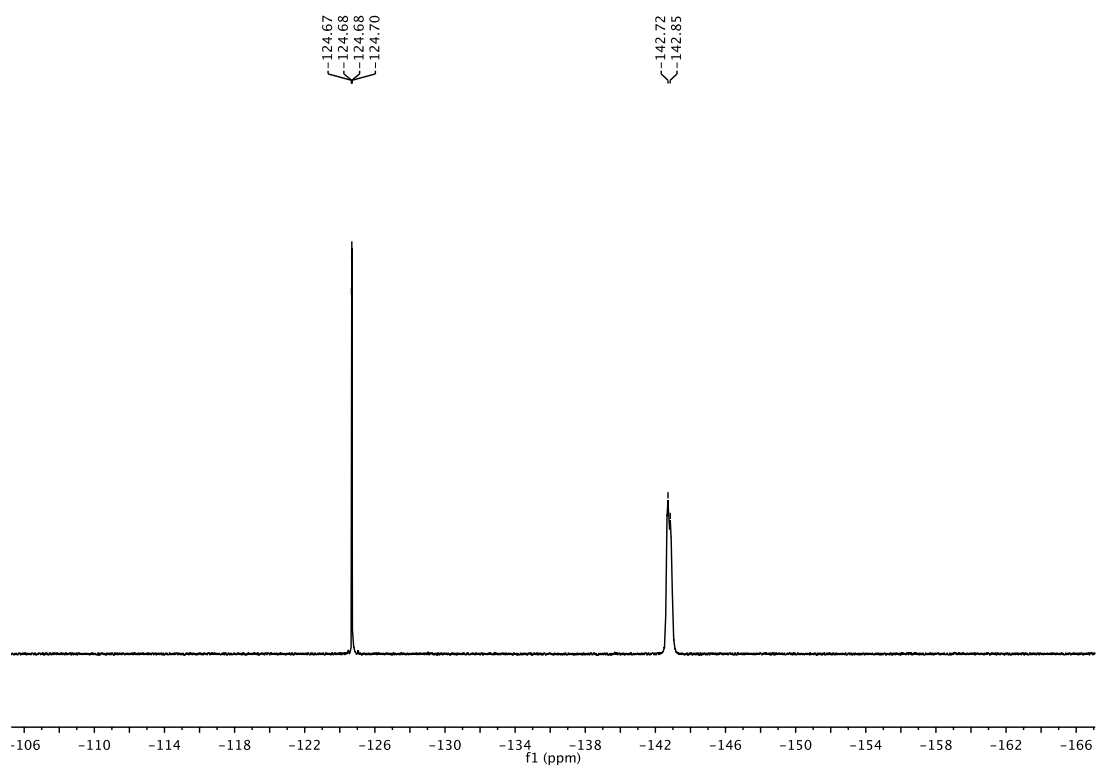
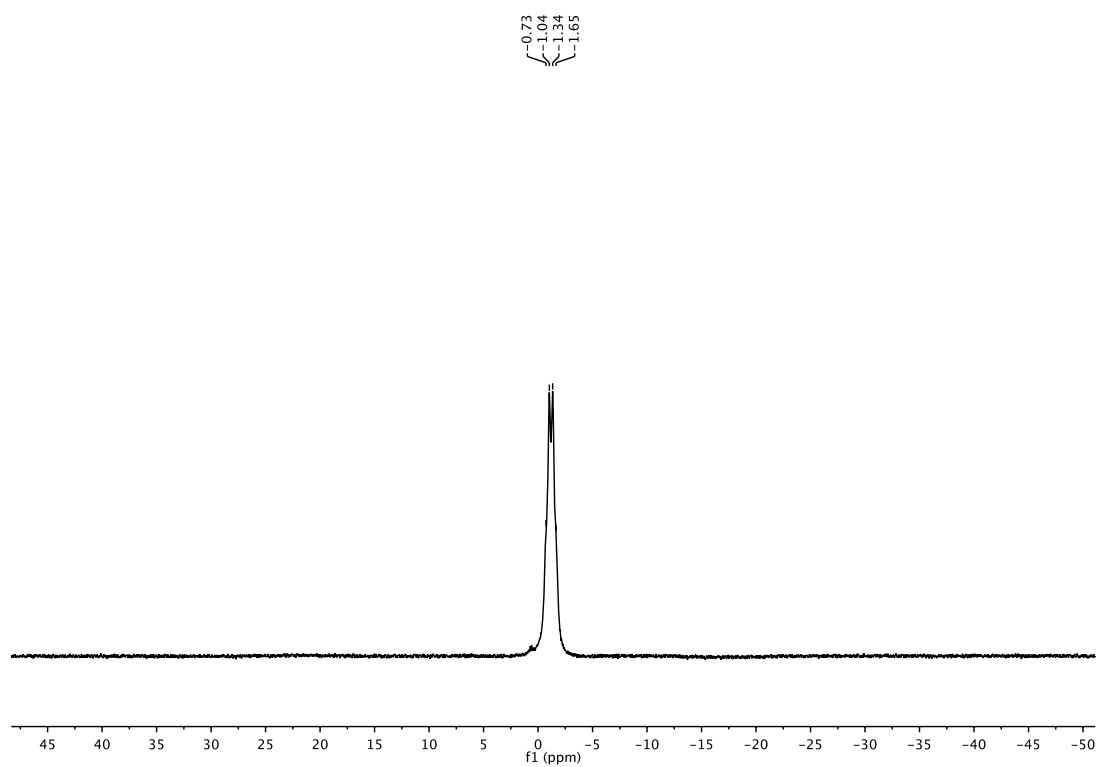


## Potassium 5-chloro-2-isonicotinoyltrifluoroborate (133)

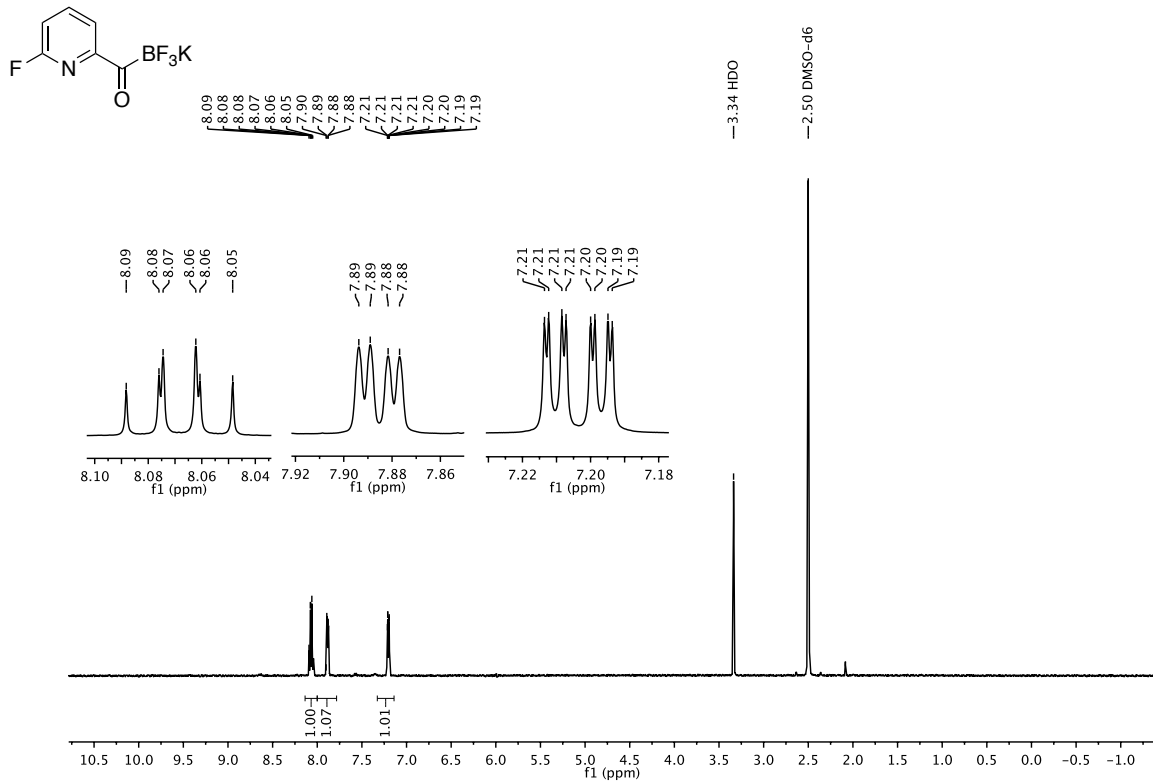
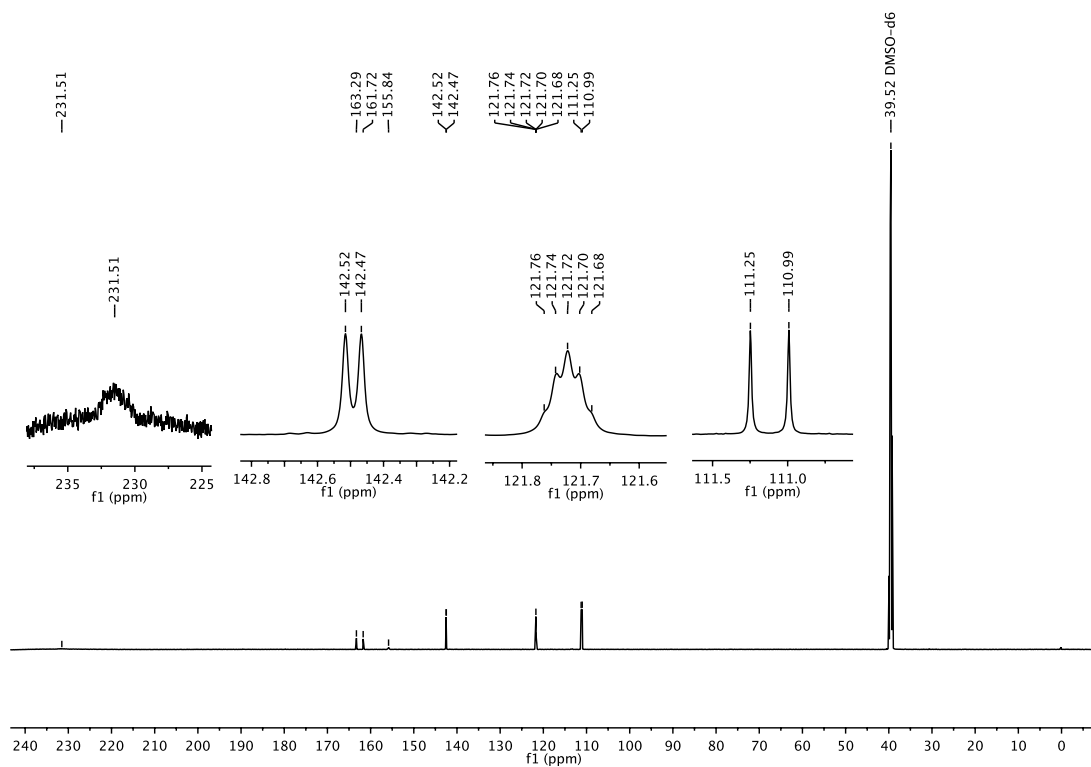
 $^1\text{H-NMR}$  (600 MHz,  $\text{DMSO-d}_6$ ) $^{13}\text{C-NMR}$  (150 MHz,  $\text{DMSO-d}_6$ )

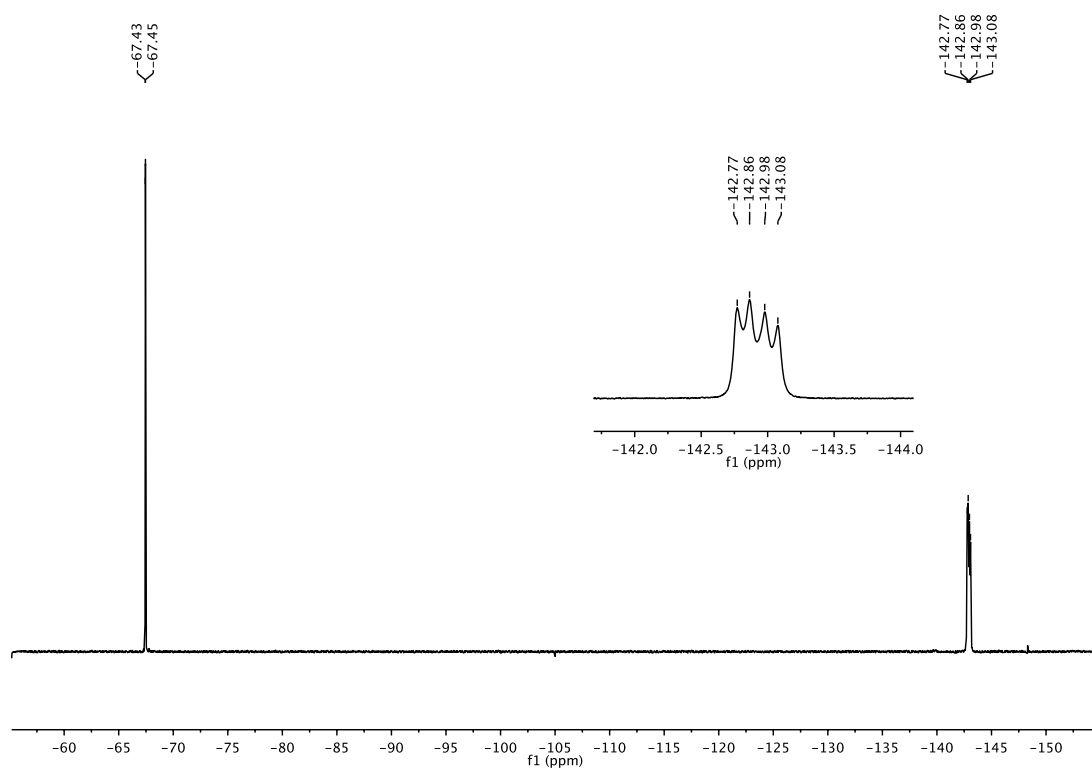
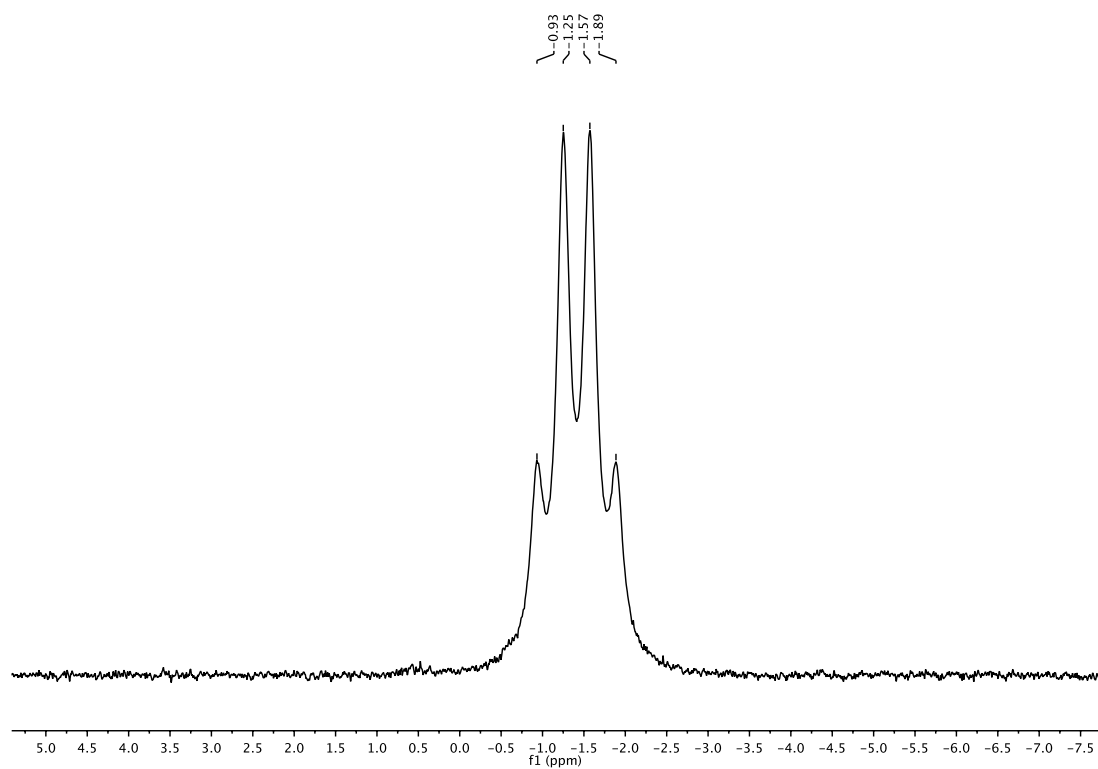
**$^{19}\text{F}$ -NMR (470 MHz,  $\text{DMSO-}d_6$ )** **$^{11}\text{B}$ -NMR (160 MHz,  $\text{DMSO-}d_6$ )**



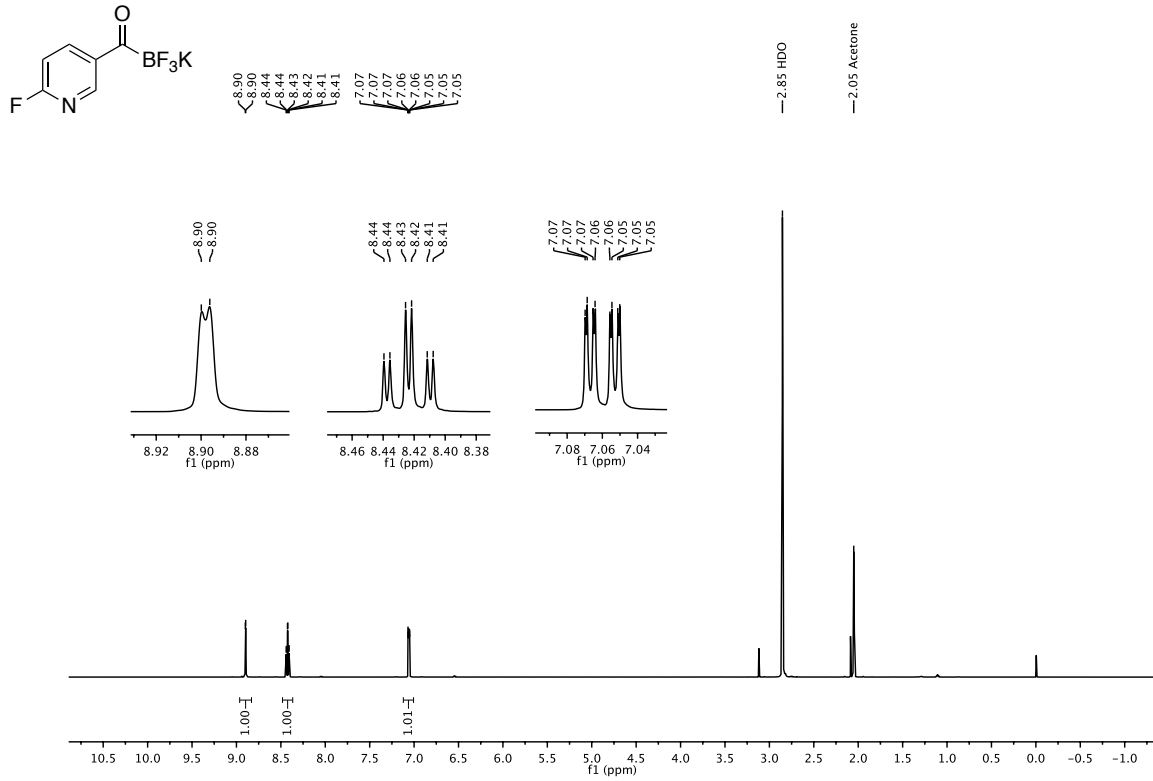
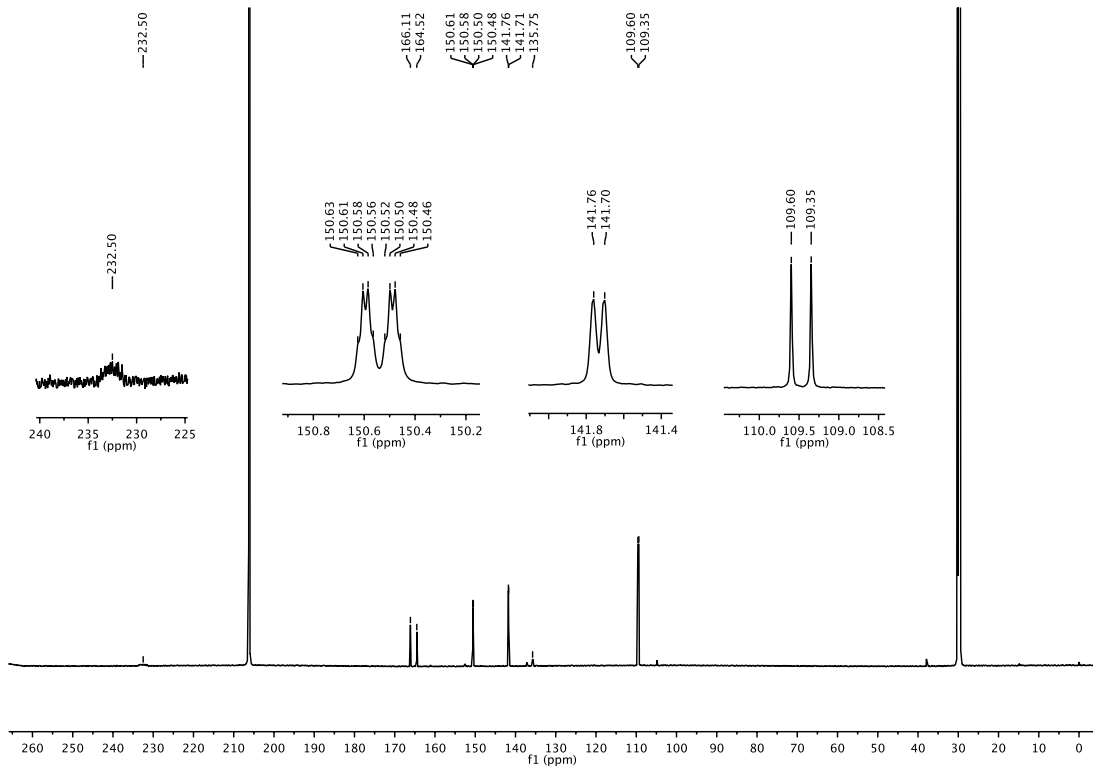
**$^{19}\text{F}$ -NMR (470 MHz,  $\text{DMSO-}d_6$ )** **$^{11}\text{B}$ -NMR (160 MHz,  $\text{DMSO-}d_6$ )**

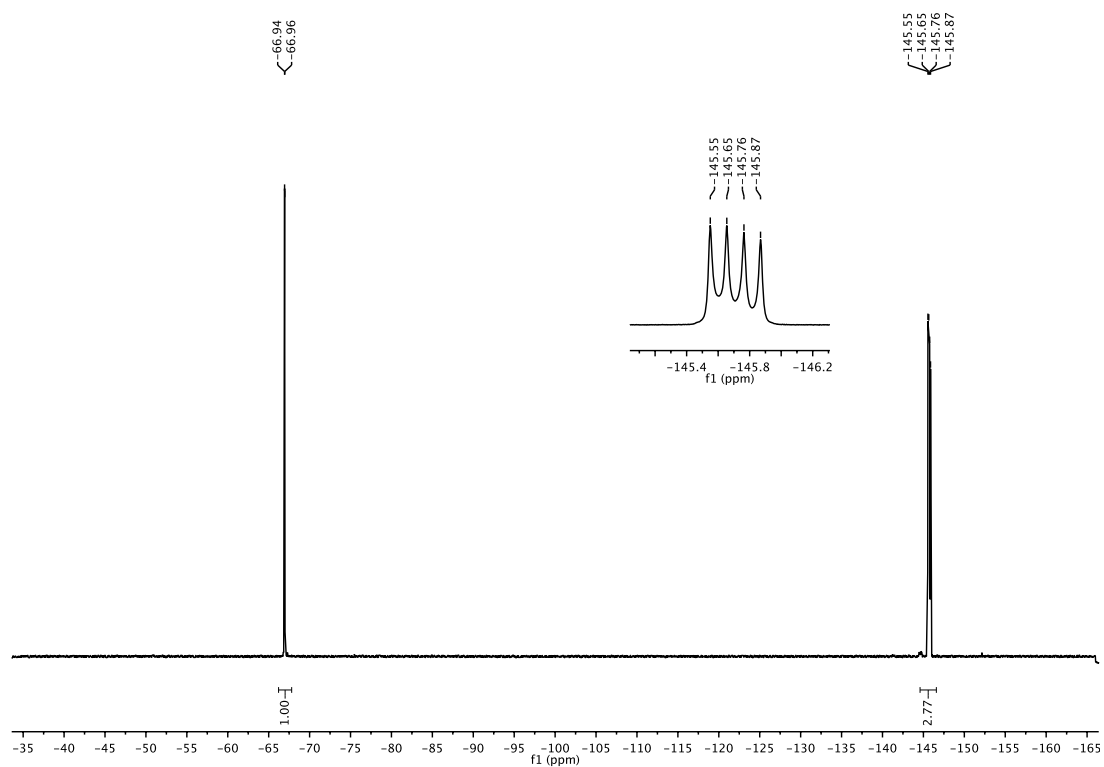
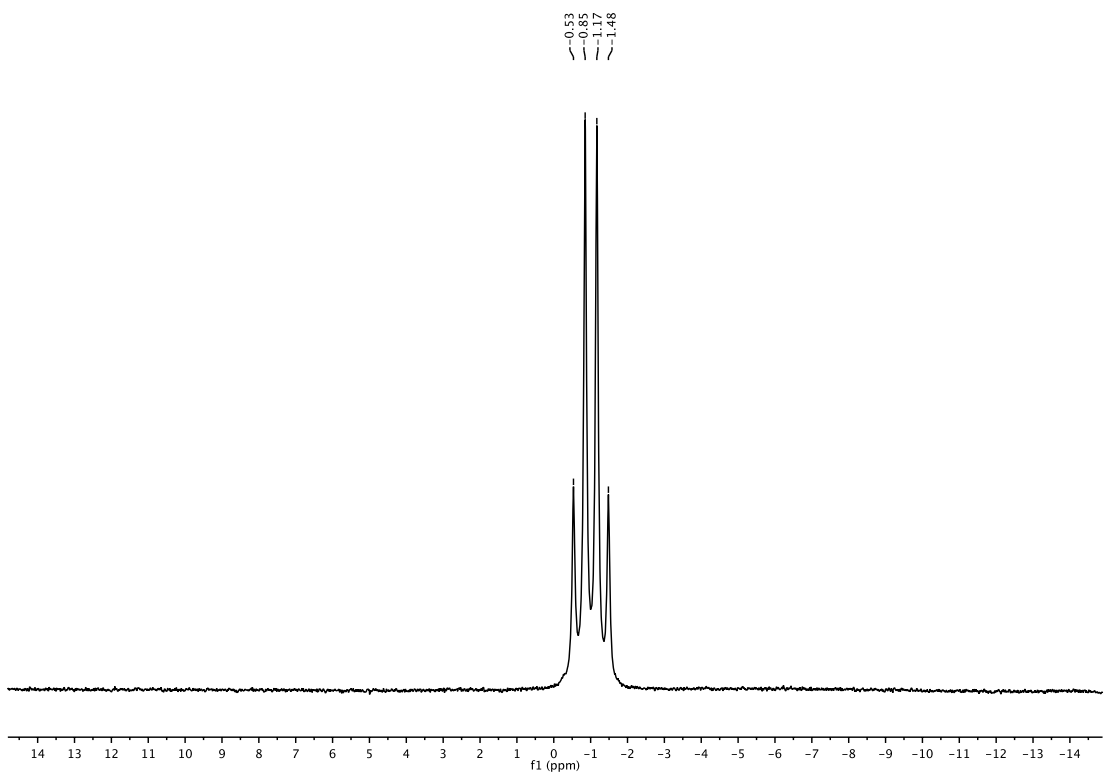
## Potassium 6-fluoro-2-isonicotinoyltrifluoroborate (136)

 $^1\text{H-NMR}$  (600 MHz,  $\text{DMSO-d}_6$ ) $^{13}\text{C-NMR}$  (150 MHz,  $\text{DMSO-d}_6$ )

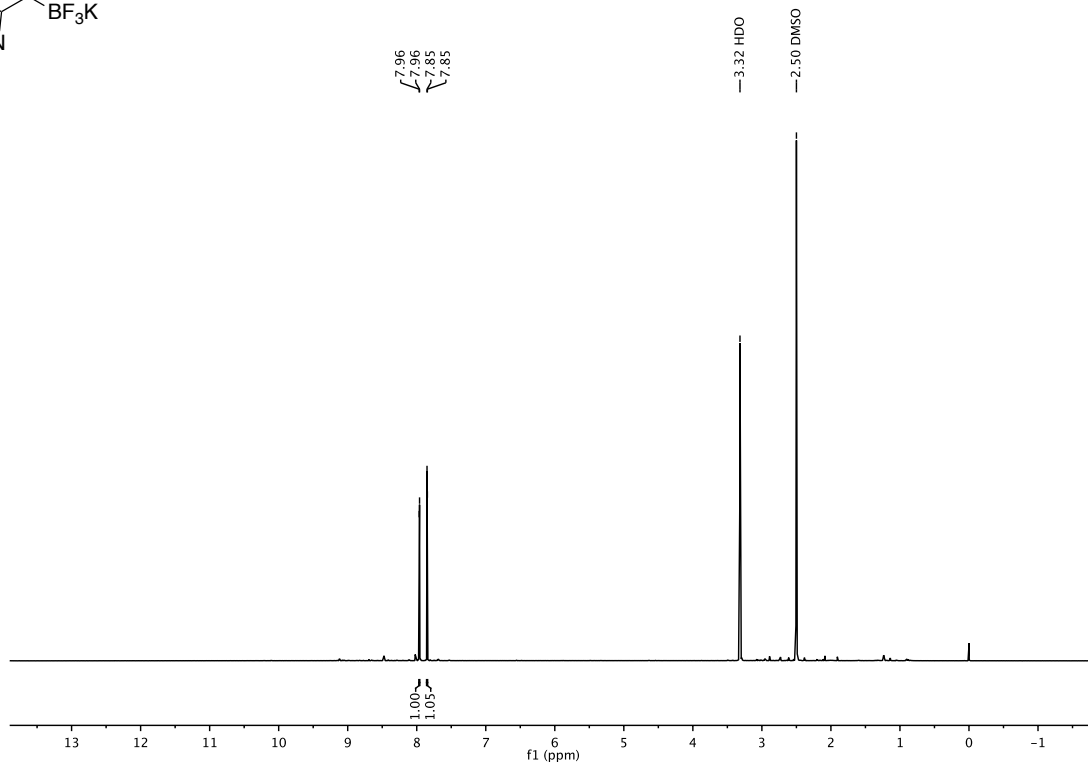
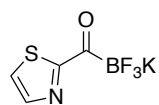
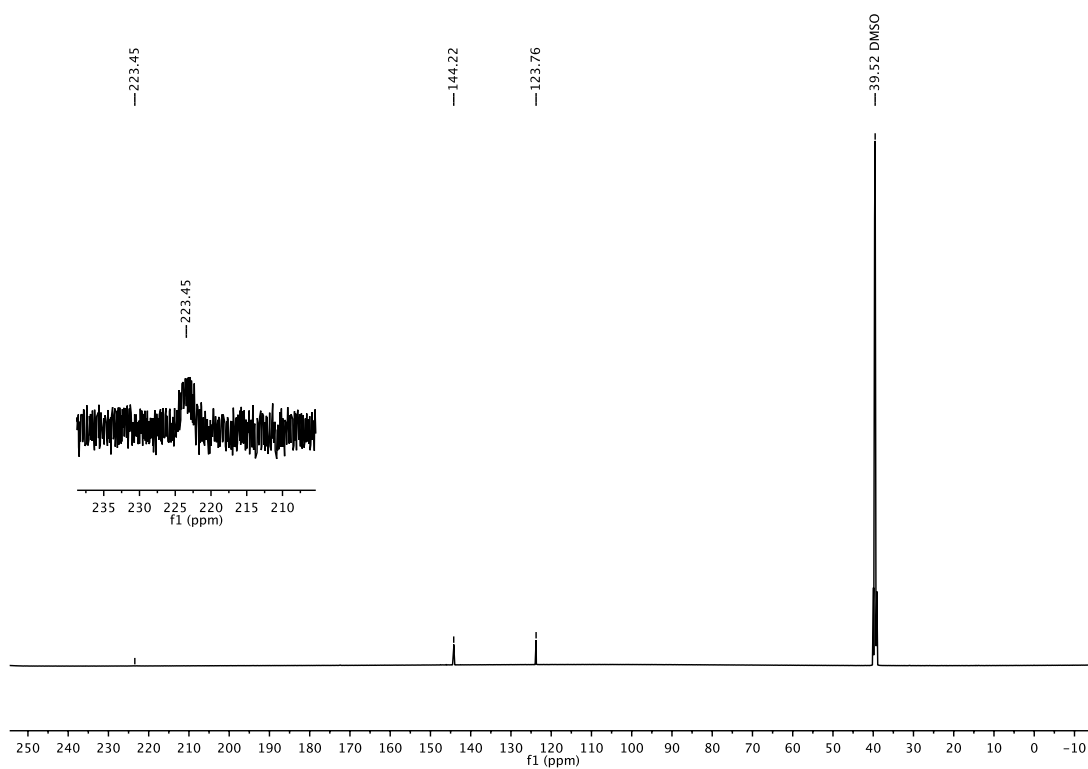
**$^{19}\text{F}$ -NMR (470 MHz,  $\text{DMSO-}d_6$ )** **$^{11}\text{B}$ -NMR (160 MHz,  $\text{DMSO-}d_6$ )**

## Potassium 2-fluoronicotinoyltrifluoroborate (156)

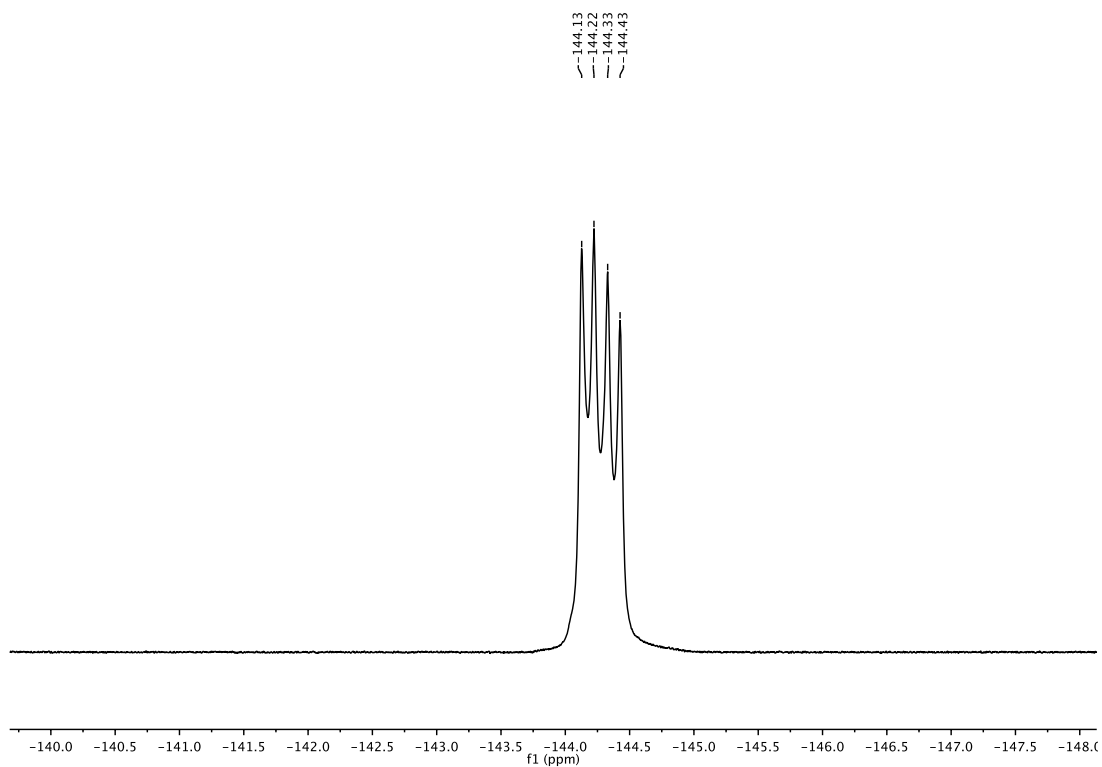
 $^1\text{H-NMR}$  (600 MHz, acetone- $d_6$ ) $^{13}\text{C-NMR}$  (150 MHz, acetone- $d_6$ )

**$^{19}\text{F}$ -NMR (470 MHz, acetone- $d_6$ )** **$^{11}\text{B}$ -NMR (160 MHz, acetone- $d_6$ )**

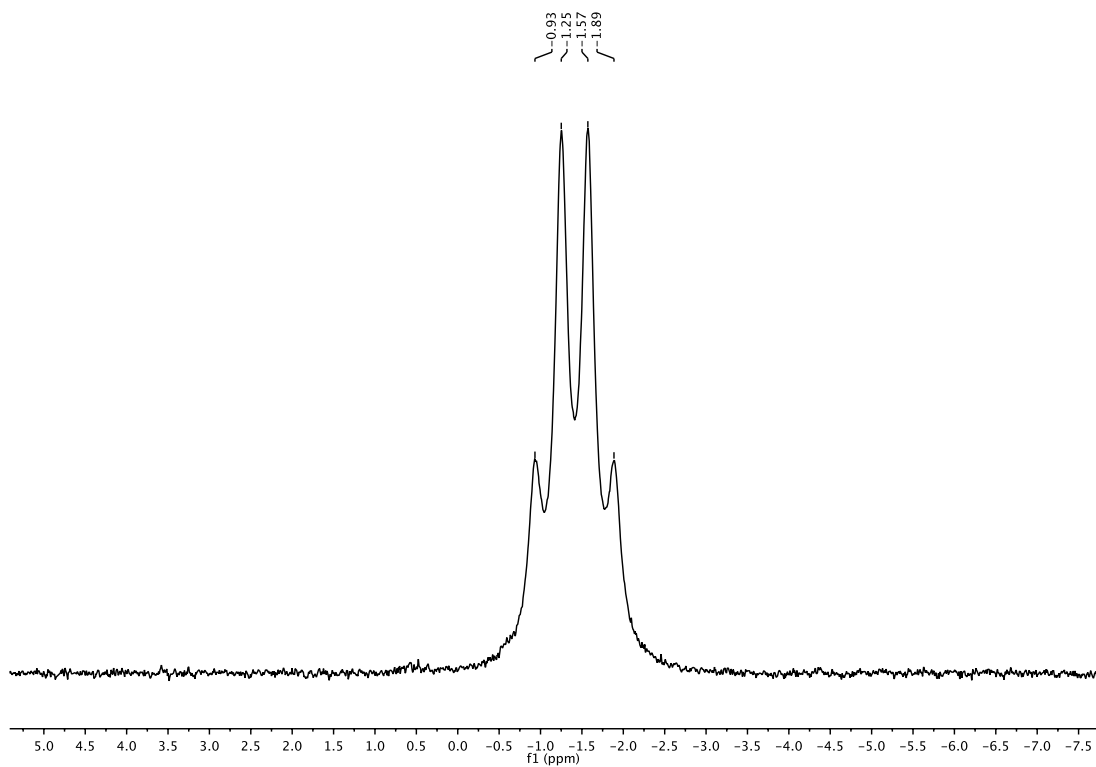


**Potassium (2-thiazolyl)methanotrifluoroborate (170)** **$^1\text{H-NMR}$  (600 MHz,  $\text{DMSO-}d_6$ )** **$^{13}\text{C-NMR}$  (150 MHz,  $\text{DMSO-}d_6$ )**

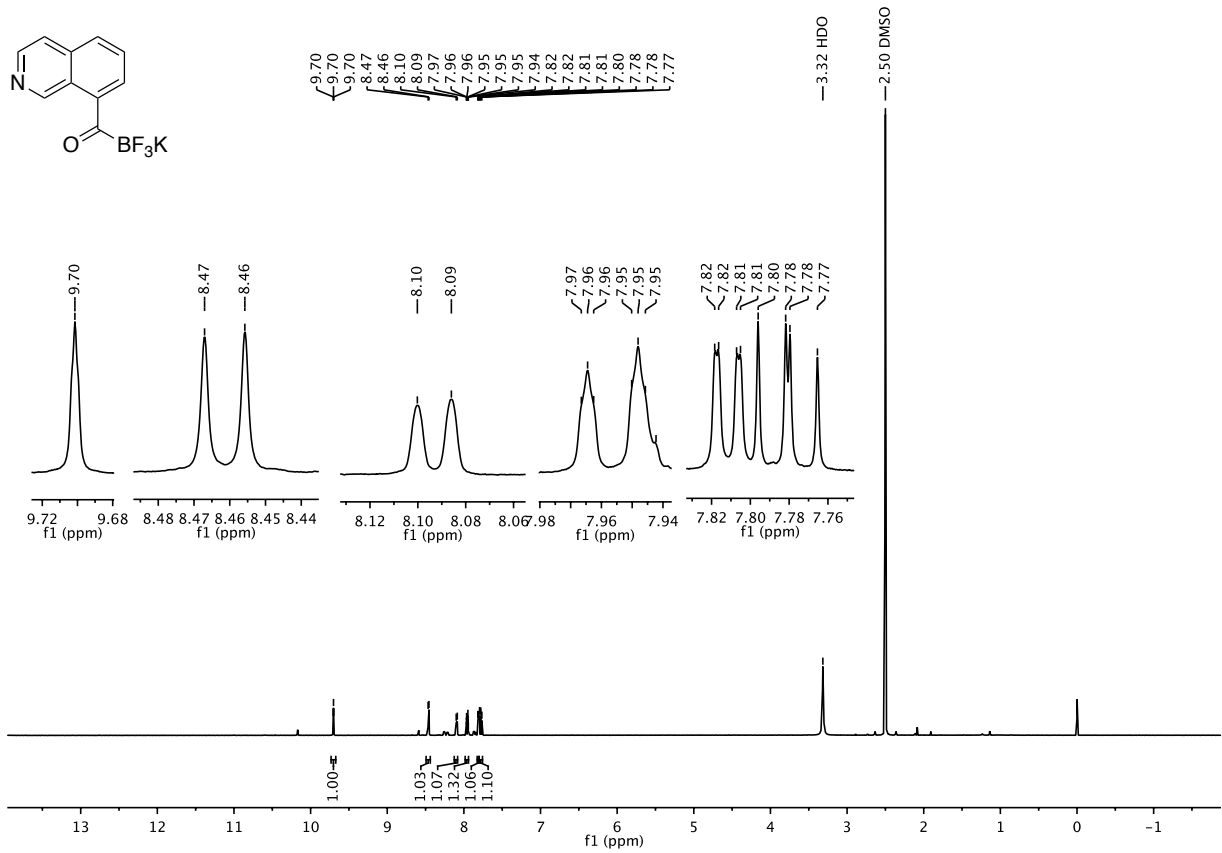
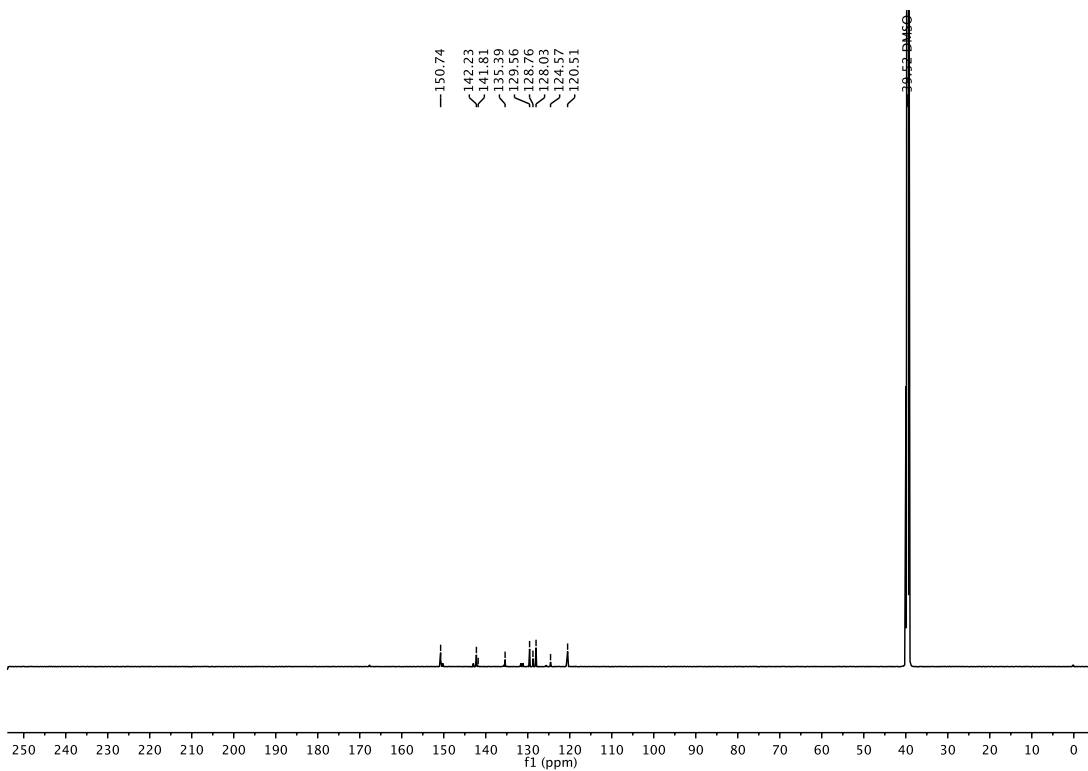
**<sup>19</sup>F-NMR (470 MHz, DMSO-d<sub>6</sub>)**

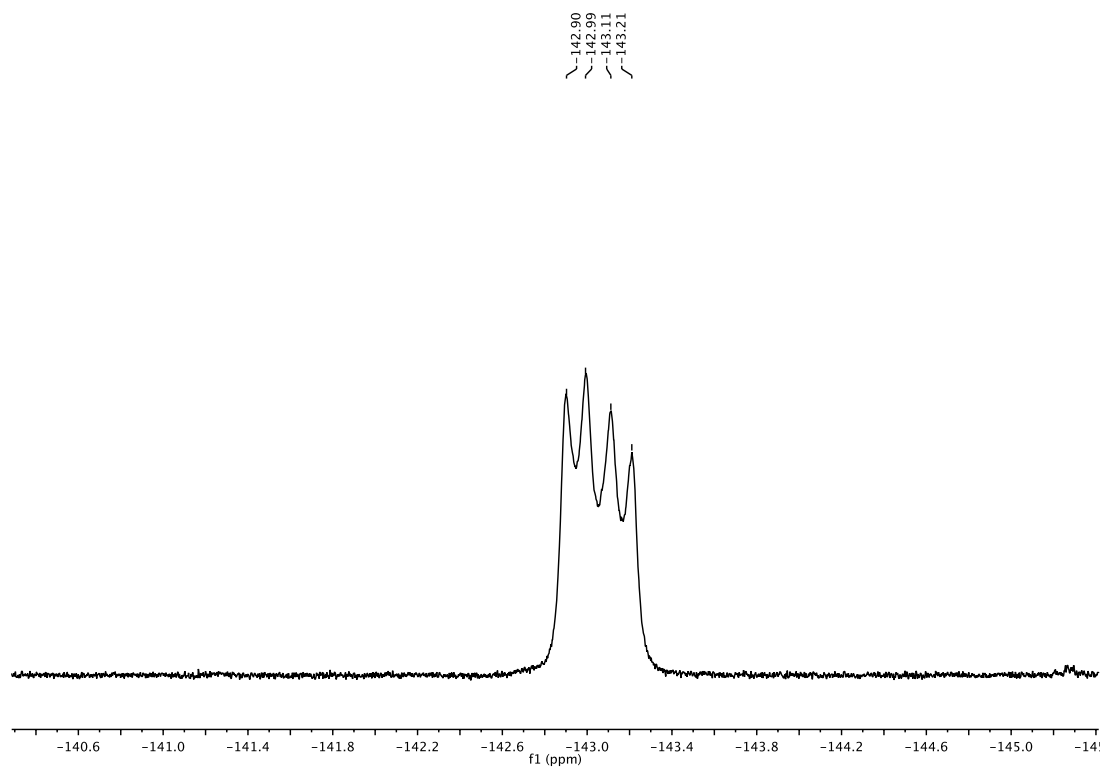
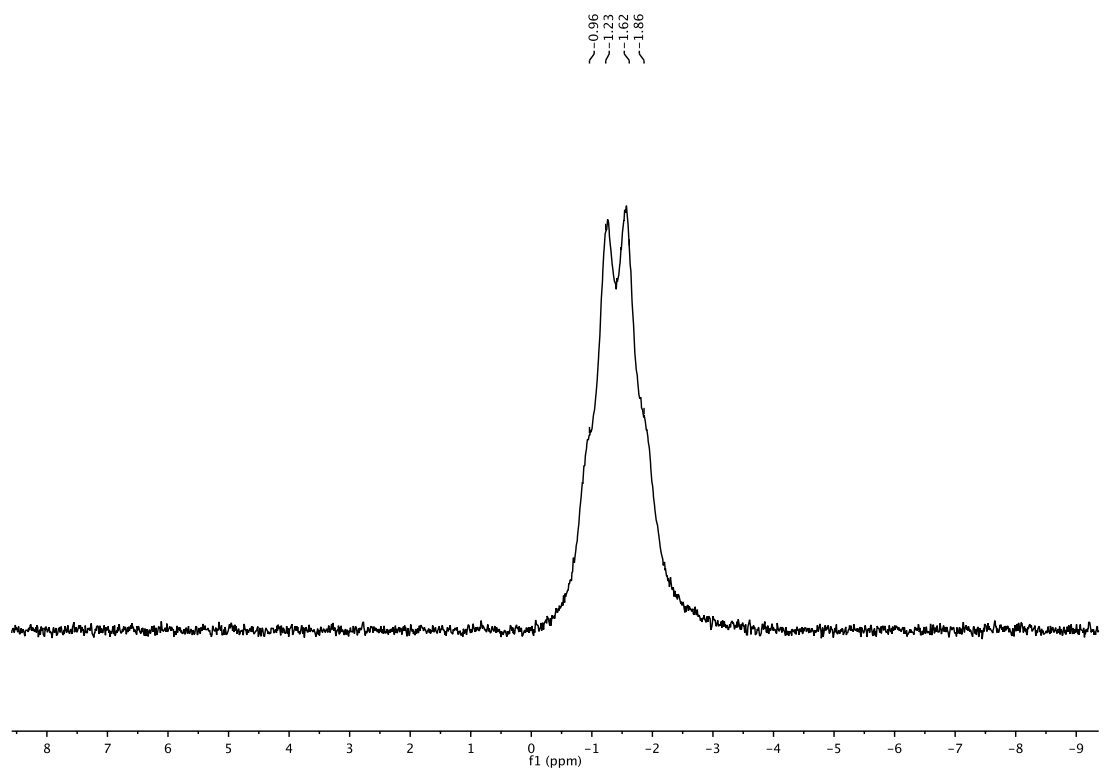


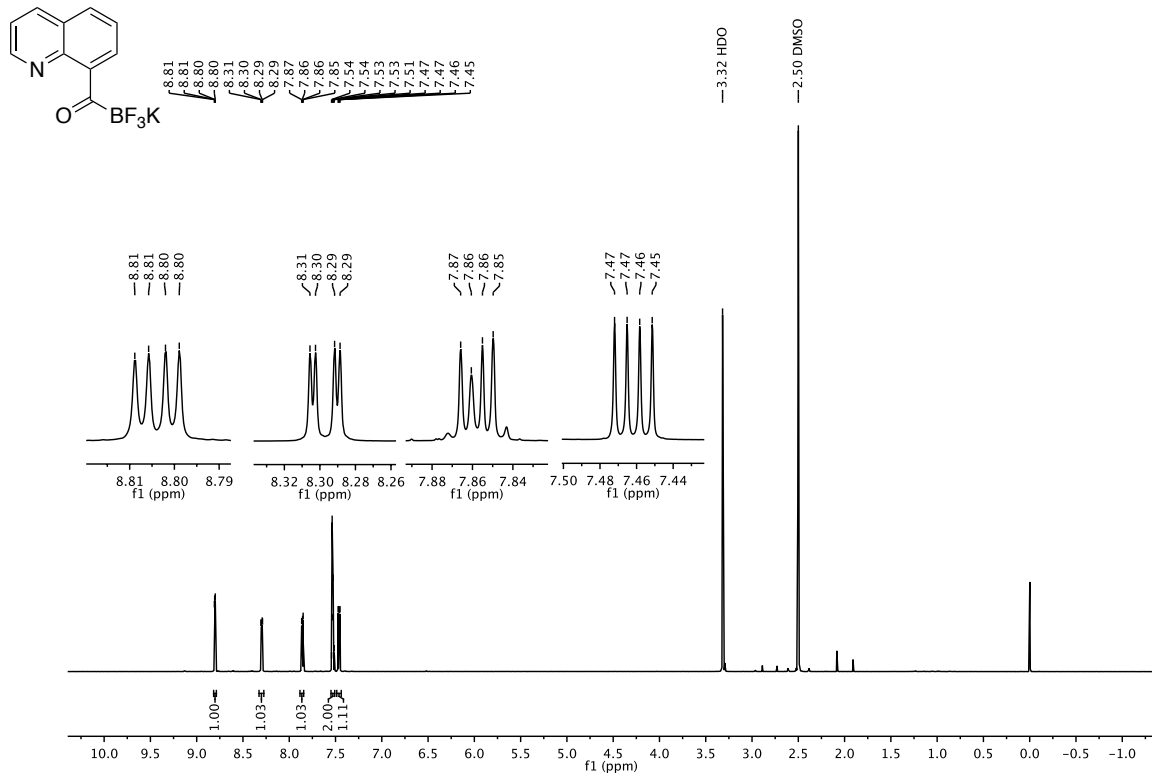
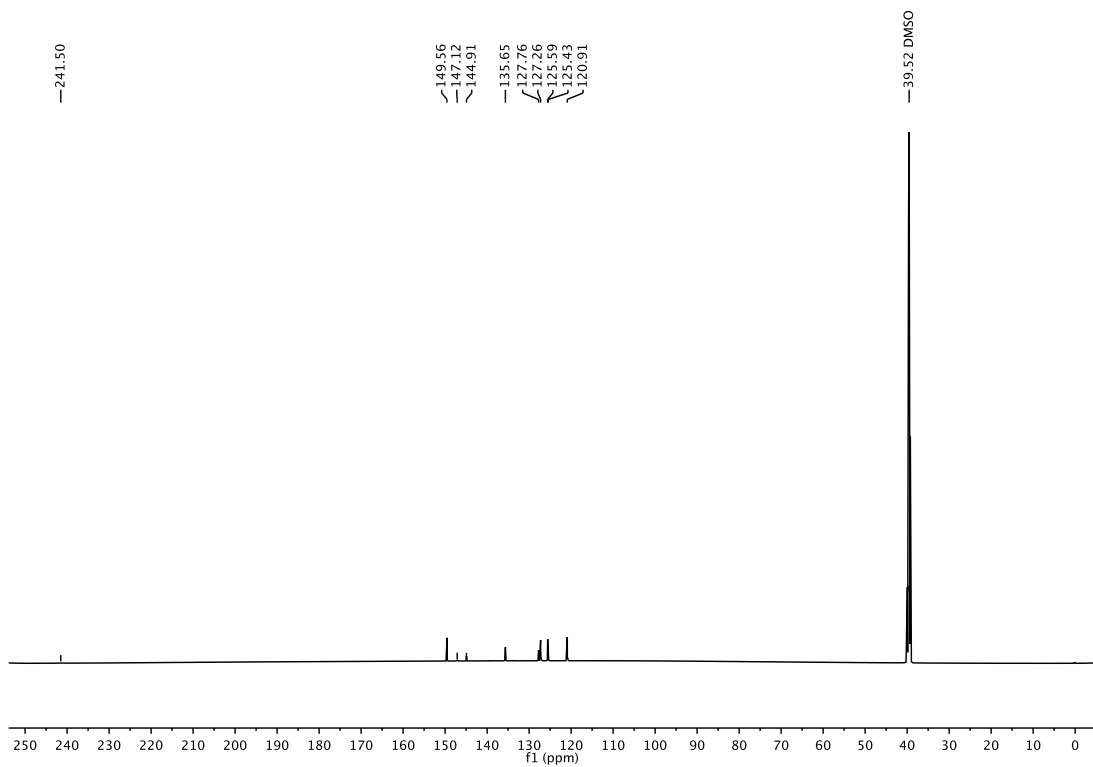
**<sup>11</sup>B-NMR (160 MHz, DMSO-d<sub>6</sub>)**

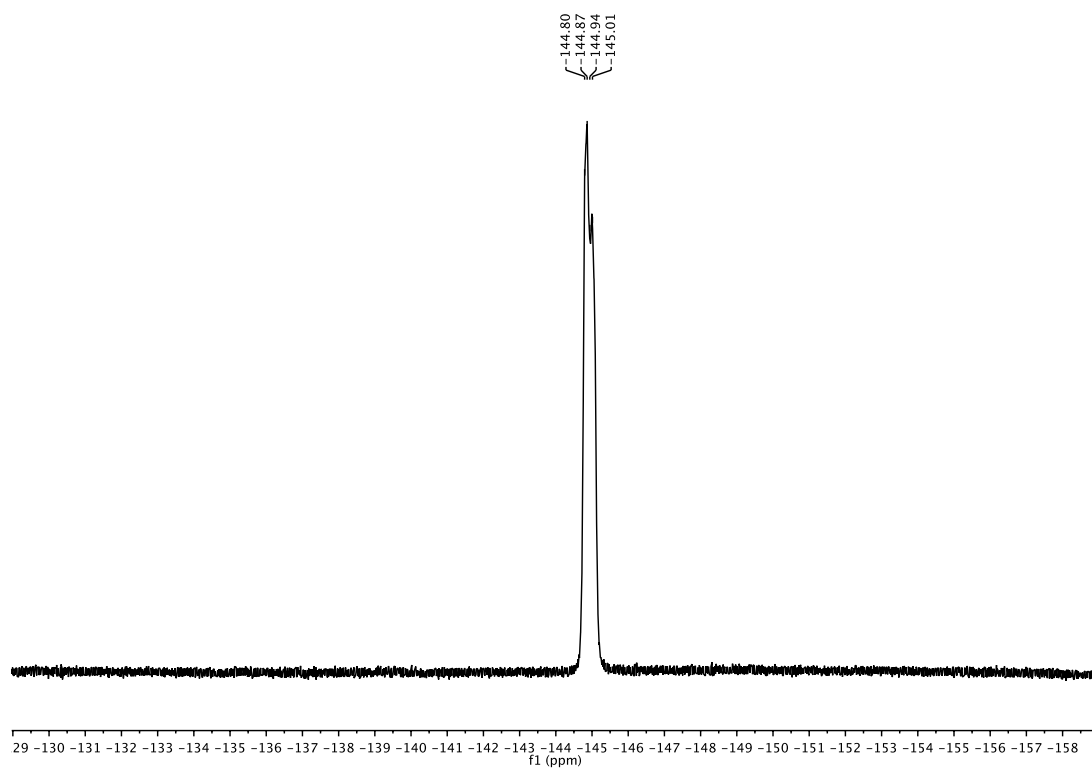
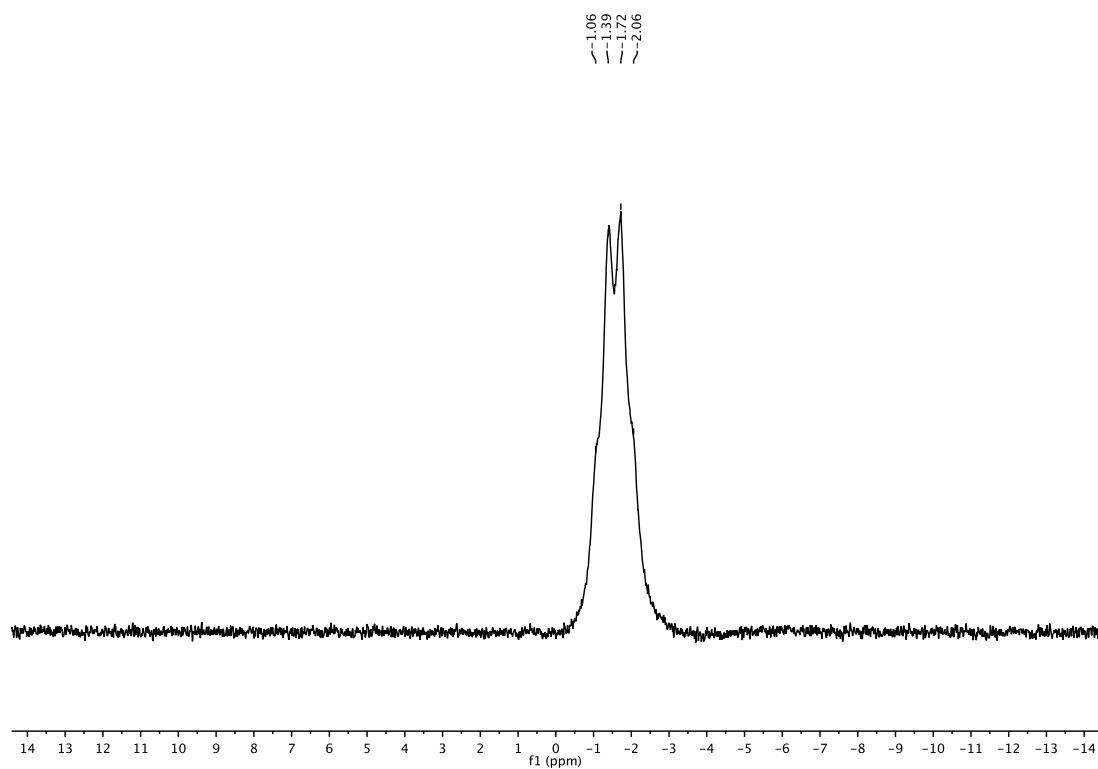


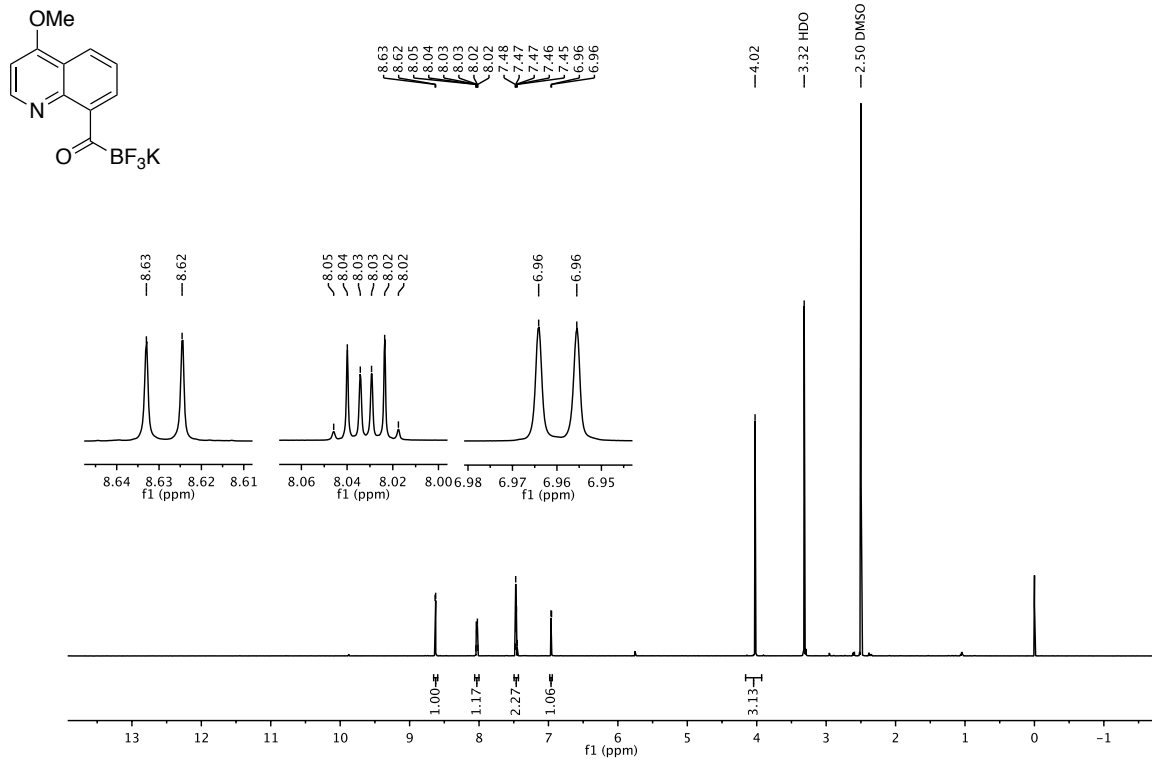
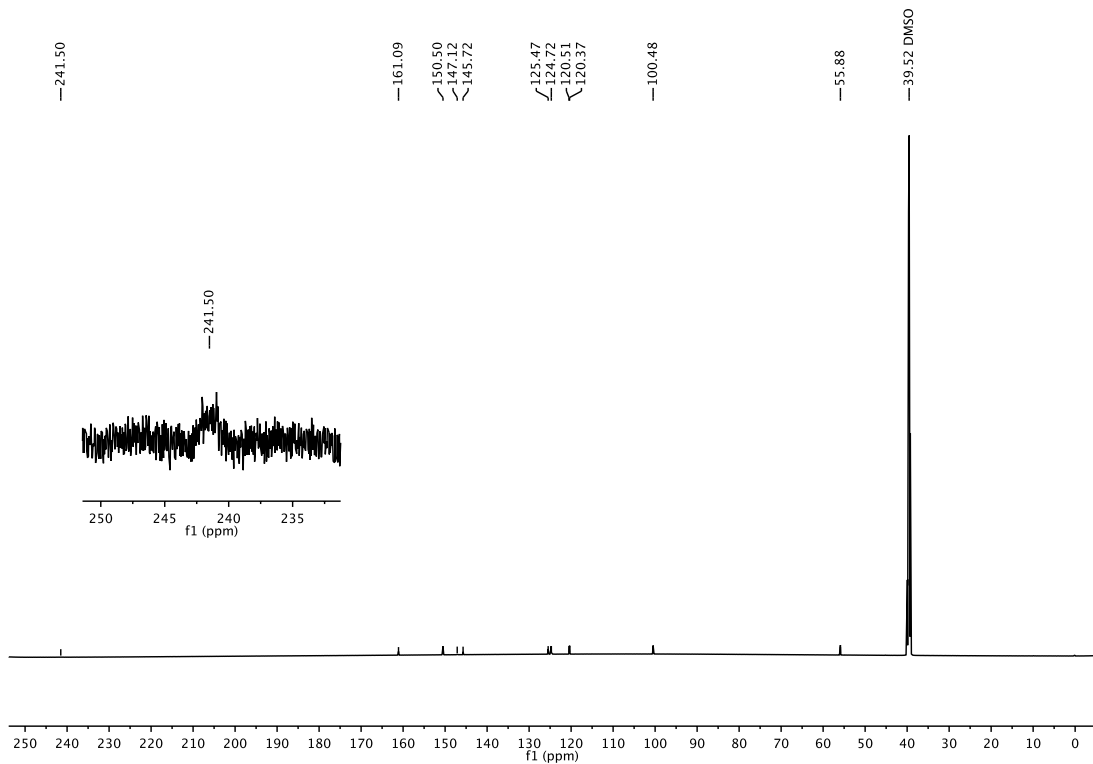
## Potassium (isoquinoline-8-yl)methanotrifluoroborate (173)

 $^1\text{H-NMR}$  (500 MHz,  $\text{DMSO-d}_6$ ) $^{13}\text{C-NMR}$  (150 MHz,  $\text{DMSO-d}_6$ )

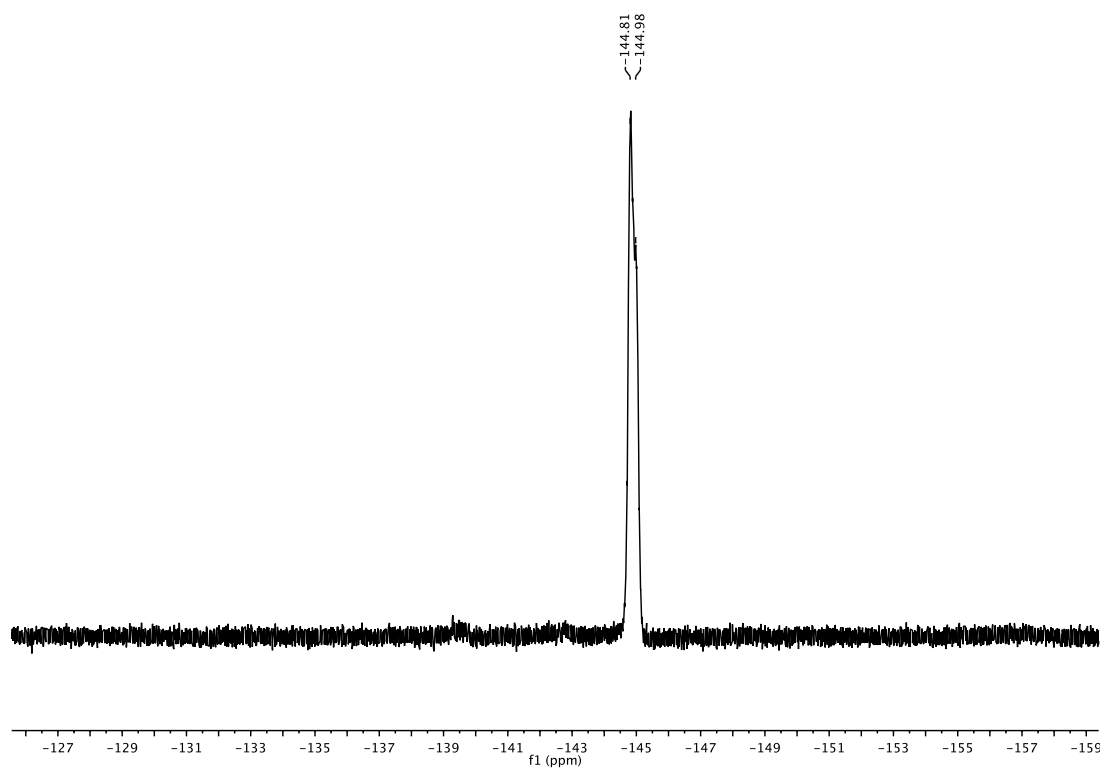
**$^{19}\text{F}$ -NMR (470 MHz,  $\text{DMSO-}d_6$ )** **$^{11}\text{B}$ -NMR (160 MHz,  $\text{DMSO-}d_6$ )**

**Potassium (quinoline-8-yl)methanonetrifluoroborate (171)** **$^1\text{H-NMR}$  (600 MHz,  $\text{DMSO-}d_6$ )** **$^{13}\text{C-NMR}$  (150 MHz,  $\text{DMSO-}d_6$ )**

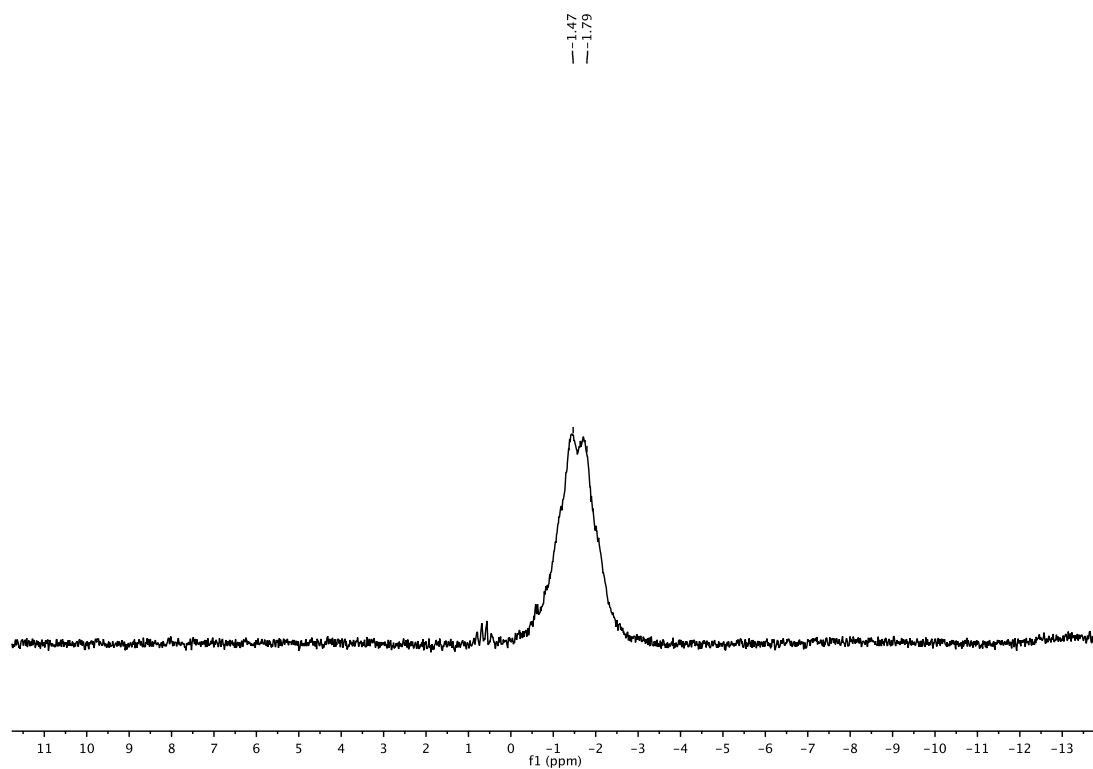
**$^{19}\text{F}$ -NMR (470 MHz,  $\text{DMSO-}d_6$ )** **$^{11}\text{B}$ -NMR (160 MHz,  $\text{DMSO-}d_6$ )**

**Potassium (4-methoxyquinoline-8-yl)methanonetrifluoroborate (174)****<sup>1</sup>H-NMR (600 MHz, DMSO-*d*<sub>6</sub>)****<sup>13</sup>C-NMR (150 MHz, DMSO-*d*<sub>6</sub>)**

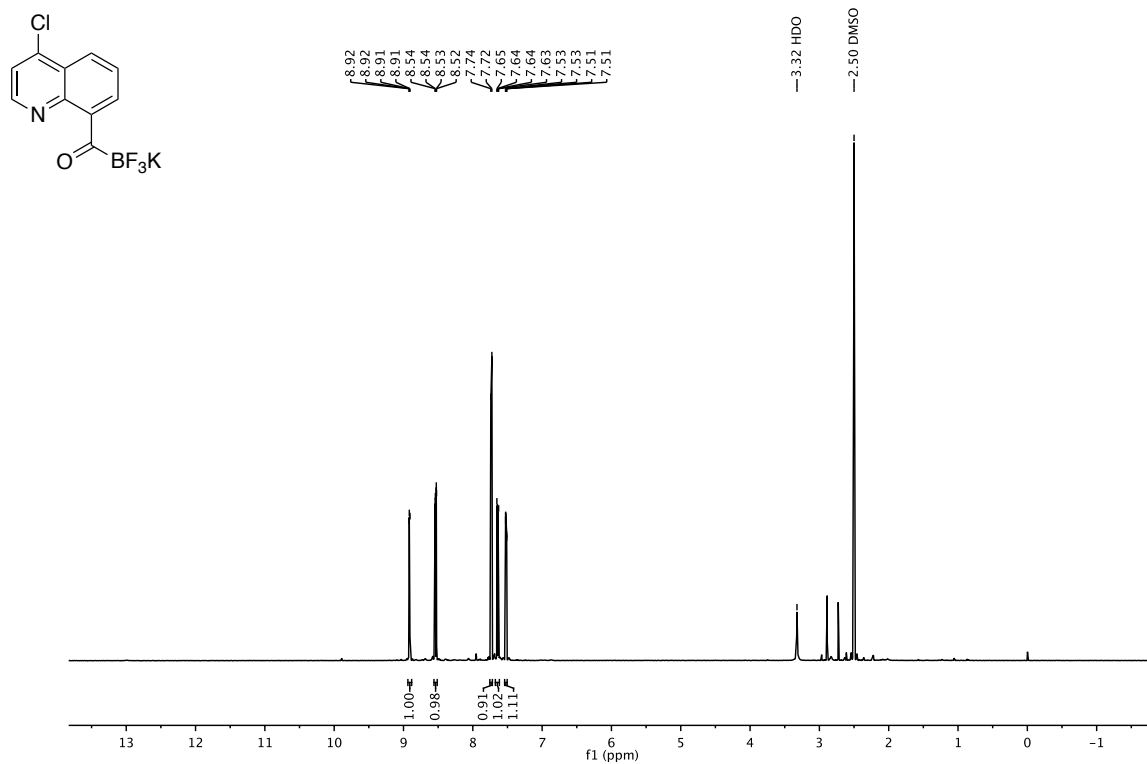
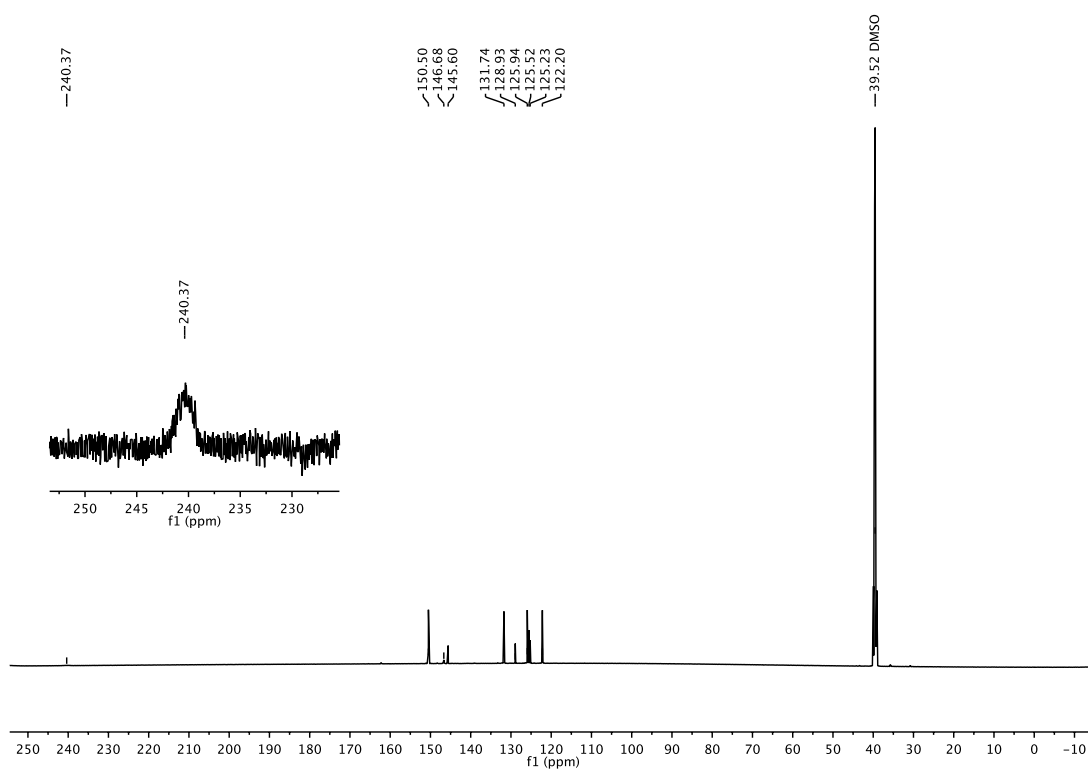
**$^{19}\text{F}$ -NMR (470 MHz,  $\text{DMSO-}d_6$ )**



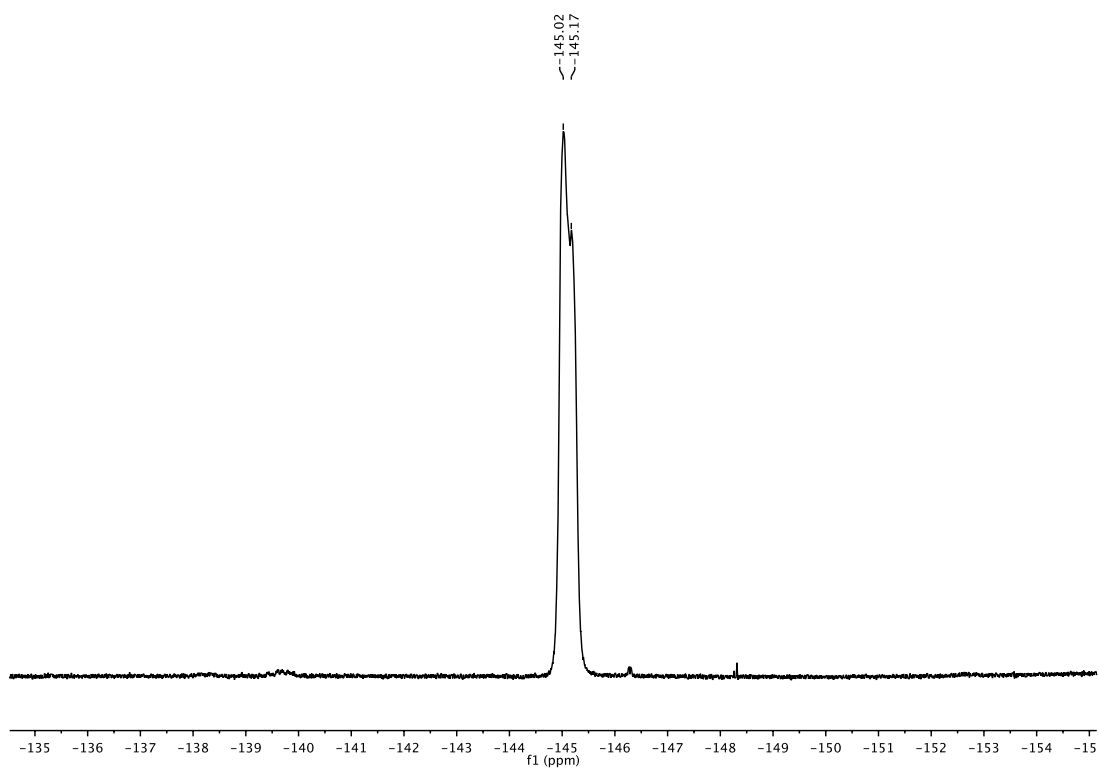
**$^{11}\text{B}$ -NMR (160 MHz,  $\text{DMSO-}d_6$ )**



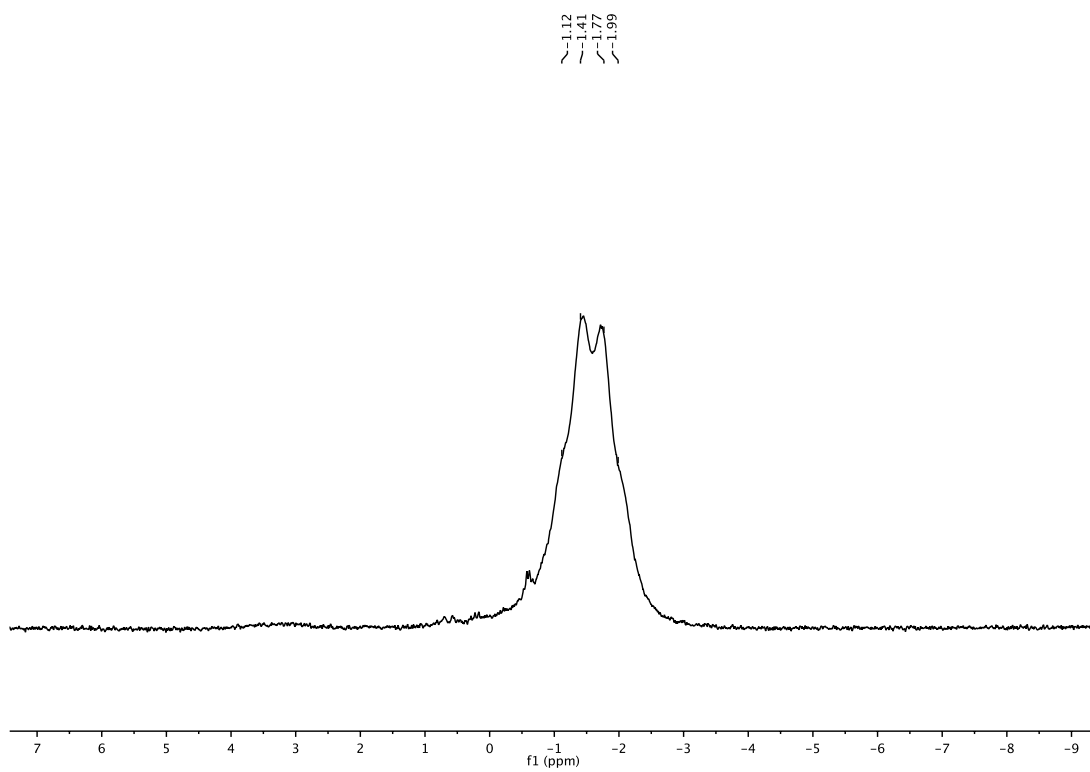


**Potassium (4-chloroquinoline-8-yl)methanonetrifluoroborate (175)****<sup>1</sup>H-NMR (500 MHz, DMSO-*d*<sub>6</sub>)****<sup>13</sup>C-NMR (150 MHz, DMSO-*d*<sub>6</sub>)**

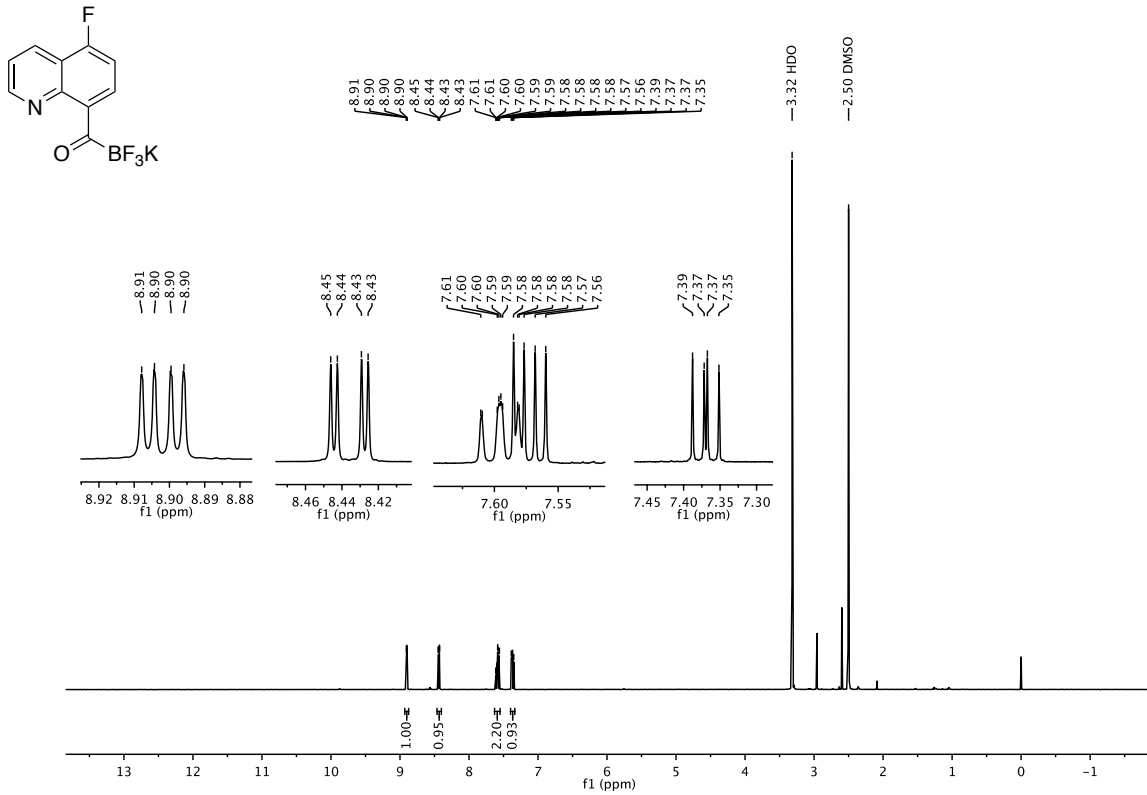
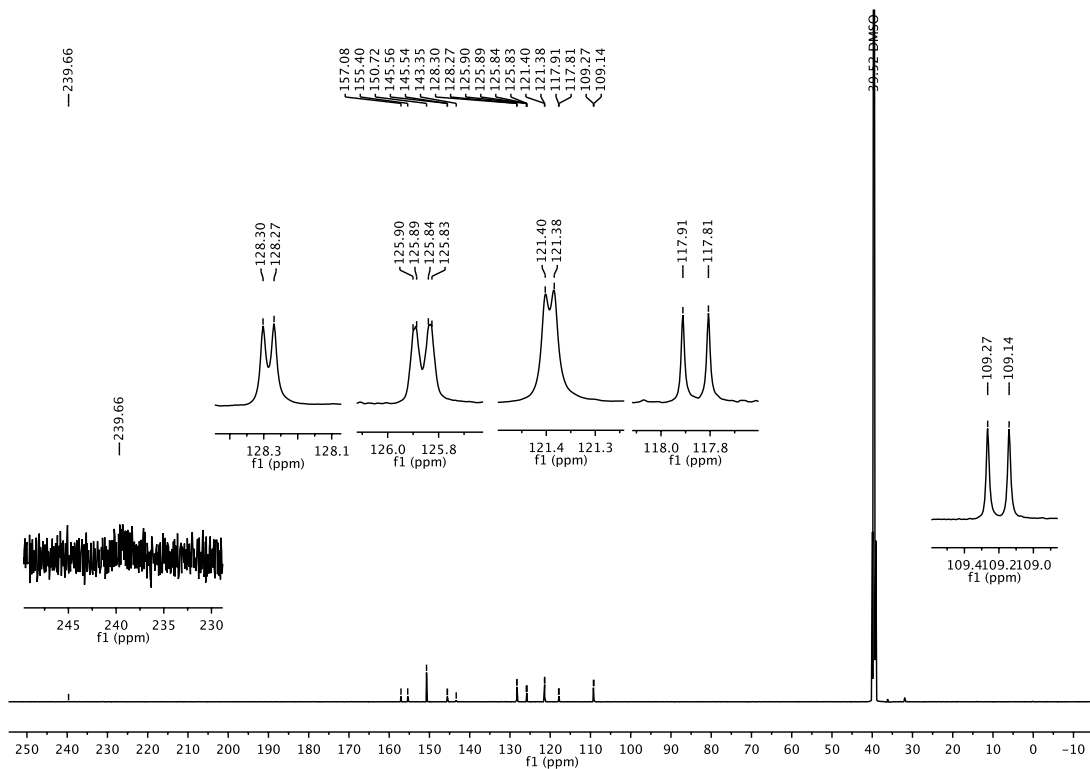
**$^{19}\text{F}$ -NMR (470 MHz, DMSO- $d_6$ )**

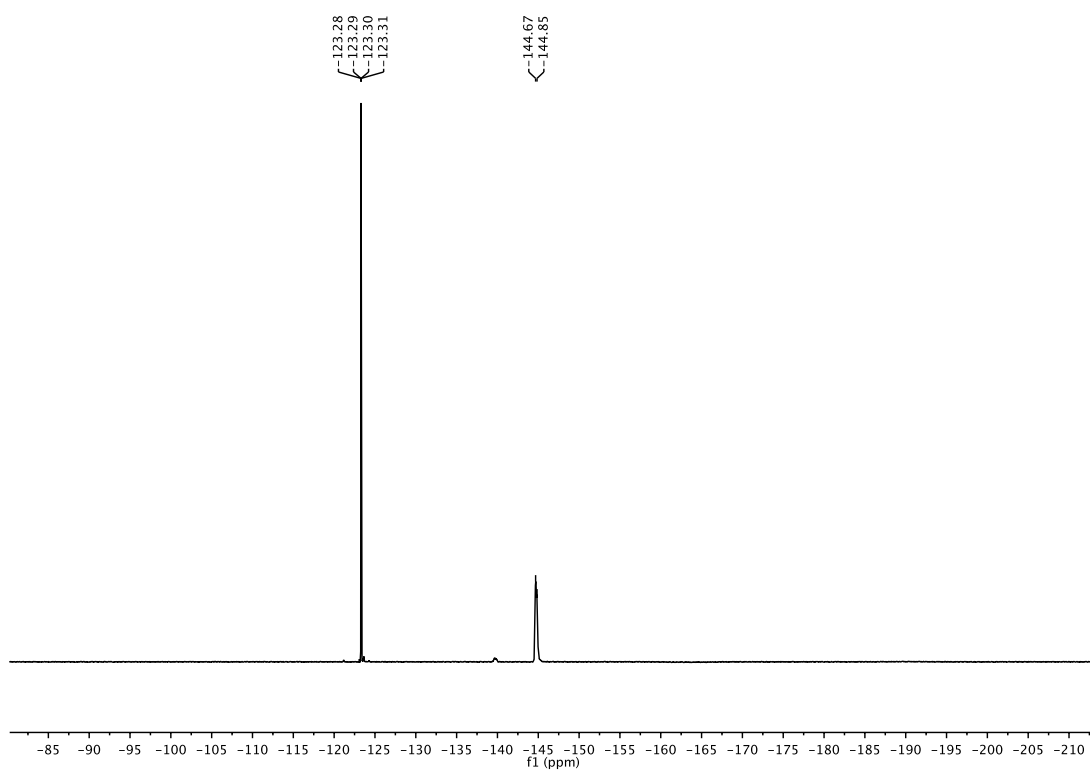
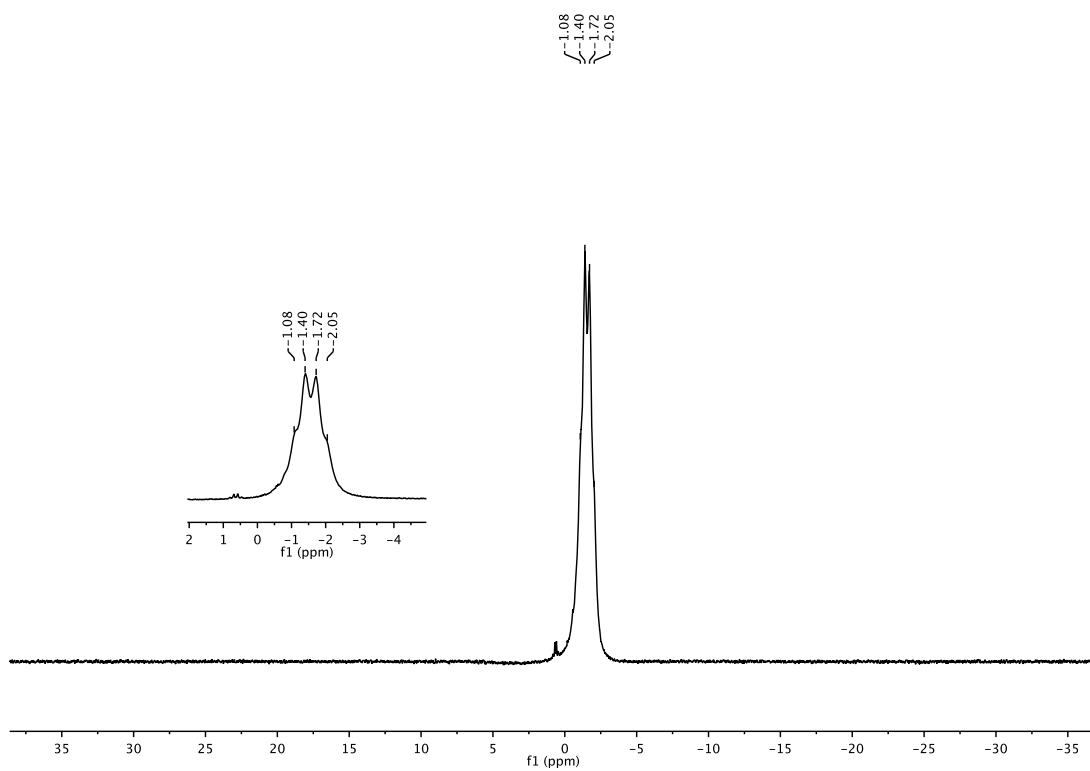


**$^{11}\text{B}$ -NMR (160 MHz, DMSO- $d_6$ )**

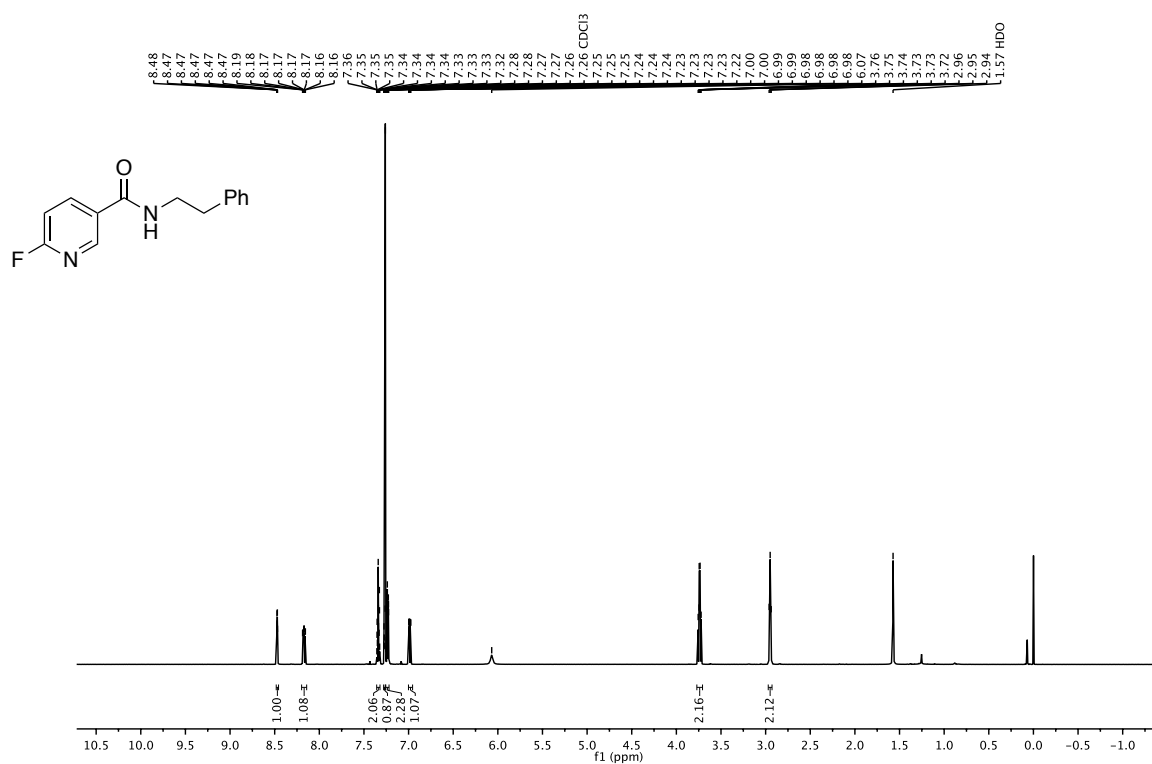
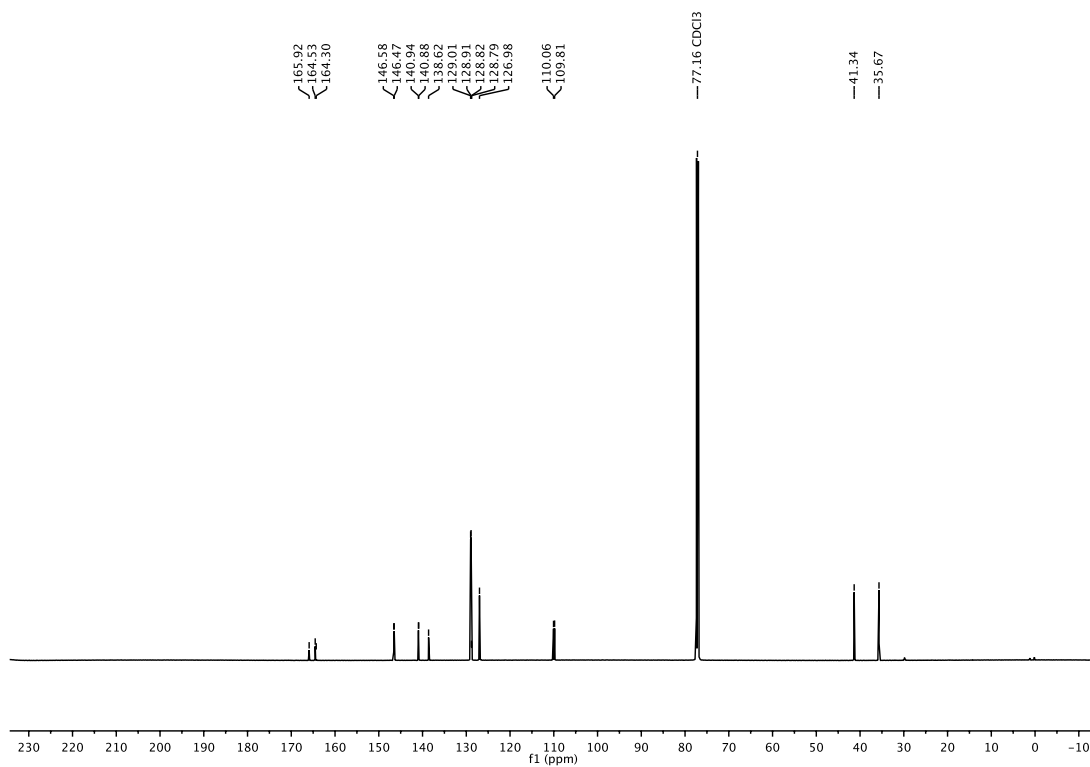


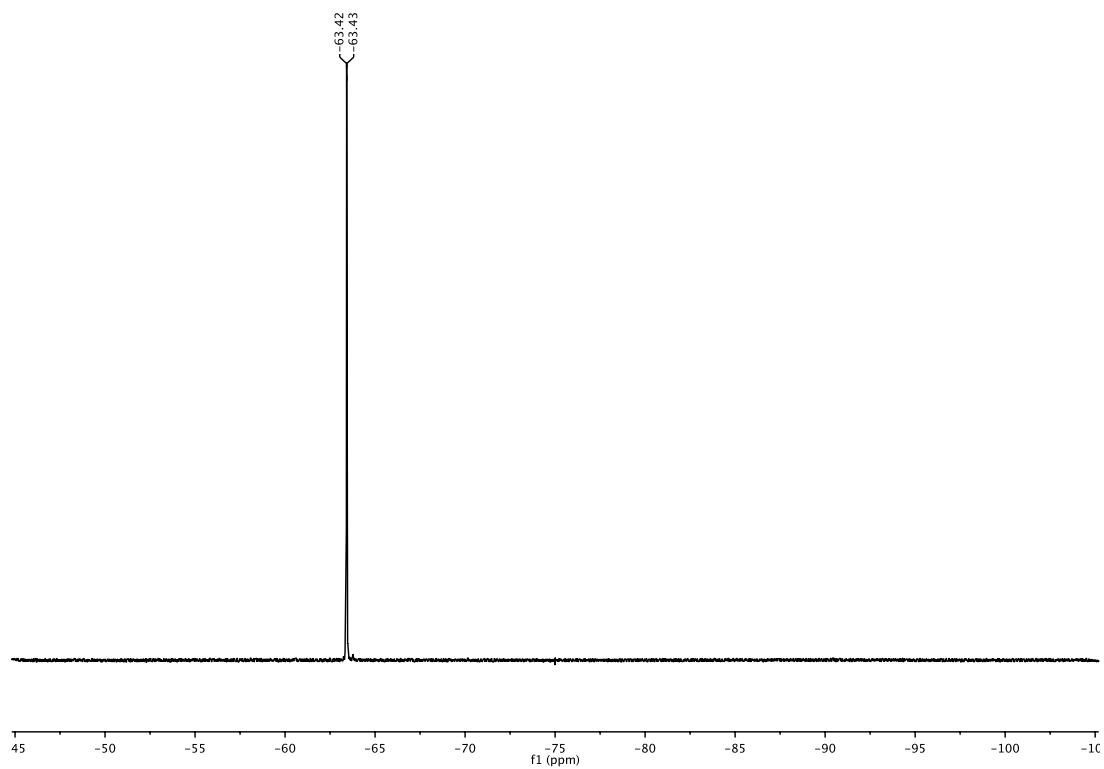
## Potassium (5-fluoroquinoline-8-yl)methanotrifluoroborate (179)

 $^1\text{H-NMR}$  (500 MHz,  $\text{DMSO-}d_6$ ) $^{13}\text{C-NMR}$  (150 MHz,  $\text{DMSO-}d_6$ )

**$^{19}\text{F}$ -NMR (470 MHz, DMSO- $d_6$ )** **$^{11}\text{B}$ -NMR (160 MHz, DMSO- $d_6$ )**



**N-(2-Phenethyl)-2-fluoro-3-picolinamide (S10)****<sup>1</sup>H-NMR (600 MHz, CDCl<sub>3</sub>)****<sup>13</sup>C-NMR (600 MHz, CDCl<sub>3</sub>)**

**$^{19}\text{F}$ -NMR (600 MHz,  $\text{CDCl}_3$ )**

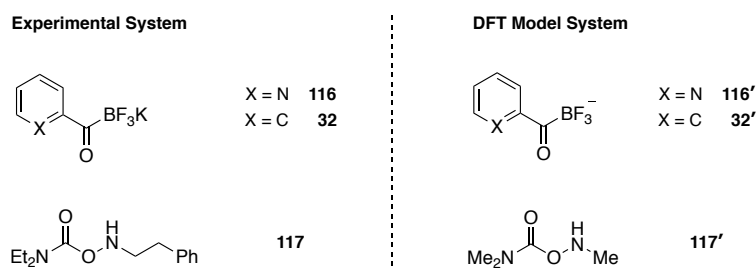
## 8.2 DFT Calculations

### 8.2.1 General Method

All calculations were performed with Gaussian09 (d1). Geometry optimization and transition state locations were conducted using the 6-31g(d) basis set in combination with the B3LYP functional. The nature of the found geometry is confirmed by analyzing the vibrational frequencies at the same level of theory. Additionally, transition states are confirmed by using IRC calculation. Single point calculations were done by using the 6-311+g(d,p) basis set with the M06-2X function with additional PCM solvation of water. 3D structures were generated by CYLview.

### 8.2.2 Model System

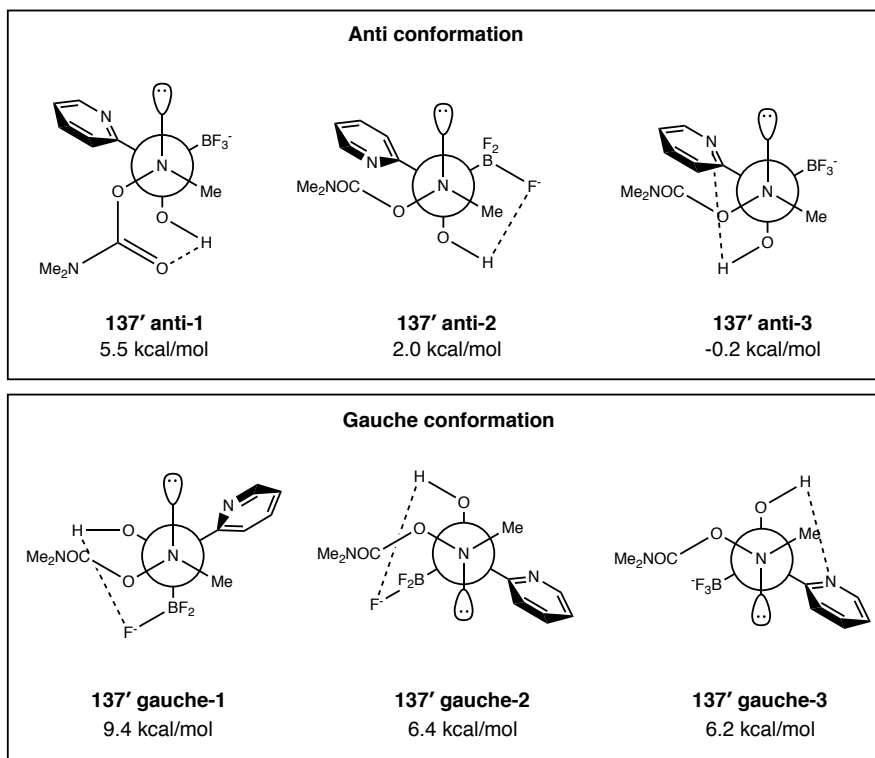
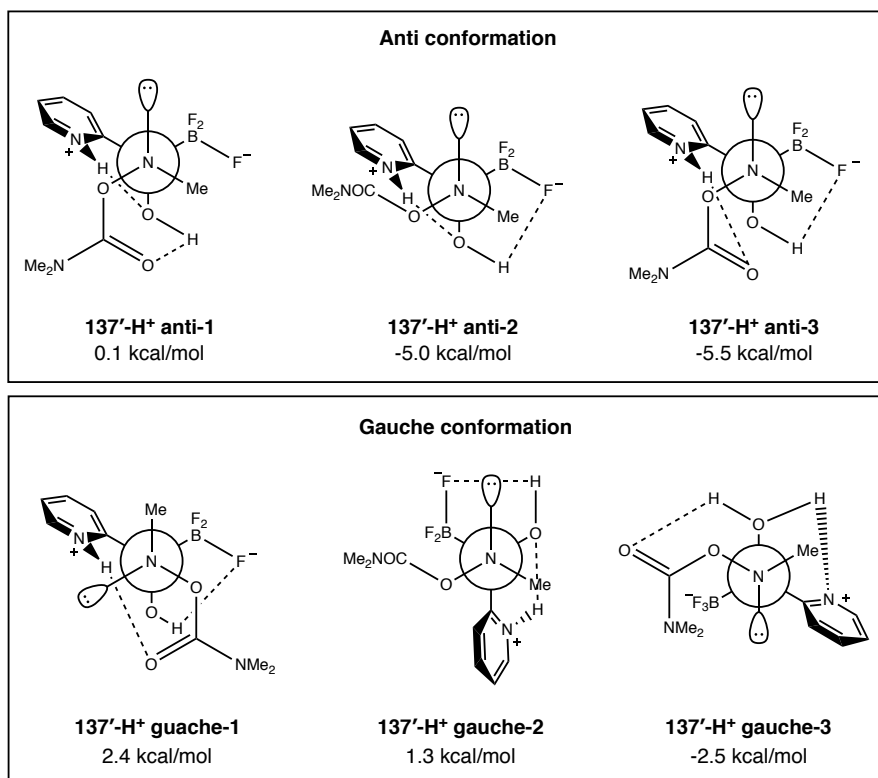
As a model system for DFT calculations of the KAT ligation the potassium acyltrifluoroborate **116** and **32** were considered without the potassium counterion resulting in acylboronate **116'** and **32'** respectively. In addition, **117** was simplified by replacing the diethylamine with a dimethylamine moiety and ethylbenzene substituent with a methyl group leading to structure **117'**.



### 8.2.3 Geometry Optimization

The lowest energy conformation of the proposed intermediate **137'** was calculated. In the following the lowest energy structures of each conformer are shown. In general, the anti conformation was found to be more energetically stable compared to the gauche conformation.



Most stable conformations of non-protonated pyridyl KAT **137'**.Most stable conformations of protonated pyridyl KAT **137'-H<sup>+</sup>**.

## 8.2.4 Cartesian Coordinates

### Hydroxylamine (117')

N 1.39157 0.12580 0.07834  
C 0.14528 -0.37257 -0.15055  
O -0.76396 0.62503 -0.41046  
O -0.15717 -1.55850 -0.15280  
N -2.11641 0.13583 -0.59841  
C -2.77892 0.18133 0.70685  
H -1.96267 -0.85032 -0.83279  
H -2.87194 1.22260 1.02664  
H -2.26341 -0.39793 1.48598  
H -3.78515 -0.22805 0.56328  
C 1.72439 1.54168 0.02186  
H 0.81676 2.14030 -0.00678  
H 2.32788 1.76703 -0.86849  
H 2.30735 1.81745 0.90946  
C 2.49753 -0.80272 0.25147  
H 2.10351 -1.81729 0.28799  
H 3.03145 -0.58382 1.18481  
H 3.20948 -0.71994 -0.58135

Thermal correction to Gibbs Free Energy = 0.117380

Sum of electronic and thermal Free Energies = -418.239343

SCF Done: E(RM062X) = -418.308547482 A.U. after 12 cycles

### Dimethylcarbamic acid

C -0.76889 -0.15474 -0.00024  
N 0.58203 0.02030 -0.00180  
O -1.45047 1.03204 0.00001  
O -1.34941 -1.22936 0.00042

H -2.38549 0.76549 0.00082  
C 1.44178 -1.15128 0.00028  
H 0.81746 -2.04360 -0.00436  
H 2.08106 -1.15778 0.89328  
H 2.08944 -1.15385 -0.88658  
C 1.23917 1.31729 0.00053  
H 1.86787 1.42589 0.89485  
H 0.49829 2.11353 -0.00918  
H 1.88384 1.41913 -0.88299

Thermal correction to Gibbs Free Energy = 0.076838

Sum of electronic and thermal Free Energies = -323.674055

SCF Done: E(RM062X) = -323.727838632 A.U. after 12 cycles

### **Dimethylcarbamate + BF<sub>3</sub>**

N -1.94302 -0.19886 -0.11521  
C -0.67941 0.42919 -0.03487  
O -0.60058 1.65316 0.00500  
O 0.29622 -0.44685 -0.03310  
C -3.12723 0.60754 0.04060  
H -2.83840 1.65288 -0.06959  
H -3.59906 0.47041 1.03152  
H -3.88138 0.34928 -0.72016  
C -2.11259 -1.62640 0.01965  
H -1.15410 -2.11434 -0.14658  
H -2.84351 -1.99856 -0.71649  
H -2.48486 -1.90880 1.02217  
B 1.78241 -0.08884 0.00611  
F 2.11533 0.64898 -1.12502  
F 2.42372 -1.33151 -0.00522  
F 2.06546 0.60174 1.17998

Thermal correction to Gibbs Free Energy = 0.071203

Sum of electronic and thermal Free Energies = -647.733695

SCF Done: E(RM062X) = -647.895425813 A.U. after 13 cycles

## K

K 0.0 0.0 0.0

SCF Done: E(RM062X) = -599.868041157 A.U. after 7 cycles

## KOH

O 0.00214 1.47398 0.00000

H -0.05767 2.43594 0.00000

K 0.00214 -0.74883 0.00000

Thermal correction to Gibbs Free Energy = -0.011046

Sum of electronic and thermal Free Energies = -675.724094

SCF Done: E(RM062X) = -675.803860897 A.U. after 11 cycles

## H<sub>2</sub>O

O 0.00000 0.11976 0.00000

H 0.76156 -0.47902 0.00000

H -0.76156 -0.47908 0.00000

Thermal correction to Gibbs Free Energy = 0.002839

Sum of electronic and thermal Free Energies = -76.406114

SCF Done: E(RM062X) = -76.4287732816 A.U. after 9 cycles

## Phenyl KAT (119')

C 3.36356 -0.51563 0.04301

C 3.05298 0.84699 0.11168

C 1.72341 1.25841 0.05596

C 0.68170 0.32715 -0.06002

C 1.00248 -1.03604 -0.13350

C 2.33521 -1.45238 -0.08249

H 4.40111 -0.84345 0.08622

H 2.57332 -2.51326 -0.14258

H 0.19720 -1.75340 -0.24588  
H 3.85136 1.58193 0.20789  
C -0.76739 0.82695 -0.10737  
O -0.91553 2.04752 -0.20136  
B -2.01738 -0.25227 0.04422  
F -1.85474 -1.29056 -0.91760  
F -3.24163 0.38807 -0.15338  
F -1.94933 -0.81224 1.34010  
H 1.44779 2.30912 0.09844

Thermal correction to Gibbs Free Energy = 0.074787

Sum of electronic and thermal Free Energies = -669.512222

SCF Done: E(RM062X) = -669.653369989 A.U. after 15 cycles

### 138' (anti-conformation)

N 3.25502 -0.41760 0.22016  
C 2.18420 -1.12010 -0.30534  
O 1.11702 -1.02462 0.51727  
O 2.24440 -1.76680 -1.33892  
N -0.18430 -1.37308 -0.14573  
C -0.39319 -2.77791 0.19986  
H -0.39625 -2.94103 1.28537  
H 0.40200 -3.35957 -0.27295  
H -1.36148 -3.06174 -0.20907  
C 3.16457 0.44898 1.38048  
H 2.12053 0.61110 1.64024  
H 3.62802 1.41995 1.15478  
H 3.68851 0.01694 2.24830  
C 4.54955 -0.54493 -0.40961  
H 4.45320 -1.22169 -1.25839  
H 5.29652 -0.94436 0.29485  
H 4.91191 0.43151 -0.76580  
C 0.15673 3.61463 -0.50971  
C -0.28539 3.28461 0.77112  
C -0.69379 1.97965 1.06232

C -0.66784 0.97953 0.08426  
C -0.23177 1.32483 -1.20571  
C 0.18163 2.62317 -1.49630  
H 0.47552 4.62977 -0.73998  
H 0.52121 2.86587 -2.50186  
H -0.21738 0.55777 -1.97193  
H -0.31352 4.04423 1.55121  
C -1.15940 -0.43320 0.39221  
O -1.29642 -0.60840 1.82224  
B -2.70669 -0.62589 -0.28819  
F -2.80181 -0.00941 -1.53336  
F -3.56290 0.01542 0.66059  
F -3.10683 -1.97178 -0.38776  
H -2.25095 -0.48224 1.96459  
H -1.02731 1.71251 2.05906

Thermal correction to Gibbs Free Energy = 0.216106

Sum of electronic and thermal Free Energies = -1087.736940

SCF Done: E(RM062X) = -1087.97772356 A.U. after 14 cycles

### **138' (gauche-conformation)**

C -2.51338 -0.64484 0.23240  
N -3.43094 0.34872 -0.08117  
O -1.36446 -0.08157 0.68199  
N -0.23298 -1.03191 0.76402  
C 0.18899 -0.95032 2.15503  
H 1.08601 -1.56138 2.24735  
H -0.61008 -1.36138 2.78171  
H 0.41345 0.07571 2.48906  
C 0.74811 -0.63947 -0.29510  
O 0.03911 -0.79194 -1.52667  
B 2.03459 -1.71995 -0.35362  
O -2.75929 -1.83258 0.14332  
F 2.63547 -1.95284 0.91221  
F 1.50490 -2.93169 -0.86406

F 3.00070 -1.21719 -1.23133  
H 0.08431 -1.75147 -1.68527  
H 0.47440 3.91965 -1.44768  
C 0.57505 1.82218 -0.96392  
C 0.95261 3.15968 -0.83113  
C 1.17515 0.81931 -0.18804  
C 1.94450 3.52548 0.08194  
H 2.24166 4.56759 0.18540  
C 2.18612 1.19721 0.70918  
C 2.56211 2.53465 0.84749  
H 2.69626 0.42455 1.27521  
H 3.35292 2.80066 1.54687  
C -3.17853 1.76787 0.07429  
H -3.58608 2.31057 -0.79057  
H -2.10797 1.95281 0.13354  
H -3.66093 2.17224 0.98027  
C -4.78917 -0.04155 -0.38555  
H -5.12241 0.42233 -1.32545  
H -5.48890 0.26804 0.40895  
H -4.81949 -1.12617 -0.48568  
H -0.18037 1.53133 -1.68570

Thermal correction to Gibbs Free Energy = 0.216643

Sum of electronic and thermal Free Energies = -1087.732149

SCF Done: E(RM062X) = -1087.97728327 A.U. after 15 cycles

### 138' TS-1

C -2.53927 -0.39871 -0.09748  
N -3.77856 0.17046 0.22487  
O -1.54738 0.12767 0.58528  
N -0.16607 -0.97811 0.71007  
C 0.14947 -0.70346 2.10128  
H 0.99875 -1.33974 2.35916  
H -0.71833 -0.97653 2.70669  
H 0.42249 0.34243 2.29815

C 0.76703 -0.62746 -0.28119  
O 0.20793 -0.86689 -1.55880  
B 2.06419 -1.84459 -0.11752  
O -2.46792 -1.29620 -0.94395  
F 2.67830 -1.75817 1.15654  
F 1.50896 -3.09600 -0.30172  
F 2.97542 -1.50841 -1.10461  
H -0.65324 -1.31383 -1.40311  
H 0.72494 3.84047 -1.69949  
C 0.74389 1.77841 -1.08194  
C 1.18236 3.10140 -1.04332  
C 1.31103 0.80282 -0.24817  
C 2.20569 3.48097 -0.17086  
H 2.55197 4.51270 -0.14242  
C 2.34788 1.19153 0.61325  
C 2.78700 2.51728 0.65365  
H 2.82826 0.43952 1.22820  
H 3.59766 2.79257 1.32626  
C -3.88852 1.32775 1.08833  
H -3.93730 2.27163 0.51802  
H -3.02350 1.36857 1.74780  
H -4.80456 1.25498 1.69212  
C -4.90827 -0.09402 -0.63996  
H -5.11343 0.74928 -1.32232  
H -5.81392 -0.26737 -0.04072  
H -4.68606 -0.98118 -1.23171  
H -0.03717 1.47060 -1.76715

Thermal correction to Gibbs Free Energy = 0.216071

Sum of electronic and thermal Free Energies = -1087.723363

SCF Done: E(RM062X) = -1087.95537641 A.U. after 16 cycles

Imaginary Frequency: -284.40  $\text{cm}^{-1}$

### 138' TS-2

C -2.78733 0.01770 0.68126



---

N -3.72765 0.40676 -0.29855  
O -1.59131 0.48538 0.45881  
N -0.27798 -0.93709 0.51084  
C -0.01431 -0.92894 1.93925  
H 0.64036 -1.77966 2.15227  
H -0.97734 -1.06023 2.43215  
H 0.47256 -0.00990 2.29035  
C 0.67300 -0.51781 -0.37105  
O 0.17598 -0.47938 -1.69775  
B 1.78667 -2.04264 -0.45239  
O -3.15147 -0.68908 1.63169  
F 0.98821 -3.01794 -1.01141  
F 2.79689 -1.62166 -1.28154  
F 2.25965 -2.38352 0.80735  
H -0.36109 -1.28634 -1.77295  
C 1.14527 1.93073 -0.77185  
C 1.48174 0.73802 -0.11473  
H 1.56995 4.02299 -1.03800  
C 1.84997 3.10722 -0.52058  
C 2.55048 0.75440 0.79216  
C 2.90646 3.11662 0.39330  
C 3.25263 1.93407 1.04734  
H 2.84523 -0.16854 1.27871  
H 3.45627 4.03513 0.58930  
H 4.08096 1.92250 1.75298  
C -5.13653 0.27327 -0.02102  
H -5.24338 -0.37333 0.85042  
H -5.66654 -0.17524 -0.87633  
H -5.61702 1.24646 0.19064  
C -3.34568 1.23464 -1.42017  
H -2.29360 1.05924 -1.64510  
H -3.49050 2.31376 -1.22910  
H -3.95533 0.97065 -2.29746  
H 0.32295 1.92111 -1.47684

Thermal correction to Gibbs Free Energy = 0.212793

Sum of electronic and thermal Free Energies = -1087.720759

SCF Done: E(RM062X) = -1087.94042261 A.U. after 17 cycles

Imaginary Frequency: -345.58 cm<sup>-1</sup>

### Phenyl Nitroene 143'

C 2.68435 -0.73236 -0.30879

N 2.67997 -0.10283 0.88834

O 1.54573 -1.53712 -0.66409

N 0.22631 -1.30292 -0.21570

C -0.28560 -2.60722 0.23399

H -0.39479 -3.26597 -0.63083

H -1.24087 -2.47556 0.73628

H 0.45331 -3.03852 0.91056

C -0.39467 -0.17023 -0.35948

C -1.84244 -0.13651 -0.04446

B 0.28941 1.33774 -0.78842

O 3.57133 -0.77026 -1.11916

F 1.45310 1.16814 -1.50913

F -0.68043 2.00923 -1.49913

F 0.52448 1.93697 0.47093

C 3.60686 1.01583 1.05492

H 4.12592 1.18856 0.11419

H 4.34034 0.79384 1.83996

H 3.03503 1.91008 1.32318

C 1.85349 -0.41099 2.04414

H 1.44849 -1.42095 1.97983

H 1.04284 0.31540 2.16180

H 2.48867 -0.37604 2.93692

C -2.32542 0.87114 0.80922

C -2.75684 -1.00823 -0.66161

C -3.68691 0.95701 1.08601

H -1.62538 1.57821 1.23834

C -4.58866 0.07921 0.47961

H -4.04734 1.72765 1.76133

C -4.12234 -0.89246 -0.40709  
H -2.40649 -1.75009 -1.37368  
H -5.65234 0.16327 0.68403  
H -4.82008 -1.55956 -0.90518

Thermal correction to Gibbs Free Energy = 0.206672

Sum of electronic and zero-point Energies = -1011.773288

SCF Done: E(RM062X) = -1011.96883826 A.U. after 14 cycles

### 143' TS-3

C -2.38195 0.97093 -0.07174  
N -3.57630 0.30012 -0.23525  
O -1.65529 0.49529 0.94417  
N 0.06292 1.07627 0.77630  
C -0.07079 2.39842 1.34929  
H 0.93302 2.83396 1.40531  
H -0.50579 2.30692 2.34571  
H -0.72874 2.97525 0.69862  
C 0.86004 0.26323 0.38875  
C 2.28659 0.29616 0.10395  
B -0.31119 -2.20973 -0.19464  
O -2.04739 1.91639 -0.79047  
F 0.89080 -2.68612 -0.49354  
F -0.79890 -2.41812 1.01629  
F -1.06864 -1.70338 -1.14842  
C -4.56033 0.82526 -1.16289  
H -4.10359 1.63528 -1.72979  
H -5.44605 1.20612 -0.63207  
H -4.89001 0.03722 -1.85336  
C -3.99336 -0.80194 0.61247  
H -4.73590 -0.48216 1.36018  
H -3.13072 -1.21917 1.12816  
H -4.45280 -1.58472 -0.00505  
C 3.10887 -0.78752 0.45443

C 2.84812 1.41231 -0.54827  
C 4.47757 -0.73093 0.20218  
H 2.67054 -1.66103 0.92207  
C 5.03097 0.37571 -0.44551  
H 5.11039 -1.56428 0.49382  
C 4.21112 1.43946 -0.83101  
H 2.20955 2.23660 -0.85144  
H 6.09578 0.40525 -0.65885  
H 4.63501 2.29705 -1.34602

Thermal correction to Gibbs Free Energy = 0.196603

Sum of electronic and thermal Free Energies = -1011.812010

SCF Done: E(RM062X) = -1011.91822669 A.U. after 16 cycles

Imaginary Frequency: -198.1756  $\text{cm}^{-1}$

#### 148'

N -4.91013 0.50688 -0.11631  
C -3.61827 0.43710 0.38855  
O -3.38517 0.17439 1.56306  
O -2.70152 0.69550 -0.54369  
N 0.77617 -1.15629 0.13603  
C -0.53756 -1.75001 0.39776  
H -1.16294 -1.76347 -0.50510  
H -1.07238 -1.18679 1.16698  
H -0.39412 -2.78099 0.72074  
C -6.01608 0.13828 0.73832  
H -5.63847 0.01838 1.75337  
H -6.48106 -0.80701 0.41326  
H -6.79379 0.91643 0.72452  
C -5.20645 0.70836 -1.51889  
H -4.30830 1.03857 -2.03646  
H -5.99050 1.47142 -1.63561  
H -5.56921 -0.21820 -1.99421  
C 4.43017 2.52535 0.11439  
C 3.26287 2.99581 -0.49141

C 2.11372 2.20709 -0.49433  
C 2.11767 0.92841 0.08006  
C 3.29123 0.46264 0.68844  
C 4.43526 1.26137 0.70737  
H 5.32774 3.14094 0.12724  
H 5.33831 0.88944 1.18684  
H 3.30575 -0.52389 1.13590  
H 3.24526 3.98099 -0.95345  
C 0.80543 0.18130 0.11792  
O -0.22466 0.90975 0.18607  
B 1.91889 -2.17363 -0.31078  
F 2.67895 -2.55040 0.81640  
F 2.72901 -1.57701 -1.27352  
F 1.27347 -3.29698 -0.83403  
H -1.76215 0.67557 -0.15050  
H 1.18902 2.57082 -0.92984

Thermal correction to Gibbs Free Energy = 0.213500

Sum of electronic and thermal Free Energies = -1087.869408

SCF Done: E(RM062X) = -1088.09871150 A.U. after 14 cycles

#### 147'

N 2.49875 -0.00110 -0.00100  
C 3.92944 0.00187 0.00108  
H 4.28225 0.59426 -0.84691  
H 4.27499 -1.03067 -0.09359  
H 4.28214 0.43205 0.94184  
C 1.34210 -0.00101 -0.00040  
C -0.75838 -1.23430 -0.00008  
C -0.06677 -0.00125 -0.00025  
H -2.69422 -2.15445 0.00024  
C -2.14620 -1.21810 0.00015  
C -0.75626 1.23330 -0.00011  
C -2.83435 0.00137 0.00028  
C -2.14403 1.21966 0.00016

H -0.20756 2.16929 -0.00018

H -3.92013 0.00233 0.00051

H -2.69042 2.15697 0.00028

H -0.21158 -2.17140 -0.00015

Thermal correction to Gibbs Free Energy = 0.104757

Sum of electronic and thermal Free Energies = -364.048603

SCF Done: E(RM062X) = -364.144743223 A.U. after 13 cycles

### **N-methylbenzamide (141')**

C -3.50238 -0.51620 -0.19950

N -2.05945 -0.67774 -0.14912

H -3.78010 0.27387 0.49913

H -3.98901 -1.45146 0.09332

H -3.85458 -0.22884 -1.19961

C -1.23424 0.38593 0.11118

H -1.66000 -1.48934 -0.59717

O -1.66887 1.50096 0.38625

C 0.24301 0.10592 0.05041

C 0.79567 -1.17372 0.20232

C 2.17727 -1.35745 0.13995

C 3.01894 -0.26480 -0.07544

C 1.09664 1.19967 -0.14477

C 2.47537 1.01491 -0.21469

H 0.15582 -2.02790 0.40817

H 2.59591 -2.35192 0.26903

H 4.09495 -0.40878 -0.12582

H 0.65438 2.18630 -0.23564

H 3.12807 1.86897 -0.37428

Thermal correction to Gibbs Free Energy = 0.121011

Sum of electronic and thermal Free Energies = -440.140660

SCF Done: E(RM062X) = -440.203928148 A.U. after 13 cycles

**Pyridyl KAT (116')**

C 3.32732 -0.56485 -0.00012  
C 2.23184 -1.42991 0.00035  
N 0.95744 -1.02759 0.00048  
C 0.71551 0.29490 0.00013  
C 1.75481 1.24067 -0.00032  
C 3.07515 0.80945 -0.00047  
H 4.34164 -0.95790 -0.00020  
H 3.89724 1.52402 -0.00085  
H 1.47530 2.28941 -0.00049  
H 2.39026 -2.50988 0.00074  
C -0.74337 0.79680 0.00026  
O -0.85824 2.02445 0.00073  
B -2.02223 -0.26705 -0.00018  
F -1.94714 -1.06269 -1.16088  
F -3.21584 0.47005 -0.00066  
F -1.94780 -1.06238 1.16080

Thermal correction to Gibbs Free Energy = 0.061500

Sum of electronic and thermal Free Energies = -685.552450

SCF Done: E(RM062X) = -685.692599165 A.U. after 14 cycles

**137' anti-1**

N -3.35108 -0.57305 0.28356  
C -2.07338 -0.86871 -0.17474  
O -1.17344 -0.70163 0.80969  
O -1.86421 -1.23519 -1.32519  
N 0.27871 -1.19433 0.70130  
C 0.21863 -2.64248 0.53705  
H -0.26313 -2.95666 -0.39552  
H -0.30040 -3.07259 1.40110

H 1.25810 -2.97425 0.51735  
C -3.59859 0.01391 1.58837  
H -2.82020 -0.29345 2.28366  
H -4.57333 -0.33016 1.95959  
H -3.61774 1.11504 1.54935  
C -4.41017 -0.43014 -0.69591  
H -4.09447 -0.91242 -1.62007  
H -4.63309 0.62909 -0.90470  
H -5.33022 -0.90482 -0.32803  
C 0.06251 3.66616 -0.04557  
C -0.20482 2.86810 -1.15286  
N 0.11383 1.56943 -1.23550  
C 0.73532 0.99723 -0.19330  
C 1.04435 1.72324 0.97312  
C 0.70562 3.06669 1.04304  
H -0.21763 4.71710 -0.03686  
H 0.94421 3.64701 1.93281  
H 1.56713 1.21651 1.77376  
H -0.70569 3.29012 -2.02627  
C 1.08017 -0.48714 -0.31354  
O 0.90157 -0.96197 -1.62831  
B 2.72716 -0.73732 0.07579  
F 2.95178 -0.43335 1.43873  
F 3.48279 0.11300 -0.73567  
F 3.07666 -2.08091 -0.15646  
H -0.00984 -0.73767 -1.89356

Thermal correction to Gibbs Free Energy = 0.204126

Sum of electronic and thermal Free Energies = -1103.775261

SCF Done: E(RM062X) = -1104.01644536 A.U. after 15 cycles



**137' anti-2**

N 3.29920 -0.27894 0.24121  
C 2.24927 -0.94749 -0.36717  
O 1.18815 -0.98836 0.46514  
O 2.32142 -1.44833 -1.47808  
N -0.10538 -1.35372 -0.20879  
C -0.24911 -2.78363 0.05449  
H -0.21517 -3.01364 1.12695  
H 0.55348 -3.30441 -0.47487  
H -1.21914 -3.07982 -0.34197  
C 3.20463 0.35790 1.54215  
H 2.16082 0.44197 1.83894  
H 3.64643 1.36339 1.49389  
H 3.74907 -0.21327 2.31161  
C 4.59589 -0.28952 -0.39660  
H 4.50150 -0.79579 -1.35717  
H 5.34240 -0.81548 0.22054  
H 4.95899 0.73608 -0.56111  
C -0.16716 3.59891 -0.44397  
C -0.63632 3.14522 0.78448  
N -0.90756 1.86245 1.06136  
C -0.72075 0.95323 0.09229  
C -0.26794 1.31864 -1.19104  
C 0.01943 2.64956 -1.45500  
H 0.03987 4.65438 -0.60544  
H 0.37996 2.94924 -2.43744  
H -0.14409 0.54704 -1.94107  
H -0.80594 3.85119 1.60007  
C -1.10406 -0.49244 0.39595  
O -1.15870 -0.71770 1.81213  
B -2.66645 -0.72981 -0.23764  
F -2.78033 -0.17507 -1.51565

F -3.50175 -0.04544 0.68492

F -3.04461 -2.08441 -0.26765

H -2.02989 -0.36316 2.05715

Thermal correction to Gibbs Free Energy = 0.203826

Sum of electronic and thermal Free Energies = -1103.785231

SCF Done: E(RM062X) = -1104.02167698 A.U. after 15 cycles

### **137' (also 137' anti-3)**

N 3.28536 -0.31332 0.10268

C 2.19746 -1.02150 -0.39189

O 1.15471 -0.91848 0.45545

O 2.23118 -1.65843 -1.43198

N -0.16913 -1.31392 -0.15352

C -0.32392 -2.72025 0.21604

H -0.23096 -2.87119 1.29946

H 0.43238 -3.29896 -0.32071

H -1.32518 -3.02095 -0.09258

C 3.26160 0.40547 1.36288

H 2.23766 0.67118 1.61968

H 3.85544 1.32476 1.26696

H 3.69041 -0.18941 2.18655

C 4.57794 -0.51902 -0.51255

H 4.43022 -1.06571 -1.44364

H 5.25416 -1.09556 0.14095

H 5.06003 0.44552 -0.72742

C -0.01714 3.59394 -0.44909

C -0.17129 3.10534 0.84198

N -0.52473 1.84126 1.11700

C -0.75432 0.99788 0.09890

C -0.62227 1.40375 -1.24166

C -0.24940 2.71150 -1.51222

H 0.27113 4.62828 -0.61893  
H -0.14370 3.04919 -2.54128  
H -0.83906 0.68668 -2.02234  
H -0.00229 3.75199 1.70393  
C -1.16047 -0.42206 0.46228  
O -1.20665 -0.56706 1.88016  
B -2.70659 -0.71955 -0.18449  
F -2.63943 -0.70488 -1.59569  
F -3.53974 0.31115 0.26925  
F -3.19055 -1.96613 0.24855  
H -0.83340 0.26398 2.23277

Thermal correction to Gibbs Free Energy = 0.204393

Sum of electronic and thermal Free Energies = -1103.784961

SCF Done: E(RM062X) = -1104.02699055 A.U. after 15 cycles

### 137' gauche-1

N 3.67293 -0.38073 -0.19462  
C 2.58133 -0.99458 0.38506  
O 1.63167 -0.06741 0.67541  
O 2.53472 -2.17871 0.67168  
N 0.28263 -0.62729 0.68213  
C -0.12843 -0.59733 2.08578  
H -0.14039 0.41182 2.51786  
H 0.55654 -1.24294 2.64198  
H -1.13419 -1.02175 2.15140  
C 3.63650 0.95304 -0.77429  
H 2.67734 1.42731 -0.57273  
H 3.78997 0.89624 -1.86347  
H 4.44410 1.57135 -0.35369  
C 4.84721 -1.17840 -0.46547  
H 4.74258 -2.13692 0.04294

H 5.75240 -0.66505 -0.10807  
H 4.96870 -1.36107 -1.54547  
C -4.43739 -1.52587 -0.34317  
C -3.29493 -2.09418 -0.90877  
N -2.07999 -1.54426 -0.85968  
C -1.93426 -0.36611 -0.22421  
C -3.02579 0.27599 0.38510  
C -4.28789 -0.30906 0.32025  
H -5.40249 -2.02142 -0.42218  
H -5.14312 0.18176 0.78164  
H -2.86316 1.21562 0.89687  
H -3.36329 -3.04999 -1.43257  
C -0.51603 0.25650 -0.22595  
O 0.05325 0.02684 -1.52501  
B -0.49808 1.90508 0.03039  
F -1.08790 2.26977 1.26903  
F -1.24748 2.45925 -1.04809  
F 0.80314 2.43948 -0.02804  
H -0.13248 0.85334 -2.00009

Thermal correction to Gibbs Free Energy = 0.205075

Sum of electronic and thermal Free Energies = -1103.771166

SCF Done: E(RM062X) = -1104.01126340 A.U. after 15 cycles

### **137' gauche-2**

N 3.49551 -0.05613 0.48042  
C 2.39092 -0.82343 0.17931  
O 1.38745 -0.54396 1.06097  
O 2.38179 -1.69158 -0.68039  
N 0.01266 -0.92536 0.77105  
C -0.10962 -2.38149 0.75399  
H -1.18212 -2.60448 0.76275

H 0.33735 -2.77422 1.67390  
H 0.34648 -2.85403 -0.11903  
C 3.38524 1.25381 1.11159  
H 2.35993 1.43050 1.42648  
H 3.65231 2.03707 0.38849  
H 4.06701 1.32350 1.97201  
C 4.68501 -0.27180 -0.31844  
H 4.69484 -1.30070 -0.67797  
H 5.57738 -0.08574 0.29396  
H 4.71640 0.40259 -1.18908  
C -4.75427 -0.03644 0.48072  
C -4.23627 -0.65035 -0.65491  
N -2.92992 -0.72405 -0.94559  
C -2.06142 -0.16613 -0.09073  
C -2.49007 0.48076 1.08696  
C -3.84565 0.54607 1.37149  
H -5.82681 -0.01178 0.66004  
H -4.19532 1.04856 2.27167  
H -1.74512 0.93337 1.72959  
H -4.90772 -1.11683 -1.37874  
C -0.56671 -0.20854 -0.39419  
O -0.36747 -0.90660 -1.61989  
B 0.02514 1.35411 -0.54847  
F 0.18116 1.98760 0.70599  
F -0.83373 2.10352 -1.35456  
F 1.29878 1.24830 -1.18989  
H 0.51900 -0.63210 -1.90698

Thermal correction to Gibbs Free Energy = 0.206648

Sum of electronic and thermal Free Energies = -1103.775471

SCF Done: E(RM062X) = -1104.01753736 A.U. after 14 cycles

**137' gauche-3**

N -3.50932 -0.03042 -0.44428  
C -2.43515 -0.85765 -0.19098  
O -1.40312 -0.53039 -1.03071  
O -2.47295 -1.81178 0.56548  
N -0.04767 -0.93401 -0.72824  
C 0.07434 -2.38877 -0.69425  
H 1.14533 -2.61725 -0.76334  
H -0.42233 -2.79531 -1.58127  
H -0.33997 -2.84675 0.20678  
C -3.36914 1.30393 -1.01261  
H -2.35316 1.45592 -1.36677  
H -3.56943 2.06240 -0.24416  
H -4.08548 1.43750 -1.83762  
C -4.71899 -0.26638 0.31571  
H -4.73672 -1.30564 0.64371  
H -5.59785 -0.05992 -0.31099  
H -4.77034 0.38242 1.20460  
C 4.73576 -0.07843 -0.48347  
C 4.20435 -0.65932 0.66050  
N 2.89063 -0.69604 0.92885  
C 2.03603 -0.14167 0.05677  
C 2.48396 0.47003 -1.12929  
C 3.84362 0.50162 -1.39609  
H 5.80936 -0.07365 -0.65431  
H 4.21471 0.97625 -2.30250  
H 1.74984 0.92224 -1.78351  
H 4.85623 -1.12230 1.40224  
C 0.55006 -0.19676 0.40432  
O 0.37944 -0.87021 1.65064  
B -0.02664 1.37869 0.54733  
F -0.07126 2.00015 -0.73174

F 0.85269 2.08643 1.37895

F -1.31829 1.36535 1.10676

H 1.27329 -1.17394 1.90348

Thermal correction to Gibbs Free Energy = 0.206616

Sum of electronic and thermal Free Energies = -1103.772632

SCF Done: E(RM062X) = -1104.01813218 A.U. after 14 cycles

### 137' TS-1

C -2.56382 -0.35062 -0.19585

N -3.79452 0.24986 0.09216

O -1.59331 0.08939 0.57568

N -0.26308 -1.04008 0.68487

C -0.04042 -0.94447 2.11839

H 0.85144 -1.53665 2.33274

H -0.91079 -1.37582 2.62358

H 0.14719 0.07582 2.46341

C 0.71437 -0.64032 -0.23267

O 0.25340 -0.89420 -1.55367

B 2.10868 -1.74764 -0.02013

O -2.47616 -1.19511 -1.09360

F 2.67481 -1.57169 1.24733

F 1.66210 -3.04473 -0.19583

F 2.99182 -1.34640 -1.01387

H -0.65608 -1.25290 -1.45939

H 2.25340 2.96170 2.04338

N 1.53740 1.32565 1.01561

C 2.05076 2.55940 1.04915

C 1.25507 0.77965 -0.17869

C 2.33243 3.31826 -0.08376

H 2.75891 4.31448 0.00643

C 1.51028 1.46913 -1.37977

C 2.05208 2.74635 -1.32760

H 1.27156 0.97985 -2.31432

H 2.25672 3.29333 -2.24653  
C -3.91546 1.34316 1.03399  
H -4.86326 1.25623 1.58457  
H -3.90759 2.32693 0.53357  
H -3.08499 1.30670 1.73670  
C -4.88467 0.08461 -0.84499  
H -5.02911 0.98116 -1.47252  
H -5.82524 -0.10199 -0.30653  
H -4.65768 -0.76484 -1.48802

Thermal correction to Gibbs Free Energy = 0.202877

Sum of electronic and thermal Free Energies = -1103.773368

SCF Done: E(RM062X) = -1103.99908258 A.U. after 16 cycles

Imaginary Frequency: -241.03 cm<sup>-1</sup>

### 137' TS-2

C -2.81720 -0.40581 0.23347  
N -3.78176 0.43808 -0.35958  
O -1.59710 0.07152 0.10880  
N -0.25548 -1.17175 0.35371  
C -0.19903 -1.25480 1.80171  
H 0.66683 -1.88420 2.03086  
H -1.12319 -1.73067 2.13203  
H -0.03911 -0.28966 2.28778  
C 0.75760 -0.60285 -0.38798  
O 0.38200 -0.62601 -1.76380  
B 2.16221 -1.77877 -0.30020  
O -3.15890 -1.45156 0.78314  
F 1.71378 -3.01252 -0.70722  
F 3.07041 -1.21387 -1.17925  
F 2.63976 -1.78921 1.00361  
H -0.57920 -0.47352 -1.73084  
N 1.50873 1.09333 1.24893  
C 1.32906 0.76472 -0.03989  
H 2.15692 2.50563 2.60110



C 2.04287 2.28371 1.53884  
C 1.72373 1.63104 -1.07821  
C 2.45012 3.20915 0.58166  
C 2.28490 2.86085 -0.76126  
H 1.58035 1.31066 -2.10140  
H 2.88593 4.16013 0.87790  
H 2.59493 3.54189 -1.55192  
C -5.17648 0.18982 -0.07173  
H -5.27306 -0.83763 0.27818  
H -5.78561 0.33132 -0.97684  
H -5.57066 0.86952 0.70554  
C -3.45293 1.77132 -0.81720  
H -4.04076 2.01604 -1.71423  
H -2.39228 1.82060 -1.05815  
H -3.67204 2.54214 -0.05628

Thermal correction to Gibbs Free Energy = 0.200858

Sum of electronic and thermal Free Energies = -1103.767831

SCF Done: E(RM062X) = -1103.98715518 A.U. after 16 cycles

Imaginary Frequency: -222.27  $\text{cm}^{-1}$

#### 146'

N 1.45342 0.62488 0.10271  
C 2.61011 1.47731 0.35978  
H 3.50913 0.86510 0.30767  
H 2.53765 1.95945 1.34386  
H 2.68043 2.28595 -0.38060  
C 0.27435 1.28258 0.16510  
O 0.17214 2.50245 0.37106  
B 1.70341 -0.89192 -0.24213  
F 0.75432 -1.32920 -1.17023  
F 2.99715 -1.00767 -0.76951  
F 1.61679 -1.67186 0.93821  
N -1.96847 1.03527 -0.73327  
C -1.02317 0.49296 0.05200

H -3.90540 0.90538 -1.42454  
C -3.17005 0.45137 -0.75757  
C -1.26403 -0.64106 0.84386  
C -3.51500 -0.66141 0.00894  
C -2.53059 -1.21513 0.82859  
H -0.45278 -1.06901 1.42068  
H -4.51799 -1.07918 -0.04124  
H -2.74395 -2.08993 1.43988

Thermal correction to Gibbs Free Energy = 0.106222

Sum of electronic and thermal Free Energies = -780.233811

SCF Done: E(RM062X) = -780.398039334 A.U. after 14 cycles

### **N-methylpicolinamide (118')**

N -1.99813 -0.65819 -0.00007  
C -3.44467 -0.60339 0.00004  
H -3.86033 -1.08977 0.89104  
H -3.86045 -1.09057 -0.89045  
H -3.73530 0.44848 -0.00039  
C -1.21696 0.45069 -0.00002  
O -1.63505 1.60707 0.00002  
N 0.64809 -1.13455 -0.00001  
C 0.26680 0.15297 -0.00002  
H 2.23811 -2.44860 0.00002  
C 1.95870 -1.39655 0.00002  
C 1.16876 1.21918 -0.00001  
C 2.93869 -0.40176 0.00002  
C 2.53183 0.93254 0.00001  
H 0.78175 2.23169 -0.00002  
H 3.99047 -0.67145 0.00002  
H 3.26470 1.73485 0.00002  
H -1.50722 -1.54414 -0.00004

Thermal correction to Gibbs Free Energy = 0.110267

Sum of electronic and thermal Free Energies = -456.197023

SCF Done: E(RM062X) = -456.250656827 A.U. after 13 cycles

**142'**

C -2.67198 0.71536 -0.31713  
N -2.64072 0.14359 0.90970  
O -1.54003 1.49011 -0.74259  
N -0.21942 1.29202 -0.28202  
C 0.29572 2.62812 0.06595  
H 0.52327 3.16862 -0.85439  
H 1.19787 2.53574 0.66274  
H -0.49501 3.14528 0.60989  
C 0.39405 0.15363 -0.36449  
C 1.84773 0.12125 -0.03408  
B -0.28642 -1.36629 -0.75239  
O -3.57950 0.71524 -1.10542  
F -1.45507 -1.22614 -1.46644  
F 0.68804 -2.04419 -1.45691  
F -0.50348 -1.94768 0.51951  
C -3.56878 -0.96038 1.15116  
H -4.11209 -1.17323 0.23261  
H -4.28149 -0.69773 1.94274  
H -2.99537 -1.84503 1.44701  
C -1.78879 0.50344 2.03196  
H -1.38234 1.50805 1.91292  
H -0.97685 -0.21942 2.16605  
H -2.40457 0.51096 2.93885  
C 2.35328 -0.96683 0.69378  
N 2.62915 1.10336 -0.51933  
C 3.72103 -1.01217 0.94888  
H 1.68194 -1.74403 1.03583  
C 4.53801 -0.00429 0.43986  
H 4.14258 -1.83410 1.52022  
C 3.94339 1.02398 -0.29446  
H 5.61192 -0.01228 0.59912  
H 4.54807 1.82254 -0.71997

Thermal correction to Gibbs Free Energy = 0.194466

Sum of electronic and thermal Free Energies = -1027.871995

SCF Done: E(RM062X) = -1028.01028946 A.U. after 14 cycles

### 142' TS-3

C 2.27753 -1.06068 -0.23328  
N 3.55688 -0.54022 -0.22962  
O 1.53704 -0.63607 0.79315  
N -0.21166 -1.14552 0.56258  
C -0.13051 -2.53037 0.96802  
H -1.15599 -2.91145 0.95234  
H 0.29358 -2.57827 1.97262  
H 0.51580 -3.04508 0.25631  
C -0.95361 -0.26518 0.22004  
C -2.40510 -0.23826 -0.00583  
B 0.64239 2.31500 0.19276  
O 1.89184 -1.85509 -1.09527  
F -0.51433 2.85532 -0.17672  
F 0.94643 2.26095 1.47311  
F 1.52076 1.98592 -0.73244  
C 4.47865 -0.91599 -1.28361  
H 4.00607 -1.67810 -1.90175  
H 5.41079 -1.31381 -0.85782  
H 4.73451 -0.04927 -1.91144  
C 4.01551 0.46184 0.71306  
H 4.91982 0.11534 1.23383  
H 3.23721 0.66123 1.44676  
H 4.26146 1.40045 0.19491  
C -2.99796 0.89150 -0.58066  
N -3.10648 -1.33165 0.35862  
C -4.37556 0.88153 -0.80063  
H -2.38438 1.74554 -0.83696  
C -5.10532 -0.24260 -0.42595  
H -4.86606 1.73973 -1.25082  
C -4.42345 -1.31913 0.15377

H -6.17979 -0.29387 -0.57363

H -4.96400 -2.21200 0.46258

Thermal correction to Gibbs Free Energy = 0.183864

Sum of electronic and thermal Free Energies = -1027.862417

SCF Done: E(RM062X) = -1027.95779165 A.U. after 14 cycles

Imaginary Frequency: -149.85  $\text{cm}^{-1}$

#### 144'

N 2.47480 0.02394 0.00015

C 3.90478 -0.03132 -0.00009

H 4.27578 0.46876 -0.89816

H 4.20305 -1.08279 -0.00072

H 4.27607 0.46775 0.89843

C 1.32201 0.04767 0.00005

N -0.64243 -1.18974 -0.00003

C -0.10992 0.04709 0.00003

H -2.39947 -2.25481 -0.00001

C -1.97097 -1.25637 0.00001

C -0.82491 1.25097 -0.00000

C -2.79625 -0.11742 -0.00002

C -2.21717 1.14949 -0.00002

H -0.32111 2.21208 -0.00001

H -3.87514 -0.23523 -0.00002

H -2.83109 2.04422 -0.00003

Thermal correction to Gibbs Free Energy = 0.092996

Sum of electronic and thermal Free Energies = -380.087762

SCF Done: E(RM062X) = -380.178418585 A.U. after 13 cycles

#### H<sup>+</sup>Pyridyl KAT (116'-H<sup>+</sup>)

C 3.30146 0.45781 0.03975

C 2.90118 -0.86743 0.05641

N 1.58564 -1.14087 0.00745

C 0.61356 -0.21475 -0.05548  
C 0.97095 1.13056 -0.08228  
C 2.32441 1.46177 -0.03237  
H 4.35729 0.69969 0.08024  
H 2.62796 2.50443 -0.05141  
H 0.18055 1.86772 -0.15386  
H 3.58338 -1.70826 0.10771  
C -0.81446 -0.84626 -0.08592  
O -0.77408 -2.07038 -0.10712  
B -2.05607 0.25212 0.02299  
F -1.79496 1.20383 -0.98990  
F -1.84844 0.84064 1.28377  
F -3.28315 -0.34547 -0.10912  
H 1.18060 -2.09641 0.00380

Thermal correction to Gibbs Free Energy = 0.076148

Sum of electronic and thermal Free Energies = -686.059745

SCF Done: E(RM062X) = -686.136804552 A.U. after 15 cycles

### **137'-H<sup>+</sup> anti-1**

N -3.60903 0.33632 0.09963  
C -2.40150 -0.15228 -0.29545  
O -1.50059 -0.15188 0.72508  
O -2.16460 -0.51682 -1.44912  
N -0.31006 -1.08262 0.68530  
C -0.80303 -2.45444 0.59801  
H -1.34488 -2.66437 -0.33172  
H -1.44769 -2.64404 1.46029  
H 0.07759 -3.09518 0.64250  
C -3.92049 0.73336 1.46626  
H -3.16725 0.34568 2.14806  
H -4.90165 0.33041 1.74430  
H -3.96014 1.82749 1.56011  
C -4.64048 0.58045 -0.89915  
H -4.27836 0.25200 -1.87169

H -4.88909 1.64928 -0.94166  
H -5.55089 0.02414 -0.64372  
C 2.12330 3.32221 0.04827  
C 2.00182 2.63671 -1.13688  
N 1.48035 1.38850 -1.12667  
C 1.08017 0.73526 -0.01539  
C 1.20548 1.40111 1.21564  
C 1.71450 2.68578 1.23975  
H 2.53584 4.32417 0.05538  
H 1.81185 3.20958 2.18620  
H 0.91122 0.87275 2.11187  
H 2.30053 3.02900 -2.10139  
C 0.70755 -0.68072 -0.23604  
O 0.47660 -0.90738 -1.62694  
B 2.24423 -1.49667 0.15432  
F 2.55786 -1.16015 1.46561  
F 3.14166 -0.95145 -0.75688  
F 2.07529 -2.85792 -0.01560  
H -0.49403 -0.78908 -1.77119  
H 1.37873 0.80584 -1.96713

Thermal correction to Gibbs Free Energy = 0.219628

Sum of electronic and thermal Free Energies = -1104.295249

SCF Done: E(RM062X) = -1104.47122835 A.U. after 14 cycles

### **137'-H<sup>+</sup> anti-2**

N 3.53531 -0.03611 0.23927  
C 2.37652 -0.24179 -0.46211  
O 1.41932 -0.79619 0.35548  
O 2.21449 0.04695 -1.63435  
N 0.21030 -1.20545 -0.37234  
C 0.25879 -2.66496 -0.42563  
H 0.25170 -3.12961 0.56922  
H 1.16855 -2.95193 -0.95818  
H -0.60566 -2.99878 -0.99973

C 3.75152 -0.44384 1.61949  
H 2.83519 -0.85124 2.03973  
H 4.06923 0.41819 2.22161  
H 4.54180 -1.20562 1.67596  
C 4.67242 0.55238 -0.44768  
H 4.37357 0.81445 -1.46150  
H 5.51026 -0.15731 -0.48951  
H 5.01330 1.45344 0.07973  
C -1.27956 3.59456 -0.06233  
C -1.63558 2.90467 1.07306  
N -1.42972 1.56889 1.12400  
C -0.91064 0.83792 0.11625  
C -0.52267 1.50938 -1.05276  
C -0.70694 2.87942 -1.13313  
H -1.43740 4.66528 -0.11657  
H -0.40761 3.40921 -2.03260  
H -0.06270 0.92931 -1.84274  
H -2.07526 3.36150 1.95128  
C -0.91574 -0.63147 0.31397  
O -0.96423 -0.87765 1.73539  
B -2.43971 -1.19537 -0.30274  
F -3.37722 -0.20925 0.00222  
F -2.68675 -2.35785 0.46086  
F -2.35802 -1.45788 -1.65281  
H -1.60651 -1.60853 1.82058  
H -1.66852 0.99953 1.94049

Thermal correction to Gibbs Free Energy = 0.218816

Sum of electronic and thermal Free Energies = -1104.303367

SCF Done: E(RM062X) = -1104.47862811 A.U. after 15 cycles

**137'-H<sup>+</sup> (also 4a'-H<sup>+</sup> anti-3)**

N -3.57028 -0.13297 -0.20152  
C -2.33516 -0.10374 0.36951  
O -1.41802 -0.77594 -0.38539



O -2.07459 0.48435 1.41869  
N -0.19113 -1.11202 0.38647  
C -0.27593 -2.55743 0.59735  
H 0.56451 -2.83975 1.23046  
H -0.24738 -3.12213 -0.34256  
H -1.20704 -2.76983 1.12826  
C -3.88499 -0.84182 -1.43541  
H -3.04193 -1.45759 -1.73915  
H -4.11632 -0.13169 -2.24076  
H -4.76325 -1.48032 -1.27853  
C -4.64551 0.64696 0.39238  
H -4.28382 1.10891 1.30940  
H -5.49830 -0.00314 0.62454  
H -4.98579 1.42690 -0.30220  
C 1.20369 3.58938 0.08801  
C 0.46843 2.79007 0.93273  
N 0.39713 1.45858 0.70740  
C 1.00562 0.83381 -0.32381  
C 1.74649 1.62211 -1.21838  
C 1.84405 2.98631 -1.01108  
H 1.27045 4.65576 0.26906  
H 2.42148 3.59689 -1.69913  
H 2.22886 1.12410 -2.04795  
H -0.08782 3.15501 1.78762  
C 0.95577 -0.65089 -0.37813  
O 0.97855 -1.07071 -1.73514  
B 2.43761 -1.20784 0.35678  
F 2.27568 -1.33586 1.72496  
F 3.43810 -0.30205 0.02601  
F 2.66000 -2.44808 -0.27634  
H 1.61049 -1.81362 -1.74239  
H -0.24836 0.87831 1.27708

Thermal correction to Gibbs Free Energy = 0.220740

Sum of electronic and thermal Free Energies = -1104.308338

SCF Done: E(RM062X) = -1104.48135607 A.U. after 15 cycles

**137'-H<sup>+</sup> gauche-1**

N 3.55851 -0.44938 -0.23974  
C 2.29249 -0.64456 0.20683  
O 1.71350 0.52601 0.58655  
O 1.74826 -1.75062 0.27134  
N 0.35180 0.34530 1.00904  
C 0.17641 1.23836 2.15298  
H 0.47974 2.26585 1.93360  
H 0.74040 0.83854 3.00097  
H -0.88966 1.24406 2.39424  
C 4.19442 0.86038 -0.31677  
H 3.44600 1.64589 -0.23935  
H 4.70864 0.95206 -1.28048  
H 4.93567 0.98697 0.48403  
C 4.37085 -1.59773 -0.60891  
H 3.76824 -2.50043 -0.52537  
H 5.24412 -1.68093 0.05179  
H 4.72703 -1.49094 -1.64113  
C -3.04835 -2.94799 -0.00336  
C -1.68015 -2.94646 0.20157  
N -1.00442 -1.78476 0.18853  
C -1.57652 -0.57895 -0.03623  
C -2.95640 -0.53679 -0.24164  
C -3.68780 -1.72194 -0.22250  
H -3.59853 -3.88180 0.01388  
H -4.76288 -1.69357 -0.37550  
H -3.42583 0.42601 -0.39277  
H -1.09522 -3.84112 0.38208  
C -0.59938 0.60018 -0.14684  
O 0.10071 0.32926 -1.35928  
B -1.32322 2.09999 -0.26898  
F -2.42219 2.18763 0.60302  
F -1.76500 2.15782 -1.62216  
F -0.39022 3.10365 -0.02931

H -0.25642 0.99452 -1.97761

H 0.03708 -1.76935 0.34803

Thermal correction to Gibbs Free Energy = 0.220682

Sum of electronic and thermal Free Energies = -1104.293527

SCF Done: E(RM062X) = -1104.46870356 A.U. after 15 cycles

### 137'-H<sup>+</sup> gauche-2

N -3.22284 -0.82259 -0.39202

C -2.54187 -0.34228 0.68629

O -1.17577 -0.55325 0.53530

O -3.03507 0.11643 1.69608

N -0.40939 0.37827 1.33396

C -0.05063 -0.28220 2.58488

H 0.47609 -1.24187 2.44930

H -0.96898 -0.44709 3.15014

H 0.58954 0.41084 3.13825

C -2.62862 -1.12183 -1.68811

H -1.59310 -0.79422 -1.72689

H -3.18101 -0.58562 -2.46998

H -2.68893 -2.19800 -1.90609

C -4.67442 -0.86306 -0.32164

H -4.98492 -0.68163 0.70645

H -5.03874 -1.84503 -0.65017

H -5.11859 -0.09481 -0.96940

C 3.97765 -1.80963 -0.39544

C 4.13872 -0.52798 0.07584

N 3.04070 0.20567 0.37253

C 1.76558 -0.21205 0.22527

C 1.57014 -1.51782 -0.25632

C 2.66842 -2.30616 -0.55299

H 4.84505 -2.41171 -0.63901

H 2.52057 -3.31635 -0.92322

H 0.55646 -1.87096 -0.38483

H 5.09891 -0.05134 0.23294

C 0.70674 0.82479 0.49249  
O 1.35695 1.89014 1.19502  
B 0.16031 1.42341 -1.03297  
F 0.37789 0.45329 -2.01938  
F 0.98416 2.55456 -1.24752  
F -1.16637 1.78954 -0.94759  
H 1.22417 2.66837 0.61974  
H 3.08239 1.15899 0.75394

Thermal correction to Gibbs Free Energy = 0.220403

Sum of electronic and thermal Free Energies = -1104.286925

SCF Done: E(RM062X) = -1104.47017015 A.U. after 16 cycles

### **137'-H<sup>+</sup> gauche-3**

N -3.60451 -0.08187 -0.30923  
C -2.43759 -0.65345 0.08724  
O -1.53423 -0.66499 -0.95117  
O -2.23451 -1.13816 1.19620  
N -0.19766 -1.11759 -0.67774  
C -0.18934 -2.56807 -0.47905  
H 0.85818 -2.88743 -0.45858  
H -0.67508 -3.03006 -1.34274  
H -0.68129 -2.88944 0.44293  
C -3.66407 0.75670 -1.50716  
H -3.17176 0.26010 -2.34230  
H -3.17555 1.72341 -1.33378  
H -4.71570 0.91831 -1.76067  
C -4.59139 0.19391 0.72879  
H -4.49807 -0.55185 1.51686  
H -5.59442 0.14446 0.29315  
H -4.43939 1.19097 1.16504  
C 4.69794 0.01507 -0.31222  
C 4.11831 -0.07140 0.93103  
N 2.77854 -0.23539 1.02833  
C 1.93857 -0.29241 -0.03060

C 2.49773 -0.19736 -1.31517  
C 3.86609 -0.05236 -1.44956  
H 5.77044 0.14022 -0.40233  
H 4.30590 0.02171 -2.43974  
H 1.82360 -0.22245 -2.16056  
H 4.66764 -0.01987 1.86319  
C 0.49881 -0.30158 0.29507  
O 0.40690 -0.75795 1.65260  
B 0.10887 1.40636 0.19274  
F 0.25651 1.79903 -1.13062  
F 1.03390 2.03029 1.03038  
F -1.19174 1.58587 0.66032  
H -0.54930 -0.72299 1.86712  
H 2.29217 -0.28507 1.92715

Thermal correction to Gibbs Free Energy = 0.221143

Sum of electronic and thermal Free Energies = -1104.295949

SCF Done: E(RM062X) = -1104.47693896 A.U. after 15 cycles

### 137'-H<sup>+</sup> TS-2

C -2.62504 -0.05255 -0.27526  
N -3.89940 0.33114 0.07330  
O -1.71310 0.19069 0.64927  
N -0.39286 -1.04238 0.60483  
C -0.21617 -1.13232 2.04343  
H 0.63309 -1.79298 2.23220  
H -1.12180 -1.57220 2.46442  
H -0.03848 -0.16745 2.53470  
C 0.57663 -0.56625 -0.23250  
O 0.20963 -0.63509 -1.58432  
B 2.09267 -1.89296 -0.12824  
O -2.39600 -0.56149 -1.38869  
F 2.57826 -1.74243 1.14845  
F 1.50430 -3.07495 -0.38930  
F 2.89356 -1.37291 -1.09599

H -0.79566 -0.72291 -1.60786  
H 2.23982 3.06626 -2.16394  
N 1.47590 1.44471 -1.12069  
C 2.17573 2.59709 -1.18922  
C 1.29998 0.70252 0.00298  
C 2.75982 3.10087 -0.05090  
H 3.32433 4.02477 -0.08986  
C 1.92133 1.17651 1.17517  
C 2.62487 2.36733 1.14531  
H 1.87720 0.58525 2.07714  
H 3.09605 2.73177 2.05333  
C -4.21664 0.95100 1.34678  
H -3.39439 0.79586 2.04245  
H -5.13023 0.50318 1.75873  
H -4.39013 2.03258 1.23739  
C -4.95866 0.30747 -0.92039  
H -4.59045 -0.19455 -1.81328  
H -5.28087 1.32670 -1.18070  
H -5.82939 -0.23552 -0.52998  
H 1.01174 0.99939 -1.92648

Thermal correction to Gibbs Free Energy = 0.216769

Sum of electronic and thermal Free Energies = -1104.284276

SCF Done: E(RM062X) = -1104.44195482 A.U. after 15 cycles

Imaginary Frequency: -296.68  $\text{cm}^{-1}$

### 137'-H<sup>+</sup> TS-1

C 2.40396 0.08454 -0.24543  
O 1.60042 -0.54285 0.60208  
N 0.16814 -1.16545 -0.25696  
C 0.50165 -2.58028 -0.17873  
H 1.43702 -2.74873 -0.71388  
H -0.31106 -3.10903 -0.68222  
H 0.57319 -2.95150 0.84885  
C -0.91907 -0.73410 0.46146

C -1.11969 0.73030 0.39231  
O -1.13449 -1.25100 1.75967  
B -2.47548 -1.30761 -0.58664  
F -2.35631 -0.60573 -1.75199  
F -2.37758 -2.66222 -0.71291  
F -3.48878 -0.89376 0.23264  
H 0.38021 0.98350 -1.01416  
N -0.43812 1.44495 -0.52988  
C -2.05235 1.40820 1.19386  
C -2.27037 2.76148 0.99703  
C -0.62867 2.76457 -0.73642  
C -1.55828 3.45947 0.00667  
H -3.00068 3.28425 1.60781  
H -1.71567 4.51731 -0.16839  
H 0.00080 3.21468 -1.49510  
H -2.59997 0.83483 1.92911  
H -0.34848 -1.01355 2.28508  
O 2.01767 0.73119 -1.23912  
N 3.73651 -0.00878 0.06607  
C 4.23574 -0.75217 1.21076  
H 5.07618 -1.38713 0.90256  
H 3.44265 -1.37728 1.61542  
H 4.59378 -0.07447 1.99954  
C 4.71152 0.77534 -0.67363  
H 5.18318 1.52694 -0.02456  
H 4.20873 1.27351 -1.50054  
H 5.50034 0.12219 -1.06885

Thermal correction to Gibbs Free Energy = 0.217053

Sum of electronic and thermal Free Energies = -1104.296669

SCF Done: E(RM062X) = -1104.45332624 A.U. after 16 cycles

Imaginary Frequency: -285.39  $\text{cm}^{-1}$

**149'-H<sup>+</sup>**

N 1.49838 0.63883 -0.13195  
C 2.67343 1.49271 -0.33994  
H 3.55127 0.85520 -0.41443  
H 2.79997 2.19022 0.49655  
H 2.55636 2.08911 -1.25009  
C 0.33553 1.30525 -0.13227  
O 0.18979 2.52992 -0.24397  
B 1.70237 -0.87794 0.24068  
F 0.88175 -1.20079 1.31752  
F 1.24242 -1.67161 -0.89626  
F 3.02773 -1.12917 0.46335  
N -1.11827 -0.71564 -0.52642  
C -0.97721 0.53323 -0.03550  
H -2.26628 -2.37791 -0.96630  
C -2.29162 -1.37783 -0.54988  
C -2.11333 1.18016 0.45309  
C -3.43438 -0.77891 -0.05577  
C -3.33680 0.52103 0.45763  
H -1.99500 2.19777 0.80321  
H -4.37650 -1.31444 -0.07301  
H -4.21871 1.01586 0.85335  
H -0.24288 -1.20749 -0.83803

Thermal correction to Gibbs Free Energy = 0.121167

Sum of electronic and thermal Free Energies = -780.745659

SCF Done: E(RM062X) = -780.842560452 A.U. after 15 cycles

**148'-H<sup>+</sup>**

N -1.41127 0.66802 -0.15832  
C -2.49587 1.65413 -0.30825  
H -2.75719 2.07488 0.66848  
H -3.36540 1.13727 -0.70631  
H -2.18983 2.46578 -0.97016



C -0.20234 1.12465 -0.09726  
C 1.07235 0.33098 -0.05985  
O 0.00233 2.43897 -0.08685  
N 2.11795 1.11983 0.25288  
C 1.21645 -1.01795 -0.38950  
C 2.50009 -1.56211 -0.33653  
C 3.33916 0.58863 0.30250  
C 3.57856 -0.75872 0.02682  
H 2.65056 -2.60848 -0.58481  
H 4.58718 -1.15592 0.08055  
H 4.14956 1.26424 0.56468  
H 0.36651 -1.61038 -0.69741  
H 0.98300 2.53678 0.04965  
B -1.88890 -0.89580 0.15407  
F -3.22458 -0.80009 0.45647  
F -1.65544 -1.63051 -1.00222  
F -1.11950 -1.32602 1.21579

Thermal correction to Gibbs Free Energy = 0.120517

Sum of electronic and thermal Free Energies = -780.748310

SCF Done: E(RM062X) = -780.838858464 A.U. after 14 cycles

### **Dimethylcarbamic acid + BF<sub>3</sub>**

C -0.68317 -0.26433 -0.06919  
O 0.29440 0.54179 -0.16917  
B 1.83552 0.15274 0.02920  
F 1.92718 -1.21454 -0.36052  
F 2.50988 0.96991 -0.81114  
F 2.08972 0.30803 1.35616  
H 0.45016 -1.74162 -0.14292  
O -0.52806 -1.57346 -0.02405  
N -1.93670 0.19618 -0.01150  
C -2.20893 1.63166 -0.01308  
H -2.79677 1.89252 0.87386  
H -2.78131 1.90120 -0.90802

H -1.27070 2.18187 -0.00316

C -3.09403 -0.69266 0.04971

H -3.63973 -0.52656 0.98555

H -2.77254 -1.73038 0.00014

H -3.76467 -0.47924 -0.79024

Thermal correction to Gibbs Free Energy = 0.085661

Sum of electronic and thermal Free Energies = -648.252581

SCF Done: E(RM062X) = -648.331785000 A.U. after 12 cycles

